PHD

Valorisation of terpenes for sustainable materials

Maltby, Katarzyna

Award date:
2020

Awarding institution:
University of Bath

Valorisation of terpenes for sustainable materials

Katarzyna Anna Maltby

A thesis submitted for the degree of Doctor of Philosophy

University of Bath

Department of Chemical Engineering

November 2019

Copyright notice

Declaration of any previous submission of the work

The material presented here for examination for the award of a higher degree by research has / ~~has not~~ been incorporated into a submission for another degree. Figure 3.35 has been previously submitted for an MRes degree at the University of Bath.

Candidate's signature

Declaration of authorship

I am the author of this thesis, and the work described therein was carried out by myself personally, with the exception of Table 3.12 and Figure 4.38 which 100% of the work was carried out by other researchers.

Candidate's signature

Table of Contents

List of figures

Chapter 1

Chapter 3

Chapter 4

Figure 3.73 in Chapter 3 and Figure 4.8 and 4.10 in Chapter 4 were reprinted from scientific journals with permission.

Thesis figure number	reference	License number
Figure 4.8	*J. Appl. Polym. Sci.,* 2017, **134**, 44958.	4587641476897
Figure 4.10	*J. Appl. Polym. Sci.,* 2017, **134**, 44958.	4587641476897
Figure 3.73	*Chem. Eur. J.,* 2011, **17**, 7549-7559.	4701000434789

List of Tables

Abstract

Current industrial processes, such as plastic production and energy sector, are strongly dependent on fossil-based feedstocks. However, these feedstocks have a limited availability and adverse environmental impact, thus developing new sustainable feedstocks is one of the biggest challenges of modern research.

Terpenes are an abundant, but currently underutilised sustainable feedstocks. In terms of availability, the two major terpene feedstocks are limonene and pinene, but industrial biotechnology processes can deliver alternative terpene feedstocks, such as β-elemene or farnesene. In this project limonene and β-elemene were investigated in epoxidation and carbonation reactions.

Epoxides are used in many branches of industry - for example in the polymer industry to produce polyethers, polycarbonates, polyesters and others. Epoxidation of β-elemene was performed using three different catalysts: Venturello polyoxometalate (**VENT**), Mizuno polyoxometalate (**MIZ**) and trifluoroacetophenone (**TFAP**). All these use H_2O_2 as a green oxidant.

It has been found that the epoxidation of β-elemene is a consecutive reaction in which monoepoxide (**BEMO**) is formed first, then the bisepoxide (**BEBO**), and with long reaction times the trisepoxide (**BETO**). Epoxidation catalysed by **VENT** can be performed in flow microreactor and it can yield **BEMO**, **BEBO** and **BETO**. However, catalyst deactivation was found to be an issue.

Epoxidation catalysed by **MIZ** can yield only **BEMO** and **BEBO**, but no **BETO**. The issues with complex catalyst degradation and high reaction dilution have to be addressed to make this reaction industrially viable. Epoxidation catalysed by **TFAP** is still to be explored with preliminary results showing it can epoxidise **BE** to **BEMO**, **BEBO** and **BETO**.

Carbonation was first studied with 1,2-limonene oxide and 8,9-limonene oxide in order to achieve cyclic carbonates. The main focus was on using one catalyst for epoxidation and carbonation. The co-operative effect of **VENT** and Bu_4NBr was observed during 1,2-limonene oxide carbonation, but it did not have significant effect on 8,9-limonene carbonation. The influence of temperature, pressure, different catalysts and the starting stereochemistry of epoxide was tested. The resultant carbonates (*trans*-1,2-limonene cyclic carbonate and 8,9-limonene cyclic carbonate) underwent thiol-ene reaction to create bi-functional carbonate compounds and opened with an excess of amine resulting in novel hydroxyurethanes.

Carbonation of β-elemene bisepoxide and trisepoxide was performed using the quaternary ammonium salt Bu_4NBr in order to produce novel cyclic carbonates. The reactivity of each epoxide was dependent on the reaction temperature. Preliminary polymerisation studies were performed on

β-elemene biscarbonate (**BEBC**), but due to the low purity of monomer these were unsuccessful in yielding polymers. However, the experiments confirmed that **BEBC** can react with an amine resulting in hydroxyurethanes. The purity of **BEBC** could be improved by a better synthesis method as the main by-product is β-elemene monocarbonate monoalcohol (**BEMCMD**) which is a result of epoxide rearranging. It might be due to inefficient CO_2 mass transfer, high reaction temperature or a complex interaction between both of those.

Carbonation of **BETO** yielded β-elemene biscarbonate monoepoxide (**BEBCMO**) and β-elemene triscarbonate (**BETC**). However, **BETC** suffered the same issues as **BEBC** and under reaction conditions a mixture of **BETC** and β-elemene biscarbonate monoalcohol (**BEBCMD**) was produced. The most interesting carbonate synthesised was **BEBCMO** as it is a bi-functional carbonate species suitable for NIPU synthesis which has an additional epoxide group available for postfunctionalisation. **BEBCMO** can be synthesised selectivity at 100 °C, which is 40 °C reduction in the reaction temperature comparing to the **BEBC** and **BETC** synthesis.

In this work, the catalytic approach to **BE** epoxidation was shown and carbonation reaction was investigated as a way of utilising epoxides and another renewable feedstock – CO_2. Carbonation was first investigated using 1,2-limonene oxide and 8,9-limonene oxide. Then the carbonation of **BEBO** and **BETO** was investigated.

Acknowledgments

First, I am grateful for the opportunity to work on this project which would not be possible without EPSRC funding, the CSCT and the invaluable supervisory team. I would like to thank my supervisors, Dr Pawel Plucinski, Prof Matthew Davidson and Dr Ulrich Hintermair for believing in me and organising my (sometimes chaotic) stream of thoughts. Before my PhD I have never run an NMR, I have never done column chromatography and never worked with high pressure reactors. It was quite a task to make a scientist from me.

I would like to acknowledge the whole CSCT community (that involves academics, students, administrative support, communications coordinators and managers), it is a privilege to work in such inspiring environment and I believe the world would be a better place if everyone was as inspiring as you.

I would like to thank an army of reviewers who read and spell checked various bits of my thesis, my posters and presentations throughout my PhD, in non-particular order: Stuart, Izzy, Maya, Steffi, Paul, Emma, Matt, Rachael, Nick, George and Andy. In the reviewing area an honourable mention is earned by Theo, who achieved unachievable and has read every single chapter of this thesis. Except experimental sections, we all know reading experimental is the worst, so I kept it as a special treat for my husband (he signed the paper, he cannot leave me now).

Thank you to NMR specialists Dr Catherine Lyall, Dr John Lowe and Dr Tim Woodman for answering all my questions about NMR spectroscopy, as a person working with natural compounds I always had many questions. I also would like to acknowledge Rémi Castaing and Shaun Reeksting for patiently answering all my questions about TG-MS, DSC, GPC and ESI-MS. Thank you for helping with my results analysis when I was really lost.

Finally, I would like to thank two heroes, who are often overlooked, but vital for many projects to be possible. I would like to thank glassblower Phil Jones for being able to repair anything from glass round bottom flask to glass microreactor and I would like to thank Paul Frith for being able to design and build anything from aluminium heating block to parallel reactor.

To my family, people who I already have mentioned and those who I overlooked,

Thank you.

Structure of this thesis

This thesis consists of 5 chapters. Each of the chapters, except Chapter 2 (Aims and Objectives), has its own reference list included at the end of the chapter.

Chapter 1 provides background information to renewable feedstocks and presents terpenes as one of the viable renewable feedstocks. It contains an overview of terpene uses and their application in renewable polymers. The polymers overview focuses on the materials synthesised from terpene epoxides and further functionalisation of terpene-derived materials, but other examples are presented as well. The chapter finishes with examples of terpene-based polymers which could find their application in sustainable coatings.

Chapter 2 includes the aims and objectives of this PhD project.

Chapter 3 and Chapter 4 are results sections. Each of them starts with an introduction which provides background information relevant to the methods used in the experiments and shows opportunities for future work. Chapter 3 and Chapter 4 contain their own sections with conclusions, future work and experimental section. Future work is not as detailed as it is going to be in the Chapter 5.

Specifically, Chapter 3 provides an inside into terpenes epoxidation and presents results from three different catalytic procedures used for epoxidation of β-elemene, a terpene feedstock available via industrial biotechnology. Chapter 4 focuses on terpene-derived cyclic carbonates. It starts with work on monofunctional limonene cyclic carbonates and continues with cyclic carbonates derived from β-elemene epoxides synthesised in Chapter 3.

Chapter 5 contains a detailed description of overall conclusions and recommended future work.

Abbreviations

Al cat – aluminium amino-tris(phenolate)

AIBN – azobisisobutyronitrile

Aliquat 336 – commercially available mixture of C8 and C10 chloride quaternary ammonium salts

inert atm. – inert atmosphere, Ar or N_2

Bu4N-X – quaternary ammonium salt X = Cl, Br, I, F

n-BuOH – n-butanol

t-BuOH – tert butyl alcohol

$CHCl_3$ – chloroform, $CDCl_3$ is an abbreviation from deuterated chloroform

CO_2 – carbon dioxide

Conv. – conversion [%]

DABCO – 1,4-diazabicyclo[2.2.2]octane $C_6H_{12}N_2$

DBU – 1,8-diazabicyclo[5.4.0]undec-7-ene $C_9H_{16}N_2$

DCM – dichloromethane

DMAP – 4-dimethylaminopyridine $C_7H_{10}N_2$

DMDO – dimethyl dioxirane

DMF – dimethylformamide

DMSO – dimethyl sulfoxide

$\overline{DP_n}$ – degree of polymerisation

Et_2O – diethyl ether

EtOAc – ethyl acetate

eq – equivalent

GC-MS – gas chromatography mass spectrometry

H_2O_2 – hydrogen peroxide

IR – infrared spectroscopy

mCPBA - meta-chloroperoxybenzoic acid

MeCN – acetonitrile

MeOH - methanol

MIZ – Mizuno catalyst $[Bu_4N]_4[\gamma\text{-}HPV_2W_{10}O_{40}]$

M(OTf) – trifluoromethanesulfonate M = Yb, Fe, Bi

MTBD – 7-methyl-1,5,7-triazabicyclo(4.4.0)dec-5-ene $C_8H_{15}N_3$

N_0 – initial number of monomer units

N – number of molecules after time t (includes monomers, oligomers and polymers)

NBS – N-bromosuccinimide

NIPU – non-isocyanate polyhydroxyurethane

NIST – National Institute of Standards and Technology

NMR – nuclear magnetic resonance

O_2 – molecular dioxygen

p – pressure [bar]

P – extend of reaction

PPNCl – bis(triphenylphosphine)iminium chloride

Priamine 1074 – biobased diamine derived from fatty acids produced by Croda

i-PrOH – isopropyl alcohol

PU – polyurethane

PW-Amberlite – heterogeneous peroxotungstophosphate catalyst immobilised on ion exchange resins

SBA-16 – mesoporous silica

t – time [h] or [min]

T – temperature [°C]

TBD – triazabicyclodecene $C_7H_{13}N_3$

TFAP – 2,2,2-trifluoroacetophenone

THF – tetrahydrofuran

UV – ultraviolet, electromagnetic radiation with wavelength from 10 nm to 400 nm

VENT – Venturello catalyst $[(C_8H_{17})_3NCH_3]_3(PW_4O_{24})$

Compounds abbreviations

Compounds abbreviations are included within the text in **bold** font. All abbreviations follow the same naming system presented on the figure below. The abbreviations of the main compounds in this thesis are included in the list below.

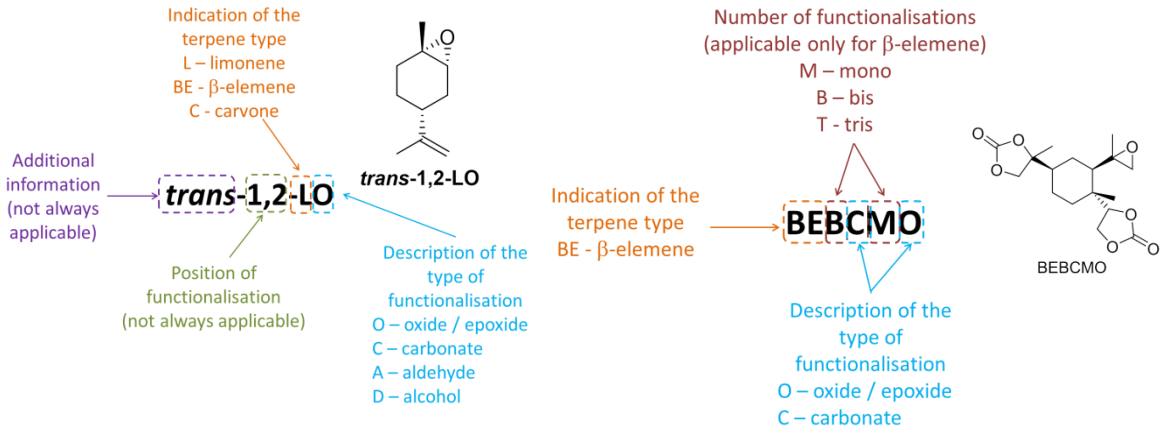

Compounds abbreviated in this thesis

Limonene-derived compounds

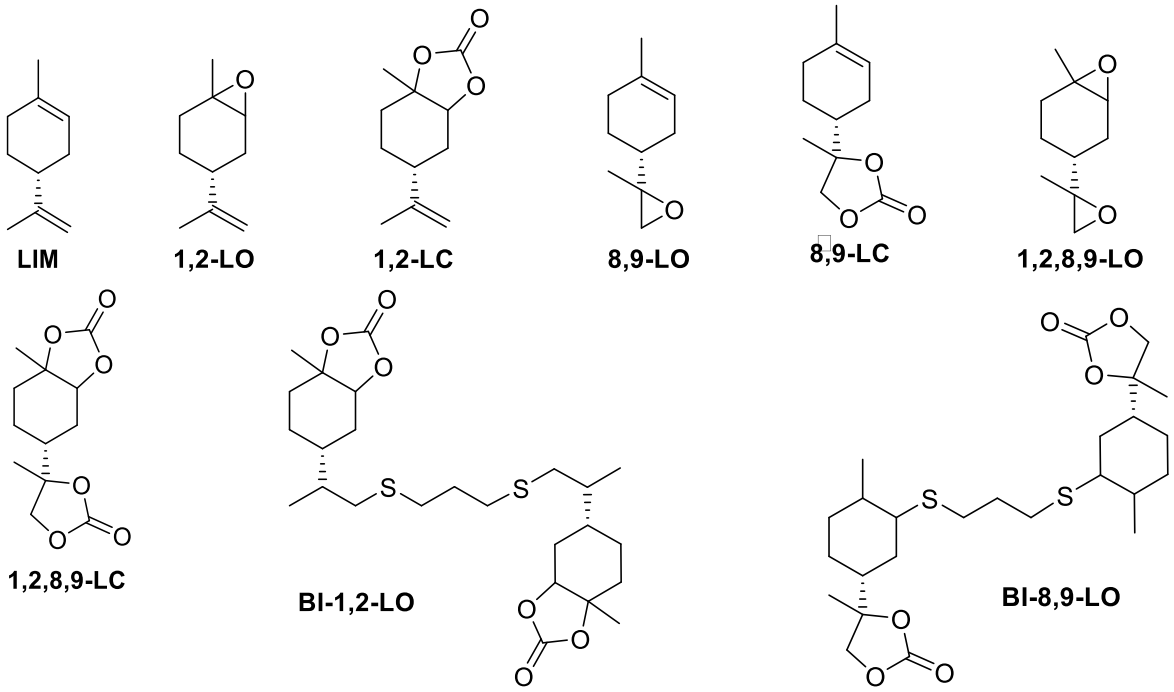

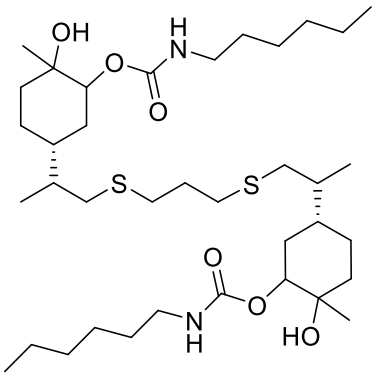

BI-1,2-LO-HU

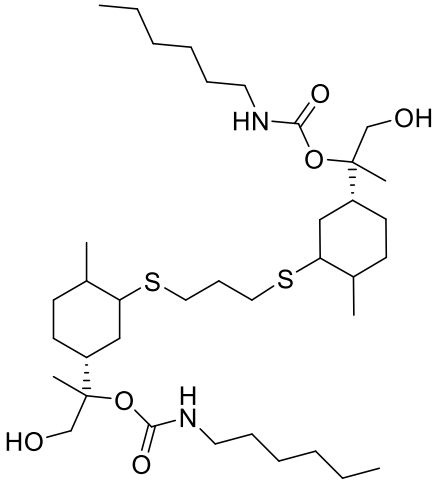

BI-8,9-LO-HU

Carvone-derived compounds

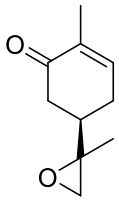

8,9-CO

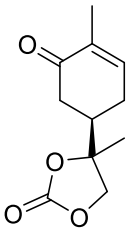

8,9-CC

β-elemene-derived compounds

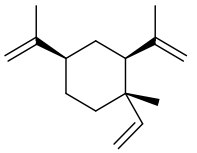

BE

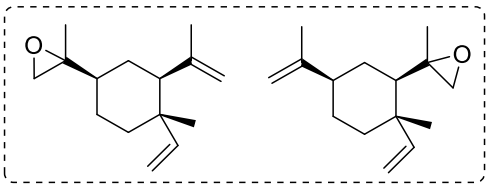

BEMO

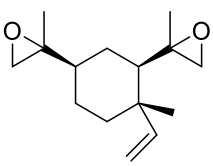

BEBO

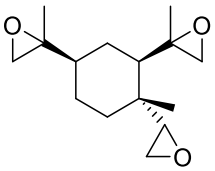

BETO

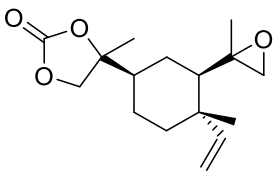

BEMCMO

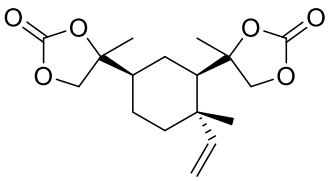

BEBC

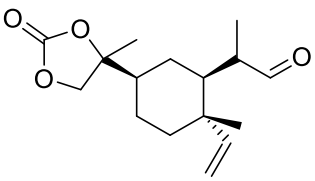

BEMCMA

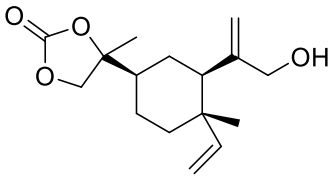

BEMCMD

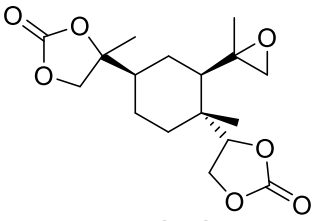

BEBCMO

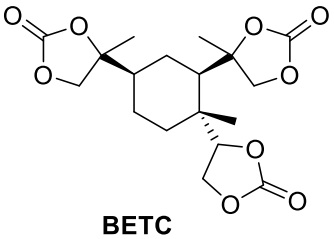

BETC

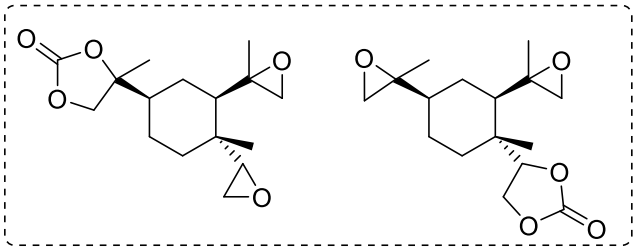

BEMCBO

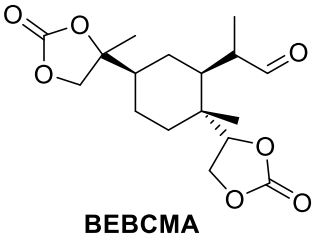

BEBCMA

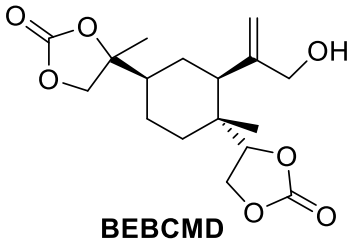

BEBCMD

1. Introduction and literature review

This section includes background information about crude oil and the petrochemical industry with focus on non-energy uses of crude oil, especially polymers. This is followed by an introduction to renewable feedstocks and renewable polymers. This section continues with terpenes, their application in industry and an overview of terpene-based polymers.

1.1 Crude oil

Our modern lifestyle highly depends on crude oil; from 2009 to 2018, the worldwide daily demand for crude oil increased by 18% and is predicted to continue to increase.[1] However, in the United Kingdom between 2004 and 2017, oil consumption experienced a general decline, with a small increase of consumption from 2014 to 2017.[2] The majority of the UK's oil demand comes from the transport sector – car travel, goods vehicles, busses and air travel. In the UK, about 10% of the overall oil consumption is dedicated to non-energy uses, where oil is used as feedstock to produce goods, for example plastics and chemicals.[3]

The oil industry is vital for maintaining our modern lifestyle; however, oil exploration and production have negative environmental impacts.[4] A great deal of effort is dedicated to reducing oil dependence via the use of renewable energy sources and renewable feedstocks. Renewable feedstocks are especially important for ensuring lower oil dependence for everyday use materials, such as polymers, which currently are mostly produced from petrochemical resources.[5]

1.2 Polymers

Polymers are well known and widely used materials. They can have diverse structures, tuneable properties and they can come from various natural or synthetic sources. Synthetic polymers have various structures and properties, thus technically, they can be used in all branches of industry.[6] Polymers are produced on a multimillion tonnes scale in form of plastics, rubbers and fibres. The world production of plastics rose by 50 % from 2002 to 2013 and in 2017 it reached 348 million metric tonnes.[7] Synthetic rubber production reached 15 million metric tonnes worldwide in 2017.[8] Synthetic fibres production reached almost 65 million tonnes worldwide in 2017.[9] Based on the production volumes, plastics have the highest environmental impact. According to the Ellen MacArthur Foundation, plastics used as packaging materials have the most significant environmental impact due to their high production volumes and disposable character.[10] However, there are also increasing global demands for other types of polymers which are used in coatings,

foams or paints, such as polyurethanes. The polyurethane global demand has increased by 25 % from 2012 to 2017 and reached 16.9 million metric tonnes in 2017, thus finding more sustainable alternatives is desirable.[11]

The use of plastics and their end of life raise substantial environmental concerns in Europe and globally. The properties of plastics that make them desirable high performance materials, such as high durability and resistance to degradation, make most plastics resistant to biodegradation in the natural environment.[12] From 1950 to 2015 about 6300 million metric tonnes of plastic waste were generated worldwide. Only 9% of plastic waste produced was recycled and 12 % was incinerated. The rest was disposed in landfill or was released into the environment.[12]

Influenced by the growing European plastic problem, in 2015 the European Commission adopted its Circular Economy Action Plan and in 2018 the European Commission released its brochure on the Strategy for Plastics in Circular Economy that included commitment to ensure all packaging plastics on the EU market are either reusable or recyclable in a cost-effective manner by 2030.[13] The brochure also indicated the importance of consumer behaviour, innovative materials and alternative feedstocks. Compostable and biodegradable plastics are of special interest.[13] Following this, SusChem, a pan-European body launched by the European Commission in 2004, released its Plastics Strategic Research Innovation Agenda, which identified areas where the circularity of plastics can be improved.[14] Circularity in terms of alternative feedstock includes using agricultural biomass, forest biomass and waste based raw materials as feedstock for bio-based polymers. The key challenges are related to inefficiencies in biomass to product processes, for example low yields, high energy demand and complexity of feedstock.[14]

1.3 Renewable feedstocks for chemicals and plastics

The use of renewable feedstocks in manufacturing has attracted increasing interest in recent years as the conversion of waste streams to high value chemical feedstocks is economically appealing. The particular application strongly depends on the type of feedstock, its availability and price.[15] The cost and availability have to match the demand for the product. Another factor in choosing renewable feedstock is its oxygen content, which is important in terms of processing.[15, 16] In general, natural products are often stereochemically and regiochemically pure which is potentially valuable for the chemical industry.[17]

Commercially, renewable feedstocks like carbohydrates, vegetable oils and lignocellulosic waste, are used in sustainable production of goods in various branches of industry. Carbohydrates like corn starch, sucrose and cassava are used in fermentation processes to produce lactic acid, propanediol, butanediol, succinic acid and terpenes.[18] Additionally, polyols which are used in food

industry can be derived via hydrogenation or hydrogenolysis of carbohydrates.[19] Vegetable oils can be used in soaps, detergents, surfactants and lubricants.[19] Lignocellulosic waste is a particularly challenging feedstock due to its ill-defined structure.[15] The fermentation of lignocellulosic material performed by the company Virent (USA) produces bio-gasoline and companies like BetaRenewables and GranBio focus on ethanol production.[18] However, lignocellulosic feedstock can be also used to produce more valuable products such as levulinic acid, furfural, sorbitol and xylitol.[20] Cellulose also has specialist application as hydrogels and flexible materials for electronics.[21]

One of the renewable feedstocks which is often neglected is carbon dioxide (CO_2). CO_2 is a naturally occurring gas in the atmosphere, but it can be considered as a sustainable source of carbon.[22, 23] CO_2 is used industrially for the synthesis of urea, salicylic acid and inorganic compounds,[22, 24] but it is also used in its supercritical state as a reaction solvent and in supercritical extractions.[25] CO_2 is also investigated in CO_2-epoxide coupling for sustainable polymers such polycarbonates and non-isocyanate polyhydroxyurethanes.[26]

It is worth noting that most renewable feedstocks have different physicochemical properties than crude oil, as most renewable feedstocks are oxygen rich solids, whereas crude oil is a non-oxygenated liquid.[27] Renewable feedstocks can provide a wide range of chemical building blocks, but they require different processing which often requires the development of new chemical strategies for depolymerisation and removing functional groups.[27] Terpenes are an example of a renewable feedstock which is similar in physicochemical properties to crude oil; they are non-oxygenated unsaturated liquid hydrocarbons. That means that well known olefin chemistry can be applied which gives terpenes an advantage over other renewable feedstocks.[28]

There is a consensus that sustainable biorefinery should focus on producing specialty or platform chemicals instead of fuel production.[27] This review will focus on renewable monomers and polymers.

1.4 Renewable polymers

Renewable polymers can be divided into three groups.[29] The first group are natural polymers, for example cellulose or starch. The second group are polymers generated via fermentation of natural resources, for example polyhydroxyalkanoates. The last group are polymers built from renewable monomers, for example polylactic acid.[29] Not all renewable polymers are biodegradable and some renewable polymers are direct drop-in replacements for fossil-based plastics, thus renewable plastics can be divided into groups based on renewability and biodegradation (Figure 1.1).[30] Often, studies assume that bio-derived polymers are biodegradable, but only limited

examples of degradability are shown.[31] Extensive research is needed to fully evaluate biodegradability and possible impacts of renewable polymers on the environment.[31]

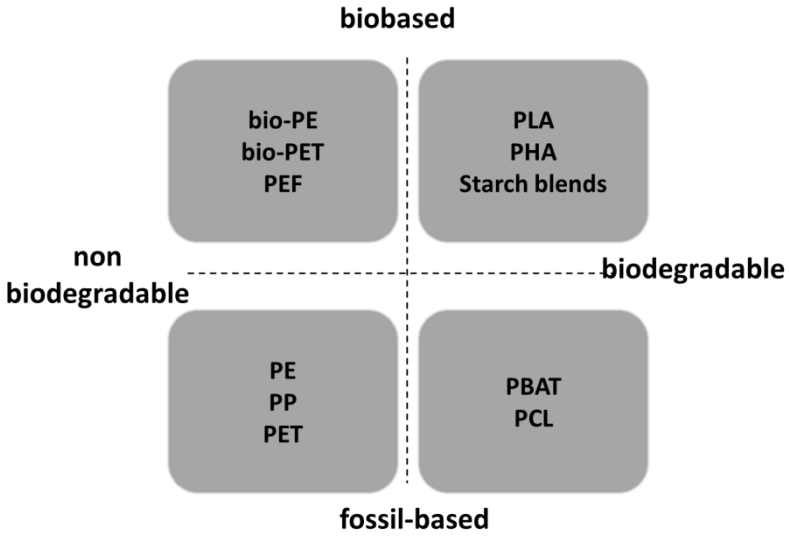

Figure 1.1 Categories of plastics based on renewability and biodegradation.[30] PE – polyethylene, PP – polypropylene, PET - polyethylene terephthalate, bio-PE – bioderived PE, bio-PET – partially bioderived PET, PEF - polyethylene furanoate, PLA – polylactic acid, PHA – polyhydroxyalkanoates, PBAT - polybutylene adipate terephthalate, PCL – polycaprolactone.

In 2018 the worldwide production of renewable plastics reached 2.11 million metric tonnes, which is less than 1% of the overall plastic production; however, market data collected by European Bioplastics predicts that global production of bioplastics will increase.[32] The production of renewable plastics is the highest in Asia, but Europe is the largest market for renewable plastics.[32] Renewable plastics are mostly utilised in the packaging sector, but other sectors like textiles, automotive, and consumer goods can also benefit from the development of renewable polymers.[32] The most widely used bioplastics are polylactic acid (PLA), polyhydroxyalkanoates (PHA), bio-based polyethylene (bio-PE) and bio-based polyethylene terephthalate (bio-PET).[32]

PLA is a commercially available aliphatic thermoplastic polyester which is derived from renewable resources such as fermented starch from corn or sugarcane. Industrially it is synthesised through ring-opening of the cyclic lactide dimer.[33] Some applications of PLA include packaging, textile and fiber.[34] Due to its non-toxicity, biocompatibility and biodegradability PLA is often considered for biomedical application.[33] The main challenges are with high temperature applications (PLA has a low glass transition temperature around 60 °C) and brittleness. Some investigations into blending PLA with other polymers in order to improve its properties and expand the range of applications have been undertaken, but blending may compromise its biodegradability.[33, 34]

PHA is produced and accumulated by microorganisms under limited nutrient growth conditions.[35] PHA was commercialised in 1970, but initially it was more expensive than other biopolymers and the high cost of PHA remains the biggest challenge in its application.[36] A recent advancement is to use waste feedstock containing sugars or fatty acids as a carbon source which can significantly reduce the cost of the polymer.[37] The composition and quality of PHA can vary depending on the bacteria culture used, the growth conditions and the amount of carbon source.[36] PHA is fully bio-derived and biodegradable with properties similar to polypropylene.[38] The main focus is on medical application, but PHA can also be used in material and packaging industries.[35, 36]

Bio-PE is produced from ethanol which can be obtained by fermentation of sugarcane and molasses. Bio-PE maintains the same properties as fossil-based PE and has the same applications, mostly in packaging.[39] The main environmental advantage is due to the large amount of CO_2 absorbed by sugarcane while growing. However, the environmental impact of bio-PE should be evaluated through life cycle analysis, because transportation of bio-ethanol can have huge impacts on its environmental benefits.[40]

Bio-PET is partially bio-derived and chemically identical to conventionally produced PET. Bio-derived ethylene glycol is used in its synthesis which results in a 20 % (by mass) bio-based PET.[41] The Plant PET Technology Collaborative aims to deliver 100 % bio-based PET, but obtaining bio-based terephthalic acid is still a challenge.[41, 42] Despite the huge market for PET the research focus has shifted to 100 % bio-based PET alternatives like polyethylene furanoate (PEF).[41] PEF has a different chemical structure than PET; instead of terephthalic acid a novel bio-based monomer is used – 2,5-furandicarboxylic acid (FDCA).[43] Despite its different chemical structure PEF is similar enough to be used in the existing PET infrastructure and can be recycled in a similar way to PET. Moreover, it has superior barrier properties and is stronger than PET, which allows for improvements in lightweight packaging.[44]

Currently a wide range of renewable monomers is being investigated in order to produce renewable polymers, for example carbohydrates and natural oils.[45] Carbohydrates include natural polymers like lignin, cellulose, chitin and starch as well as sugars like glucose.[29, 46] Natural oils include vegetable oils, seed oils and terpenes.[29, 46] The next section will focus on terpenes and terpene-derived monomers which are subject of intensive research and some promising, renewable polycarbonates and polyesters can be synthesised on lab scale. However, terpene-derived materials are not limited to polycarbonates and polyesters.[47]

1.5 Terpenes as a renewable feedstock

Terpenes are an abundant, but currently underutilised, family of natural products. Depending on the number of isoprene units, terpenes can be classified as a monoterpenes, sesquiterpenes etc. (Figure 1.2).[48] In the 1950s terpenes were harvested by tapping live pine trees.[49] This process has been replaced by recovering crude sulfate turpentine from paper mills, from which pure α- and β-pinene are isolated by vacuum distillation and desulfurization.[49] Other extraction methods include cold-pressing, steam distillation and solvent extraction.[19] However, all of these conventional extraction techniques have drawbacks including long extraction times and high energy consumption.[50] Research has focused on improving efficiency of terpene extraction, for example intensification of limonene extraction from orange peel can be achieved by using microwave extraction which significantly improves the yield of limonene.[50]

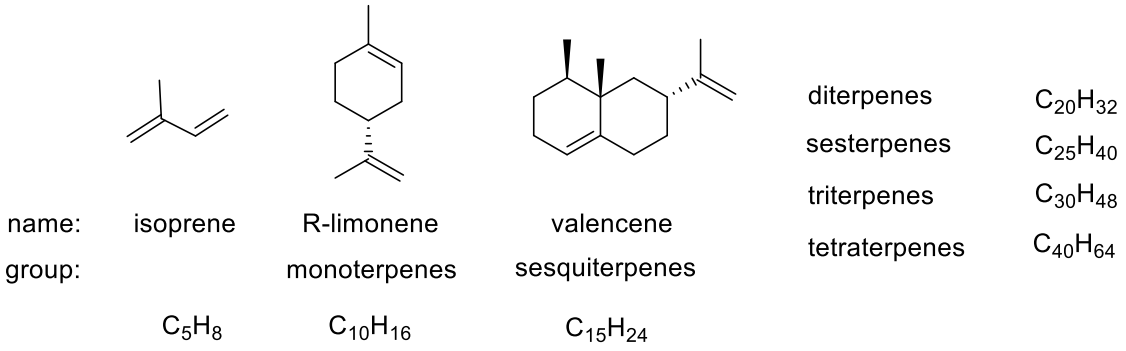

Figure 1.2 Terpene classification depending on the number of isoprene units.[48]

In terms of availability, the two major terpene feedstocks are limonene and pinene. Limonene can be extracted from orange peel, a waste material from the production of orange juice. In 2014, about 50 000 – 75 000 tonnes of limonene were produced globally, but this amount can theoretically increase to 125 000 tonnes per year based on the availability of citrus peel waste.[51] Pinene is a main component of turpentine, a waste stream from the wood and paper industry.[52] The global production of turpentine in 2014 was 440 000 – 505 000 tonnes, of which approximately 60 % was α-pinene and 20 % β-pinene.[51] Additionally, large scale industrial biotechnology provides geographically flexible supplies of terpenes via fermentation of plant sugars and cellulose waste.[53, 54] Some commercial examples include β-elemene produced by Isobionics[55] and farnesene produced by Amyris (Figure 1.3).[56]

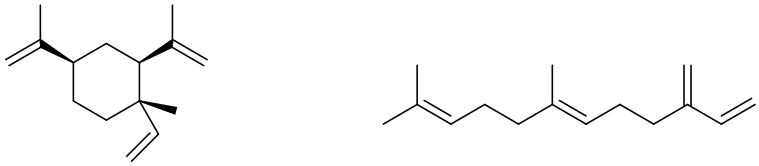

Figure 1.3 Structure of β-elemene (produced by Isobionics) and trans-β-farnesene (produced by Amyris).

Terpenes are already used in industry in fine chemical production, for example the aldol condensation of citral and acetone (Figure 1.4). This condensation forms pseudoionone which is the first step of β-ionone synthesis, which is used in pharmaceutical industry for example in vitamin A synthesis.[19, 57] The production of camphor, which is used in the pharmaceutical and cosmetics industry, requires camphene, which is produced via isomerization of α-pinene. Camphene is also used in the fragrance industry and as a food additive.[19, 58]

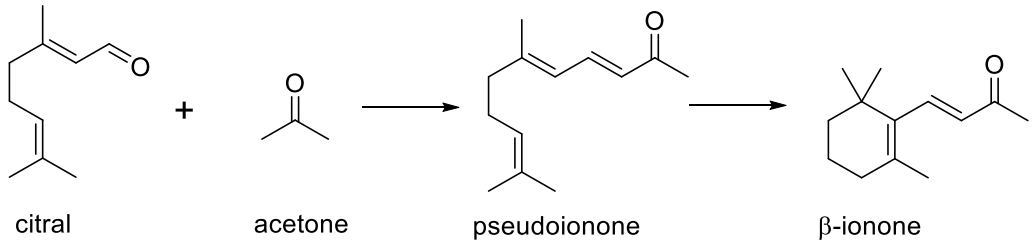

Figure 1.4 Aldol condensation of citral and acetone.[19]

The key markets for terpene-derived products have been identified by Tsolakis *et al.* as flavours and fragrances, pharmaceuticals, fuels and polymers.[59] The flavour and fragrance industry is currently the main market in terms of use of terpenes; it is a high value market, but uses relatively low volumes of terpenes.[59] Pharmaceutical products derived from terpenes need more large-scale trials[60, 61] and improvements in synthetic processes to reduce costs.[59, 62] Fuels from terpenes are interesting because of exceptional volumetric net heat of combustion, low volatility and compatibility with existing infrastructure, but have challenges due to high viscosity and inefficient supply of terpenes.[59, 63, 64] The polymer market has high potential and, with the current interest in renewable polymers, terpenes could be interesting monomers. However, difficulties occur when transforming research to industrial scale production.[59] Currently only limited examples of terpene-based polymers are industrially available; polyisoprene products are a natural rubber substitute[65] and terpene resins are used as adhesives, polymer additives and coatings.[66, 67]

1.6 Terpene-based monomers for the synthesis of polymers

Polyolefins

Terpene structures are rich in double bonds which makes them an obvious choice for cationic, anionic or radical polymerisation. One of the major terpene feedstocks, pinene, has been investigated for cationic polymerisation. Pinene has two isomers, α-pinene and β-pinene (Figure 1.5). Due to steric hindrance of the endocyclic double bond in α-pinene, cationic polymerisation gave poor results.[48]

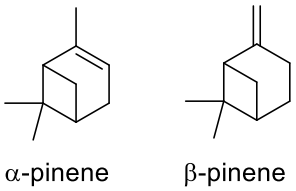

Figure 1.5 Structures of α-pinene and β-pinene.

β-Pinene is more reactive in cationic polymerisation than α-pinene. A plausible mechanism of β-pinene polymerisation is depicted in Figure 1.6.[68-70] The most effective catalysts ($AlCl_3$ and ethylaluminium dichloride) resulted in low molecular weight polymers (4 kg mol^{-1}) with unsatisfactory thermal properties (T_g < 65 °C).[69] Thus, commercially available poly(β-pinene)s are used in limited applications, mostly in pressure sensitive adhesives or hot-melt coatings.[66]

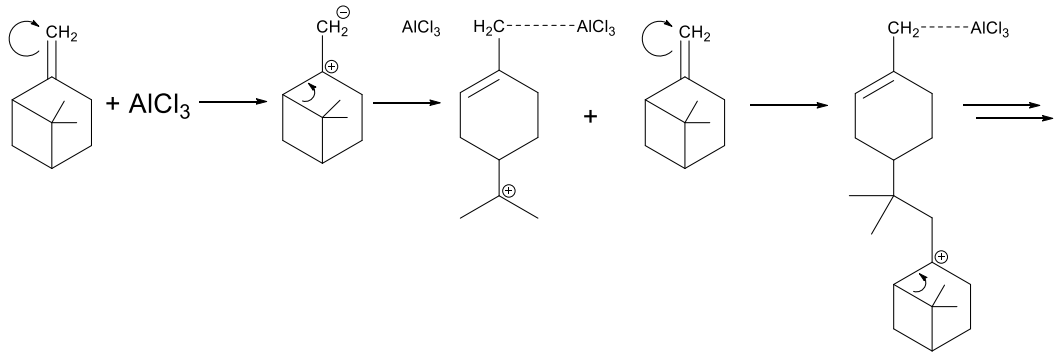

Figure 1.6 Plausible mechanism of cationic polymerisation of β-pinene using $AlCl_3$.[70]

Polymerisation of β-pinene using a catalytic system based on $AlCl_3$ etherates, such as $AlCl_3(OPh_2)$ and $AlCl_3(EtOAc)_{0.8}$, allowed a slight improvement in molecular weight (13.8 kg mol^{-1}) and glass transition temperature (T_g = 86 °C).[69] The reaction proceeds at room temperature with 1 mol % $AlCl_3$ etherate co-initiator which would make this reaction industrially viable.

An alternative strategy for improving terpene polymer properties could be copolymerisation of terpenes and other natural oils. Limonene and myrcene have been copolymerized with tung oil using BF_3 as a co-initiator (Figure 1.7).[71] Depending on the terpene and its weight percentage,

different polymer properties can be achieved. The Young's modulus decreases with increasing addition of terpene additives, whereas the glass transition temperature is a function of the type of terpene co-monomer and its weight content.[71]

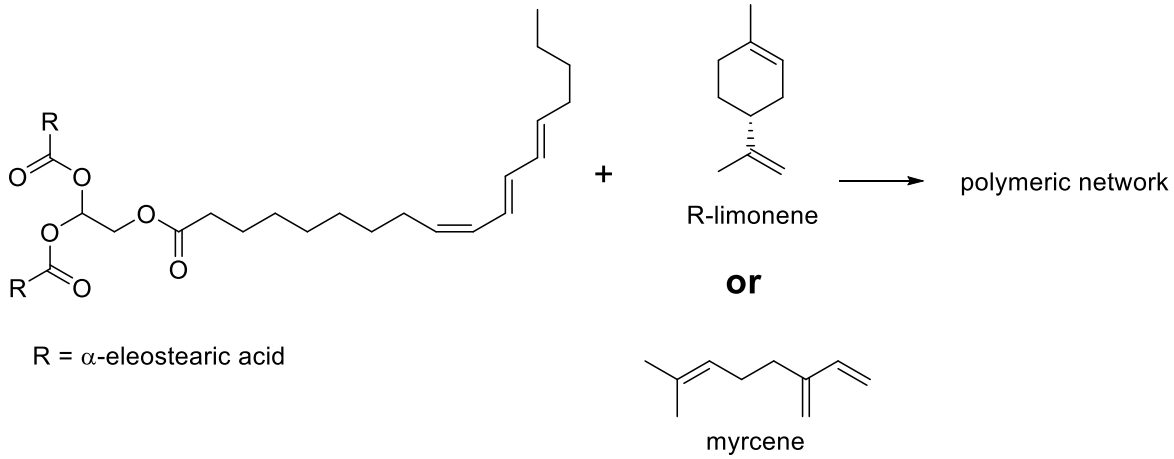

Figure 1.7 Cationic polymerisation of tung oil and terpenes using BF_3.[71]

Polyesters

Aoshima *et al.* investigated copolymerisation of aldehydes derived from terpenes with isobutyl vinyl ether (IBVE) using $EtSO_3H/GaCl_3$ as an initiator and 1,4-dioxane as the Lewis acid (Figure 1.8).[72] These copolymers are especially interesting due to their selective acid stability. In neutral and base conditions the copolymers were stable; however, in mild acidic conditions they undergo degradation. Moreover, the products of the degradation can be potentially polymerised.[72]

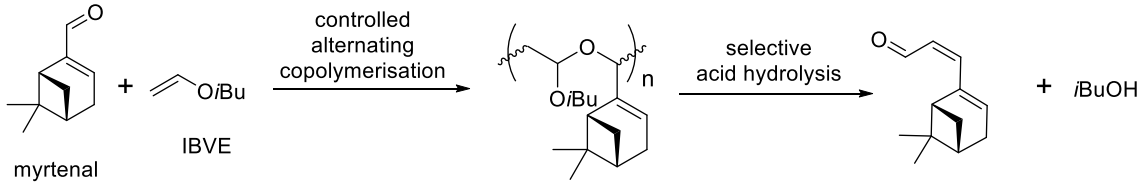

Figure 1.8 Copolymerisation of myrtenal with isobutyl vinyl ether (IBVE) and acid hydrolysis of the obtained polymers.[72]

The menthol derivative (-)-menthone was used in polyester synthesis catalysed by a zinc-alkoxide catalyst (Figure 1.9).[73] First, a cyclic terpenoid with a ketone group is transformed via Baeyer-Villiger oxidation into a lactone. Then the lactone undergoes ring opening polymerisation to form an aliphatic polyester. The synthesised polymers had molecular weights up to 91 kg mol^{-1} and a dispersity (Đ) of 1.1. The thermal analysis of those polymers was not reported.

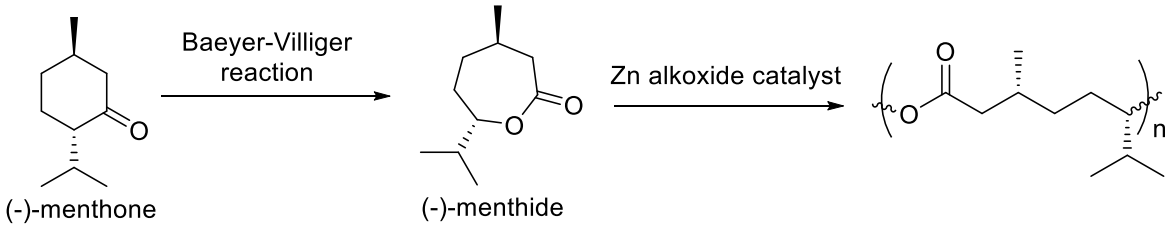

Figure 1.9 Polyesters synthesised from menthone.[73]

Dihydrocarvone, a terpene which occurs in the essential oils of caraway and dill,[74] was also used in the synthesis of polyesters (Figure 1.10). The synthesised polyesters had a glass transition temperature below -20 °C, a maximum molecular weight of 59 kg mol^{-1} and a low Đ.[75] The reactive alkene side groups could be further functionalised by epoxidation or radical induced crosslinking.

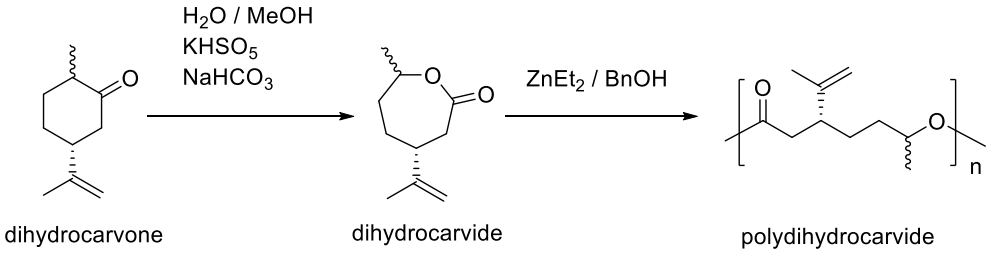

Figure 1.10 Synthesis of polyesters from dihydrocarvone.[75]

Polyesters derived from menthone and dihydrocarvone are scientifically interesting, but the supply of these terpenes is limited, thus polyesters derived from more available terpene feedstock are desirable.[76] This issue has been addressed by Quilter *et al.* by developing a four-step process whereby one of the major terpene feedstocks, β-pinene, is converted into 4-isopropylcaprolactone, which can be further used in polymerisation (Figure 1.11).[76] The highest molecular weight obtained was in the range of 30 kg mol^{-1}. The resultant polyesters were gels with low glass transition temperatures.

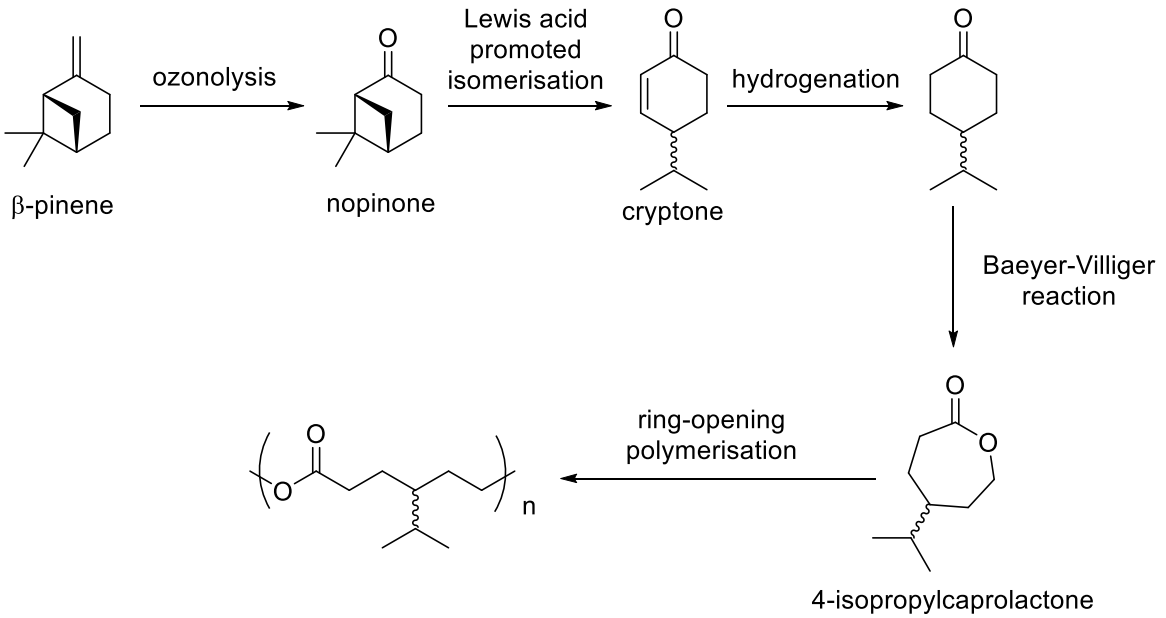

Figure 1.11 Polyesters derived from β-pinene.[76]

An alternative route to polyesters is the ring-opening copolymerisation of epoxides and anhydrides. The general reaction scheme is depicted in Figure 1.12. Terpene-based epoxides (limonene oxide, limonene dioxide and α-pinene oxide) have been copolymerized with various anhydrides. This copolymerisation reaction usually requires metal-based complexes as catalysts and is usually run in solvents.[77-79] Examples of terpene-derived polyester via epoxide and anhydride polymerisation are presented in Table 1.1.

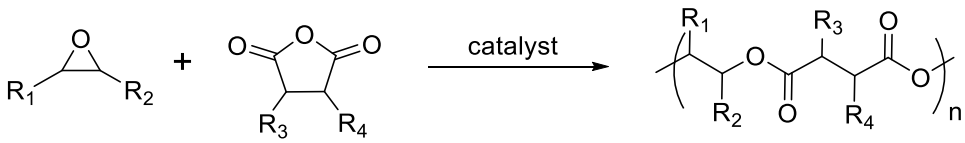

Figure 1.12 General reaction scheme for epoxide anhydride polymerisation.

Table 1.1 Examples of reported copolymerisation of terpene oxides with anhydrides.

Epoxide	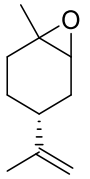 limonene oxide		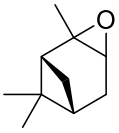 α-pinene oxide	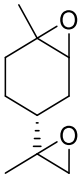 limonene bisepoxide	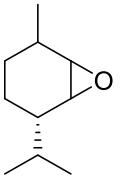 menthene oxide
Anhydride	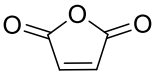	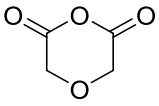	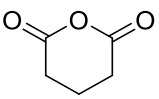	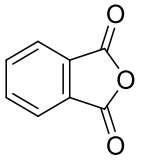	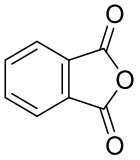
M_n [kg mol^{-1}]	12	36	8.4	8.7	12.7
Đ	1.1	1.2	1.2	1.94	1.20
T_g [°C]	62	54	not reported	59	165
reference	77		78	79	79

Polyamides

Building on previous menthone research,[73] Winnacker *et al.* have synthesised polyamides derived from menthone (Figure 1.13).[80] The corresponding oximes and lactams were successfully synthesised; however, separation of the two regio-isomers is difficult. Two procedures have been attempted for polymerisation: an anionic and an acid-catalysed procedure. The polymerisation procedure strongly affected the molecular weight of the polymers. GPC analysis showed average molecular weights in the range of 0.3 – 2.8 kg mol^{-1}. The oligomers produced were yellow-coloured solids, hardly soluble in common organic solvents, but they were soluble in formic acid or hexafluoroisopropanol. Further research is required to improve the molecular weight distribution of these polymers.

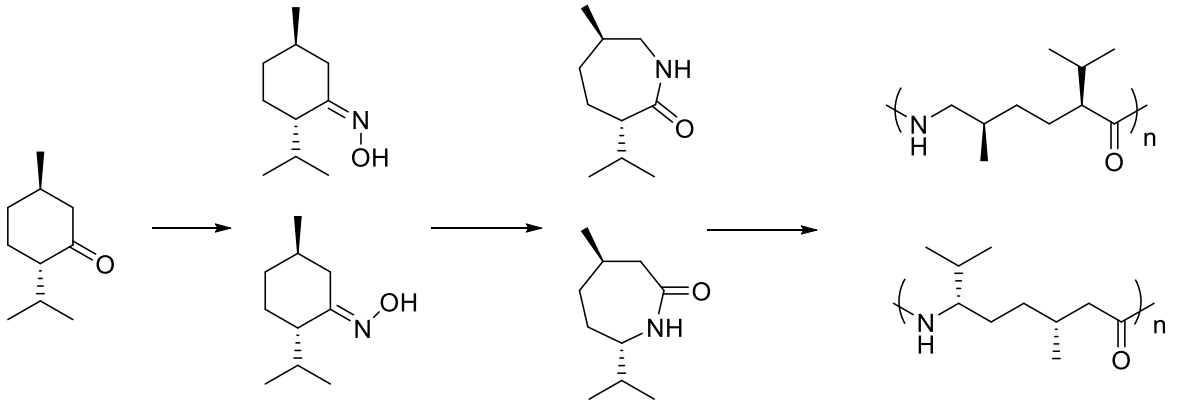

Figure 1.13 Route to polyamides from menthone.[80]

Polysulfides and thiol-ene addition

Crockett *et al.* investigated the production of the polysulfide made from limonene and sulfur (Figure 1.14) in the vulcanisation reaction.[81] The synthesised material was used as coating, for moulding solid devices and cleaning mercury salts from water and soil. Considering that the polymer is synthesised from two waste streams, it is an inexpensive material, which is highly attractive for removing metals from water and building sensors.[81]

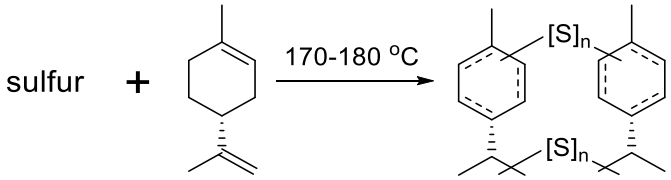

Figure 1.14 Synthesis of sulfur-limonene polysulfide.[81]

A presence of double bonds in their structures makes terpenes an interesting feedstock for thiol-ene reactions. Thiol-ene reactions have been applied in order to produce new monomers[82] or polymers.[83] Meier *et al*. were the first research group which applied thiol-ene chemistry to terpenes, and they synthesised new terpene-derived monomers and polymers (Figure 1.15).[82] The synthesised polymers had low glass transition temperature (between -9 and -10 °C) with a maximum molecular weight of 10 kg mol^{-1} and a Đ of 1.65 - 1.79. In order to produce higher molecular weight polymers, terpene-derived polymers needed to be copolymerized with longer alkyl chains. This reaction improved the molecular weight to 24 kg mol^{-1} and increased the Đ to 2.47. The resultant polymers had a lower glass transition temperature of -45 °C.[82]

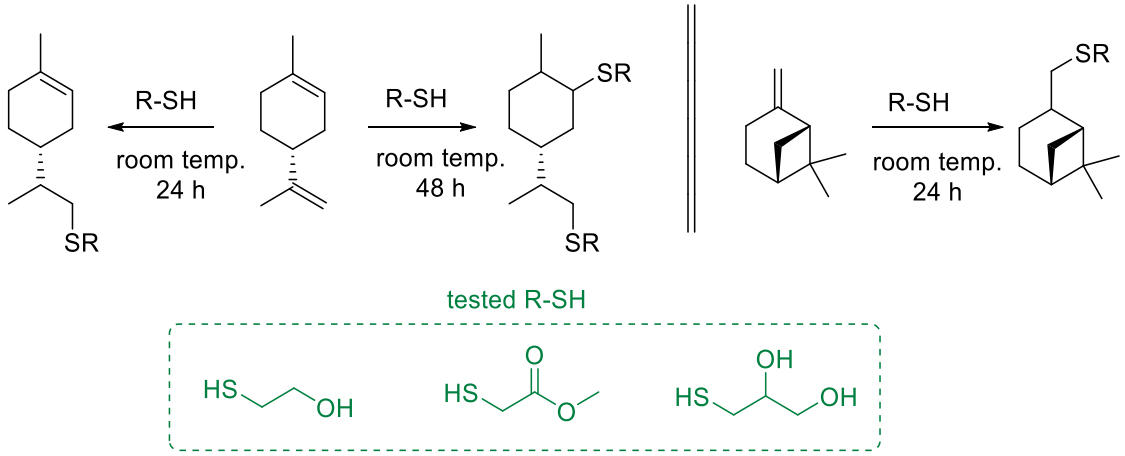

Figure 1.15 New monomers synthesised by Meier et al.[82]

The same research group continued with copolymerisations of terpene-derived monomers with castor oil (Figure 1.16).[83] The resultant polymers were mostly insoluble in THF and HFIP, thus probably had higher molecular weights than previously published polymers. The only soluble polymer sample showed a M_n of 31.8 kg mol^{-1} and Đ of 2.20. Polyether polysulfides and polyether

polysulfones could be potentially interesting for polyethylene replacement due to their thermal properties, but further research is required.[83] Limonene-based poly(thioether) networks have also been investigated by the Johansson group.[84] They achieved high yields of thermoset polymers with tuneable thermo-mechanical properties.

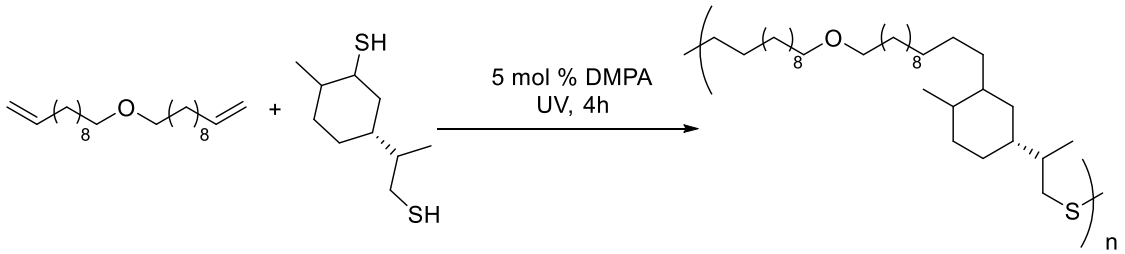

Figure 1.16 Polyether polysulfide synthesised from limonene dithiol and di-10-undecenyl ether.[83]

Polyethers

In 1985, Aikins and Williams reported polyethers derived from 1,2-limonene oxide, α-pinene oxide and β-pinene oxide (Figure 1.17).[85] All oxides reacted in radiation-induced cationic polymerisation yielding corresponding polyethers. The highest molecular weight was obtained for poly(limonene oxide) and it was equal to 2.8 kg mol^{-1}. This value is significantly smaller than the threshold for the lowest M_n for economically viable radiation polymerisation process - 10 kg mol^{-1}.[85] In comparison to previously reported catalytic cationic polymerisation products of these monomers, the synthesised polyethers had higher molecular weight and the synthesis was conducted in milder conditions and higher selectivity. However, the properties of the polymers were insufficient to be industrially viable.[85]

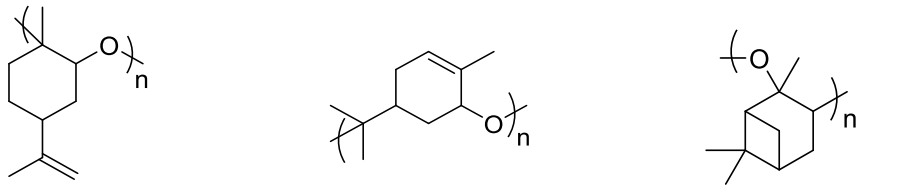

Figure 1.17 Polyethers produced from terpene oxides.[85]

Polycarbonates

Polycarbonates can be synthesised in the copolymerisation of CO_2 and epoxides which is currently investigated by a large number of research groups. The most widely investigated reactions are of CO_2 and cyclohexene oxide or reactions of CO_2 and propylene oxide.[86] Additionally, the increased interest in using renewable epoxides in polycarbonate synthesis was noticed.[87]

The first copolymerisation of limonene oxide and carbon dioxide was reported in 2014 by Coates *et al.*[88] The Coates group used β-diiminate zinc acetate complexes for the copolymerisation of carbon dioxide and a mixture of limonene oxide isomers (Figure 1.18). The study showed that only the *trans* isomer of limonene oxide undergoes reaction yielding polycarbonates.

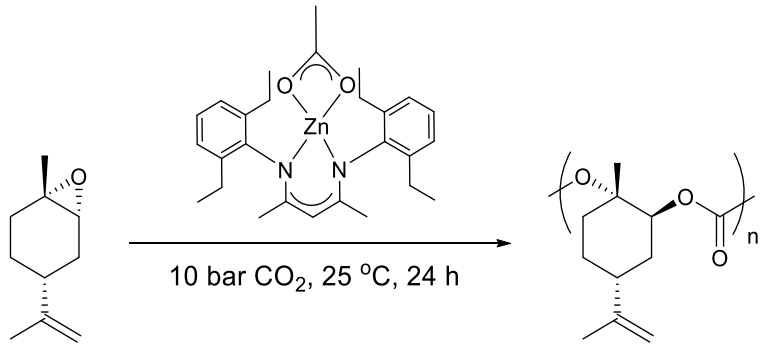

Figure 1.18 Synthesis of polylimonene carbonate.[88, 89]

The Coates discovery was further investigated by Greiner *et al.*[89] They developed a method of removing the catalyst from the reaction mixture which lowers the usage of organic solvents. Moreover, they indicated that a commercially available limonene oxide is uneconomical for the reaction in which only the *trans* isomer is reactive. This is because the commercially available limonene oxide consists of only 57 % *trans*-limonene oxide. They investigated an alternative route for limonene oxide synthesis, which gave a mixture consisting of 80 % *trans*-limonene oxide (Figure 1.19). However, it is a stoichiometric synthesis which is undesirable due to the large waste production.

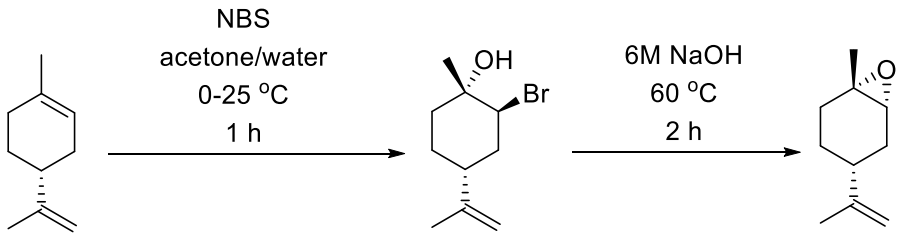

Figure 1.19 Synthesis of trans-limonene oxide.[89]

This work improved the polylimonene carbonate synthesis and resulted in a polymer with high molecular weight (above 100 kg mol^{-1}, Đ 1.13) and interesting physical properties, which makes polylimonene carbonate a valuable bio-based replacement for currently used polymers derived from fossil fuels. Polylimonene carbonate synthesised by Greiner *et al.* has high carbonate content, a high glass transition temperature (130 °C), low density (1.08 g cm^{-3}), high scratch resistance, good transparency and mechanical properties between polystyrene and bisphenol A (BPA) polycarbonate. All these properties could be potentially interesting for use as packaging materials or green coating materials.[89]

An alternate approach to the modification of polymer properties was presented in the work of Sablong *et al.*[90] They reported copolymerisation of CO_2 and 1,2,8,9-limonene dioxide catalysed by a zinc β-diiminate complex yielding a copolymer with epoxide on the isopropenyl group - polylimonene-8,9-oxide carbonate. The catalyst used for polymerisation was highly selective to *trans*-1,2-limonene oxide and did not affect the oxirane in the 8,9-position. The structure of the synthesised polymer and potential functionalization are presented in Figure 1.20. Depending on the functionalization, the glass transition temperature is easily tuneable to a maximum of 146 °C by conversion of the 8,9-oxirane to a cyclic carbonate group. The functionalized polymers were tested as coatings, showing good acetone resistance and attractive mechanical properties.[90]

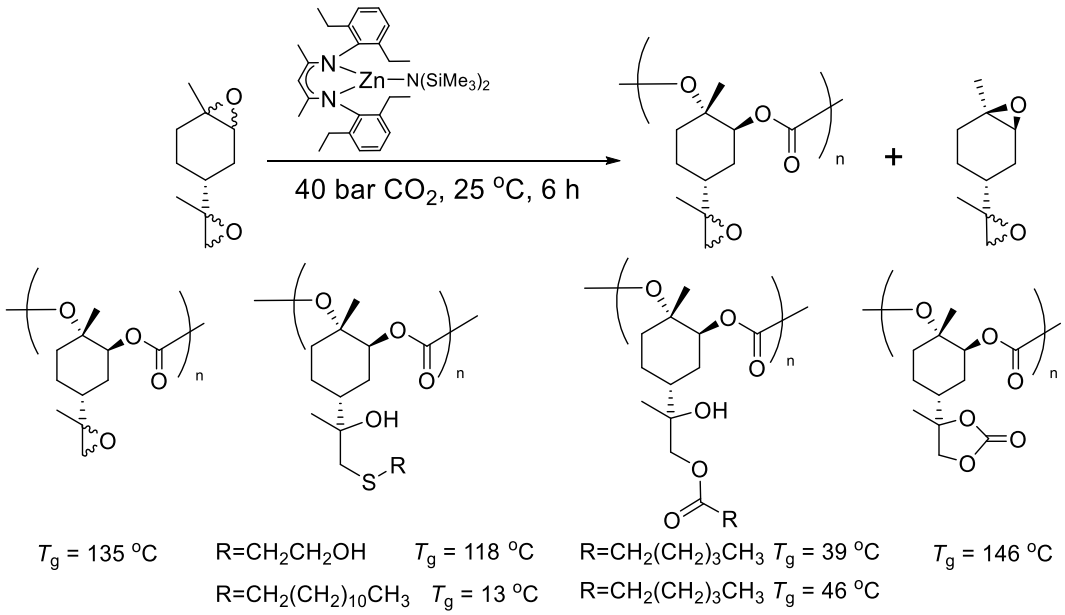

Figure 1.20 Synthesis of polylimonene-8,9-oxide carbonate and its possible functionalization.[90]

The other catalyst widely tested for copolymerisation of 1,2-limonene oxide and CO_2 is aluminium amino-tris(phenolate).[91, 92] Kleij *et al.* tested aluminium amino-tris(phenolate) with PPNCl as co-catalyst and achieved polymers with molecular weight in the range of 2.4 - 10.6 kg mol^{-1}. The highest molecular weight was achieved using pure *cis*-1,2-LO at 45 °C and 5 bar CO_2 in a Fischer-Porter reactor (Figure 1.21). The resultant polymer was stereoregular. The main difference between the Kleij catalyst system and the system described by Coates *et al.* (Figure 1.18) is that the Kleij catalyst system converts *cis*-1,2-LO whereas the Coates catalyst was highly selective to *trans*-1,2-LO. However, the Kleij catalyst system showed lower activity than the Coates catalyst.[91, 92]

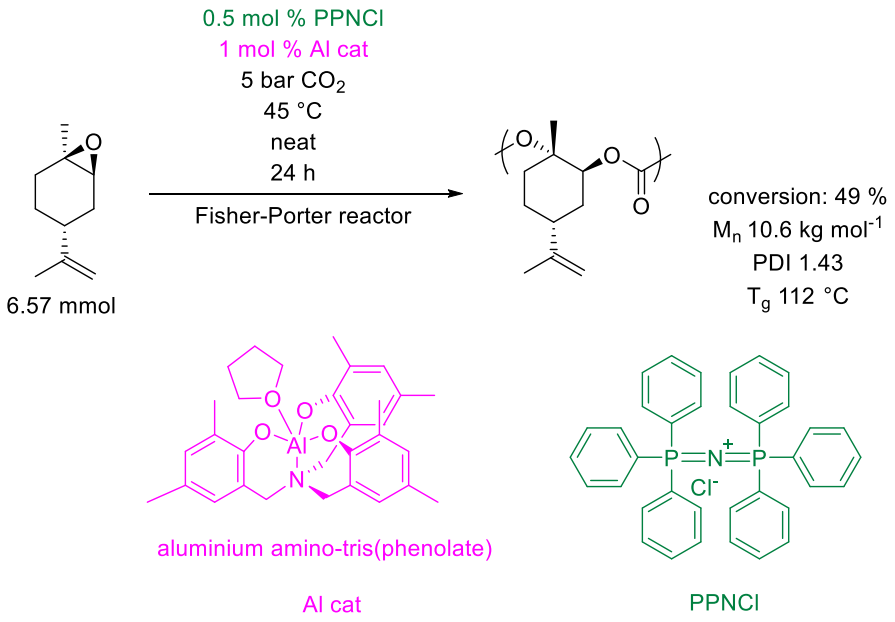

Figure 1.21 Polylimonene carbonate synthesised by Kleij et al.[91] The reaction scheme depicts the synthesis starting from sterically pure cis-1,2-LO.

Building on this research[91] and the research of Sablong *et al.*,[90] Kleij *et al.* investigated post-polymerisation functionalisation of polylimonene carbonate in order to increase the thermal properties.[92] They oxidised the remaining alkene group using mCPBA and sequentially reacted it with CO_2 resulting in polylimonene dicarbonate (Figure 1.22). The oxidation process did not affect the carbonate linkages in the polymer and the carbonation reaction reached over 99 % conversion while using PPNCl at 73 °C. The functionalisation of high molecular weight polylimonene carbonate samples (10-15 kg mol^{-1}) allowed polylimonene dicarbonate exhibiting a T_g value of 178 °C. Interestingly, the high molecular weight polylimonene carbonate prepared from a commercial mixture of *cis* and *trans*-1,2-LO performed similarly to the high molecular weight carbonate from only *cis*-1,2-LO. That is an improvement comparing to the Coates catalyst, as utilising both 1,2-LO isomers is more economically viable.

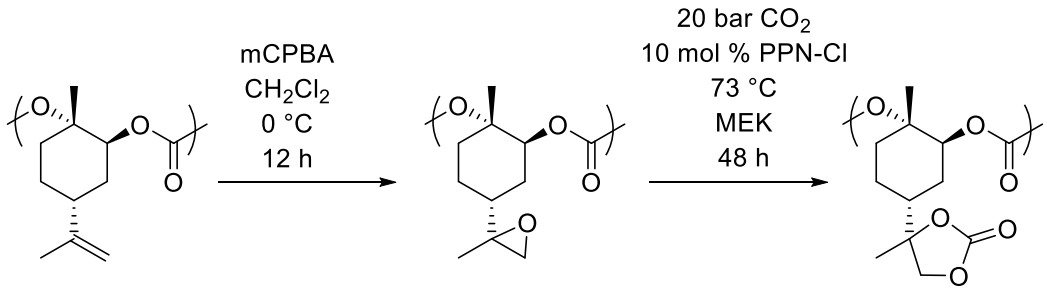

Figure 1.22 Functionalisation of polylimonene carbonate via oxidation with mCPBA and carbonation.[92]

The initial investigation of the uses of polylimonene carbonate in coatings was conducted by Koning *et al.*[93] They copolymerised limonene oxide with CO_2 using a β-diiminate zinc-bis(trimethylsilyl)amido complex (see Figure 1.20 for the structure of the catalyst) achieving polylimonene carbonate with a molecular weight up to 66 kg mol^{-1} and Đ of 1.2-1.3. Then, the resultant polylimonene carbonate was reacted with various polyols to produce dihydroxyl polycarbonate resins with M_n in the range of 2.3 - 4.0 kg mol^{-1} (Figure 1.23). MALDI-ToF-Mass Spetrometry showed that polycarbonate resins were a mixture of linear and cyclic polymeric species. The dihydroxyl polycarbonate resins were cured using hexamethylene diisocyanate trimer and yielded polylimonene carbonate coatings. The resultant coatings showed relatively low resistance to acetone and poor mechanical stability. This was likely due to insufficient crosslinking.

Modifications of the isopropenyl group were proposed to improve the crosslinking degree, for example functionalising the isopropenyl group with 2-hydroxy-1-ethanethiol or 6-hydroxy-1-hexanethiol.[93, 94] An improvement in acetone resistance and high hardness was observed. However, the coatings did not show good reverse impact resistance.[94]

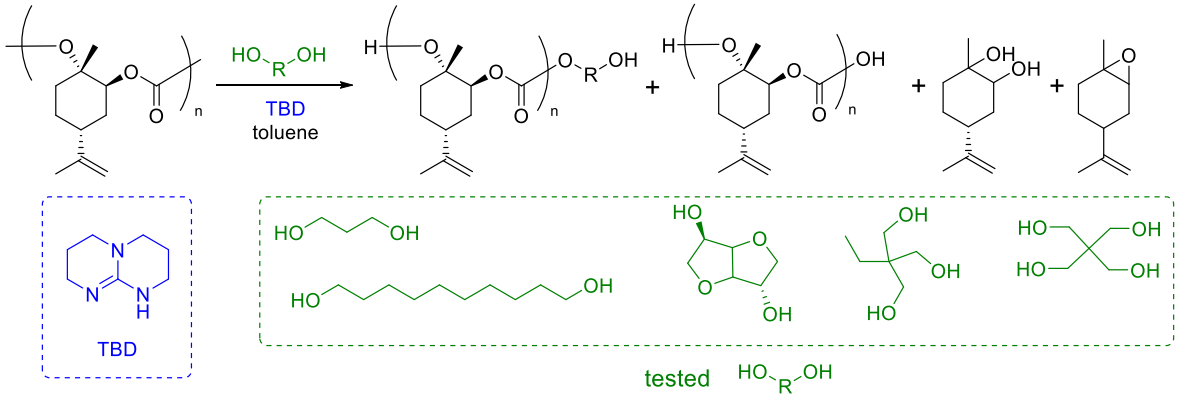

Figure 1.23 Degradation of high molecular weight polylimonene carbonate via transcarbonation.[93]

Koning *et al.* investigated the depolymerisation of polylimonene carbonate and polylimonene-8,9-oxide carbonate (Figure 1.24).[95] They used TBD as a depolymerisation catalyst, which was inspired by their previous work on dihydroxyl polylimonene carbonate resins (see Figure 1.23). TBD catalysed the depolymerisation of limonene-based polycarbonates yielding epoxides, which proved that limonene-based polycarbonates can be fully recycled into their monomers. The reaction was highly selective towards epoxides and no formation of cyclic carbonates was observed by infrared spectroscopy (IR) and gas chromatography-mass spectrometry (GC-MS). The stereoselectivity of decomposing polylimonene carbonate into *trans*-1,2-LO was related to the higher content of *trans*-1,2-LO than *cis* isomer in the starting polymer. The rate of degradation was strongly dependent on the temperature, at 80 °C no degradation was observed, but at 110 °C almost full decomposition to

the starting epoxides was observed. This work demonstrated that polylimonene carbonate and polylimonene-8,9-oxide can be developed into recyclable bio-derived polymers.

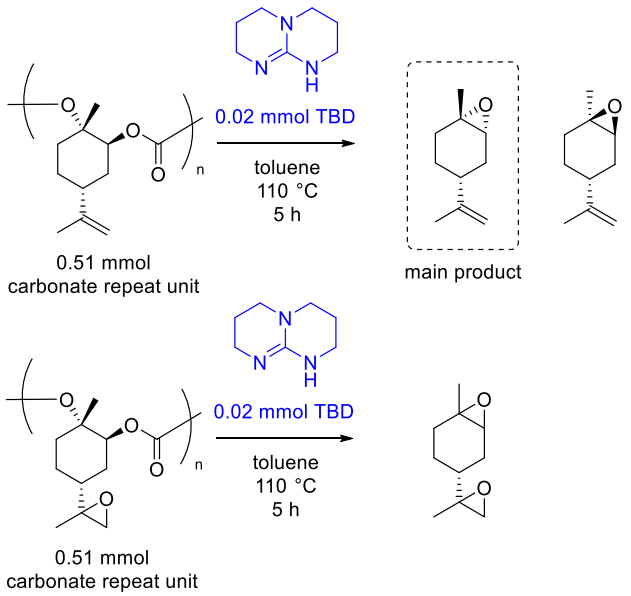

Figure 1.24 Depolymerisation of polylimonene carbonate and polylimonene-8,9-oxide carbonate in the presence of TBD.[95]

Cyclic carbonates from terpene oxides

In addition to polycarbonates, cyclic carbonates are a possible product of the reaction of CO_2 and epoxides. Various catalytic systems have been investigated in the synthesis of cyclic carbonates.[96] The synthesis of cyclic carbonates from terpene feedstocks was recently published for cyclic and acyclic terpenes and terpenoids (Figure 1.25).[97] A more detailed introduction to terpene-derived cyclic carbonates is included in Chapter 4.

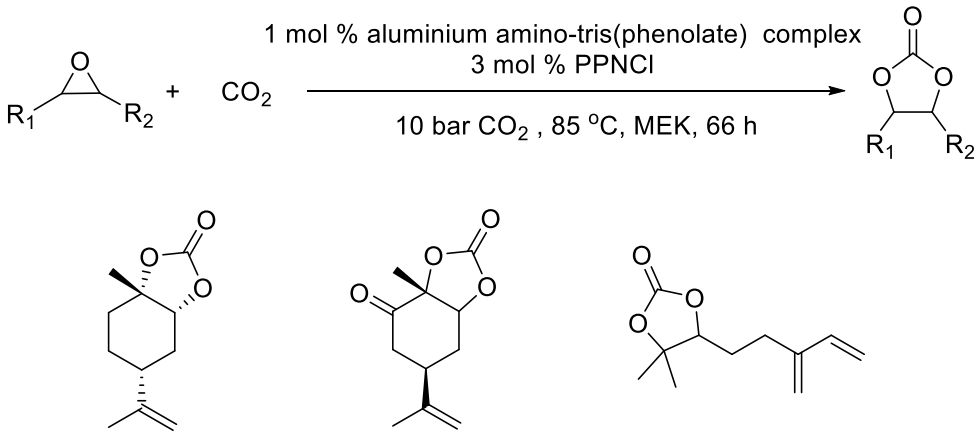

Figure 1.25 Synthesis of 5-membered cyclic carbonates using aluminium amino-tris(phenolate) complex and examples of synthesised compounds.[97]

Cyclic carbonates can potentially be used as polar aprotic solvents, electrolytes in lithium-ion batteries, monomers for polymer production or intermediates for chemical synthesis.[96] A literature search has found that some application of terpene-derived cyclic carbonates were published for 1,2,8,9-limonene dicarbonate, which was used in non-isocyanate polyurethanes synthesis.[98, 99] However, the full potential of terpene-derived cyclic carbonates is still unexplored.

Non-isocyanate polyurethanes

Non-isocyanate polyurethanes (NIPU) are expected to replace polyurethanes.[100] Their mechanical and chemical properties are similar, but NIPU do not involve toxic chemicals in the production process. Moreover, the synthesis of NIPU allows the incorporation of CO_2 into bio-based monomers.[100]

The first terpene to be used for bio-based synthesis of NIPU was limonene, as utilized by Bähr *et al*.[98] The synthesis involves two steps; first, carbonation of 1,2,8,9-limonene dioxide, and subsequently ring opening polymerisation of the cyclic carbonates (Figure 1.26). The properties of the obtained polymer can be tuned by using different amines to open the carbonate rings. The synthesised NIPU can be used as a terpene-based material or as an additive for blends with other biopolymers.[98]

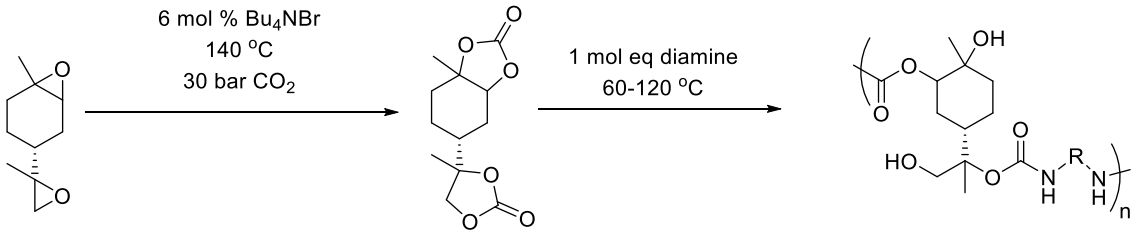

Figure 1.26 Synthesis of polyurethanes from 1,2,8,9-limonene dioxide.[98]

1.7 Terpene-derived polymers in coatings

From the previous section it is clear that a significant part of the terpene-derived polymers is investigated for application in coatings, for example polysulfides,[81] non-isocyanate polyurethanes,[98] polylimonene carbonate and polylimonene-8,9-oxide carbonate.[89, 90, 93, 94, 101, 102] Commercially, Pinova, a company based in the USA, provides polyterpene resins made from α – pinene which can be used in paints, coatings and waterproofing agents.[66]

Polymeric coatings are present in many branches of industry including food packaging, health care, automotive and architecture. The British Coatings Federation (BCF) indicated three main sectors of the UK coating industry: paint and coatings, printing inks, and wallcovering; from which the paint and coatings sector is the most significant based on sales value.[103] According to Statista, the market

value of coatings worldwide in 2017 reached over 152 billion U.S. dollars, about 20 % of it was European market value.[104]

A review paper published by Cunningham *et al.* highlighted that the manufacturers of coatings are committed to improve the sustainability of their products; they are especially interested in biosourced, biodegradable, compostable and recyclable materials.[105] These improvements could benefit in many stages of production and can contribute to using less toxic starting materials, more energy efficient processes with fewer volatile organic compounds emitted or more durable products with potentially better end of life scenario.[105] Moreover, BCF's Sustainable Development Policy published in 2016 shows strong commitment of the UK coating industry to economic, environmental and social elements of sustainable development.[106] While they achieved significant improvement in recycling and waste reduction, they are dedicated to further improvements which will include looking into renewable derived raw materials and formulation ingredients, focusing on a circular economy of the UK coating industry and further improvement on waste management.[106]

According to Cunningham *et al.* two of the most important challenges in coating applications are their solvent and corrosion resistance.[105] Microbial growth in waterborne coatings is another, more specific challenge to be addressed. Cunningham *et al.* also mentioned that industry would be interested in reducing the use of toxic chemicals, such as isocyanate or epoxy amine crosslinkers, and finding more sustainable alternatives.[105]

The direct comparison between commercial coatings and lab-scale research samples is challenging, because commercial coatings are a complex mixture which contains additives like pigments, thickening agents, anti-foaming and levelling agents.[101] Additionally, commercial coatings are often application specific and each of them have some drawbacks, for example elastomer polyurethane/polyurea coatings and polyester coatings exhibit adhesion problems, acrylic coatings have moderate chemical resistance and epoxy and polyester systems show poor exterior robustness.[101]

Greiner *et al.* investigated the mechanical and physical properties of polylimonene carbonate films (the polymerisation conditions were previously described in the polycarbonates section, for the reference see Figure 1.18 and 1.19).[89] The tensile properties showed behaviour between polystyrene and bisphenol A (BPA) polycarbonate. The pencil hardness test showed that the polylimonene carbonate film is resistant to pencil B, which is a moderate scratch resistance and a significant improvement over BPA polycarbonate (8B or softer). On the other hand acrylic coatings can resist a pencil as hard as 5H. The T_g of 130 °C might be interesting where contact with hot water is necessary. The optical testing showed no absorbance of light in the visible region, the films were highly transparent. The authors did not suggest in which application polylimonene carbonate

would be the best, but highlighted many promising properties. Some properties, such as hardness, tensile strength, glass transition temperature and transparency, are comparable to the properties of BPA polycarbonate.

The properties of polylimonene carbonate coatings can be improved by crosslinking via thiol-ene reactions (Figure 1.27).[101] The crosslinked polylimonene carbonate coatings were applied on aluminium substrate using solvent casting. The aluminium substrates were chosen as aluminium is a commonly used substrate in the paint industry and is often used in standards for mechanical testing of new coatings.[101] The resultant coatings were transparent, with no visible colour and exhibited excellent adhesion (0 in Gitterschnitt test, where 0 means best adhesion and 5 means poor adhesion). The organic solvent resistance was tested using acetone, all samples showed moderate or good acetone resistance, good acetone resistance was shown by highly crosslinked samples. The tested coatings performed significantly better in pencil hardness tests than not crosslinked samples, achieving scratch resistance of 2H (not crosslinked samples of M_n above 100 kg mol^{-1} were able to withstand pencil B). König hardness (pendulum hardness test) was lower with higher amount of crosslinking, which might be caused by the presence of thiol groups which increase plasticity.[101] The coatings did not perform well in the reverse impact test, samples showed delamination and brittle fracture. The authors indicated that toughness is a problem even for commercially available coatings and with further research, the low reverse impact performance should not prevent crosslinked polylimonene carbonate coatings from industrial applications, although further research is required.[101] Sablong *et al.* also investigated crosslinked polylimonene carbonate in coating applications.[102] Instead of using a UV initiator, they used a thermal initiator. Thermal initiated crosslinking yielded coatings exhibiting similar performance to the UV initiated crosslinking, high scratch resistance, good acetone resistance, moderate pendulum hardness and unsatisfactory performance in the reverse impact tests.

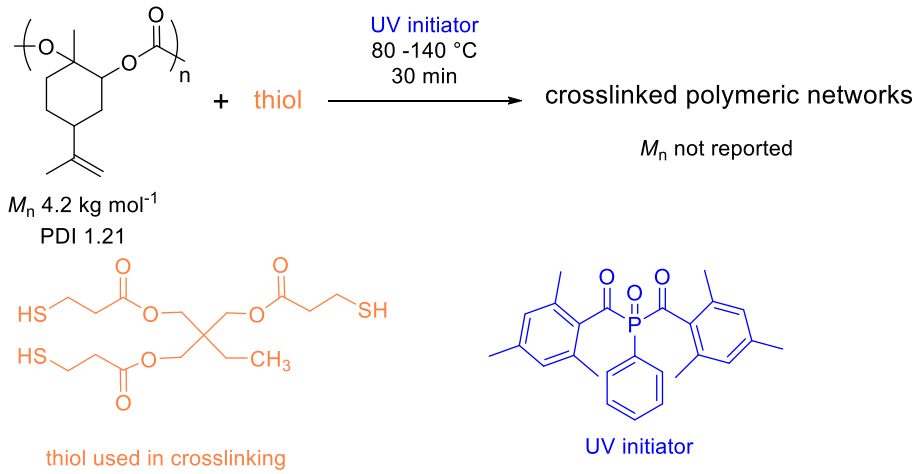

Figure 1.27 Thiol crosslinked polylimonene carbonate coatings.[101]

Terpene-based NIPU were also investigated in coating applications. Carbonated pentaerythritol glycidyl ether (PGC) and limonene biscarbonate were cured with 1,5-diaminopentane (Figure 1.28).[99] The resultant coatings were transparent and clear. Small additions of limonene biscarbonate (up to 30 wt %) increased the T_g, improved stiffness and strength of the coatings without compromising elongation at break. Higher addition of limonene biscarbonate results in coatings with unsatisfactory mechanical properties, the coatings became too brittle to do any mechanical testing. The increase of brittleness was attributed to high rigidity of limonene biscarbonate units and lower crosslinking with increasing content of limonene biscarbonate.[99] Increasing NIPU stiffness is crucial in the development of bio-based polyurethane coatings without addition of epoxy resins, thus small additions of limonene biscarbonate can improve NIPU's stiffness allowing them to be used as coatings.[99] NIPU thermosets with 30 % limonene biscarbonate and 70 % PGC showed a T_g of 58 °C (100% PGC shows a T_g of 41 °C), Young's modulus of 4040 MPa (100 % PGC shows 3390 MPa), tensile strength of 88 MPa (100 % PGC shows 70 MPa) and 2.49 % elongation at break (100 % PGC shows 2.51 %). Although fully terpene-based NIPU struggle with issues related to low reactivity of endocyclic carbonates, the use of terpene-based thermosets additives to fully bio-based NIPU thermosets showed unexplored potential.

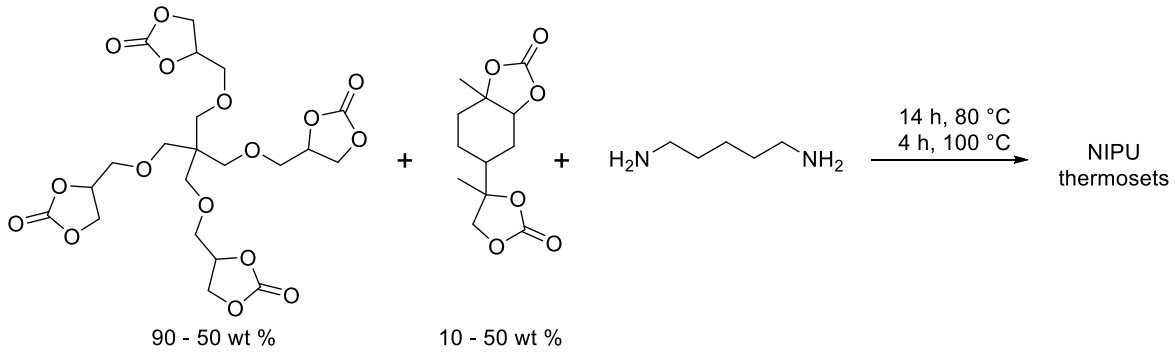

Figure 1.28 Biobased NIPU thermosets investigated as coatings.[99]

Although this review focuses mostly on polymers which can be synthesised from epoxides, it is worth noting that acrylic coatings can be derived from terpene-based acrylates and methacrylates.[107] Acrylic coatings are mostly used in architectural coatings and paints as they give good colour retention.[107] Howdle *et al.* reported a new approach to synthesise a range of acrylates and methacrylates from widely available terpene feedstocks (Figure 1.29).[107] The resultant monomers were polymerised via radical polymerisation achieving M_n in the range of 4 – 24 kg mol^{-1}. T_g was strongly dependent on M_n and it was in the range of 12 – 141 °C. Poly(carvone methacrylate) was investigated as a powder coating using trimethylolpropane tris(3-mercapto-propionate) (Figure 1.30). The obtained coatings were transparent and highly glossy with moderate

smoothness (smoothness 2 – 3, where 1 is the roughest and 10 the smoothest). The coatings also had high acetone resistance, König hardness of 185 s and in the pencil hardness test they were able to withstand pencil 2B. The coatings showed excellent adhesion to metal (0 in Gitterschnitt test) but they showed some delamination.

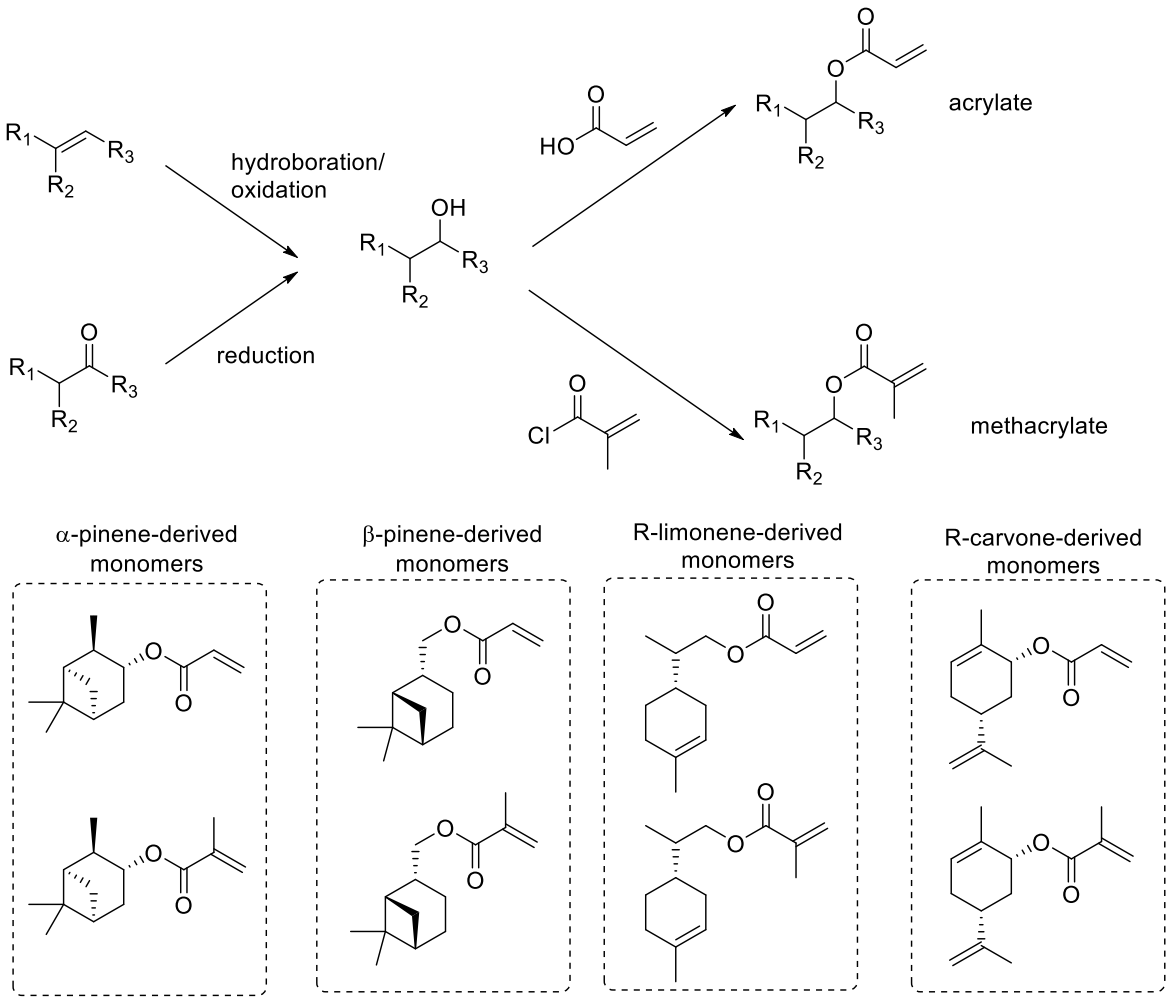

Figure 1.29 Novel acrylates and methacrylates.[107]

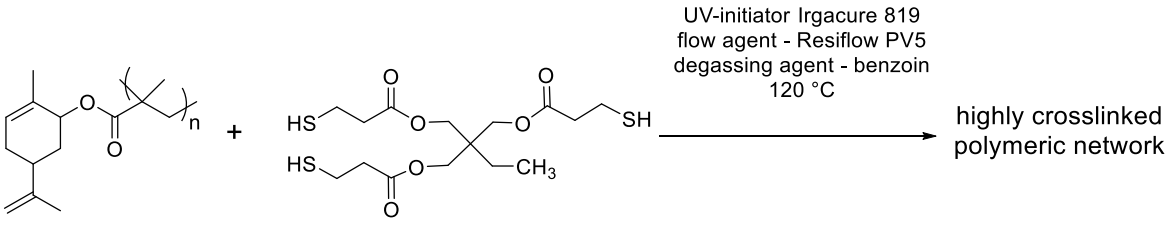

Figure 1.30 Powder coating prepared using poly(carvone methacrylate).[107]

To summarise, terpene-derived polymers have been explored as coatings and they show potential to be bio-derived alternatives to currently available coatings. The properties depend directly on the structure of the polymer, with highly crosslinked polymers being scratch resistant and exhibiting good acetone resistance. Mülhaupt *et al.* showed that terpene-derived NIPU thermosets can

increase the T_g and stiffness of coatings without affecting elongation at break, as long as they are used as an additive in an appropriate mass ratio. All examples cited in this section demonstrate that with further research terpene-derived polymers can have applications in industrial coatings, either as new coatings or additives improving coatings' properties.

1.8 Summary

Modern lifestyle highly depends on crude oil. This has a negative environmental impact, thus a great effort is dedicated to reduce crude oil dependence. Renewable feedstocks, such as carbohydrates, lignocellulosic waste and plant oils, are investigated in order to produce everyday use materials without relying on the availability of crude oil. Polymers are an example of everyday use materials which are present in all branches of industry. Increasing environmental concerns related to polymers use, production and end of life forced the development of more sustainable alternatives to current polymers. One strategy to improve the sustainability of polymers is using renewable feedstocks, for example terpenes.

As it is shown in this literature review, terpenes have been successfully implemented in polymer synthesis. Due to their diverse structures, terpenes can be used in the synthesis of polyethers, polysulfides, polyesters, polycarbonates and others. Most of these publications describe materials derived from limonene, which is understandable, as limonene is one of the biggest terpenes feedstocks. However, other terpenes, such as menthone, pinene and dihydrocarvone receive increasing attention which can lead to new materials with unexplored properties. Often application of terpene-derived polymers are inhibited due to inadequate availability of the terpene or high cost of the starting terpene which limits the polymer's applications to high value products.[108] Therefore, the use of terpenes derived via industrial biotechnology could help with improving the availability of terpenes and lowering their price.

Properties of terpene-derived polymers vary depending on the type of polymer. It is essential to compare the properties of synthesised polymers to the properties of currently used polymers. Renewable polymers should be industrially applicable. This means that the properties and the production process should be easy to implement for the large scale production as well as more sustainable than the current processes.[109]

Currently, terpene-derived polymers were mostly investigated in polymeric coating applications showing promising properties. The UK coating industry is interested in bio-derived alternatives for the current polymeric coatings. The coatings which have good solvent and corrosion resistance are of special interest. Additionally, possibilities to reduce the use of toxic chemicals are also vital for the UK coating industry to achieve their sustainability goals. Terpene-derived polymers have

potential to be bio-derived alternatives for current polymeric coatings. Preliminary research showed promising properties of terpene-derived coatings, but further research is required to allow industrial applications of terpene-derived polymers.

The aims and objectives of this thesis are included in Chapter 2. However, to summarise, the main focus of this work was on delivering novel terpene-based epoxides and cyclic carbonates, which could be used for producing polymers such as polycarbonates and NIPU. Both of those polymer types can be used in the coatings industry. Additional types of epoxides and carbonates can expand the available terpene-derived polymers and potentially provide bio-derived alternatives to some currently used polymers.

1.9 References

1. Statista, Daily demand for crude oil worldwide from 2006 to 2019 (in million barrels)*, https://www.statista.com/statistics/271823/daily-global-crude-oil-demand-since-2006/, (accessed 25/01/2019).
2. Statista, Oil consumption in the United Kingdom (UK) between 2004 to 2017 (in 1,000 barrels daily), https://www.statista.com/statistics/332028/oil-consumption-in-the-united-kingdom-uk/, (accessed 25/01/2019).
3. GOV.UK, Digest of UK Energy Statistics 2018 Chapter 3: Petroleum, https://assets.publishing.service.gov.uk/government/uploads/system/uploads/attachment_data/file/729403/Ch3.pdf, (accessed 25/01/2019).
4. Fisheries Research Services, Environmental Impacts of the Oil and Gas Industries, https://www2.gov.scot/uploads/documents/ae09environmental.pdf, (accessed 28/01/2019).
5. International Energy Agency, *The Future of Petrochemicals. Towards more sustainable plastics and fertilisers*.
6. M. Peplow, *Nature*, 2016, **536**, 266-268.
7. Statista, Production of plastics worldwide from 1950 to 2017, http://www.statista.com/statistics/282732/global-production-of-plastics-since-1950/, (accessed 04/02/2019).
8. Statista, Synthetic rubber production worldwide from 2000 to 2018 (in 1,000 metric tons), https://www.statista.com/statistics/280536/global-natural-rubber-production/, (accessed 4/02/2019).
9. Statista, Global chemical fiber production from 2000 to 2017, by fiber type (in 1,000 metric tons), https://www.statista.com/statistics/271651/global-production-of-the-chemical-fiber-industry/, (accessed 4/02/2019).
10. World Economic Forum, Ellen MacArthur Foundation and McKinsey & Company, *The New Plastics Economy — Rethinking the future of plastics*, 2016.
11. Statista, Polyurethane demand worldwide from 2012 to 2027 (in million tons), https://www.statista.com/statistics/747004/polyurethane-demand-worldwide/, (accessed 4/02/2019).
12. R. Geyer, J. R. Jambeck and K. L. Law, *Sci. Adv.*, 2017, **3**, e1700782.

13. European Commission, A European Strategy For Plastics In A Circular Economy, http://ec.europa.eu/environment/circular-economy/pdf/plastics-strategy-brochure.pdf, (accessed 11/04/2019).
14. SusChem, Plastics Strategic Research and Innovation Agenda in a Circular Economy, http://www.suschem.org/publications, (accessed 7/02/2019).
15. P. N. R. Vennestrøm, C. M. Osmundsen, C. H. Christensen and E. Taarning, *Angew. Chem. Int. Ed.*, 2011, **50**, 10502-10509.
16. C. H. Christensen, J. Rass-Hansen, C. C. Marsden, E. Taarning and K. Egeblad, *ChemSusChem*, 2008, **1**, 283-289.
17. A. J. Ragauskas, C. K. Williams, B. H. Davison, G. Britovsek, J. Cairney, C. A. Eckert, W. J. Frederick, J. P. Hallett, D. J. Leak, C. L. Liotta, J. R. Mielenz, R. Murphy, R. Templer and T. Tschaplinski, *Science*, 2006, **311**, 484-489.
18. K. Sanford, G. Chotani, N. Danielson and J. A. Zahn, *Curr. Opin. Biotechnol.*, 2016, **38**, 112-122.
19. J. L. F. Monteiro and C. O. Veloso, *Top. Catal.*, 2004, **27**, 169-180.
20. J. S. Luterbacher, D. Martin Alonso and J. A. Dumesic, *Green Chem.*, 2014, **16**, 4816-4838.
21. Y. Zhu, C. Romain and C. K. Williams, *Nature*, 2016, **540**, 354-362.
22. M. Aresta and A. Dibenedetto, *Dalton Trans.*, 2007, 2975-2992.
23. B. Ochiai and T. Endo, *Prog. Polym. Sci.*, 2005, **30**, 183-215.
24. A. W. Kleij, M. North and A. Urakawa, *ChemSusChem*, 2017, **10**, 1036-1038.
25. R. A. Sheldon, *Chem. Commun.,* 2008, 3352-3365.
26. A. J. Kamphuis, F. Picchioni and P. P. Pescarmona, *Green Chem.*, 2019, **21**, 406-448.
27. N. Brun, P. Hesemann and D. Esposito, *Chem. Sci.*, 2017, **8**, 4724-4738.
28. A. Behr and L. Johnen, *ChemSusChem*, 2009, **2**, 1072-1095.
29. P. B. Smith and G. F. Payne, in *Renewable and Sustainable Polymers*, eds. P. B. Smith and G. F. Payne, American Chemical Society, Washington, DC, 2011, pp. 1-10.
30. European Bioplastics, Bioplastic materials, https://www.european-bioplastics.org/bioplastics/materials/, (accessed 11/02/2019).
31. T. P. Haider, C. Volker, J. Kramm, K. Landfester and F. R. Wurm, *Angew. Chem. Int. Ed.*, 2019, **58**, 50-62.
32. European Bioplastics, Bioplastics market data, https://www.european-bioplastics.org/market/, (accessed 11/02/2019).
33. M. Nofar, D. Sacligil, P. J. Carreau, M. R. Kamal and M.-C. Heuzey, *Int. J. Biol. Macromol.*, 2019, **125**, 307-360.
34. R. Siakeng, M. Jawaid, H. Ariffin, S. M. Sapuan, M. Asim and N. Saba, *Polym. Compos.*, 2019, **40**, 446-463.
35. A. K. Singh, J. K. Srivastava, A. K. Chandel, L. Sharma, N. Mallick and S. P. Singh, *Appl. Microbiol. Biotechnol.*, 2019, **103**, 2007-2032.
36. H. Pakalapati, C.-K. Chang, P. L. Show, S. K. Arumugasamy and J. C.-W. Lan, *J. Biosci. Bioeng.*, 2018, **126**, 282-292.
37. S. Rodriguez-Perez, A. Serrano, A. A. Pantión and B. Alonso-Fariñas, *J. Enviro. Manage.*, 2018, **205**, 215-230.
38. S. S. Costa, A. L. Miranda, M. G. de Morais, J. A. V. Costa and J. I. Druzian, *Int. J. Biol. Macromol.*, 2019, **131**, 536-547.
39. Braskem, I'm Green Polyethylene, http://plasticoverde.braskem.com.br/site.aspx/Im-greenTM-Polyethylene, (accessed 11/04/2019).
40. W. Saibuatrong, N. Cheroennet and U. Suwanmanee, *J. Clean. Prod.*, 2017, **158**, 319-334.
41. A. Prieto, *Microb. Biotechnol.*, 2016, **9**, 652-657.
42. The Coca Cola Company, Plant PET Technology Collaborative, https://www.coca-colacompany.com/stories/meet-our-partners-plant-pet-technology-collaborative, (accessed 11/04/2019).

43. Corbion, FDCA for PEF, https://www.corbion.com/bioplastics-o/products/fdca-for-pef, (accessed 12/04/2019).
44. Corbion, The future of plastics is biobased, https://www.corbion.com/bioplastics/fdca, (accessed 12/04/2019).
45. G. Lligadas, J. C. Ronda, M. Galià and V. Cádiz, *J. Polym. Sci. Part A: Polym. Chem.*, 2013, **51**, 2111-2124.
46. A. Gandini and T. M. Lacerda, *Prog. Polym. Sci.*, 2015, **48**, 1-39.
47. A. W. Kleij, *ChemSusChem*, 2018, **11**, 2842-2844.
48. A. J. D. Silvestre and G. Alessandro, in *Monomers, Polymers and Composites from Renewable Resources*, eds. M. Belgacem and A. Gandini, 1 edn., 2008, ch. 2, pp. 17-38.
49. M. B. Erman and B. J. Kane, *Chem. Biodiversity*, 2008, **5**, 910-919.
50. T. M. Attard, B. Watterson, V. L. Budarin, J. H. Clark and A. J. Hunt, *New J. Chem.*, 2014, **38**, 2278-2283.
51. M. Goldsworthy and NNFCC, personal communication.
52. J. J. McKetta*, Encyclopedia of Chemical Processing and Design*, ed. J. J. McKetta, W. A. Cunningham, Marcel Dekker Inc., 1994, pp. 138.
53. K. R. Benjamin, I. R. Silvab, J. P. Cherubimc, D. McPheea and C. J. Paddon, *J. Braz. Chem. Soc.*, 2016, **27**, 1339-1345.
54. V. J. Martin, D. J. Pitera, S. T. Withers, J. D. Newman and J. D. Keasling, *Nat. Biotechnol.*, 2003, **21**, 796-802.
55. Isobionics, Natural Beta Elemene, http://www.isobionics.com/index-Beta%20Elemene.html, (accessed 12/04/2019).
56. Amyris, trans-beta-farnesene, http://farnesene.net/, (accessed 12/04/2019).
57. G. L. Parker, L. K. Smith and I. R. Baxendale, *Tetrahedron*, 2016, **72**, 1645-1652.
58. *US Pat.*, US5826202A, 1998.
59. N. Tsolakis, W. Bam, J. S. Srai and M. Kumar, *J. Clean. Prod.*, 2019, **222**, 802-822.
60. T. Bach, *Eur. Urol. Suppl.*, 2010, **9**, 814-818.
61. A. M. Sabogal-Guáqueta, E. Osorio and G. P. Cardona-Gómez, *Neuropharmacology*, 2016, **102**, 111-120.
62. N. Q. Liu, W. Schuehly, M. von Freyhold and F. van der Kooy, *Ind. Crops Prod.*, 2011, **34**, 1084-1088.
63. H. A. Meylemans, R. L. Quintana and B. G. Harvey, *Fuel*, 2012, **97**, 560-568.
64. F. Millo, S. Bensaid, D. Fino, S. J. Castillo Marcano, T. Vlachos and B. K. Debnath, *Fuel*, 2014, **138**, 134-142.
65. Kraton, Sustainable Products, http://kraton.com/sustainability/sustainproducts.php, (accessed 12/04/2019).
66. PINOVA, Polyterpene Resins, http://www.pinovasolutions.com/polyterpene-resins, (accessed 12/04/2019).
67. Yasuhara Chemical, Terpene Resins, https://www.yschem.co.jp/english/products/resin/index.html, (accessed 12/04/2019).
68. J. Lu, M. Kamigaito, M. Sawamoto, T. Higashimura and Y.-X. Deng, *Macromolecules*, 1997, **30**, 22-26.
69. N. A. Kukhta, I. V. Vasilenko and S. V. Kostjuk, *Green Chem.*, 2011, **13**, 2362-2364.
70. W. J. Roberts and A. R. Day, *J. Am. Chem. Soc.*, 1950, **72**, 1226-1230.
71. B. Sibaja, J. Sargent and M. L. Auad, *J. Appl. Polym. Sci.*, 2014, **131**, 41155.
72. Y. Ishido, A. Kanazawa, S. Kanaoka and S. Aoshima, *Macromolecules*, 2012, **45**, 4060-4068.
73. D. Zhang, M. A. Hillmyer and W. B. Tolman, *Biomacromolecules*, 2005, **6**, 2091-2095.
74. D. L. J. Opdyke, *Fd. Cosmet. Toxicol.*, 1980, **18**, 665-666.
75. J. R. Lowe, M. T. Martello, W. B. Tolman and M. A. Hillmyer, *Polym. Chem.*, 2011, **2**, 702-708.

76. H. C. Quilter, M. Hutchby, M. G. Davidson and M. D. Jones, *Polym. Chem.*, 2017, **8**, 833-837.
77. R. C. Jeske, A. M. DiCiccio and G. W. Coates, *J. Am. Chem. Soc.*, 2007, **129**, 11330-11331.
78. C. Robert, F. de Montigny and C. M. Thomas, *Nat. Comm.*, 2011, **2**, 586.
79. L. Peña Carrodeguas, C. Martín and A. W. Kleij, *Macromolecules*, 2017, **50**, 5337-5345.
80. M. Winnacker, S. Vagin, V. Auer and B. Rieger, *Macromol. Chem. Phys.*, 2014, **215**, 1654-1660.
81. M. P. Crockett, A. M. Evans, M. J. Worthington, I. S. Albuquerque, A. D. Slattery, C. T. Gibson, J. A. Campbell, D. A. Lewis, G. J. Bernardes and J. M. Chalker, *Angew. Chem. Int. Ed.*, 2016, **55**, 1714-1718.
82. M. Firdaus, L. Montero de Espinosa and M. A. R. Meier, *Macromolecules*, 2011, **44**, 7253-7262.
83. M. Firdaus, M. A. R. Meier, U. Biermann and J. O. Metzger, *Eur. J. Lipid Sci. Technol.*, 2014, **116**, 31-36.
84. M. Claudino, J.-M. Mathevet, M. Jonsson and M. Johansson, *Polym. Chem.*, 2014, **5**, 3245-3260.
85. J. A. Aikins and F. Williams, in *Ring-Opening Polymerisation*, ed. J. E. McGrath, ACS Symposium Series; American Chemical Society, Washington, DC, 1985, vol. 286, ch. 24, pp. 335-359.
86. M. Taherimehr and P. P. Pescarmona, *J. Appl. Polym. Sci.*, 2014, **131**, 41141.
87. K. Yao and C. Tang, *Macromolecules*, 2013, **46**, 1689-1712.
88. C. M. Byrne, S. D. Allen, E. B. Lobkovsky and G. W. Coates, *J. Am. Chem. Soc.*, 2004, **126**, 11404-11405.
89. O. Hauenstein, M. Reiter, S. Agarwal, B. Rieger and A. Greiner, *Green Chem.*, 2016, **18**, 760-770.
90. C. Li, R. J. Sablong and C. E. Koning, *Angew. Chem. Int. Ed.*, 2016, **55**, 11572-11576.
91. L. Pena Carrodeguas, J. Gonzalez-Fabra, F. Castro-Gomez, C. Bo and A. W. Kleij, *Chem. Eur. J.*, 2015, **21**, 6115-6122.
92. N. Kindermann, À. Cristòfol and A. W. Kleij, *ACS Catal.*, 2017, **7**, 3860-3863.
93. C. Li, R. J. Sablong and C. E. Koning, *Eur. Polym. J.*, 2015, **67**, 449-458.
94. C. Li, S. van Berkel, R. J. Sablong and C. E. Koning, *Eur. Polym. J.*, 2016, **85**, 466-477.
95. C. Li, R. J. Sablong, R. A. T. M. van Benthem and C. E. Koning, *ACS Macro Lett.*, 2017, **6**, 684-688.
96. J. W. Comerford, I. D. V. Ingram, M. North and X. Wu, *Green Chem.*, 2015, **17**, 1966-1987.
97. G. Fiorani, M. Stuck, C. Martín, M. M. Belmonte, E. Martin, E. C. Escudero-Adán and A. W. Kleij, *ChemSusChem*, 2016, **9**, 1304-1311.
98. M. Bähr, A. Bitto and R. Mülhaupt, *Green Chem.*, 2012, **14**, 1447-1454.
99. V. Schimpf, B. S. Ritter, P. Weis, K. Parison and R. Mülhaupt, *Macromolecules*, 2017, **50**, 944-955.
100. B. Nohra, L. Candy, J.-F. Blanco, C. Guerin, Y. Raoul and Z. Mouloungui, *Macromolecules*, 2013, **46**, 3771-3792.
101. T. Stößer, C. Li, J. Unruangsri, P. K. Saini, R. J. Sablong, M. A. R. Meier, C. K. Williams and C. Koning, *Polym. Chem.*, 2017, **8**, 6099-6105.
102. C. Li, M. Johansson, R. J. Sablong and C. E. Koning, *Eur. Polym. J.*, 2017, **96**, 337-349.
103. British Coatings Federation, Industry Statistics, https://www.coatings.org.uk/Statistics/Industry_Statistics_public.aspx, (accessed 05/09/2019).
104. Statista, Market value of coatings worldwide in 2017 and 2018, by region (in million U.S. dollars), https://www.statista.com/statistics/878011/regional-coatings-market-value-global/, (accessed 05/09/2019).

105. M. F. Cunningham, J. D. Campbell, Z. W. Fu, J. Bohling, J. G. Leroux, W. Mabee and T. Robert, *Green Chem.*, 2019, **21**, 4919-4926.
106. British Coatings Federation, Sustainable Development, https://www.coatings.org.uk/Sustainable_Development.aspx, (accessed 05/09/2019).
107. M. F. Sainz, J. A. Souto, D. Regentova, M. K. G. Johansson, S. T. Timhagen, D. J. Irvine, P. Buijsen, C. E. Koning, R. A. Stockman and S. M. Howdle, *Polym. Chem.*, 2016, **7**, 2882-2887.
108. R. Ciriminna, M. Lomeli-Rodriguez, P. Demma Cara, J. A. Lopez-Sanchez and M. Pagliaro, *Chem. Commun.*, 2014, **50**, 15288-15296.
109. A. Llevot, P.-K. Dannecker, M. von Czapiewski, L. C. Over, Z. Söyler and M. A. R. Meier, *Chem.: Eur. J.*, 2016, **22**, 11510-11521.

2. Aims and objectives

The aim of this project was to develop new methods that could lead to sustainable processes for the manufacture of new terpene-based monomers. Methods used focused on catalytic routes using benign reagents and solvents as well as continuous processing where appropriate.

From the wide range of terpene feedstocks, the main focus of the project was on limonene and β-elemene. Limonene is one of the most widely available terpenes, whereas β-elemene, which is not widely available as a natural feedstock but has recently become more available via industrial biotechnology.

The main aim was to synthesise, characterise and assess the suitability of new terpene-derived monomers for sustainable polymers. New monomers included epoxides, cyclic carbonates or thiol-functionalised carbonates. Some of the synthesised monomers were used in preliminary polymerisation studies in order to evaluate their potential for polymer synthesis.

Specific objectives for the project included:

i. Developing a sustainable protocol for β-elemene epoxidation. The development process was based on previous research conducted on limonene epoxidation. The products of interest included β-elemene monoepoxide, β-elemene bisepoxide and β-elemene trisepoxide, most of which were unknown in literature.
ii. If successful, sustainable epoxidation protocols were further explored by transferring into flow processes using microreactors.
iii. Developing catalytic routes to mono-functionalised cyclic carbonates from limonene with understanding of the various factors affecting the synthesis, such as temperature, pressure, catalytic systems, the substitution and the stereochemistry of the epoxide.
iv. Explore the potential of monofunctionalised limonene cyclic carbonates for non-isocyanate polyurethanes.
v. Utilising the findings from limonene mono-functionalised cyclic carbonates (iii) for the synthesis of novel β-elemene cyclic carbonates from their epoxides. Identifying challenges in β-elemene cyclic carbonates synthesis and choosing the cyclic carbonate with the most promising chemical properties for polymer synthesis.
vi. Explore the potential of β-elemene cyclic carbonates in non-isocyanate polyurethane synthesis.

3. Terpenes epoxidation

This chapter contains a short introduction to alkene epoxidation, sustainability issues related to industrial processes and factors important in green epoxidation processes. Previously reported terpene epoxidations are then explored with a special focus on limonene, as it contains di - and tri - substituted double bonds which are characteristic of terpene structures. A new terpene feedstock, β-elemene, is introduced and the three chosen catalytic epoxidation protocols to epoxidise it are discussed in more detail.

The results section is focused on β-elemene epoxidation and is divided into three sections: Venturello catalyst epoxidation, Mizuno epoxidation and trifluoroacetophenoene catalysed epoxidation. Conclusions and experimental sections are provided at the end of the chapter.

3.1 Introduction

3.1.1 Alkene epoxidation

Olefin epoxidation is a highly important reaction in various branches of industry. Epoxides are valuable intermediates for the synthesis of fine chemicals, pharmaceuticals and polymers.[1] Two major industrial epoxidation products are ethylene oxide and propylene oxide. Ethylene oxide is mainly used to produce ethylene glycol and surface-active agents.[1, 2] Propylene oxide is mainly used to produce polyurethane polyols and propylene glycols.[1, 2] Here, we focus on propylene oxide production because it is one of the major industrially produced epoxides, with a production volume of 8 million tonnes annualy.[3]

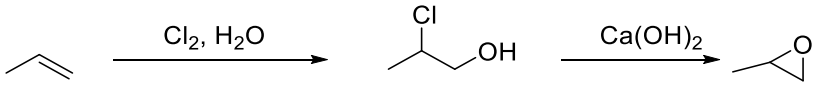

Figure 3.1 Production of propylene oxide via chlorohydrin route.[3]

Current industrial epoxidation methods are often long established, use stoichiometric reagents and generate large amounts of waste.[3] Figure 3.1 depicts one of the main industrial methods of producing propylene oxide. For each tonne of propylene oxide, 2 tonnes of $CaCl_2$ are produced alongside approximately 40 tonnes of waste water containing $CaCl_2$. Moreover, newly built plants using this technology require very high initial investment, thus new construction would not currently be considered.[3] Other available methods of producing propylene oxide require the use of organic peroxides and they suffer from the same issues: substantial waste production and high initial investment needed (Figure 3.2).[3] Further developments in industrial propylene oxidation were focused on minimising the amount of waste produced and introducing new catalysts.[4-6]

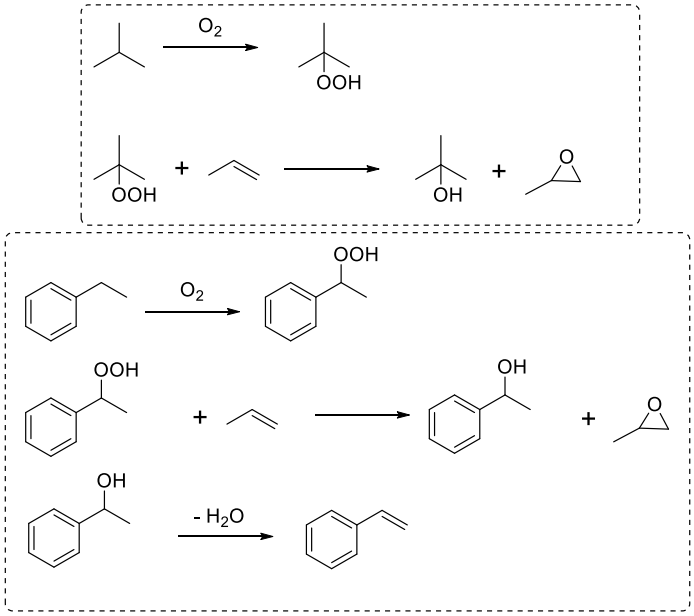

Figure 3.2 Hydroperoxidation routes to propylene oxide.[3]

3.1.2 Sustainability issues and green processes

M. Poliakoff and P. Licence identified the main sustainability issues with current industrial manufacturing: waste and the dependence on finite petroleum highlighting the importance of renewable feedstocks.[7] The overall developments in epoxidation are focused on atom efficient catalytic processes with H_2O_2 as an oxidant which can help with waste issues.[8]

Greener processes often involve reducing the amount of solvent used, as it is a significant greenhouse gas emission factor. For example, use of organic solvents accounts for 50 % of greenhouse gas emissions from the pharmaceutical industry.[9] Catalysis receives significant interest as a way of moving forward from stoichiometric unselective reagents towards more selective reactions and milder reaction conditions.[9]

Many academically investigated and industrial processes are batch processes, mostly due to the well understood reaction conditions, lower investment needed and the equipment being already widely available.[10] However, flow reaction conditions can provide many advantages such as increased productivity, safety and better process control which can improve repeatability, especially for exothermic reactions where heat control is crucial.[10] Moreover, novel flow reactors provide many innovative solutions like improved mixing via static mixers, geometric designs providing dynamic mixing and improved heat transfer solutions, all of which can translate to energy savings.[10] Flow reactors also allow for the integration of multiple reaction steps, purification

and separation into one continuous process which potentially can reduce the use of energy and waste production.[11]

Green processes should be scalable to have the greatest impact.[11] Scalability of flow processes is easier than for batch processes. In flow, the easiest way to increase productivity is to increase the operating time of the reactor. In batch, the same reaction would have to be run in multiple batches or the reactor size would have to be increased, which might require changing reaction conditions and new optimisation.[11]

Summarising, flow catalytic processes can be considered greener than batch processes by fulfilling many of the green chemistry principles, such as: atom economy, less hazardous chemical syntheses and safer solvents. This makes flow processes in general greener than batch processes in terms of meeting needs and minimising excess waste.[9, 11]

3.1.3 Green epoxidation

Green epoxidations often focus on replacing stoichiometric oxidants by greener oxidants such as hydrogen peroxide (H_2O_2) or oxygen (O_2).[12] The usage of molecular dioxygen often requires a stoichiometric amount of reductant and it is constrained due to safety concerns and selectivity issues.[12] H_2O_2 is easy to handle, as it can be obtained as 30 % aqueous solution, and it yields water as the only by-product, thus H_2O_2 is more widely used in green oxidations.

Catalysts widely used for epoxidation with H_2O_2 include transition metal complexes, perfluoroketone catalyst, arsenic and selenium catalysts and polyoxometalates.[8] Renewable feedstocks used for epoxidation include vegetable oils, furfuryl derivatives and terpenes.[13-15] The epoxidation of terpenes is of particular interest in the flavour and fragrance industry.[1] However, a growing interest in terpenes as renewable feedstocks for polymer production (see Section 1.6) has driven research on catalytic terpenes epoxidation.

3.1.4 Epoxidation of terpenes

The industrial epoxidation of terpenes is still under development, with only limited terpene epoxides available on the market. Nitrochemie currently offers 1,2-limonene oxide, 1,2,8,9-limonene oxide and α-pinene oxide.[16] Currently, terpenes are used mostly in the flavour and fragrance industry, thus there is no need for a large volume of terpenes. Academically investigated methods include stoichiometric and catalytic methods.

Stoichiometric methods

A novel stoichiometric method using in-situ generated dimethyl dioxirane (DMDO) under ultrasound conditions was developed by Kaliaguine and coworkers.[17] DMDO was generated via the reaction of acetone with potassium peroxymonosulfate, $KHSO_5$ (commercial name: Oxone). The

epoxidation used sodium bicarbonate as a pH buffer (Figure 3.3). This method is highly selective and was demonstrated to work on other terpenes. It is worth noting that for each 1.68 g of limonene diepoxide product, 4 g of $NaHCO_3$ was used as pH buffer, 3.5 g $KHSO_4$ was produced as a product of Oxone reduction and 31 g acetone was used, resulting in an E factor of 23 (excluding water).[18] For comparison, the average values of E factors for various industries are 1 – 5 for bulk chemicals, 5 – 50 for the fine chemicals industry and 25 – 100 for the pharmaceutical industry. [18] Although this method is selective and extremely fast, the amount of waste should be reduced before it can be considered as a green epoxidation.

A different approach to Oxone epoxidation was shown by Bhat *et al.* They epoxidised terpenoids, such as α-terpineol, geranyl acetate and others, using Oxone and camphor as an oxidant.[19] The reaction was sensitive to pH (pH 4–5 or 7–8 depending on the substrate used) and required 0 °C reaction temperature.

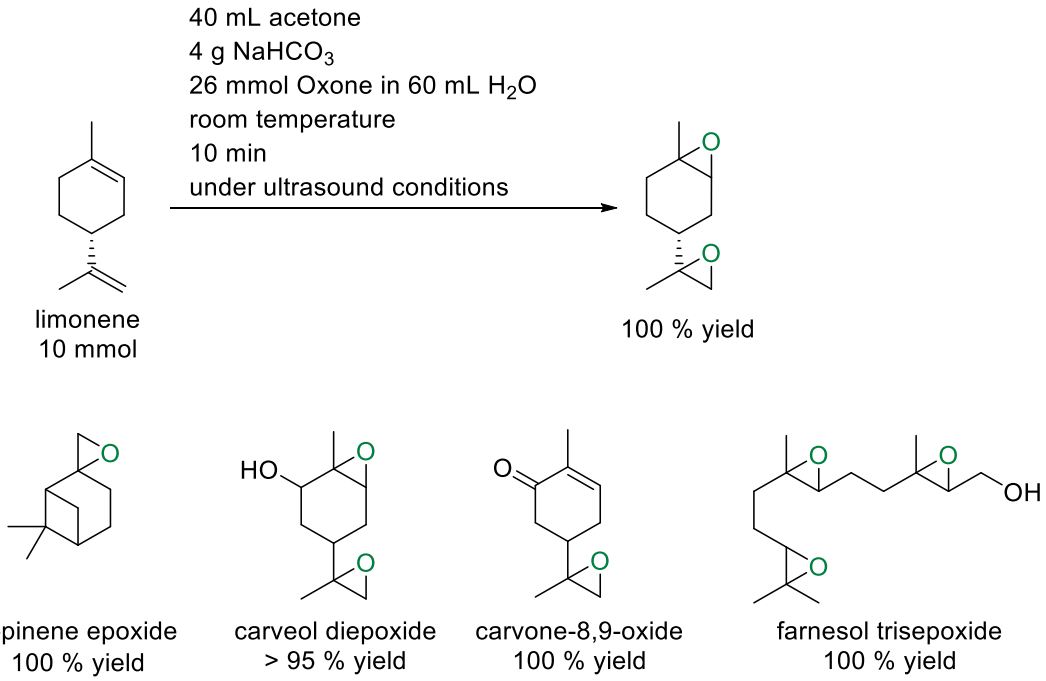

Figure 3.3 In situ generated DMDO oxidation of limonene and examples of other oxidised terpenes.[17]

Homogeneous catalysts

A number of investigations into homogeneous catalytic terpene epoxidation have been carried out using the biphasic Ishii-Venturello system.[20-22] This consists of a peroxotungstophosphate in combination with a quaternary ammonium salt, which acts as a phase transfer catalyst. The performance of the Ishii-Venturello system was evaluated in comparison to traditional oxidation routes, such as ion-exchange resins and peroxyacetic acid by Yadav *et al.*[23] The Ishii-Venturello system performed significantly better than ion exchange resins, providing 100 % conversion and 89

% selectivity after 5 h (ion exchange resins achieved only 42 % conversion and 71 % selectivity in 6 h). Peroxyacetic acid achieved 79 % conversion and 96 % selectivity in 5 h. It is worth noting that the optimal reaction temperature for peroxyacetic acid was 25 °C (40 °C lower than for the Ishii-Venturello system).[23]

The first report of terpene epoxidation was the catalytic epoxidation of monoterpenes using H_2O_2 and peroxotunstophosphate catalyst with cetyl-pyridinium cation $[C_5H_5N^+(CH_2)_{15}CH_3]_3[PW_4O_{24}]$, published by Ishii *et al.* The scope of substrates tested and the corresponding yields are shown in Figure 3.4.[20]

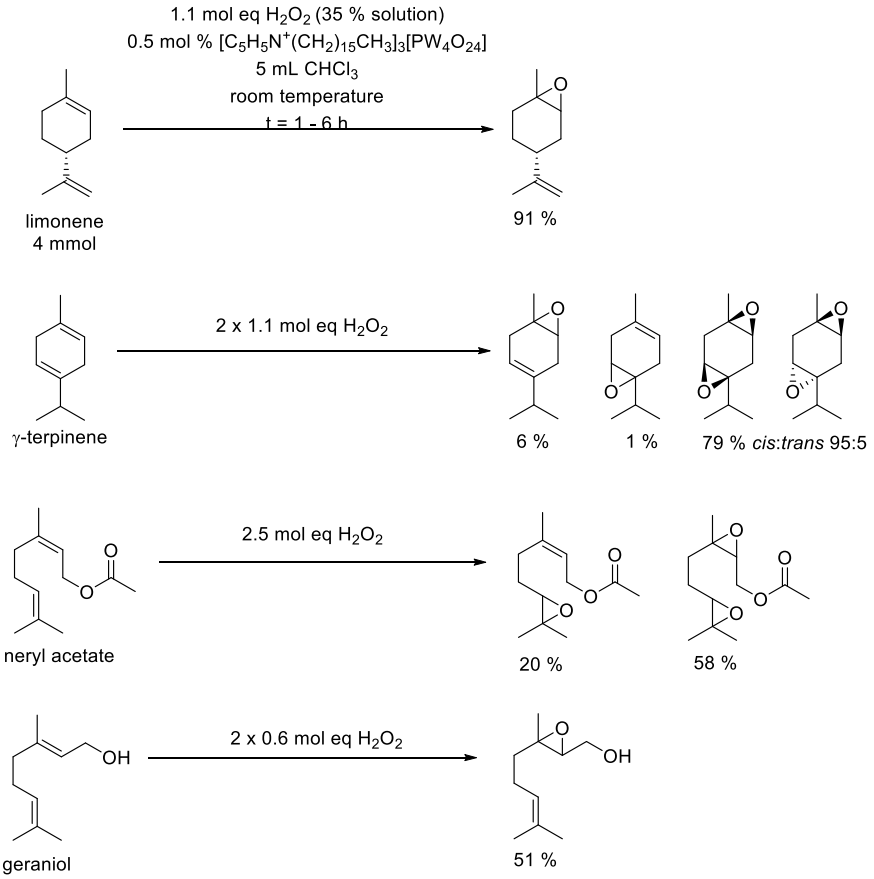

Figure 3.4 Examples of a wide range of terpenes and terpenoids epoxidised by the Ishii-Venturello-type catalyst, $[C_5H_5N^+(CH_2)_{15}CH_3]_3[PW_4O_{24}]$.[20] Examples included in the original study, but not reproduced in the figure: geranyl acetate, citral, nitrile, nerol, linalool.

The further developments of Ishii-Venturello catalysis in terpenes epoxidation were presented by Clark *et al.*,[24] who used conditions developed by Noyori *et al.*[25] and studied an in-situ created peroxotungstophosphate in terpene epoxidation. After 2 h reaction time, they achieved 94 % conversion and 81 % selectivity to 1,2-limonene oxide (Figure 3.5).

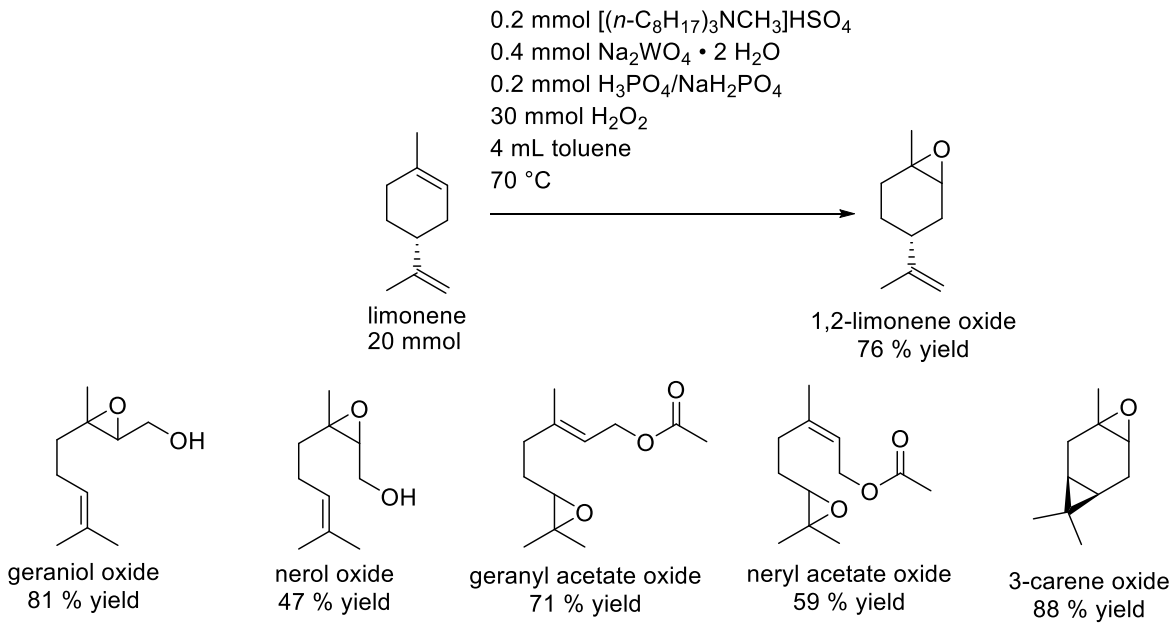

Figure 3.5 Terpene epoxidation using in situ generated peroxotungstophosphate.[24]

In the work reported by Clark *et al.* Na_2SO_4 was used to increase the ionic strength of the aqueous phase, resulting in decreased water content in the organic phase and decreasing the rate of hydrolytic decomposition of epoxide. Further investigations into the effect of salts on terpene epoxidation was carried out by Sato *et al.*[26] A range of inorganic salts, such as sulfates, carbonates, nitrates and chlorides were added to the reaction to protect acid-sensitive epoxides. Of these, Na_2SO_4 resulted in the highest yield of epoxides.

In 1998, the first attempt to use methyltrioxorhenium CH_3ReO_3 (MTO) and H_2O_2 in terpenes epoxidation was done (Figure 3.6).[27] Other terpenes investigated included α-pinene, β-pinene, linalool, geranyl and neryl acetates. Although the catalyst loading is low (up to 0.2 mol %), MTO is an expensive catalyst based on one of the 8 geologically scarcest metals.[28] Moreover, the presence of toxic co-catalyst pyridine or a mixture of pyridine and cyanopyridine and chlorinated solvents were needed. Although the epoxides yields are high, the sustainability of this system is questionable. The more recent reports focused on expanding the scope of epoxidised terpenes and changing base adducts.[29, 30] The more revolutionary work within MTO epoxidation was microencapsulating MTO and base adduct in polystyrene in order to reduce the amount of base adduct needed and simplify catalyst recovery.[31] Although this was a significant improvement, the use of organic solvent (1:1 MeCN:CH_2Cl_2) remains an issue.

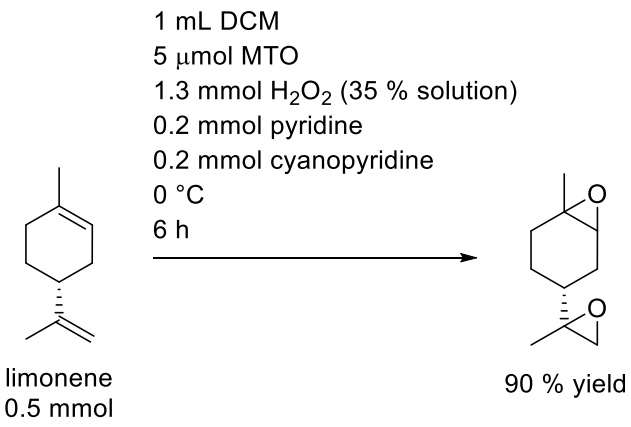

Figure 3.6 Epoxidation of limonene catalysed by MTO.[27]

All of the presented homogeneous catalysts showed selectivity to 1,2-limonene oxide or to 1,2,8,9-limonene bisepoxide. Some procedures reported a mixture of 1,2-limonene oxide and 8,9-limonene oxide. The selective epoxidation of the 8,9-position is a challenge due to its electron-deficiency. Mizuno *et al.* developed an epoxidation procedure employing a bulky polyoxometalate $[C_4H_9N]_4[\gamma\text{-}HPV_2W_{10}O_{40}]$, which sterically excludes the 1,2-position.[32] The procedure was conducted in 1:1 MeCN:t-BuOH, low temperature and short reaction times (Figure 3.7). To this day it is the only selective limonene (**LIM**) epoxidation yielding 8,9-limonene oxide (**8,9-LO**). A more detailed description of this catalyst is provided in Section 3.1.7.

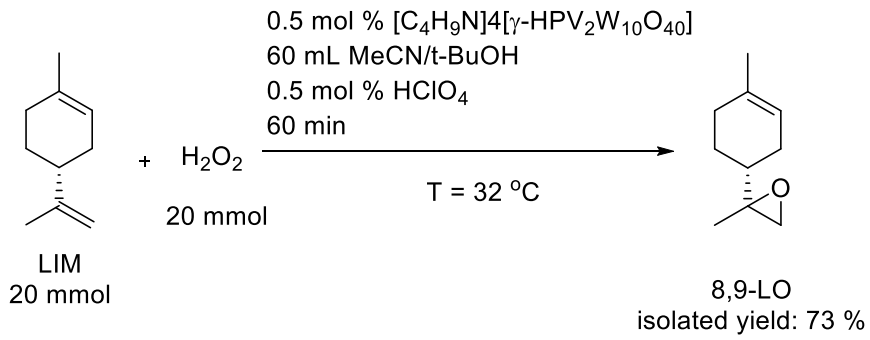

Figure 3.7 Limonene epoxidation using Mizuno catalyst.[32]

All homogeneous catalysts presented contained transition metal, as traditionally transition metal-based catalysts are the most widely studied. However, metal-based catalysts can be costly and some can be toxic. A metal free epoxidation is possible by using an organocatalyst.[33] The first LIM epoxidation performed organocatalytically was reported by Kokotos *et al.* (Figure 3.8).[34] This procedure is extensively described in Section 3.1.7.

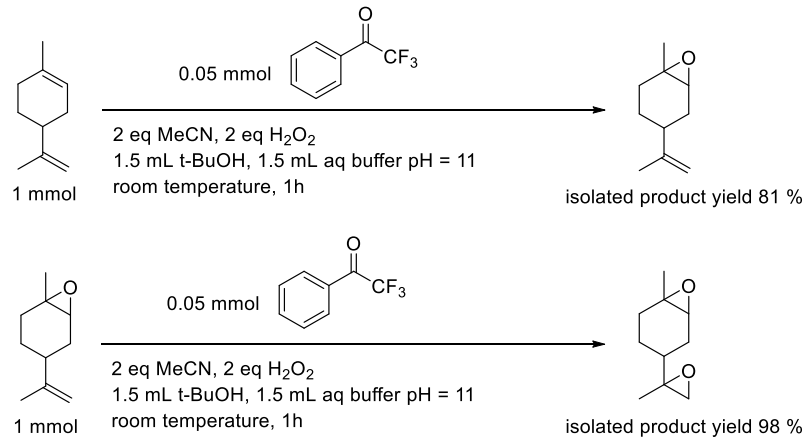

Figure 3.8 Limonene and 1,2-limonene oxide epoxidation using an organocatalyst.[34]

Heterogeneous catalysts

The further developments of Ishii-Venturello catalysis in terpene epoxidation were presented by Jacobs *et al.*,[35] who developed a heterogeneous peroxotungstophosphate catalyst (PW-Amberlite). PW-Amberlite is a catalyst synthesised via the immobilization of a phosphotungstate complex on Amberlite ion-exchange resins. In biphasic conditions, this catalyst epoxidised a wide range of terpenes and allowed for easier catalyst-epoxide separation than the homogeneous counterpart. The reaction required longer reaction times, but maintained high selectivity. For example, limonene was epoxidised at 38 °C in 24 h giving 84 % conversion and 93 % selectivity of epoxides (Figure 3.9). Additionally, it was the first high yielding α-pinene oxidation which was achieved by adjusting pH of the reaction to 4.2 using (aminomethyl)phosphonic acid.[35] They also found that although peroxotunstophosphate can be formed *in-situ* from Na_2WO_4, H_2O_2 and (aminomethyl)phosphonic acid, the preformed version of polyoxometalate $[PW_4O_{24}]^{3-}$ shows higher rates of reaction. PW-Amberlite was slower than the homogeneous phosphotungstate systems, but the catalyst was recovered by simple filtration and the reused catalyst achieved 82 % conversion and 92 % epoxide selectivity.[35] The same catalytic system was also applied to other terpenes, such as geraniol, nerol, 3-carene, geranyl and neryl acetate.

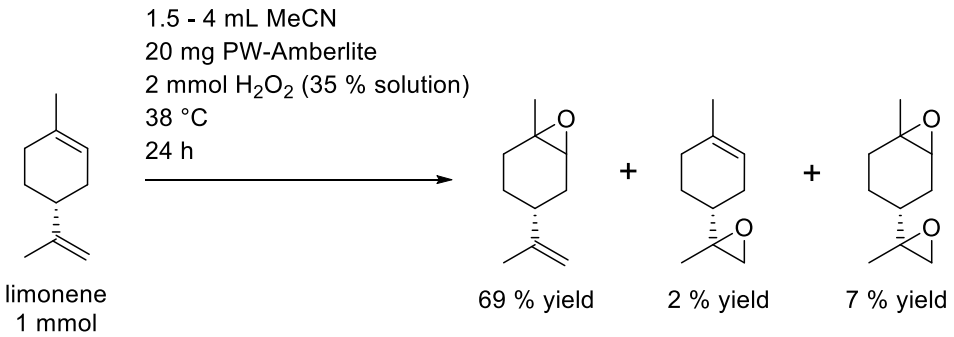

Figure 3.9 PW-Amberlite catalysed limonene epoxidation.[35]

The work on the PW-Amberlite catalyst was continued by other research groups.[36-40] Kinetic studies revealed that the reaction was first order with respect to limonene, oxidant and catalyst. The epoxide product poisons the catalyst and inhibits reaction at 160 turnovers; however, full activity was recovered after treating the PW-Amberlite catalyst with acetone.[40]

A further investigation into the PW-Amberlite catalyst was performed in a triphasic system created by reducing the amount of solvent.[38] The influence of mass transfer, reaction temperature, MeCN, limonene, water and H_2O_2 concentration were investigated. High stirring speed of 1000 rpm and small catalyst particle size (up to 425 μm) was applied to ensure no mass transfer limitations. The maximum initial reaction rate was found at 71 wt % MeCN and 18 wt % H_2O_2. Under these conditions, a rate 6.5 times faster than PW-Amberlite epoxidation in biphasic system was achieved.[38]

Other examples of heterogeneous limonene epoxidation catalysts are presented in Table 3.1. All of them require the use of organic solvents and suffer from low selectivity. The yield of 1,2-limonene oxide (**1,2-LO**) varied between 30 – 73 %. Other products included 8,9-limonene oxide (**8,9-LO**) or limonene bisepoxide (**1,2,8,9-LO**). None of the heterogeneous catalysts display high selectivity towards 8,9-limonene oxide.

Three out of five presented catalysts contain titanium in their structure (Table 3.1 Entry 1, 2, 4) which is consistent with catalysts investigated in industry.[3] A commercial TiO_2 photocatalyst with O_2 as the oxidant yielded 48 % **1,2-LO** after 2 h reaction (Table 3.1 Entry 1),[41] which is exceptionally fast for a heterogeneous catalyst. However, high reaction dilutions were required. Titanium on mesoporous silica SBA-16 (Table 3.1 Entry 2) required using tert-butyl hydroperoxide which is not classified as a green oxidant. Moreover, it required strictly controlled reaction conditions, particularly over the amount of hydroperoxide, to avoid autodecomposition of the hydroperoxide. Ti on mesoporous molecular sieves (Table 3.1 Entry 4) showed low selectivity towards epoxide and an excess of limonene was necessary to avoid Ti leaching into the reaction mixture.

Other catalysts presented consist of Alumina (Al_2O_3), and an organo-layered double hydroxide. Alumina (Table 3.1 Entry 3) provided yield comparable to that previously published for PW-Amberlite, but required a high reaction temperature of 80 °C and high concentration of H_2O_2. The organo-layered double hydroxide (Table 3.1 Entry 5), a catalyst of similar structure to naturally occurring hydrotalcite, showed a high **1,2-LO** yield of 73 % after 2 h reaction, but it required the presence of 6 mol equivalents of dicyanobenzene and 20 mol equivalents of H_2O_2 to achieve high epoxide yield. Dicyanobenzene is directly involved in the catalytic cycle by reacting with H_2O_2, creating peroxycarboximidic acid.

Table 3.1 Examples of heterogeneous catalysts for limonene epoxidation.

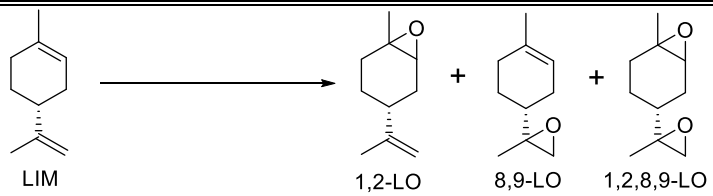

Entry	Catalyst (loading)	LIM [mmol]	Solvent	T [°C]	Oxidant	t [h]	Yield [%]	Ref
1	Silylated commercial TiO_2 photocatalyst P25 (loading not reported)	0.005	5 mL MeCN	20	1 bar O_2	2	48 (**1,2-LO**)	41
2	3D pore structure Ti/SBA-16 7.3 % Ti (300 mg)	6.2	10 mL MeCN	75	11.2 mmol TBHP[a] in decane	24	67 (**1,2-LO**)	42
3	Alumina (0.17 g)	2.7	5 mL EtOAc	80	7.5 mmol 70 % H_2O_2	6	62 (**1,2-LO**) 8 (**8,9-LO**) 12 (**1,2,8,9-LO**)	43
4	Ti-MCM-41[b] 1.27 % Ti (40 mg)	4.32	3 mL MeCN	70	1.17 mmol 35 % H_2O_2	7	30[c] (**1,2-LO** and **8,9-LO**) 5 (**1,2,8,9-LO**)	44
5	Organo-LDH[d]	6.2	80 mL MeOH And 34 mmol 1,2-dicyanobenzene	65	121 mmol 35 % H_2O_2	2	Up to 73 (**1,2-LO**)	45

a) Ti on mesoporous molecular sieves b) tert-Butyl hydroperoxide c) an excess of limonene was used, percentage yield was calculated by comparing the amount of epoxides produced to the amount of H_2O_2 used d) organo-LDH – organo-layered double hydroxide in this study dodecylsulphate and dodecylbenzensulphonate intercalated into Mg/Al-LDH

From all presented heterogeneous catalysts, PW-Amberlite was the most promising and the most widely studied. It is an inexpensive and easy to prepare catalyst which does not require any co-catalysts. It provides a high yield of **1,2-LO**, uses H_2O_2 as an oxidant and it can operate under bi- and tri-phasic conditions. Although the reaction time was long (24 h), it can operate at relatively low temperature (38 °C).

3.1.5 Epoxidation of β-elemene

β-elemene (Figure 3.10) is a sesquiterpene which occurs in nature in small quantities, for example in ginger, juniper and caraway herb and root.[46] A natural feedstock is not widely available, but recently this sesquiterpene was produced by Isobionics via industrial biotechnology through a fermentation processes.[47] β-elemene has not been widely investigated in the published literature, likely due to its low availability. The examples of its use and functionalisation occur mostly in medical literature as anti-tumor agent.[48] No examples of the use of β-elemene in catalytic oxidation or polymer synthesis were found.

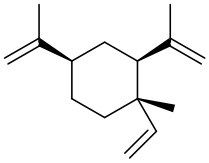

Figure 3.10 Structure of β-elemene.

The only published example of β-elemene oxidation was reported in 1973, where epoxidation and ozonolysis of the molecule was investigated.[49] Epoxidation was performed with peracetic acid, and occured mostly on the least sterically hindered 1-methylethyl group (Figure 3.11). Ozonolysis of β-elemene yielded multifunctional ketones and a ketoaldehyde. Multiple ozonolysis steps were needed to obtain full conversion of the alkene functionalities, with the alkene at the vinyl position being the least reactive.[49]

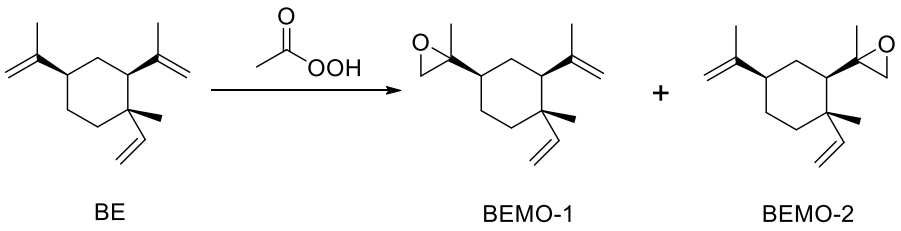

Figure 3.11 β-elemene epoxidation using peracetic acid. The ratio between BEMO-1 and BEMO-2 was 9:1.[49]

3.1.6 Relevant work in the Plucinski, Davidson and Bull groups

In the previous work, the epoxidation of limonene using Ishii-Venturello chemistry was investigated. We used the Venturello catalyst (**VENT**) which consists of Aliquat 336 (a commercial mixture of C8 and C10 quaternary ammonium chloride salts) as a phase transfer catalyst and a $[PW_4O_{24}]^{3-}$ anion. **VENT** was shown to give 83 % conversion and 90 % selectivity towards **1,2-LO** in a flow microreactor with an integrated static mixer with 10 minutes residence time (Figure 3.12).[24] This reaction proceeds in mild conditions with no solvent, which makes it highly interesting when considering the green chemistry principles.

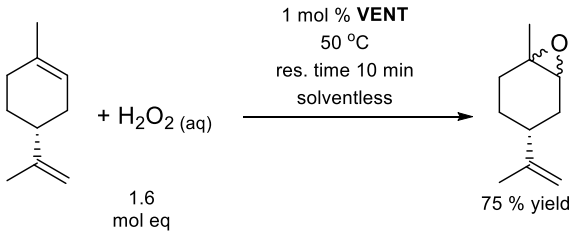

Figure 3.12 Flow epoxidation of LIM using microreactors performed in the Plucinski group.[50]

This work was further developed by W. Cunningham, who expanded the scope of terpenes epoxidised in flow (Figure 3.13).[51]

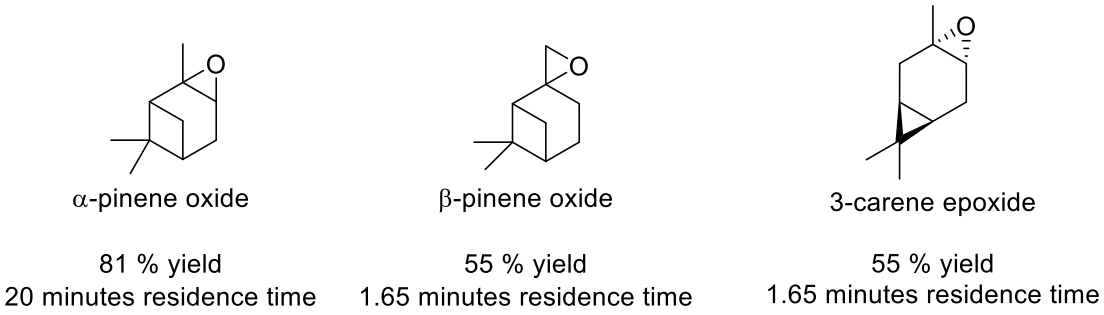

Figure 3.13 Expanded scope of terpenes epoxidised in flow by Cunningham.[51]

Preliminary studies on β-elemene (**BE**) epoxidation have been done by M. Hutchby and W. Cunningham.[51, 52] M. Hutchy used mCPBA as an oxidant and by varying the amount of mCPBA he was able to synthesise β-elemene monoepoxide (**BEMO**), bisepoxide (**BEBO**) and trisepoxide (**BETO**) (Figure 3.14). W. Cunningham used **VENT** as a catalyst, and in batch conditions he was able to achieve 60 % yield of bisepoxide (Figure 3.15).

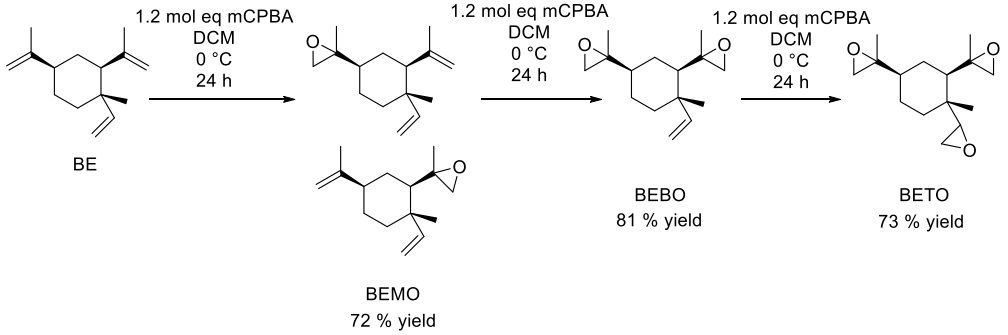

Figure 3.14 Batch epoxidation of β-elemene using mCPBA performed by M. Hutchby.[52]

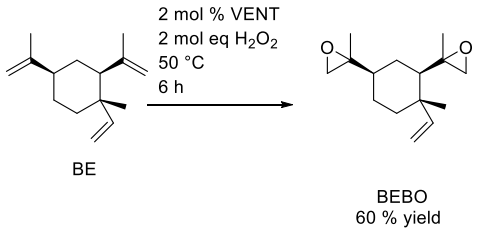

Figure 3.15 β-elemene epoxidation using VENT in batch conditions performed by W. Cunningham.[51]

3.1.7 Catalytic epoxidation protocols chosen for β-elemene epoxidation

Three catalytic systems were chosen for further studies on BE epoxidation. First, **VENT** which is a polyoxometalate previously studied within the Plucinski group. Second, **MIZ** which is a highly selective **LIM** epoxidation catalyst yielding exclusively **8,9-LO**. Third, **TFAP** which is a commercially available organocatalyst.

Venturello catalyst VENT

Tungsten-based polyoxometalates are one of the most efficient epoxidation catalysts[40] and as it was previously shown in this literature review, the Ishii-Venturello systems were widely tested in terpenes epoxidation on a wide range of substrates.

It was chosen due to is relatively easy synthesis from Na_2WO_4 and H_2O_2,[21] and previous experience of working with it within the Plucinski and Bull groups. **VENT** can operate in solventless conditions and previous studies with limonene showed high conversions and high epoxide yields. A 60 % yield of **BEBO** using **VENT** in a batch oxidation reactor has been achieved.[51] It is expected that the use of flow microreactors can increase the selectivity and efficiency of the bi-phasic reaction as it was previously observed for limonene and farnesene.

Mizuno catalyst MIZ

Mizuno *et al.* conducted an extensive study on using $[Bu_4N]_4[\gamma\text{-}HPV_2W_{10}O_{40}]$ **(MIZ)**, as an epoxidation catalyst.[32] The same catalyst can also be used for the hydroxylation of alkanes,[53] oxidative bromination of alkenes, alkynes and aromatics.[54] Mizuno *et al.* investigated changing the central heteroatom of the anion from Si^{4+} to P^{5+}, various reaction solvents, other vanadium species, such as $VO(acac)_2$, $VOSO_4$, $NaVO_3$, V_2O_5, and changing the oxidant from H_2O_2 to organic hydroperoxides.[32] They found that the P^{5+} heteroatom significantly improves the catalyst's performance in the epoxidation reaction. The most efficient reaction solvent was a 1:1 mixture of MeCN and t-BuOH, yielding 84 % epoxide in comparison to MeCN alone yielding 70 % and t-BuOH only 8 %. It was also found that $HClO_4$ is a proton source, which is required to create the active bis-μ-hydroxo site of {OV-(μ-OH)$_2$-VO} from {OV-(μ-O) (μ-OH)-VO}. A low activity with organic hydroperoxides (epoxide yield < 1 %), such as tert-butyl hydroperoxide and cumene

hydroperoxide was explained by steric hindrance of the active site of bulky **MIZ**. The developed reaction conditions and the scope of substrate are presented in Figure 3.16. For limonene epoxidation, **MIZ** exhibited outstanding selectivity towards **8,9-LO** with no **1,2-LO** observed. This has been attributed to steric constraints at the active site.

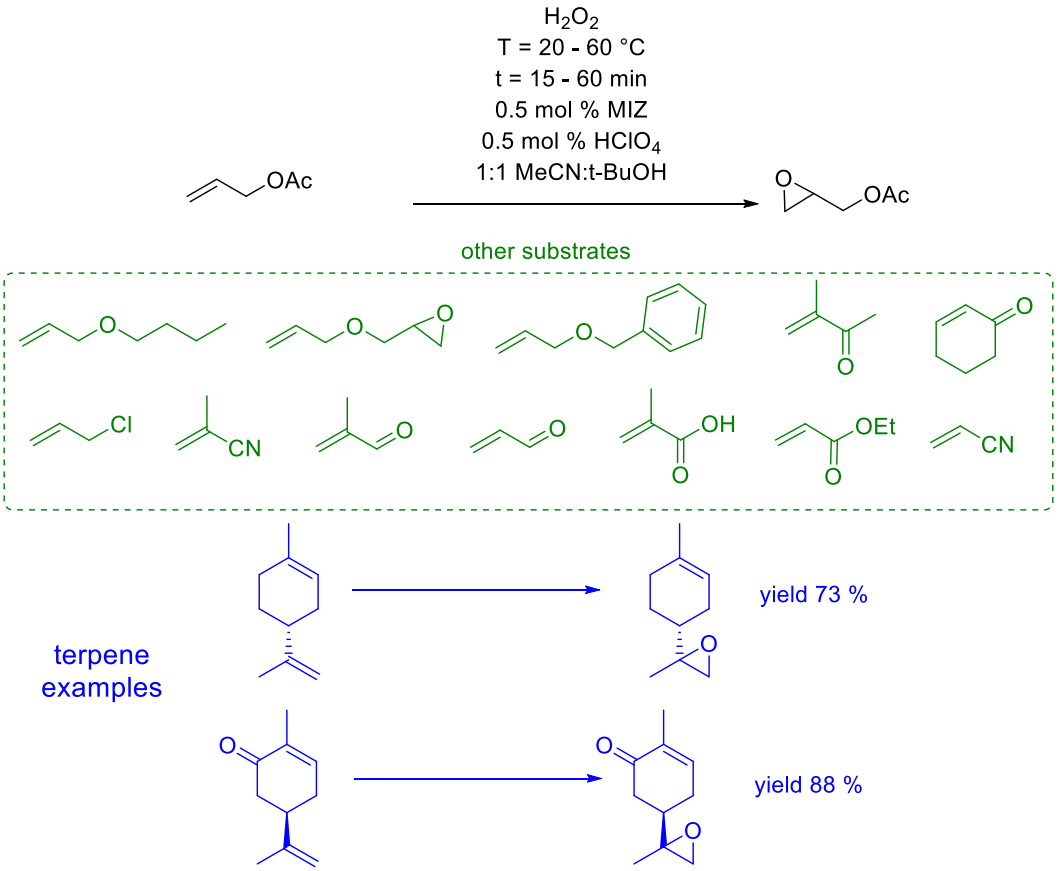

***Figure 3.16 The wide range of substrates tested by Mizuno et al.*[32]**

MIZ was chosen for further study in β-elemene epoxidation due to its unusual regioselectivity. Since **BE** has three double bonds it would be interesting to see if unusual β-elemene monoepoxides or bisepoxides regioisomers were possible to synthesise. These have not yet been achieved via other epoxidation routes (Figure 3.17). **MIZ** is also highly selective and requires a short reaction time; 15 minutes usually provides full conversion. The reaction optimisation will focus on scaling up the reaction and reducing the amount of solvent used.

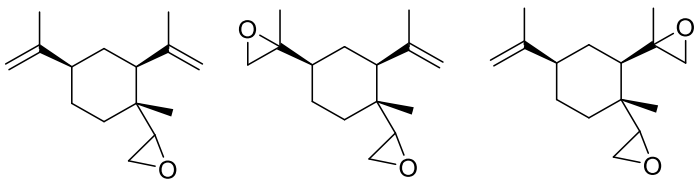

Figure 3.17 Unusual BE epoxide regioisomers not synthesised yet.

Trifluoroacetophenone (TFAP) organocatalyst

A commercially available organocatalyst, 2,2,2-trifluoroacetophenone (**TFAP**), was reported to epoxidise a wide range of olefins, such as cyclic olefins, disubstituted and trisubstituted olefins, monosubstituted styrenes, electrondeficient alkenes, natural steroid cholesterol and terpenes.[34] Other ketones were tested, but **TFAP** was the most efficient due to high carbonyl activation (when the CF_3 group was replaced by CF_2Cl, the yield of epoxide decreased from > 99 % to 92 %). When acetophenone was employed the epoxide yield decreased dramatically to 12 %, thus the perfluoroalkyl moiety was crucial for activity in epoxidation reactions.

In the absence of H_2O_2 and MeCN, no reaction was observed and it has been confirmed that H_2O_2 is an oxidant in this epoxidation, but MeCN is vital as it is directly involved in the reaction mechanism (Figure 3.18).[34] In the presence of water, the ketone is transformed to its hydrate form and in the reaction with H_2O_2 and peroxycarboximidic acid (formed from MeCN at pH 11) goes on to form perhydrate, which is further activated by peroxycarboximidic acid.

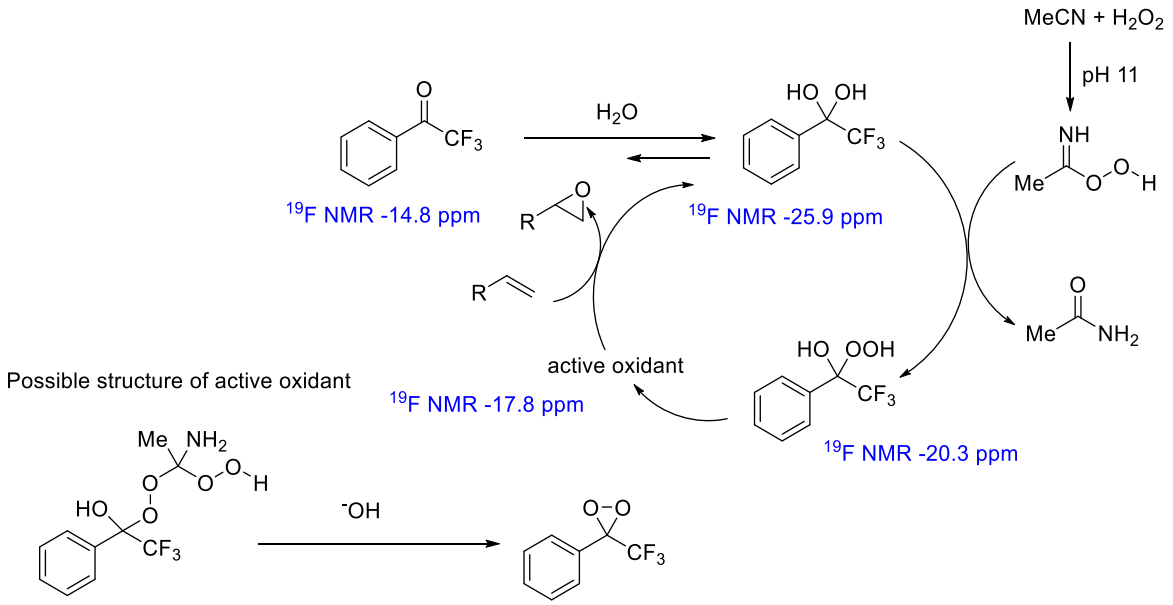

Figure 3.18 Reaction mechanism proposed by Kokotos et al. and relevant ^{19}F NMR spectroscopy data.[34]

TFAP was chosen for further investigation in β-elemene epoxidation due to its good performance in the epoxidation of limonene and 1,2-limonene oxide (see Figure 3.8). The bi-phasic reaction could be potentially performed in flow to improve mass transfer, but preliminary batch optimisation studies must first be done focusing on finding the most optimal solvent and reducing the dilution.

3.2 Results and discussion

3.2.1 Venturello

The polyoxometalate based phase transfer catalyst, Venturello catalyst (**VENT**), was previously used within the group with various terpenes for batch epoxidation and epoxidation using flow reactors.[51] In this research, **VENT** is used as catalyst for the flow epoxidation of **BE** with an aim of developing a protocol for catalytic and selective delivery of **BE** epoxides.

Most of the flow epoxidation conditions were replicated from previous experiments on flow epoxidation of farnesene. The replicated conditions are a reaction temperature of 50 °C and 1.6 molar equivalents of H_2O_2 per double bond. The reaction set up (Figure 3.19) consists of 2 syringe pumps and 2 microreactors. One syringe pump delivers a mixture of **VENT** and olefin, the other syringe is loaded with H_2O_2.

The microreactors are commercially available from Little Things Factory and they have integrated preheating channels and a static mixer.[55] The reaction temperature is maintained via a heating jacket which is built into the structure of the reactor. In the two reactor setup the outlet of the first reactor is connected to the sampling outlet 3 of the second reactor (see labelled picture in Figure 3.19) and the biphasic reaction mixture is collected via sampling outlet 1 of the second reactor. Due to the positioning of the connection between the reactors, the overall reaction volume of the two reactors is 7.5 mL (not double the volume of one reactor). This type of connection ensures that the geometry of the reactor is maintained throughout the whole experiment.

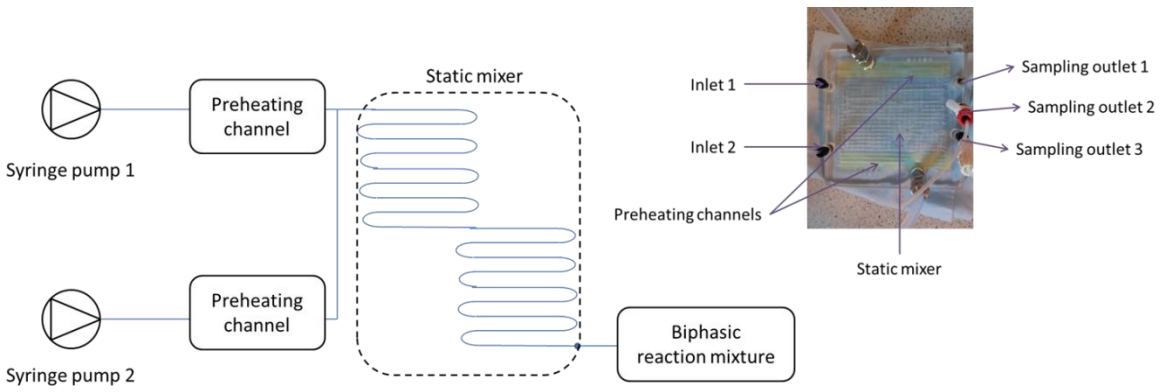

Figure 3.19 Reaction set up and labelled photograph of the Little Things Factory reactor.[55]

Preliminary batch studies

Preliminary batch reactions have been studied to determine the starting catalyst loading and possible product distribution (Figure 3.20). The epoxidation reaction is highly exothermic, thus the batch reactions were run in chloroform, rather than solventless, to prevent overheating. The reactions were maintained at 50 °C using an aluminium heating block.

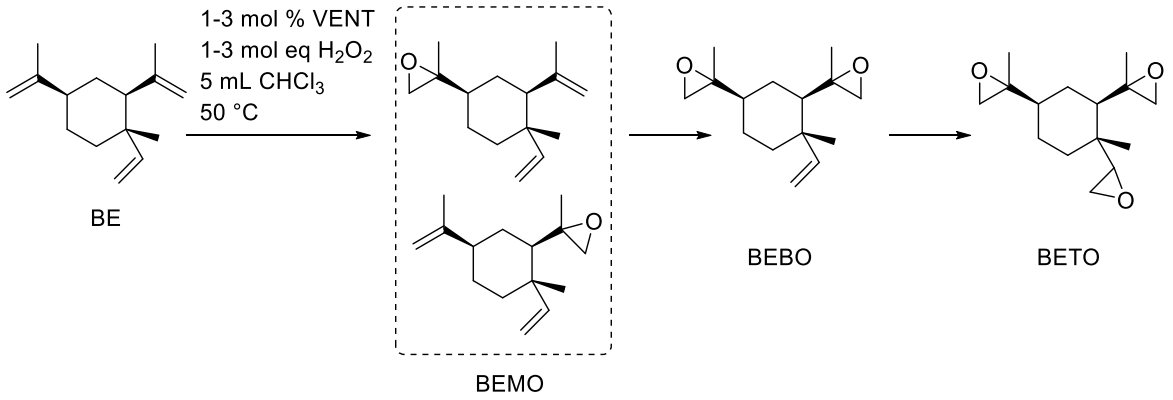

Figure 3.20 Reaction conditions of preliminary batch studies.

During this experiment, the GC-FID analysis method was used, in which the molar fractions of each compound are based on relating the area of β-elemene (or its oxides) to the sum of areas of all detected peaks. The different response factor to oxygenated products was applied based on calibration curves obtained for **BEMO**, **BEBO** and **BETO**. This method does not provide a precise conversion level or yield since it does not account for by-products which do not show on GC-FID. However, the relative ratio between products and disappearance of BE peak on GC-FID provides a good indication of the main reaction products. The purpose of this experiment was to choose initial conditions for epoxidation using flow reactors. In the later stages of the project, the GC-FID was further developed and the concentrations of **BE**, **BEMO**, **BEBO** and **BETO** were calculated based on the mesitylene internal standard. The regioselectivity was confirmed by ^{1}H NMR spectroscopy and it was consistent with previous finding of the Davidson and Bull groups.[51, 52]

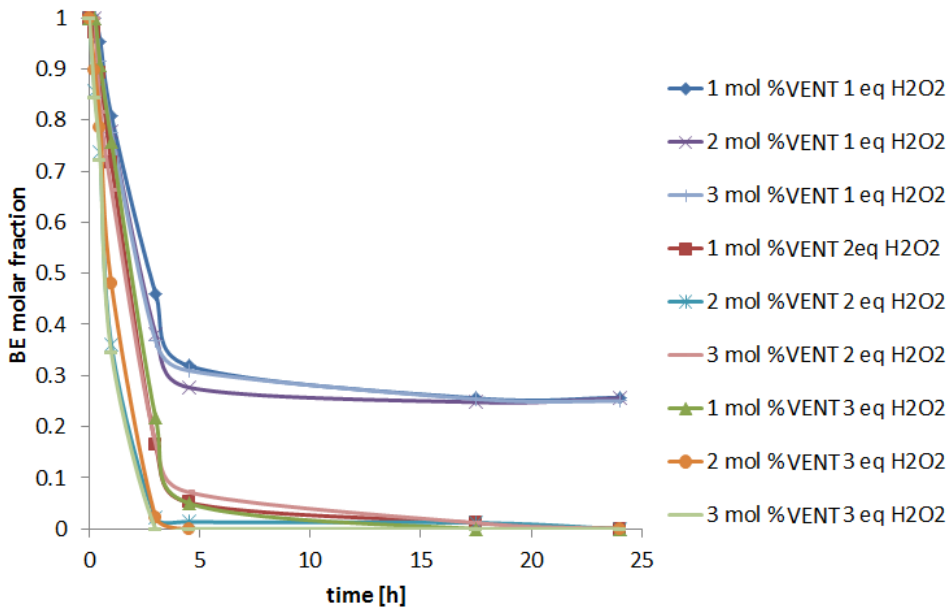

Figure 3.21 Preliminary batch epoxidation of BE catalysed by VENT. Reaction conditions: 0.5 g BE, 1-3 mol % VENT, 5 mL chloroform, 1-3 mol eq H_2O_2, 50 ℃.

Figure 3.21 depicts changes in the **BE** molar fraction depending on the amount of the catalyst and molar equivalents of H_2O_2 used. If only one molar equivalent of H_2O_2 was used (in respect to the amount of **BE**) complete conversion of **BE** was not achieved, presumably due to the epoxidation reaction running out of oxidant. **BE** consumption when 1 eq H_2O_2 was used was unrelated to the amount of catalyst used.

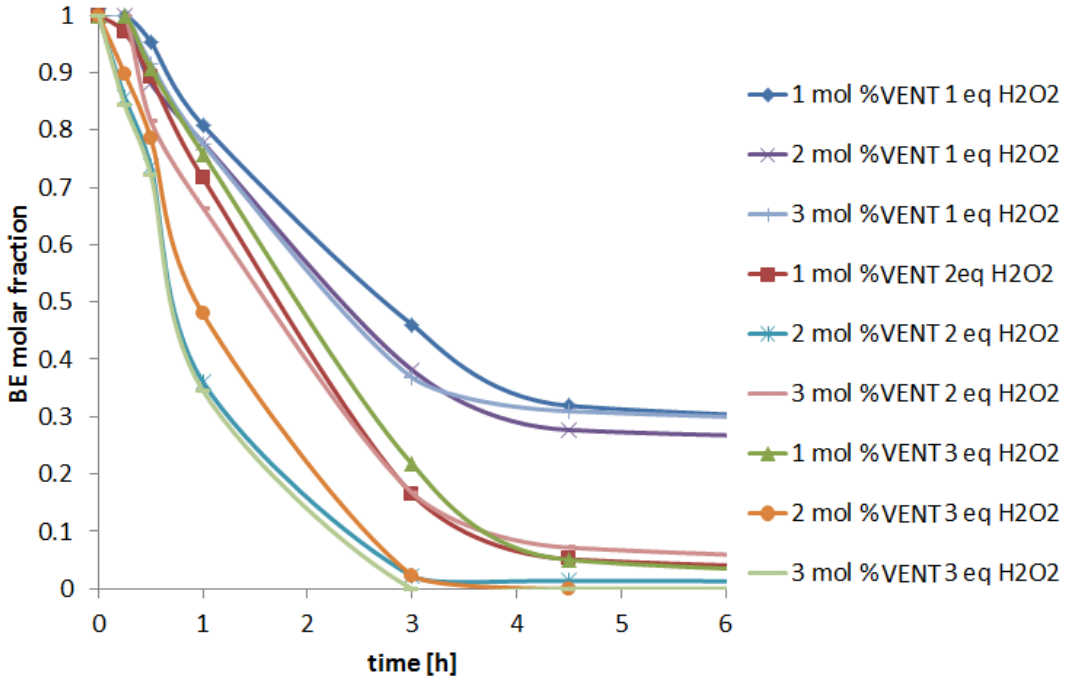

Figure 3.22 Changes in BE molar fraction in 0 – 6 h under reaction conditions previously stated.

The highest conversions were observed for 2 mol % **VENT** with 2 or 3 equivalents H_2O_2; the use of 3 mol % **VENT** with 3 equivalents H_2O_2 was equally efficient (Figure 3.22). For the reactions with the highest conversion, after 3 h almost full conversion of **BE** was observed. The product composition after 3 h reaction time for the highest conversion reactions are presented in Figure 3.23. The main product of the reaction was **BEBO**, but some concentration of **BETO** was observed. Both of these epoxides are potentially useful for polymers and cyclic carbonates synthesis as described in Chapter 4. The increase in the catalyst loading increased **BE** consumption and the yield of **BEBO** and **BETO** by up to 5 %. However, considering the applied analysis method these changes have not been considered as significant.

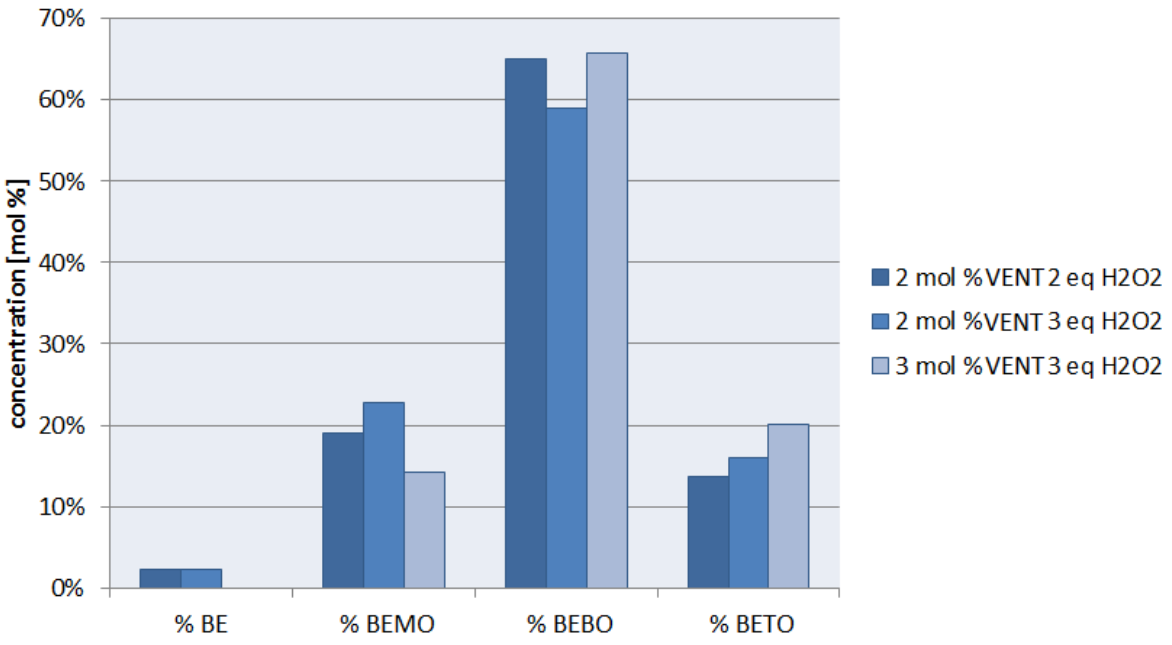

Figure 3.23 The product composition at 3 h reaction time for the reactions with the highest conversion.

The preliminary batch studies showed that the amount of available H_2O_2 was more significant for the reaction than the catalyst loading. The tested catalyst loading included 1, 2 or 3 mol % **VENT** and showed that increasing the catalyst loading from 1 to 2 mol % improved **BE** conversion. However, the further increase from 2 to 3 mol % did not show significant changes in **BE** conversion or product distribution. Therefore, the chosen starting reaction conditions were 50 °C, residence time of 33.2 min, 2 mol % **VENT** (in regard to the amount of **BE**) and 3.2 molar equivalent of H_2O_2 (in flow reaction conditions an excess is used). Previous work in the Plucinski group has determined that 1.6 mol H_2O_2 eq per double bond is needed in a flow set up to achieve high conversion at shorter reaction times.[50-52] For all of the tested batch reactions, the first indication of **BETO** was observed after 3 h reaction with no **BETO** detected at 2 h. It indicated that **BETO** synthesis is signifcantly slower and it needs a longer reaction time, which might mean **BETO** is not achievable in flow epoxidation catalysed by **VENT**.

Flow experiment without catalyst - mass loss and error analysis

To identify any analysis errors and to check whether mass transfer between phases will affect the analysis, a flow epoxidation experiment was performed without the addition of **VENT**, but with Aliquat 336 instead. As previously stated, **VENT** consists of polyoxometalate and a phase transfer catalyst, Aliquat 336 is the phase transfer catalyst which is used in **VENT**. Adding Aliquat 336 by itself should allow for mass transfer between phases, but from previous research done in Plucinski group it is known that Aliquat 336 by its own do not catalyse epoxidation. From each outlet of the reactor three samples were taken and analysed by GC-FID. The changes in **BE** molar fraction, i.e. the ratio between the concentration at the specific residence time and the initial concentration, depending on the residence time are presented in Figure 3.24. Since no **VENT** was added, the **BE** molar fraction should stay at 1. Small variations were attributed to analysis error.

Overall, most of the samples did not deviate from 1 by more than 6 %, thus overall error assigned to GC-FID analysis is 6 % per each compound analysed by GC-FID. For the reactions in which more than one compound is analysed, for example where **BE**, **BEMO** and **BEBO** are analysed, the overall error on cumulative molar fraction can be up to 18 %.

To investigate mass transfer between phases, an NMR sample was taken from the aqueous phase and diluted with D_2O. The NMR spectrum did not show any signals which could be attributed to **BE** or mesitylene (the GC-FID standard used). These results suggest that the organic phase is not transported to the aqueous phase in significant quantities.

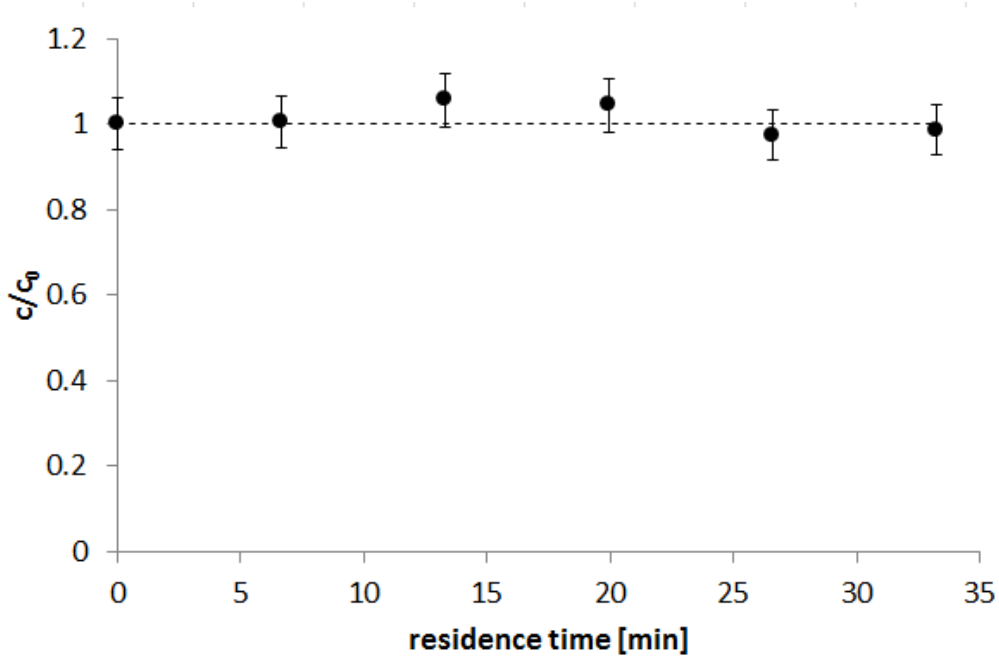

Figure 3.24 Changes of BE molar fraction at different residence times. Experimental conditions: reactor volume 7.5 mL, 50 °C, BE with 2 mol % Aliquat 336 (17.6 mg per 1 mL BE) and 10 mol % mesitylene (0.06 mL per 1 mL BE) as an internal standard, 30 % H_2O_2 with pH adjusted to 7 using aqueous 1M NaOH, flow rate of organic phase: 0.093 mL/min, flow rate of aqueous phase: 0.133 mL/min.

Flow epoxidation with various amount of hydrogen peroxide

From the preliminary batch studies it was shown that the amount of H_2O_2 is crucial for high conversion and high yields of epoxides. The flow epoxidation experiments were conducted with 2.24, 3.2 and 4.8 molar equivalents of H_2O_2 (Figure 3.25), the excess of H_2O_2 was controlled by changing the volumetric ratios between the organic and aqueous phases, maintaining the same overall flow rate with an exception for the experiment with 2.24 eq H_2O_2 (see Table 3.2). An excess of H_2O_2 is used to ensure that the reaction is not limited by the availability of H_2O_2. Indeed, the higher the excess of H_2O_2, the higher conversion of **BE**. However, despite the higher conversion of reaction with 4.6 mol equivalent H_2O_2, it does not improve the yields of epoxides (Figure 3.28 and Table 3.2) suggesting presence of high boiling diols. Although the mass balance has an error of up to 16 % (Figure 3.25-3.27) it is still within previosly identified experimental error of 6 % per compound.

Table 3.2 Reaction conditions for epoxidation in microreactors with variable amount of H_2O_2 in the range of 2.24 – 4.8 molar equivalents.

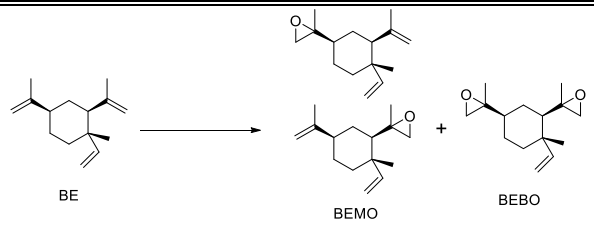

Entry	H_2O_2 mol eq	Aqueous phase[a] [mL/min]	Organic phase [mL/min][b]	Overall flowrate [mL/min]	Residence time [min]	molar fraction		
						BE	BEMO	BEBO
1	4.8	0.154	0.072	0.226	33.2	0.39	0.38	0.13
2	3.2	0.133	0.093	0.226	33.2	0.52	0.39	0.16
3	2.24	0.093	0.093	0.186	32.3	0.57	0.28	0.18

Specific reaction conditions are presented below reaction progress graphs Figure 3.25 – 3.28.
a) 30 % H_2O_2 pH adjusted to 7 using 1 M NaOH
b) β-elemene, 2 mol % VENT, 10 mol % mesitylene as an internal standard for GC-FID

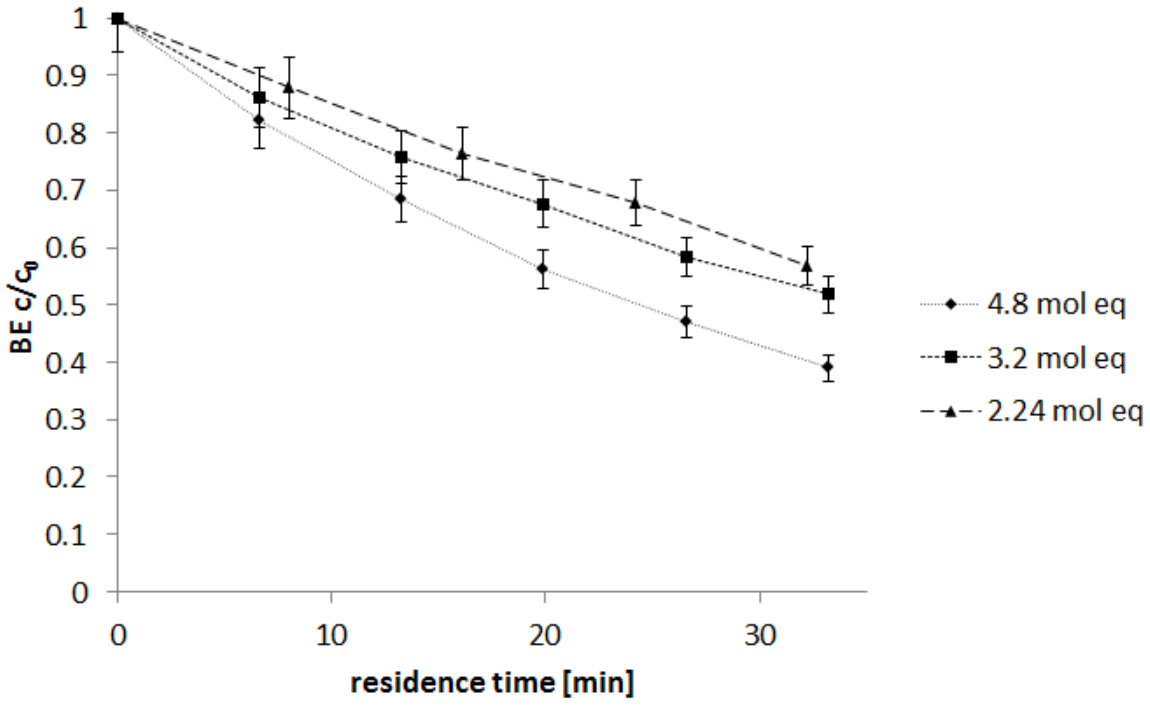

Figure 3.25 Changes in BE molar fraction depending on the excess of H_2O_2 used. Experimental conditions: reactor volume 7.5 mL, 50 °C, BE with 2 mol % VENT and 10 mol % mesitylene dissolved in it, 30 % H_2O_2 with pH adjusted to 7 using aqueous 1M NaOH. Corresponding flow rates of organic and aqueous phases are presented in Table 3.2.

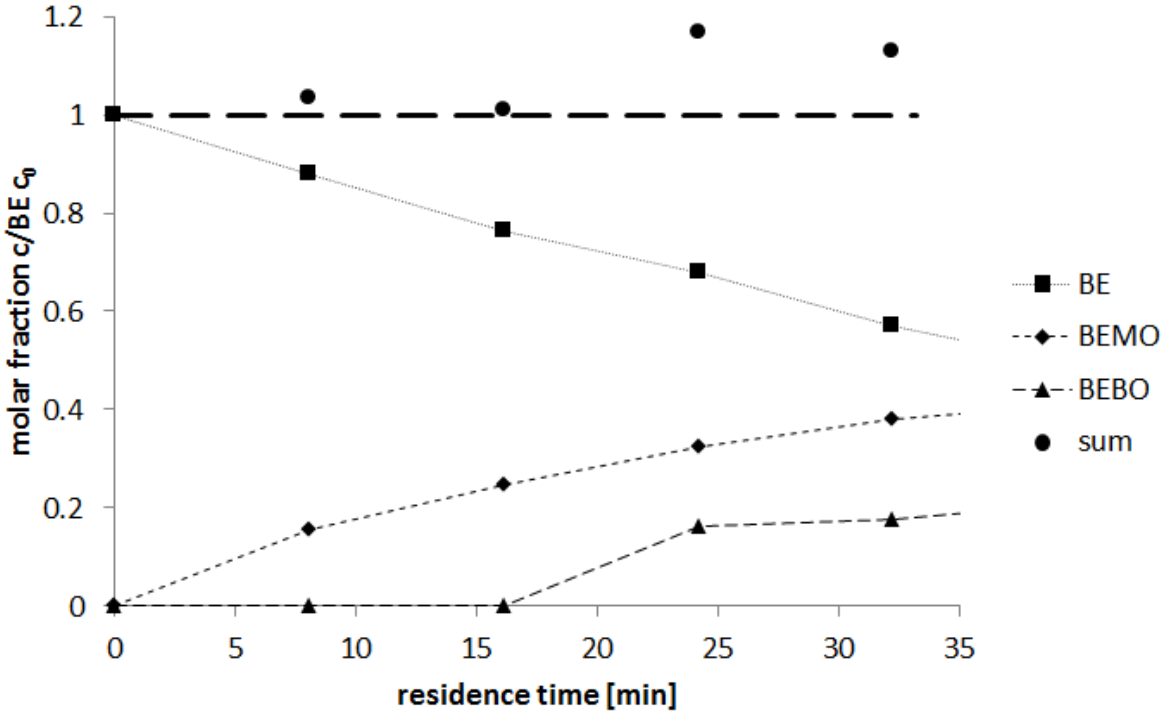

Figure 3.26 Reaction progress represented as molar fraction of compounds with 2.24 eq H_2O_2 used. Experimental conditions: reactor volume 7.5 mL, 50 °C, BE with 2 mol % VENT and 10 mol % mesitylene, 30 % H_2O_2 with pH adjusted to 7 using aqueous 1M NaOH, organic phase flow rate: 0.093 mL min^{-1}, aqueous phase flow rate: 0.093 mL min^{-1}.

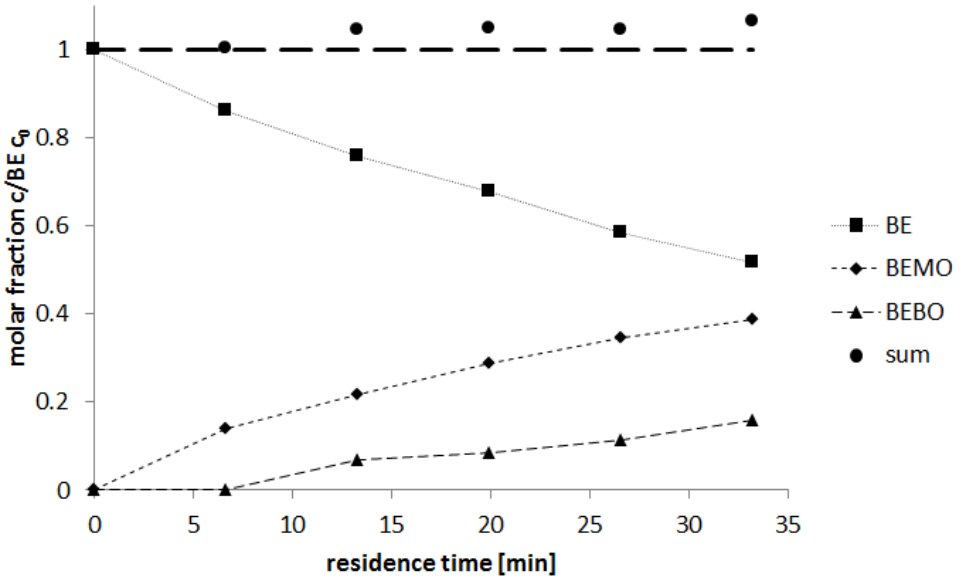

Figure 3.27 Reaction progress represented as molar fraction of compounds with 3.2 eq H_2O_2 used. Experimental conditions: reactor volume 7.5 mL, 50 °C, BE with 2 mol % VENT and 10 mol % mesitylene, 30 % H_2O_2 with pH adjusted to 7 using aqueous 1M NaOH, organic phase flow rate: 0.093 mL min^{-1}, aqueous phase flow rate: 0.133 mL min^{-1}.

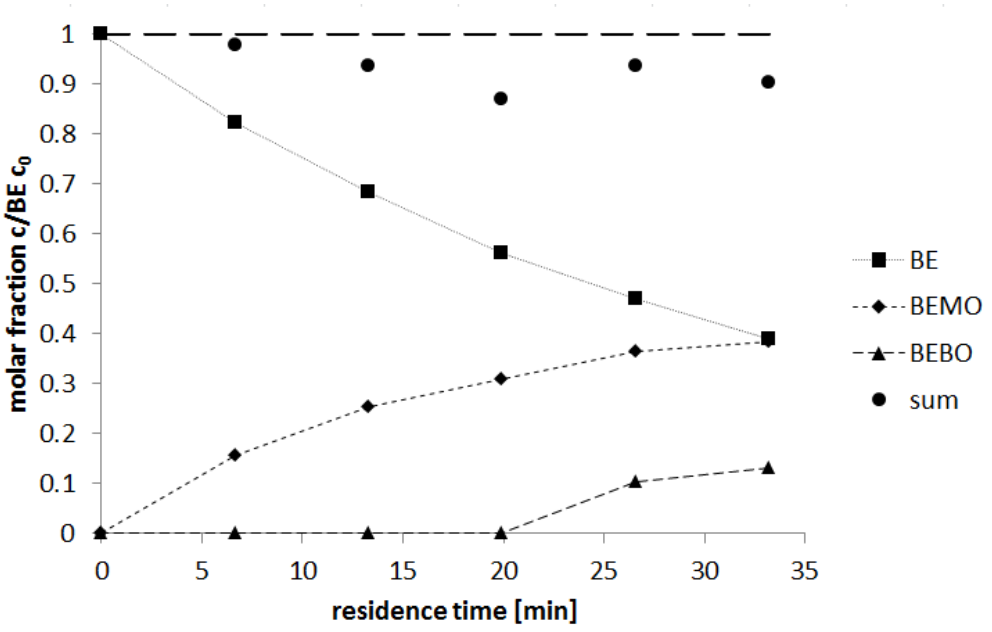

Figure 3.28 Reaction progress represented as molar fraction of compounds with 4.8 eq H_2O_2 used. Experimental conditions: reactor volume 7.5 mL, 50 °C, BE with 2 mol % VENT and 10 mol % mesitylene, 30 % H_2O_2 with pH adjusted to 7 using aqueous 1M NaOH, organic phase flow rate: 0.072 mL min^{-1}, aqueous phase flow rate: 0.154 mL min^{-1}.

In Table 3.2 the results are presented as the molar fractions of the compounds. The conversion of BE can be calculated from the molar fraction using Equation 3.1. BEMO and BEBO molar fractions directly correspond to yield and can be recalculated into selectivity using Equation 3.2.

$$conversion = 1 - BE\ molar\ fraction \tag{3.1}$$

$$selectivity = \frac{BEMO\ or\ BEBO\ molar\ fraction}{1 - BE\ molar\ fraction} \tag{3.2}$$

Comparing the flow results to analogous batch experiments conducted at the same conditions with the same excess of H_2O_2 (Table 3.3) there is no significant difference in conversion and product distribution when 3.2 eq H_2O_2 were used. However, there was a significant improvement of conversion and epoxide yield when 4.8 eq H_2O_2 were used in flow epoxidation. This is probably caused by the restricted interfacial area between the two phases in the batch reactor. In a microreactor, H_2O_2 has a larger interfacial area between the two phases, which allows for improved phase transfer catalysis (Figure 3.29).

Table 3.3 Results of batch experiments corresponding to the same conditions as flow experiments.

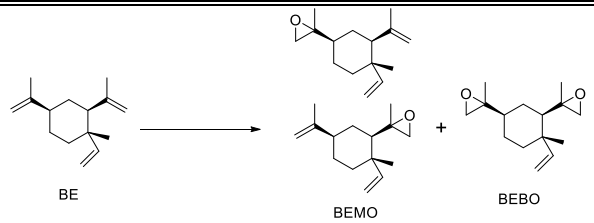

			Compounds molar fractions					
			Batch epoxidation			Flow epoxidation		
Entry	**H_2O_2 eq**	**Time [min]**	**BE**	**BEMO**	**BEBO**	**BE**	**BEMO**	**BEBO**
1	3.2	33	0.54	0.43	0.11	0.52	0.39	0.16
2	4.8	33	0.70	0.28	0	0.39	0.38	0.13

Batch reaction conditions: 4.3 mmol BE, 13.76 or 20.64 mmol H_2O_2 as 30 % solution, 2 mol % VENT, 10 mol % mesitylene, 50 °C. Flow reaction conditions the same as in Figure 3.27 and 3.28

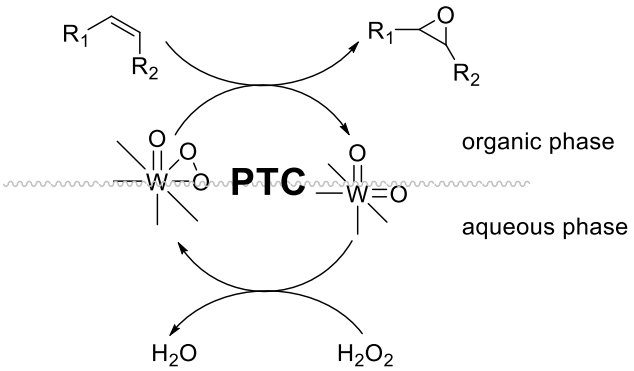

Figure 3.29 Phase transfer catalysis mechanism.[56]

Flow epoxidation with various overall flow rates

The effect of varying flow rates (0.226 – 0.452 mL min^{-1}) was also investigated, the results of which are presented in Figure 3.30. The volumetric ratios between the two phases of the reaction were constant for all the flow rates and the geometry of the reactor was not changed. The specific reaction conditions are included in the figure captions. Lower flow rates provide longer residence times, therefore the conversion should be proportionally higher. The tested flow rates in the range of 0.226 – 0.452 mL min^{-1} correspond to residence time of 33.2 – 18.5 min respectively. The lowest flow rate tested (0.226 mL min^{-1}) achieved 48 % conversion in 33.2 min residence time. The highest flow rate used (0.452 mL min^{-1}) achieved 35 % conversion in 16.5 min residence time, the reduction of residence time by 50 % from 33.2 to 16.5 min reduced conversion by only 13 %. This results suggest the **BE** epoxidation is reaction limited and not mass transfer limited.[38, 57]

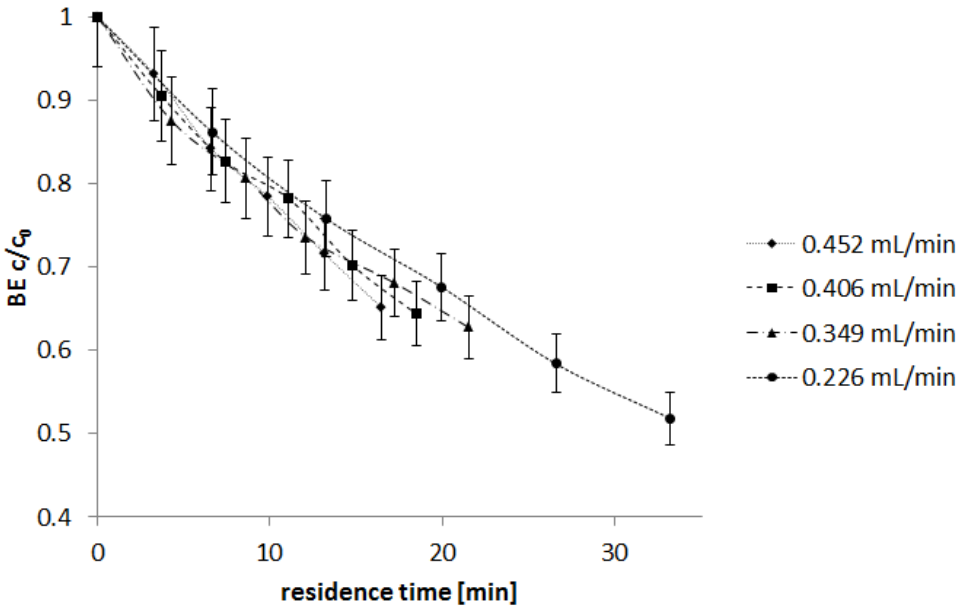

Figure 3.30 Changes in BE molar fraction depending on the residence time. Experimental conditions: reactor volume 7.5 mL, 50 °C, BE with 2 mol % VENT and 10 mol % mesitylene, 3.2 mol eq 30 % H_2O_2 with pH adjusted to 7 using aqueous 1M NaOH.

A large excess of H_2O_2 was used for the **BE** epoxidation, thus it can be assumed that reaction follows a pseudo first order reaction rate (Equation 3.3). The graph of $\ln BE\ \frac{c}{c_0}$ versus residence time is presented in Figure 3.31. The linear dependence of $\ln BE\ \frac{c}{c_0}$ against time confirms that the reaction follows pseudo first order reaction kinetics, and the apparent kinetic constant is equal to the slope of linear dependence. No significant changes within k_1 were observed within the range of flow rates tested (Figure 3.32) indicating that the reaction is within a kinetically controlled catalytic process. This result is consistent with previous findings of Plucinski group on limonene epoxidation, which also followed pseudo first order reaction kinetics in respect to limonene, which were also kinetically limited.[50]

$$\ln\frac{c}{c_0} = -k_1 t \tag{3.3}$$

where:

$\frac{c}{c_0}$ – molar fraction [-]

k_1 – apparent kinetic constant [min^{-1}]

t – residence time [min]

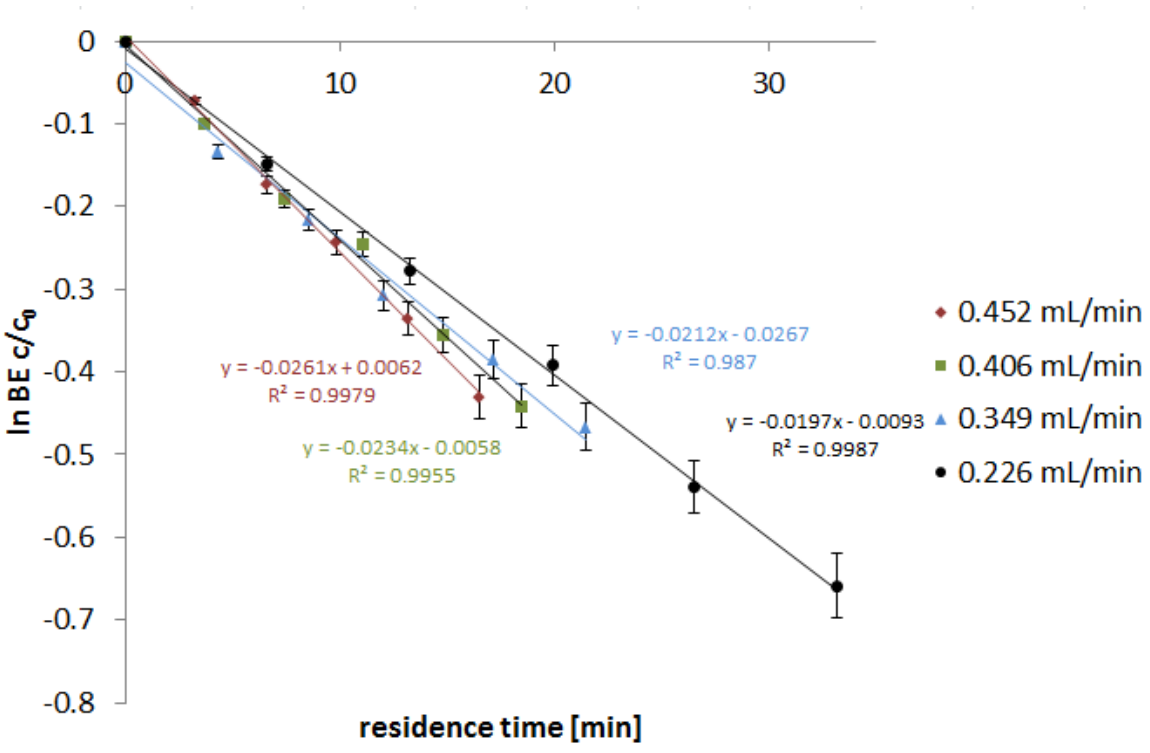

Figure 3.31 Changes in $\ln(\frac{c}{c_0})$ in relation to the residence time.

Experimental conditions: reactor volume 7.5 mL, 50 °C, BE with 2 mol % VENT and 10 mol % mesitylene, 3.2 mol eq 30 % H_2O_2 with pH adjusted to 7 using aqueous 1M NaOH.

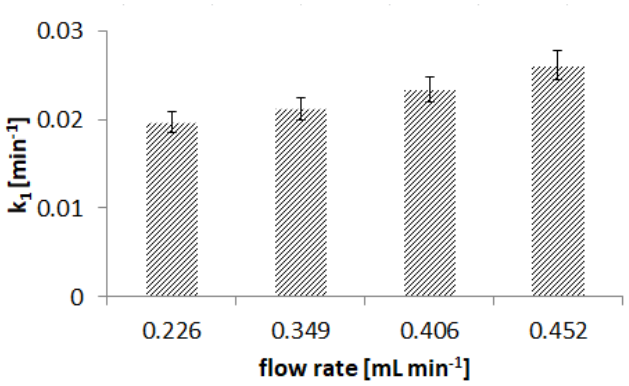

Figure 3.32 Calculated apparent rate constant k_1 and its relation to the overall flowrate.

Selectivity towards epoxides, which according to the GC-FID results was close to 100 %, was not affected by the changes in flow rates (Table 3.4). However, the yield of epoxides was influenced by different flow rates proportionally to the length of residence time (Figure 3.33 and 3.34). The composition of products was always the same with the main product being **BEMO** and **BEBO** as the second largest product. No **BETO** was observed, which is consistent with preliminary batch studies in which the first presence of **BETO** was observed only after longer reaction times of minimum 3 h.

Table 3.4 Results of BE epoxidation in various flowrates.

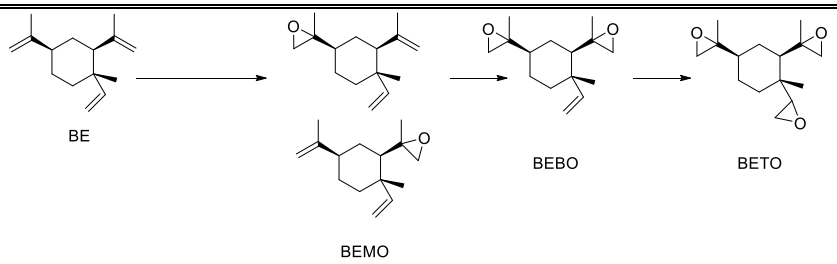

Entry	Flow rate [mL min^{-1}]	Residence time [min]	Molar fraction				Overall molar fraction
			BE	BEMO	BEBO	BETO	
1	0.452	16.5	0.65	0.33	0.10	0	1.08
2	0.406	18.5	0.64	0.31	0.09	0	1.05
3	0.349	21.5	0.63	0.34	0.11	0	1.08
4	0.226	33.2	0.52	0.38	0.16	0	1.06

Reaction conditions reactor volume 7.5 mL, 50 °C, BE with 2 mol % VENT and 10 mol % mesitylene dissolved in it, 3.2 mol eq 30 % H_2O_2 with pH adjusted to 7 using aqueous 1M NaOH.

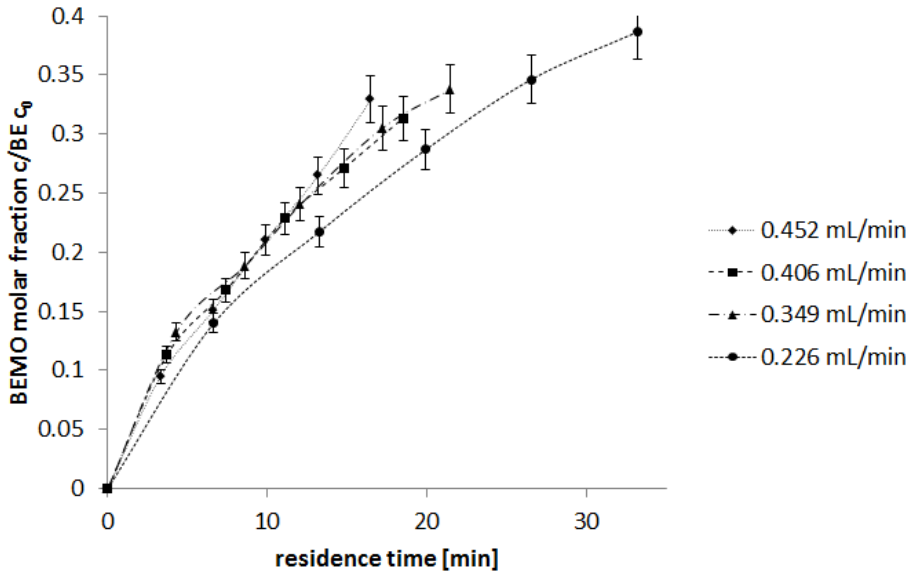

Figure 3.33 Changes of BEMO molar fraction depending on the residence time. Experimental conditions stated in Figure 3.31.

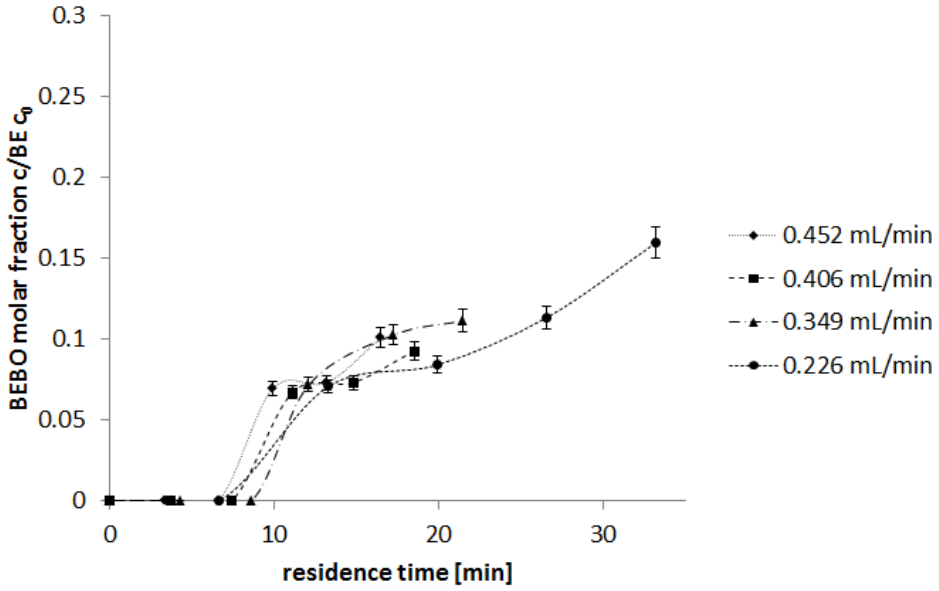

Figure 3.34 Changes of BEBO molar fraction depending on the residence time. Experimental conditions stated in Figure 3.31.

In summary, it was found that mass transfer does not affect conversion and epoxide yield in the range of flow rates tested. The distribution of products suggests **BE** epoxidation is a consecutive reaction, with **BEMO** forming fist and **BEBO** second, **BETO** was not observed in flow set up. However, the residence time was too short to be able to obtain full conversion profile and further model reaction kinetics was not performed. The consecutive epoxidation is supported by previously observed results within the Plucinski group for farnesene epoxidation (Figure 3.35).[58]

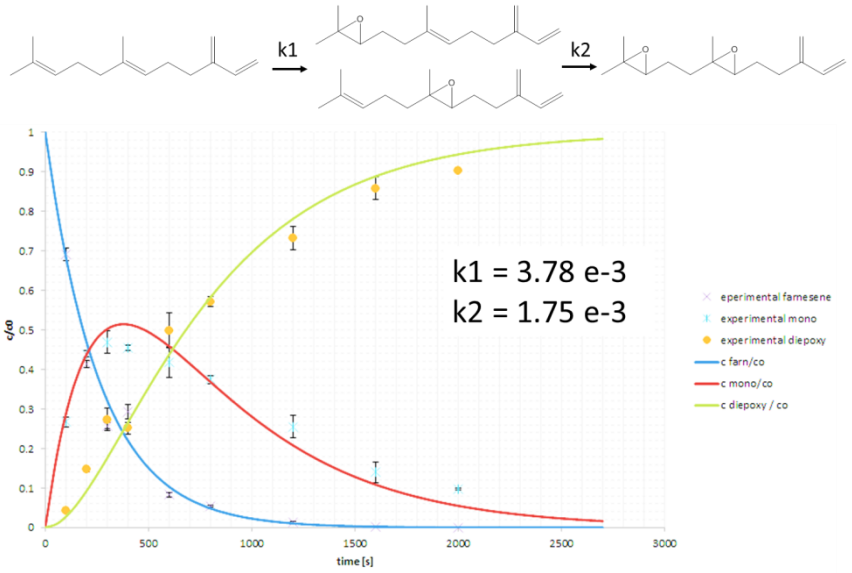

Figure 3.35 Results of farnesene epoxidation obtained within the Plucinski group.[58] These results are presented for information purposes and are not part of this thesis.

Flow epoxidation with longer residence time

Longer residence times were achieved by collecting and recovering the epoxidation reaction mixture from the reactor after the first reaction and recycling it as a feed for another reaction. Collection of the reaction mixture was started after the reactor achieved steady state. The steady state was ensured by collecting three samples from each outlet and ensuring that the conversion at a set point of the reactor does not change over time. The recovered bi-phasic reaction mixture was separated in a semi-continuous manner; the separation was performed using a glass separating funnel cooled by an ice pack. The aqueous phase was periodically removed from the separating funnel approximately every 30 min to reduce the possibility of the two phases reacting further. The recovered two phases were reused as a feed for another reaction. The reuse of phases was stopped when the volume of organic phase was insufficient to perform another experiment. The minimum volume of the organic phase to perform one experiment in the flow reactor (7.5 mL volume) is 12 mL.

The long residence time experiments were performed using 2.24 and 3.32 molar eq H_2O_2. Molar distributions of **BE**, **BEMO** and **BEBO** are presented in Figure 3.36 and 3.37. No **BETO** formation was observed on GC-MS or GC-FID. This confirms the hypothesis from the previous section that the **BE** epoxidation is a consecutive reaction.

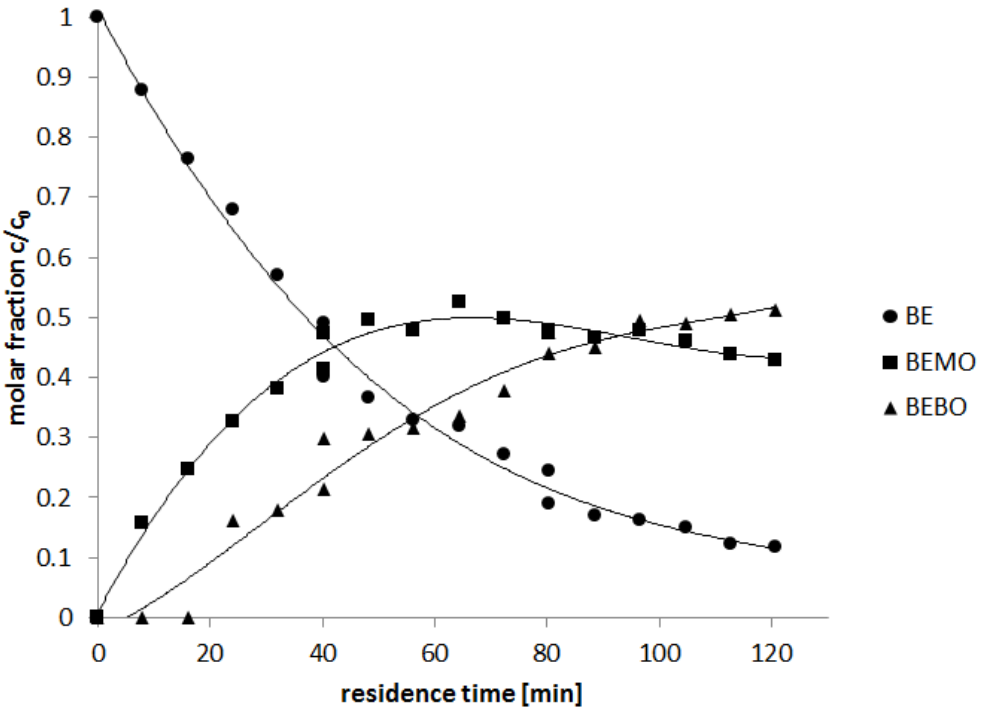

Figure 3.36 Reaction progress represented as molar fraction of compounds with 2.24 eq H_2O_2 used. Experimental conditions: reactor volume 7.5 mL, 50 °C, BE with 2 mol % VENT and 10 mol % mesitylene, 30 % H_2O_2 with pH adjusted to 7 using aqueous 1M NaOH, organic phase flow rate: 0.093 mL min^{-1}, aqueous phase flow rate: 0.093 mL min^{-1}. No BETO was observed. The trend lines are fitted using excel polynomial function and are presented as a guidance only.

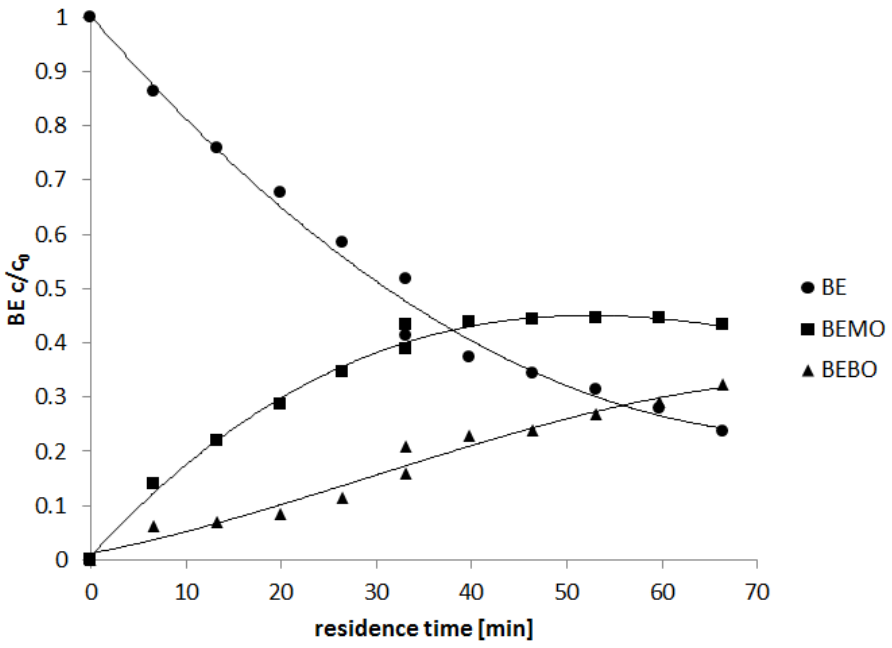

Figure 3.37 Reaction progress represented as molar fraction of compounds with 3.2 eq H_2O_2 used. Experimental conditions: reactor volume 7.5 mL, 50 °C, BE with 2 mol % VENT and 10 mol % mesitylene dissolved in it, 30 % H_2O_2 with pH adjusted to 7 using aqueous 1M NaOH, organic phase flow rate: 0.093 mL min^{-1}, aqueous phase flow rate: 0.133 mL min^{-1}. The trend lines are fitted using excel polynomial function and are presented as a guidance only.

In Table 3.5 the conditions of flow experiments and the molar fraction at the longest residence time are presented. The long residence time of 120.9 min improved **BE** conversion to 88 % and the yield of **BEBO** to 51 % - the highest observed under all flow reactions conditions tested. The shorter residence time of 66.4 min provided **BE** conversion lower by 12 % which shows the conversion is dependent on the residence time, but that it is not a linear dependence. The yield of **BEBO** increased from 16 % to 32 % upon doubling the residence time (from 33.2 min to 66.4 min) which suggest a more linear dependence for **BEBO** formation than **BE** conversion.

Table 3.5 Composition of products at the longest residence times achieved for 2.24 eq H_2O_2 and 3.2 eq H_2O_2

	Flow rate [mL/min]					Molar fraction		
Entry	**Aqueous phase**	**Organic phase**	**Overall**	**H_2O_2 eq**	**Residence time [min]**	**BE**	**BEMO**	**BEBO**
1	0.093	0.093	0.186	2.24	120.9	0.12	0.43	0.51
2	0.133	0.093	0.226	3.2	66.4	0.24	0.43	0.32

Experimental conditions for 2.24 mol eq H_2O_2: reactor volume 7.5 mL, 50 °C, BE with 2 mol % VENT and 10 mol % mesitylene, 30 % H_2O_2 with pH adjusted to 7 using aqueous 1M NaOH, organic phase flow rate: 0.093 mL min^{-1}, aqueous phase flow rate: 0.093 mL min^{-1}.
Experimental conditions for 3.2 mol eq H_2O_2: reactor volume 7.5 mL, 50 °C, BE with 2 mol % VENT and 10 mol % mesitylene dissolved in it, 30 % H_2O_2 with pH adjusted to 7 using aqueous 1M NaOH, organic phase flow rate: 0.093 mL min^{-1}, aqueous phase flow rate: 0.133 mL min^{-1}.

Based on the previous results, the molar fraction of BE was recalculated to fit pseudo first order reaction kinetics (Figure 3.38). After each cycle, a jump in the molar fraction of BE is visible between two cycles of the same reaction. This is likely due to insufficient cooling during phase separation and further epoxidation reaction occurring between two phases in the collecting flask prior to recycle to the rector. Although the results from each cycle can be described as straight line, the slope of each line is slightly different with each cycle. The changes are even more visible in the experiment with 2.24 molar eq H_2O_2. The changes in the slope of lines indicate changes in the apparent kinetic constant which shows that a change in the catalyst activity occurs. Venturello-type catalysts are known to almost fully deactivate after 500 turnovers, but the deactivation process is not fully understood.[59]

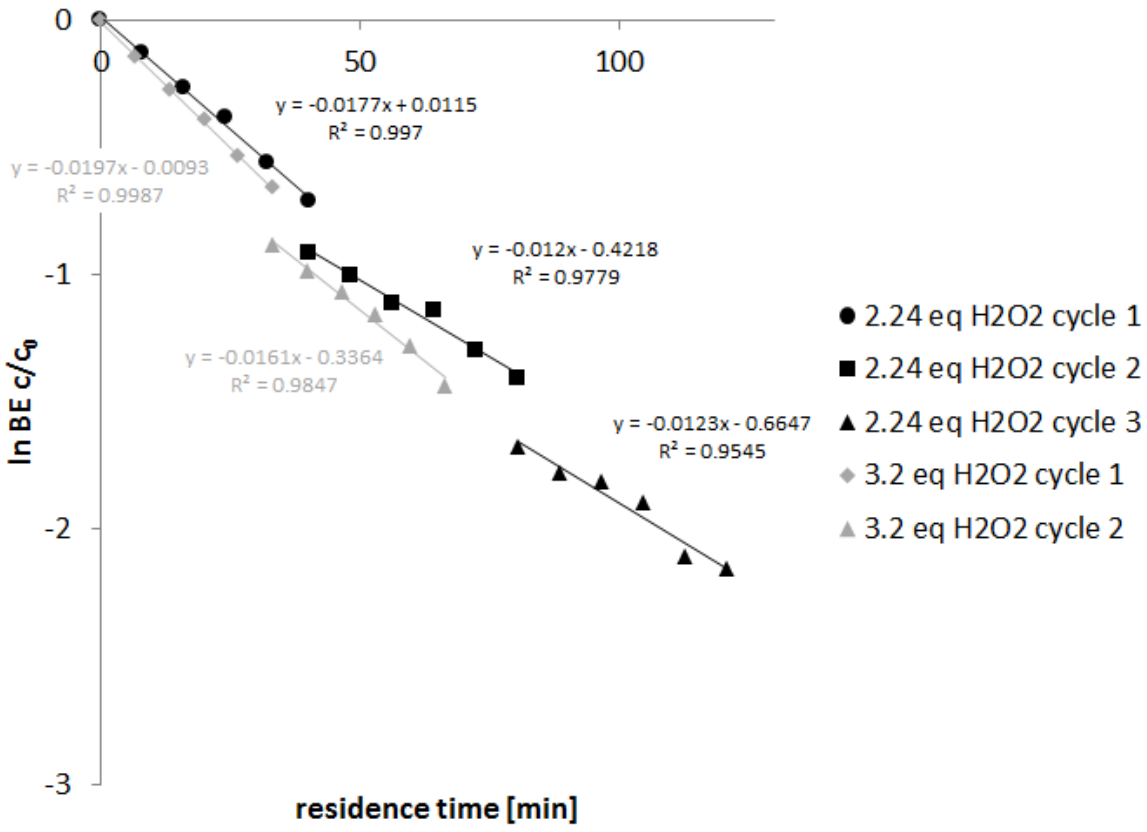

Figure 3.38 Changes of $ln(\frac{c}{c_0})$ obtained from long residence time experiments.

Summary of VENT epoxidation

The preliminary batch reactions showed that the amount of H_2O_2 is crucial to obtain high epoxide yields, but they also suggested that **BETO** formation is too slow for flow epoxidation.

The flow experiments with variable amount of H_2O_2 confirmed that the excess of H_2O_2 is necessary to obtain high epoxide yields. Comparing to batch reactions conducted with the same excess of H_2O_2, no significant improvement was observed when 3.2 mol eq H_2O_2 were used in flow and significant improvement was observed when 4.8 mol eq was used in flow.

BE conversion followed pseudo first order reaction model. Varying the overall flow rate showed that the apparent kinetic constant does not depend on flow rate, suggesting that the reaction is kinetically limited not mass transfer limited.

Experiments with longer residence time confirmed that **BE** epoxidation is a consecutive reaction with **BEMO** being produced first and **BEBO** second. No **BETO** was observed in flow reactions which confirmed results from preliminary batch epoxidations. Experiments with longer residence time showed that apparent kinetic constant changes over time suggesting catalyst degradation.

3.2.2 Mizuno

β-elemene oxidation with Mizuno catalyst

Mizuno catalyst (**MIZ**) is a bulky polyoxometalate $[Bu_4N]_4[\gamma HPV_2W_{10}O_{40}]$ which was previously used in limonene epoxidation resulting in high selectivity towards the electron-deficient double bond. Its regioselectivity is related to its bulky shape which sterically excludes the 1,2-position on limonene.[32] In this project, **BE** was epoxidised using **MIZ** and the reaction conditions developed for limonene epoxidation were applied (Figure 3.39).[32] The special interest was on the **MIZ** regioselectivity effect, but NMR analysis confirmed that no unusual **BEMO** or **BEBO** regioisomers were observed (see Figure 3.17). The NMR analysis is presented in Figure 3.40 and the diagnostic peaks are the signals from alkene groups via ^{1}H NMR spectroscopy.

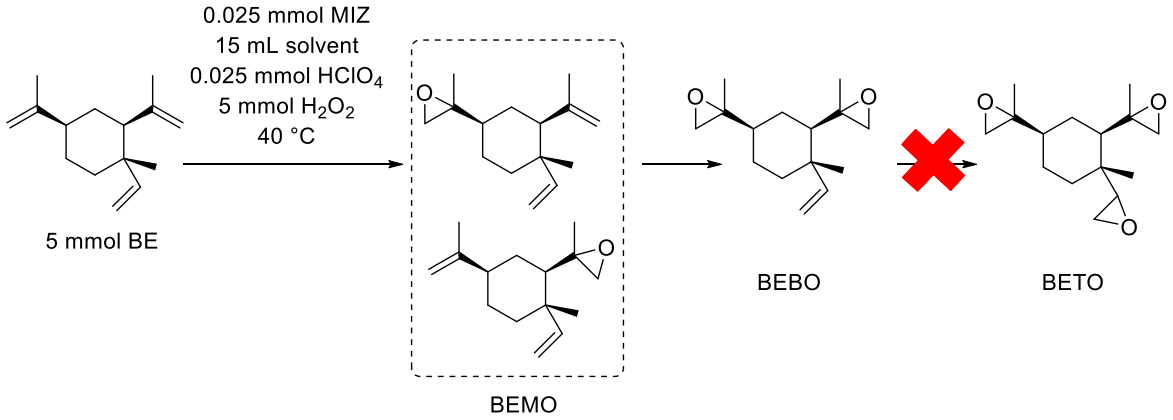

Figure 3.39 Epoxidation of BE catalysed by MIZ.

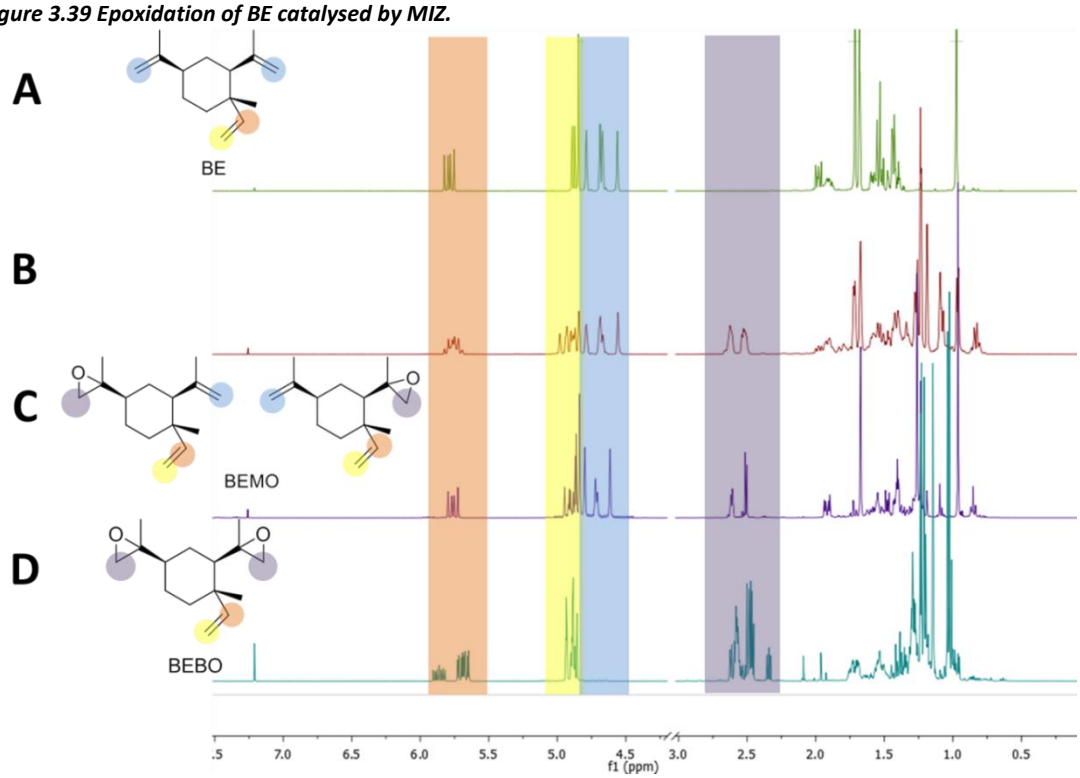

Figure 3.40 Changes in ^{1}H NMR spectra of A - β-elemene, B – crude reaction mixture from MIZ epoxidation (Figure 3.39) after evaporating solvent in vacuo C – pure BEMO D – pure BEBO.

The first **BE** epoxidation was done using 1 mol eq H_2O_2 (Figure 3.39). Considering **BE** has three double bonds which are available for epoxidation, the reaction was limited by the amount of H_2O_2 and conversion was incomplete (Figure 3.41). The products were a mixture of **BEMO** and **BEBO**, with **BEMO** being the main product.

The H_2O_2 mass balance presented in the Figure 3.41 is based on the calculated value using Equation 3.4. The direct measurement of the H_2O_2 concentration was not performed due to limitations of the equipment available. The variation in H_2O_2 concentrations in Figure 3.41 were caused by experimental error related to GC-FID measurements of **BE**, **BEMO** and **BEBO**.

$$1 = [H_2O_2]_t + BEMO + 2 \cdot BEBO \tag{3.4}$$

Where:

$[H_2O_2]_t$ – H_2O_2 concentration at the time t

$BEMO$ - β-elemene monoepoxide concentration

$BEBO$ - β-elemene bisepoxide concentration

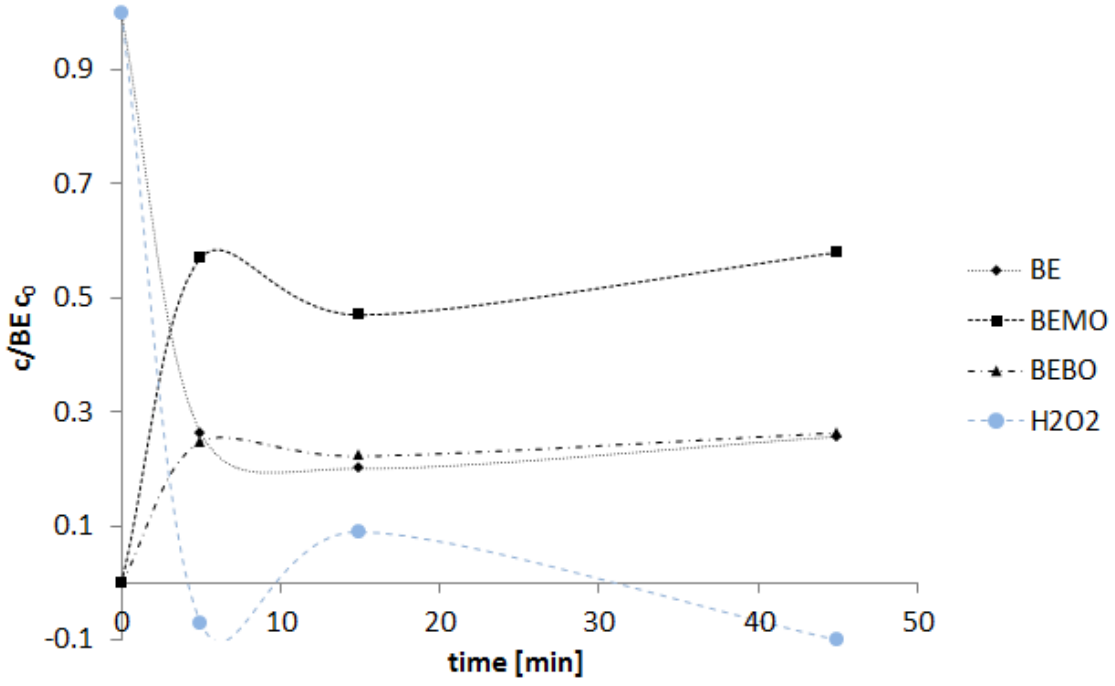

Figure 3.41 Changes in BE molar fraction versus reaction time. Reaction conditions: 5 mmol BE, 15 mL 1:1 MeCN:t-BuOH, 0.025 mmol MIZ, 0.025 mmol $HClO_4$, 5 mmol H_2O_2 (30% solution used).

Error analysis

All experiments were analysed using GC-FID. An aliquot from the reaction mixture was taken and diluted to the desired concentration using methanol. The external mesitylene standard was added to the GC-FID sample. The molar fractions are calculated by referencing all samples to the sample taken before the start of the reaction. A control experiment was carried out using identical conditions, but without a catalyst to determine the analysis error (Figure 3.42). No epoxide peaks were detected without catalyst presence. The error calculated in the GC-FID analysis using mesitylene as an external standard is 10 % per analyte, the same analysis error was assumed for limonene epoxidation and β-elemene epoxidation.

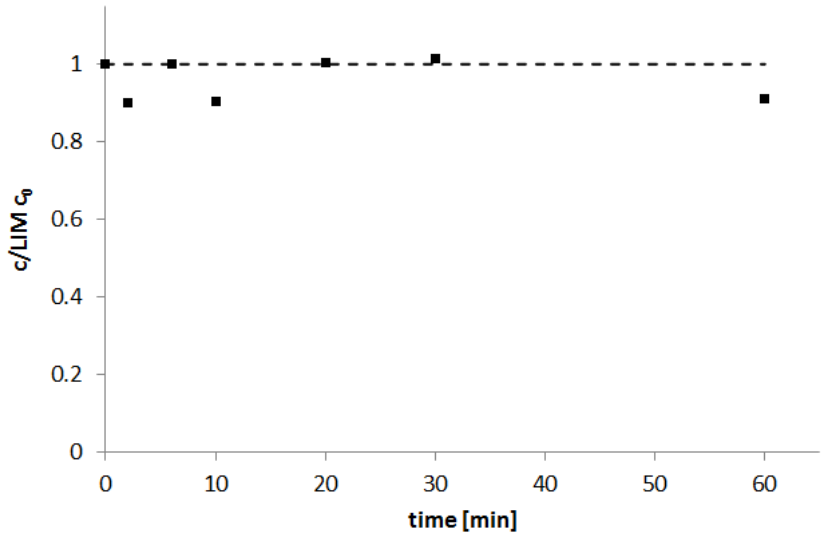

Figure 3.42 Changes in limonene concentration due to analysis. Reaction conditions: 5 mmol limonene, 15 mL solvent (1:1 t-BuOH and MeCN), 5 mmol H_2O_2, 50 ℃.

β-elemene epoxidation catalysed by MIZ with various amounts of H_2O_2

A surprising result was achieved by varying the amount of H_2O_2 used. The more H_2O_2 that was used, the lower the conversion that was achieved (Figure 3.43). Additionally, the yield of epoxide was lower with 2 and 3 molar eq H_2O_2 used, with no BEBO observed even after 45 min reaction time (Table 3.6). No BETO was observed in the reactions with 1-3 molar eq H_2O_2. These results suggest that the initial concentration of H_2O_2 has a negative effect on the catalyst, reducing its activity.

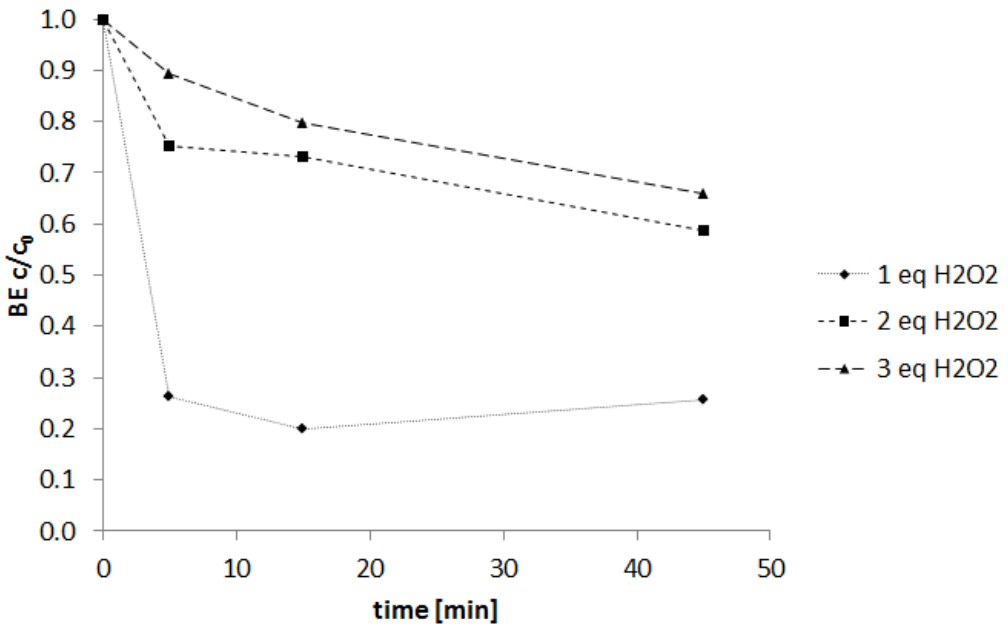

Figure 3.43 Changes in BE molar fraction depending on the molar equivalents of H_2O_2 used. Reaction conditions: 5 mmol BE, 15 mL 1:1 MeCN:t-BuOH, 0.025 mmol MIZ, 0.025 mmol $HClO_4$, 5-15 mmol H_2O_2 (30% solution used).

Table 3.6 Composition of BE, BEMO, BEBO and BETO at 45 min reaction time depending on the amount of H_2O_2 used.

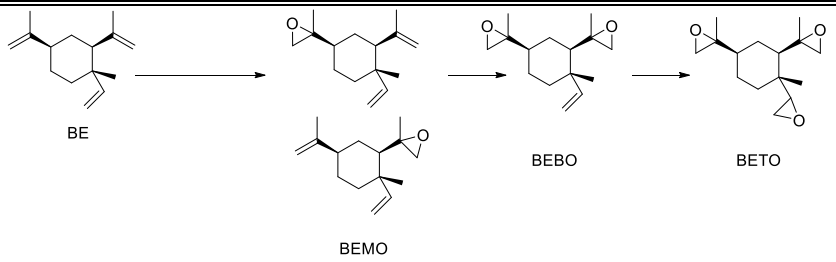

Entry	Molar equivalent H_2O_2	Molar fraction			
		BE	BEMO	BEBO	BETO
1	1	0.26	0.58	0.26	0
2	2	0.59	0.16	0	0
3	3	0.66	0.09	0	0

Reaction conditions: 5 mmol BE, 15 mL solvet (1:1 t-BuOH:MeCN), 0.5 mol % MIZ, 0.5 mol % $HClO_4$, 5-15 mmol H_2O_2 (indicated in the table – 30 % solution was used), 40 °C, 45 min reaction time

A supplementary experiment was performed to check whether the catalyst was reactivated with an addition of fresh H_2O_2 after 45 min (Figure 3.44). A slight drop of BE and BEMO concentration was observed, but no additional BEBO was produced. The changes in BE and BEMO are within experimental error, but additional catalyst-substrate interaction which might not be visible by GC-FID cannot be ruled out. A likely explanation is that under the reaction conditions the catalyst structure undergoes irreversible changes, hindering the catalyst activity. The results suggest that the changes to the structure are accelerated by high concentration of H_2O_2.

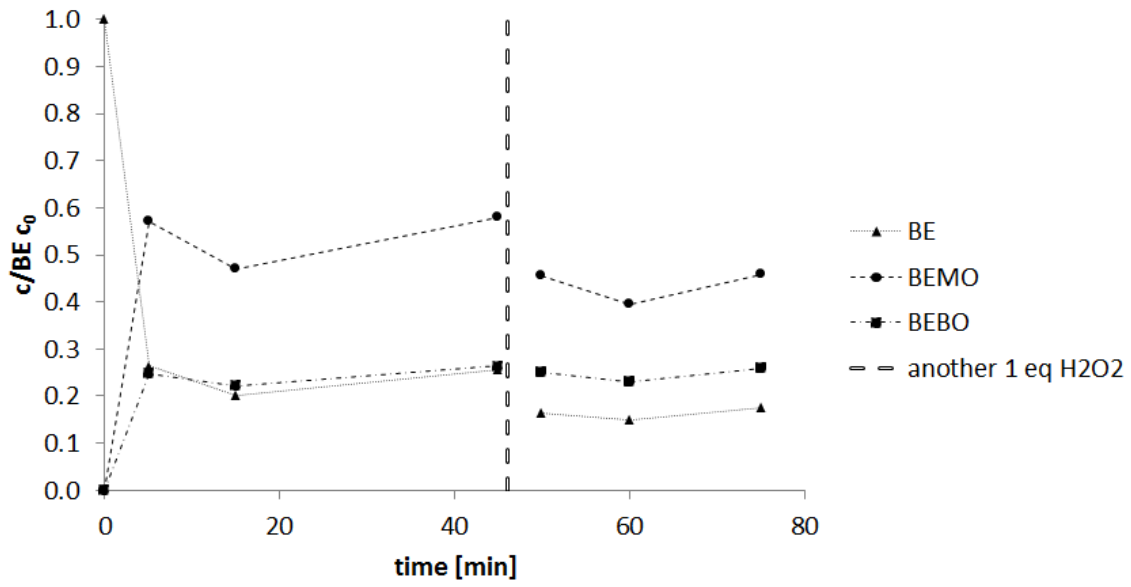

Figure 3.44 Changes in BE, BEMO and BEBO composition under reaction conditions. At 45 min reaction time additional 1 eq H_2O_2 was added. Reaction conditions: 5 mmol BE, 15 mL 1:1 MeCN:t-BuOH, 0.025 mmol MIZ, 0.025 mmol $HClO_4$, 10 mmol H_2O_2 added in two portions, first at 0 min and second at 45 min (30% solution used).

The reaction with higher catalyst loading (1 mol %) and 2 molar eq H_2O_2 was performed to check whether the higher catalyst loading is beneficial for increasing the yield of **BEBO** (Figure 3.45). Comparing to the standard reaction conditions (0.5 mol % MIZ and 1 mol eq H_2O_2) it lowered the conversion by 8 %, which is within the experimental error previously calculated. However, the yield of both epoxides (**BEMO** and **BEBO**) significantly decreased (Table 3.7). Results of this experiment confirmed the previous hypothesis that the amount of H_2O_2 introduced at the beginning of the reaction has significant influence on the catalyst structure and its performance in the epoxidation reaction. Although the large mass loss of 24 % is still within experimental error previously assumed, it might also suggest other reactions occurring which are not possible to follow on GC-FID.

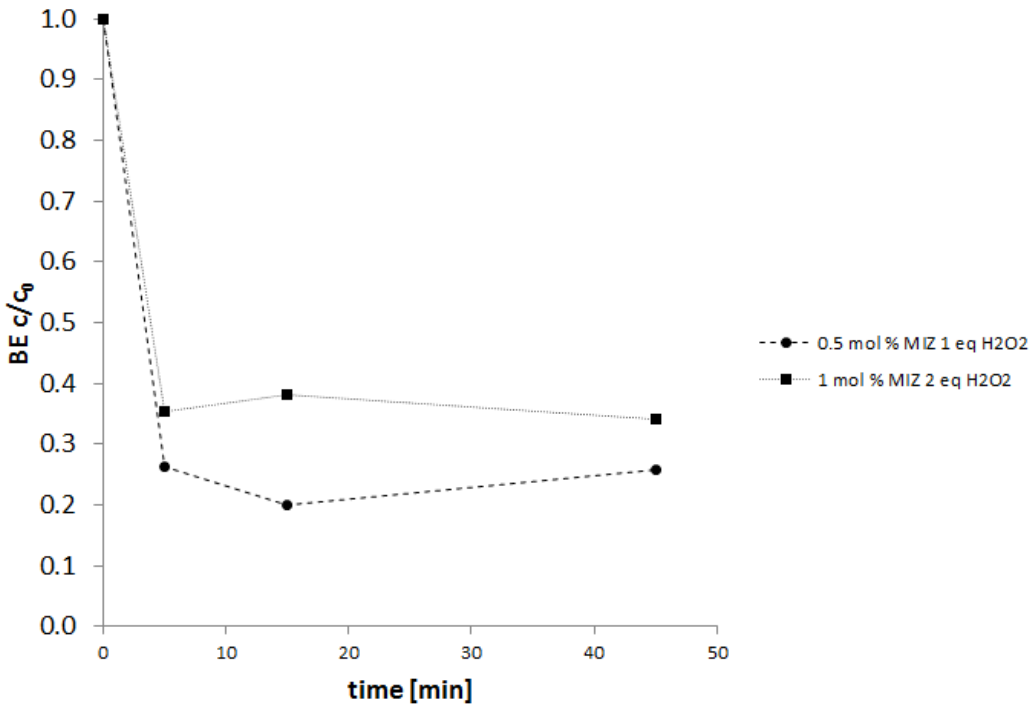

Figure 3.45 Changes in BE molar fraction during the reaction catalysed by 0.5 mol % with 1 eq H_2O_2 and reaction catalysed by 1 mol % MIZ with 2 eq H_2O_2.

Table 3.7 Molar fraction of BE, BEMO and BEBO at 45 min reaction time with 0.5 – 1 mol % MIZ and 1 – 2 mol eq H_2O_2 was used, results correspond to Figure 3.45.

Entry	MIZ [mol %]	Molar equivalent H_2O_2	Molar fraction				
			BE	BEMO	BEBO	BETO	sum
1	0.5	1	0.26	0.58	0.26	0	1.1
2	1	2	0.34	0.28	0.14	0	0.76
Reaction conditions: 5 mmol BE, 15 mL solvet (1:1 t-BuOH:MeCN), 0.5 - 1 mol % MIZ (indicated in the table), 0.5 - 1 mol % $HClO_4$ (equimolar to the amount of catalyst), 5-10 mmol H_2O_2 (indicated in the table – 30 % solution was used), 40 °C, 45 min reaction time							

Varying the amount of β-elemene

Varying the amount of **BE** was an alternative approach to increase the yield of epoxides, rather than changing the amount of H_2O_2 (Table 3.8). By varying the amount of **BE** between 5 mmol and 1.5 mmol, the **BE** conversion rose up to 100 %. The yield of epoxides was also greater than in the standard reaction conditions, with the yield of **BEBO** increased up to 63 %. However, upon reducing the quantity of **BE** by over three times, resulting in over 3 mol eq H_2O_2 in the reaction mixture, no **BETO** was observed. Another interesting observation is a significant mass loss in reactions with high yields of epoxides (Table 3.8 and Figure 3.46). For the reaction with 1.5 mmol **BE** the mass loss reached over 30 %, which even with the previously calculated experimental error of 10% per compound is a significant mass loss. No additional peaks were visible on GC-MS, but

potential by-products such as high boiling β-elemene diols or aldehydes were expected to be too high boiling to be visible on GC-FID. Potentially, the presence of hydroxyl radicals can facilitate the rearrangements of epoxides or the production of some polymeric products as well.

Table 3.8 Molar fraction of BE, BEMO, BEBO and BETO at 45 min reaction time in the reaction with 1.5 – 5 mmol BE.

Entry	BE [mmol]	MIZ [mol %]	Molar equivalent H_2O_2	Molar fraction				
				BE	BEMO	BEBO	BETO	sum
1	5	0.5	1	0.26	0.58	0.26	0	1.10
2	2.5	1	2	0.02	0.25	0.58	0	0.85
3	1.5	1.67	3.33	0	0.06	0.63	0	0.69

Reaction conditions: BE (the amount indicated in the table), 15 mL solvent (1:1 t-BuOH:MeCN), 0.5 – 1.5 mol % MIZ (it is the same amount by mass – 90mg, but since the amount of BE changes it is different molar %), 0.5 – 1.5 mol % $HClO_4$ (the same amount by mass, but since the amount of BE changes it is a different molar %), 5 mmol H_2O_2 (30 % solution was used), 40 °C, 45 min reaction time

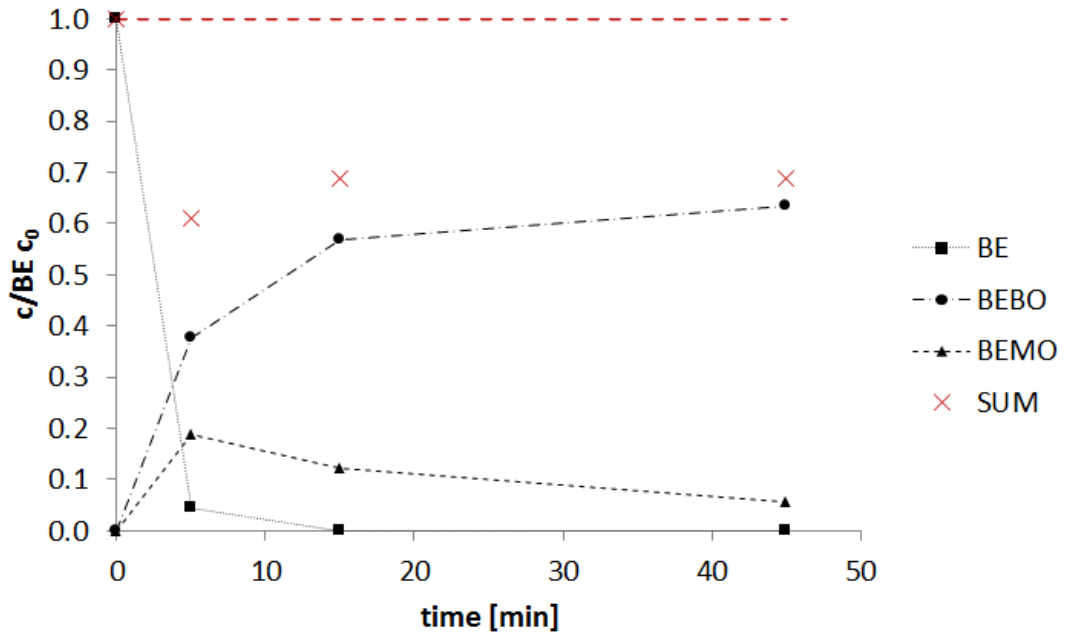

Figure 3.46 Reaction progress of BE epoxidation catalysed by MIZ when 1.5 mmol BE was used. Reaction conditions: 1.5 mmol BE, 15 mL solvent, 40 °C, 1.5 mol % MIZ, 1.5 mol % $HClO_4$. The red dashed line is a theoretical mass balance and the red crosses correspond to sum of molar fractions of the compounds detected on GC-FID.

MIZ catalysed epoxidation of β-elemene monoepoxide and β-elemene bisepoxide

Further investigations into MIZ reactivity towards different β-elemene epoxides were performed starting from **BEMO** or **BEBO** as a substrate (Figure 3.47 and Figure 3.48). However, even with long reaction times of 100 min, no presence of **BETO** was observed. Considering all of the data presented, it can be concluded that it is not possible to obtain **BETO** via H_2O_2 epoxidation catalysed by **MIZ**. It was also observed that the rate of reaction significantly decreased when **BEMO** was used as substrate for the epoxidation (Table 3.9 Entry 1 and 2). Moreover, significant

mass loss of 16 % was observed if **BEBO** was used as an epoxidation substrate. It might suggest some interaction between the catalyst and epoxides, which could also explain the mass losses previously observed.

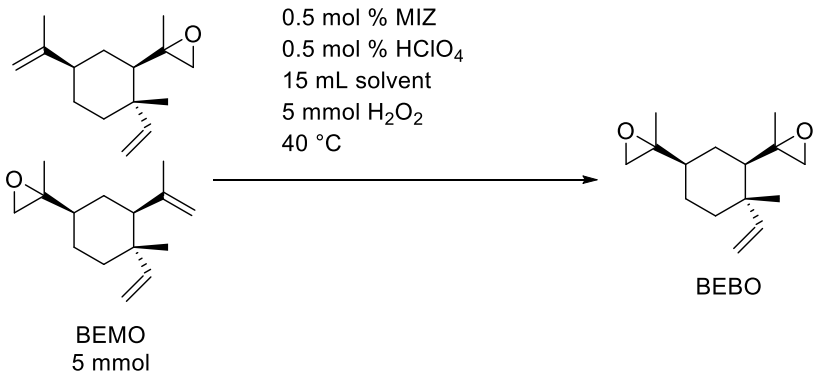

Figure 3.47 MIZ epoxidation of BEMO. The reaction conditions correspond to the previous BE epoxidation.

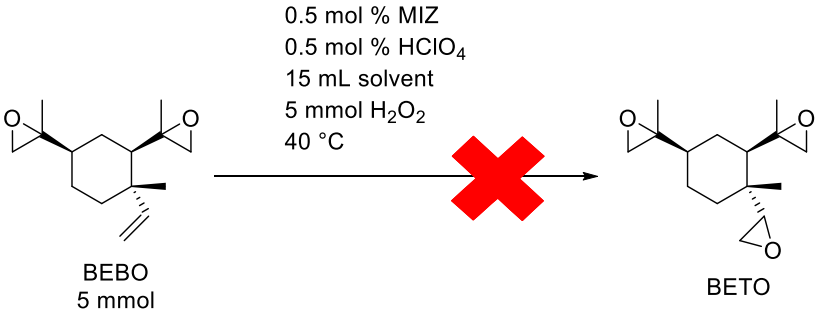

Figure 3.48 MIZ epoxidation of BEBO. The reaction conditions correspond to the previous BE epoxidation.

Table 3.9 The molar fractions of BE, BEMO, BEBO and BETO in the epoxidations shown in Figure 3.47 and Figure 3.48 and the previously stated BE epoxidation.

Entry	substrate	Molar fraction				
		BE	BEMO	BEBO	BETO	Sum
1[a]	5 mmol BE	0.26	0.58	0.26	0	1.1
2	5 mmol BEMO	0	0.72	0.31	0	1.03
3	5 mmol BEBO	0	0	0.84	0	0.84

Reaction conditions: substrate indicated in the table, 15 mL solvent (1:1 t-BuOH:MeCN), 0.5mol % MIZ, 0.5 mol % $HClO_4$, 5 mmol H_2O_2 (30 % solution was used), 40 °C, 100 min reaction time
a) 45 min reaction time

3.2.3 Further investigation into Mizuno epoxidation with limonene as a substrate

Since **BE** is a complicated substrate with multiple oxidation products, the epoxidation catalysed by MIZ was further investigated using limonene as a model substrate (Figure 3.49) to compare to the previously published work by Mizuno *et al.*[32] The published data indicates exclusive regioselectivity towards **8,9-LO**.

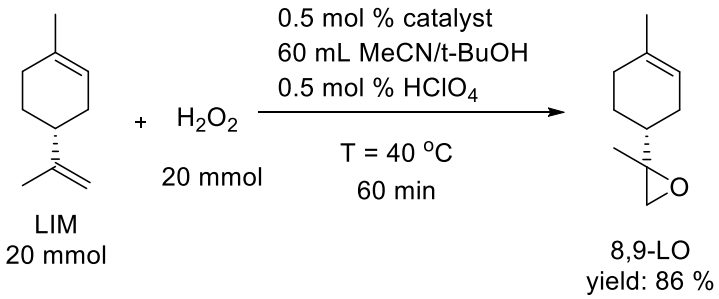

Figure 3.49 Limonene epoxidation performed according to published results,[32] yield analysed by GC-FID, the yield is comparable to previously published 73 % isolated yield.

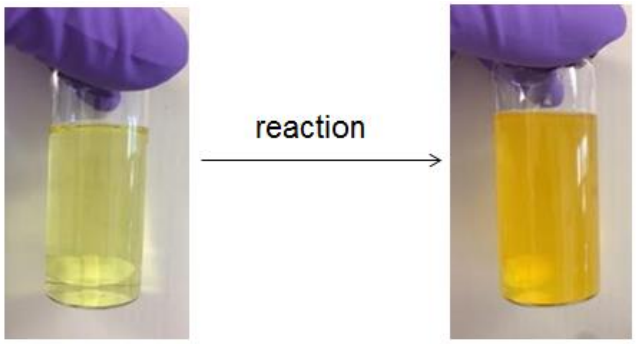

Figure 3.50 Changes in reaction mixture appearance after adding H_2O_2.

The previous findings of this report indicated that the concentration of H_2O_2 has a significant influence on the epoxidation reaction, thus from this point all epoxidation compared on the same chart or in the same table were performed on the same day from the same batch of H_2O_2 to ensure the concentration of H_2O_2 was constant. In special cases, H_2O_2 was titrated directly before experiments. It is worth noting that the reaction mixture changed colour immediately after adding H_2O_2 and became less clear. Since both the substrate and the product are colourless clear oils, the colour probably come from the vanadium species present in solution (Figure 3.50). The colour change is independent of the olefin epoxidised and always occurs after H_2O_2 addition.

Catalyst stability in solution

Catalyst stability in solution was investigated by premixing **MIZ** with solvent, acid, limonene, H_2O_2 or a various combination of those, mixing it at reaction temperature of 40 °C for 1 h and starting the epoxidation by adding H_2O_2 (Figure 3.51). When **MIZ** was premixed with solvent, acid and H_2O_2 the start of reaction was measured from the time of limonene addition. During the standard epoxidation procedure without premixing, **MIZ**, acid and limonene were dissolved in the reaction solvent and immediately after achieving reaction temperature, H_2O_2 was added in one portion. There was no significant difference in performance between the standard conditions and **MIZ** premixed with reaction solvent, acid and limonene. However, when the **MIZ** catalyst was premixed with solvent, acid and H_2O_2 changes of **LIM** concentration were observed, but no corresponding **8,9-LO** was produced (Figure 3.52).

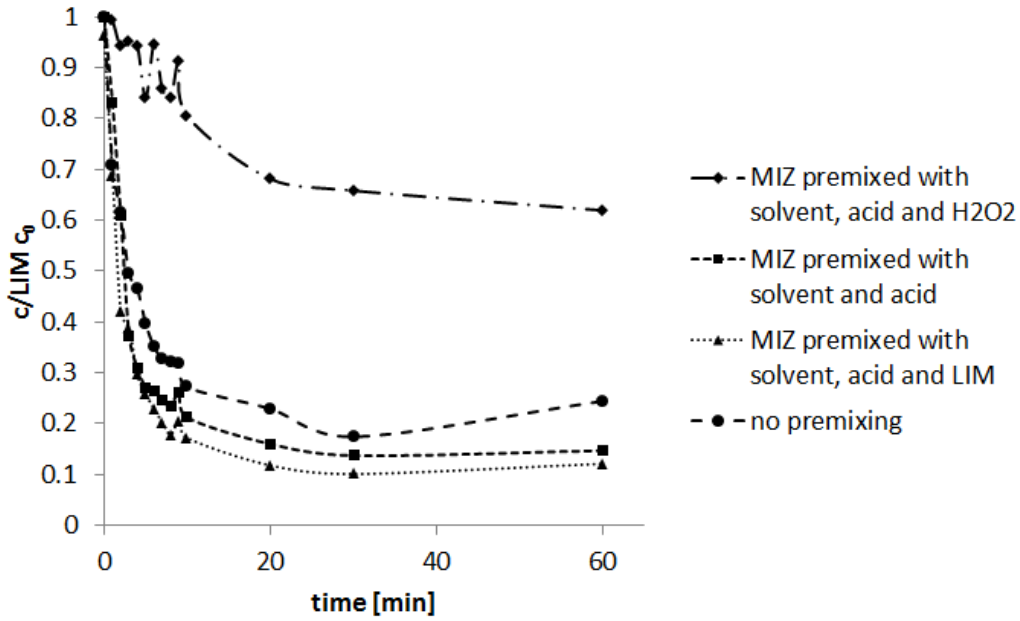

Figure 3.51 Changes in LIM molar fraction, depending on premixing the catalyst with solvent, acid, limonene and H_2O_2 in various combinations. Reaction conditions: 5 mmol LIM, 5 mmol H_2O_2, 0.025 mmol MIZ, 0.025 $HClO_4$, 15 mL 1:1 MeCN:t-BuOH, 40 °C.

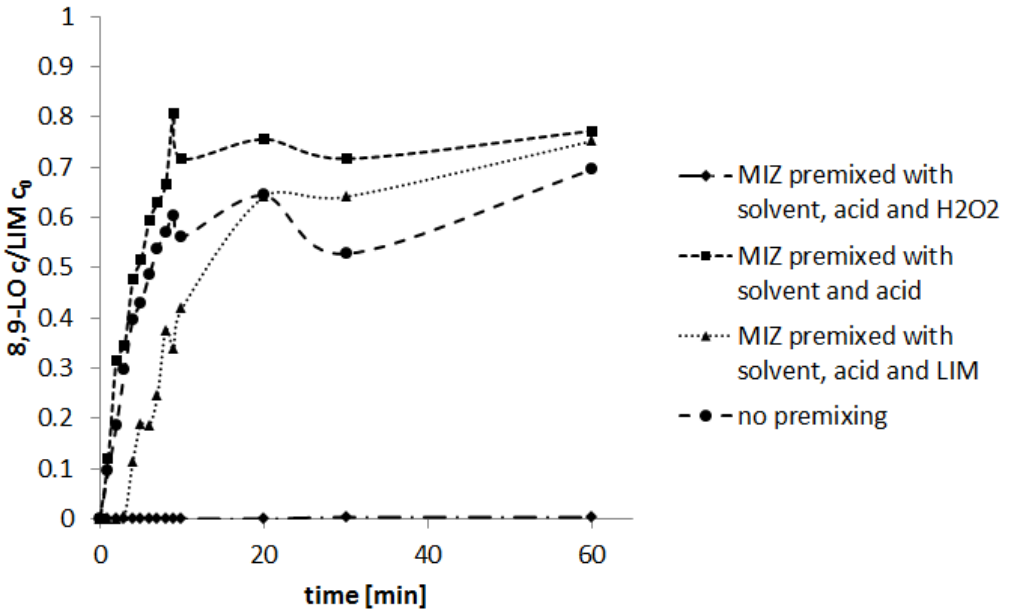

Figure 3.52 Changes in 8,9-LO molar fraction, depending on premixing the catalyst with solvent, acid, limonene and H_2O_2 in various combinations. Reaction conditions: 5 mmol LIM, 5 mmol H_2O_2, 0.025 mmol MIZ, 0.025 $HClO_4$, 15 mL 1:1 MeCN:t-BuOH, 40 ℃.

The previous results suggest that H_2O_2 causes MIZ to decompose, even without the presence of substrate (LIM), suggesting unproductive H_2O_2 decomposition. A supplementary experiment was performed where MIZ was premixed with solvent, acid and H_2O_2 for an hour and then LIM and additional H_2O_2 were added (Figure 3.53). Further LIM mass loss was observed, but no corresponding epoxides were observed via GC-MS (Figure 3.54). The lack of products detected on GC-MS, changes in the colour of the reaction mixture, and the cloudiness of solution, suggest there are some unidentified interactions between limonene, MIZ and H_2O_2.

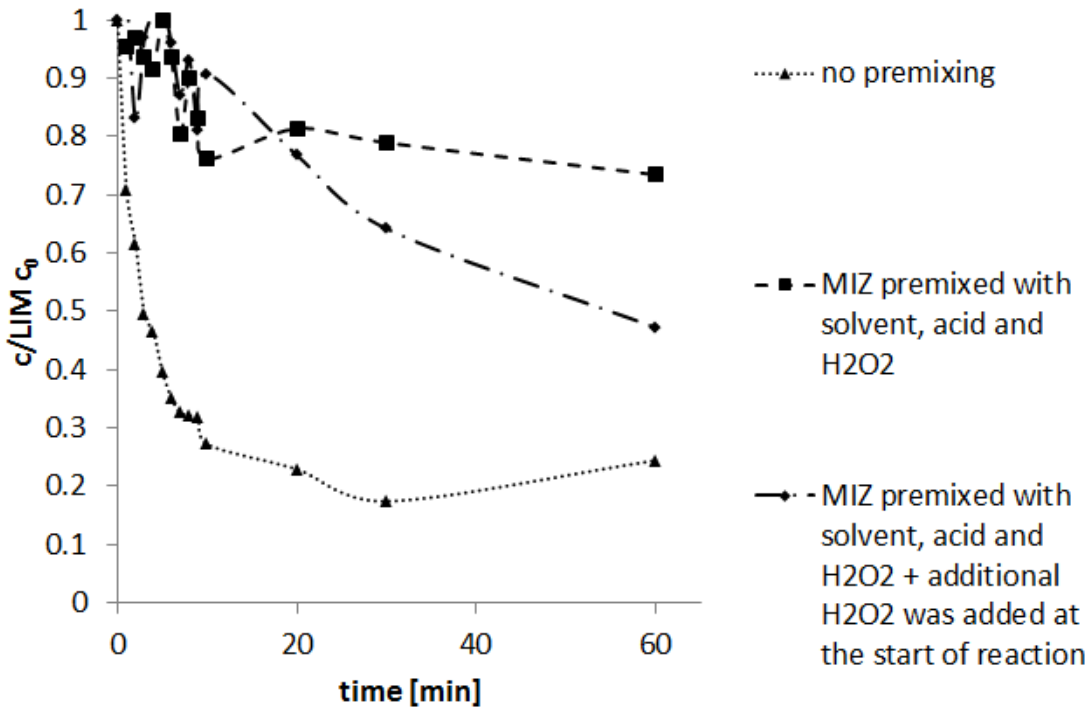

Figure 3.53 Changes in LIM molar fraction, depending on premixing the catalyst with solvent, acid, limonene and H_2O_2 in various combinations. Reaction conditions: 5 mmol LIM, 2 x 5 mmol H_2O_2 (5 mmol added during premixing, and additional 5 mmol was added at the start of reaction at the same time as limonene), 0.025 mmol MIZ, 0.025 $HClO_4$, 15 mL 1:1 MeCN:t-BuOH, 40 ℃.

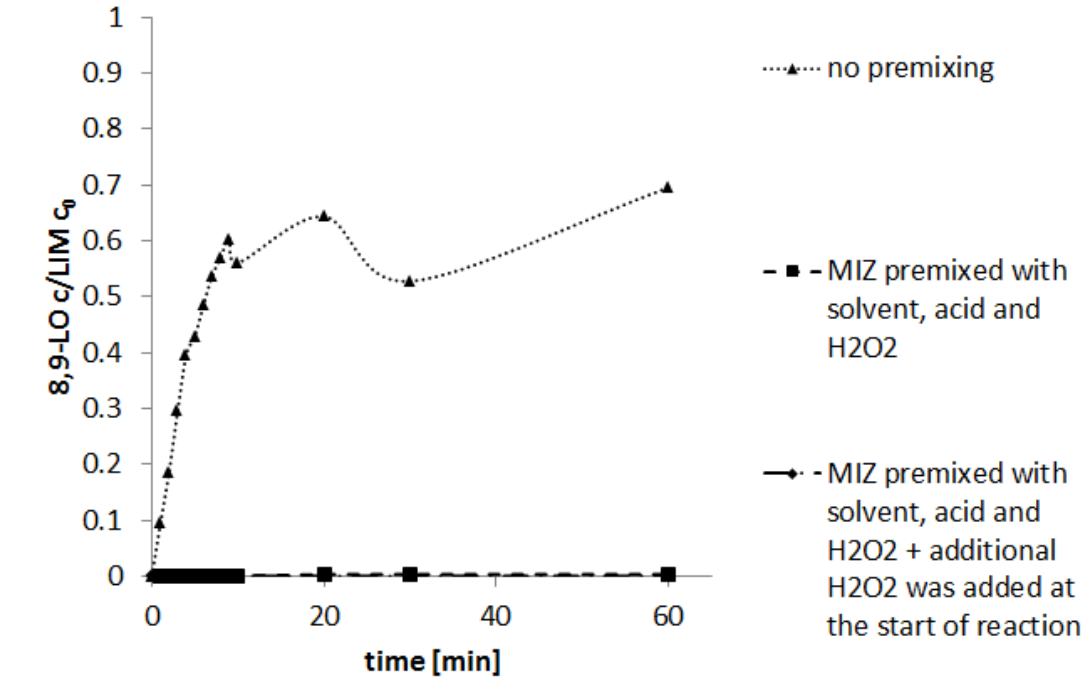

Figure 3.54 Changes in 8,9-LO molar fraction, depending on premixing the catalyst with solvent, acid, limonene and H_2O_2 in various combinations. Reaction conditions: 5 mmol LIM, 2 x 5 mmol H_2O_2 (5 mmol added during premixing, and additional 5 mmol was added at the start of reaction at the same time as limonene), 0.025 mmol MIZ, 0.025 $HClO_4$, 15 mL 1:1 MeCN:t-BuOH, 40 ℃.

In summary, the results presented showed that **MIZ** epoxidation is sensitive to the amount of H_2O_2 added. The catalyst was stable in solution until H_2O_2 was added, H_2O_2 was decomposed even in the absence of olefin. Further investigation included optimising the amount of solvent used, catalyst poisoning by organic aldehydes and diols, product inhibition and changing the concentration of H_2O_2 solutions used.

Varying the amount of solvent needed for limonene epoxidation

Under the standard epoxidation procedure, 0.81 mL **LIM** is dissolved in 15 mL solvent which is a high dilution undesirable for future scale up attempts. To investigate the influence of solvent (1:1 MeCN:t-BuOH) quantities, experiments using 15 mL, 5 mL and 1 mL of solvent were run. Each experiment was set up twice, the first experiment was used to get information on reaction progress via GC-FID and the second experiment was to investigate the changes of temperature in the reaction mixture during reaction. All samples were homogeneous and clear before adding H_2O_2.

As epoxidations are highly exothermic reactions, it was anticipated that the large volume of solvent helps to maintain the reaction temperature. Indeed, when 5 mL solvent was used the addition of H_2O_2 increased the reaction temperature by 15 °C, compared to a 5 °C increase when 15 mL solvent was used (Figure 3.55). However, the variation of 15 °C in the reaction temperature should not cause thermal decomposition of catalyst, as the reported epoxidations using **MIZ** operate well in temperatures of up to 60 °C.[32] There were no reports of the epoxidation reaction at higher temperatures.

A surprising result observed for the reaction mixture with 1 mL solvent, was that the addition of H_2O_2 caused the reaction mixture to split into two liquid phases (Figure 3.56). A change of colour from yellow to dark red-orange was observed and the reaction temperature increased by 6 °C. The split into two liquid phases, solid precipitation and low temperature increase indicated that the reaction did not occur. However, the reaction was still heated and the final GC-MS and NMR spectroscopy samples were taken after 1h at 40 °C. Samples from each phase were analysed qualitatively by GC-MS and NMR spectroscopy, and no detectable concentration of **8,9-LO** was observed on either of the analytical techniques. The reaction mixture consisted mostly of unreacted limonene and reaction solvent (Figure 3.56). The solid precipitation was not identified, but it is probably a vanadium species originated from **MIZ** decomposition.

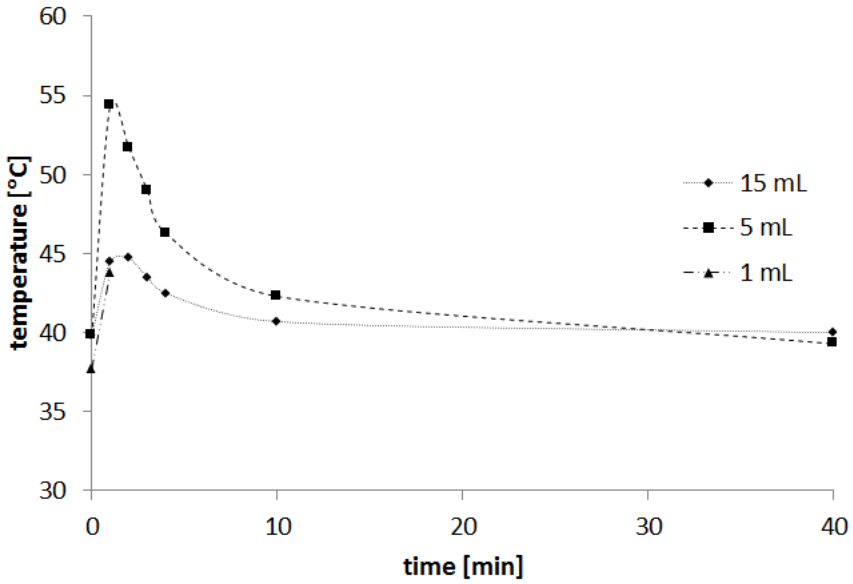

Figure 3.55 Changes the temperature of reaction mixture in the batch reactor. Reaction conditions: 5 mmol LIM, 2 x 5 mmol H_2O_2 (5 mmol added during premixing, and additional 5 mmol was added at the start of reaction at the same time as limonene), 0.025 mmol MIZ, 0.025 $HClO_4$, 1 - 15 mL 1:1 MeCN:t-BuOH, 40 °C.

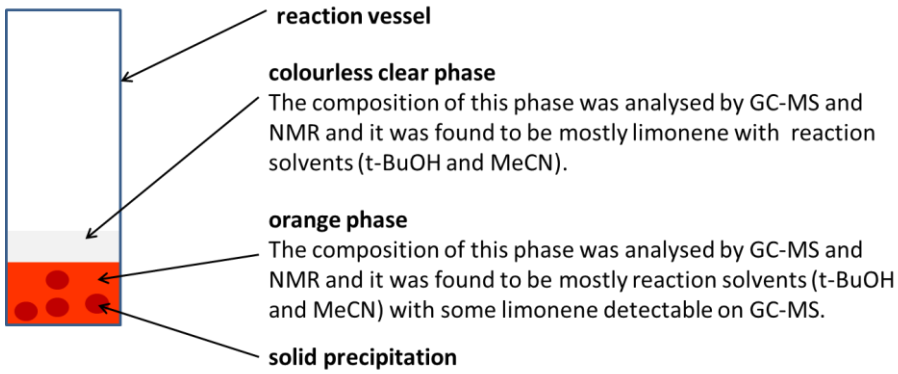

Figure 3.56 Phase separation in a vessel with 1mL reaction solvent used after adding H_2O_2.

Reaction progress was monitored for experiments with 15 mL solvent and 5 mL solvent (Figure 3.57). It was expected that the reduced amount of solvent will cause the reaction to progress faster due to lower dilution of substrates; a potential decrease of selectivity was expected as well. However, the results showed that in lower dilution conversion decreased by 40 %. The catalyst remained highly regioselective with no **1,2-LO** observed on GC-MS, but a drop of selectivity to **8,9-LO** was observed with additional signals observed on GC-MS. The additional signals were not assigned to any of the previously known compounds and a NIST library search did not show any match to known compounds.

In the original paper, the concentration of catalyst was varied between 0.00083 mmol mL^{-1} and 0.0017 mmol mL^{-1}, the reactions in this work use 0.025 mmol **MIZ** in 15 mL solvent which

corresponds to 0.0017 mmol mL^{-1} – the maximum concentration reported in the paper. Based on the results presented in this section, **MIZ** cannot work efficiently under more concentrated conditions.

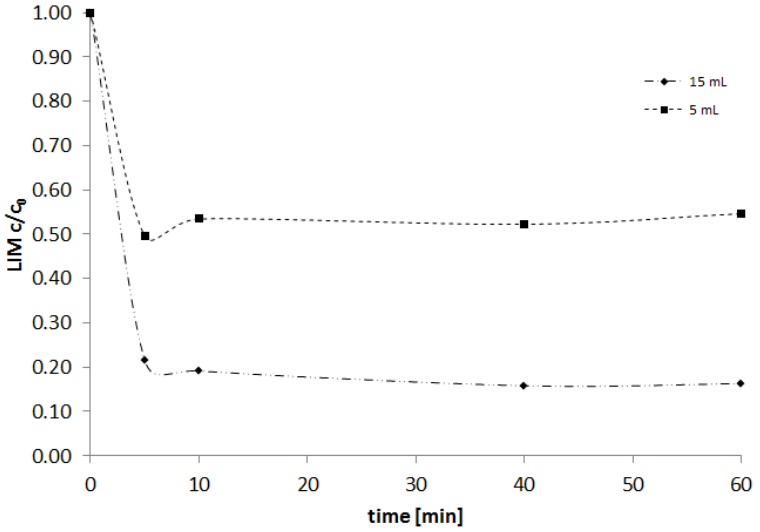

Figure 3.57 Changes in LIM molar fraction over reaction time, depending on the amount of solvent used. Reaction conditions: 5 mmol LIM, 5 mmol H_2O_2, 0.025 mmol MIZ, 0.025 $HClO_4$, 15 mL 1:1 MeCN:t-BuOH, 40 ℃.

Scale up of the reaction can be achieved by adjusting the amount of solvent accordingly to the amount of **LIM** used. The reaction on a 60 mmol scale was performed and the crude reaction mixture was analysed by NMR spectroscopy using the diagnostic peaks highlighted in Figure 3.58. The reaction achieved 91 % **LIM** conversion and 96 % selectivity to **8,9-LO** after a 60 min reaction. It is worth noting that for 60 mmol **LIM** (8.16 g), 180 mL solvent was needed. Although this epoxidation method is highly selective and relatively fast, the high dilution remains a significant hindrance to its industrial application.[9]

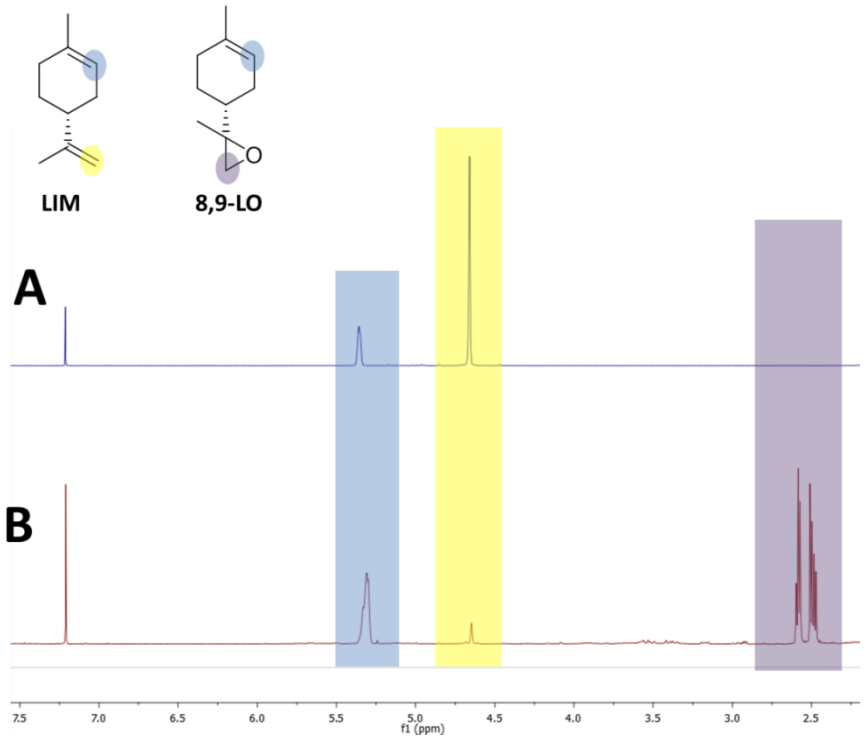

Figure 3.58 Changes in ^{1}H NMR spectroscopy for LIM epoxidation catalysed by MIZ. Spectrum A – pure LIM, B – reaction mixture after evaporation of solvent.

MIZ catalyst poisoning with organic aldehydes and diols

An experiment to check if common epoxidation by-products affect the performance of the **MIZ** catalyst was designed. The corresponding diols and aldehydes in the 8,9 position of **LIM** are not commercially available and their synthesis was beyond scope of this project. The catalyst poisoning by organic diols and aldehydes was tested by adding common organic compounds to the 5 mmol **LIM** used for epoxidation, 0.5 mmol ethylene glycol was used as a diol and 0.5 mmol benzaldehyde was added as an aldehyde (Figure 3.59).

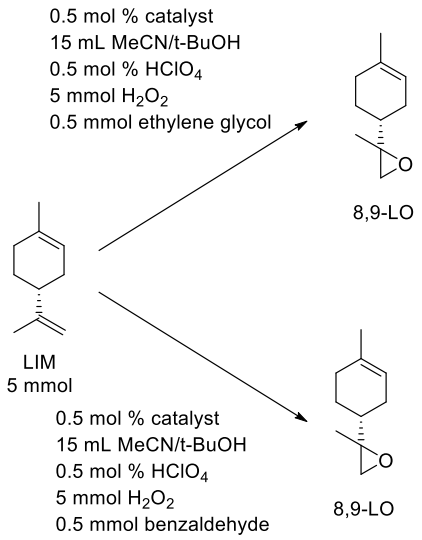

Figure 3.59 Experiment for the determination of catalyst poisoning with ethylene glycol and benzaldehyde.

In Figure 3.60, the consumption of limonene under these reaction conditions is shown, revealing no significant effect on limonene consumption. Unfortunately, it was not possible to obtain quantitative values for the production of **8,9-LO**, due to the interference of benzaldehyde and ethylene glycol peaks with those of **8,9-LO** via GC-FID analysis. However, the qualitative analysis confirms that the catalyst retained high selectivity towards **8,9-LO** (Figure 3.61).

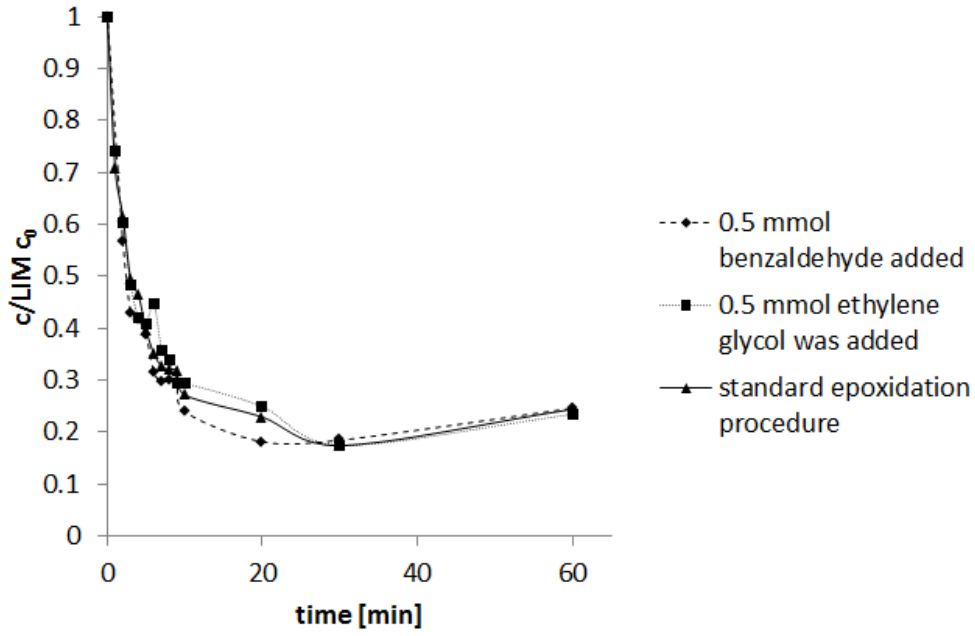

Figure 3.60 Changes in LIM molar fraction over reaction time with ethlene glycol or benzaldehyde addition. Reaction conditions: 5 mmol LIM, 5 mmol H_2O_2, 0.025 mmol MIZ, 0.025 $HClO_4$, 15 mL 1:1 MeCN:t-BuOH, 40 ℃, 0.5 mmol benzaldehyde or ethylene glycol.

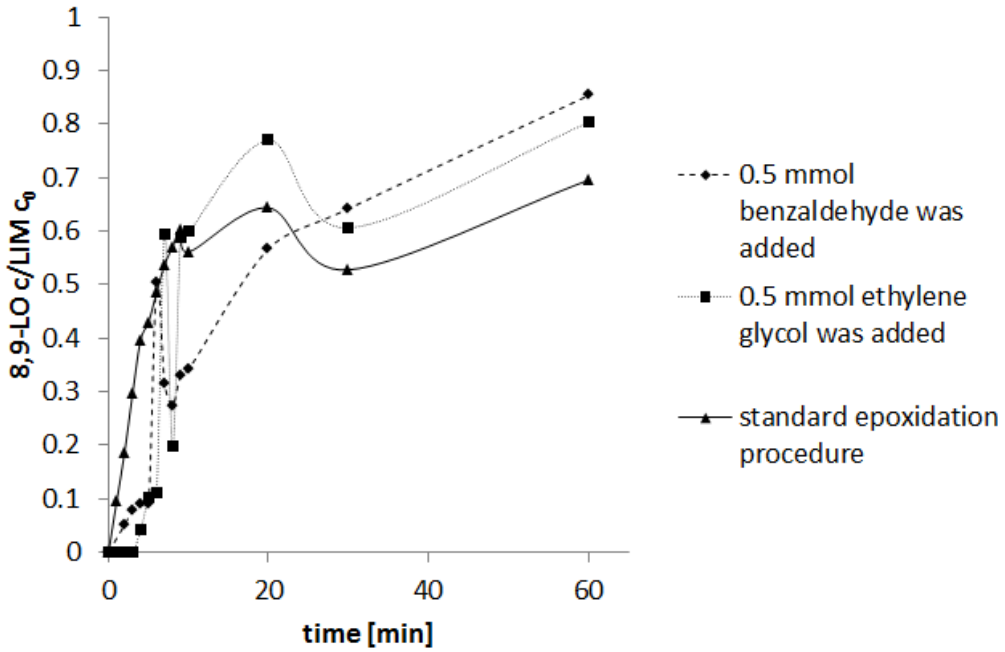

Figure 3.61 Qualitative GC-FID results representing changes in 8,9-LO molar fraction in epoxidation reactions with an addition of ethylene glycol or benzaldehyde. The results cannot be considered as quantitative due to interactions of ethylene glycol and benzaldehyde with 8,9-LO peaks.

The lack of interactions between ethylene glycol and benzaldehyde are depicted in Figure 3.62, where the relation between reaction rate and LIM concentration is shown. The curves overlap and show the same slope, with the small changes in the slope are attributed to the large error of experimental data.

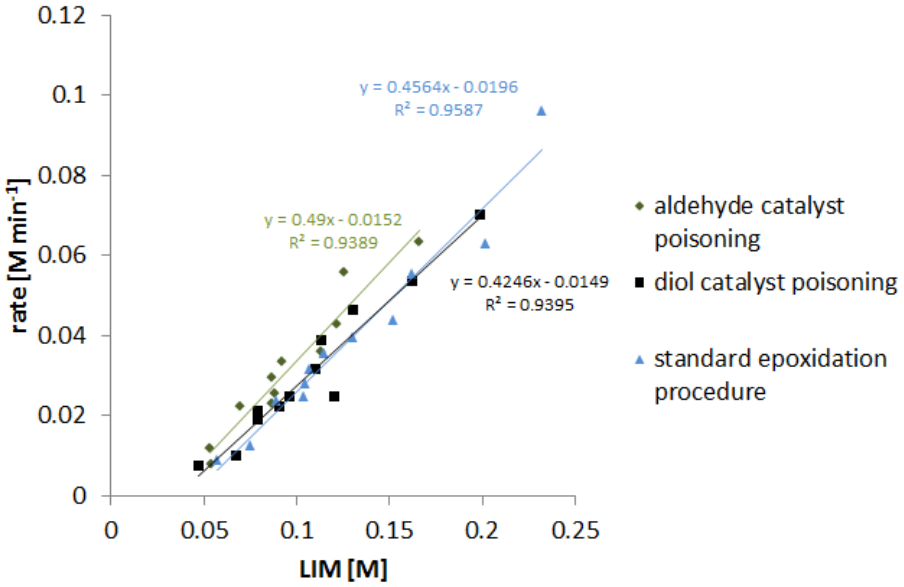

Figure 3.62 Changes in rate calculated from changes in LIM concentrations in epoxidation reactions with an addition of ethylene glycol or benzaldehyde. Reaction conditions: 5 mmol LIM, 5 mmol H_2O_2, 0.025 mmol MIZ, 0.025 $HClO_4$, 15 mL 1:1 MeCN:t-BuOH, 40 ℃, 0.5 mmol benzaldehyde or ethylene glycol.

The influence of varying concentration of hydrogen peroxide

In the previous section it was found that H_2O_2 concentration has a significant influence on the epoxidation rate, thus two different concentrations of H_2O_2 were used in the LIM epoxidation. Since H_2O_2 is a sensitive reagent and can degrade over time, for this experiment H_2O_2 was titrated immediately beforehand. The titration procedure is available in the Section 3.4.8.

Figure 3.63 shows a significant improvement in limonene conversion by using 50 % H_2O_2 which clarifies the previous findings, suggesting water content has significant impact on reaction rate (Figure 3.64). The more concentrated H_2O_2 also resulted in a higher TON (Figure 3.65), which was calculated using Equation 3.5.

$$TON = \frac{8{,}9 - LO\ [mmol]}{MIZ\ [mmol]} \tag{3.5}$$

Where:

TON – turnover number [-]

$8{,}9 - LO$ – the number of 8,9-LO molecules produced [mmol]

MIZ – the number of MIZ molecules, corresponds to the initial amount [mmol]

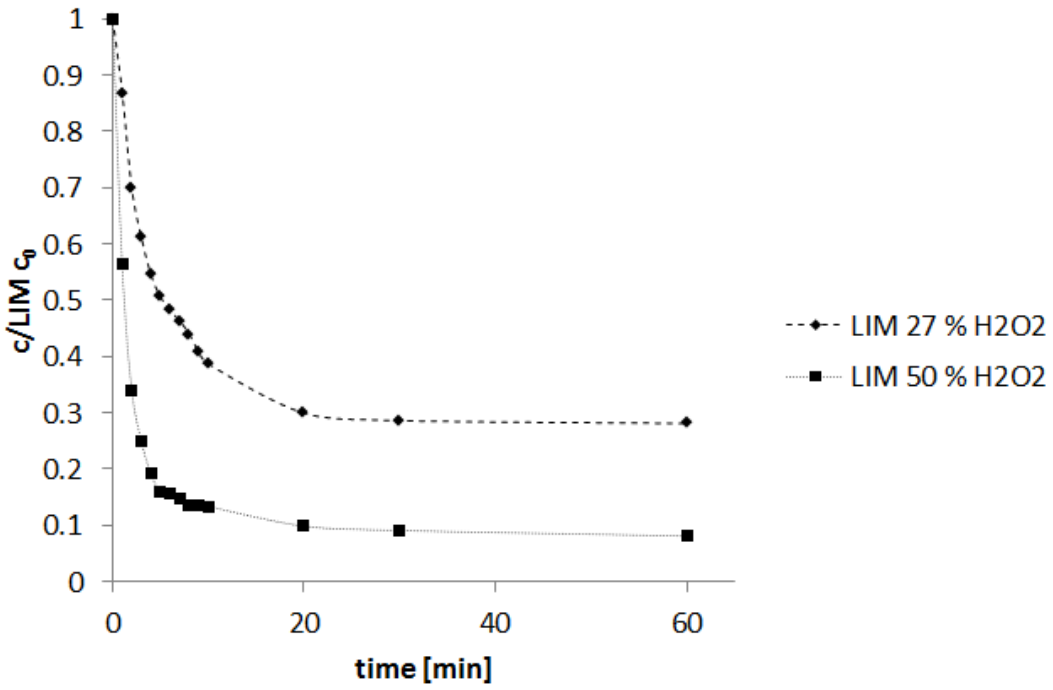

Figure 3.63 Changes in LIM molar fraction in reaction using 27 % H_2O_2 and 50 % H_2O_2. Reaction conditions: 5 mmol LIM, 0.025 mmol MIZ, 0.025 mmol $HClO_4$, 5 mmol H_2O_2 (but different concentration solutions were used), 40 ℃, 15 mL solvent 1:1 MeCN:t-BuOH.

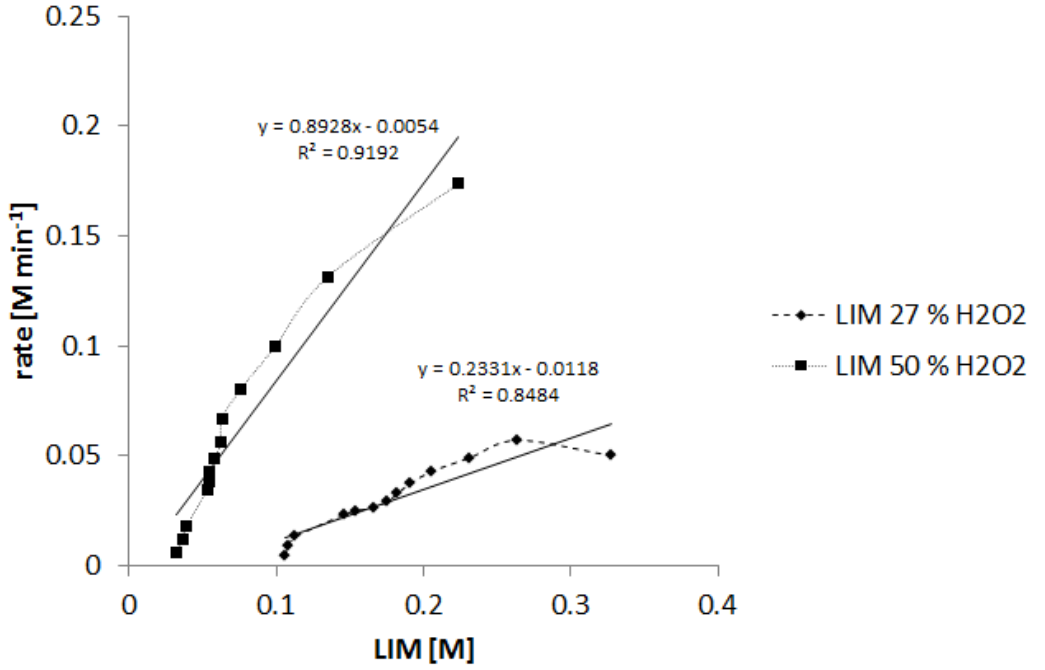

Figure 3.64 Changes in rate of reaction when 27 % and 50 % solution of H_2O_2 were used. The rate was calculated based on changes in LIM concentration. Reaction conditions: 5 mmol LIM, 0.025 mmol MIZ, 0.025 mmol $HClO_4$, 5 mmol H_2O_2 (but different concentration solutions were used), 40 ℃, 15 mL solvent 1:1 MeCN:t-BuOH.

The reaction using 27 % H_2O_2 achieved 160 TON and the reaction using 50 % H_2O_2 achieved 207 TON (Figure 3.65). The cumulative TON was calculated using **8,9-LO** concentrations. If **8,9-LO** is the only product of **LIM** epoxidation, the changes in **LIM** concentration should be proportional to TON achieved. Results presented in Figure 3.65 showed that under these reaction conditions the correlation is linear within experimental error. These results are consistent with the results published by Mizuno *et al.* in which the highest reported TON for **MIZ** was achieved by using 60 % H_2O_2 resulting in 210 TON.[32]

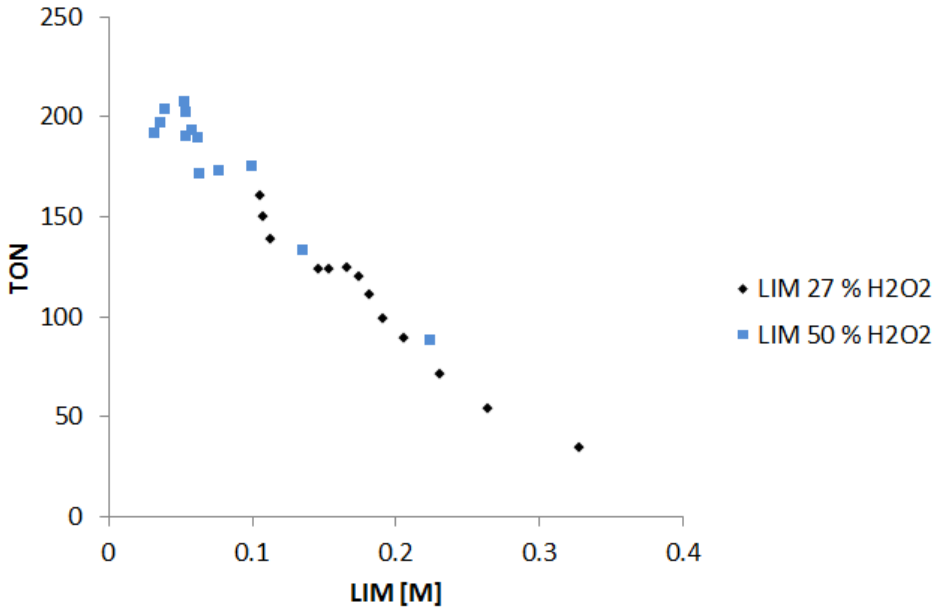

Figure 3.65 Cumulative TON achieved in LIM epoxidation versus LIM concentration.

A complementary experiment was performed to check if the use of 50 % H_2O_2 can further extend the TON achieved by **MIZ**. The epoxidation reaction was set up using more **LIM** and H_2O_2, but the same amount of catalyst as previously (0.025 mmol). Table 3.10 shows the conditions of all experiments with various concentration of H_2O_2. Although the limonene consumption and rate of reaction increase with increasing H_2O_2 concentration (Figure 3.66 and Figure 3.67 green curves) the overall limonene consumption and rate of reaction were lower than for experiments with 5 mmol LIM used (Figure 3.66 and Figure 3.67 black curves). The rate of reaction decreases in the order **5 mmol LIM 50 % H_2O_2** > **7 mmol LIM 50 % H_2O_2** > **5 mmol LIM 27 % H_2O_2** > **7 mmol LIM 27 % H_2O_2**, which corresponds to the increasing concentration of water **0.586 M** > **0.799 M** > **1.56 M** > **2.11 M**.

Table 3.10 Summary of LIM epoxidation using 27 % and 50 % solutions of H_2O_2.

Entry	Volume of reaction[a]	LIM [mmol]	H_2O_2 [mmol]	H_2O_2 conc.[b]	H_2O[c] [mmol]	MIZ [mmol]	TON
1	16.93	7	7	27 %	35.7	0.025	44
2	16.53	7	7	50 %	13.2	0.025	134
3	16.38	5	5	27 %	25.6	0.025	160
4	16.10	5	5	50 %	9.44	0.025	207

a) volume of reaction is calculated as the sum of reaction solvent volume, limonene volume and H_2O_2 volume b) commercially available H_2O_2 concentration used for experiment c) the amount introduced to reaction with H_2O_2 Reaction conditions: 5 or 7 mmol LIM, 0.025 mmol MIZ, 0.025 mmol $HClO_4$, 5 or 7 mmol H2O2 (30 % or 50 % H_2O_2 solution was used), 15 mL 1:1 MeCN:t-BuOH, 40 °C.

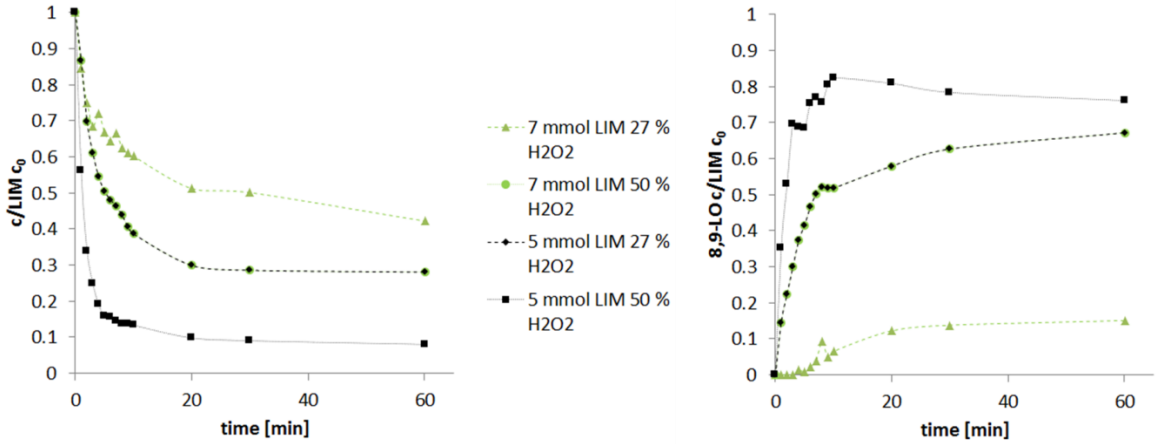

Figure 3.66 Changes in LIM (left) and 8,9-LO (right) molar fraction in reaction using 27 % H_2O_2 and 50 % H_2O_2 and in reactions using 5 mmol and 7 mmol LIM. Reaction conditions were described in Table 3.10: 5 or 7 mmol LIM, 0.025 mmol MIZ, 0.025 mmol $HClO_4$, 5 or 7 mmol H_2O_2 (but different concentration solutions were used), 40 ℃, 15 mL solvent 1:1 MeCN:t-BuOH.

It is worth noting that independently of the amount of substrate used (Figure 3.66) the reaction was very rapid and in around 15 min provided maximum achieved conversion, after which the reaction progress plateaued with no further changes observed. Larger concentrations of both substrates (**LIM** and H_2O_2) did not improve the rate of reaction (Figure 3.66 and 3.77, green triangles) suggesting that the starting concentration of water is an inhibiting factor.

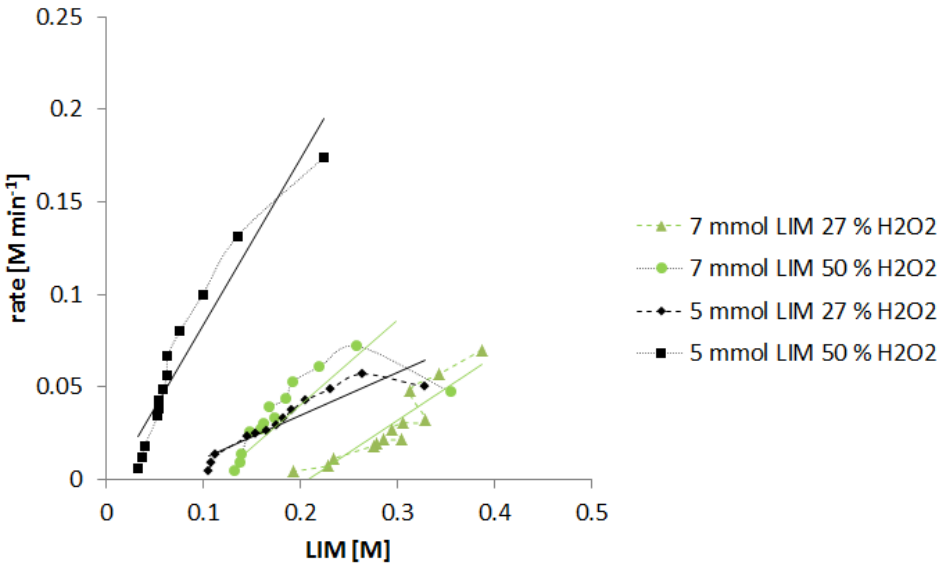

Figure 3.67 Changes in rate of reaction for reactions using 27 % H_2O_2 and 50 % H_2O_2 and for reactions using 5 mmol and 7 mmol LIM. Reaction conditions are described in Table 3.10: 5 or 7 mmol LIM, 0.025 mmol MIZ, 0.025 mmol $HClO_4$, 5 or 7 mmol H_2O_2 (but different concentration solutions were used), 40 ℃, 15 mL solvent 1:1 MeCN:t-BuOH.

Given the linear relationship between **LIM** and rate, surprising changes in the rate of **8,9-LO** production and TON were observed (Figure 3.68 and Figure 3.69). If **8,9-LO** was the only product of the reaction, the graphical correlation between TON and **LIM** molar concentration should give a straight line, since in theory 1 molecule of **LIM** reacts to give 1 molecule of **8,9-LO**. However, for reactions in which 7 mmol **LIM** was used, the curve looks more exponential than linear (Figure 3.69 orange and green curve), suggesting that limonene is involved in another catalytic cycle, rather than just epoxidation. The maximum achieved TON decreased in the order **5 mmol LIM 50 % H_2O_2** > **5 mmol LIM 27 % H_2O_2** > **7 mmol LIM 50 % H_2O_2** > **7 mmol LIM 27 % H_2O_2** (Figure 3.69), which might be explained by side reactions occurring.

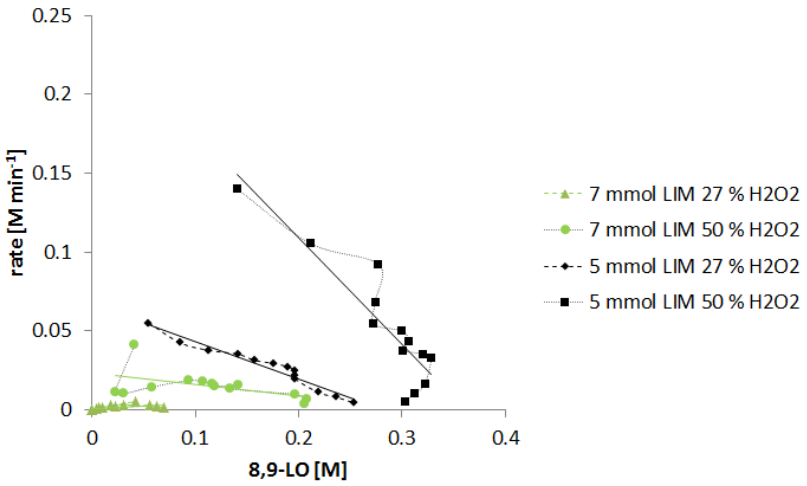

Figure 3.68 Changes in rate of reaction calculated using 8,9-LO concentrations for reactions using 27 % H_2O_2 and 50 % H_2O_2 and for reactions using 5 mmol and 7 mmol LIM. Reaction conditions are described in Table 3.10: 5 or 7 mmol LIM, 0.025 mmol MIZ, 0.025 mmol $HClO_4$, 5 or 7 mmol H_2O_2 (but different concentration solutions were used), 40 ℃, 15 mL solvent 1:1 MeCN:t-BuOH.

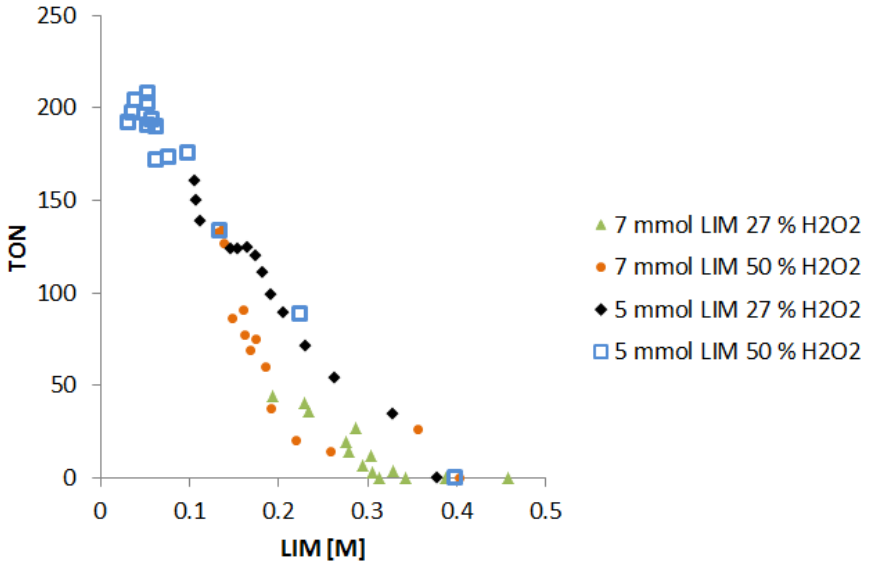

Figure 3.69 Cumulative TON changes versus LIM concentration in reaction using 27 % H_2O_2 and 50 % H_2O_2 and in reactions using 5 mmol and 7 mmol LIM. Reaction conditions were described in Table 3.10: 5 or 7 mmol LIM, 0.025 mmol MIZ, 0.025 mmol $HClO_4$, 5 or 7 mmol H_2O_2 (but different concentration solutions were used), 40 ℃, 15 mL solvent 1:1 MeCN:t-BuOH.

Product inhibition

Based on the rate equation written out using elementary step rate constants, the relationship between substrate concentrations depends on stoichiometry. If there is no catalyst deactivation or product inhibition, the rate at a given concentration should not change as long as a difference between the initial molar concentration of substrates is the same.[60] The conditions of two experiments which were performed for **LIM** epoxidation in order to determine if product inhibition or catalyst deactivation appears are presented in Table 3.11. Figure 3.70 depicts the correlation between reaction rate and **LIM** concentration. Since the rate curves do not overlap, that indicates that either product inhibition or catalyst deactivation occurs.

Table 3.11 Reaction conditions for experiment to determine product inhibition. The same concentration of catalyst was used, a small variation in reaction volume is related to the different volume of substrate added. The volume varies by 2 % which was assumed to not change MIZ concentration significanly.

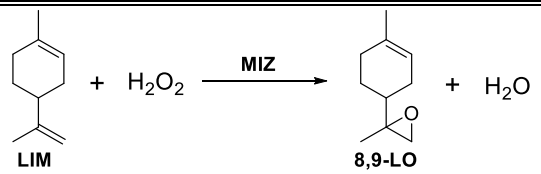

Entry	Volume of reaction[a]	MIZ [mmol/M]	LIM [mmol/M]	H_2O_2 [mmol/M]
1	15.81 mL	0.025/0.00158	5/0.316	5/0.316
2	16.13 mL	0.025/0.00155	7/0.434	7/0.434

a) For calculation the volume of reaction solvent and limonene was taken, it does not account for changes in volume caused by addition of H_2O_2. Reaction conditions: 5 or 7 mmol LIM, 0.025 mmol MIZ, 0.025 mmol $HClO_4$, 5 or 7 mmol H_2O_2 (30 % solution), 40 °C, 15 mL solvent (1:1 MeCN:t-BuOH).

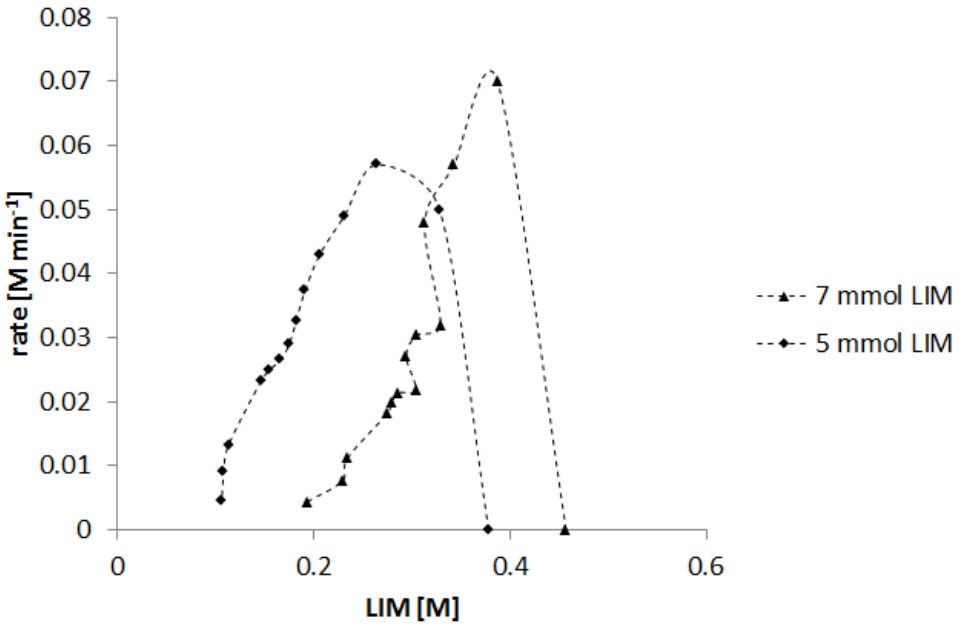

Figure 3.70 Changes in rate of reaction using different starting concentrations of LIM and H_2O_2. Reaction conditions: 5 or 7 mmol LIM, 0.025 mmol MIZ, 0.025 mmol $HClO_4$, 5 or 7 mmol H_2O_2 (30 % solution), 40 °C.

To check for product inhibition two the same reactions were set up, but starting from different conversion points.[60] The first experiment was started using 5 mmol **LIM** which is the standard epoxidation procedure, this point corresponds to conversion 0%. The second experiment was started using 4 mmol **LIM** and 1 mmol **8,9-LO**, which corresponds to 20 % conversion. It is necessary to recreate the same conditions as seen at 20 % conversion, which means the amount of H_2O_2 and water had to be adjusted accordingly. The amount of water was adjusted not only for what would be produced as a result of oxidation, but also what would be introduced into reaction with a 30% solution of H_2O_2.

In Figure 3.71 the correlation between the rate of reaction and the **LIM** concentration is shown for both reactions. The curves do not overlay, indicating catalyst deactivation.[60] Had the curves overlaid, this would have indicated product inhibition due to the rate of reaction being dependent on substrate-product ratio. In Figure 3.71 the two curves do not overlay, which indicates **MIZ** deactivation.

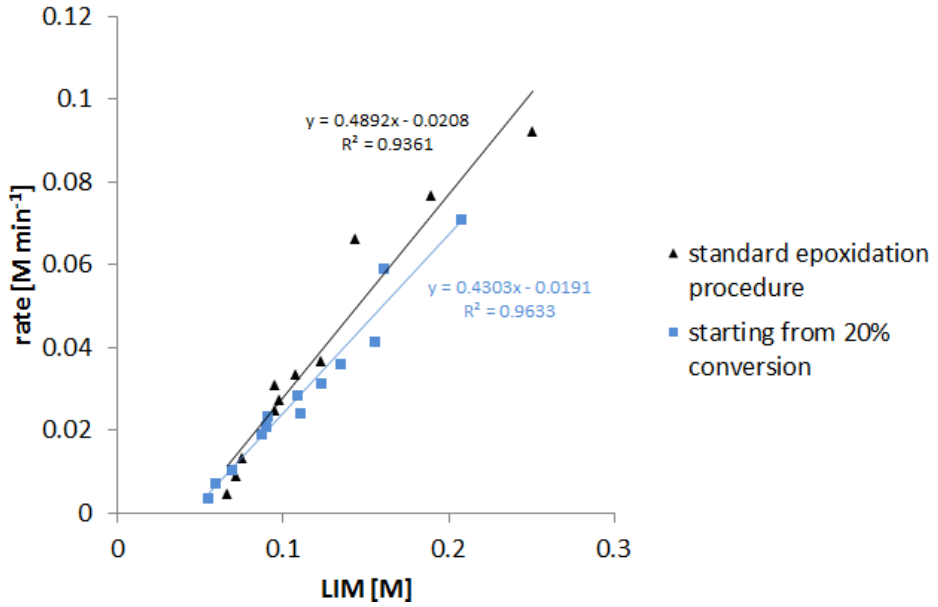

Figure 3.71 Changes in rate of reaction when changing the starting point of reaction. Reaction conditions for reaction starting at 20 % conversion: 40 ℃, 15 mL solvent (1:1 MeCN: t-BuOH) 0.025 mmol MIZ, 0.025 mmol $HClO_4$ 4 mmol LIM, 1 mmol 89 LO, 4 mmol H_2O_2 as 30% solution (0.416 mL 30% solution), 1 mmol water + additional water as it was 30% solution (0.062 mL overall). The standard epoxidation procedure: 0.025 mmol MIZ, 0.025 mmol $HClO_4$, 15 mL solvent, 5 mmol LIM, 5 mmol H_2O_2 (0.52 mL 30% solution).

A complementary experiment was performed in which the amount of water was not adjusted, so only 4 mmol H_2O_2 (30% solution) was used with no additional water added, but with the addition of **8,9-LO**. The relation between reaction rate and **LIM** concentration is shown in Figure 3.72 The rate of reaction with an addition of **8,9-LO** but without water (Figure 3.72 green series) is faster, suggesting that the amount of water in the reaction has impact on the catalyst deactivation.

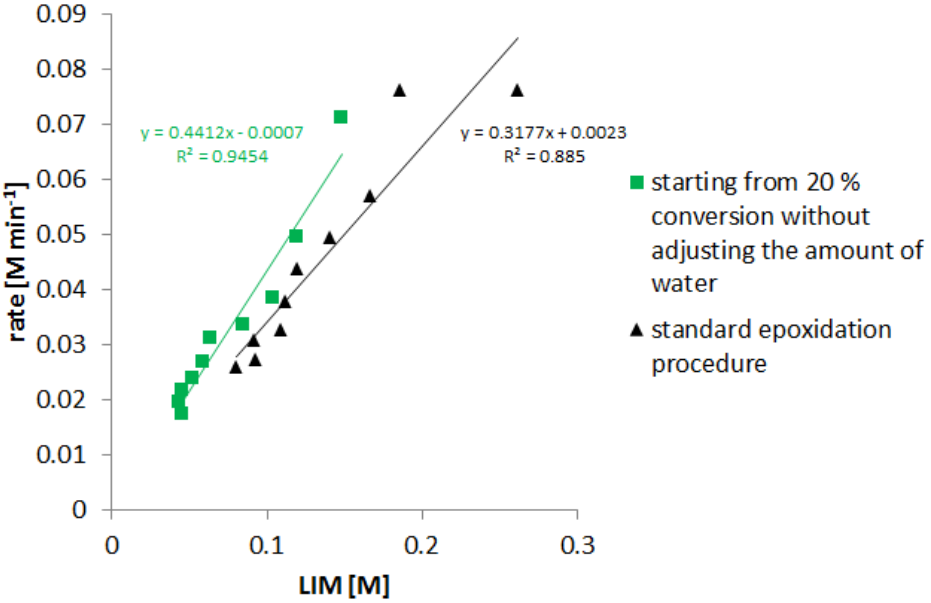

Figure 3.72 Changes in rate of reaction. Reaction conditions for reaction starting at 20 % conversion: 40 ℃, 15 mL solvent (1:1 MeCN: t-BuOH) 0.025 mmol MIZ, 0.025 mmol $HClO_4$ 4 mmol LIM, 1 mmol 89 LO, 4 mmol H2O2 as 30% solution (0.416 mL 30% solution), 1 mmol water (0.018 mL overall). The standard epoxidation procedure: 0.025 mmol MIZ, 0.025 mmol $HClO_4$, 15 mL solvent, 5 mmol LIM, 5 mmol H_2O_2 (0.52 mL 30% solution).

In summary, the results presented showed that reducing the amount of solvent is not possible, with the reduced volume of solvent leading to lower conversion. The experiments with ethylene glycol and benzaldehyde did not show catalyst poisoning with organic diols and aldehydes. The results with more concentrated H_2O_2 solution improved TON up to 210, but the attempts to achieve further improvement were not successful. Product inhibition experiments showed that **8,9-LO** does not inhibit reaction, but water does. The next sections focus on ^{31}P and ^{51}V NMR spectroscopy of **MIZ** and looking into possible products of deactivation. It was hypothesised that **MIZ** can isomerise to the β-isomer of **MIZ** under reaction conditions, thus the β-isomer was synthesised and its performance in the epoxidation reaction was tested.

^{31}P NMR and ^{51}V NMR of MIZ

Figure 3.73 depicts the mechanism for epoxidation catalysed by **MIZ** proposed by Mizuno *et al.*[32] with the corresponding ^{51}V NMR shifts for different forms of the polyoxometalate obtained from the supporting information to the original paper.[32] In another publication by Mizuno *et al.* where **MIZ** was used for hydroxylation of alkanes, the ^{51}V NMR shifts of compound I, II and III (Figure 3.73) are reported as -578 ppm, -539 ppm and -630 ppm respectively.[53] In this report, the abbreviation **MIZ** corresponds to $[Bu_4N]_4[\gamma\text{-}HPV_2W_{10}O_{40}]$. The compound I depicted in Figure 3.73 corresponds to **MIZ** protonated by $HClO_4$ – $[\gamma\text{-}H_2PV_2W_{10}O_{40}]^{3-}$.

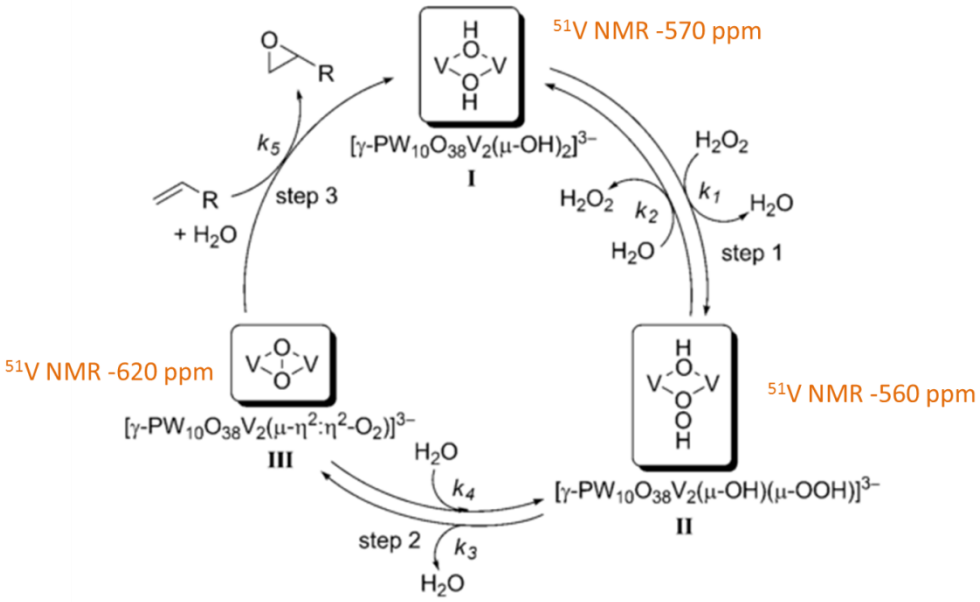

Figure 3.73 Epoxidation mechanism proposed by Mizuno et al.[32] Alternative ^{51}V NMR shifts, which are I -578 ppm, II -539 ppm, III -630 ppm are available from another Mizuno et al. publication[53] (picture reproduced, with permission, from Mizuno et al.[32]).

The **MIZ** catalyst was analysed by ^{31}P NMR and ^{51}V NMR, the samples were prepared in 1:1 MeCN and t-BuOH and run without locking. Some of the NMR analysis for the **MIZ** polyoxometalate is reported at pH 2, thus two NMR samples at different pH were prepared to check how much ^{31}P NMR and ^{51}V NMR signals shift at different pH values. The first sample was prepared with no pH adjustment (pH 6-7 using paper pH strips or pH 5.4 using pH meter), the second sample was prepared with pH adjustment using 3M aqueous HCl (pH 0 using paper pH strip and pH meter).

^{31}P NMR spectra are presented in Figure 3.74, a shift of 0.2 ppm was observed with changing pH. Both samples of **MIZ** showed a single peak at -13.90 or -14.10 ppm (depending on pH) which is slightly different than the previously published data (-14.3 ppm).[32] However, a different publication by Mizuno *et al*. reported shift of -14.1 ppm in MeCN.[54]

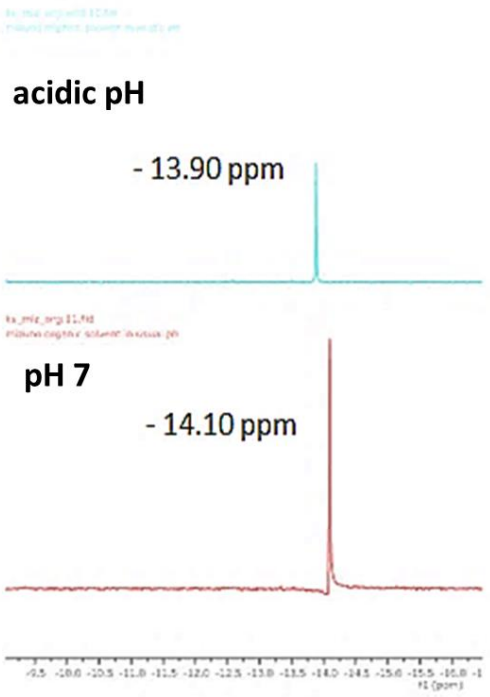

Figure 3.74 ^{31}P NMR of MIZ dissolved in 1:1 MeCN:t-BuOH. The top spectrum: acidic pH, bottom: 6-7 pH.

^{51}V NMR are presented in Figure 3.75. Although no changes in shifts were observed with changing pH, an additional peak at -364 ppm was observed at highly acidic pH and the ratio between the peaks at -581 and -673 ppm changed. In the previously reported data, ^{51}V NMR analysis for **MIZ** was reported as a single peak at -570 ppm[32] or -581 ppm[54] or -580 ppm.[53] The obtained data is consistent with previously reported data. However, it was not possible to assign the peak at -673 ppm which remains an unsolved vanadium species. The small peak at -542 ppm possibly corresponds to a $[\beta\text{-}HPV_2W_{10}O_{40}]^{4-}$ species which was mentioned by Mizuno et al., but they did not report a corresponding ^{51}V NMR signal.[32] A different source reported -544.2 ppm and -555.2 ppm for $Cs_5[\beta\text{-}PV_2W_{10}O_{40}]$.[61]

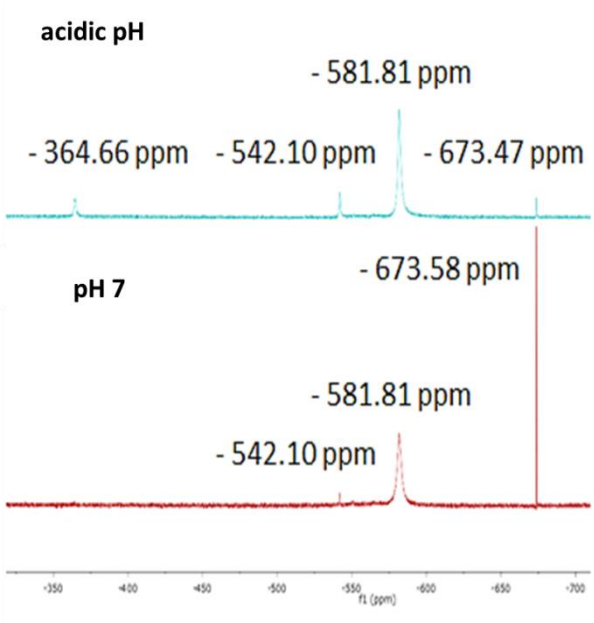

Figure 3.75 ^{51}V NMR of MIZ dissolved in 1:1 MeCN:t-BuOH. The top spectrum: acidic pH, bottom: 6-7 pH.

To further understand changes in the **MIZ** structure under reaction conditions the ^{51}V NMR and ^{31}P NMR measurements were taken after the addition of each reagent to the reaction. An NMR sample was taken directly from the reaction mixture and was run without any deuterated solvent (Figure 3.76). Although the samples were prepared immediately during epoxidation, due to issues with the NMR spectrometer, they were analysed 24 h after they were prepared. A fresh sample of **MIZ** (Figure 3.76 spectrum 1) was prepared to compare to the 24 h sample (Figure 3.76 spectrum 2) and check whether any changes occurred during the 24 h lapse. No significant difference was observed. Spectrum 3 was taken after **MIZ** was dissolved in the solvent (1:1 MeCN:t-BuOH) and limonene was added to the reaction. Until now, no significant changes in ^{31}P NMR were observed. The spectra showed a single peak which shifted from -14.19 to -14.36 ppm which corresponds to the shift reported for **MIZ**. Spectrum 4 represents the sample taken after acid ($HClO_4$) addition. The single peak shifted to -13.98 which corresponds to the **MIZ** signal at acidic pH (see Figure 3.74), thus it is possibly a protonated version of **MIZ** – $[\gamma H_2PV_2W_{10}O_{40}]^{3-}$. Spectrum 5 corresponds to a sample taken after H_2O_2 addition to the reaction. After H_2O_2 addition, extra peaks at -13.32 and -13.36 ppm appeared, but they do not correspond to any other reported species. Additionally, the intensity of peaks is lower and a solid precipitated in the NMR tube.

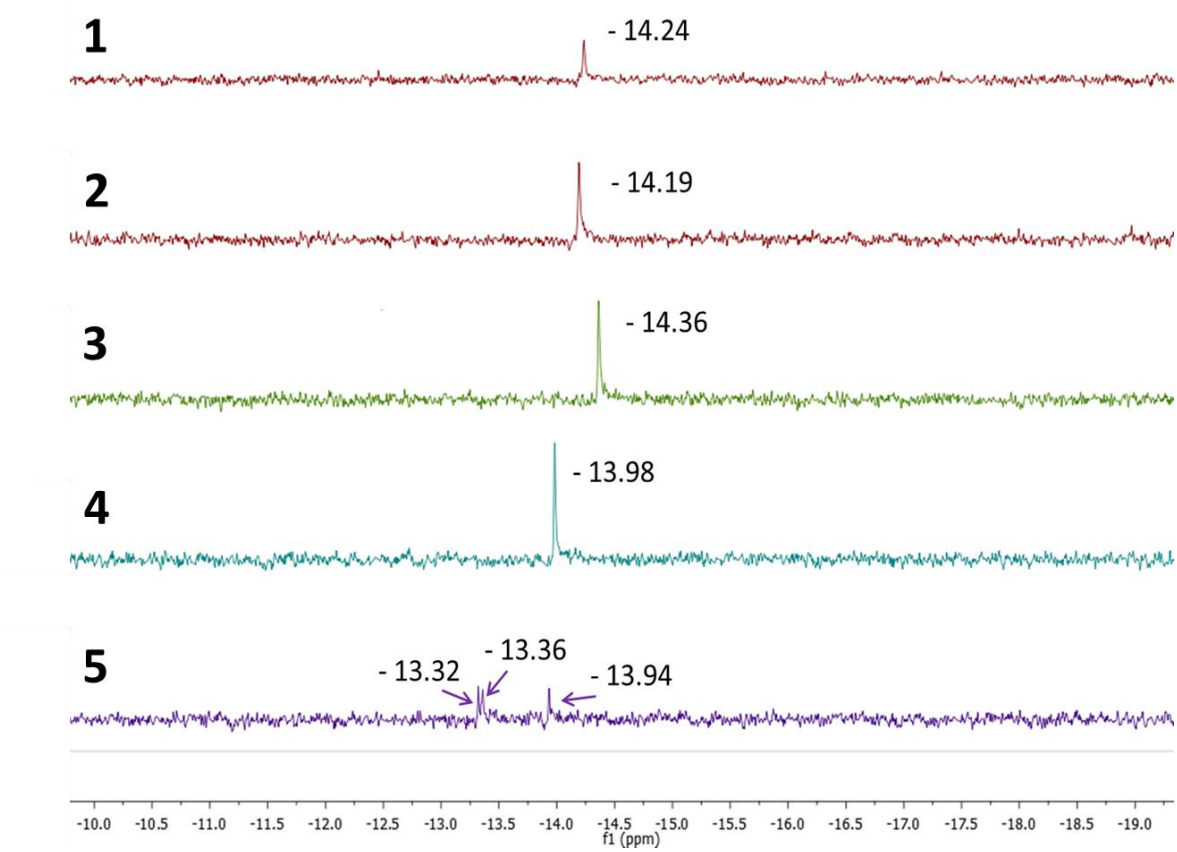

Figure 3.76 ^{31}P NMR of MIZ dissolved in 1:1 MeCN:t-BuOH. Spectrum 1 – fresh MIZ sample prepared immediately before analysis, 2 – 24 h old sample MIZ 3 – 24 h old sample MIZ and LIM 4 –24 h old sample MIZ, LIM and $HClO_4$, 5 - after H_2O_2 addition.

^{51}V NMR spectra are presented in Figure 3.77, with no changes observed between the fresh **MIZ** sample and the 24 h sample (Spectrum 1 and 2). The addition of limonene (Spectrum 3) also did not cause any changes. Spectrum 4 corresponds to a sample taken after acid addition. A small shift of 0.3 ppm was observed, but the reported literature reports a larger shift of 3 ppm from -581 ppm to -578 ppm for the protonated form of **MIZ**.[53] Although, the shift does not correspond exactly to the reported data (-578 ppm), it is still assumed to be a protonated form of **MIZ**. Another change observed in Spectrum 4 was that the intensity of the peak at -674 ppm increased. Spectrum 5 corresponds to a sample taken after H_2O_2 addition. The peak at -582 ppm shifted to -549 ppm which might correspond to a $[\beta\text{-}HPV_2W_{10}O_{40}]^{4-}$ or $[\beta\text{-}H_2PV_2W_{10}O_{40}]^{3-}$ species, since it is very close to the -544 and -555 ppm values previously reported for $Cs_5[\beta\text{-}PV_2W_{10}O_{40}]$.[61] However, the peak at -549 ppm cannot be assigned with a full certainty. It is worth noting that the intensity of the peak at -674 ppm is as strong as it was in Spectrum 4.

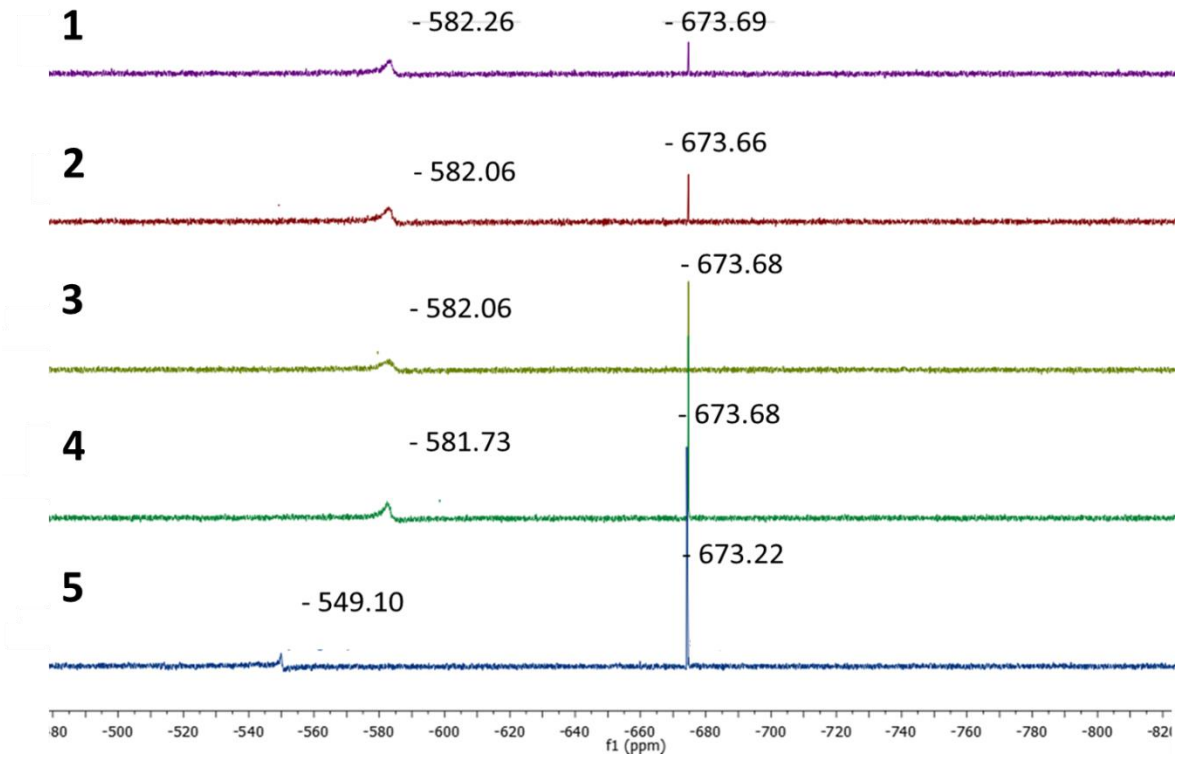

Figure 3.77 ^{51}V NMR of MIZ dissolved in 1:1 MeCN:t-BuOH. Spectrum 1 – fresh MIZ sample prepared immediately before analysis, 2 – 24 h old sample MIZ 3 – 24 h old sample MIZ and LIM 4 –24 h old sample MIZ, LIM and $HClO_4$, 5 - after H_2O_2 addition.

These results are consistent with previous results where the catalyst was stable in solution until H_2O_2 was added to the reaction. In the samples analysed by ^{31}P NMR and ^{51}V NMR (Figure 3.76 and Figure 3.77) the significant changes were also observed after H_2O_2 addition and no significant changes were observed when limonene or $HClO_4$ were added, thus there is no evidence of limonene strongly binding to the catalyst.

Limonene epoxidation using β-isomer of Mizuno catalyst

Mizuno et al. mentioned the presence of a β-isomer of **MIZ** which is a by-product of the **MIZ** synthesis.[32] Another source indicated that $Cs_5[\gamma\text{-}PV_2W_{10}O_{40}]$, which is a precursor to obtain **MIZ** - $[Bu_4N]_4[\gamma\text{-}HPV_2W_{10}O_{40}]$, is stable at pH 2 in the presence of excess vanadium ions $[VO_2]^+$, and in the absence of excess vanadium an isomerisation to the darker orange $Cs_5[\beta\text{-}PV_2W_{10}O_{40}]$ occurs. Since the epoxidation reaction does not take place at pH 2 and no additional $[VO_2]^+$ is present, it is expected that under reaction conditions **MIZ** can isomerise to the orange β-isomer, which would also explain the change in colour under the reaction conditions. In this report, the β-isomer of **MIZ** was prepared according to a literature procedure[61] to check if it is active in the epoxidation of **LIM** (Figure 3.78).

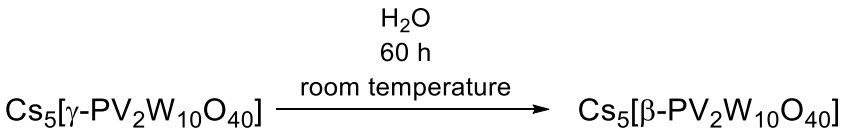

Figure 3.78 Synthesis of $Cs_5[\beta\text{-}PV_2W_{10}O_{40}]$ according to the literature procedure.[61]

The NMR spectroscopy samples were prepared by dissolving the synthesised $Cs_5[\beta\text{-}PV_2W_{10}O_{40}]$ in water at pH 1 and showed a single peak on ^{31}P NMR at -13.5 ppm and two peaks on ^{51}V NMR at -543 ppm and -554 ppm which corresponds to the data published in the literature: ^{31}P NMR at pH 4 -12.85 ppm and ^{51}V NMR at pH 3.5 -544 and -555 ppm. The slightly different shift in the ^{31}P NMR was attributed to the different pH of the NMR spectroscopy sample reported in the literature. IR analysis is available in the Experimental section.

To allow solubility in an organic solvent, the Cs^+ counter ion in $Cs_5[\beta\text{-}PV_2W_{10}O_{40}]$ had to be changed to Bu_4N^+. Cation exchange in the original Mizuno paper was performed at pH 2 with the presence of $[VO_2]^+$. The pH adjustment and the addition of $[VO_2]^+$ were probably a way to stabilise the γ-isomer and prevent isomerisation to β-isomer. In this work, the β-isomer was the compound of interest, thus the pH was not adjusted and no additional vanadium species were added. The cation exchange was performed in water with Bu_4N-Cl. The γ-isomer and β-isomer have characteristic colours (Figure 3.79) which is consistent with previously published literature.[61]

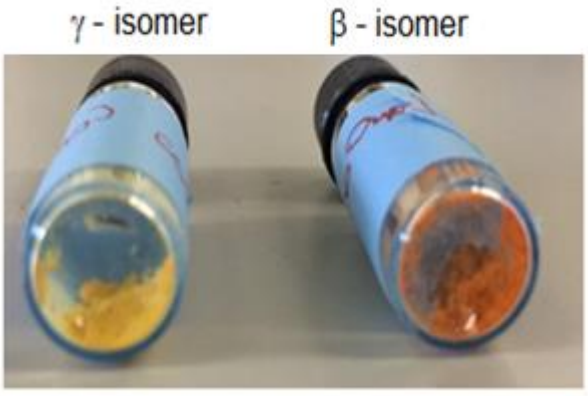

Figure 3.79 Colour change between γ and β - isomer of MIZ.

The resultant orange solid was insoluble in water and soluble in organic solvents such as the 1:1 mixture of MeCN and t-BuOH used in the epoxidation reaction. The IR spectra still shows the diagnostic peaks for $[\beta\text{-}PV_2W_{10}O_{40}]^{5+}$ (Figure 3.80). ^{31}P NMR showed two peaks at -13.24 and -13.55 ppm (Figure 3.81). There are no reports of β-isomer analysis in organic solvents, but the reported shift in water is -13.5 ppm.[61] The detected peaks were within the range of the ^{31}P NMR shift reported for the β-isomer, but the presence of two peaks suggested it was not a single compound, and was potentially a mixture of $[\beta\text{-}PV_2W_{10}O_{40}]^{5-}$, $[\beta\text{-}HPV_2W_{10}O_{40}]^{4-}$ or

$[\beta\text{-}H_2PV_2W_{10}O_{40}]^{3-}$. ^{51}V NMR shifts previously reported for the β isomer were at -543 and -554 ppm in aqueous solution.[61] The synthesised β-isomer sample showed three peaks at -535 ppm, -539 ppm and -556 ppm on ^{51}V NMR (Figure 3.82), which is within the same range as previously reported shifts in aqueous solution. However, the additional peak at -535 ppm is an unknown compound which might be a different protonation of the β-isomer, but it could also correspond to an unknown vanadium species.

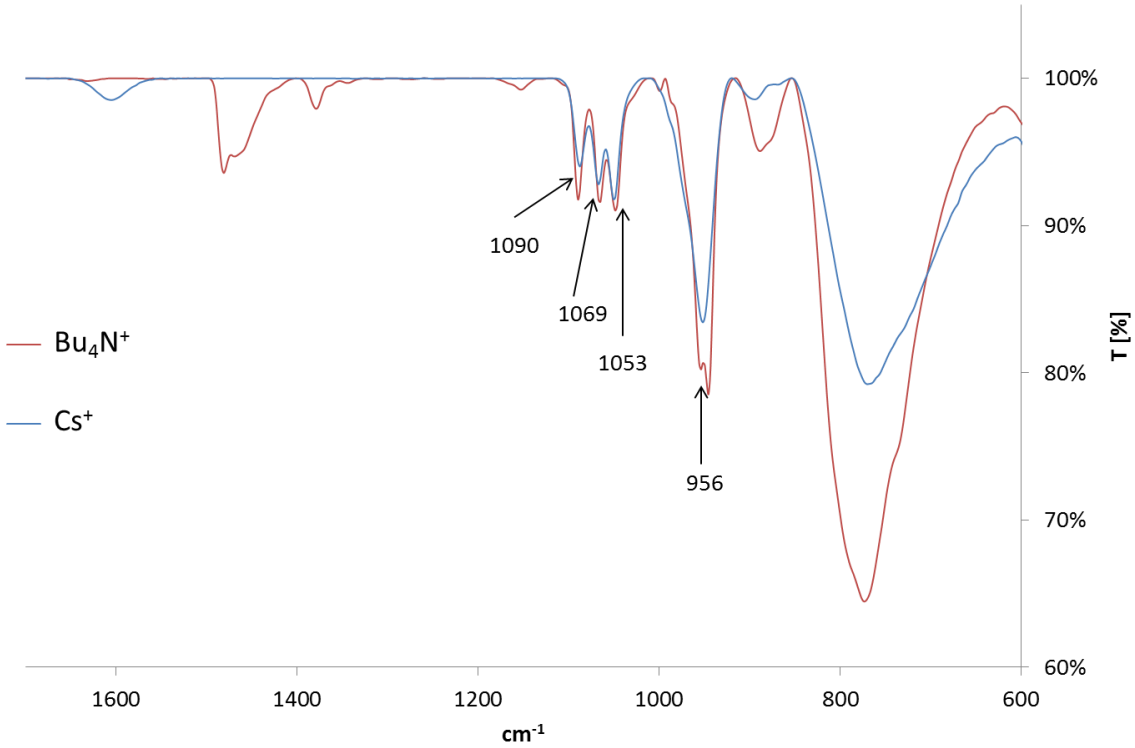

Figure 3.80 Changes in IR spectra for the synthesised β-isomer with Cs^+ and Bu_4N^+. Reported IR data for $Cs_5[\beta\text{-}PV_2W_{10}O_{40}]$: 1090(m), 1068(m), 1058(m), 976(s,sh), 960(s), 890(m), and 794 (vs, br).[61]

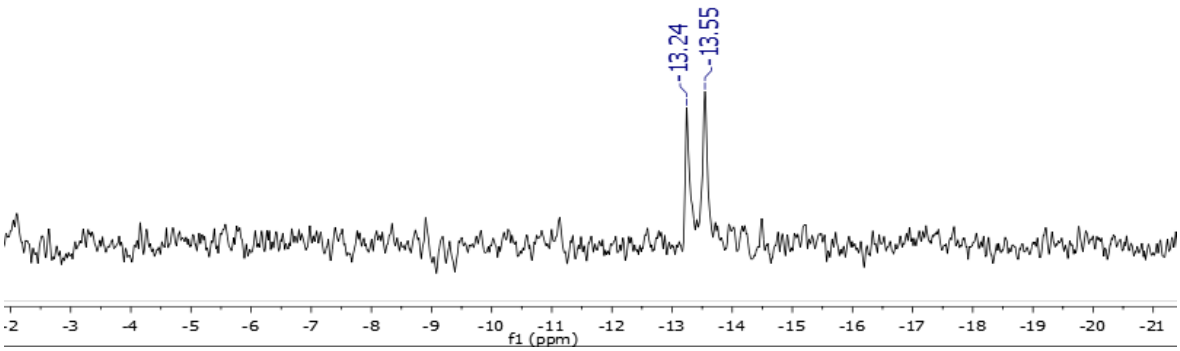

Figure 3.81 ^{31}P NMR of synthesised β-isomer. No reports of β - isomer in organic medium, but the data reported in aqueous solution for $Cs_5[\beta\text{-}PV_2W_{10}O_{40}]$ is -13.5 ppm.[61]

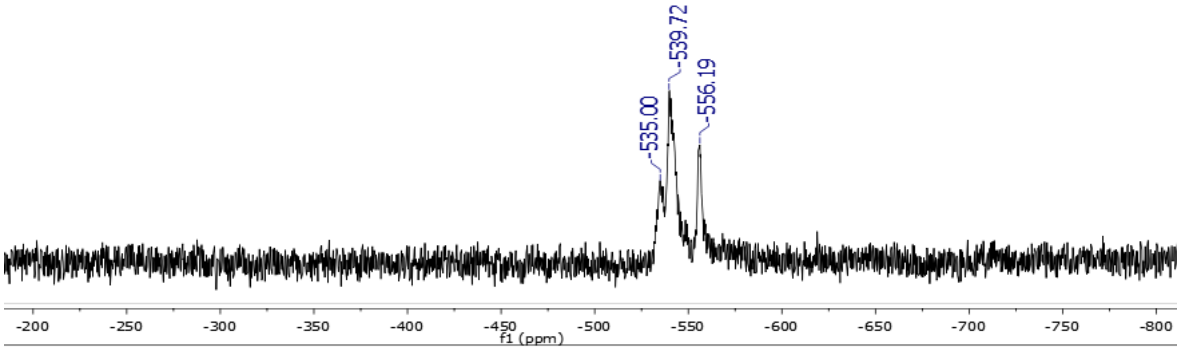

Figure 3.82 ^{51}V NMR of the synthesised β-isomer, no reports of β - isomer in organic medium is available, but in aqueous solution for $Cs_5[\beta\text{-}PV_2W_{10}O_{40}]$ was reported -543 and -554 ppm.[61]

The analysis of the synthesised β-isomer confirmed it was β-isomer, but its protonation state was unknown. The synthesis potentially yielded $[Bu_4N]_5[\beta\text{-P } V_2W_{10}O_{40}]$, $[Bu_4N]_4[\beta\text{-HP } V_2W_{10}O_{40}]$, $[Bu_4N]_3[\beta\text{-}H_2P\ V_2W_{10}O_{40}]$ or a mixture of all of those.

Comparing the obtained β-isomer analysis to the previously unresolved peaks from Figure 3.76 and 3.77 no correlation was found, thus it cannot be confirmed that the β-isomer is created under the reaction conditions. Although based on the presented results the β-isomer cannot be proven to be a reason for catalyst deactivation, the synthesised β-isomer was used in **LIM** epoxidation to confirm it is not active in the **LIM** epoxidation (Figure 3.83). Since the protonation state of the synthesised β-isomer was not known, 2 mol eq $HClO_4$ were used in respect to the β-isomer of **MIZ**. Mizuno *et al.* previously reported that $HClO_4$ added to the reaction does not co-catalyse the reaction, but it is a proton source for the formation of a bis-μ-hydroxo site in **MIZ** and an excess of $HClO_4$ does not affect the conversion or yield of products.[32]

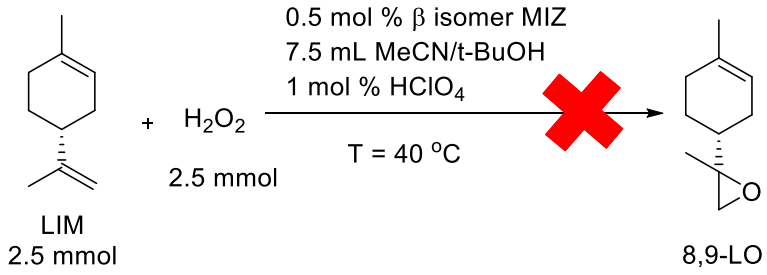

Figure 3.83 LIM epoxidation catalysed by β - isomer MIZ.

The **LIM** consumption and **8,9-LO** production were shown in Figure 3.84 and Figure 3.85 respectively. Although the small mass loss of **LIM** of up to 6 % was shown, no production of **8,9-LO** was observed confirming that the β isomer **MIZ** is not reactive in the **LIM** epoxidation reaction. It is worth noting that the mass loss reported is still within the experimental error.

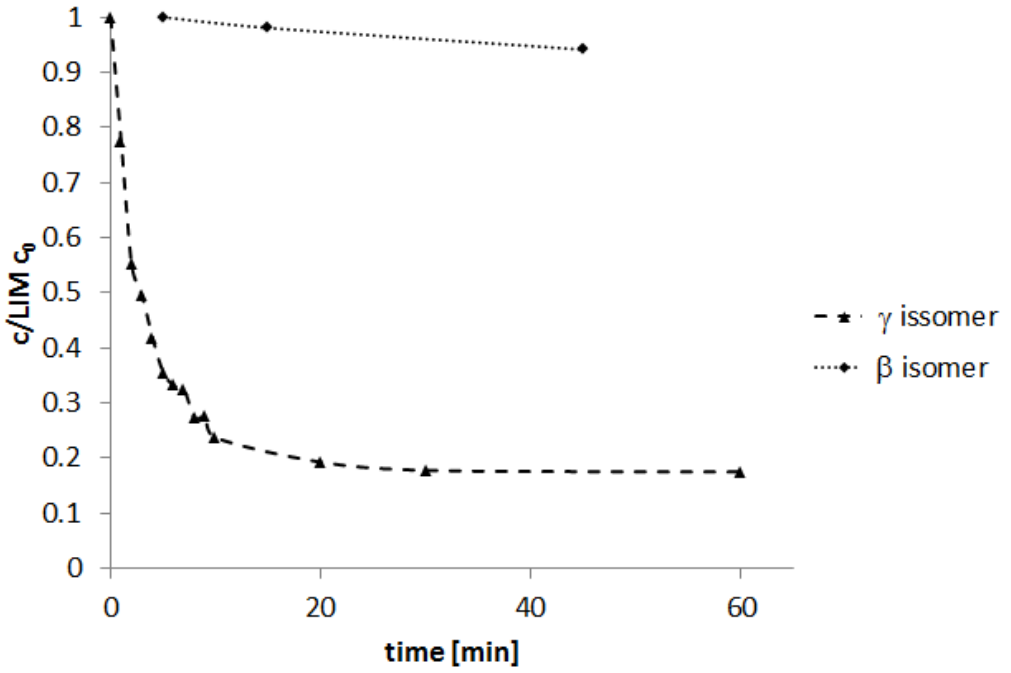

Figure 3.84 LIM epoxidation catalysed by β - isomer MIZ. Reacion conditions presented in Figure 3.83.

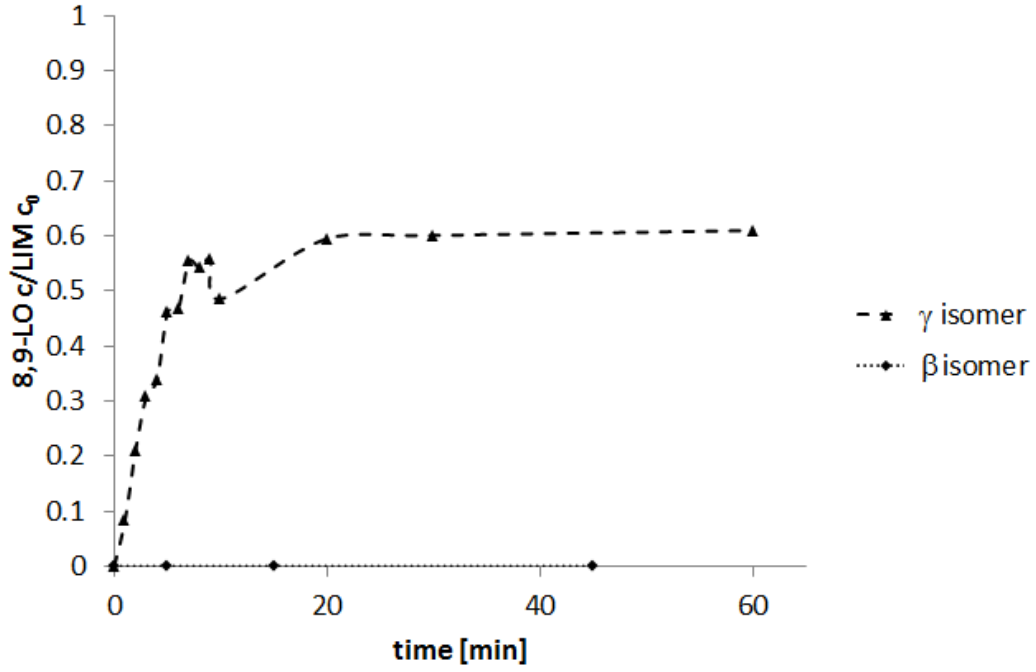

Figure 3.85 Changes in 8,9-LO molar fraction in LIM epoxidation catalysed by β - isomer MIZ. Reacion conditions presented in Figure 3.83.

Summary of MIZ epoxidation

BE can be successfully oxidised using **MIZ** and the possible oxidation products include **BEMO** and **BEBO**. However, if **BETO** is the desired product of epoxidation, **MIZ** is not an appropriate catalyst since it did not yield **BETO** under any reaction conditions tested.

Although **MIZ** epoxidation is highly selective and fast (about 15 min reaction time) it has not been further studied in a flow reactor due to possible catalyst deactivation and solid precipitation. Various experiments were performed to find the cause of catalyst deactivation. **MIZ** catalyst was stable in solution until H_2O_2 was added. It has been confirmed that the stability of the catalyst was negatively affected by water concentration and higher TON was achieved when 50 % H_2O_2 solution was used instead of 30 %. Organic diols and aldehydes did not affect **MIZ** performance, suggesting there is no catalyst poisoning by common epoxidation by-products. It has been proposed that under reaction conditions **MIZ** isomerises to β-isomer **MIZ**, but it could not be concluded that the β-isomer was produced during reaction conditions. However, it has been confirmed that the β-isomer **MIZ** is not active in the **LIM** epoxidation reaction.

The scale up of the reaction also proved problematic due to the high dilution of the epoxidation reaction, but attempts to reduce the amount of solvent were unsuccessful. The current epoxidation conditions use the highest reaction concentration previously published for the **MIZ** catalyst and the reaction can be scaled up if the amount of solvent is proportionally scaled up as well.

3.2.4 Preliminary epoxidation studies using trifluoroacetophenone (TFAP)

Preliminary studies on **TFAP** were undertaken. First, a reaction which was previously reported for limonene was performed to replicate published results and ensure the reaction set up, commercially bought catalyst and oxidant are of appropriate quality (Figure 3.86). For the purpose of this analysis it was assumed no **8,9-LO** is formed, since the original paper does not mention its formation under these reaction conditions. However, the region of ^{1}H NMR spectrum where epoxide signals corresponding from **8,9-LO** would appear was too crowded to exclude **8,9-LO** formation. Further qualitative GC-MS analysis showed the presence of **8,9-LO**. Although it was not analysed quantitatively, **1,2-LO** was definitely the main product. The analysis showed 69 % conversion and 82 % selectivity (56 % yield) which is significantly lower than 81 % isolated yield reported.[34] It is worth noting that NMR analysis was done with an assumption no **8,9-LO** is present, thus the 56 % yield slightly differ from real value. Since selectivity remained high, it is possible that the variation in H_2O_2 concentration caused this issue. Other solvents were tested including iPrOH, EtOAc and n-BuOH with only i-PrOH yielding comparable results.

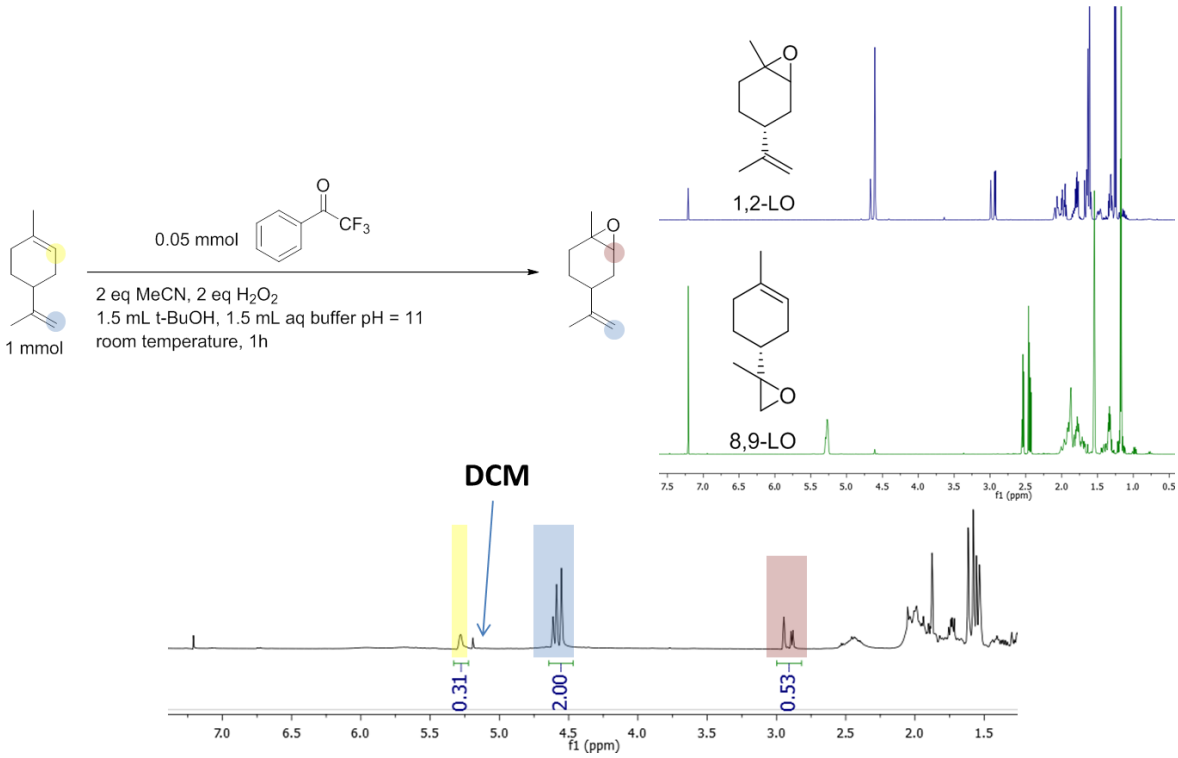

Figure 3.86 ^{1}H NMR spectroscopy of crude organic phase extracted from LIM epoxidation using TFAP. After reaction organic layer was extracted with DCM and solvent was evaporated in vacuo, then an NMR sample was prepared in $CDCl_3$.

Further investigation of **TFAP** catalysed epoxidation could be carried out using flow NMR, which is able to provide in-situ information about catalyst species in the reaction system.[62] However, the reaction volume would have to be increased to at least 25 mL of organic phase. The scale up of the reaction to 25 mL t-BuOH proved challenging (Figure 3.87). The reaction was analysed by NMR spectroscopy and GC-FID with an external mesitylene standard. NMR spectra were not usable since the reaction solvent overlapped with the limonene and product signals. GC-FID analysis showed that only 29 % conversion was achieved after a 75 min reaction. Further investigation of this reaction should be a part of future work, but a possible reason for lower yields could be insufficient mass transfer between organic and aqueous phases.

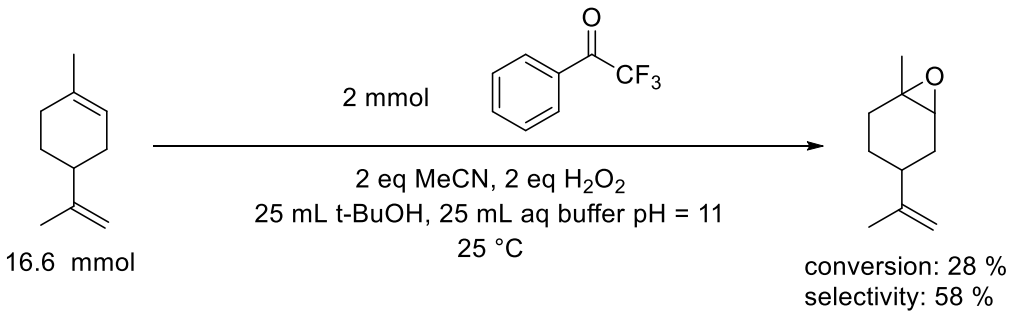

Figure 3.87 A large scale epoxidation of LIM using TFAP.

This catalyst was also investigated for **BE** epoxidation (Figure 3.88). This experiment was performed before GC-FID analysis was developed for **BE** epoxidation, thus it was analysed using ^{1}H NMR spectroscopy. The reaction showed 49 % conversion of alkene bonds and showed 99 % selectivity towards epoxy groups yielding 49 % of epoxide products which are a mixture of **BEMO** and **BEBO**. No **BETO** was produced as no disappearance of the alkene in the vinyl double bond was observed (Figure 3.88 yellow). Via ^{1}H NMR it is not possible to determine the ratio between **BEMO** and **BEBO**, but it is possible to see that no significant disproportion of alkene groups (Figure 3.88 green) was shown, suggesting that both regioisomers of **BEMO** are produced in about 1:1 ratio.

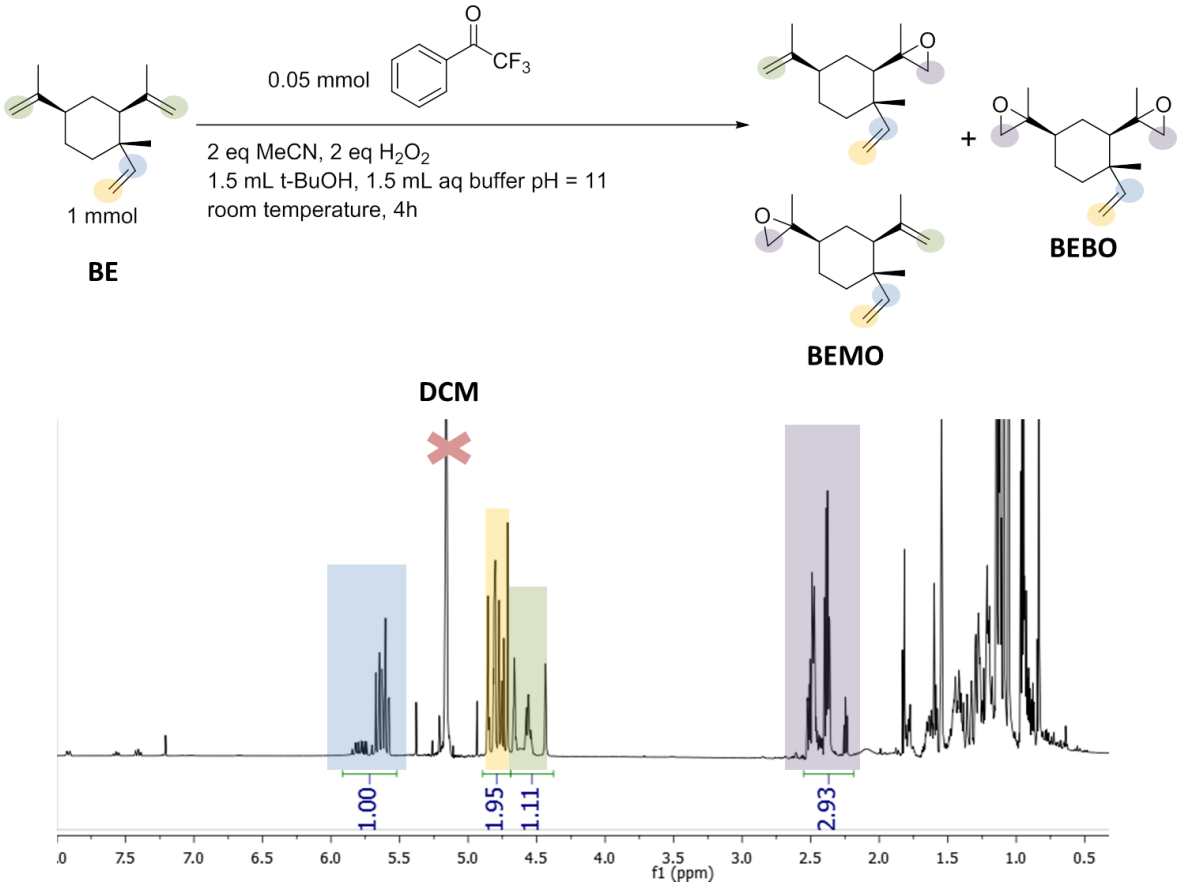

Figure 3.88 ^{1}H NMR spectrum and reaction scheme of BE epoxidation catalysed by TFAP.

Marc Hutchby within the Davidson group and the Bull group further investigated **TFAP** catalysed epoxidation of **BE** and proposed to change the solvent to MeCN (Table 3.12).[34] With an increased amount of **TFAP** (10 mol % instead of 5 mol %) and high excess of H_2O_2 (10 mol eq) **BE** can be epoxidised to the trisepoxide.[52] Hutchby's results indicated that higher concentrations of MeCN and an excess of H_2O_2 improve epoxides yields, which is consistent with findings of Kokotos *et al.* as it has been indicated MeCN has a crucial role in a catalytic cycle.[34]

Table 3.12 Marc Hutchby's results[52] This data is not part of this thesis it is presented for information purposes only.

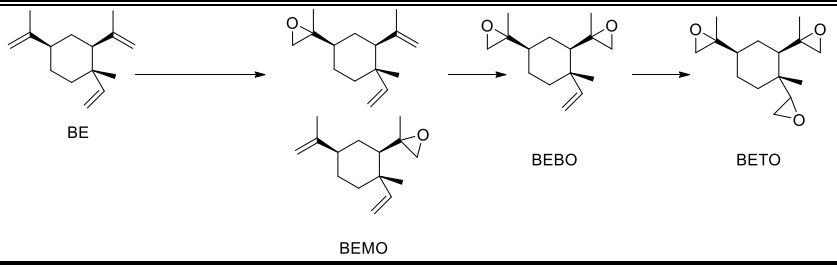

				Yield[a] [%]		
Entry	**BE [mmol]**	**H_2O_2 [mmol]**	**TFAP [mmol]**	**BEMO**	**BEBO**	**BETO**
1	5	20	0.5	67	19	-
2	5	30	0.5	-	82	6
3	5	50	0.5	-	30	61

a) total isolated yield after column chromatography
Reaction conditions: 20 mL MeCN, 20 mL aq buffer solution pH 11, room temperature, time not reported

3.3 Conclusions and future work

The Venturello catalyst is the most widely studied epoxidation catalyst within the Plucinski group. In this research it was found that it can selectively epoxidise **BE**. **BE** epoxidation is a consecutive reaction with **BEMO** being the first product and **BEBO** second. **BETO** was not observed in the flow reaction set up as it requires long reaction times not achievable in flow reactor. The experiment with varying flow rates (0.226 – 0.452 mL min^{-1}) showed that the reaction is kinetically limited and not mass transfer limited. It was also shown that an excess of H_2O_2 is needed in order to achieve high epoxide yields. As high excess of H_2O_2 was used, the pseudo first order reaction model was applied and it was found that the **BE** rate of reaction can be described as pseudo first order reaction. However, with longer residence times (above 33.2 min) it was observed that the rate of reaction changes over time indicating catalyst deactivation or product inhibition. Further studies into catalyst deactivation and improving **BEBO** yield are recommended to make this system a green protocol for **BE** epoxidation.

The Mizuno catalyst is the only reported catalyst which shows exclusive selectivity towards **8,9-LO** in limonene epoxidation, thus it was hypothesised that it might allow an unusual monoepoxide and bisepoxide formation when applied to **BE** epoxidation. No unusual products were observed, the epoxidation catalysed by **MIZ** yielded **BEMO** and **BEBO**. **BETO** was not observed in any of the tested reaction conditions showing **MIZ** inactivity towards the vinyl double bond in the **BE** structure. The presented results showed **MIZ** deactivation and high sensitivity to water content. The β-isomer of **MIZ** was synthesised and it was confirmed that it does not catalyse the **BE** epoxidation. However, no evidence has been found that the β-isomer is a plausible explanation for **MIZ** deactivation under reaction conditions. While **MIZ** is highly selective and shows high

reaction yields, it is not recommended for scale up or flow epoxidation since it exhibits complex catalyst deactivation behaviour and high dilution of the reaction is necessary.

Although only preliminary studies on **TFAP** catalysed **BE** epoxidation were done, it is a promising catalyst for **BE** epoxidation. It differs from other tested catalyst as it can selectively provide **BETO** in high yields as was shown by M. Hutchby.[52] The issues in the reaction scale up should be addressed in future work. The **TFAP** catalysed epoxidation mechanism has been well described by Kokotos *et al.*[34] and could be investigated by flow NMR to further understand it.[62]

The comparison among three catalysts investigated in **BE** epoxidation is presented in Table 3.13. All of the tested catalysts were homogeneous and **TFAP** was the only catalyst commercially available. Only **VENT** allowed running a solventless reaction and it was the only catalyst tested in flow. As **TFAP** is also a biphasic reaction it should be further develop and applied in a flow reaction set up.

Table 3.13 Comparison among three tested catalysts VENT, MIZ and TFAP.

Entry		VENT	MIZ	TFAP
1	**Catalyst synthesis and availability**	Easy to scale up, large amount of DCM used	Highly sensitive to pH and quality of CsOH solution	Commercially available
2	**Catalyst appearance**	Very viscous yellow-green oil	Yellow solid	Clear oil
3	**Use of solvent**	none	1:1 MeCN:t-BuOH	t-BuOH and aqueous pH buffer MeCN – part of catalytic cycle
4	**Epoxides produced**	BEMO BEBO and after long reaction times BETO	BEMO and BEBO	BEMO, BEBO and BETO
5	**Scale up**	Possible to run in flow set up making scale up easy. Catalyst instability should be addressed	Reaction is homogeneous and it operates in high dilutions – difficult scale up	Not tested, but as it is a biphasic reaction it might benefit from the use of microreactors
6	**Product purification**	Biphasic reaction, epoxides would have to be purified from VENT	Homogeneous reaction, the catalyst precipitates from the reaction mixture upon removing reaction solvents *in vacuo*	Biphasic reaction, the epoxides would have to be purified from the reaction solvent, MeCN and TFAP

3.4 Experimental

3.4.1 General consideration

All reagents and NMR solvents were sourced from Sigma Aldrich, Alfa Aesar or Fischer Scientific. All solvents, except NMR solvents, were sourced from VWR and used as received. β-elemene was kindly provided by Isobionics.

GC-MS spectra were recorded on a Shimadzu GC-2010 Plus with FID and TIC detectors using a BP20 polar column, 30 m x 0.25 mm x 0.25 µm (max temp. 260/280 °C).
Sample preparation: For experiments with mesitylene as an internal standard, the sample was taken from the reaction aliquot and diluted with methanol. For experiments where an external standard was used, a 20 µL aliquot was taken from the reaction and diluted in 1 mL MeOH. It was then further diluted by taking 50 µL and diluting in 1 mL MeOH, then 150 µL mesitylene 0.384 mM solution was added. 0.384 mM mesitylene solution was prepared by dissolving 120 mg mesitylene in 1 mL MeOH, and further diluting by taking 20 µL and dissolving it in 1 mL MeOH, and the last step of dilution by adding 160 µL to 8 mL MeOH. 150 µL of 0.384 mM mesitylene solution was added per sample.
GC method for limonene and limonene oxides analysis: The sample was injected at 250 °C in split mode with a split ratio 1:10. The column oven temperature was set at 80 °C, where it was kept for 2 min, then it was increased by 10 °C min^{-1} from 80 to 260 °C where it was kept for 2 min. The carrier gas – helium, was in the linear velocity control mode, with the linear velocity set at 40 cm sec^{-1}. The FID had a temperature of 300 °C. Ar was used as the make up gas at a flow rate 30 mL min^{-1}. The hydrogen flow rate was set at 40 mL min^{-1} and the air flow rate at 400 mL min^{-1}. For the TIC detector, the ion source was set at 200 °C and the interface temperature was set at 250 °C. The detector voltage was relative to the tuning result.
GC method for β-elemene and β-elemene oxides analysis: The sample was injected at 250 °C in split mode with a split ratio 1:10. The column oven temperature was set at 100 °C, where it was kept for 2 min, then it was increased by 10 °C min^{-1} from 100 to 260 °C, where it was kept for 8 min. Carrier gas – helium, was in the linear velocity control mode, with the linear velocity set at 40 cm sec^{-1}. The FID had temperature of 300 °C, Ar was used as the make up gas at a flow rate 30 mL min^{-1}. The hydrogen flow rate was set at 40 mL min^{-1} and the air flow rate at 400 mL min^{-1}. For the TIC detector, the ion source was set at 200 °C and the interface temperature was set at 250 °C. The detector voltage was relative to the tuning result.

NMR spectra were obtained on a Bruker Avance III 400 MHz, Agilent ProPulse 500 MHz, Brucker Avance III 500 MHz and Bruker Avance II + 500 MHz Ultrashield equipped with a broadband observe probe. All NMR spectra were referenced against a solvent peak (chloroform-d ^{1}H NMR: 7.26 ppm ^{13}C {^{1}H} NMR 77.16 ppm).

IR spectra were recorded on a Bruker ALPHA II Fourier transform spectrometer fitted with an ATR accessory. The number of scans was set to 24 and the resolution was set to 4 cm^{-1}.

3.4.2 Venturello catalyst (VENT) preparation

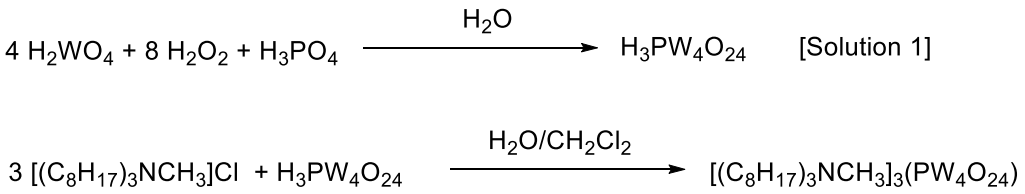

The Venturello catalyst for olefin epoxidation was prepared according to the original Venturello preparation method with minor changes.[21] 25g tungstic acid was suspended in 80 mL 30 wt % H_2O_2 solution and stirred for 30 min at 70 °C leading to a colour change from yellow to light green. The light green solution was cooled down to room temperature and 6 mL 40 % phosphoric acid was added, followed by 20 min stirring. Next, the solution was diluted with 220 mL distilled water and stirred for another 15-20 min (this solution is further referred as a Solution 1).

For the cation exchange, the commercially available Aliquat 336 was used, which is an ammonium salt mixture consisting mostly of methyltrioctylammonium chloride. 21 g Aliquat 336 was dissolved in 400 mL DCM and the resulting solution was added dropwise to Solution 1 under magnetic stirring, followed by 30 min additional stirring. The resulting bi-phasic mixture was separated using a separating funnel. The organic phase was collected and washed with 2x150 mL saturated NaCl water solution. After washing, the organic solution was dried over $MgSO_4$, filtered and evaporated *in vacuo*. The yield of resulting yellow oil varied between 26 and 29g (67 % -74 %).

3.4.3 β-elemene epoxidation in microreactor

Epoxidation was carried out in two microreactors with preheating channels and an integrated static mixer (2 x Little Things Factory, XXL-ST-04, 4.5 mL reaction volume. Note that to connect two reactors together 1/3 volume of one reactor has to be lost resulting in an overall reactor volume of 7.5 mL). The reaction was carried out at 50 °C. The temperature was controlled by a recirculating

heat exchanger (Fisher Scientific ISO UK 6200). The substrates were delivered to the reactor using syringe pumps. The first syringe was charged with 30 wt % H_2O_2 solution with the pH adjusted to 7 using 1M NaOH. The second syringe was charged with pure BE containing 2 mol % Venturello catalyst and 10 mol % mesitylene as an internal GC-FID standard. Both syringes were made of glass. The flow rates of each phase and the residence time are reported in the relevant captions of charts and tables. Products were analysed by GC-FID. Information about conversion and selectivity can be found in the charts and tables presented in results section.

3.4.4 Mizuno catalyst preparation

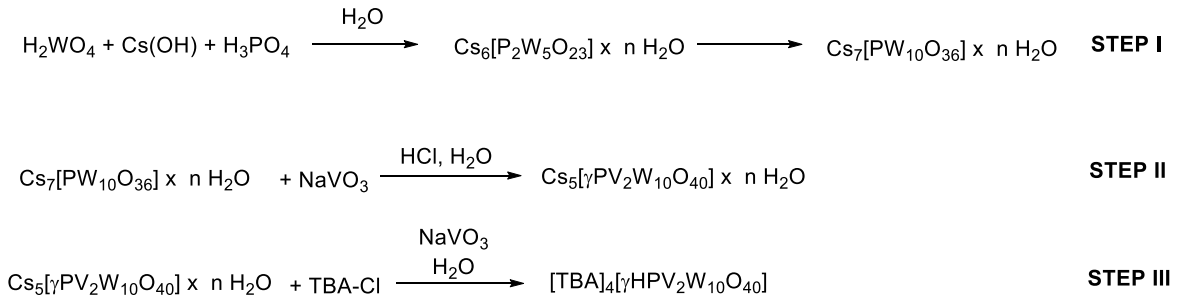

STEP I $Cs_7[PW_{10}O_{36}]$ x nH_2O preparation: Following the previously published method,[61] 6 g of tungstic acid was added to 40 mL water under magnetic stirring, resulting in a yellow slurry. 50 wt %. Aqueous CsOH was added dropwise to the slurry under vigorous stirring until pH = 13 (about 11 mL CsOH solution). After CsOH addition, the mixture become cloudy, thus it was filtered over celite yielding a clear colourless filtrate. The pH of the filtrate was adjusted to 7 by adding 85 % H_3PO_4 dropwise (usually about 2.1 mL acid). The solution was stirred for 1 h, filtered again and cooled down in a refrigerator overnight. The resulting white solid ($Cs_6[P_2W_5O_{23}]$ x nH_2O) was recovered by filtration and refluxed in water for 24 h. The mass ratio between the solid and water was 1:2 respectively. After reflux, the white solid ($Cs_7[PW_{10}O_{36}]$ x nH_2O) was separated by filtration.

Note: The batch of CsOH solution has a crucial impact on the synthesis. The reported synthesis was carried out with Alfa Aesar™ Cesium hydroxide, 50% w/w aq. soln., 99% (metals basis) stored and packed under inert atmosphere.

STEP II $Cs_5[\gamma PV_2W_{10}O_{40}]$ x nH_2O preparation: Following the previously published method,[61, 63, 64] 0.1 g sodium metavanadate ($NaVO_3$) was dissolved in 4 mL water by heating to 70 °C. The solution was cooled down to room temperature and 3 M HCl was added dropwise to adjust the pH to 0.8. The solution became yellow, which indicated the presence of $[VO_2]^+$. 1.25 g $Cs_7[PW_{10}O_{36}]$ was slowly added to the yellow solution. The solution was stirred for an additional 30 min and filtered yielding a yellow solid ($Cs_5[\gamma PV_2W_{10}O_{40}]$ x nH_2O). The resulting yellow solid (γ isomer) is

stable at pH 2 and in the presence of $[VO_2]^+$. In the absence of $[VO_2]^+$, isomerisation to β-isomer occurs which has an orange colour.[61]

STEP III $[TBA]_4[\gamma HPV_2W_{10}O_{40}]$ preparation: Following the previously published method,[32] 0.145 g of $NaVO_3$ was dissolved in 120 mL water at 70 °C, cooled down to room temperature and acidified to pH 2 using 3 M HCl (about 0.8 mL 3 M HCl was needed). 3.8 g $Cs_5[\gamma\text{-}PV_2W_{10}O_{40}]$ was added. The resulting solution was filtered in order to remove insoluble solids and 1.55 g TBA-Cl was added in one portion. The reaction was stirred for 10 min and filtered, yielding yellow solid which will be referred as the Mizuno catalyst (**14**). IR analysis results were in accordance with previously published data.[32, 61]

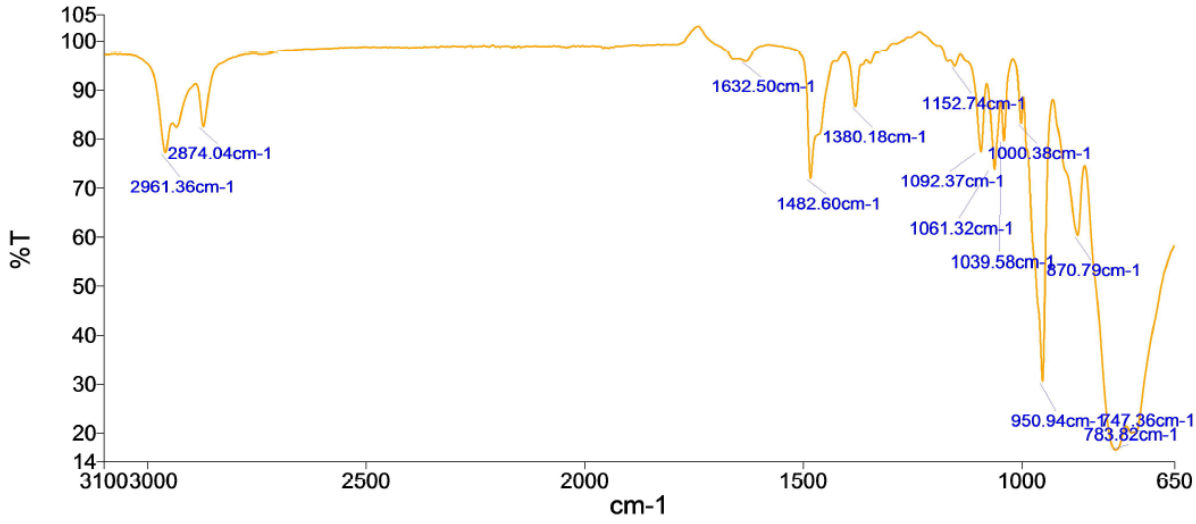

Figure 3.89 IR of the final Mizuno catalyst $[Bu_4N]_4[\gamma HPV_2W_{10}O_{40}]$.

3.4.5 Batch epoxidation using Mizuno catalyst

5 mmol olefin (**BE** or **LIM**), 0.025 mmol **MIZ**, a magnetic stirrer bar and 15 mL solvent (1:1 MeCN:t-BuOH) were placed in a 25 mL glass vial with a plastic cap. The catalyst was activated by adding 0.025 mmol 70 % $HClO_4$. The mixture was warmed up to 40 °C using an aluminium heating block and 5 mmol of H_2O_2 was added to the reaction mixture in one portion (H_2O_2 was used as 30 % or 50 % aqueous solution). The reaction was periodically followed by GC-FID. To separate **MIZ** from the reaction mixture, organic solvents were removed *in vacuo* until a precipitate of the catalyst was formed. 20 mL Et_2O was added to the resulting mixture and **MIZ** was filtered from the precipitate, followed by evaporation of Et_2O. In this experiment the resultant olefin was not purified, but generally it can be purified using column chromatography. The reaction set up is shown in Figure 3.90.

Figure 3.90 Batch MIZ epoxidation reaction set up.

3.4.6 β isomer MIZ preparation

The β-isomer was synthesised according to the literature procedure[61] starting from $Cs_5[\gamma\text{-}PV_2W_{10}O_{40}]$, which was prepared according to procedure described in Section 3.4.4.
3.3 g of $Cs_5[\gamma\text{-}PV_2W_{10}O_{40}]$ was stirred with 100 mL water for 60 h. This was cooled down to 0 °C and passed through a celite filter. The volume was reduced to 25 mL using rotary evaporator and then cooled down for 1 h at 0 °C. An orange solid crashed out of solution and was collected (1.11 g, orange solid). The solid was dissolved in 25 mL water at 25 °C, passed through a celite filter and evaporated to dryness. The procedure yielded 0.544 g orange solid which was further identified by IR (Figure 3.93) and NMR spectroscopy (Figure 3.91 and 3.92) as $Cs_5[\beta\text{-}PV_2W_{10}O_{40}]$.

0.466 g of $Cs_5[\beta\text{-}PV_2W_{10}O_{40}]$ was dissolved in 15 mL water. 0.190 g tetrabutylammonium chloride was added and everything was stirred for 5 min and filtered. The procedure yielded 0.255 g orange solid which was analysed by IR (Figure 3.94) and NMR spectroscopy (Figure 3.95 and 3.96).

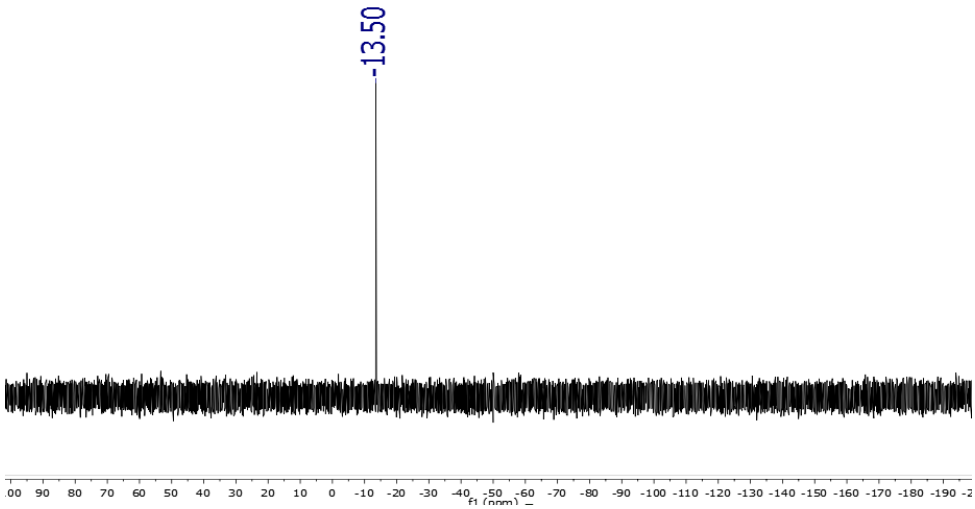

Figure 3.91 ^{31}P NMR spectroscopy of β-isomer MIZ with Cs^+ as a cation, run in H_2O at 25 ℃ without locking, reported value: ^{31}P NMR - 12.85 (aqueous solution, pH 4, 30°C).[61]

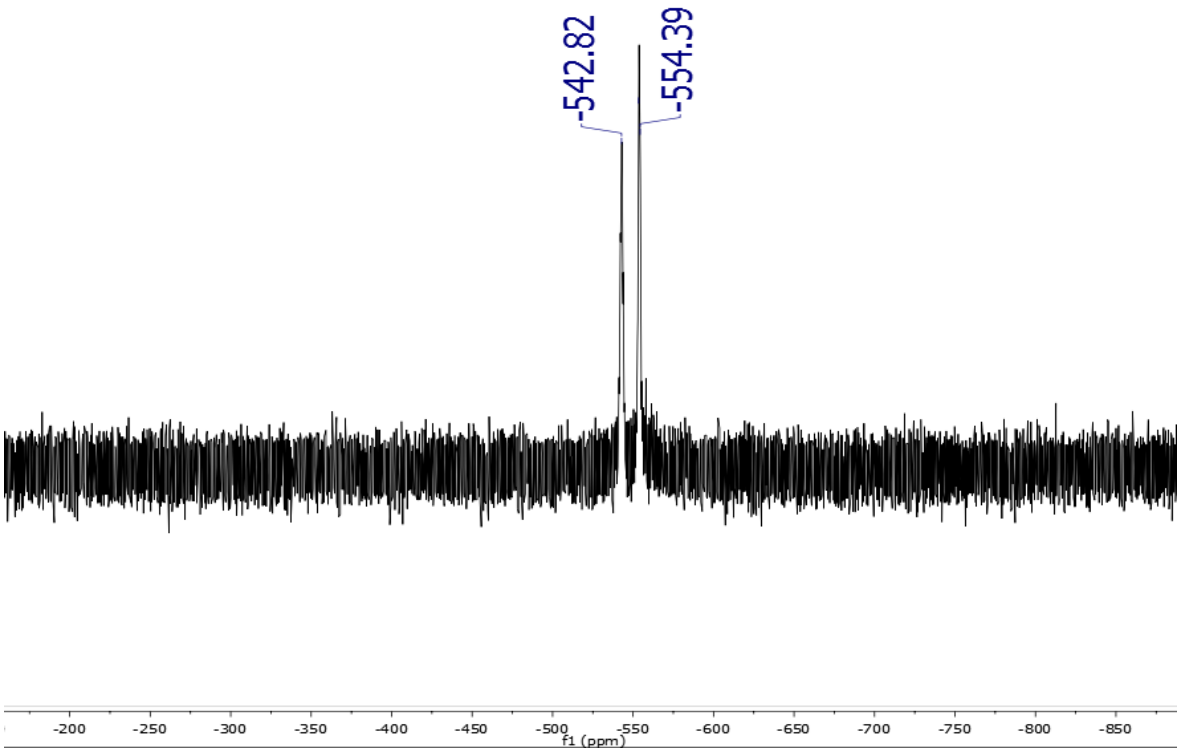

Figure 3.92 ^{51}V NMR spectroscopy of β-isomer MIZ with Cs^+ as a cation, run in H_2O at 25 ℃ without locking. Reported value: ^{51}V NMR (-544.2, -555.2 with $^2J_{VOV}$ ~2OHz. pH 3.5, 30 ℃).[61]

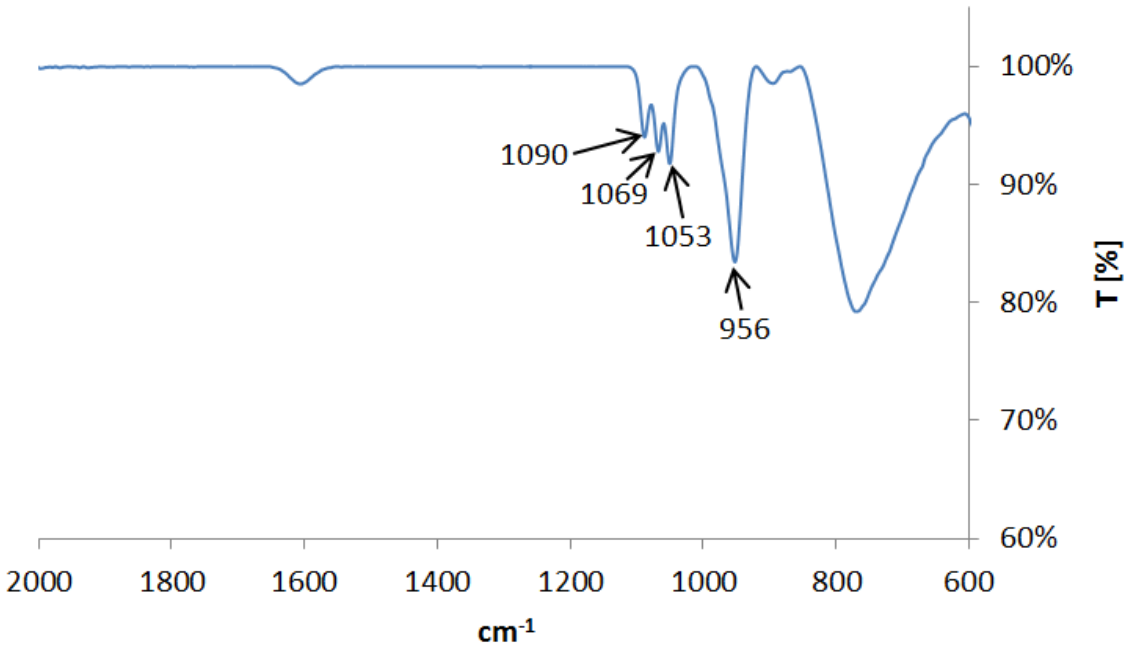

Figure 3.93 IR of β-isomer MIZ with Cs^+ as a cation, reported: IR (medium =mineral oil, range= 1600-650cm-'): 1090(m), 1068(m), 1058(m), 976(s,sh), 960(s), 890(m), and 794 (vs, br).

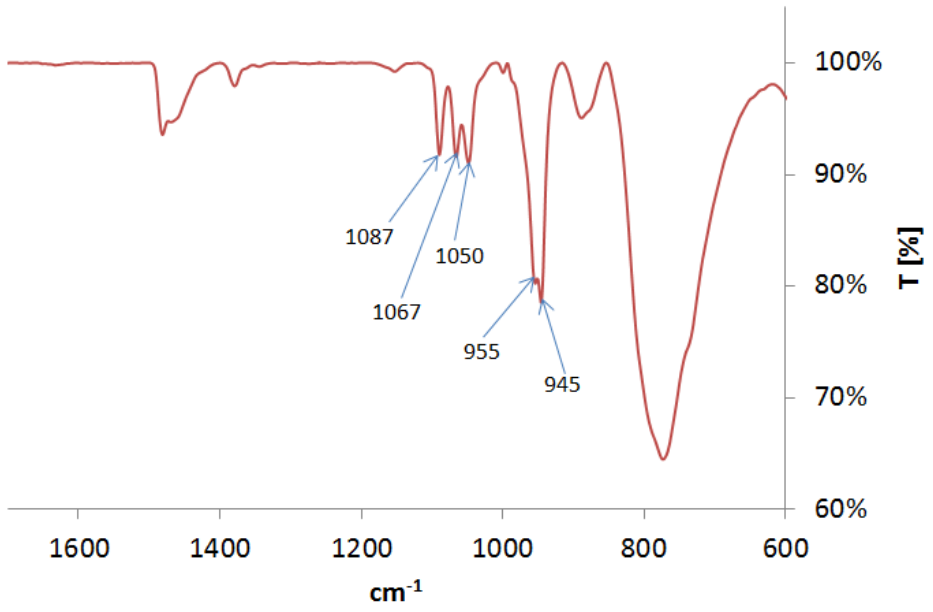

Figure 3.94 IR of β isomer MIZ with Bu_4N^+ as a cation. IR reported for MIZ with Cs^+ cation: IR (medium =mineral oil, range=1600-650 cm^{-1}): 1090(m), 1068(m), 1058(m), 976(s,sh), 960(s), 890(m), and 794 (vs, br).[61]

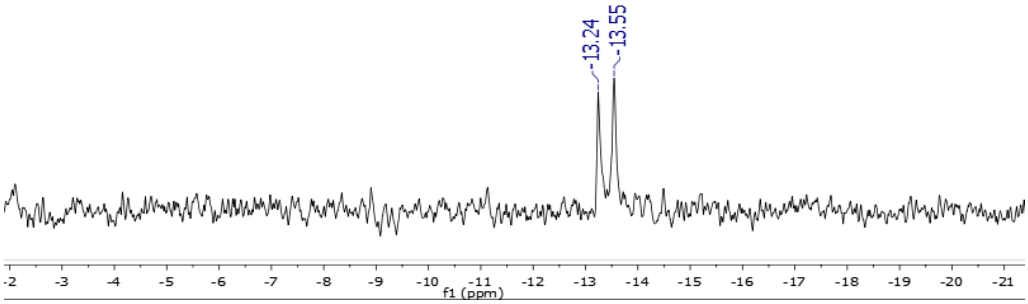

Figure 3.95 ^{31}P NMR spectroscopy of β isomer MIZ with Bu_4N^+ as a cation, no reports of β isomer in organic medium but in aqueous medium it was -13.5 ppm.

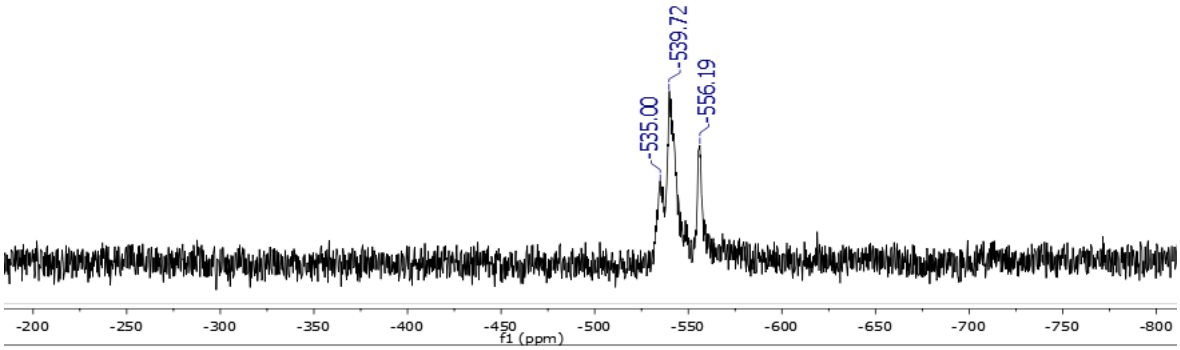

Figure 3.96 ^{51}V NMR spectroscopy of β isomer MIZ with Bu_4N^+ as a cation, no reports of β isomer in organic medium but in aqueous medium it was -543 and -554 ppm.

3.4.7 Epoxidation using organocatalyst TFAP

Epoxidation was performed according to the previously published procedure.[34] 1 mmol of olefin (**LIM** or **BE**) was placed in a 10 mL round bottom flask, and 1.5 mL t-BuOH, 5 mol % **TFAP** and 1.5 mL aqueous pH buffer were added. Then 2 mmol MeCN was added and the epoxidation was started by adding 2 mmol 30 % H_2O_2. The reaction was run at room temperature (19 °C).

To prepare 250 mL pH buffer solution: 20.725 g K_2CO_3 and 4.25 mg EDTA tetrasodium salt were diluted to 250 mL with water. The resultant solution is 0.6 M K_2CO_3, 4 x 10^{-5} M EDTA tetrasodium salt and it maintains pH 11 under reaction conditions.

3.4.8 H_2O_2 titration

$$5\ H_2O_{2\,(aq)} + 2\ MnO_4^-{}_{(aq)} + 6\ H^+_{(aq)} \longrightarrow 5\ O_{2\,(g)} + 2\ Mn^{2+}_{(aq)} + 3\ H_2O_{(aq)}$$

Titration was performed according to the previously reported procedure.[65] 0.0197 M solution of $KMnO_4$ was prepared by dissolving 0.388 g of potassium permanganate (2.46 mmol) in 125 mL of distilled water. This solution will be further referred as the titrant.

According to the reported procedure, the aliquot taken for titration should contain between 1.7 and 2.3 mmol of H_2O_2. 30 µL of 30 % H_2O_2 was diluted with 26 mL water; if 60 % H_2O_2 was used, 30 µL of 60 % H_2O_2 was diluted in 52 mL water. This solution was acidified with 2.6 mL diluted sulfuric acid (4 mL concentrated acid : 16 mL water).

The titrant was placed in a burette, a H_2O_2 aliquot was put in a 100 mL beaker and was titrated with permanganate solution until a faint pink colour persist for at least 30 seconds. The colour was checked against a white ceramic tile. To get statistically significant results, the titration has to be repeated 3 times. The titrant was freshly prepared in bulk and use for all titrations The H_2O_2 aliquot was prepared separately for each titration. For the calculation of results it is worth noting 1 mmol permanganate reacts with 2.5 mmol H_2O_2.

Table 3.14 H_2O_2 titration

TITRATION NUMBER	1	2	3
0.0197 M $KMnO_4$ used	5.40 mL	5.40 mL	5.35 mL
H_2O_2 concentration calculated	27 %	27 %	27 %

Example calculation:

$$5.40\ mL\ \times 0.0197\ M = 0.106\ mmol\ KMnO_4$$
$$0.106\ mmol\ \times 2.5 = 0.266\ mmol\ H_2O_2\ (9\ mg)$$
$$mass\ of\ 30\ \mu L\ of\ 30\ \%\ H_2O_2 = 0.033\ g$$

$$\frac{9\ mg}{33\ mg} = 27\ \%$$

The mass of 30 % H_2O_2 *solution is experimental data which is consistent with the theoretical value calculated based on density.*

3.4.9 Compounds characterisation

8,9-limonene oxide (8,9-LO)

8,9-limonene oxide		**8,9-LO** is a previously known compound[32, 66]
		mixture of isomers:
4R,8R-8,9-LO	**4R,8R-8,9-LO**	^{1}H NMR (400 MHz, $CDCl_3$) δ = 5.32 (m, 1H), 2.62 – 2.57 (m, 1H), 2.53 – 2.47 (2xd, 1H), 1.93 (m, 5H), 1.60 (m, 3H), 1.22 (m, 5H).
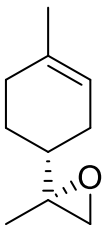	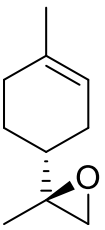	^{13}C {^{1}H} NMR (101 MHz, $CDCl_3$) δ = 134.1, 133.9, 120.1, 119.9, 59.4, 59.2, 53.4, 52.7, 40.2, 39.7, 30.4, 30.1, 27.5, 27.5, 25.0, 24.9, 23.5, 23.4, 18.8, 18.1.

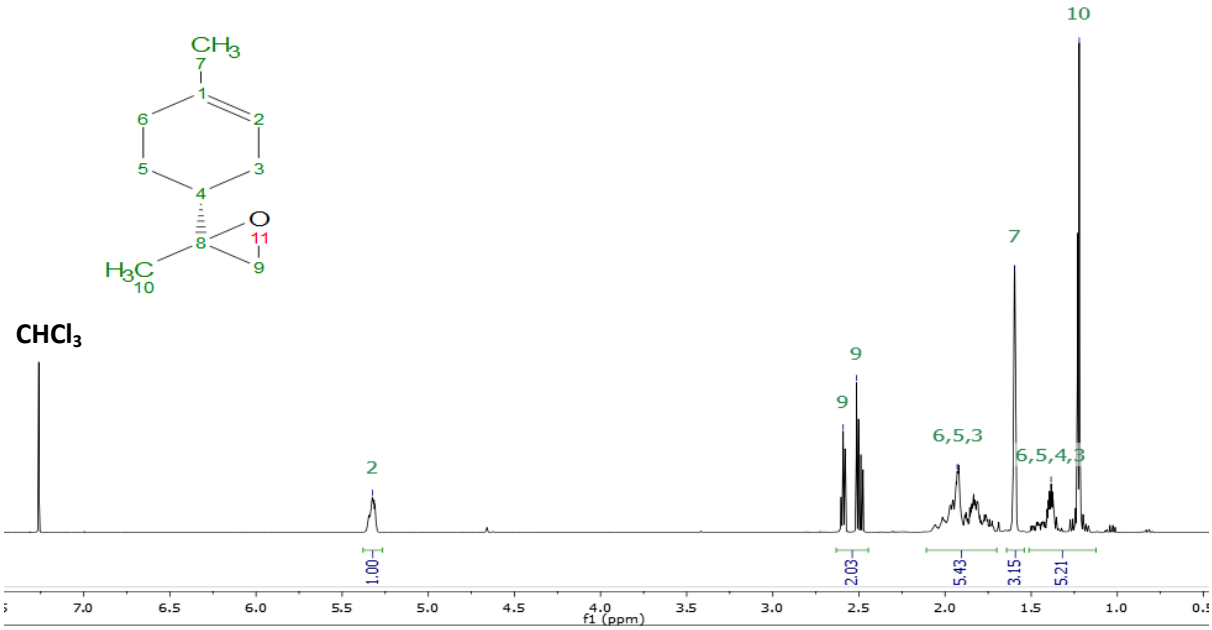

Figure 3.97 ^{1}H NMR spectrum of 8,9-LO.

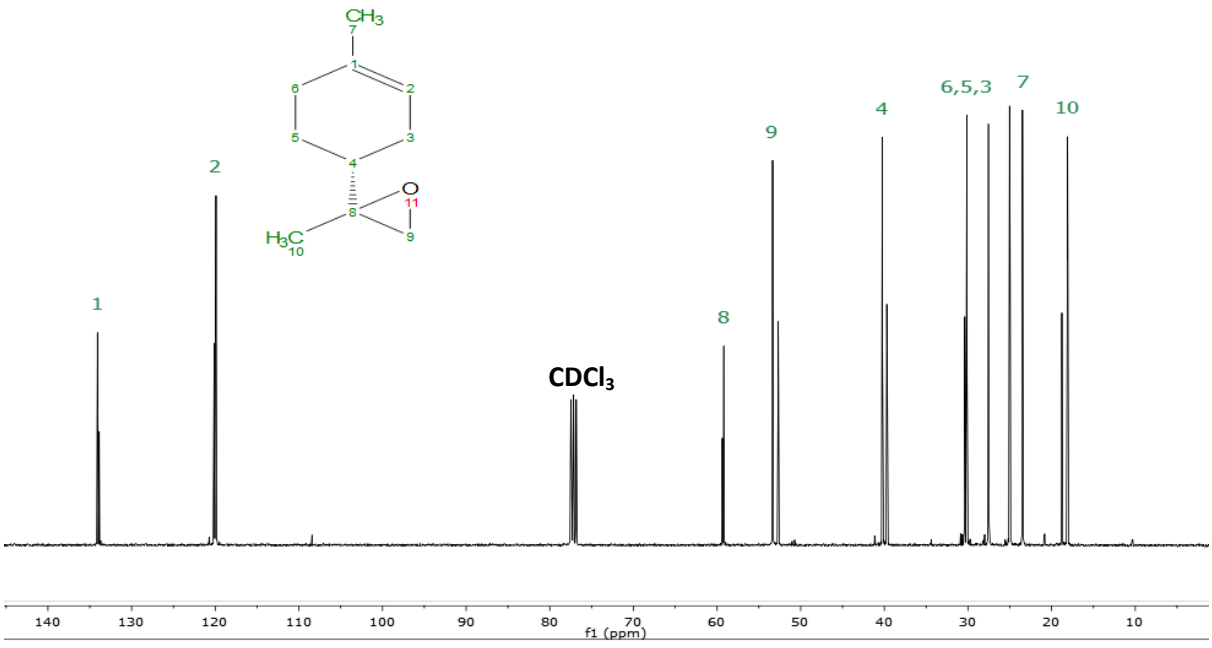

Figure 3.98 ^{13}C {^{1}H} NMR spectrum of 8,9-LO.

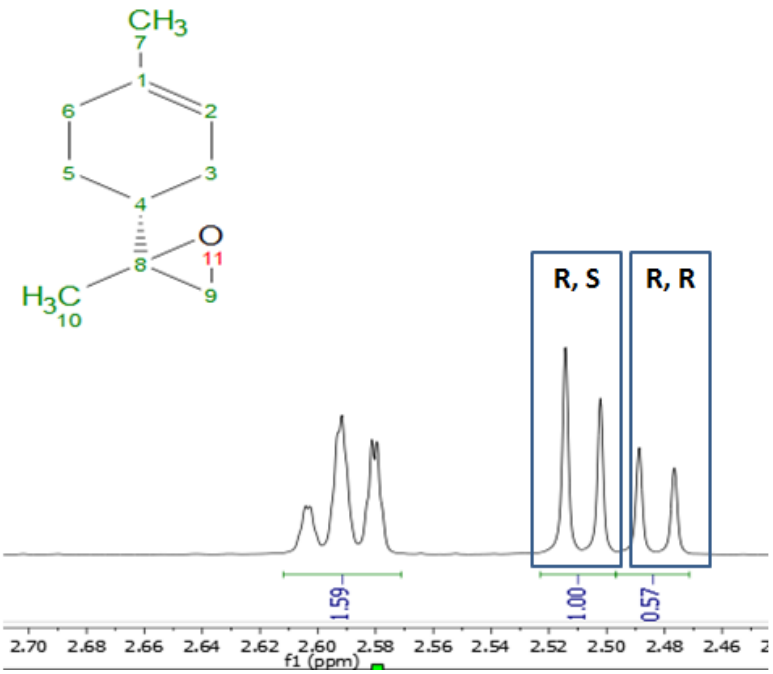

Figure 3.99 ^{1}H NMR spectra of protons in position 9 with characteristic stereoisomers peaks.[66]

β elemene (BE)

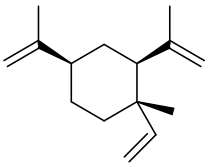

BE

^{1}H NMR(400 MHz, $CDCl_3$): δ = 5.84 (dd, 1H, J=17.4, 10.9 Hz), 4.99 – 4.86 (m, 2H), 4.86 – 4.57 (m, 4H), 2.09 – 1.88 (m, 2H), 1.81 – 1.68 (m, 6H), 1.68 – 1.36 (m, 6H), 1.02 (s, 3H) ppm

^{13}C{^{1}H} NMR (101 MHz, $CDCl_3$) δ = 150.4, 147.8, 112.3, 110.0, 108.4, 53.00, 45.9, 40.1, 39.9, 33.1, 27.0, 24.9, 21.2, 16.8.

As BE is an industrially available compound, no other analysis was performed.

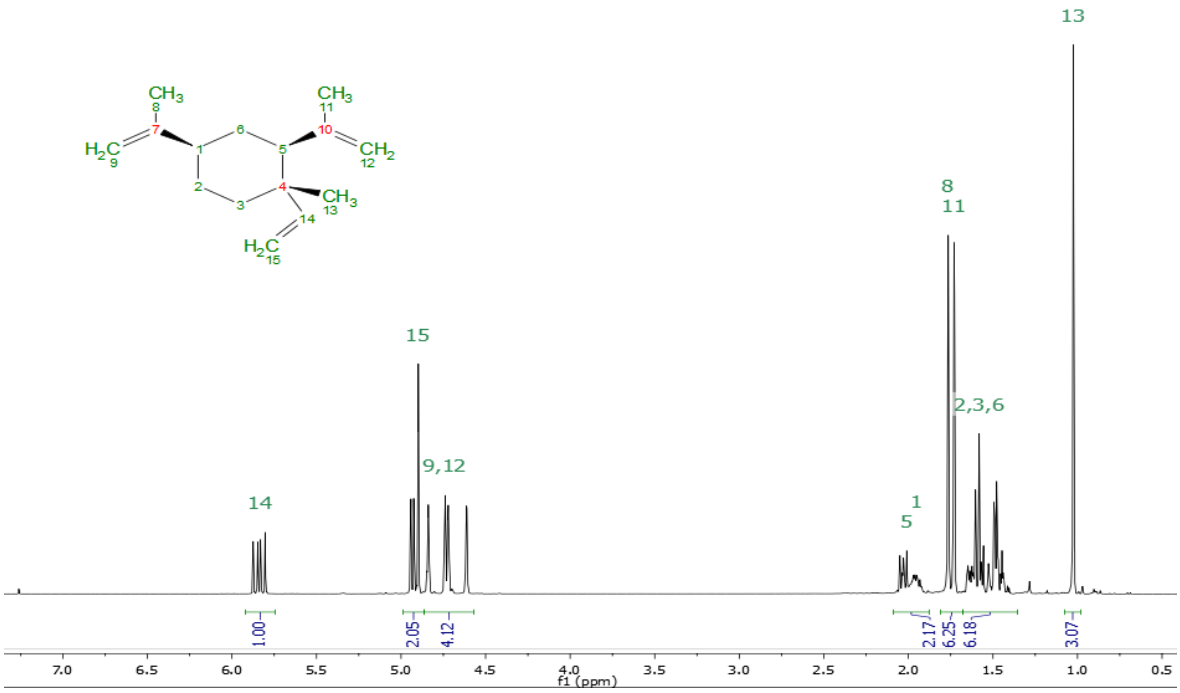

Figure 3.100 ^{1}H NMR spectroscopy of BE.

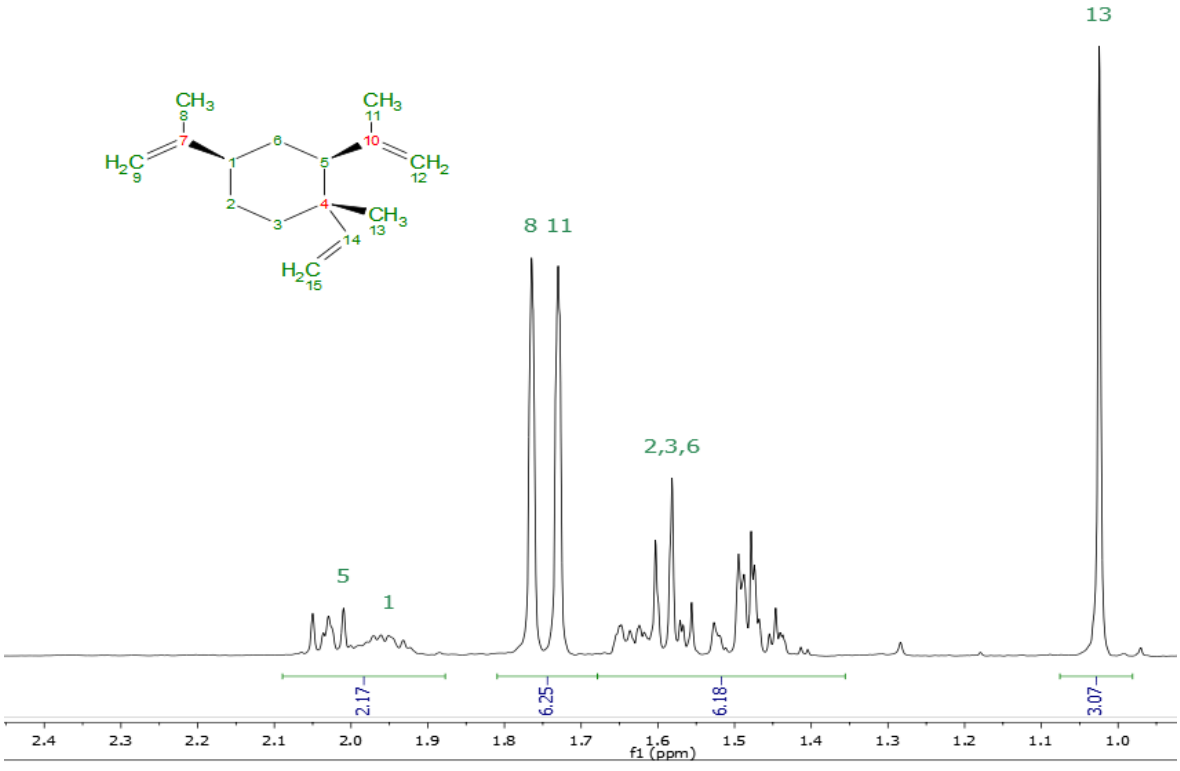

Figure 3.101 ^{1}H NMR spectroscopy of BE in the region of 2.4 – 0.9 ppm.

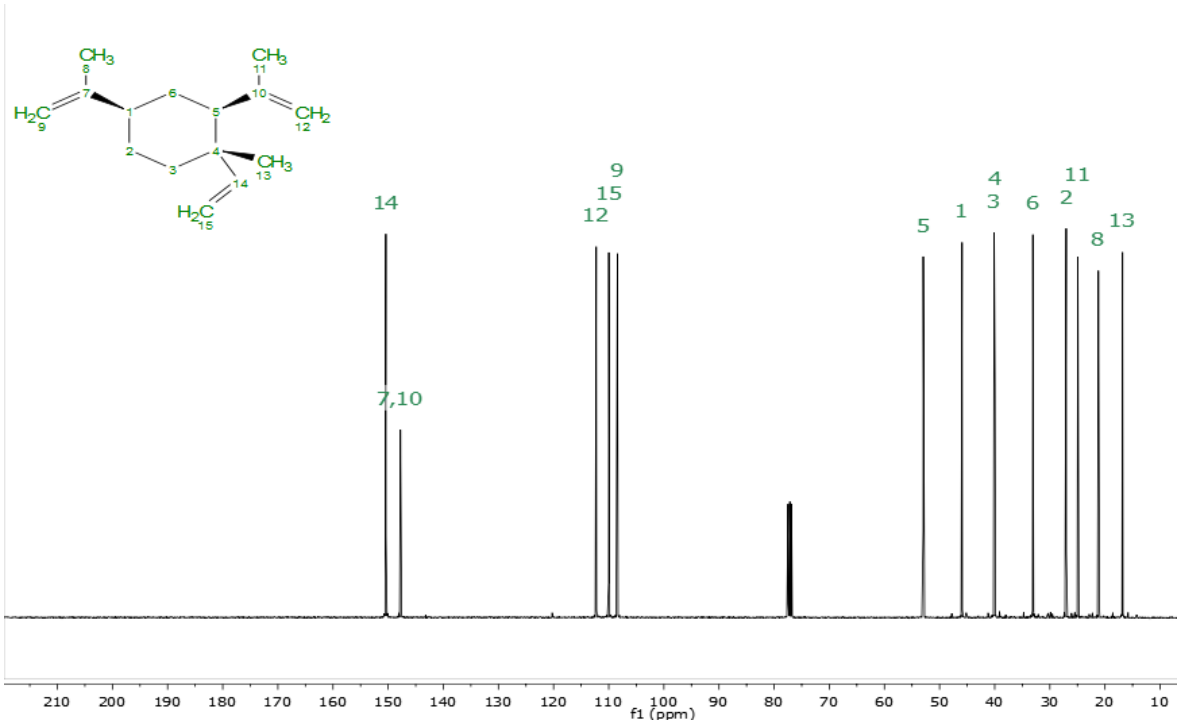

Figure 3.102 $^{13}C\{^{1}H\}$ NMR spectroscopy of BE.

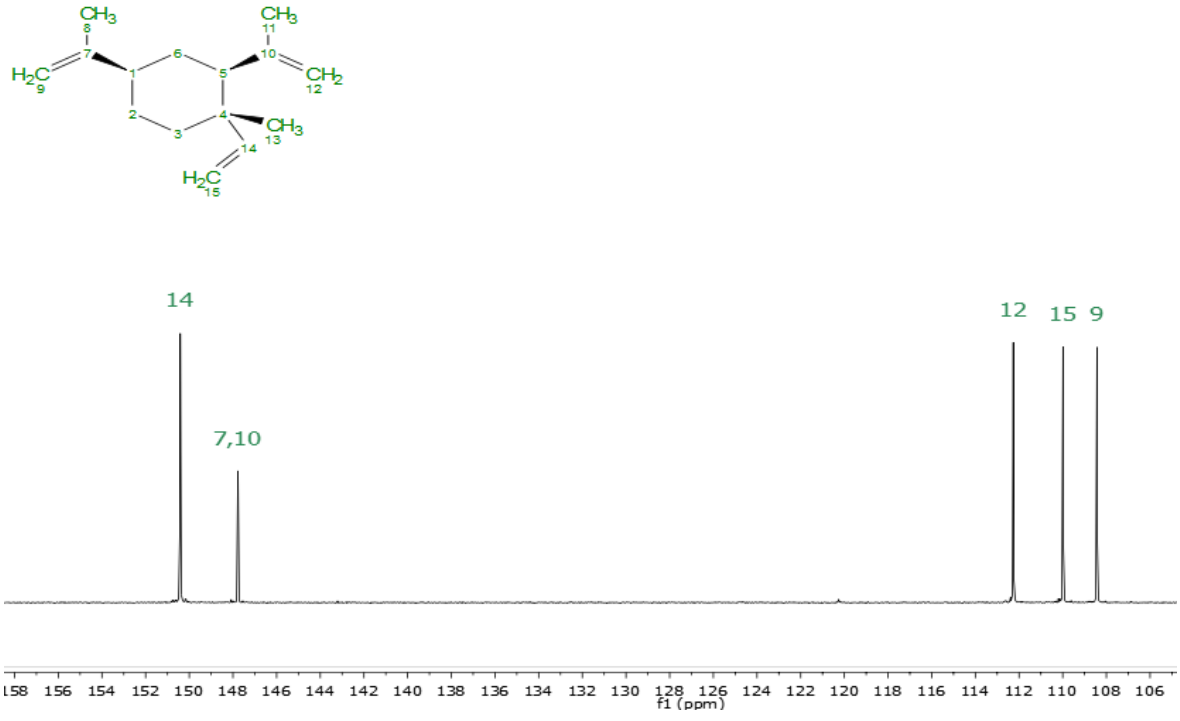

Figure 3.103 $^{13}C\{^{1}H\}$ NMR spectroscopy of BE in the range of 154 – 106 ppm.

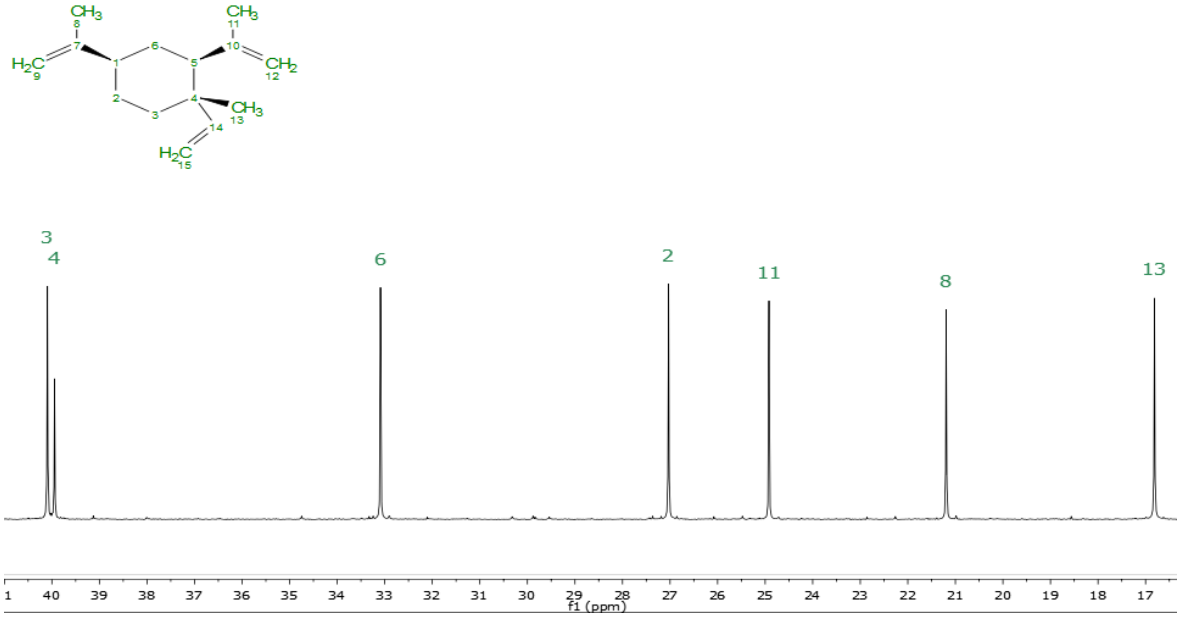

Figure 3.104 $^{13}C\{^{1}H\}$ NMR spectroscopy of BE in the range of 41 – 16.5 ppm.

β elemene monoepoxide (BEMO)

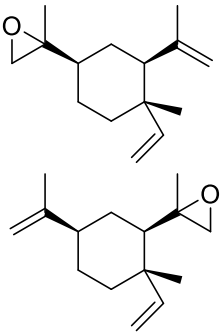

BEMO

^{1}H NMR(400 MHz, $CDCl_3$): δ = 5.78 (m, 1H), 5.05 – 4.85 (m, 2H), 4.70 (m, 2H), 2.70 – 2.35 (m, 2H), 2.00 – 0.78 (m, 17H) ppm

^{13}C{^{1}H} NMR (101 MHz, $CDCl_3$) δ = 150.6, 150.1, 150.1, 149.5, 147.5, 147.5, 112.4, 112.3, 110.7, 110.1, 110.1, 109.8, 108.6, 108.6, 59.5, 58.7, 58.1, 56.3, 53.6, 53.4, 53.4, 53.3, 52.5, 52.3, 51.5, 45.5, 45.3, 44.7, 44.6, 41.8, 41.3, 40.0, 40.0, 39.5, 39.4, 39.4, 30.0, 29.5, 29.4, 27.1, 26.8, 24.9, 24.9, 24.0, 23.5, 22.6, 21.2, 21.1, 20.0, 18.6, 18.5, 17.6, 17.3, 16.7, 16.7.

Without selective synthesis of the regioisomers it is not possible to assign any diagnostic peaks for the regioisomers. This compound was previously synthesised within the Davidson group, thus MS and IR was not done.

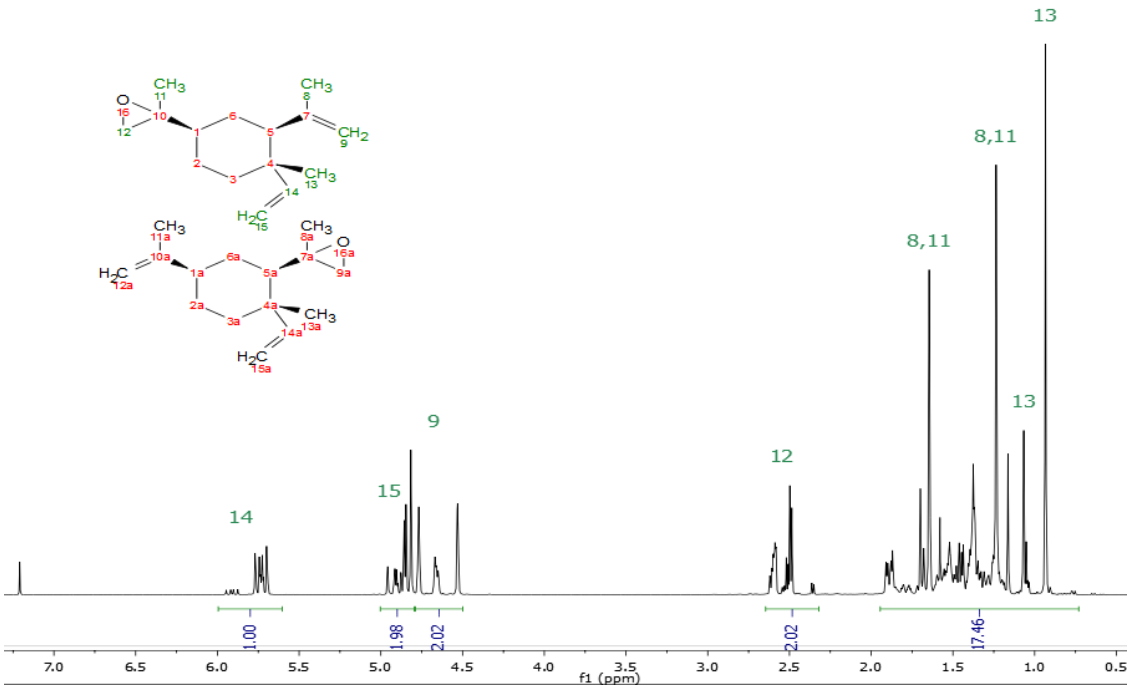

Figure 3.105 ^{1}H NMR spectroscopy of BEMO.

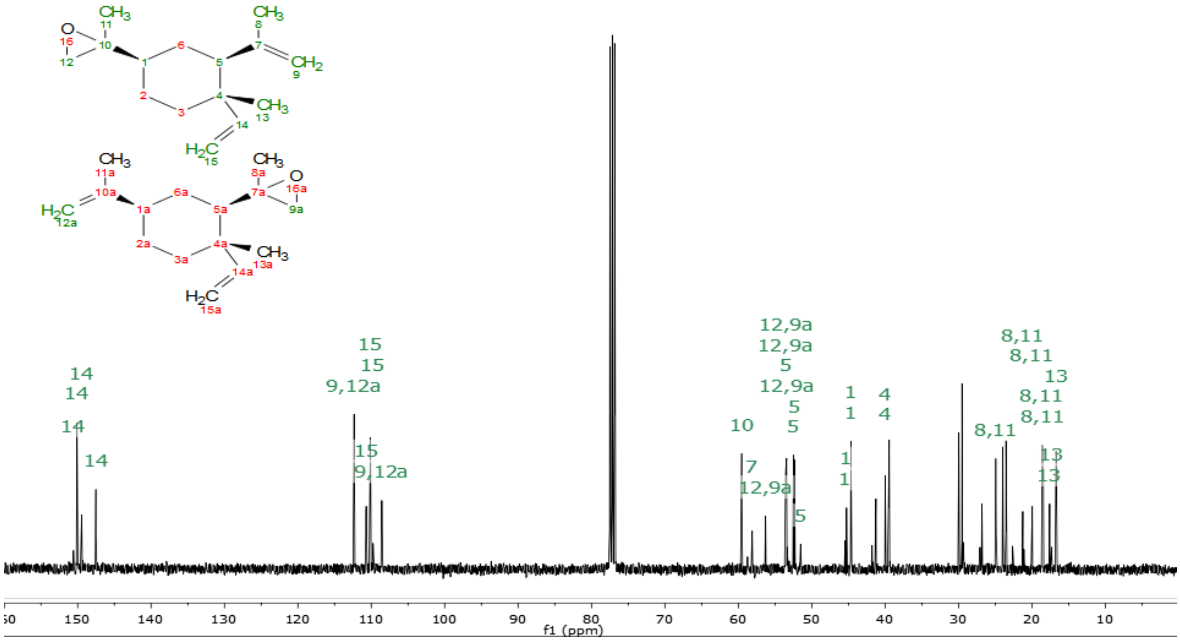

Figure 3.106 $^{13}C\{^{1}H\}$ NMR of BEMO.

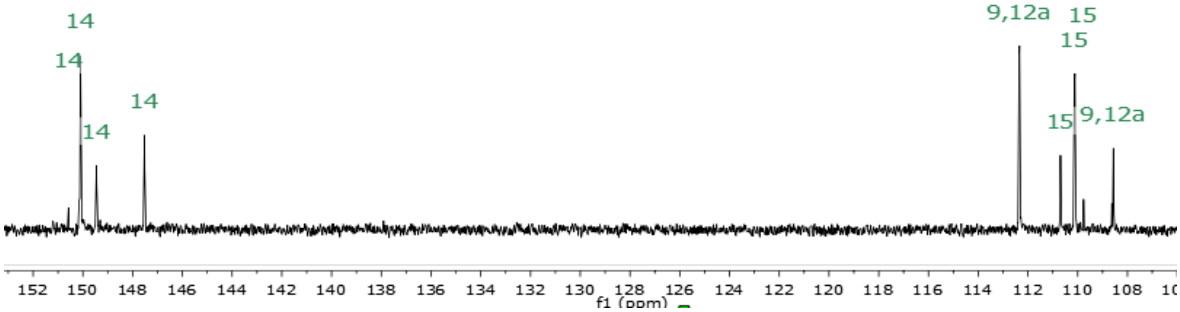

Figure 3.107 $^{13}C\{^{1}H\}$ NMR of BEMO in the region of 152 – 107 ppm.

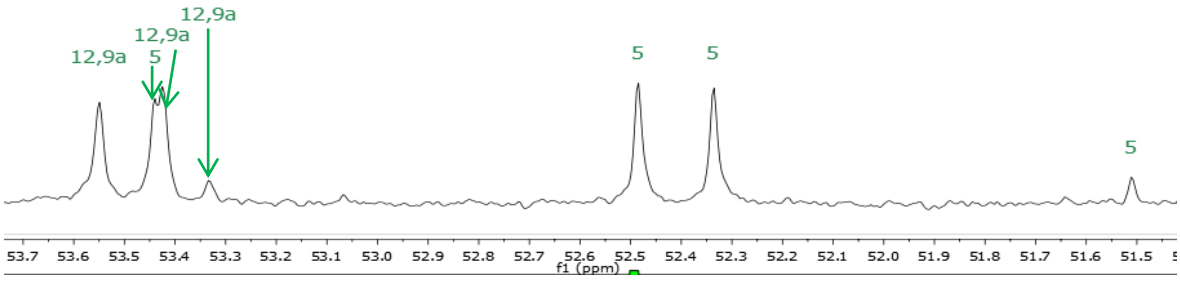

Figure 3.108 $^{13}C\{^{1}H\}$ NMR of BEMO in the region of 53.7 – 51.5 ppm.

β-elemene bisepoxide (BEBO)

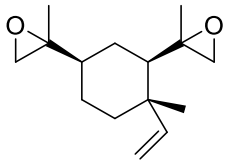

BEBO

^{1}H NMR(400 MHz, $CDCl_3$): δ = 5.74 (m, 1H), 5.05 – 4.85 (m, 2H), 2.73 – 2.33 (m, 4H), 1.86 – 0.98 (m, 17H) ppm

^{13}C{^{1}H} NMR (101 MHz, $CDCl_3$) δ = 150.3, 150.2, 149.2, 149.0, 110.8, 110.8, 109.9, 109.9, 59.4, 59.4, 59.3, 58.6, 58.5, 58.0, 56.3, 56.1, 53.6, 53.4, 53.4, 53.1, 53.0, 52.8, 51.1, 50.9, 44.2, 44.1, 44.1, 43.3, 41.2, 41.2, 40.7, 40.6, 40.0, 39.4, 39.3, 26.5, 26.1, 26.0, 26.0, 24.0, 23.6, 23.5, 23.2, 23.0, 22.4, 20.0, 19.8, 19.3, 18.5, 18.5, 18.4, 17.5, 17.5, 17.3, 17.1.

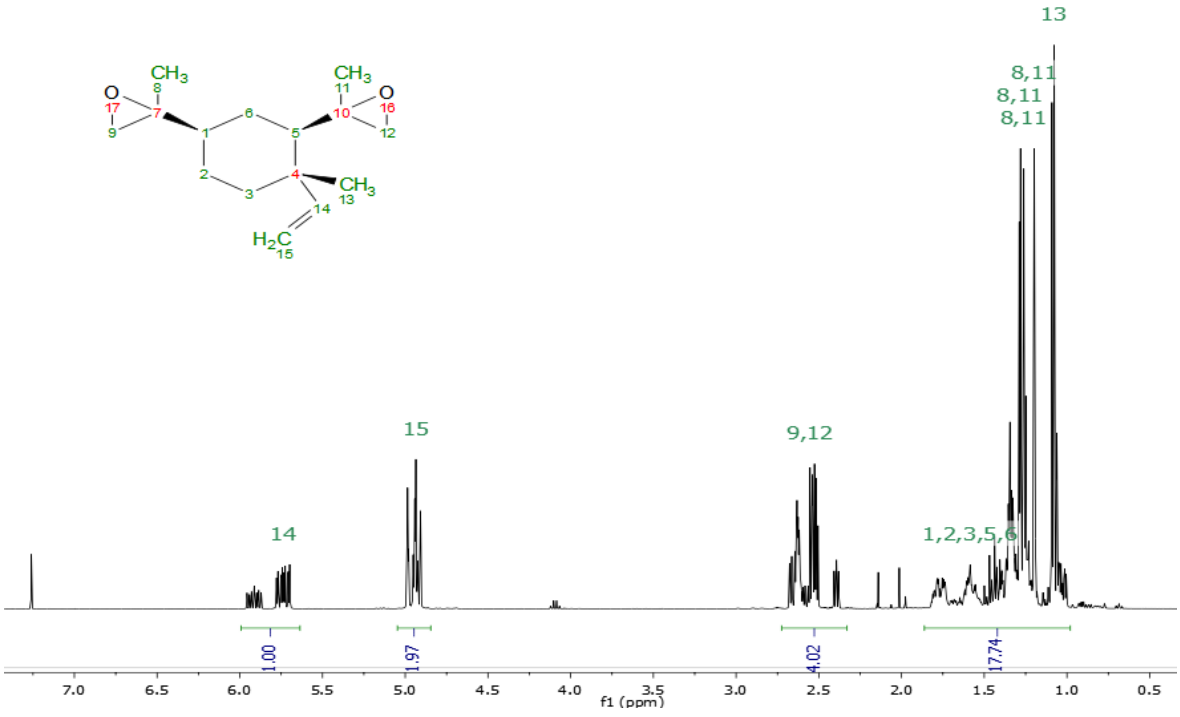

Figure 3.109 ^{1}H NMR spectroscopy of BEBO.

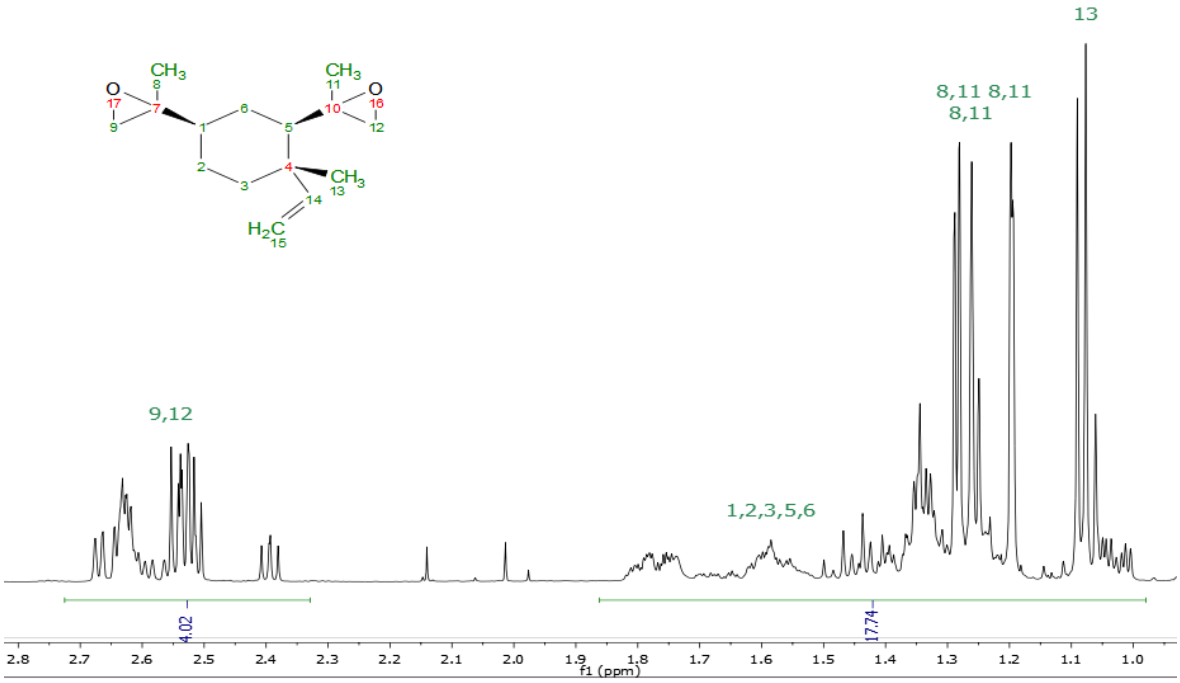

Figure 3.110 ^{1}H NMR spectroscopy of BEBO in the range of 2.8 – 1.0 ppm.

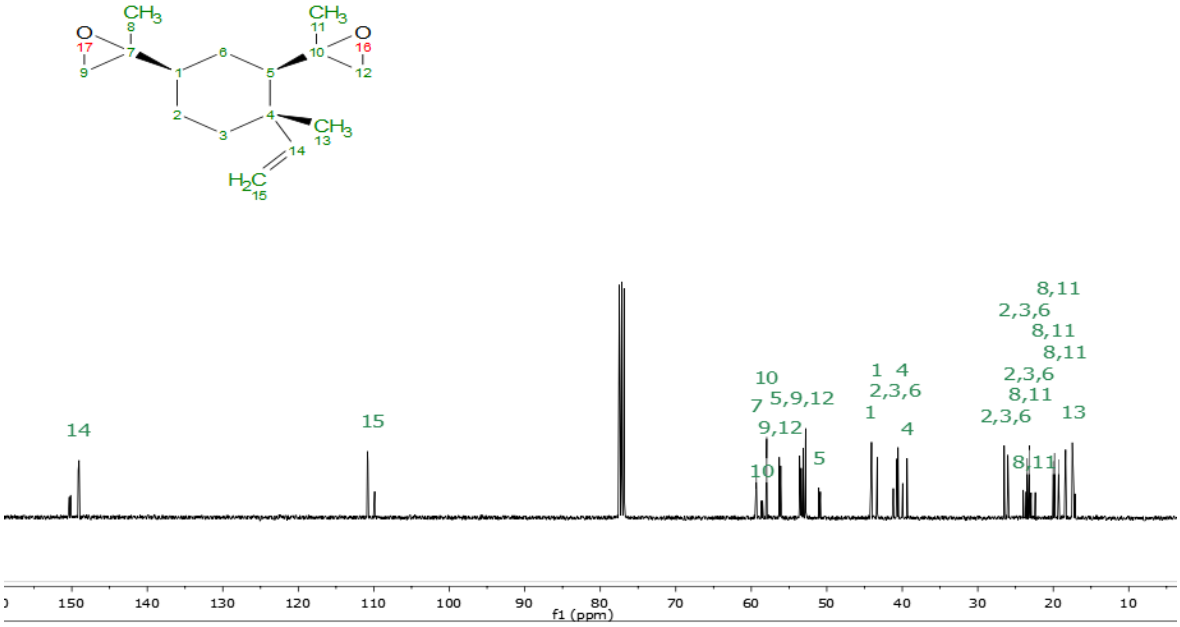

Figure 3.111 ^{13}C{^{1}H} NMR spectroscopy of BEBO.

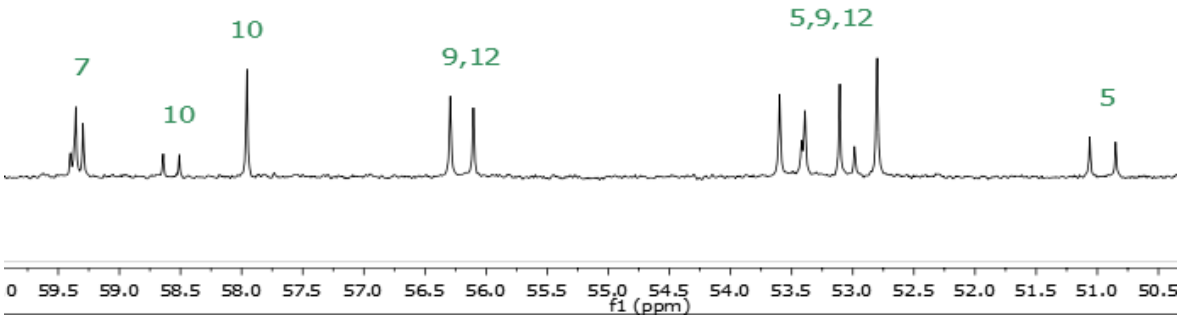

Figure 3.112 $^{13}C\{^{1}H\}$ NMR spectroscopy of BEBO in the range of 60 – 50 ppm.

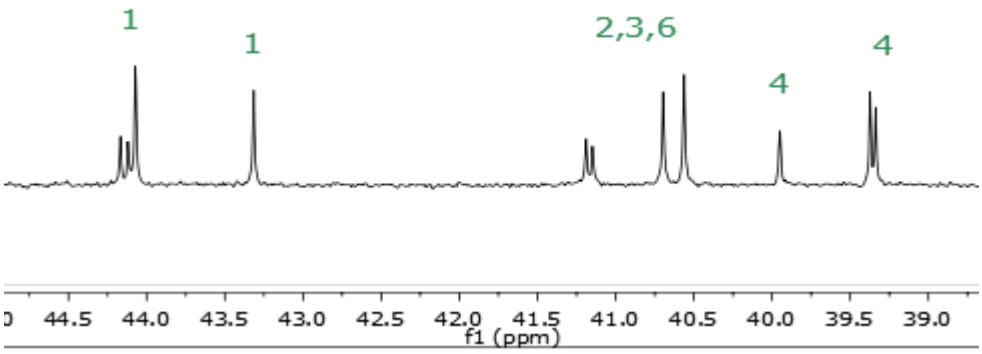

Figure 3.113 $^{13}C\{^{1}H\}$ NMR spectroscopy of BEBO in the range of 45 – 39 ppm.

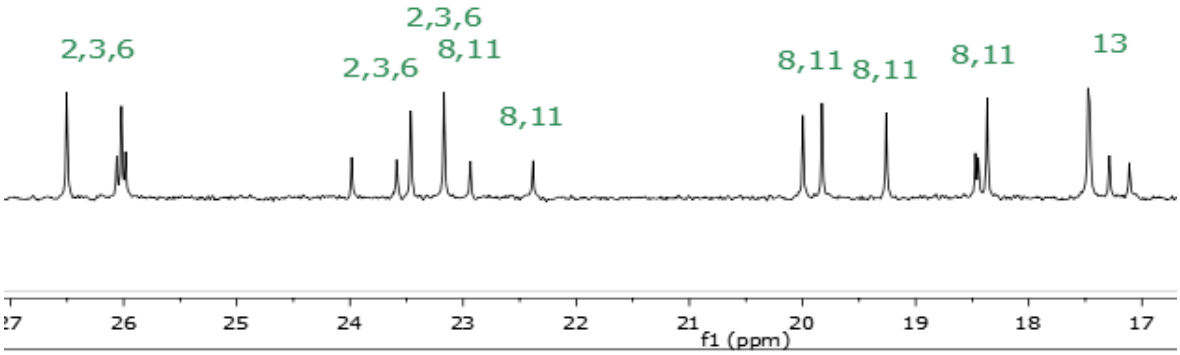

Figure 3.114 $^{13}C\{^{1}H\}$ NMR spectroscopy of BEBO in the range of 27 – 17 ppm.

β-elemene trisepoxide(BETO)

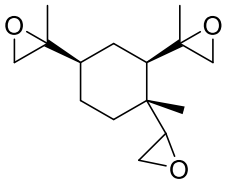

BETO

^{1}H NMR(400 MHz, $CDCl_3$): δ = 2.96 – 2.39 (m, 7H), 1.93 – 1.03 (m, 15H), 0.96 – 0.74 (m, 3H) ppm

$^{13}C\{^{1}H\}$ NMR (101 MHz, $CDCl_3$) δ = 60.1, 60.1, 59.8, 59.4, 59.3, 59.3, 59.3, 59.2, 59.2, 58.1, 58.0, 57.4, 57.3, 56.5, 56.4, 55.5, 55.3, 53.9, 53.7, 53.6, 53.5, 52.9, 52.7, 50.5, 50.2, 44.4, 44.3, 44.1, 43.7, 43.1, 43.1, 42.3, 37.4, 37.3, 36.4, 36.4, 36.2, 36.2, 35.1, 34.9, 26.5, 26.4, 25.9, 23.0, 22.8, 22.7, 22.6, 20.3, 20.1, 19.5, 19.4, 19.3, 18.5, 18.3, 15.2, 15.1, 13.2, 13.1.

MS-ESI^{+}:
Calculated $[M + Na]^{+}$ = 275.1618
Found $[M + Na]^{+}$ = 275.1641

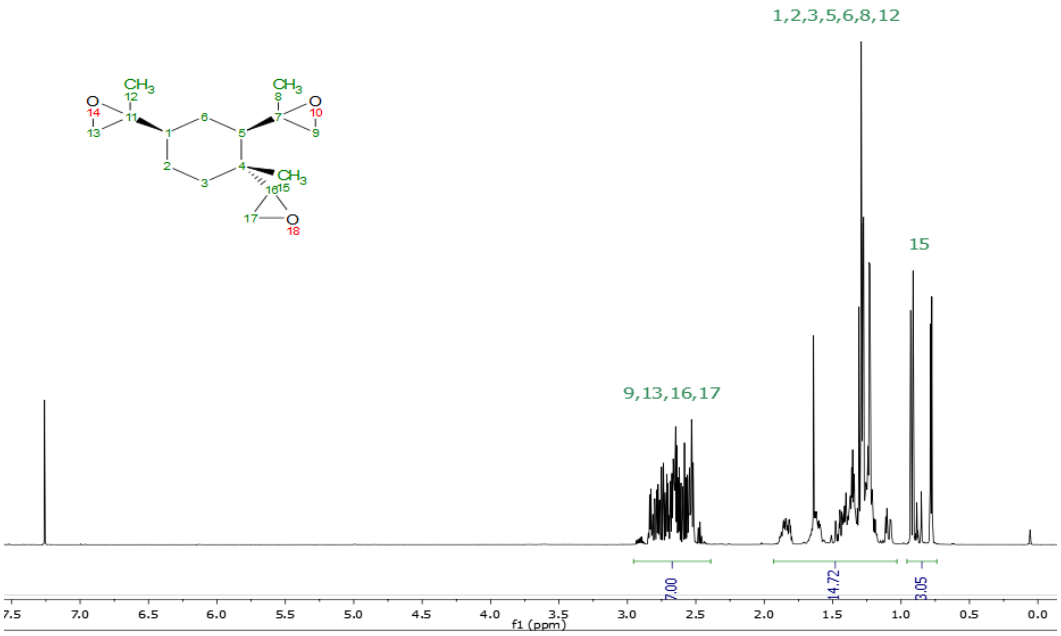

Figure 3.115 ^{1}H NMR spectroscopy of BETO. A signal at 1.64 ppm was assigned to water, no crosspeaks to any carbons were visible on HSQC from this impurity.

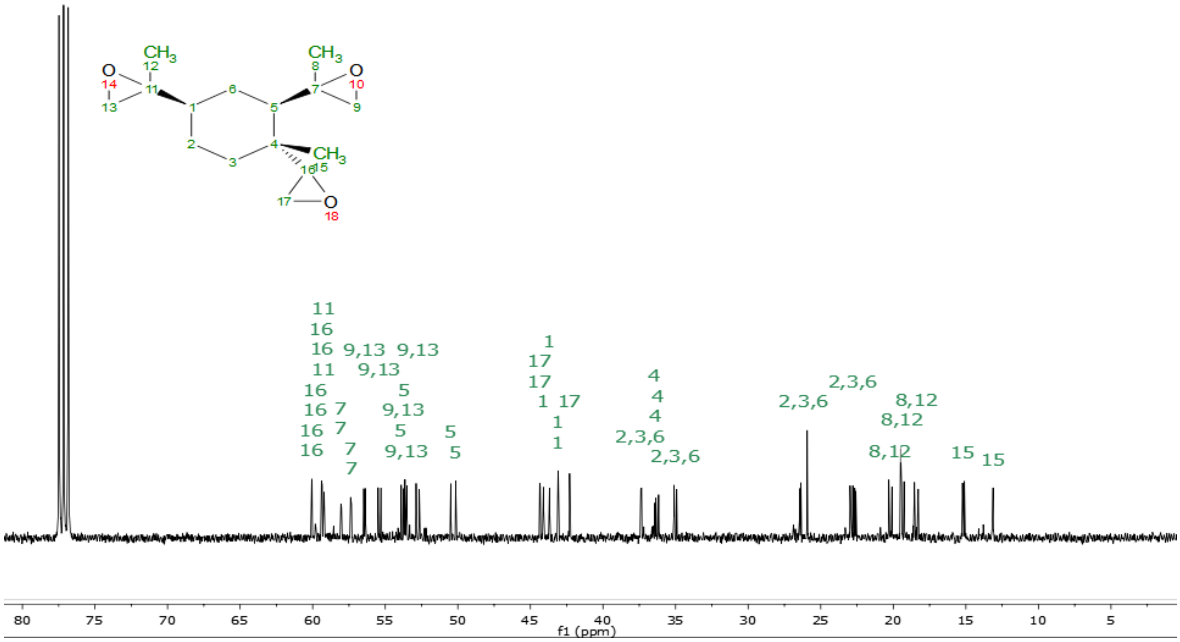

Figure 3.116 $^{13}C\{^{1}H\}$ NMR spectroscopy of BETO.

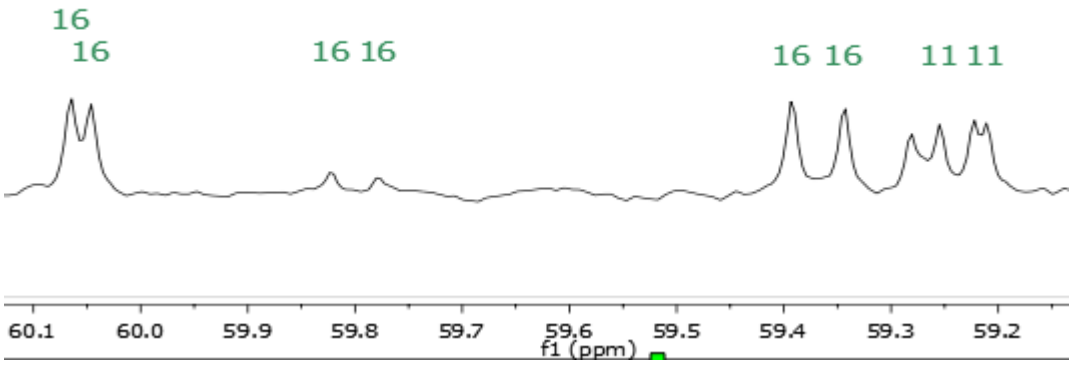

Figure 3.117 $^{13}C\{^{1}H\}$ NMR spectroscopy of BETO in the range of 60.1 – 59.2 ppm.

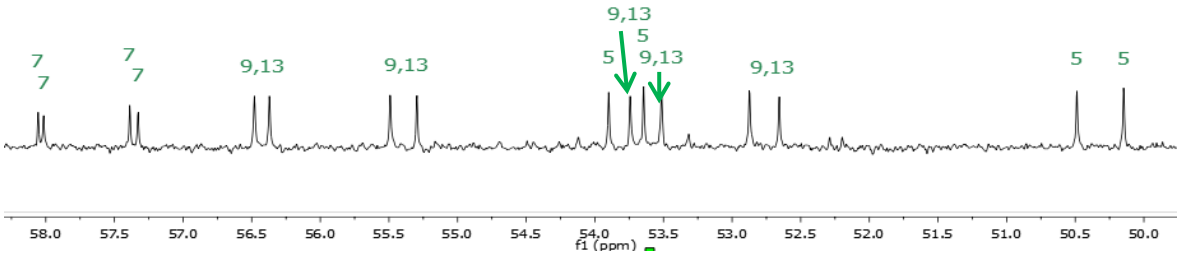

Figure 3.118 $^{13}C\{^{1}H\}$ NMR spectroscopy of BETO in the range of 58 – 50 ppm.

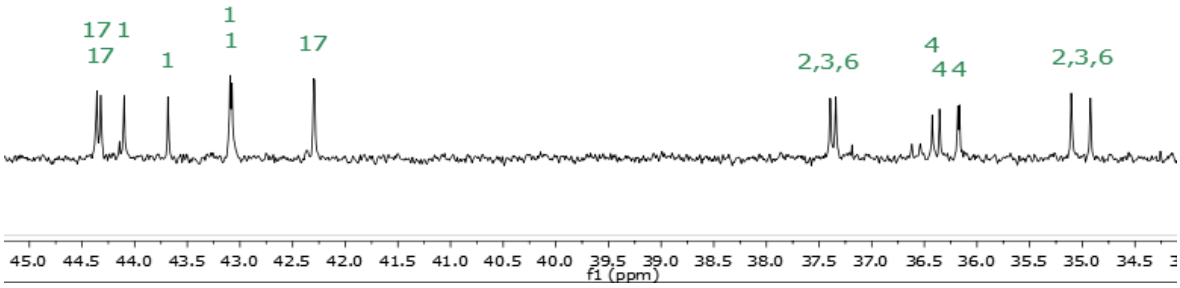

Figure 3.119 $^{13}C\{^{1}H\}$ NMR spectroscopy of BETO in the range of 45 – 34 ppm.

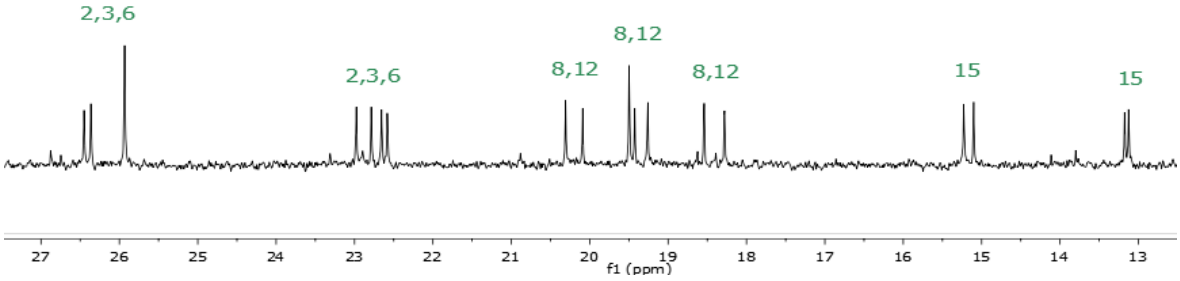

Figure 3.120 $^{13}C\{^{1}H\}$ NMR spectroscopy of BETO in the range of 27 – 13 ppm.

3.5 References

1. S. T. Oyama, in *Mechanisms in Homogeneous and Heterogeneous Epoxidation Catalysis*, ed. S. T. Oyama, Elsevier, Amsterdam, 2008, pp. 3-99.
2. S. A. Hauser, M. Cokoja and F. E. Kühn, *Catal. Sci. Technol.*, 2013, **3**, 552-561.
3. F. Cavani and J. H. Teles, *ChemSusChem*, 2009, **2**, 508-534.
4. J. K. F. Buijink, J. J. M. van Vlaanderen, M. Crocker and F. G. M. Niele, *Catal. Today*, 2004, **93-95**, 199-204.
5. T. A. Nijhuis, M. Makkee, J. A. Moulijn and B. M. Weckhuysen, *Ind. Eng. Chem. Res.*, 2006, **45**, 3447-3459.
6. R. A. Sheldon, *Chem. Commun.*, 2008, 3352-3365.
7. M. Poliakoff and P. Licence, *Nature*, 2007, **450**, 810.
8. I. W. C. E. Arends and R. A. Sheldon, *Top. Catal.*, 2002, **19**, 133-141.
9. L. Rogers and K. F. Jensen, *Green Chem.*, 2019, **21**, 3481-3498.
10. N. Kloye., S. Falß, Manuel Holtkamp, A. Prokofyeva, T. Bieringer, N. Kockmann, in *Handbook of Green Chemistry*, ed. A. A. Lapkin, Wiley-VCH Verlag GmbH & Co. KGaA, 2018, vol. 12, pp. 153-190.
11. S. G. Newman and K. F. Jensen, *Green Chem.*, 2013, **15**, 1456-1472.
12. K. P. Bryliakov, *Chem. Rev.*, 2017, **117**, 11406-11459.
13. S. J. Poland and D. J. Darensbourg, *Green Chem.*, 2017, **19**, 4990-5011.
14. S. M. Danov, O. A. Kazantsev, A. L. Esipovich, A. S. Belousov, A. E. Rogozhin and E. A. Kanakov, *Catal. Sci. Technol.*, 2017, **7**, 3659-3675.
15. K. A. D. Swift, *Top. Catal.*, 2004, **27**, 143-155.

16. Nitrochemie, Oxidation Products, https://www.nitrochemie.com/en/nitrochemie/produkte_und_kompetenzen/oxidationsprodukte/index.php, (accessed 16/11/2019).
17. L. Charbonneau, X. Foster and S. Kaliaguine, *ACS Sustain. Chem. Eng.*, 2018, **6**, 12224-12231.
18. R. A. Sheldon, *Green Chem.*, 2017, **19**, 18-43.
19. R. D. Gaikwad, S. S. Kabiraj and S. V. Bhat, *Flavour Frag. J.*, 2016, **31**, 350-355.
20. S. Sakaguchi, Y. Nishiyama and Y. Ishii, *J. Org. Chem.*, 1996, **61**, 5307-5311.
21. C. Venturello and R. Daloisio, *J. Org. Chem.*, 1988, **53**, 1553-1557.
22. C. Venturello, E. Alneri and M. Ricci, *J. Org. Chem.*, 1983, **48**, 3831-3833.
23. G. D. Yadav and D. V. Satoskar, *J. Am. Oil Chem. Soc.*, 1997, **74**, 397-407.
24. G. Grigoropoulou and J. H. Clark, *Tetrahedron Lett.*, 2006, **47**, 4461-4463.
25. K. Sato, M. Aoki, M. Ogawa, T. Hashimoto and R. Noyori, *J. Org. Chem.*, 1996, **61**, 8310-8311.
26. H. Hachiya, Y. Kon, Y. Ono, K. Takumi, N. Sasagawa, Y. Ezaki and K. Sato, *Synthesis*, 2012, **44**, 1672-1678.
27. A. L. P. de Villa, D. E. De Vos, C. C. de Montes and P. A. Jacobs, *Tetrahedron Lett.*, 1998, **39**, 8521-8524.
28. M. L. C. M. Henckens, P. P. J. Driessen and E. Worrell, *Resour. Conserv. Recy.*, 2014, **93**, 1-8.
29. M. E. Amato, F. P. Ballistreri, A. Pappalardo, G. A. Tomaselli, R. M. Toscano and G. T. Sfrazzetto, *Molecules*, 2013, **18**, 13754-13768.
30. T. Michel, M. Cokoja, V. Sieber and F. E. Kühn, *J. Mol. Catal. A: Chem.*, 2012, **358**, 159-165.
31. R. Saladino, A. Andreoni, V. Neri and C. Crestini, *Tetrahedron*, 2005, **61**, 1069-1075.
32. K. Kamata, K. Sugahara, K. Yonehara, R. Ishimoto and N. Mizuno, *Chem.: Eur. J.*, 2011, **17**, 7549-7559.
33. I. Triandafillidi, D. I. Tzaras and C. G. Kokotos, *ChemCatChem*, 2018, **10**, 2521-2535.
34. D. Limnios and C. G. Kokotos, *J. Org. Chem.*, 2014, **79**, 4270-4276.
35. A. L. Villa de P, B. F. Sels, D. E. De Vos and P. A. Jacobs, *J. Org. Chem.*, 1999, **64**, 7267-7270.
36. R. Barrera Zapata, A. L. Villa and C. Montes de Correa, *Ind. Eng. Chem. Res.*, 2009, **48**, 647-653.
37. R. B. Zapata, A. L. Villa, C. M. de Correa, L. Ricardez-Sandoval and A. Elkamel, *Ind. Eng. Chem. Res.*, 2010, **49**, 8369-8378.
38. R. Barrera Zapata, A. L. Villa and C. Montes de Correa, *Ind. Eng. Chem. Res.*, 2006, **45**, 4589-4596.
39. R. B. Zapata, A. L. Villa, C. M. d. Correa and C. T. Williams, *Appl. Catal. A-Gen.*, 2009, **365**, 42-47.
40. A. d. L. Villa de P, F. Taborda A and C. Montes de Correa, *J. Mol. Catal. A: Chem.*, 2002, **185**, 269-277.
41. R. Ciriminna, F. Parrino, C. De Pasquale, L. Palmisano and M. Pagliaro, *Chem. Commun.*, 2018, **54**, 1008-1011.
42. L. Charbonneau and S. Kaliaguine, *Appl. Catal. A-Gen.*, 2017, **533**, 1-8.
43. A. J. Bonon, Y. N. Kozlov, J. O. Bahú, R. M. Filho, D. Mandelli and G. B. Shul'pin, *J. Catal.*, 2014, **319**, 71-86.
44. M. V. Cagnoli, S. G. Casuscelli, A. M. Alvarez, J. F. Bengoa, N. G. Gallegos, N. M. Samaniego, M. E. Crivello, G. E. Ghione, C. F. Pérez, E. R. Herrero and S. G. Marchetti, *Appl. Catal. A-Gen.*, 2005, **287**, 227-235.
45. M. a. A. Aramendía, V. Borau, C. Jiménez, J. M. Luque, J. M. Marinas, J. R. Ruiz and F. J. Urbano, *Appl. Catal. A- Gen.*, 2001, **216**, 257-265.
46. A. M. Adio, *Tetrahedron*, 2009, **65**, 5145-5159.

47. Isobionics, Natural Beta Elemene, http://www.isobionics.com/index-Beta%20Elemene.html, (accessed 12/04/2019).
48. Z. Jiang, J. A. Jacob, D. S. Loganathachetti, P. Nainangu and B. Chen, *Front. Pharmacol.*, 2017, **8**:105.
49. A. F. Thomas, C. Vial, M. Ozainne and G. Ohloff, *Helv. Chim. Acta*, 1973, **56**, 2270-2279.
50. M. Vezzoli, unpublished work.
51. W. Cunningham, PhD Thesis, University of Bath, 2018.
52. M. Hutchby and W. Cunningham, unpublished work.
53. K. Kamata, K. Yonehara, Y. Nakagawa, K. Uehara and N. Mizuno, *Nature Chem.*, 2010, **2**, 478.
54. K. Yonehara, K. Kamata, K. Yamaguchi and N. Mizuno, *Chem. Commun.*, 2011, **47**, 1692-1694.
55. LTF, Microreactor XXL-ST-04, http://www.ltf-gmbh.com/produkte/xxl_st-04_en.html, (accessed 14/09/2016).
56. M. Makosza, in *Phase-Transfer Catalysis*, American Chemical Society, 1997, vol. 659, ch. 4, pp. 41-51.
57. B. P. Mason, K. E. Price, J. L. Steinbacher, A. R. Bogdan and D. T. McQuade, *Chem. Rev.*, 2007, **107**, 2300-2318.
58. K. Smug, MRes Dissertation, Univeristy of Bath, 2015.
59. D. C. Duncan, R. C. Chambers, E. Hecht and C. L. Hill, *J. Am. Chem. Soc.*, 1995, **117**, 681-691.
60. D. G. Blackmond, *Angew. Chem. Int. Ed.*, 2005, **44**, 4302-4320.
61. P. J. Domaille, in *Inorg. Synth.*, eds. G. Hervéa and A. Téazéa, John Wiley & Sons, Inc., 1990, vol. 27, pp. 96-104.
62. A. M. R. Hall, P. Dong, A. Codina, J. P. Lowe and U. Hintermair, *ACS Catal.*, 2019, **9**, 2079-2090.
63. W. H. Knoth and R. L. Harlow, *J. Am. Chem. Soc.*, 1981, **103**, 1865-1867.
64. P. J. Domaille and R. L. Harlow, *J. Am. Chem. Soc.*, 1986, **108**, 2108-2109.
65. titrations.info, Hydrogen peroxide titration, http://www.titrations.info/permanganate-titration-hydrogen-peroxide, (accessed 26/08/2018).
66. R. M. Carman, J. J. Devoss and K. L. Greenfield, *Aust. J. Chem.*, 1986, **39**, 441.

4. Cyclic carbonates from limonene oxides and β-elemene oxides

This chapter includes introduction, results and experimental sections regarding all cyclic carbonate work done within this project. The introduction details the challenges and opportunities related to cyclic carbonates and non-isocyanate polyhydroxyurethanes (NIPU). The results section is divided into three parts: first,limonene carbonates and their synthesis from limonene using a single catalytic system for both the epoxidation and carbonation reactions; second, novel cyclic carbonates derived from β-elemene – a promising terpene feedstock derived via industrial biotechnology processes; third, attempts to synthesise cyclic carbonates from farnesene and carvone.

4.1 Introduction

Cyclic carbonates can be synthesised through the reaction of carbon dioxide with epoxides[1] or diols[2] using homogeneous or heterogeneous catalysts (Figure 4.1). CO_2 is a greenhouse gas generated in large quantities via fuel combustion and industrial processes, but CO_2 is also an abundant carbon feedstock.[3] Using CO_2 in chemical synthesis has received increasing attention as a supplementary strategy to its geological storage.[4] Epoxides are easily accessible via stoichiometric and catalytic routes that have been described in Chapter 3.

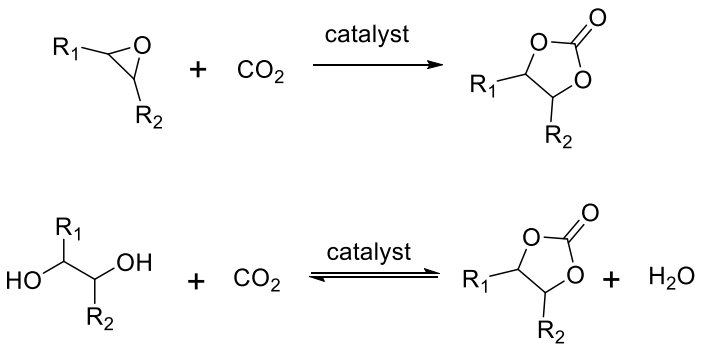

Figure 4.1 Synthesis of 5-membered cyclic carbonates starting from CO2 and epoxides or diols.

4.1.1 Homogeneous catalysts for the synthesis of cyclic carbonates from CO_2 and epoxides

Quaternary ammonium salts are commonly used as homogeneous catalysts in the synthesis of 5-membered cyclic carbonates from CO_2 and epoxides.[5] The main role of quaternary ammonium salt is to open the epoxide to form a bromo-alkoxide, which can react with CO_2 and give a cyclic carbonate product (Figure 4.2).[6]

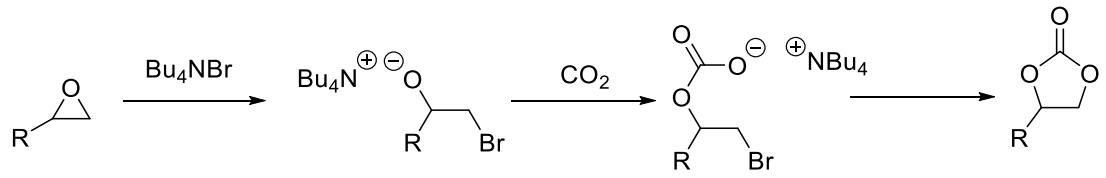

Figure 4.2 Cyclic carbonates formation using quaternary ammonium salt Bu4NBr as catalyst.[6]

However, other homogeneous catalysts can be used, for example metal halides, ionic liquids, polyoxometalates, salen complexes, salphen complexes or others.[3, 7] Lewis acid catalysts (for example metal salen or salphen complexes) are often used in combination with an additional halide source. Lewis acids can preactivate the epoxide resulting in milder reaction conditions (Figure 4.3).[3] On the other hand, polyoxometalates can be considered as a Lewis acidic catalyst, but the reaction mechanism proposed for cyclic carbonates synthesis catalysed by polyoxometalates postulates the double activation of monomers (Figure 4.4).[8, 9] It has been postulated that transition metal polyoxometalates can coordinate CO_2[10, 11] and the combination of a quaternary ammonium salt and polyoxometalates shows synergistic effect on cyclic carbonate synthesis.[8]

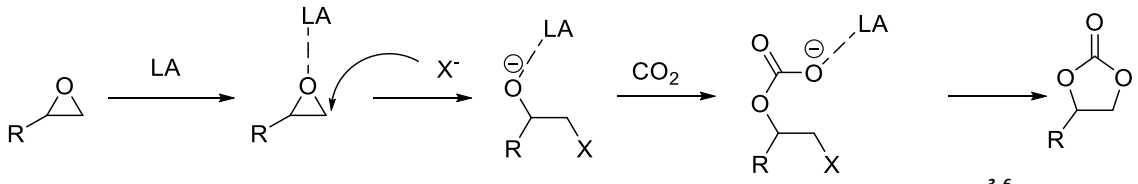

Figure 4.3 Combination of Lewis acid (LA) and halide (X-) catalyst in the cyclic carbonates synthesis.[3, 6]

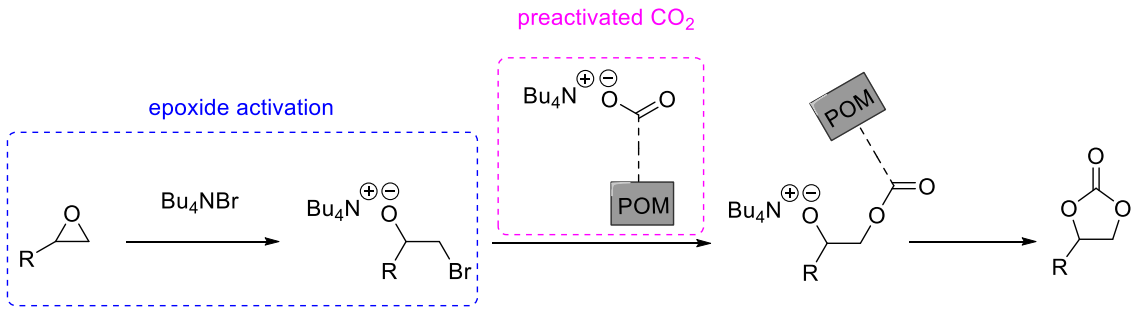

Figure 4.4 Dobuble activation of epoxide and CO2 via quaternary ammonium salt and polyoxometalate.[8, 9]

Yasuda *et al.* have reported the reactivity of a catalyst consisting of a quaternary ammonium salt cation and a polyoxometalate anion $[\alpha\text{-}SiW_{11}O_{39}Mn]^{6-}$ in the synthesis of propylene carbonate from propylene oxide.[9] They found that different substitution of the transition metal in the polyoxometalate and the length of the chain of the quaternary ammonium salt cation has a significant effect on the activity. Tetraheptylammonium cation $[(n\text{-}C_7H_{15})_4N]^+$ was 4 times more active than tetrabutylammonium cation $[(n\text{-}C_4H_9)_4N]^+$, retaining high selectivity towards cyclic carbonates. Moreover, the quaternary ammonium salt of polyoxometalate $[(n\text{-}C_7H_{15})_4N]_6[\alpha\text{-}SiW_{11}O_{39}Mn]$ was 8 times more active than tetraheptylammonium bromide $(n\text{-}C_7H_{15})_4NBr$.

Leitner *et al.* differ to Yasuda *et al.* as the former report a combined catalytic system comprised of a quaternary ammonium salt cation, a polyoxometalate anion and a quaternary ammonium bromide, such as Bu_4NBr, as a co-catalyst.[8] They found that the bromide and polyoxometalate catalysts have different functions in the mechanism of the cyclic carbonate synthesis. The bromide preactivates the epoxide by creating bromo-alkoxide and polyoxometalate coordinates to CO_2, thus combining these two catalysts can yield more carbonates and make the reaction stereoselective (see Figure 4.4).[8]

The catalytic systems mentioned above require high pressure (above 30 bar CO_2) and high temperature (above 120 °C). North *et al.* have reported aluminium(salen) complexes and aluminium(salphen) complexes which can operate at room temperature and low pressure, yielding cyclic carbonates from terminal epoxides.[12, 13] These aluminium complexes (Figure 4.5) operate with tetrabutylammonium bromide as a co-catalyst.

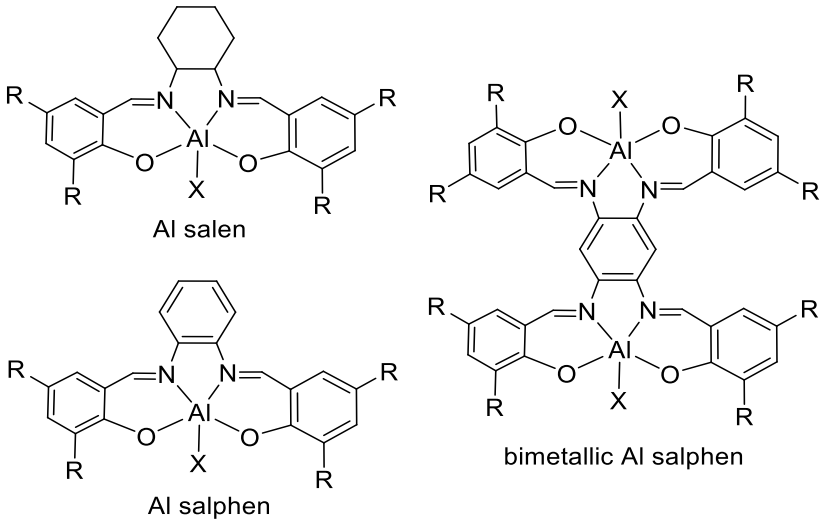

Figure 4.5 The general structure of Al(salen) complexes[12, 13] R=tert butyl, X=Cl, acetate or tosyl.

Another class of catalysts which can operate at lower temperature and lower CO_2 pressure are aluminium amino-tris(phenolate)s.[14] Aluminium amino-tris(phenolate)s require use of a solvent and nucleophilic co-catalyst. Kleij *et al.* reported the synthesis of cyclic carbonates using aluminium amino-tris(phenolate) with different aryl substituents. The most effective catalysts had methyl and t-butyl groups, but other groups were tested as well (Figure 4.6).

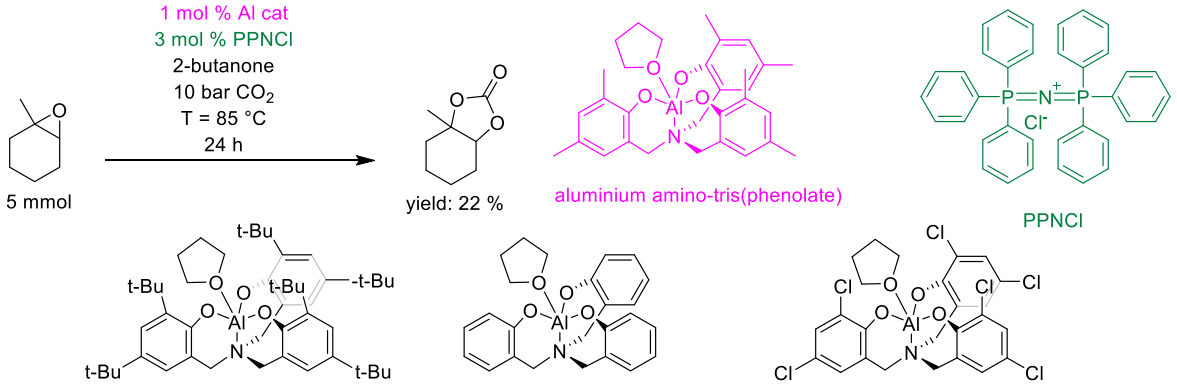

Figure 4.6 Cyclic carbonates synthesis catalysed by aluminium amino-tris(phenolate).[14]

4.1.2 Industrially important cyclic carbonates and polyurethanes

Currently, the industrially favoured cyclic carbonates are ethylene carbonate and propylene carbonate. They can be used as organic solvents, electrolyte solvents for lithium ion batteries, and monomers for the production of polycarbonates and polyurethanes.[1]

Polyurethanes are used as adhesives, coatings, sealants, rigid and flexible foams, textile fibres and in various medical applications.[15] In 2016 the sales volume of polyurethanes in the United Kingdom reached over 136 000 tonnes and it is predicted to grow.[16] Polyurethanes are typically synthesised by the polyaddition between a polyol and polyisocyanate (Figure 4.7).[17] Current polyurethane research is focused on replacing monomers with bio-derived alternatives and making the synthesis safer.[17] The safety concerns arise from the use of isocyanates which are a toxic and volatile substance produced via phosgenation of diamines – isocyanates are a direct health risk for industrial process operators.[17] The use of cyclic carbonates allows the synthesis of non-isocyanate polyhydroxyurethanes, which can be an alternative, safer solution to the conventional polyurethane synthesis.[17]

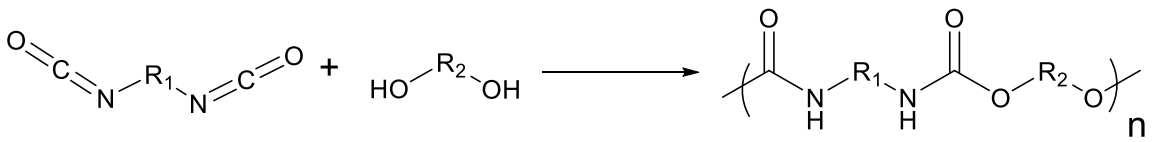

Figure 4.7 Synthesis of polyurethanes from polyol and polyisocyanate.

4.1.3 Non-isocyanate polyhydroxyurethanes (NIPU), their synthesis and applications

Non-isocyanate polyhydroxyurethanes (NIPU) are synthesised by polyaddition of bicyclic or multifunctional carbonates to di- or polyfunctional diamines (Figure 4.8). The reaction favours the formation of secondary hydroxyl groups.[17] Depending on reactants, NIPU can be classified as linear NIPU (from bicyclic carbonates and diamines) or hybrid networks (from multifunctional carbonates and amines).[17] The main challenges with NIPU synthesis are the low reactivity of carbonates during aminolysis and low molecular weight of resultant polymers.[18]

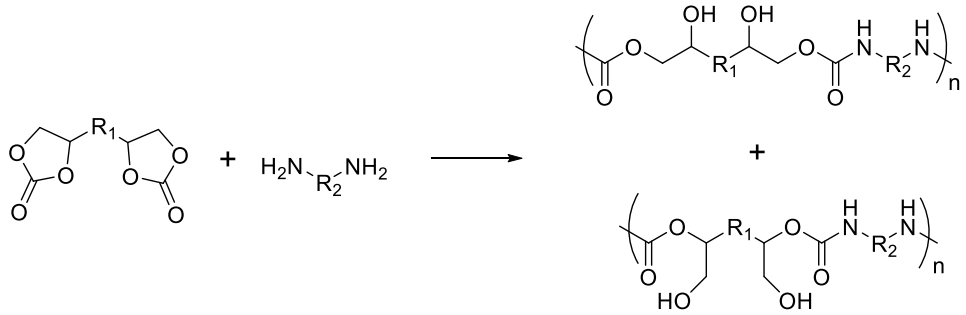

Figure 4.8 Non-isocyanate polyhydroxyurethanes synthesis from bicyclic carbonate and diamine.

The reaction conditions can strongly affect conversion and the properties of the resultant polymers. Polyaddition of bicyclic carbonates and diamines can proceed with no catalyst at room temperature, but it is generally slow.[19] Elevating the temperature (to about 100 °C) and extending reaction times (24 h or more) can increase the rate of the reaction, however, it is worth noting that too high temperature can cause decrease of selectivity due to side reactions.[20]

Usually, aminolysis of 5-membered cyclic carbonates is conducted at elevated temperatures. The barriers to high conversion are high viscosity and changes in stoichiometry due to side reactions.[21] Viscosity increases during polymerisation, limiting diffusion of monomers, which can inhibit achieving high conversion and prevent high molecular weights. Side reactions causing changes in stoichiometry include amine carbonation, and formation of CO_2 and urea (Figure 4.9).[21]

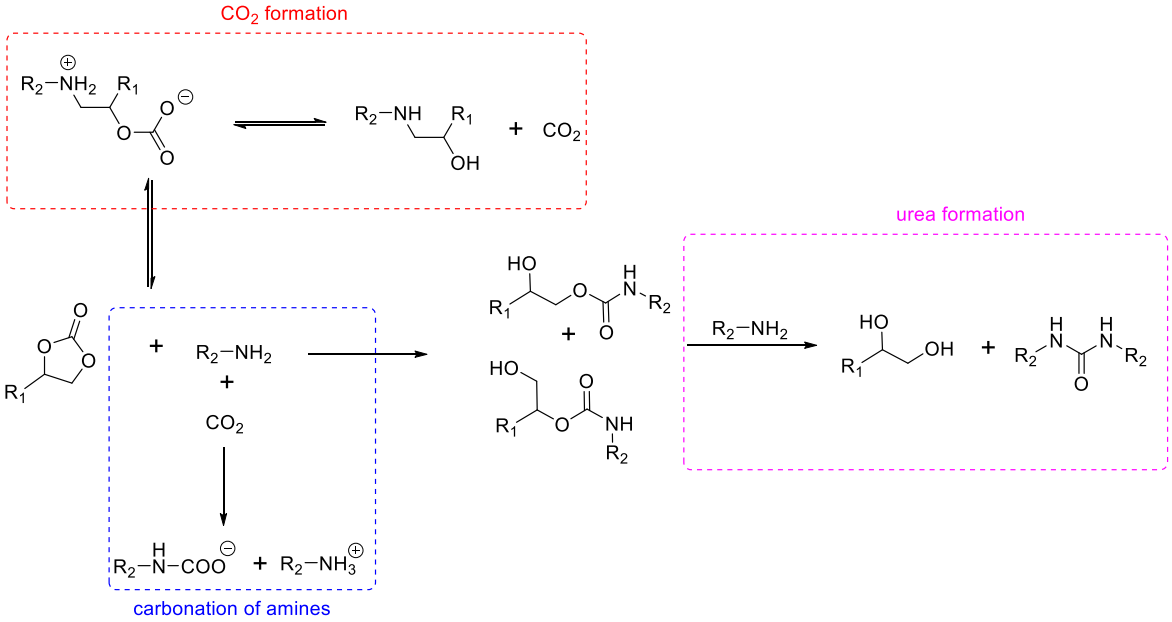

Figure 4.9 Side reactions affecting stoichiometry of reagents.[21]

Changes in amine concentration can cause changes in stoichiometry, resulting in lower molecular weights of polymers. Figure 4.10 presents the possible degree of polymerisation calculated from the extent of reaction using Carothers' equation (Carothers equation for two monomers of functionality not greater than two in equimolar ratio Equation 4.1).[18, 22] The degree of polymerisation is equal to the number of monomer units in a polymer molecule. In the case of NIPU it is the overall number of carbonate units and amine units. For example, for an extent of reaction equal to 90 % the degree of polymerisation is equal to 10, which consist of 5 carbonate units and 5 amine units.

$$\overline{DP_n} = \frac{1}{1-P} \tag{4.1}$$

where:

$\overline{DP_n} - degree\ of polymerisation$

$P - \ extent\ of\ reaction$

$$P = \frac{N_0 - N}{N_0} \tag{4.2}$$

where:

$N_0 - initial\ number\ of\ monomer\ units$

$N - number\ of\ molecules\ after\ time\ t\ (includes\ monomers, oligomers\ and\ polymers)$

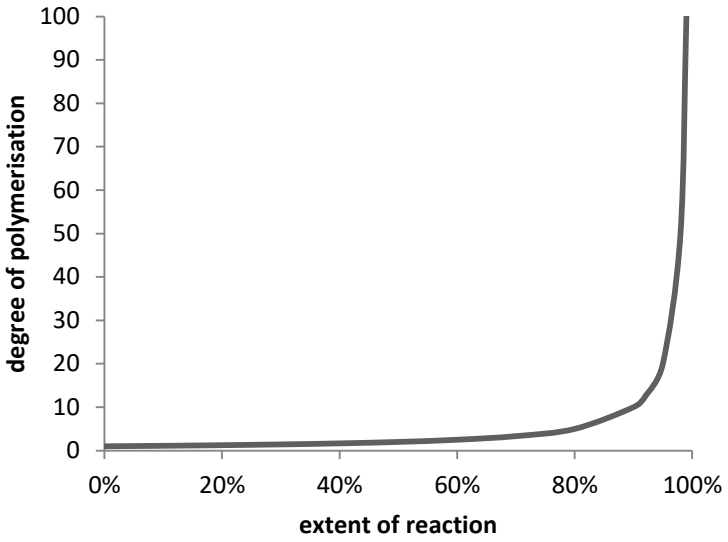

Figure 4.10 Degree of polymerisation calculated from Carothers' equation.

Additionally, it has been postulated that low molecular masses can be explained by the presence of strong hydrogen bonds (Figure 4.11).[18] NIPU, unlike conventional PU, contain hydroxyl functionalization in the polymer chain, which results in more hydrogen bonding in NIPU than PU. Furthermore, hydrogen bonding in NIPU can be a reason for gelation of the system.[18] Protic additives (like protic solvents and plasticisers) can help recover chain mobility by competing with intra- and inter-chain hydrogen bonds (Figure 4.11). Moreover, protic additives increase positive charge on carbonyl carbon and can facilitate aminolysis of cyclic carbonates.[18, 19]

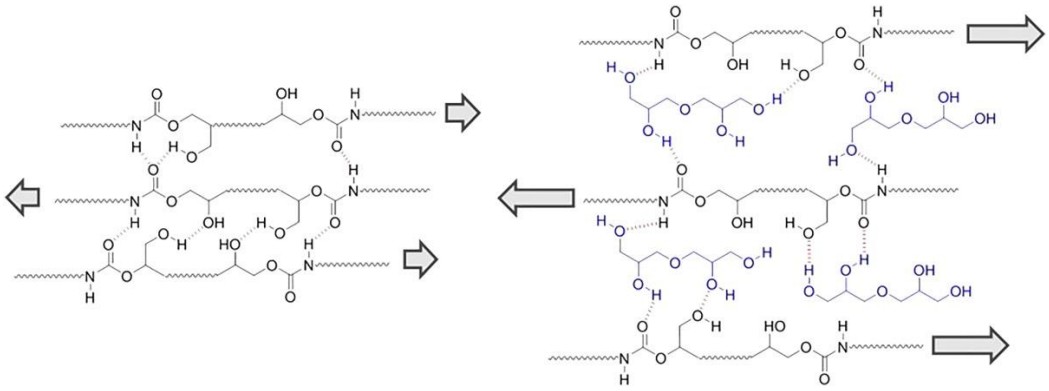

Figure 4.11 The effect of adding plasticiser to NIPU (picture reproduced, with permission, from Blain et al. [18]).

It has been postulated that reaction between cyclic carbonates and amines can be catalysed by various inorganic Lewis acids and organocatalysts.[19] Theoretically, inorganic Lewis acids should increase the electrophilicity of cyclic carbonate.[20] A variety of inorganic Lewis acids have been tested, including halide metal salts such as $MgBr_2$, $FeCl_3$, LiCl, LiF; quaternary ammonium salts such as Bu_4NCl and trifluoromethanesulfonate salts such as $Yb(OTf)_3$, $Fe(OTf)_3$ and $Bi(OTf)_3$.[19, 20] All of them increase carbonate conversion, and moderate Lewis acids (for example LiF and LiCl)

activate the carbonyl group resulting in higher molecular weight polymers.[20] Stronger Lewis acids, for example $CaCl_2$, can affect basicity of the amino group resulting in lower conversion.[20] Basic additives can theoretically increase nucleophilicity of amines, but basic additives such as CaH_2 and K_2CO_3 resulted in lower molecular weight polymers while maintaining high carbonate conversion suggesting hydrolysis of the carbonate ring.[20] However, inorganic metal salts often cause undesired colour changes and turbidity, thus organocatalysts present an attractive alternative.[19]

The organocatalysts tested in aminolysis of cyclic carbonates include phosphines, nitrogen containing bases, phosphazenes and thioureas.[19] In the reaction presented in Figure 4.12 phosphines provided poor results, conversion was no different than in the uncatalysed reaction. Phosphazenes showed some rate enhancement, but conversion was just slightly higher than the uncatalysed reaction. Nitrogen containing bases and thioureas performed the best, and among them TBD provided the highest conversion.[19] The high activity of TBD can be explained by its bifunctional activity; it can activate carbonate and amine.[23] Thioureas generally show lower performance than TBD,[23] but at the conditions presented on Figure 4.12 they showed similar activity to TBD.[19] In the reaction presented on Figure 4.12, none of the tested catalysts significantly influenced regioselectivity of products.[19]

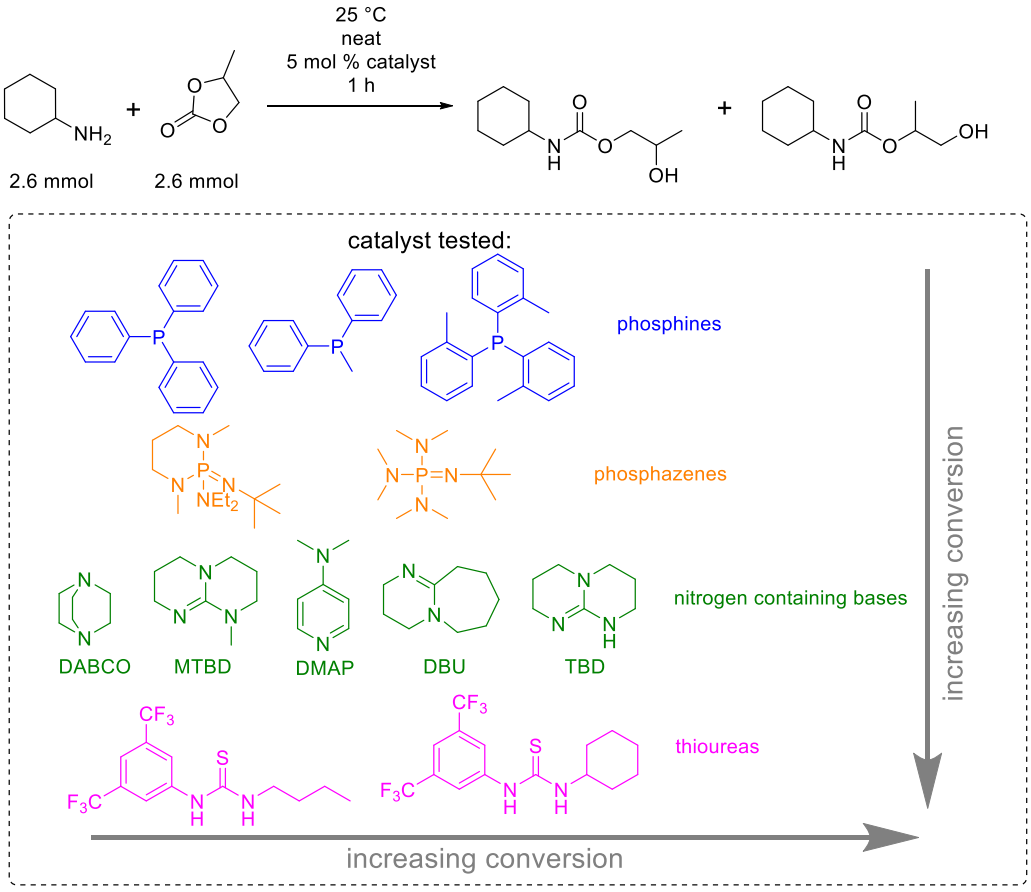

Figure 4.12 Organocatalysts tested by Blain et al. [19]

Most conventional polyurethane synthesis is carried out neat, thus many NIPU syntheses are also reported neat. There are some reports including solvents, and the most commonly used solvents are DMSO, THF, DMF, MeOH.[17, 19, 24] It has been postulated that the polarity of the solvent can influence the reaction kinetics by increasing the positive charge on the carbonyl carbon. The increase of positive charge is attributed to hydrogen bonding between solvent molecules and oxygen atoms in cyclic carbonate.[21] An example of solvent effects on aminolysis of cyclic carbonates is presented in Figure 4.13, where methanol shows superior performance.

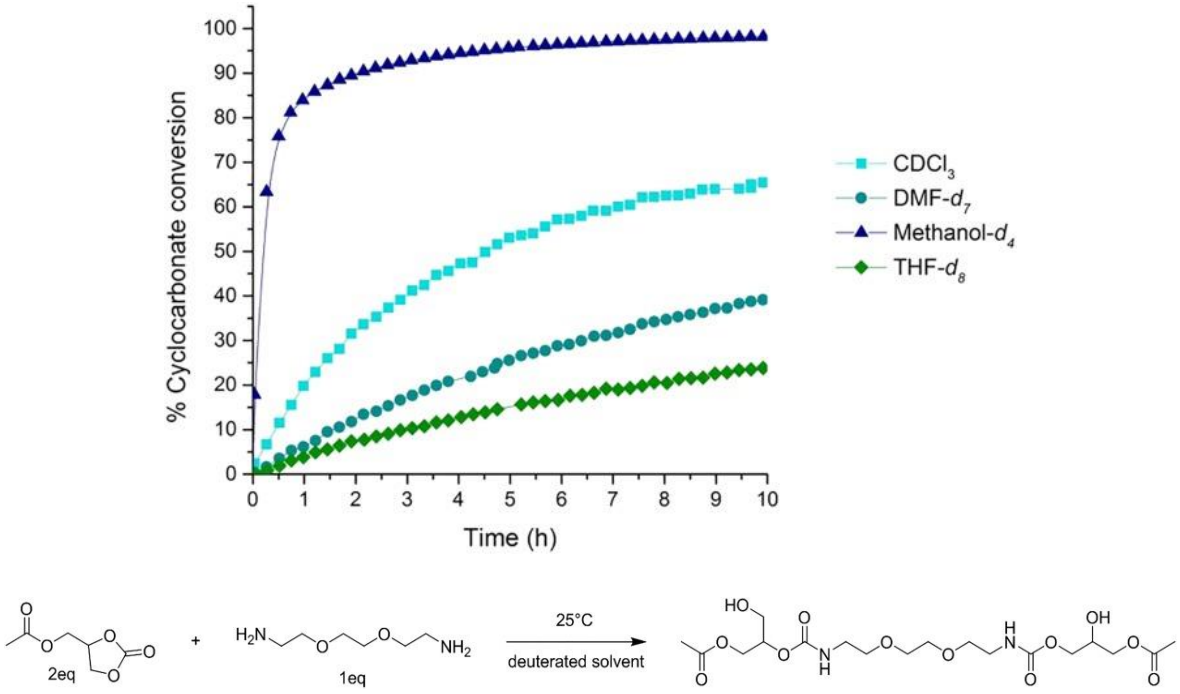

Figure 4.13 Solvent effect on cyclic carbonate aminolysis studied by Blain et al.[18] Figure and reaction scheme reproduced, with permission, from Blain et al.[18]

In addition to reaction conditions, the structure of the cyclic carbonate has a crucial role in the rate of reaction. In general, 5-membered cyclic carbonates are less reactive than 6- or 7-membered cyclic carbonates. This is attributed to differences in ring strain, since the ring strain energy is the lowest for 5-membered cyclic carbonates.[21, 24] The substituents of cyclic carbonates also affect their reactivity, with the effect depending on the type of substituent, its position and steric hindrance.[21, 24] Cyclic carbonates with ester substituents undergo reaction more quickly than ether substituents and ether substituents are more reactive than alkyl substituents.[21, 24] However, ester functionalization on cyclic carbonates can lead to decrease of the molecular weight of the resulting polymer due to side reactions between ester groups and amines.[21] In general, electron withdrawing substituents increase the electrophilicity of the carbonyl group, thus carbonates with electron withdrawing groups close to the carbonyl group will be more reactive with amines (Figure 4.14).[25, 26] Since the electronic

effect of substituents reduces with the distance between substituents and carbonyl group, the hydrogen bonding between substituents and amines might be another explanation for changing cyclic carbonate reactivity.[24]

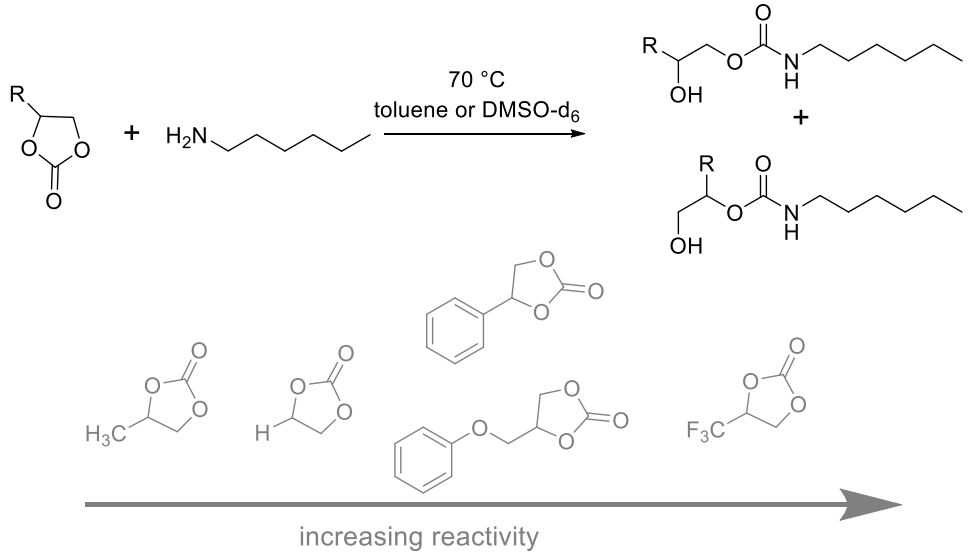

Figure 4.14 Increasing reactivity of cyclic carbonates depending on substituents.[26]

The choice of amine can strongly affect not only the properties of the resultant NIPU, but also conversion. Conversion is the highest for the least hindered and most nucleophilic amines, such as butyl amine and cyclohexylmethyl amine. The sterically demanding amines such as cyclohexyl amine react slower (Figure 4.15).[19] Example of properties, which can be affected by the choice of amine, are hardness and tensile strength. The highest hardness and tensile strength occur for short chain diamines and the lowest for diamines with longer chains. This is due to differences in cross-linking density and hydrogen bonding.[27]

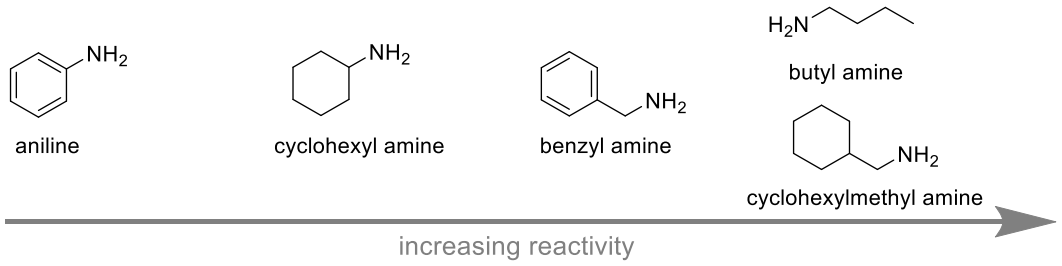

Figure 4.15 Reactivity of amines in aminolysis of cyclic carbonates based on results published in Ref [19].

The lack of control over regioselectivity of ring opening with amines contributes to difficulties in controlling NIPU properties. Due to the complicated mixture of isomers obtained as a result of poor regioselectivity, NIPU often are amorphous.[28] The strategies for controlling regioselectivity are still limited, but one possibility could be using bulky amines and substituted cyclic carbonates in the presence of an organocatalyst (Figure 4.16).[29] This procedure was also tested for terpene-derived carbonates (Figure 4.17).[29]

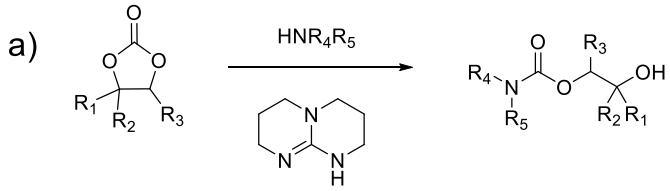

amine	Conv. [%]	I [%]	II [%]
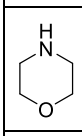	>99	<1	>99
	>99	<1	>99
	>99	<1	>99

Figure 4.16 TBD catalysed cyclic carbonate ring opening a) general reaction scheme b) the reported example along with the table with results for tested amines[29]
The catalyst (TBD) free reactions yielded mixturse of isomer I and isomer II in ratios of approximately 60:40 respectively. The catalyst free reaction with pyrrolidine showed slightly different ratio of isomer I: isomer II 46:54

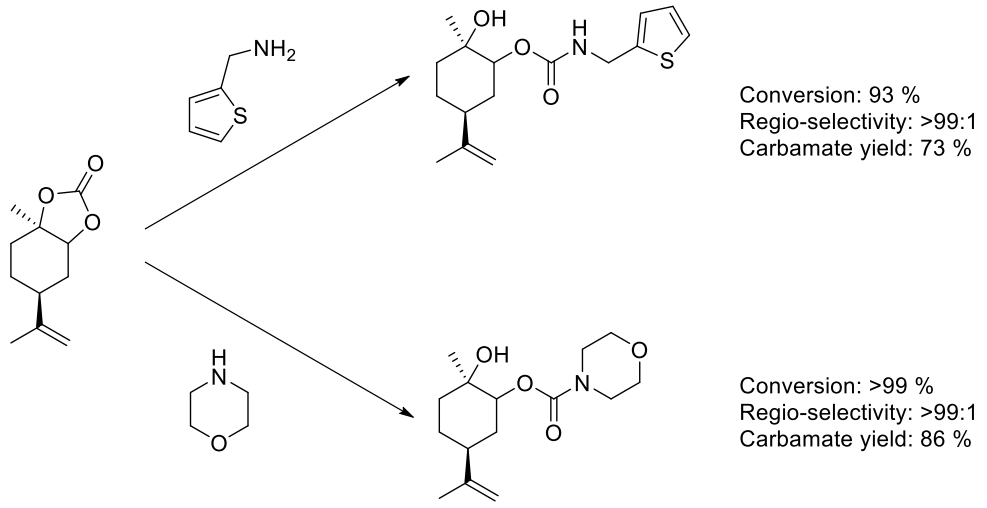

Reaction conditions: 0.5 mmol carbonate, 1 mmol amine, 20 mol % TBD, neat, room temperature, 18 h

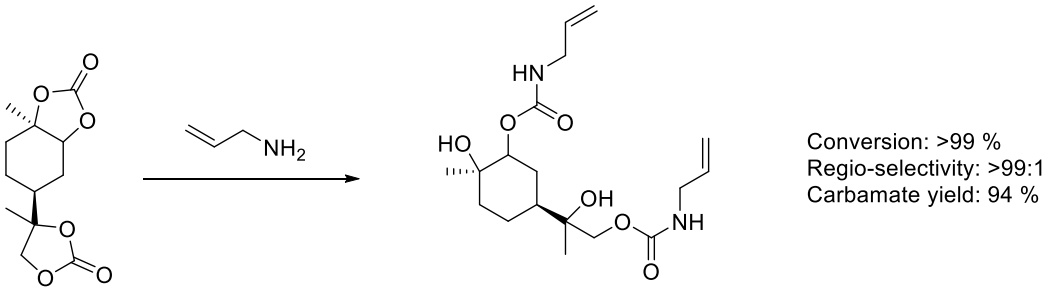

Reaction conditions: 0.5 mmol carbonate, 2 mmol amine, 20 mol % TBD, neat, room temperature, 18 h

Figure 4.17 Regio-selective ring opening examples of terpene-derived cyclic carbonates.[29]

NIPU can replace PU in many current applications, such as coatings, foams, adhesives and sealants; reviews on this topic are widely available.[4, 17, 21, 27, 30] NIPU can achieve lower porosity, lower water absorption, enhanced abrasive resistance, and improved thermal and chemical resistance compared to conventional polyurethanes.[27, 30] Moreover, NIPU coatings exhibit low volatile organic compound levels, which is of interest for industry due to stricter safety regulations.[30, 31] However, the curing process for NIPU coatings usually requires elevated temperature due to slow reaction rates between cyclic carbonates and amines, which may limit their uses in room temperature applications.[27] Furthermore, NIPU's water and chemical resistance allow them to be used as sealants for protection of electronic devices, aircraft components and as glues compatible with wide range of materials.[27] Foaming of NIPU was initially challenging due to the lack of gas released during the synthesis. The proposed foaming strategies use blowing agents such as poly(methylhydrogenosiloxane).[28] Despite a lot of promising properties, NIPU often are yellow or can change colour to yellow when exposed to UV which limits their uses in transparent coatings.[27, 30]

Biodegradation studies of NIPU are very limited.[28] Biodegradation of conventional polyurethanes has been studied and, in some cases, they can be degraded by fungi, bacteria and enzymes.[32, 33] The presence of urethane and ester linkages allows enzymes, such as ureases and esterases, to degrade the polymer. Polyurethanes with ether linkages proved to be difficult to degrade due to ether linkages being inaccessible for enzymes.[32] Biodegradation can occur only if the active site of the enzyme can access the relevant chemical bond. The overall biodegradability will depend on polymer structure, the level of cross-linking, molecular weight and hydrophobicity.[28] Moreover, it is still more economically viable to dispose of polyurethanes rather than to recycle them.[28]

4.1.4 Terpene-derived cyclic carbonates

The first example of terpene derived cyclic carbonates was limonene biscarbonate which was synthesised from limonene bisepoxide and CO_2 catalysed by a quaternary ammonium salt.[34] The synthesised limonene biscarbonate was used for NIPU synthesis (Figure 4.18), the work was further continued to develop NIPU coatings based on limonene biscarbonate and pentaerythritol glycidyl ether.[35]

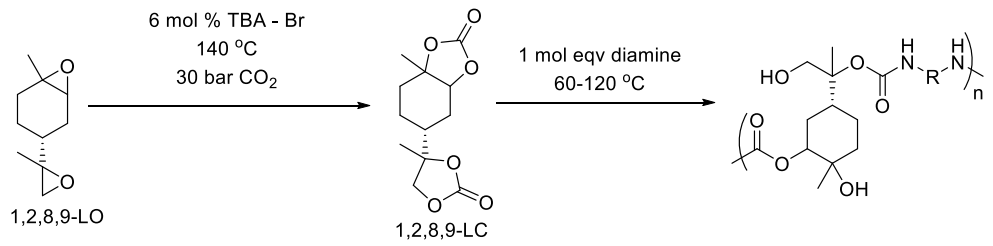

Figure 4.18 The synthesis of linear NIPUs from limonene bisepoxide.[34]

Since then, more examples of terpene derived carbonates have been published (Figure 4.19).[14] Kleij *et al.* investigated coupling of CO_2 and terpene epoxides using aluminium amino-tris(phenolate) as catalyst. A combination of Lewis acidic aluminium amino-tris(phenolate) and nucleophilic PPNCl allowed reduction of reaction temperature and pressure comparing to using only a quaternary ammonium salt as a catalyst. The highly substituted terpene epoxides present a particular challenge in bio-based cyclic carbonates, because a greater degree of substitution causes the reaction to proceed more slowly.[14] Cyclic terpene-based epoxides exhibited high selectivity toward cyclic carbonates, whereas acyclic terpene-based epoxides showed poor selectivity towards cyclic carbonates. The acyclic terpene-based epoxides were more susceptible to epoxide rearrangement and undesired, uncontrolled polymerisation.[14] The synthesised monofunctional cyclic carbonates have not been used in NIPU synthesis in published literature.

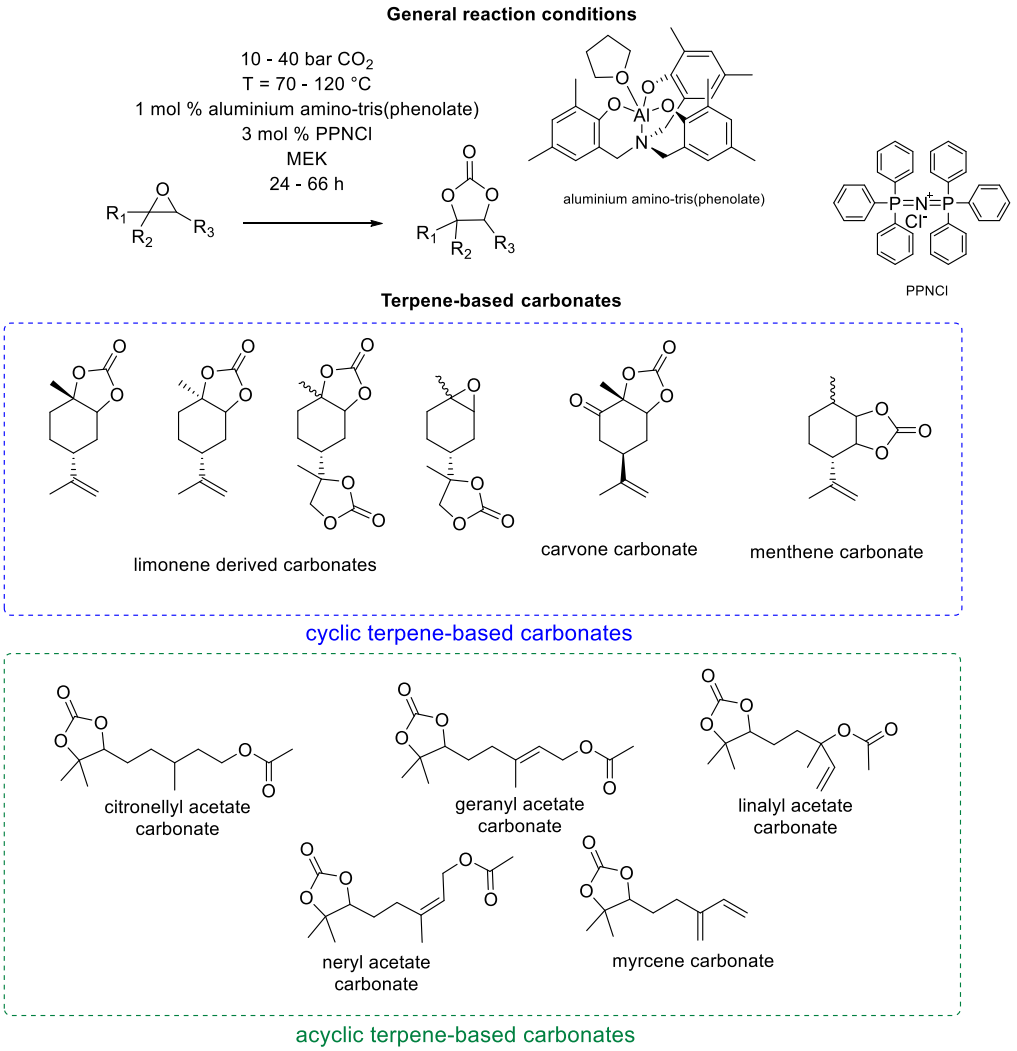

Figure 4.19 Terpene-derived cyclic carbonates present in literature.[14]

Purification of synthesised cyclic carbonates is also challenging, usually requiring column chromatography.[14] Alternatively, the carbonates can be used without purification,[14, 34] but any impurities in cyclic carbonates will cause yellowing of the corresponding NIPU.[34, 35] Crystallisation

of terpene-derived cyclic carbonates could be a solution for their purification, but only limited examples appear in the literature.[14, 35] Additionally, the synthesis of acyclic terpene-based carbonates is especially challenging due to side reactions resulting in the rearrangement of starting epoxide under the reaction conditions. The undesired side reactions produced polyethers, alcohols and ketones. This effect is not caused by the terpene scaffold structure, as the same by products were also observed for a non-functionalised trisubstituted epoxide – trimethyloxirane.[14] Moreover, terpene scaffolds which contain a diene unit are exceptionally difficult to transform to the corresponding carbonate and purify. For example, myrcene-derived carbonate was synthesised in low yields due to additional side reactions, possibly radical, resulting in a complicated mixture of products containing polymers.[14]

Despite issues with synthesis, most terpene-based cyclic carbonates are derived from natural resources, thus they are renewable feedstocks, but their availability is limited. It is important to move forward to terpene feedstocks delivered via industrial biotechnology, a more flexible approach that is able to provide higher volumes of terpenes than natural resources. For example, Amyris built a multimillion tonne sugar cane processing plant which could be used for farnesene production.[36]

Many terpene-derived cyclic carbonates presented are mono-functionalised, but NIPU synthesis requires at least bi-functionalised species. Strategies to prepare bi-functional cyclic carbonates could be based on thiol-ene chemistry, as demonstrated by Tomita *et al.* (Figure 4.20).[37] Terpenes, which contain multiple double bonds, can be easily functionalised via thiol-ene chemistry, as demonstrated by Meier's group.[38]

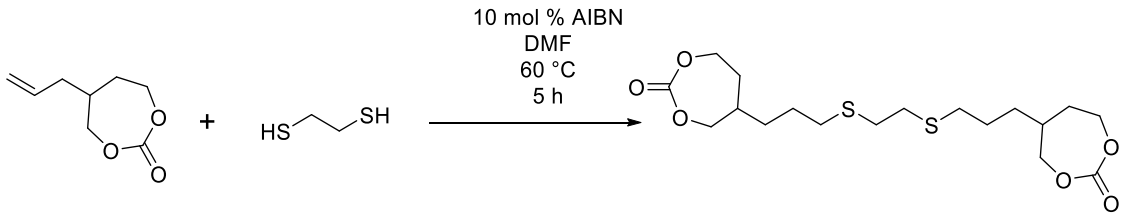

Figure 4.20 Strategy for synthesis of bifunctional species from mono functional carbonates.[37]

4.1.5 Relevant prior work in the Davidson and Plucinski groups

In the groups' previous work,[39-41] the epoxidation of limonene using the Venturello catalyst (**VENT**) was shown to give 83 % conversion and 90 % selectivity towards 1,2-limonene oxide in a flow microreactor with an integrated static mixer with 10 minutes residence time (Figure 4.21). **VENT** is an oxidation catalyst consisting of phase transfer catalyst (Aliquat 336) and tungsten based polyoxometalate $[PW_4O_{24}]^{3-}$.The epoxidation reaction proceeds in mild conditions with no solvent, making it highly promising in the context of green chemistry.

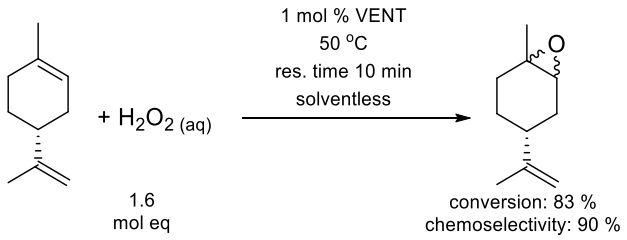

Figure 4.21 Limonene epoxidation. VENT – Venturello catalyst.[39-41]

Following this, a preliminary investigation into the use of epoxides in cyclic carbonate synthesis was undertaken using cyclohexene oxide as a model reactant. Some reports found polyoxometalates an effective catalyst for cyclic carbonates synthesis. Since **VENT**, the catalyst used for limonene oxidation, is a polyoxometalate we decided to investigate if **VENT** can be used for oxidation and cyclic carbonates synthesis. Using the same catalyst for oxidation and cyclic carbonates synthesis has potential to reduce unit operations necessary to obtain cyclic carbonates (Figure 4.22).

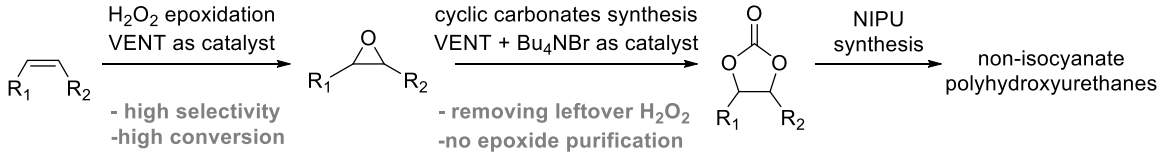

Figure 4.22 The general concept of using VENT as epoxidation and carbonation catalyst.

For the evaluation of **VENT** in producing cyclic carbonates, cyclohexene oxide (**CHO**) was chosen as a model. We applied reaction conditions developed by Leitner *et al.* to investigate if **VENT** has an impact on cyclohexene cyclic carbonate (**CHC**) synthesis.[8] Three catalysts have been investigated and as reported in Table 4.1 Entry 2 **VENT** is an efficient catalyst for CO_2 insertion. Moreover, **VENT** shows higher reactivity than Bu_4NBr which is usually used in such reactions (Table 4.1 Entry 3). However, a combined catalytic system consisting of Bu_4NBr and **VENT** showed the highest conversion (97 %), whilst maintaining the high selectivity seen with Bu_4NBr (Table 4.1 Entry 1). **CHO** did not undergo any reaction in the absence of a catalyst (Table 4.1 Entry 4).

Table 4.1 CHCC synthesis from CHO catalysed by VENT and Bu_4NBr.[42]

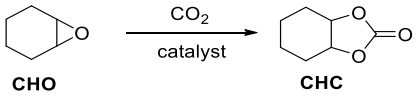

CHO CHC

Entry	Catalyst	T [°C]	p[a] [bar]	t [h]	Conv[b] [%]	Selectivity[b] CHC [%]
1	2 mol % VENT+ 3 mol % Bu_4NBr	120	75	4	97	84
2	2 mol % VENT	120	75	4	78	69
3	3 mol % Bu_4NBr	120	75	4	60	88
4	none	120	75	4	0	-

Reaction conditions: 6.3 mmol CHO; 10 mol % biphenyl as an internal standard a) pressure of CO_2 at 40 °C b) conversion and selectivity calculations based on ^{1}H NMR spectroscopy

4.2 Results and discussion

4.2.1 Cyclic carbonates from limonene oxides

Cyclic carbonates from commercially available 1,2-limonene oxide

Following these encouraging **CHO** results, three catalytic systems were tested on commercially available 1,2-limonene oxide (**1,2-LO** 57:43 *trans*:*cis*) in order to evaluate the difference between CO_2 insertion catalysed by Bu_4NBr and by combined catalytic system consists of Bu_4NBr and **VENT** (Table 4.2). Initially 3 mol % Bu_4NBr was applied at 30 bar CO_2 which gave high conversion, but the selectivity was poor (20 %) with a higher pressure improving selectivity to 41 % (Entry 2, p = 75 bar). The addition of 2 mol % **VENT** to 3 mol % Bu_4NBr at higher CO_2 pressures improved conversion and selectivity (Entry 3). However, as this catalytic system applies to 5 mol % catalyst loading, a reaction at the same CO_2 pressure and with 5 mol % Bu_4NBr was tested. Improved conversion was achieved, but selectivity was still below 60% (Entry 4). ^{1}H NMR analysis of the crude reaction mixture showed disproportion of the isomer ratio in **1,2-LO** after the reaction. This suggested that isomers react in different ways and possibly only one isomer is reactive. This theory was confirmed by NMR analysis; in all the catalytic systems attempted, one isomer of the cyclic carbonates is dominant which indicated that only ***trans*-1,2-LO** is active in the CO_2 insertion. The same observation was previously reported by Kleij and co-workers.[14] Considering plausible mechanisms of double inversion pathway in the CO_2 insertion (Figure 4.23), it is clear that nucleophilic attack on the ***cis*-1,2-LO** is inhibited due to steric hindrance, thus only traces of ***cis*-1,2-LC** were observed.

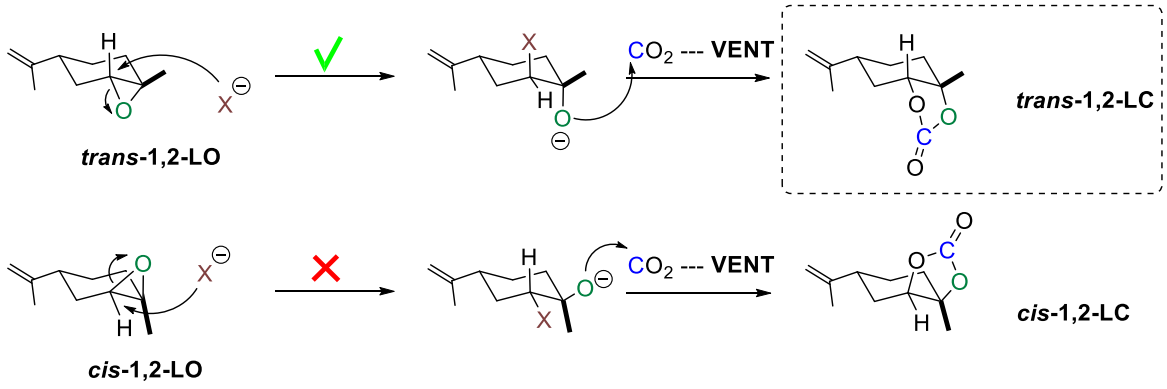

Figure 4.23 Proposed mechanism of CO_2 insertion.[8, 14]

Table 4.2 The synthesis of 1,2-LC from commercially available 1,2-LO.

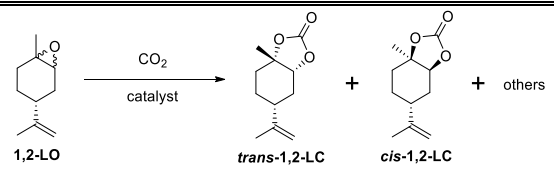

Entry	Catalyst	T [°C]	p[a] [bar]	Conv[b] [%]	Selectivity[c] 1,2-LC [%]	*trans*: *cis* 1,2-LC
1	3 mol % Bu_4NBr	140	30	79	20	96:4
2	3 mol % Bu_4NBr	140	75	61	41	94:6
3	2 mol % VENT + 3 mol % Bu_4NBr	140	75	73	53	92:8
4	5 mol % Bu_4NBr	140	75	95	52	95:5

Reaction conditions: 2.3 mmol **1,2-LO**; 10 mol % biphenyl as an internal standard, 24 h;
a) pressure of CO_2 at 40 °C b) conversion and selectivity calculations based on ^{1}H NMR spectroscopy
c) selectivity corresponds to chemoselectivity which includes *cis*- and *trans*-1,2-LC isomer

The influence of 1,2-limonene oxide stereochemistry on the cyclic carbonate synthesis

To investigate further, the isomers of **1,2-LO** were separated according to previously reported methods.[43, 44] As expected, the *cis* isomer did not show good selectivity to ***cis*-1,2-LC** (Table 4.3 Entry 1) (Figure 4.24). The *trans* isomer showed excellent selectivity to ***trans*-1,2-LC** (Entry 5 and 6) (Figure 4.25). Applying a longer reaction time (Entry 4 and 5) resulted in high conversion and high selectivity.

Table 4.3 The behaviour of different mixtures of cis-1,2-LO and trans-1,2-LO in the CO_2 insertion

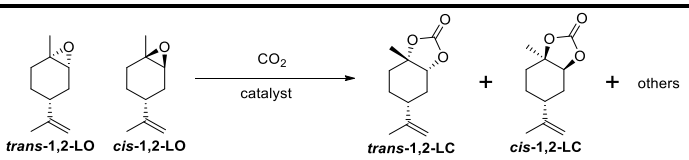

Entry	*trans*:*cis* 1,2-LO	t [h]	Conv[a] [%]	*trans*:*cis* 1,2-LO after reaction	Selectivity[b] 1,2-LC [%]	*trans*: *cis* 1,2-LC
1	0:100	24	60	0:100	12	0:100
2	13:87	24	80	13:87	26	55:45
3	57:43	24	83	33:67	64	99:1
4	97:3	24	91	91:9	85	99:1
5	97:3	4.5	60	96:4	95	98:2
6	100:0	4.5	61	100:0	89	100:0

Reaction conditions: 4.6 mmol **1,2-LO**, 3 mol % Bu_4NBr, 2 mol % **VENT**, 10 mol % biphenyl as an internal standard, 140 °C, 75 bar CO_2 at 40 °C
a) conversion and selectivity calculations based on ^{1}H NMR spectroscopy b) selectivity corresponds to chemoselectivity and includes *cis*- and *trans*-1,2-LC

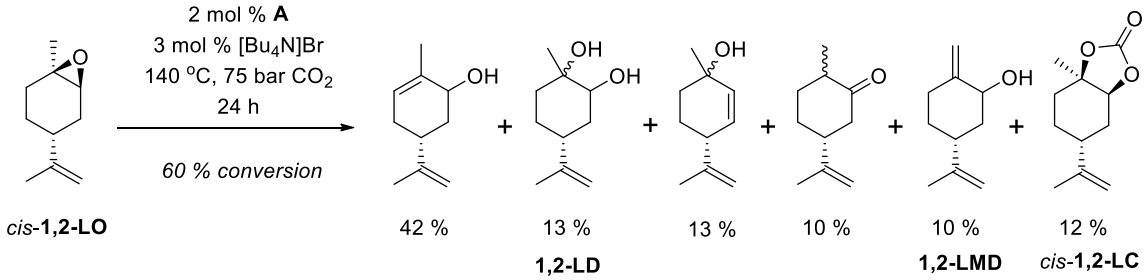

Figure 4.24 CO_2 insertion to cis-1,2-LO. Products were identified by GC-MS, selectivity of cis-1,2-LC was calculated by NMR spectroscopy, the rest of the products were calculated by GC-MS.

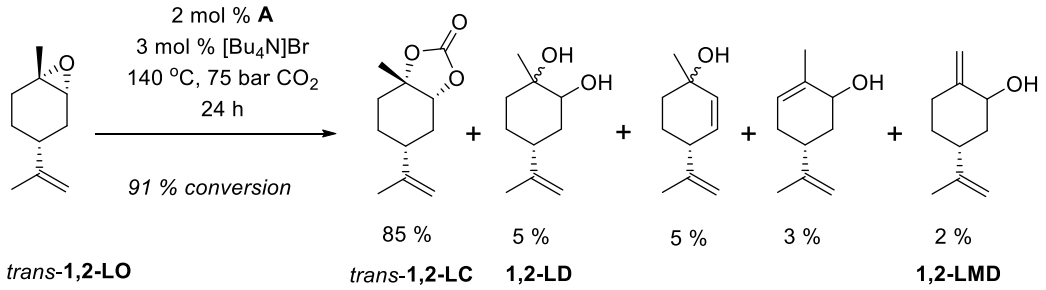

Figure 4.25 CO_2 insertion to trans-1,2-LO. Products were identified by GC-MS, selectivity of trans-1,2-LC was calculated by NMR spectroscopy, the rest of products were calculated by GC-MS.

Reaction conversion profiles of ***trans*-1,2-LO** and a commercial sample of **1,2-LO** (57:43 *trans*:*cis*, obtained from Sigma Aldrich) (Figure 4.26) were obtained using stainless steel autoclaves charged with the same reaction mixture but stopping at different times. The conversion for commercial **1,2-**

LO is slightly lower than for ***trans*-1,2-LO** presumably due to the *cis* isomer inhibiting catalysis. The ^{1}H NMR spectrum of **1,2-LO** and by-products is complex and to move the investigation forwards only ***trans*-1,2-LO** was used in the following investigation into the CO_2 epoxide insertion.

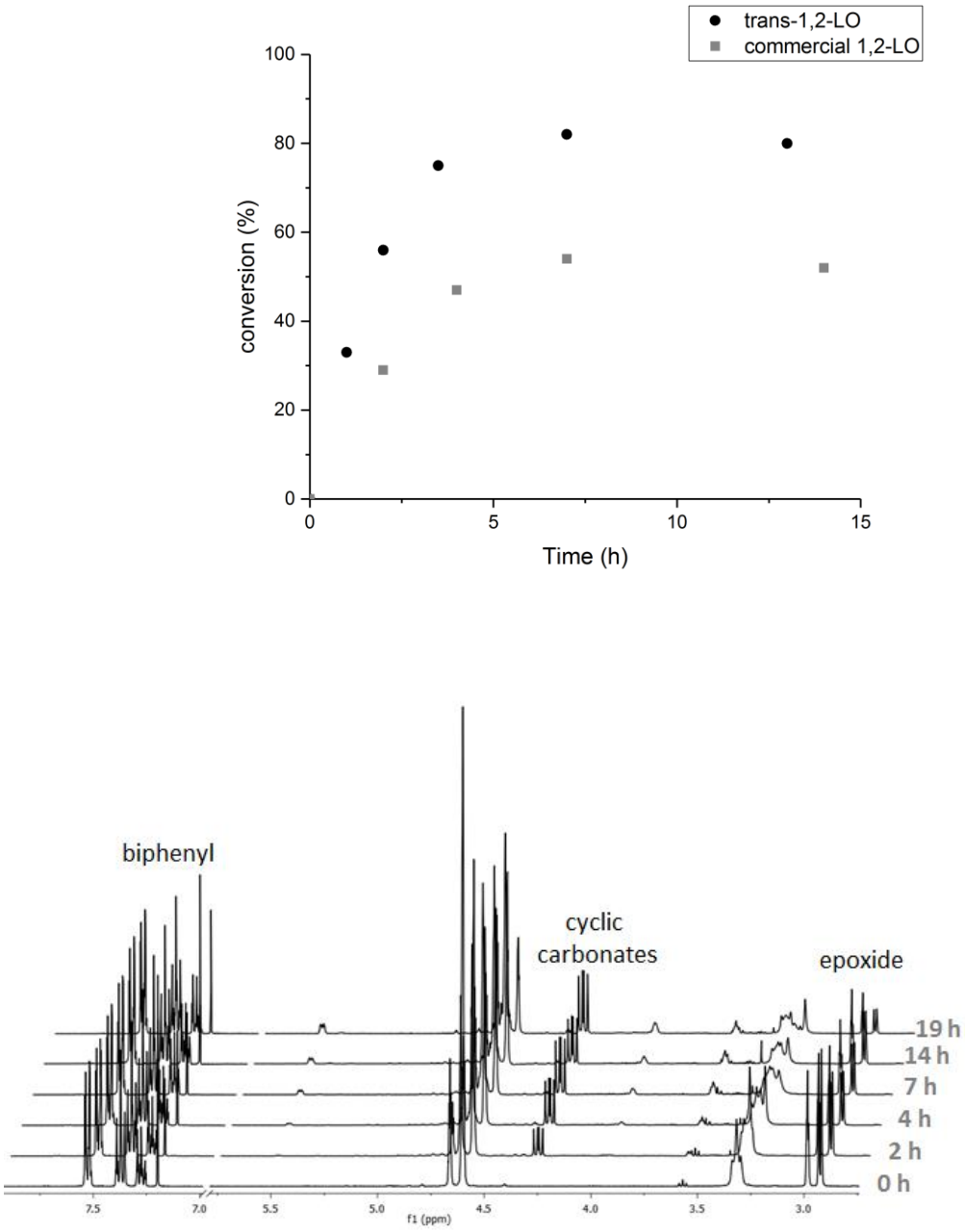

Figure 4.26 Top: Reaction profiles at 140 °C and 75 bar CO_2, 2.83 mmol 1,2-LO, 2 mol % VENT, 3 mol % Bu_4NBr, 10 mol % biphenyl as an internal standard. The commercial 1,2-LO was sourced from Sigma Aldrich, trans-1,2-LO has been synthesised in the procedure described in Experimental section, it is optically 100 % trans-1,2-LO which contains 10 % impurities (See Figure 4.73) Bottom: ^{1}H NMR spectra run in $CDCl_3$ on 400 Mhz spectrometer, showing reaction progress. The presented spectra correspond to data points collected for commercial 1,2-LO (57:43 trans:cis).

Stereochemisty studies using NOESY experiment

NOESY experiment and analysis have been done with assistance from University of Bath NMR spectroscopy specialist – Catherine Lyall

The previously described results lead to the conclusion that the synthesised **1,2-LC** should consist of mostly one optical isomer. The two possible products are ***trans*-1,2-LC** and ***cis*-1,2-LC**. Since reactions with ***trans*-1,2-LO** showed significantly higher selectivity to cyclic carbonates **than *cis*-1,2-LO**, **the 1,2-LC** synthesised from the commercial mixture should consist of ***trans*-1,2-LC**. This conclusion was supported by NMR spectroscopy.

The crude reaction mixture from reaction of commercially available **1,2-LO** and CO_2 was purified by column chromatography and **1,2-LC** was successfully separated from the mixture and submitted to NMR spectroscopy (Figure 4.27).

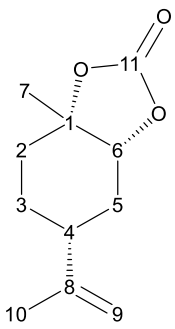

	^{1}H NMR	^{13}C NMR
1	---	82.0
2	H2 (2H) 1.60; 2.26	32.8
3	H3 (2H) 1.40; 1.65	25.5
4	H4 (1H) 1.89	39.6
5	H5 (2H) 1.39; 2.21	33.9
6	H6 (1H) 4.35	80.4
7	H7 (3H) 1.42	25.9
8	---	147.3
9	H9 (2H) 4.68; 4.72	110.1
10	H10 (3H) 1.68	20.4
11	---	154.7

Figure 4.27 NMR spectroscopy assignments for the obtained 1,2-LC.

In the NOESY experiment (Figure 4.28), a proton at H9 from the alkene group at 4.68 ppm showed interaction with a proton at H3and H4 and the proton at H5 (Figure 4.28, blue dot). This indicates that all of these protons are on the same side of the molecule and confirms the position of alkene group.

Hydrogen at position H6 (Figure 4.28 B, red dot) interacts with a methyl group at position H7, one hydrogen at H5 and significantly the hydrogen atom H4. H4 has fixed stereochemistry, thus the NOESY interaction between H6 and H4 is an excellent indicator of the **1,2-LC** stereochemistry. Therefore, it can be confidently stated that the commercially available mixture of **1,2-LO** yields cyclic carbonates consisting of mostly ***trans*-1,2-LC**. This is consistent with previous findings of other research groups.[14]

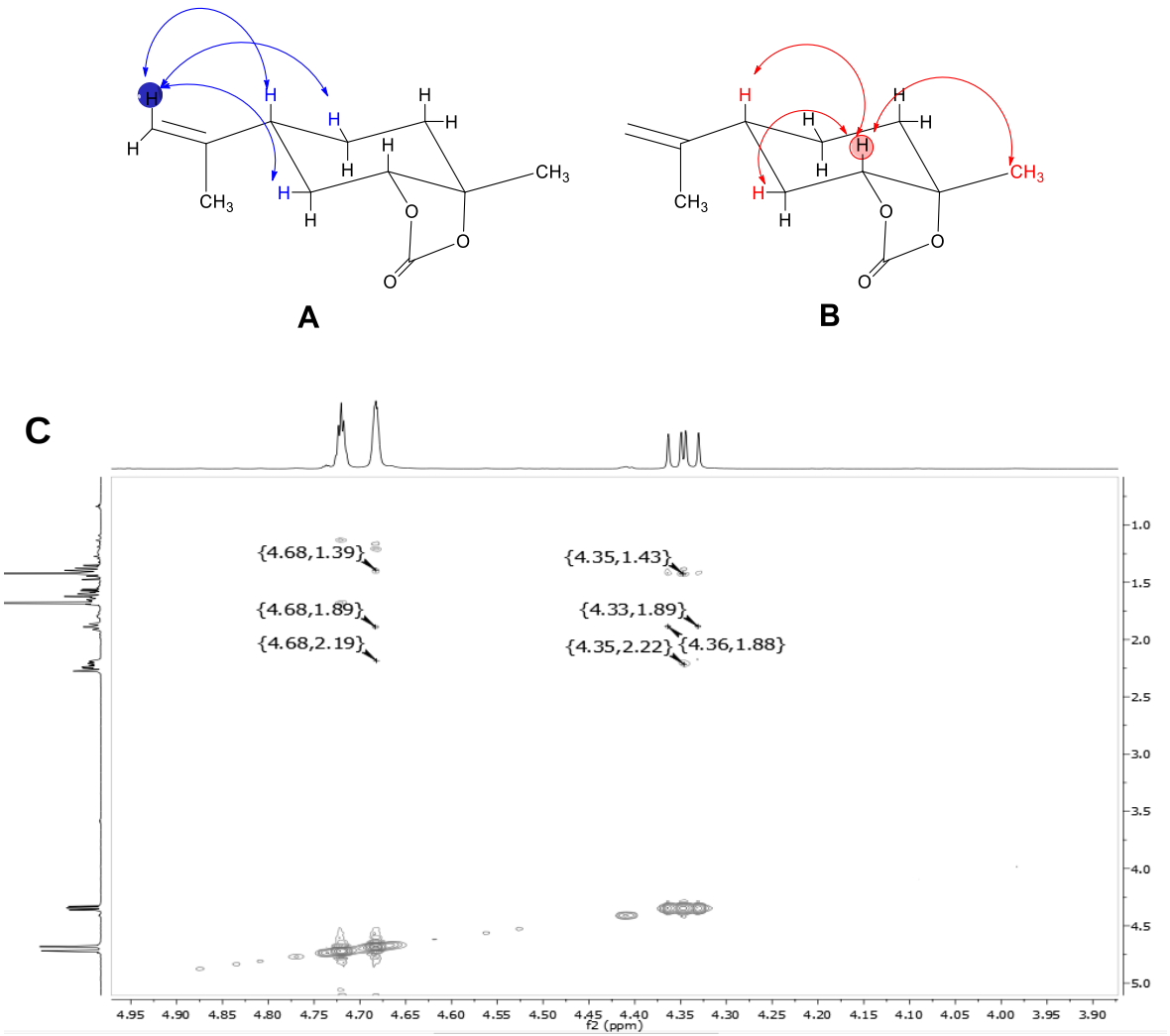

Figure 4.28 The key NOESY interactions of 1,2-LC A) ^{1}H-^{1}H NOESY interactions confirming alkene orientation B) ^{1}H-^{1}H NOESY interaction confirming 1,2-LC stereochemistry, C) ^{1}H-^{1}H NOESY spectrum .

Further investigation of cyclic carbonates synthesis from trans-1,2-limonene oxide

The temperature of the reaction was varied from 40-140 °C (Table 4.4) and it was quickly seen that conversion strongly depends on temperature, with the fastest reaction observed at 140 °C. A drop in the reaction temperature by 20 °C resulted in lower conversion, but the reaction maintained high selectivity. The reaction at 80 °C showed significantly lower conversion and selectivity and the reaction at 40 °C did not yield cyclic carbonates at all. This is consistent with the data reported for carbonation of limonene bisepoxide in which the conversion was high for reactions at 140 and 120 °C but conversion at 100 °C was significantly lower.[34] High reaction temperatures are typical for cyclic carbonate synthesis catalysed by quaternary ammonium salts; however, the optimum reaction temperature strongly depends on the epoxide used.[8, 9, 45, 46] For ***trans*-1,2-LO**, conversion increased with higher temperature and the high selectivity of reaction was not reduced up to 140 °C.

Table 4.4 The influence of temperature on trans-1,2-LC synthesis.

Entry	Catalyst	T [°C]	t [h]	Conv[a] [%]	Selectivity *trans*-1,2-LC[%]	*trans*: *cis* 1,2-LC
1	VENT+Bu_4NBr	140	4.5	65	80[b]	100:0
2	VENT +Bu_4NBr	120	4.5	42	78	100:0
3	VENT +Bu_4NBr	80	4.5	10	45	100:0
4	VENT +Bu_4NBr	40	4.5	5	0	-

Reaction conditions: 1.73 mmol ***trans*-1,2-LO** (see Figure 4.73), 2 mol% **VENT**, 3 mol % Bu_4NBr, 10 mol % biphenyl as an internal standard, stirrer speed 300 rpm, 75 bar CO_2 at 40 °C
a) conversion and selectivity calculations based on ^{1}H NMR spectroscopy, b) other possible products are presented in Figure 4.25

Pressure influence on carbonation of trans-1,2-limonene oxide

The influence of pressure on the ***trans*-1,2-LC** synthesis was investigated (Table 4.5). An autoclave was pressurised in the range of 20 - 75 bar CO_2, which corresponds to CO_2 density in the range of 0.037 – 0.238 g mL^{-1}. The results showed that selectivity strongly depends on the available CO_2. At high CO_2 densities between 0.149 and 0.238 g mL^{-1} (60 – 70 bar) the conversion and selectivity remains high. However, the reaction at a lower CO_2 density of 0.059 g mL^{-1} (30 bar) showed significantly lower selectivity whilst retaining the same level of conversion. In atmospheric pressure of air, the formation of cyclic carbonates was minor. According to GC-MS analysis of crude reaction mixture, at lower CO_2 densities the yield of side products from epoxide hydrolysis and dehydratation of 1,2-limonene diol (Figure 4.29 presents possible dehydration products previously reported by other research group) was higher than the yield of cyclic carbonates (Table 4.5 Entry 5).

Table 4.5 The influence of pressure on trans-1,2-LC synthesis.

Entry	Catalyst	T [°C]	p[a] [bar]	t [h]	Conv[b] [%]	Selectivity *trans*-1,2-LC[%]	*Trans*: *cis* 1,2-LC
1	VENT+Bu_4NBr	140	75	4.5	68	76	1:0
2	VENT +Bu_4NBr	140	60	4.5	62	79	1:0
3	VENT +Bu_4NBr	140	30	4.5	65	55	1:0
4	VENT +Bu_4NBr	140	20	4.5	45	35	1:0
5	VENT +Bu_4NBr	140	atm[c]	4.5	16	25[d]	1:0

Reaction conditions: 2.16 mmol ***trans*-1,2-LO** (see Figure 4.73), 2 mol% **VENT** , 3 mol % Bu_4NBr, 10 mol % biphenyl as an internal standard, stirrer speed 300 rpm
a) pressure of CO_2 at 40 °C b) conversion and selectivity calculations based on ^{1}H NMR spectroscopy c) atmospheric pressure – air d) low concentration of product, the carbonyl signal does not appear on $^{13}C\{^1H\}$ NMR spectroscopy but the ^{1}H NMR spectroscopy shows characteristic *dd* at 4.30 ppm, the main by products were identified by GC-MS (Figure 4.24 compounds 1,2-LD and 1,2-LMD)

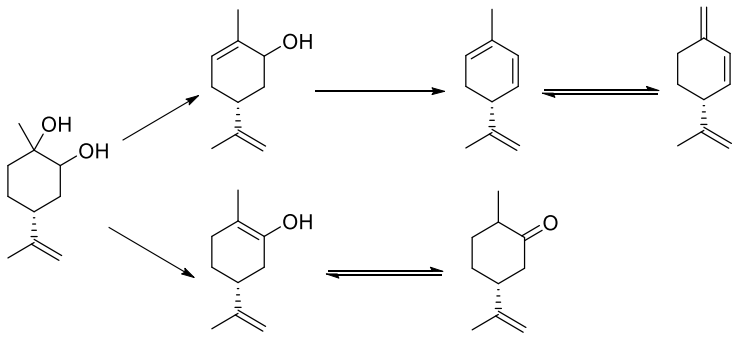

Figure 4.29 Possible products of 1,2-limonene diol dehydration.[47]

Phase behaviour during the carbonation reaction

The phase behaviour was investigated using a high pressure viewing cell autoclave equipped with a sapphire glass window. At 40 °C and atmospheric pressure the reaction mixture was a homogeneous phase with the catalyst fully dissolved in the liquid (Figure 4.30 A). When the autoclave was pressurised with CO_2, the mixture significantly increased in volume and created a three phase system (Figure 4.30 B). Although not analysed quantitatively, the lower phase likely consisted mainly of the heavy catalyst, which is CO_2 insoluble. The middle phase was an expanded liquid phase of limonene oxide with dissolved CO_2. The upper phase was a supercritical CO_2 ($scCO_2$) phase, probably with some limonene oxide. Upon increasing the temperature, the solubility of CO_2 in the reaction mixture decreased and the volume of the expanded liquid decreased (Figure 4.30 C). The catalyst separation stopped occurring and the reaction changed colour from light yellow to dark brown. The change of colour could possibly mean that **VENT** is not stable under the reaction conditions. It is worth noting **VENT** is a complex mixture of polyoxometalates and its thermal stability is not known, thus identifying the active species in the carbonation reaction is challenging.

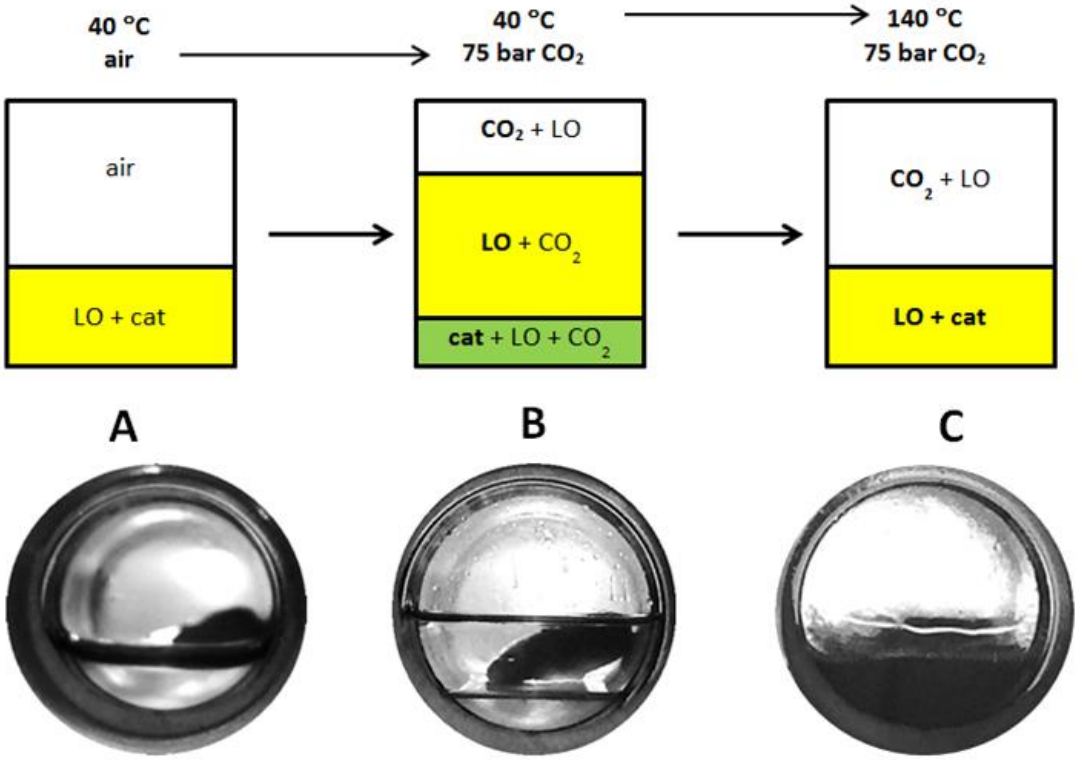

Figure 4.30 Phase behaviour experiment using high pressure viewing cell. The object visible in the pictures is a magnetic stirrer bar. The species in bold is the main compound of the phase.
LO – limonene oxide, cat – catalyst: 2 mol % VENT and 3 mol % Bu_4NBr.

Variation in catalyst loading and halide counterion

Most of the experiments were conducted using **VENT** at a loading of 2 mol % with 3 mol % of Bu_4NBr. However, the general epoxidation conditions originally done within the group use only 1 mol % **VENT**. The effect of reducing the amount of **VENT** was studied, and when changing from 2 mol % to 1 mol % (Table 4.6 Entry 1-3), the conversion decreased by 12% with no significant changes in selectivity. It is possible to use 5 mol % **VENT** without any addition of Bu_4NBr (Table 6 Entry 4), but the use of 5 mol % **VENT** is undesirable due to the unfavourable mass ratio – 5 mol % **VENT** is equal to 80 mass % of reaction mixture.

Next, different halide salts were investigated as the co-catalyst for CO_2 insertion (Table 4.6 Entry 5-13). Often, the most active salt for cyclic carbonate synthesis is the bromide salt due to its well-balanced nucleophilic properties and leaving group character.[8] However, for ***trans*-1,2-LC** synthesis the most active and selective appeared to be Bu_4NCl (Table 4.6 Entry 5 and 9). The same effect was observed for the combined catalytic system consisting of **VENT** and Bu_4NCl. Bu_4NI, which is a weaker nucleophile, is perhaps unsurprisingly the least active catalyst. Since previously reported literature confirms that Bu_4NF is not selective towards cyclic carbonates,[8] Bu_4NF was not tested in this work.

Yasuda *et al*. found that quaternary ammonium salts with longer alkyl chains are more active in cyclic carbonate synthesis. However, the change of Bu_4NCl for Aliquat 336 (a commercial mixture of C8 and C10 quaternary ammonium chloride salts) did not result in any significant change in activity (Table 4.6 Entry 5 and 8). In the absence of a catalyst, the carbonation of ***trans*-1,2-LO** did not proceed (Table 4.6 Entry 14).

Table 4.6 The synthesis of trans-1,2-LC catalysed by various catalysts.

Entry	Catalyst	t [h]	Conv[a] [%]	Selectivity *trans*-1,2-LC[%]	*Trans*: *cis* 1,2-LC
1	2 mol % VENT+ 3 mol % Bu_4NBr	4.5	68	76	1:0
2	1 mol % VENT +3 mol % Bu_4NBr	4.5	56	77	1:0
3	1 mol % VENT + 3 mol % Bu_4NBr	24	91	64	1:0
4	5 mol % VENT	4.5	83	72	1:0
5	3 mol % Bu_4NCl	4.5	35	82	1:0
6	3 mol % Bu4NBr	4.5	45	59	1:0
7	3 mol % Bu_4NI	4.5	15	52	1:0
8	3 mol % Aliquat 336[b]	4.5	34	69	1:0
9	2 mol % VENT + 3 mol % Bu_4NCl	4.5	83	78	1:0
10	2 mol % VENT + 3 mol % Bu_4NI	4.5	55	39	1:0
11	2 mol % VENT + 3 mol % Bu_4NCl	24	93	74	1:0
12	2 mol % VENT + 3 mol % Bu_4NBr	24	96	55	1:0
13	2 mol % VENT + 3 mol % Bu_4NI	24	98	67	1:0
14	none	4.5	-[c]	-	-

Reaction conditions: 2.0-2.6 mmol ***trans*-1,2-LO** (see Figure 4.73), 140 °C, 75 bar CO_2 at 40 °C, 10 mol % biphenyl as an internal standard, stirrer speed 300 rpm
a) conversion and selectivity calculations based on ^{1}H NMR spectroscopy b) Aliquat 336 is commercial mixture of C8 and C10 quaternary ammonium salts with predominating N-methyl-N,N,N-trioctylammonium chloride c) 5 % mass loss

Integrated epoxidation and carbonation of 1,2-limonene cyclic carbonate

Next, **VENT** was used in epoxidation and carbonation to yield **1,2-LC** in two step reaction (Figure 4.31). Limonene therefore was epoxidised in flow microreactor to **1,2-LO**. The resulting bi-phasic solution was separated and the organic phase was used in CO_2 insertion without any purification after the addition of 3 mol % Bu_4NBr to the mixture (Figure 4.31). Pleasingly, after 24 h, 85 % of **1,2-LO** had reacted with 42 % selectivity to ***trans*-1,2-LC**. It is worth noting **1,2-LO** synthesised via **VENT** catalysed epoxidation is a mixture of two stereoisomers (42 % *trans* and 58 % *cis*), 42 % selectivity to ***trans*-1,2-LC** corresponds to 85 % of available ***trans*-1,2-LO** which has been transformed into ***trans*-1,2-LC**. Mono functionalised **1,2,-LC** was isolated by column chromatography; however, recrystallisation of these terpene-derived cyclic carbonates has been shown by others as an alternative purification method.[14, 35]

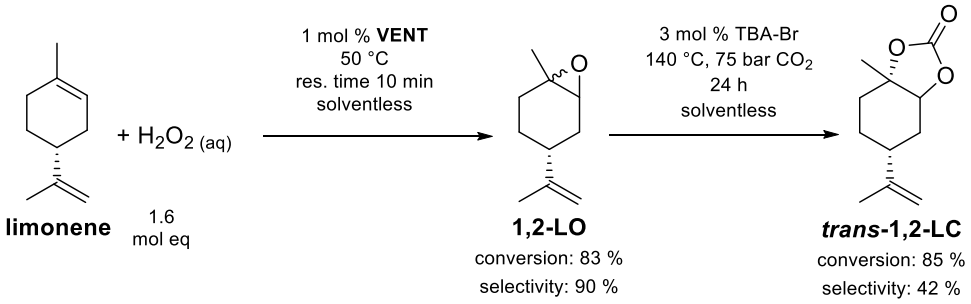

Figure 4.31 Two-steps synthesis of cyclic carbonates from limonene without purification of 1,2-LO. res. time – residence time; selectivity is chemoselectivity.

The synthesis and characterisation of 8,9-limonene cyclic carbonate

Cyclic carbonate formation at the 1,2 position of limonene has been widely investigated, mostly due to the ease and availability of epoxidising the more active, electron-rich double bond. The selective formation of 8,9 functionalised analogue is a challenge, due to difficult selective epoxidation at 8,9 position. To combat this challenge, a catalyst which sterically exclude 1,2 position is needed. Mizuno has reported a procedure employing polyoxometalate based catalyst along with H_2O_2 as an oxidant to provide 100% regioselectivity towards 8,9-limonene oxide.[48] The epoxidation catalyst consist of quaternary ammonium cation (Bu_4N^+) and divanadium substituted phosphotungstate polyoxometalate anion $[\gamma\text{-}HPV_2W_{10}O_{40}]^{4-}$, this catalyst will be furthered referred as **MIZ**. While **1,2-LO** has been previously used for cyclic carbonates synthesis,[14] **8,9-LO** is an unexplored yet reagent. Carbonation of **8,9-LO** is much more facile than **1,2-LO**, at 140 °C, high conversion was achieved even after shorter reaction times (Table 4.7 Entry 1-3). Thus, the catalytic activity of different catalyst was tested in lower temperature and shorter reaction time (Entry 3). In contrast to **1,2-LO**, **8,9-LO** is less sterically hindered, thus the nucleophilic attack is favourable on both isomers. No significant difference in the stereoisomers ratio was observed after the reaction with any slight changes within range of the experiment and ^{1}H NMR spectroscopy error. While **VENT** can catalyse formation of **8,9-LC**, the effect of adding **VENT** has lower impact than for **1,2-LC** (Entry 4 and 5). However, using an alternative polyoxometalate catalyst MIZ, the catalyst used in the limonene epoxidation yielding **8,9-LO**, completely changed the selectivity of the carbonation reaction. The reaction with **MIZ** yielded 8,9-limonene aldehyde (**8,9-LA**) and no cyclic carbonates were detected by NMR spectroscopy. The formation of **8,9-LA** was independent of the presence of CO_2, but the yield did vary depending on the batch of polyoxometalate catalyst (Entry 7 and 8). Due to high catalyst loading and inconsistent yields this reaction has not been considered as a viable aldehyde synthesis. High conversion and high selectivity to **8,9-LC** can be obtained by using 3 mol % Bu_4NBr as a catalyst (Entry 1).

Table 4.7 Carbonation of 8,9-LO.

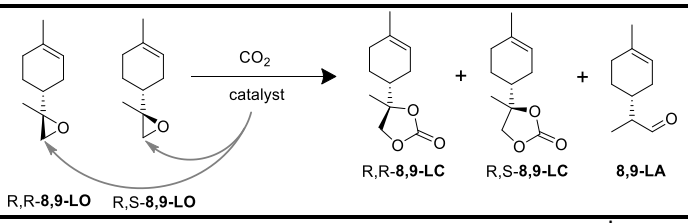

Entry	Catalyst	T [°C]	p[a] [bar]	t [h]	R,S:R,R 8,9-LO after reaction	Conv[b] [%]	Selectivity 8,9-LC[%]	R,S:R,R 8,9-LC[c]
1	3 mol % Bu_4NBr	140	75	2.5	54:46	80	96	70:30
2	3 mol % Bu_4NBr	120	75	4.5	58:42	76	91	65:35
3	3 mol % Bu_4NBr	120	75	2.5	59:41	52	99	67:33
4	3 mol % Bu_4NBr + 2 mol% VENT	120	75	2.5	64:36	68	98	73:27
5	2 mol % VENT	120	75	2.5	64:36	46	86	83:17
6	3 mol % Bu_4NBr + 2 mol % MIZ	120	75	2.5	61:39	57	76	63:37
7	2 mol % MIZ	120	75	2.5	62:38	63[d]	0[e]	-
8	2 mol % MIZ	120	atm[f]	2.5	56:44	75[g]	0[h]	-
9	No catalyst	120	75	2.5	63:37	-[i]	-	-

Reaction conditions: 2.3 mmol **8,9-LO** (starting stereochemistry 63:37 R,S:R,R), 10 mol % biphenyl as an internal standard, stirrer speed 300 rpm
a) pressure of CO_2 at 40 °C b) conversion and selectivity calculations based on ^{1}H NMR spectroscopy c) calculated based on ^{1}H NMR spectroscopy using doublet at 4.25 ppm, the overlapping doublets were deconvoluted using MestReNova d) up to 63% depending on the batch of **MIZ**
e) reaction yields **8,9-LA**, 50% selectivity f) atmospheric pressure of air g) 53-75 % depending on the batch of **MIZ** h) reaction yields **8,9-LA**, 47% selectivity i) 6.5 % mass loss

Thiol-ene click reactions and opening with amines; proof of concept

In constrast to 1,2,8,9-carbonate, the use of monofunctional terpene-derived cyclic carbonates in NIPU synthesis is still an unexplored area of research. In this work, the monofunctional cyclic carbonates **1,2-LC** and **8,9-LC** have been used to prepare bifunctional species using thiol-ene click reactions. The bifunctional species were furthered reacted with hexylamine (Figure 4.32). Dithiol addition on **1,2-LC** was performed using method developed by Meier et al.,[38] and no radical initiator was needed. However, **8,9-LC**, which contains an endocyclic double bond in its structure, required the use of radical initiator and a longer reaction time. The bi-functional cyclic carbonate species **BI-1,2-LC** and **BI-8,9-LC** were reacted with an excess of hexylamine resulting in ring opening of cyclic carbonates. The IR spectra of the products showed almost complete consumption of cyclic carbonates (Figure 4.33). Carbonyl signals on $^{13}C\{^1H\}$ NMR spectroscopy shifted to 157.2 ppm (**BI-1,2-LC-HU**) and 157.5 ppm (**BI-8,9-LC-HU**), the shift is consistent with reported data for other hydroxyurethanes[29] and it suggest ring opening of cyclic carbonates (the ^{1}H NMR and ^{13}C NMR spectroscopy results are available in Section 4.4.10). **BI-1,2-LC-HU** and **BI-8,9-**

LC-HU were analysed by ESI-MS after evaporating an excess of amine, the analysis confirmed the presence of sodium adduct of mass 725.4690 g mol^{-1} and 725.4624 g mol^{-1} respectively. The synthesised hydroxyurethanes **BI-1,2-LC-HU** and **BI-8,9-LC-HU** demonstrate the unexplored potential of monofunctionalised terpene-derived cyclic carbonates. In this experiment an excess of hexyl amine was used to create a model substrate, but **BI-1,2-LC** and **BI-8,9-LC** could be reacted with diamines creating linear NIPU.

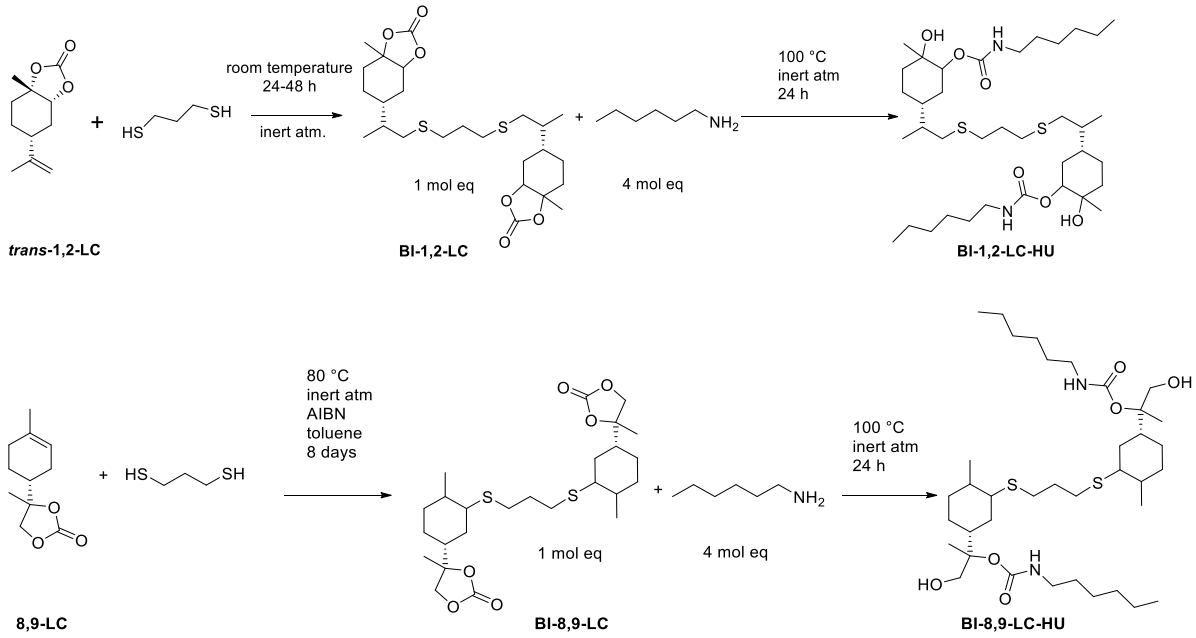

Figure 4.32 Synthesis of bifunctional species from 1,2-LC and 8,9-LC via radical addition. The resulted bi-functional cyclic carbonate species were reacted with hexylamine resulting in hydroxyurethanes BI-1,2-LC-HU and BI-8,9-LC-HU.

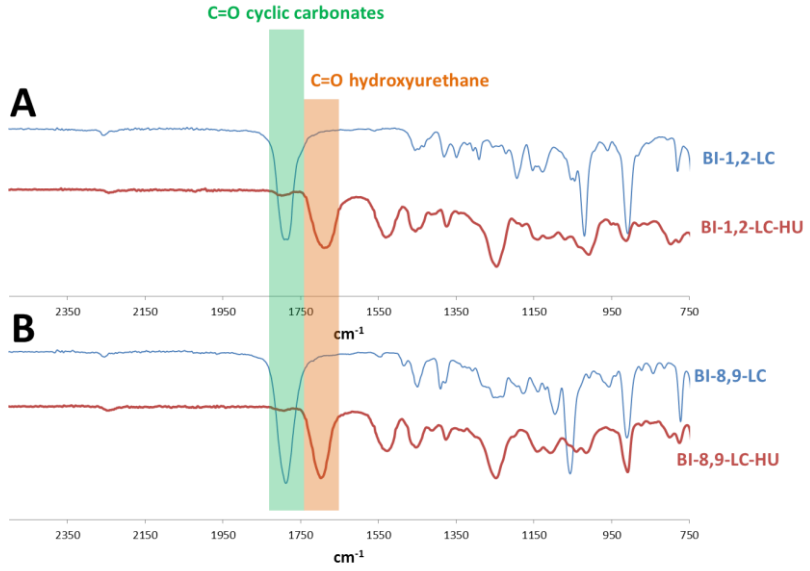

Figure 4.33 IR spectra before and after ring opening with hexylamine. A: synthesis of BI-1,2-LC-HU (before and after reaction), B: synthesis of BI-8,9-LC-HU (before and after reaction). Blue line – bifunctional cyclic carbonate species BI-1,2-LC (top) and BI-8,9-LC (bottom), red line – BI-1,2-LC-HU (A) and BI-8,9-LC-HU (B) after evaporating the excess amine.

4.2.2 Cyclic carbonates from β - elemene oxides

β - elemene oxides

β - elemene (**BE**) has three double bonds and in theory all of them can be epoxidised (Figure 4.34), giving an opportunity for multifunctional terpene-derived cyclic carbonates. Additionally, **BE** is produced via industrial biotechnology which means its production can be scaled up.[49, 50] For the purpose of this study **BE** was epoxidised using mCPBA and purified using column chromatography or distillation, but in Chapter 3 a number of catalytic epoxidation methods were presented that are applicable to **BE**. β - elemene monoepoxide (**BEMO**) is always synthesised as a mixture of regioisomers in a roughly 1:1 ratio. β - elemene bisepoxide (**BEBO**) exists as one regioisomer, but each epoxide functionality has two stereoisomers. β - elemene trisepoxide (**BETO**) is the hardest to obtain due to the low reactivity of the electron deficient double bond in the vinyl group. Each epoxide functionality results in two stereoisomers which makes **BETO** a complex mixture of 8 possible stereoisomers.

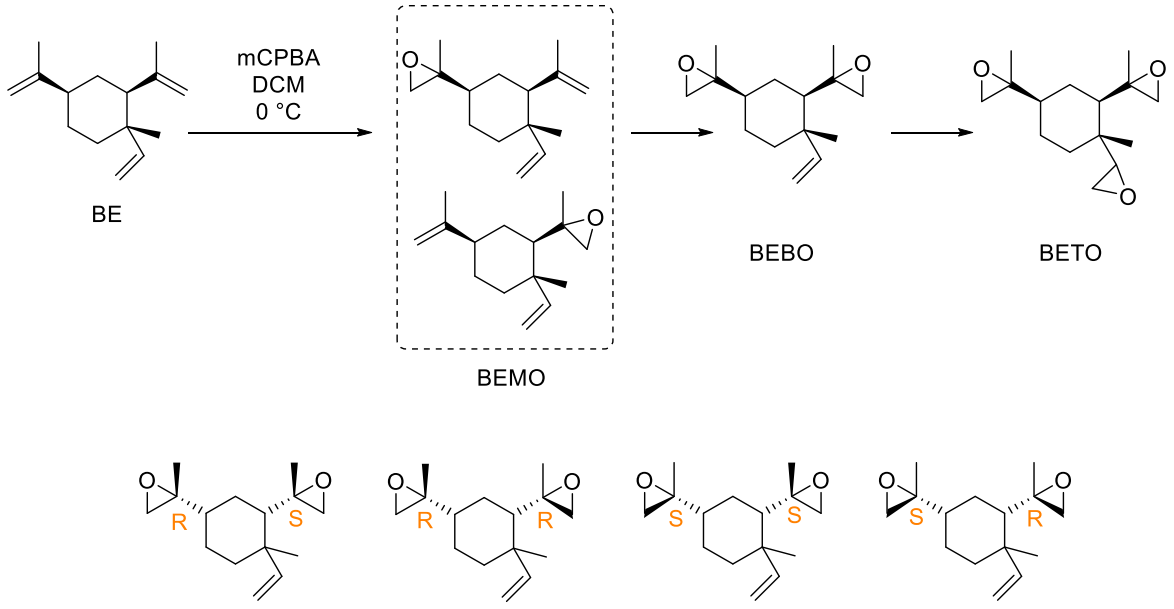

Figure 4.34 β-elemene oxidation using mCPBA. The final product depends on the excess of mCPBA used. The BEBO stereoisomers are drawn as an example.

β - elemene cyclic carbonates from β - elemene bisepoxide

Novel bi-functional and mono-functional cyclic carbonates have been synthesised from **BEBO** using a quaternary ammonium salt as catalyst. To improve CO_2 mass transfer, all carbonations were run in high pressure reactors, pressurised to 50 bar at 40 °C, corresponding to a CO_2 density of 0.113 g/mL. The design of the carbonation reactor does not allow for adding a sparger, thus high pressure CO_2 is the best solution for the set up used in this experiment. Since the phase behaviour

during reaction, and **BEBO** volumetric expansion in high pressure CO_2 is not known, the CO_2 density was not increased any further to avoid overloading the carbonation reactor. Depending on reaction temperature, the reaction of **BEBO** with CO_2 yielded different products (Table 4.8).

Table 4.8 Results of carbonation of BEBO in temperature range 100 – 160 °C.

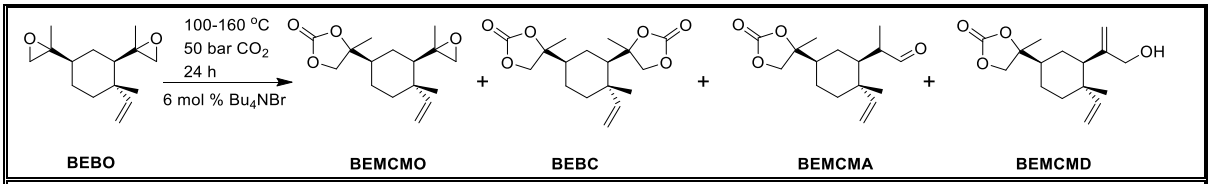

BEBO BEMCMO BEBC BEMCMA BEMCMD

Entry	T [°C]	p [bar]	t [h]	Yield CC[a] [%]	Yield ALD[b] [%]	Column chromatography yield [%]		
						BEMCMO	BEBC + BEMCMD	BEMCMA
1	140	50	24	71	18	14	50[c]	21
2	140	50	1.5	19	2	nd[d]	nd	nd
3	130	50	24	79	10	nd[d]	nd	nd
4	120	50	24	57	5	67[e]	19[f]	2
5	120	50	65	82	14	7	38[g]	7
6	100	50	24	50	0	84	5[h]	0
7	160	50	24	58	16	nd[d]	nd	nd

Reaction conditions: 1 g BEBO, 6 mol % Bu_4NBr a) yield of cyclic carbonate groups based ^{1}H NMR spectroscopy b) yield of aldehyde group based ^{1}H NMR spectroscopy c) 42 % BEBC 58 % BEMCMD d) nd - not done e) 94 % BEMCMO 6 % BEMCMA f) 43 % BEBC 57 % BEMCMD g) 41 % BEBC 59 % BEMCMD h) 85 % BEBC 15 % BEMCMD.

At high reaction temperatures for 24 h in the range of 130 – 140 °C (Table 4.8 Entry 1 and 3) the reaction yielded the highest amount of carbonate species. The separation by column chromatography (Entry 1) yielded two fractions. The first fraction consisted mostly of the β-elemene monocarbonate monoepoxide **BEMCMO** and aldehyde impurities. The second fraction was believed to be the biscarbonate **BEBC**, since MS confirmed its formation. However, the more detailed NMR spectroscopy analysis showed additional alkene signals via ^{1}H NMR spectroscopy (Figure 4.35) suggesting that it was a mixture of **BEBC** and monocarbonate monoalcohol BEMCMD. The full analysis of pure **BEMCMD** was not conducted, but the partial NMR spectroscopy assignments were made, based on the 2D NMR spectra of the **BEBC** and **BEMCMD** mixture (Figure 4.36).

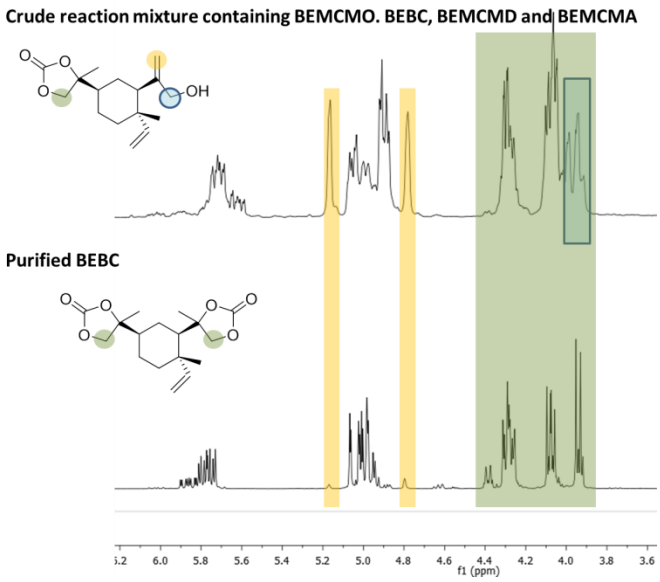

Figure 4.35 ^{1}H NMR (CDCl3, 400 MHz) spectra of crude reaction mixture and purified BEBC. The top spectrum contains characteristic signals for BEMCMD.

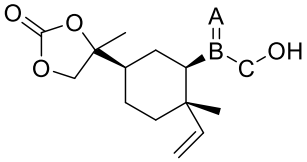

^{1}H NMR	^{13}C{H} NMR
A CH_2 5.11; 4.73	**A** CH_2 111.2; 111.1
B C_q -----	**B** C_q 150.5
C CH_2 3.92; 3.88	**C** CH_2 67.0

MS ESI-TOF+
Calclated $[M+Na]^+$ = 303.1572
Found $[M+Na]^+$ = 303.1595

Figure 4.36 Partial assignments of BEMCMD using NMR spectroscopy. obtained from mixture of BEBC and BEMCMD and results of mass spectrometry obtained from a mixture of BEBC and BEMCMD.

In general, high reaction temperatures caused an increase in **BEMCMA** production (Table 4.8 Entries 1-3 and 7). The reaction at 140 °C and 1.5 h reaction time (Entry 2) was performed to check if aldehyde production was directly correlated to high reaction temperature or high conversion of epoxides and an increased viscosity of reaction. NMR spectroscopy analysis confirmed that even with short reaction times, low concentrations of aldehyde species were produced, showing that the aldehyde production starts at low conversion. The reaction at 160 °C (Entry 7) showed similar aldehyde production as the reaction at 140 °C, and additionally the yield of carbonate species was lower, suggesting other by-products which were not further identified due to the complexity of NMR spectra. It is worth noting that high mass loss was observed during the purification of reaction mixtures obtained at high reaction temperatures indicating that the high functionality leads to higher polarity making column chromatography difficult.

At lower temperature, in the range of 100 – 120 °C (Entry 4-6), the main product after a 24 h reaction time was **BEMCMO**. With extended reaction time, it is possible to increase the yield of **BEBC** at 120 °C (Entry 5), but as a mixture with **BEMCMD**. Additionally the concentration of aldehyde species increases. As for previous reactions with high **BEBC** content, after purification a very low yield of the fraction rich in **BEBC** and **BEMCMD** was obtained. The low yield of **BEBC** and **BEMCMD** was attributed to difficulties in performing column chromatography, since the concentration of carbonate species according to NMR analysis was high. **BEMCMO** recovery on column chromatography is usually higher yielding, thus it is believed the main product of reaction at 120 °C with extended reaction time was a mixture of **BEBC** and **BEMCMD**.

The regioselectivity of **BEMCMO** and **BEMCMA** was confirmed by NMR spectroscopy analysis. The epoxide signals in **BEMCMO** show the same shifts as corresponding epoxide group in **BEBO** (56.3 56.2 53.0 52.7 via $^{13}C\{H\}$ NMR spectroscopy). The regioselectivity of **BEMCMA** was confirmed using $^{13}C\{H\}$ NMR spectroscopy (Figure 4.37).

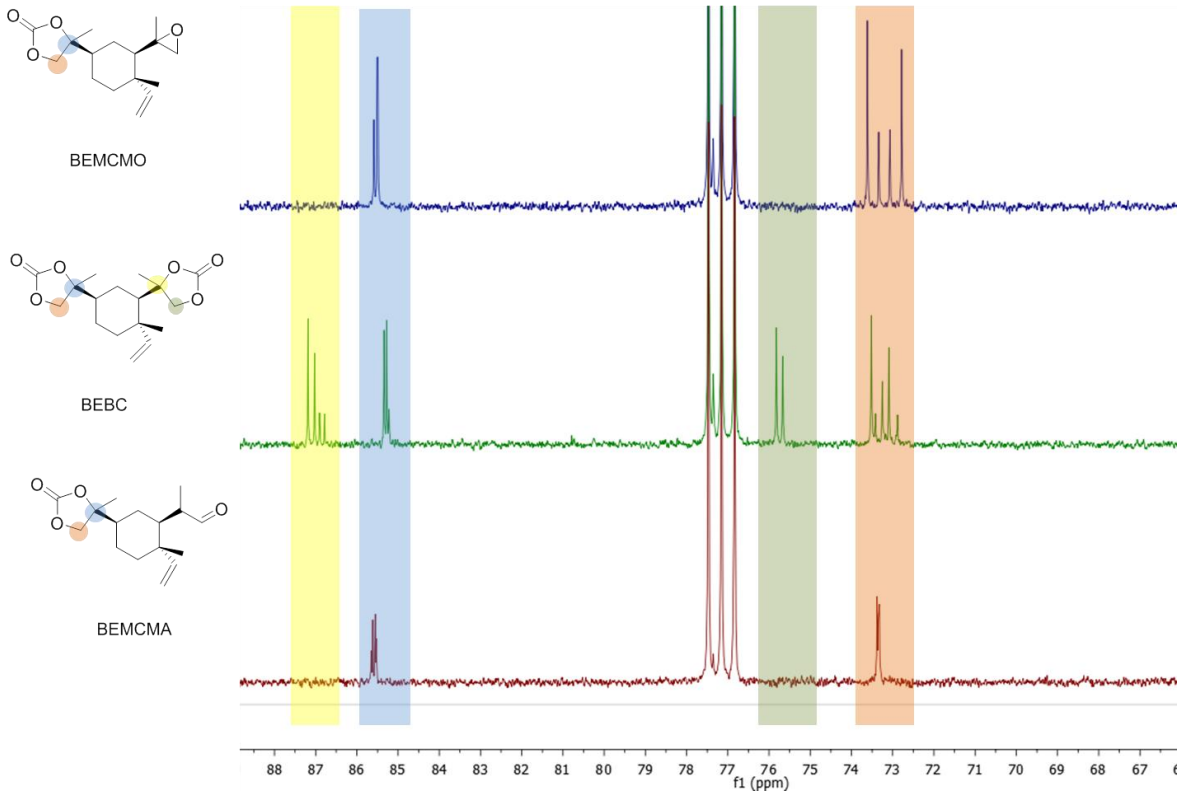

Figure 4.37 $^{13}C\{^{1}H\}$ NMR (101 MHz, $CDCl_3$) spectroscopy of BEMCMO, BEBC and BEMCMA in region of 88 – 67 ppm confirming regioselectivity of BEMCMA.

Testing other catalysts to allow process improvement was beyond the scope of this thesis, but other members of the Davidson research group showed it is possible to synthesised β-elemene carbonates at lower temperatures and lower CO_2 pressure.[51] S. Federle within her MRes project investigated aluminium amino-tris(phenolate) catalyst in β-elemene derived cyclic carbonates synthesis.[51] Aluminium amino-tris(phenolate) was previously used in terpene-derived cyclic carbonates synthesis and allowed reducing temperature and CO_2 pressure.[14] Figure 4.38 presents S. Federle's work with corresponding yields of products. The data was entirely obtained by S. Federle and is presented in this thesis only for information purposes.

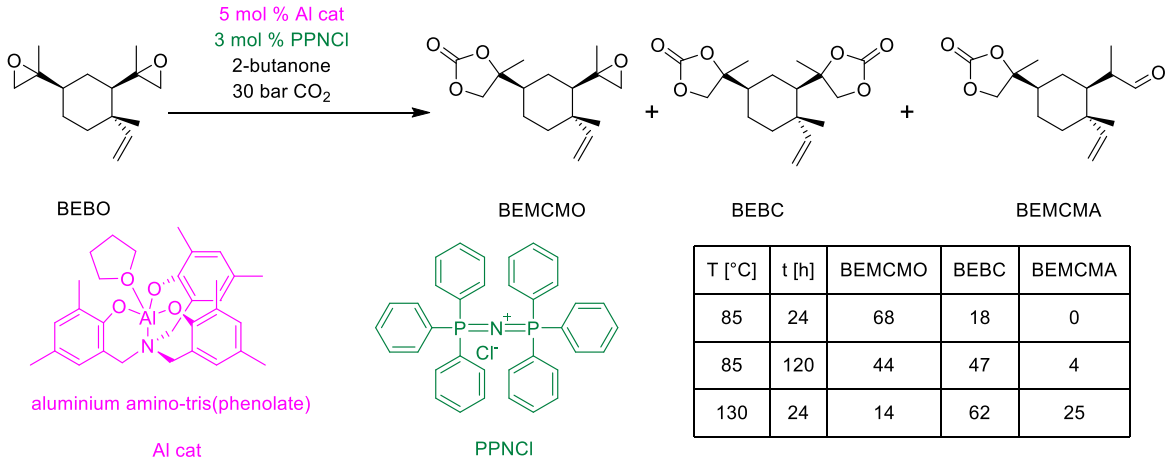

T [°C]	t [h]	BEMCMO	BEBC	BEMCMA
85	24	68	18	0
85	120	44	47	4
130	24	14	62	25

Figure 4.38 β-elemene derived cyclic carbonates synthesised using Aluminium amino-tris(phenolate) as a catalyst for carbonation reaction.[51]

At different reaction conditions aluminium amino-tris(phenolate) can yield polycarbonates, as it was presented for limonene polycarbonate.[52, 53] In this PhD project, the synthesis of β-elemene derived polycarbonates catalysed by aluminium amino-tris(phenolate) was investigated, but no polymer products were observed. Some small concentrations of cyclic carbonates were detected. The data is included in Section 4.6 Appendix.

Preliminary studies to NIPU synthesis from β - elemene biscarbonate

β-elemene biscarbonate (**BEBC**) was synthesised at 140 °C and 50 bar CO_2, but none of the purification methods used were satisfactory. Purification methods included crystallisation and column chromatography, distillation was discarded due to the high boiling point of cyclic carbonate species. Crystallisation in various organic solvents did not yield any crystals. Gel crystallisation was attempted,[54] but again no crystals were obtained. Column chromatography struggled to separate **BEBC** and **BEMCMD**, and the mass loss during purification makes it an undesirable method. Due to difficulties with **BEBC** purification the crude reaction mixture was used in NIPU synthesis with no further purification, as has been previously done in the literature for limonene

derived cyclic carbonates.[34] The content of cyclic carbonate, in the crude reaction mixture was calculated using ^{1}H NMR spectroscopy (Figure 4.39). The spectrum was referenced using the vinyl CH proton (yellow region on the figure) and integrating the carbonate region between 4.22 and 3.54 ppm (green region on the figure). The integration of this region indicates 3.20 protons and by comparing it to 4 protons (which is the maximum achievable result) it can be assumed that the carbonate content was 80 %. It is worth noting that the real value is smaller, because signals from **BEMCMD** overlap with carbonate region. Also the cyclic carbonate content includes monofunctional species such as **BEMCMA** and **BEMCMD** which can be quantified. The estimated content of **BEBC** is about 47 % **BEBC**.

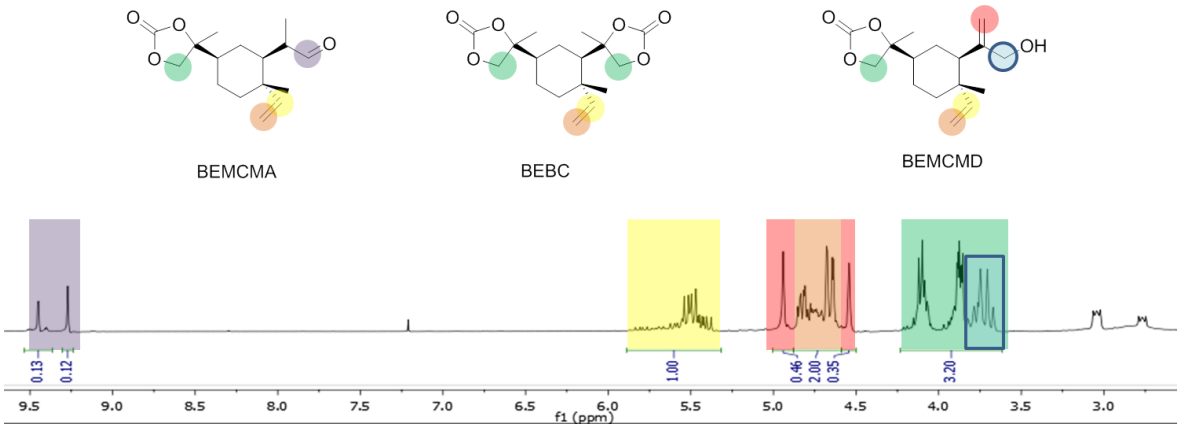

$$BEBC\ content = \frac{overal\ carbonate\ integration - BEMCMA * 2 - BEMCMD}{carbonate\ integration\ if\ 100\ \%\ pure}$$

$$= \frac{3.20 - (0.25 * 2) - (0.46 + 0.35)}{4} = \frac{1.89}{4} = 47\ \%$$

Figure 4.39 Crude reaction mixture ^{1}H NMR spectrum used for calculation of carbonate content.

The first attempt of NIPU synthesis was conducted at 100 °C in solventless conditions under Ar atmosphere. The diamines used in the synthesis are depicted in Figure 4.40. Priamine 1074 was obtained from Croda and it is a biobased diamine derived from fatty acids which is liquid at room temperature.[55] Isophorone diamine is often used as a hardener in NIPU synthesis, it contains one primary and one secondary amine which have different reactivity towards the ring opening of cyclic carbonates.[34] isophorone diamine is also liquid at room temperature. The other two amines (1,8-diaminooctane and 1,4-diaminobutane) are highly nucleophilic amines which should be highly reactive in aminolysis of cyclic carbonates,[19] both of them are solids at room temperature. The choice of amine was influenced by the choice of amine used for limonene cyclic carbonates in previously published literature.[34, 35]

As it is shown in Figure 4.40, each sample will be abbreviated as NIPU-[amine used for BEBO ring opening], for example the sample synthesised in the reaction of **BEBO** with Priamine 1074 is further refered as **NIPU-PRI**, sample synthesised in the reaction of BEBO with 1,8-diamonooctane is further refered as **NIPU-C8**.

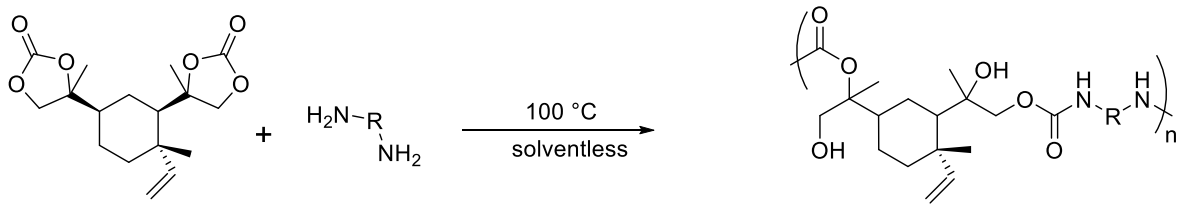

Amine		Sample Name
Priamine 1074 MW 533	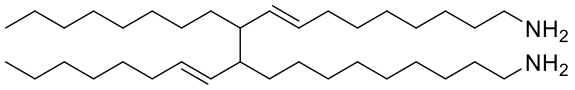	**NIPU-PRI**
isophorone diamine MW 170	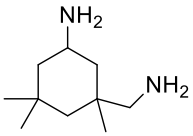	**NIPU-IP**
1,8 - diaminooctane	MW 144 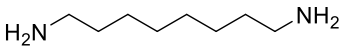	**NIPU-C8**
1,4-diaminobutane	MW 88 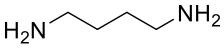	**NIPU-C4**

Figure 4.40 The reaction of a mixture containing mostly BEBC and BEMCMD and various amines at 100 °C.

All synthesised samples were yellow/brown colour with **NIPU-IP** showing slightly less colouration than the other samples. At 100 °C all of the samples were highly viscous liquids which stopped the magnetic stirrer from rotating (Figure 4.41). Upon cooling down, **NIPU-IP** and **NIPU-C8** became solid, **NIPU-PRI** was an extremely viscous liquid and **NIPU-C4** was a viscous liquid. Due to its complexity ^{1}H NMR spectroscopy analysis is not the best available method for monitoring this reaction (Figure 4.42). However, it is worth noting that aldehyde impurities disappeared, which indicated some side reactions, possibly imine condensation. The ^{13}C NMR spectroscopy (Figure 4.43) shows a shift in carbonyl signal, where 154 ppm is characteristic for cyclic carbonates and 157 ppm was previously reported for NIPU and hydroxyurethanes.[56] IR analysis indicated whether full conversion of cyclic carbonates was achieved (Figure 4.44), as cyclic carbonates have a characteristic signal around 1800 cm^{-1}, the characteristic signal for BEBC is at 1789 cm^{-1}. All samples showed some conversion of cyclic carbonate species with **NIPU-C8** and **NIPU-C4** showing the complete disappearance of the signal at 1789 cm^{-1}, indicating full conversion of cyclic carbonates.

NIPU-PRI NIPU-IP NIPU-C8 NIPU-C4

Figure 4.41 Pictures of produced NIPU samples at the end of reaction in the reaction vessel.

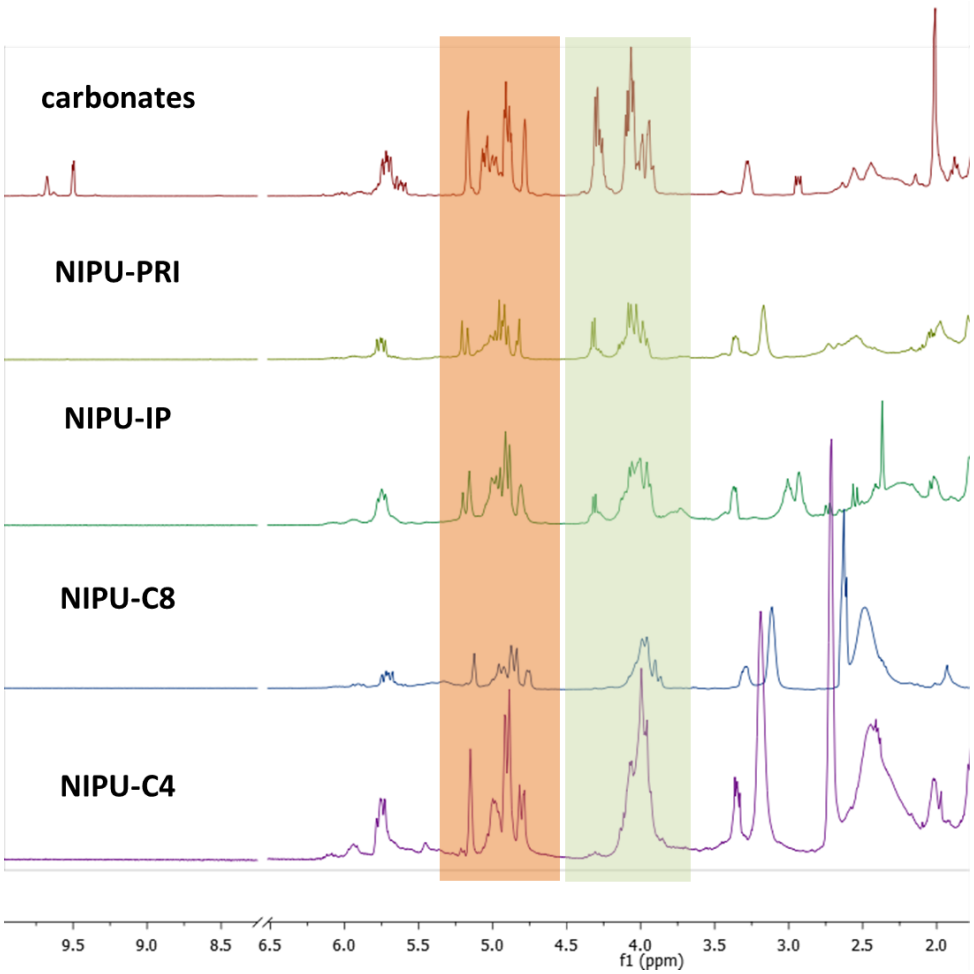

Figure 4.42 ^{1}H NMR (400 MHz, $CDCl_3$) spectrum of carbonates used for NIPU synthesis and spectra of crude reaction mixture after NIPU synthesis.Green area – carbonates functionality (note that carbonate region can contain signals from CH_2–OH originating from BEMCMD), Orange area – alkene region.

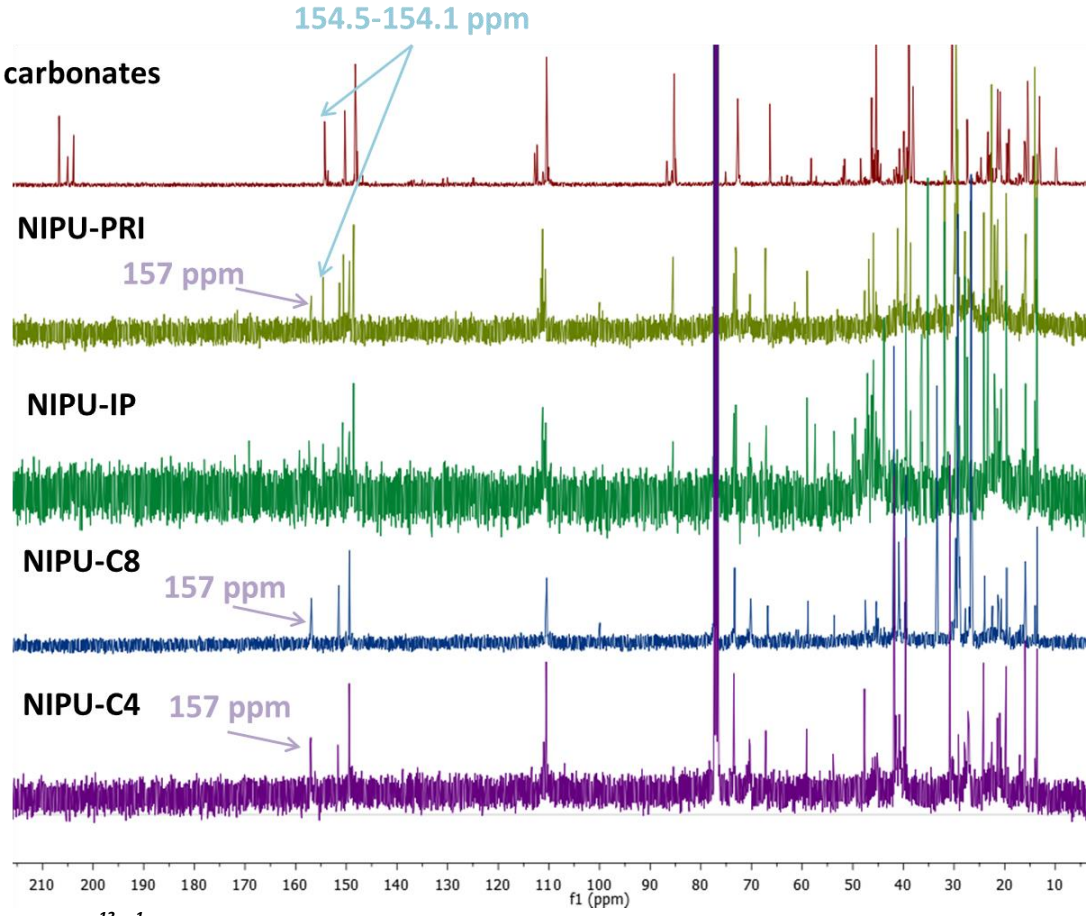

Figure 4.43 $^{13}C\{^{1}H\}$ NMR (101 MHz, $CDCl_3$)spectra of carbonates used for NIPU synthesis and NIPU samples. Signal at 154 ppm is characteristic for cyclic carbonates and signal at 157 ppm corresponds to opened cyclic carbonates.

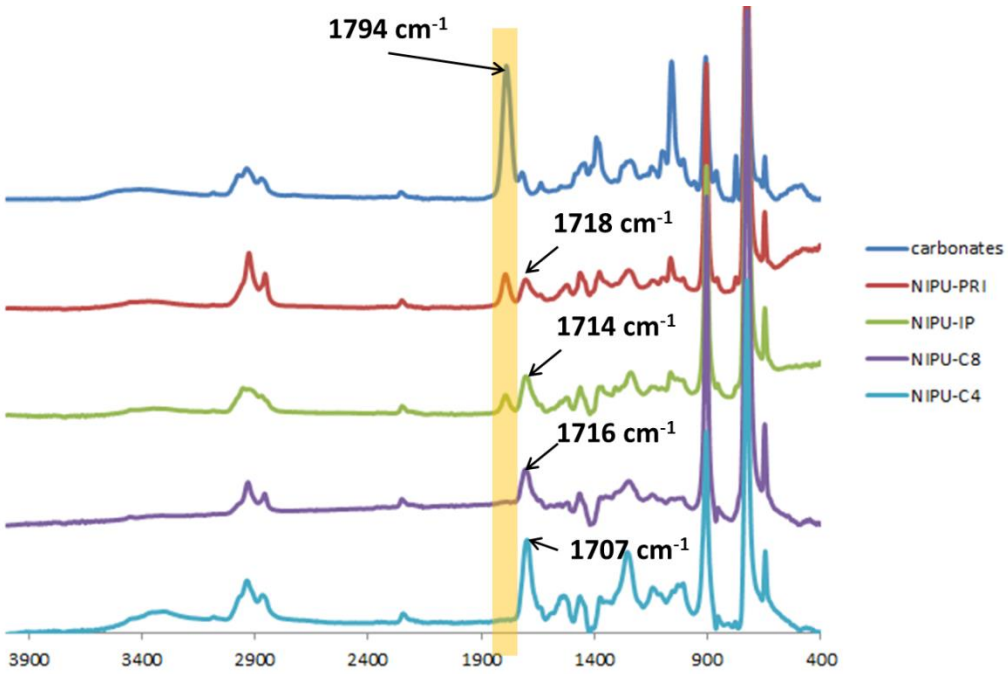

Figure 4.44 ATR-IR in the range 400 – 4000 cm^{-1}. The highlighted region corresponds to cyclic carbonates, the signals at around 1700 cm^{-1} are the urethane signals. The NH stretch is expected to be at 1535 cm^{-1} but the region is crowded and it was not highlighted.[57]

The analysis of molecular weight (M_n) was performed using GPC with a polystyrene standard (Table 4.9). Based on the GPC results, all synthesised NIPU samples had a Đ in the range of 1.2 – 1.6 which are similar to values previously reported for unpurified 1,2,8,9-limonene carbonate. However, M_n results calculated against the polystyrene standard suggest all synthesised NIPUs were small molecules, possibly consisting of one unit of carbonates and one unit of amine. The NIPU-C4 sample showed a M_n lower than a starting carbonate monomer. Considering that GPC showed low M_n, ESI-MS was used to further investigate the structure of synthesised NIPU samples (Table 4.10). The sample **NIPU-C4** was not tested due to the toxicity of the amine. All samples contained molecules consisting of one unit of amine and one unit of carbonate species.

Based on all analyses, the linear β-elemene derived NIPU have not been synthesised. Considering the low purity of **BEBC** and a high content of **BEMCMD** it is not surprising that the synthesis of NIPUs did not yield satisfactory results. Additionally, due to impure monomer the stoichiometry between carbonates and amines was imbalanced. However, these results do indicate that NIPU materials are accessible via reaction of amines with **BEBC**.

Table 4.9 GPC results.

	GPC of crude reaction mixture polystyrene standard	
Sample name	**M_n [g mol^{-1}]**	**Đ**
Carbonates	n/a	n/a
NIPU-PRI	1757	1.5
NIPU-IP	534	1.4
NIPU-C8	648	1.6
NIPU-C4	214	1.2

Table 4.10 ESI - mass spectrometry results.

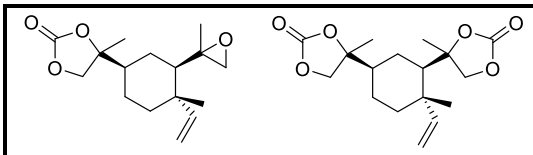

BEMCMO
Exact Mass: 280.1675

BEBC
Exact Mass: 324.1573

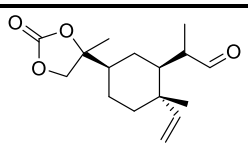

BEMCMA
Exact Mass: 280.1675

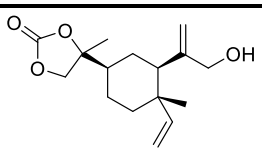

BEMCMD
Exact Mass: 280.1675

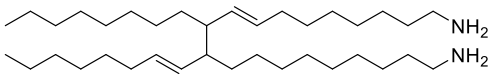

PRI
Exact Mass: 532.5696

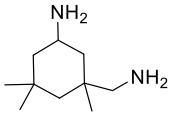

IP
Exact Mass: 170.1783

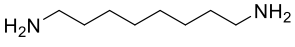

C8
Exact Mass: 144.1626

		Calculated	Found
ESI-MS of sample NIPU-PRI	**$C_{52}H_{97}N_2O_4$** [PRI+BEMCMO or BEMCMA or BEMCMD+H]$^+$	813.7448	813.7450
	$C_{53}H_{97}N_2O_6$ [PRI+BEBC+H]$^+$	857.7347	857.7368
ESI-MS of sample NIPU-IP	**$C_{26}H_{47}N_2O_4$** [IP+BEMCMO or BEMCMA or BEMCMD+H]$^+$	451.3536	451.3622
	$C_{37}H_{68}N_4Na_1O_6$ [IP+BEBC+IP+Na]$^+$	687.5037	687.5317
ESI-MS of sample NIPU-C8	**$C_{24}H_{45}N_2O_4$** [C8+BEMCMO or BEMCMA or BEMCMD+H]$^+$	425.3379	425.3446

β - elemene cyclic carbonates derived from β - elemene trisepoxide

The previous carbonation studies were performed on **BEBO**, but the synthesis of bi-functional carbonate species from **BEBO** required elevated temperature due to the low reactivity of the sterically hindered epoxide group. The less sterically hindered epoxide group was fully reacted at 100 °C and 24 h reaction time. This difference in reactivity indicates that steric hindrance of the epoxide might have an influence on its reactivity.

BETO has three epoxide groups and two of them are less sterically crowded than the slowly reacting epoxide group of **BEBO**. Since the bi-functional carbonate species are more interesting for

NIPU synthesis than mono-functional carbonate species, **BETO** was used in carbonation reaction to investigate if it is possible to synthesise bi-functional carbonate species at lower temperature.

BETO was synthesised using mCPBA (Figure 4.45), but the electron deficient vinyl group is less reactive to mCPBA oxidation than other β-elemene double bonds, resulting in longer reaction time and by-product formation, such as diols and aldehydes. Additionally, purification of **BETO** shows issues, the yield of column chromatography was significantly lower than the yield observed for **BEBO** and attempts of distillation at reduced pressure were unsuccessful. Moreover, **BETO** is more viscous than **BEBO** which might be a problem for large scale processing. However, if **BETO**'s additional epoxide group allows synthesis of bi-functional carbonate species at lower reaction temperatures and high selectivity, it might be beneficial to overcome issues related to **BETO**. The purification issues might be addressed by a different **BETO** synthesis and the issues related to processing a viscous compound can potentially be overcome by adding solvent from a wide range of green solvents.

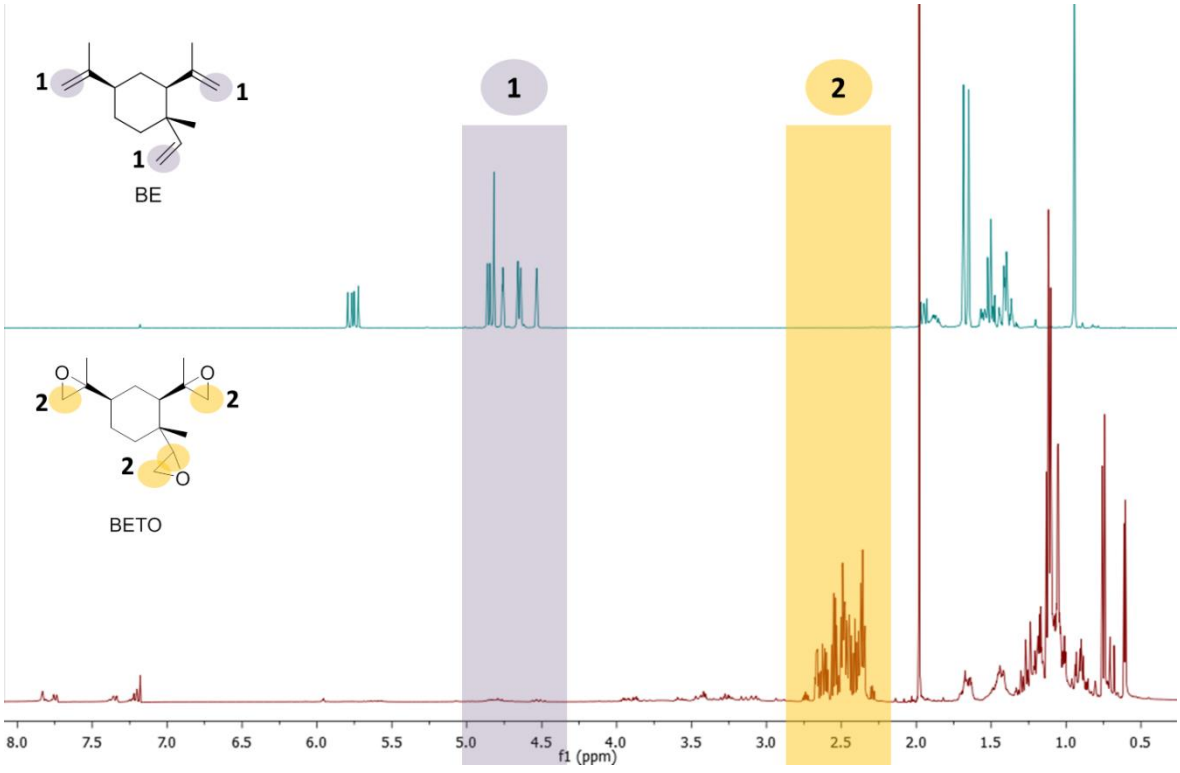

Figure 4.45 Epoxidation of BE to BETO. Top: β-elemene Bottom: β-elemene trisepoxide. The disappearance of all double bonds (1) shows that β-elemene was fully oxidised and replaced by epoxide peaks (2). The impurities from mCPBA are visible around 7.30-7.70 ppm and acetone at 2.0 ppm. Acetone was removed before carbonation using high vacuum pump, but impurities from mCPBA were not possible to remove.

First, the reaction of **BETO** at 100 °C was performed (Figure 4.46). As expected, not all epoxide groups reacted (Figure 4.47). Conversion and yield calculations are constrained by the complexity of the NMR spectra. None of the diagnostic methyl groups are resolved from other signals and the signal of the vinyl group double bond at 6 ppm is not present in **BETO** spectra, which makes referencing NMR spectroscopy signals impossible without adding an external standard. It is worth noting that working with an external standard and extremely viscous reaction mixture creates additional difficulties in obtaining quantitative results. Conversion can be roughly estimated by assuming that integration of the epoxide groups, cyclic carbonate groups and aldehyde peaks totals 7 protons, which is the number of protons present in **BETO** epoxides groups (Figure 4.48). Following carbonation at 100 °C, only traces of aldehyde groups were detected, and the ^{1}H NMR spectroscopy signal was too small to integrate, thus only epoxide groups, cyclic carbonates and impurities at 4.93-4.76 ppm were taken into consideration. A rough estimation of conversion and yields shows conversion of 56 % epoxy groups and about 52 % yield to cyclic carbonate groups. The reaction was purified by column chromatography and the main product of reaction was biscarbonate monoepoxide **BEBCMO**. The products of the reaction were identified using NMR spectroscopy, ESI-MS and IR.

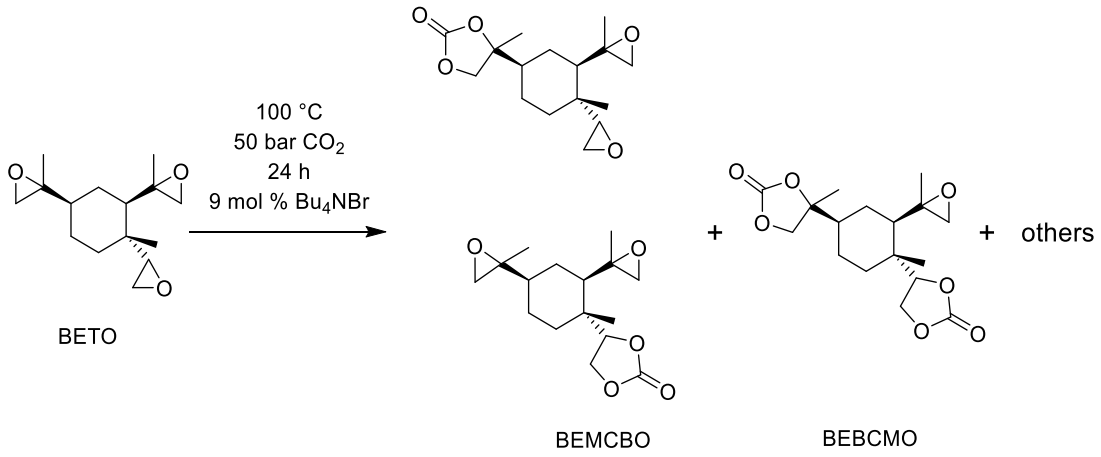

Figure 4.46 The carbonation of BETO at 100 °C, 50 bar CO_2, 24 h, 9 mol % Bu_4NBr.

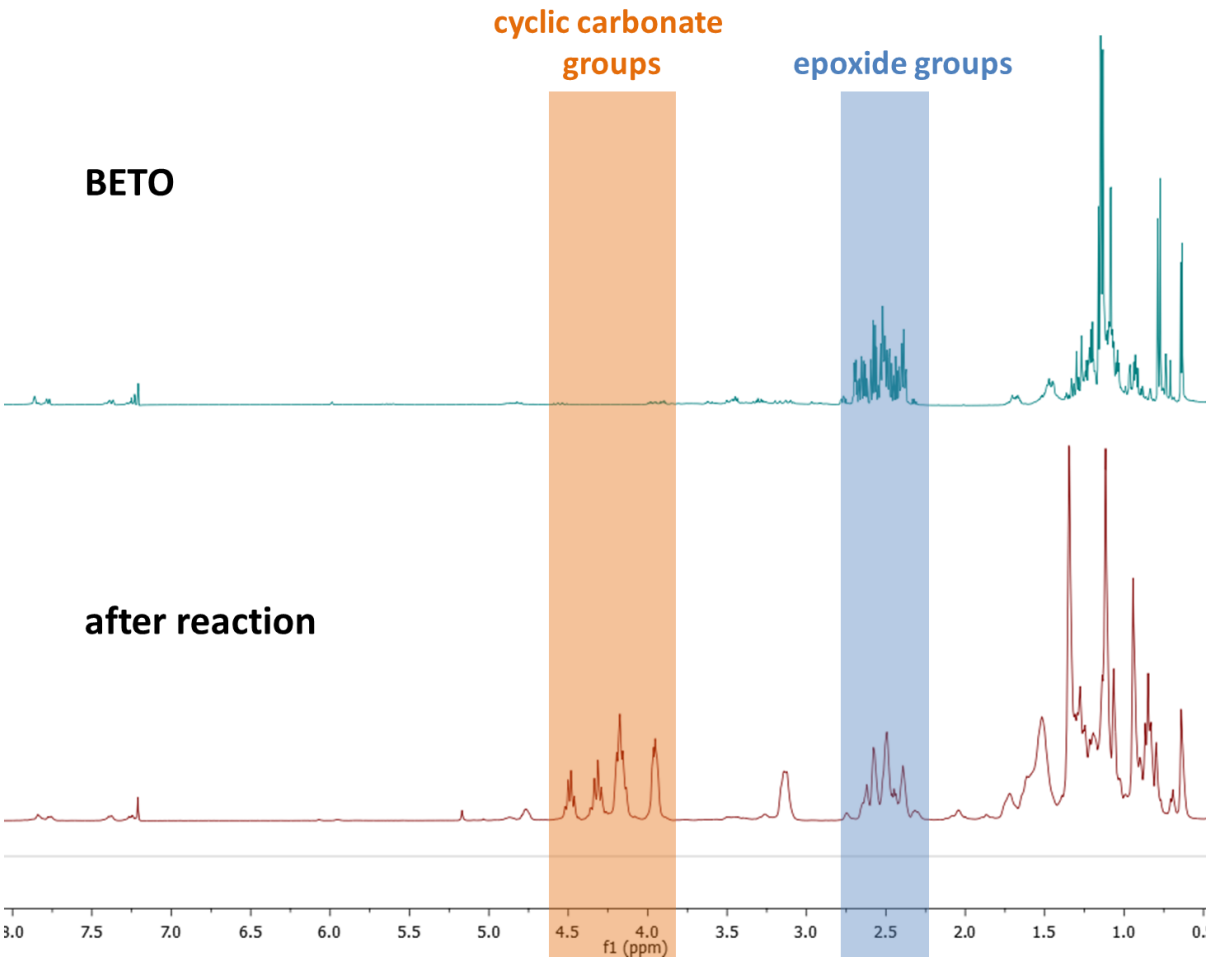

Figure 4.47 ^{1}H NMR spectroscopy of the carbonation of BETO at 100 °C, 50 bar CO_2, 24 h, 9 mol % Bu_4NBr.

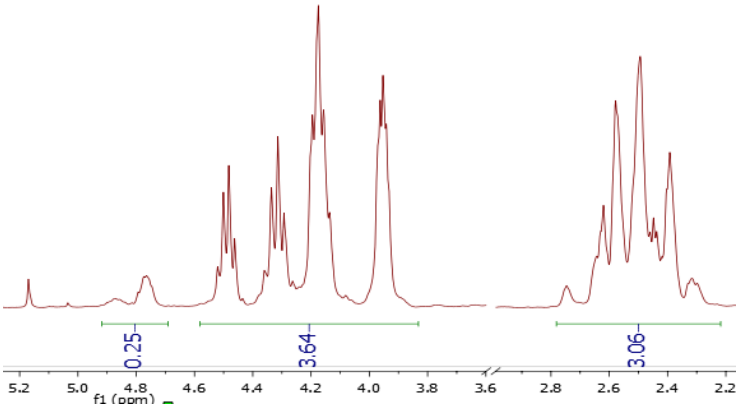

$$conversion\ of\ epoxide\ groups = 1 - \frac{3.06}{7} = 56\ \%$$

$$yield\ of\ cyclic\ carbonates\ groups = \frac{3.64}{7} = 52\ \%$$

Figure 4.48 Conversion and yield estimation for BETO carbonation at 100 °C.

The regioselectivity of **BEBCMO** was confirmed by NMR spectroscopy using 2D experiments and DEPT135 (Figure 4.49 and 4.51). All epoxide signals (purple, 2.5 – 2.8 ppm) show correlation on HSQC with carbons at 54.4 – 57.0 ppm which correspond to the signals of the corresponding epoxide group in **BETO**. Additionally, in the HMBC, the epoxide protons show correlation to only one CH_3 group at 19.8 – 20.6 ppm. The CH carbonate peak (orange) is distinctive from other signals as it is the only CH environment from the carbonate groups, and it correlates to CH carbon at 83.6 and 83.7 ppm. The CH_2 (blue and yellow) were assigned based on additional information from HMBC where the yellow CH_2 group correlates to the CH carbon (orange) and the blue CH_2 group correlates to the CH_3 carbon at 21.7 ppm.

The findings of the NMR spectroscopy are consistent with the hypothesis that the most sterically hindered epoxide group will not react at 100 °C. It is also consistent with previous results presented for **BEBO**, in which it has been found that higher temperature is necessary to react both epoxides. Considering the complexity of carbonyl signal at 154.4 – 154.8 ppm on ^{13}C {^{1}H} NMR spectroscopy, **BEBCMO** is expected to be a mixture of most, if not all, possible stereoisomers (Figure 4.50).

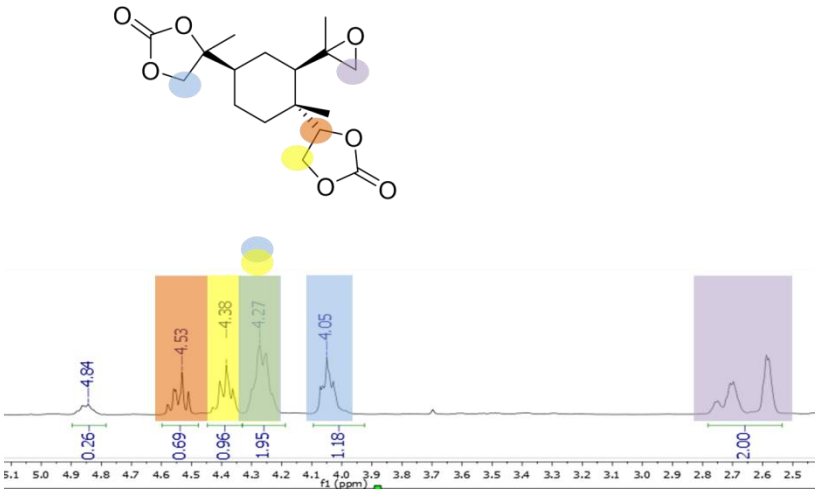

Figure 4.49 Assignments of key signals of BEBCMO on ^{1}H NMR spectroscopy of purified BEBCMO sample.

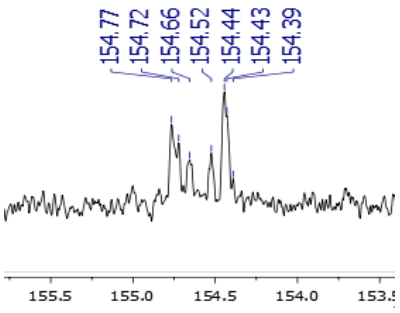

Figure 4.50 BEBCMO carbonate C=O signal on $^{13}C\{H\}$ NMR spectroscopy of purified sample.

The signal at 4.84 ppm is believed to be an impurity since it did not show any correlation to the carbonates signals at 154.4 – 154.8 ppm on the HMBC spectrum. The impurity is still present in the **BEBCMO** sample after purification by column chromatography, and possibly it was some structure with hydroxy groups, which might be a result of epoxide ring opening or epoxide rearrangements. However, the structure of the impurity has not been fully resolved. Other signals from this impurity must overlap with either carbonate groups or the epoxide, but no obvious interactions were observed on by 2D NMR spectroscopy.

The formation of **BEMCBO** was confirmed by ESI-MS which detected signals at 297.2 and 319.2 g mol^{-1} corresponding to $[M+H]^+$ and $[M+Na]^+$ adducts respectively. The regioselectivity was analysed by NMR spectroscopy, the analysis showed it is a mixture of regioisomers with one species being dominant in the mixture (Figure 4.51). The full assignments were not performed due to insufficient quality of NMR spectra.

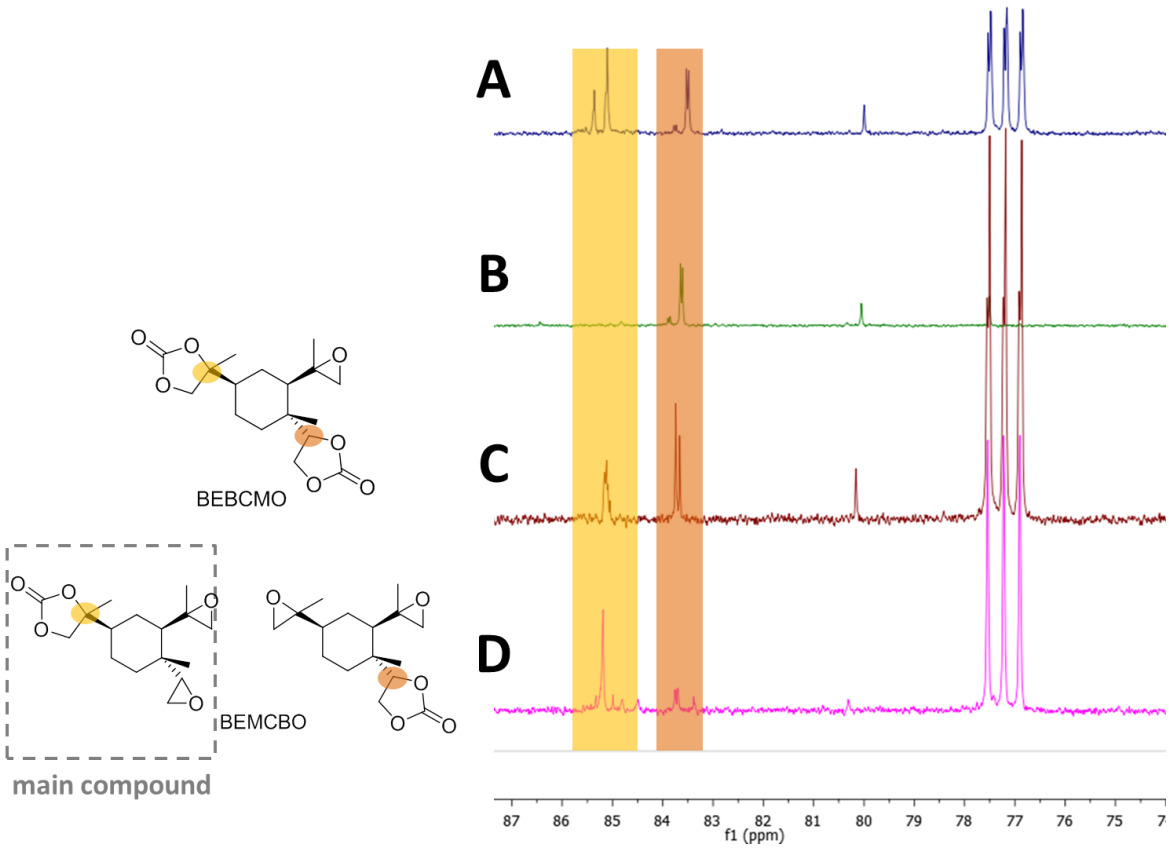

Figure 4.51 Changes in $^{13}C\{^1H\}$ NMR spectroscopy for BEBCMO, BEMCBO and crude reaction mixture.
A – $^{13}C\{H\}$ NMR spectrum of crude reaction mixture containing BEBCMO and BEMCBO;
B – DEPT135 of crude reaction mixture containing BEBCMO and BEMCBO;
C – $^{13}C\{H\}$ NMR spectroscopy of purified BEBCMO;
D – $^{13}C\{H\}$ NMR spectroscopy of purified BEMCBO.
All spectra were referenced against chloroform residue at 77.16 ppm, the signal at 80.1 ppm corresponds to the unidentified by-product.

The second reaction with **BETO** was performed at 140 °C (Figure 4.52) with an assumption that all epoxides can react at high temperature giving cyclic carbonates. Unfortunately, not all epoxide groups reacted (Figure 4.53), the conversion and yield estimation is presented in Figure 4.54. The yield of cyclic carbonates groups increased to 67 %. The yield of aldehyde groups increased to 2 % and other by products were visible on a crude reaction mixture spectrum.

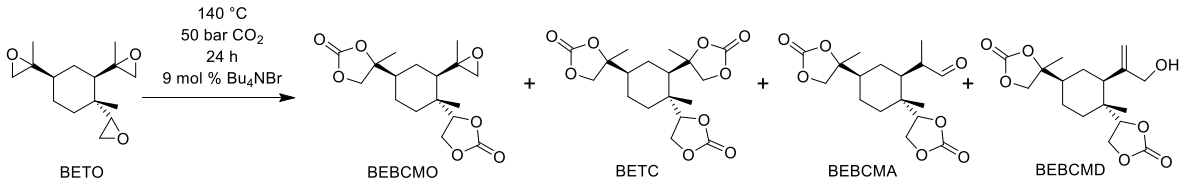

Figure 4.52 The carbonation of BETO at 140 °C, 50 bar CO_2, 24 h,9 mol % Bu_4NBr.

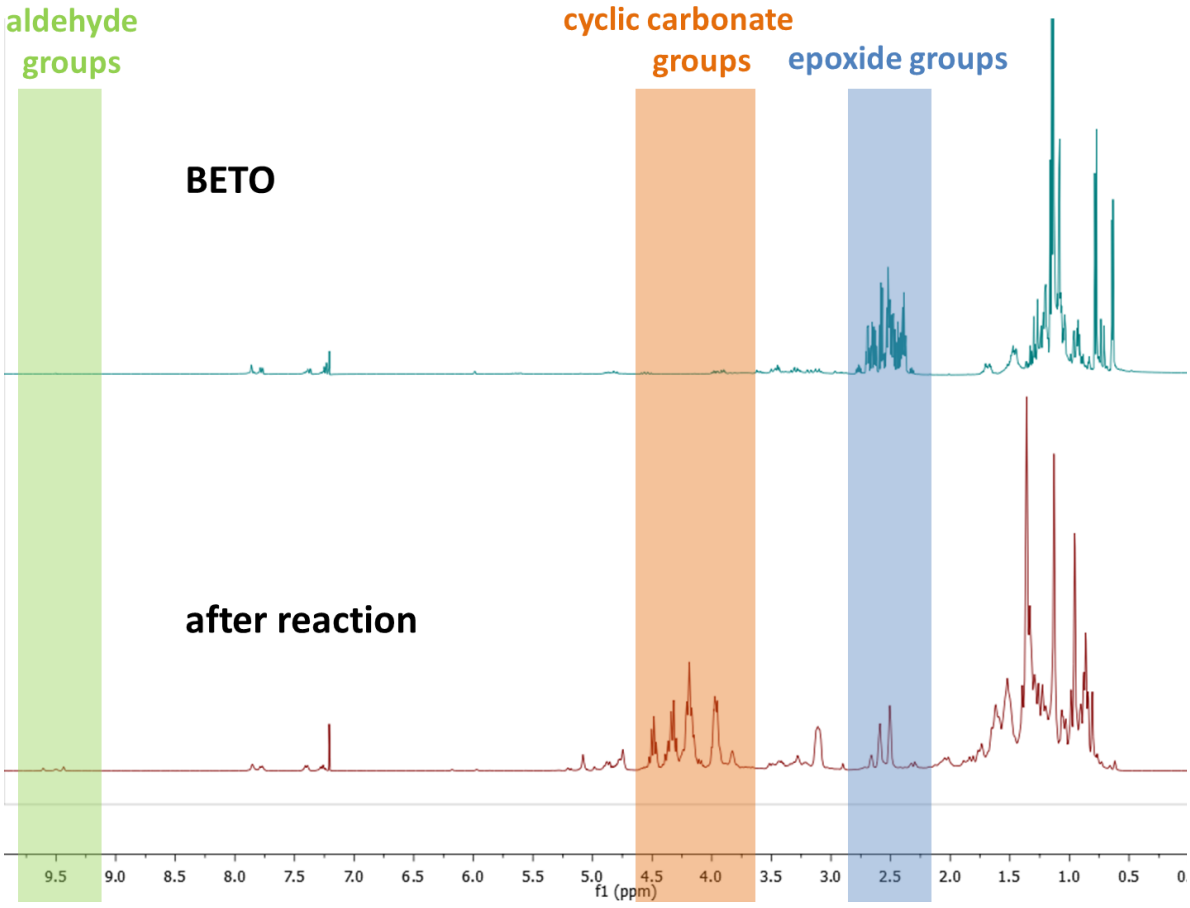

Figure 4.53 ^{1}H NMR spectrum of the carbonation of BETO at 140 °C, 50 bar CO_2, 24 h,9 mol % Bu_4Br.

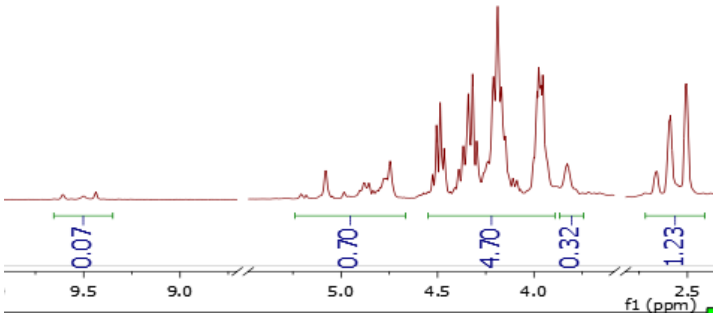

$$conversion\ of\ epoxide\ groups = 1 - \frac{1.23}{7} = 82\ \%$$

$$yield\ of\ cyclic\ carbonates\ groups = \frac{4.70}{7} = 67\ \%$$

$$yield\ of\ aldehyde\ groups = \frac{0.07 * 2}{7} = 2\ \%$$

Figure 4.54 Conversion and yield estimation for BETO carbonation at 140 ℃.

The reaction mixture was purified by column chromatography and two fractions were separated. The first one was identified as **BEBCMO**, as NMR spectroscopy was consistent with the sample obtained from reaction at lower temperature. The second fraction was analysed by IR, ESI-MS and NMR spectroscopy. IR confirms the formation of cyclic carbonates by the characteristic C=O stretch at 1785 cm^{-1}. ESI-MS confirmed formation of **BETC** by detecting a signal at 407.1364 g mol^{-1} which corresponds to sodium adduct of **BETC**. However, NMR spectroscopy analysis was unclear and the full assignments of **BETC** were not possible. The further NMR spectroscopy and ESI-MS analysis showed presence of impurity **BEBCMD** and the partial NMR spectroscopy assignments with ESI-MS results are presented in Figure 4.55.

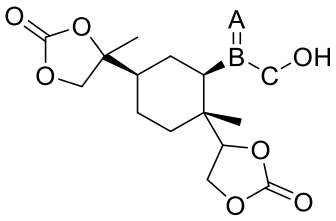

^{1}H NMR

A CH_2 5.22; 4.88
B C_q -----
C CH_2 3.95

$^{13}C\{H\}$ NMR

A CH_2 114.3
B C_q 149.0
C CH_2 66.7

MS ESI-TOF+
Calclated $[M+Na]^+$ = 363.1420
Found $[M+Na]^+$ = 363.1457

Figure 4.55 BEBCMD, NMR spectroscopy partial assignments and ESI-MS results.

The composition of a mixture recovered from a chromatography column which contains **BETC** and **BEBCMD** was estimated using ^{1}H NMR spectroscopy (Figure 4.56). The composition was estimated to be 33 % **BETC** and 67 % **BEBCMD**. The **BEBCMD** formation is not surprising since a similar effect was described previously for **BEBC** and **BEMCMD**. It is not clear if the by-product formation is a result of increased viscosity, lack of CO_2, high reaction temperature or a complex interplay of multiple factors.

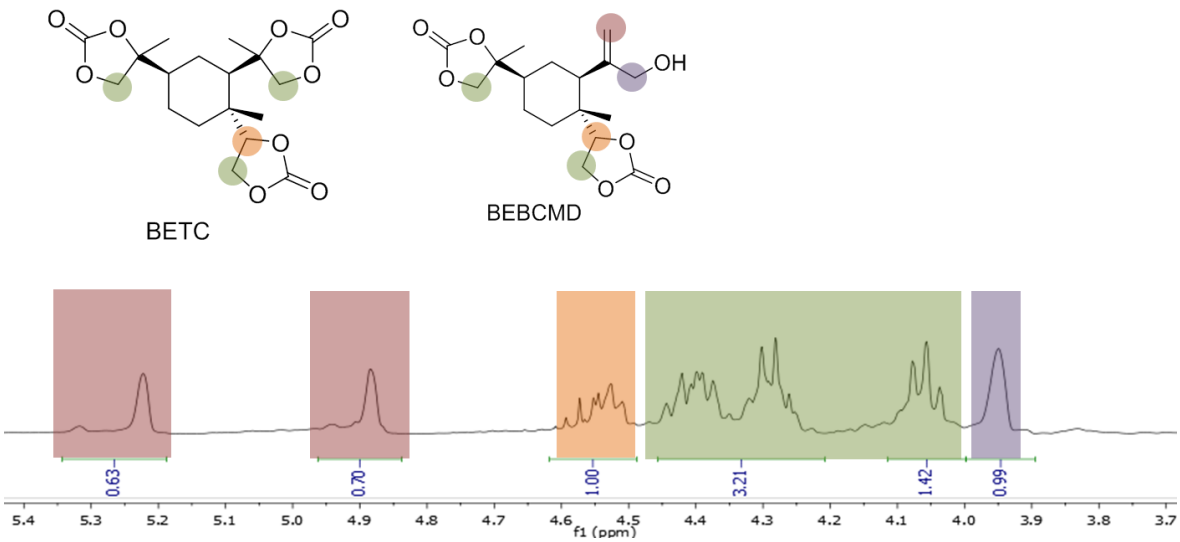

$$BEBCMD\ content = \frac{alkene\ signals}{alkene\ signals\ if\ sample\ consist\ of\ 100\%\ BEBCMD} = \frac{1.33}{2} = 67\ \%$$

Figure 4.56 ^{1}H NMR (400 MHz, $CDCl_3$) spectrum of a mixture of BETC and BEBCMD.

4.2.3 Examples of other terpene-derived cyclic carbonates

Carvone cyclic carbonates and their stereochemical behaviour

Carvone is a terpene isolated from spearmint and it is structurally similar to limonene. The main difference is in their ring structure; limonene contains a cyclohexene ring while carvone contains a cyclohexenone ring (Figure 4.57). This change makes the 8,9 position favourable for epoxidation with mCPBA yielding carvone-8,9-oxide (**8,9-CO**), whereas in limonene mCPBA oxidation favours 1,2 position under the same reaction conditions. The epoxidation of the 1,2 position in carvone is possible via alkaline H_2O_2 epoxidation and it yields carvone-1,2-oxide (**1,2-CO**).[58]

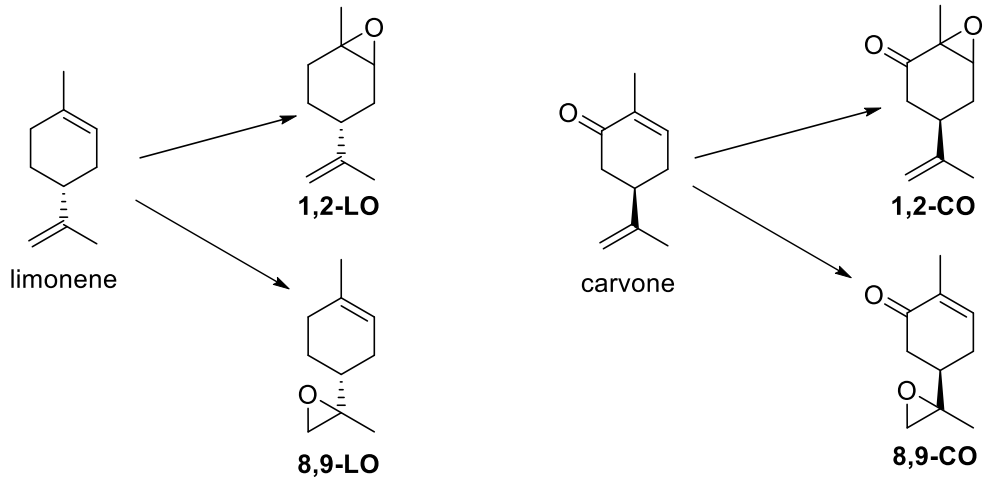

Figure 4.57 Structures of limonene, carvone and their epoxides.

1,2-CO and **8,9-CO** can react with CO_2 and yield corresponding cyclic carbonates. Carvone 1,2-cyclic carbonate (**1,2-CC**) has been synthesised by Fiorani *et al.*[14] and carvone 8,9-cyclic carbonate (**8,9-CC**) has been synthesised in this work (Figure 4.58). Here, **8,9-CC** has been synthesised via carbonation of **8,9-CO** using Bu_4NBr as catalyst (Figure 4.59). The reaction is as rapid as for **8,9-LO** and after 1.5 h showed full conversion with selectivity over 90 %. **1,2-CC** and **8,9-CC** show similar stereochemistry behaviour to **1,2-LC** and **8,9-LC**. Carvone 1,2-oxide (**1,2-CO**) yields mostly one cyclic carbonate isomer (**1,2-CC**) and carvone 8,9-oxide (**8,9-CO**) yields two isomers of cyclic carbonates (**8,9-CC**).

Selective carbonation of **1,2-LO** towards ***trans*-1,2-LC** is caused by the steric hindrance of epoxide in 1,2-position constraining the nucleophilic attack on it. Unlike **1,2-LC**, the stereoselectivity of **1,2-CC** is a result of selective epoxidation of carvone in 1,2-position which yields only one isomer of epoxide,[58] not due to the steric hindrance of the epoxide. Since epoxidation of the 1,2 position is a stereoselective process, the carbonation also yielded mostly one isomer of cyclic carbonates. In comparison, epoxidation at the 8,9 position yields a mixture of **8,9-CO** isomers and carbonation yields corresponding cyclic carbonates isomers in a ratio of approximately 54:46. The changes in ^{1}H NMR spectroscopy between carvone, **8,9-CO** and **8,9-CC** are shown in Figure 4.60.

1,2-CC
G. Fiorani *et al.* [14]

8,9-CC
This work

Figure 4.58 Carvone cyclic carbonates, on the left: carvone cyclic carbonate previously published by Fiorani et al.[14]; on the right: carvone cyclic carbonate synthesised in this work.

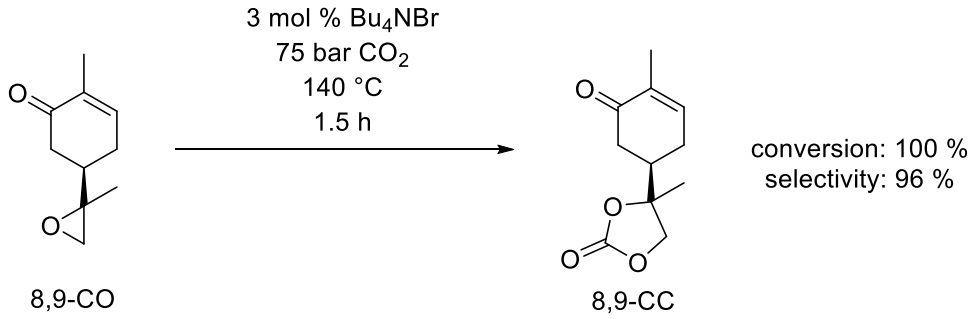

Figure 4.59 The synthesis of 8,9-CC from 8,9-CO using Bu_4NBr as a catalyst.

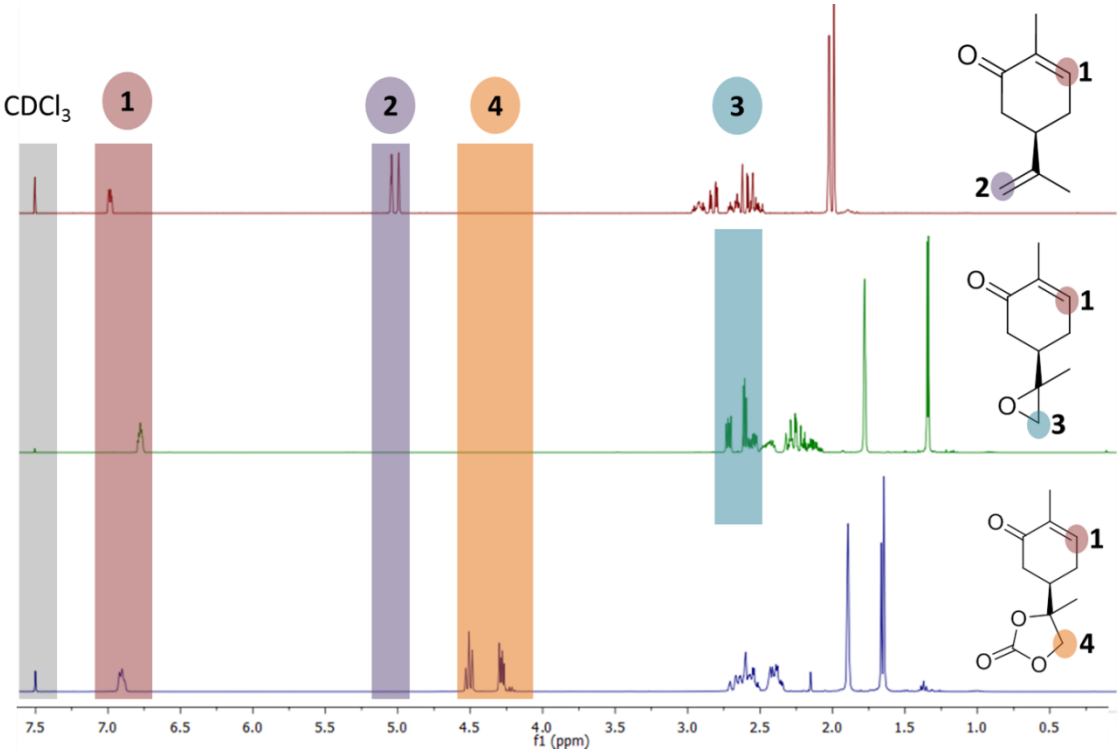

Figure 4.60 ^{1}H NMR spectra of carvone, 8,9-CO and 8,9-CC.

Farnesene cyclic carbonates

Farnesene is an acyclic terpene derived via industrial biotechnology by the American company Amyris. It is an interesting feedstock because of its potential multimillion tonne scale availability.[36] Moreover, farnesene can be epoxidised using the same flow epoxidation as limonene epoxidation – solventless epoxidation catalysed by **VENT** using a microreactor. Figure 4.61 presents the group's previous work which resulted in a protocol for highly selective epoxidation of farnesene. After 33 min residence time, 100 % conversion and about 90 % selectivity to farnesene bisepoxide (**FBO**) was achieved.

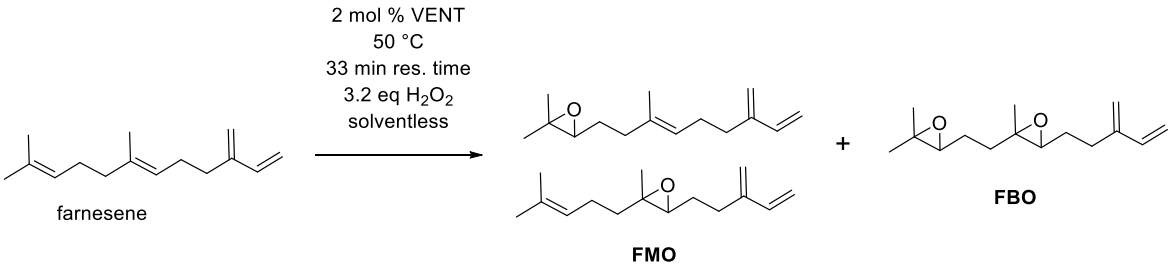

Figure 4.61 Flow epoxidation of farnesene using microreactor. VENT – Venturello catalyst, 2 mol % with respect to the amount of farnesene; res. time – residence time.
This epoxidation reaction is not part of this PhD thesis, farnesene epoxidation was previously studied within the Plucinski group.[39, 40, 59]

The synthesis of farnesene cyclic carbonates was attempted using **FBO** from the epoxidation mixture without any further purification (Figure 4.62). The changes in ^{1}H NMR spectra are presented in Figure 4.63; spectrum A is a pure sample of farnesene, spectrum B is an organic phase recovered from the epoxidation reaction and spectrum C is a crude reaction mixture after attempted carbonation. These NMR spectra suggest the organic phase recovered from epoxidation contained mostly **FBO**, but other compounds were visible by TLC (unreacted farnesene and **FMO**, possibly some other uncharacterised epoxidation by-products). The carbonation attempt presented on Figure 4.62 resulted in a complex mixture of polymeric products (Figure 4.35 spectrum C). In spectrum C, it is clear that the signal in the 2.5-3.0 region, corresponding to epoxide protons, has decreased in intensity; however, the complexity of this spectrum suggests there is a mixture of products, not necessarily just cyclic carbonates. The mixture recovered from the carbonation reactor had a foam-like structure, and was hardly soluble in organic solvents (Figure 4.34). With an excess of chloroform, it was possible to dissolve it in order to obtain a sample suitable for NMR spectroscopy, but unfortunately, the concentration was too low to obtain satisfactory ^{13}C{^{1}H} NMR spectra. The mixture recovered from the carbonation reactor was mildly soluble in THF in low concentrations, allowing for GPC to be performed, which showed a polymeric species of M_n = 12 900 g mol^{-1} and Đ = 2.80.

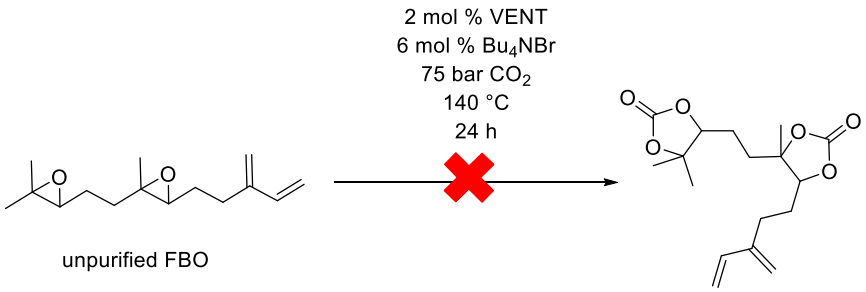

Figure 4.62 Reaction of unpurified organic layer from epoxidation with CO_2 in the presence of Bu_4NBr. The unpurified organic layer mostly contained FBO, but unreacted farnesene and FMO were present in the reaction mixture. VENT was used as the epoxidation catalyst.

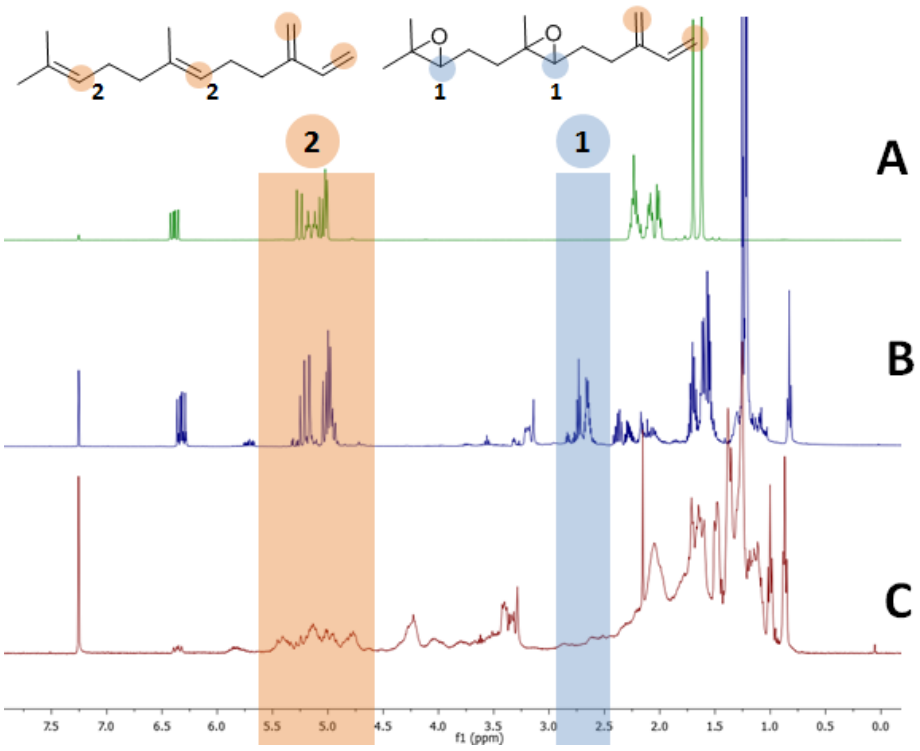

Figure 4.63 Changes in ^{1}H NMR spectra between farnesene (A), unpurified organic layer from epoxidation which contained mostly FBO (B) and a complex reaction mixture produced via carbonation presented on Figure 4.32 (C).

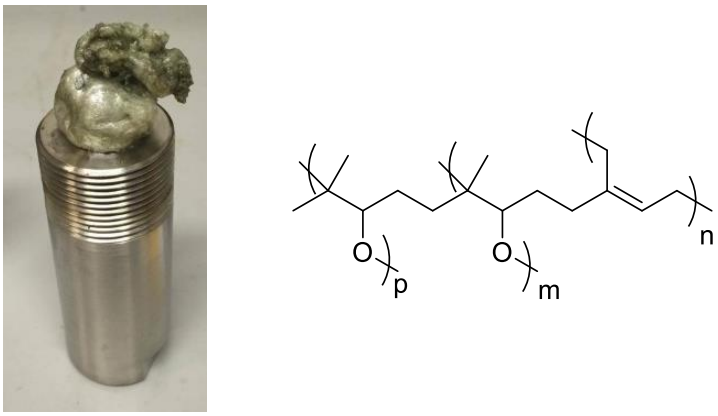

Figure 4.64 Mixture recovered from carbonation reactor had a foam-like structure. ^{1}H NMR spectroscopy results are presented in Figure 4.33 spectrum C, GPC analysis showed M_n = 12 900 g mol^{-1} and Đ = 2.80. The polymer structure was not further investigated, but some possible structures are presented.[60-62]

Another attempt to prepare farnesene cyclic carbonates involved reacting purified **FBO** with CO_2 in the presence of Bu_4NBr. Purification of **FBO** proved to be difficult - multiple attempts of distillation under reduced pressure resulted in polymerisation of **FBO** within the distillation apparatus. Purified **FBO** was obtainable via column chromatography, however, the yield was lower than expected. This may be due to reaction of **FBO** on silica, since this has been previously reported in the literature for myrcene.[14] Carbonation of **FBO** was attempted at 120 °C for 24 h, resulting in a poorly soluble mixture, which due to its insolubility could not be analysed. To reduce

the side reactions, carbonation at 100 °C and a shorter reaction time of 5 h was performed (Figure 4.65), but no signals which could be assigned to cyclic carbonates were visible on ^{1}H NMR spectroscopy or $^{13}C\{^{1}H\}$ NMR spectroscopy (Figure 4.66 and 4.67).

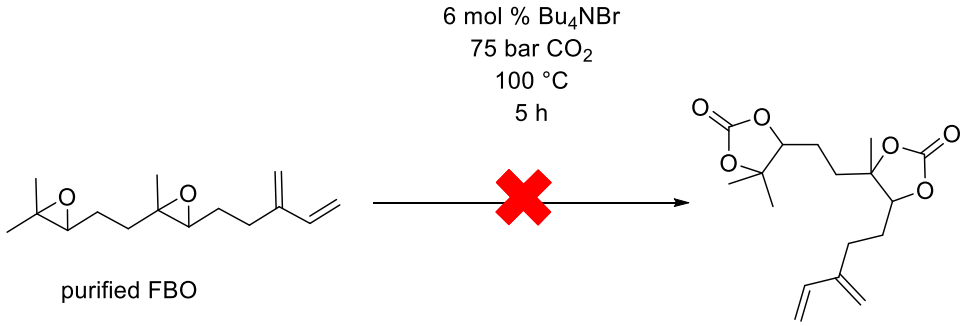

Figure 4.65 Carbonation of purified FBO catalysed by Bu_4NBr at 100 °C and 5 h reaction time. No visible signs of cyclic carbonates were observed on ^{1}H NMR spectroscopy and $^{13}C\{^{1}H\}$ NMR spectroscopy.

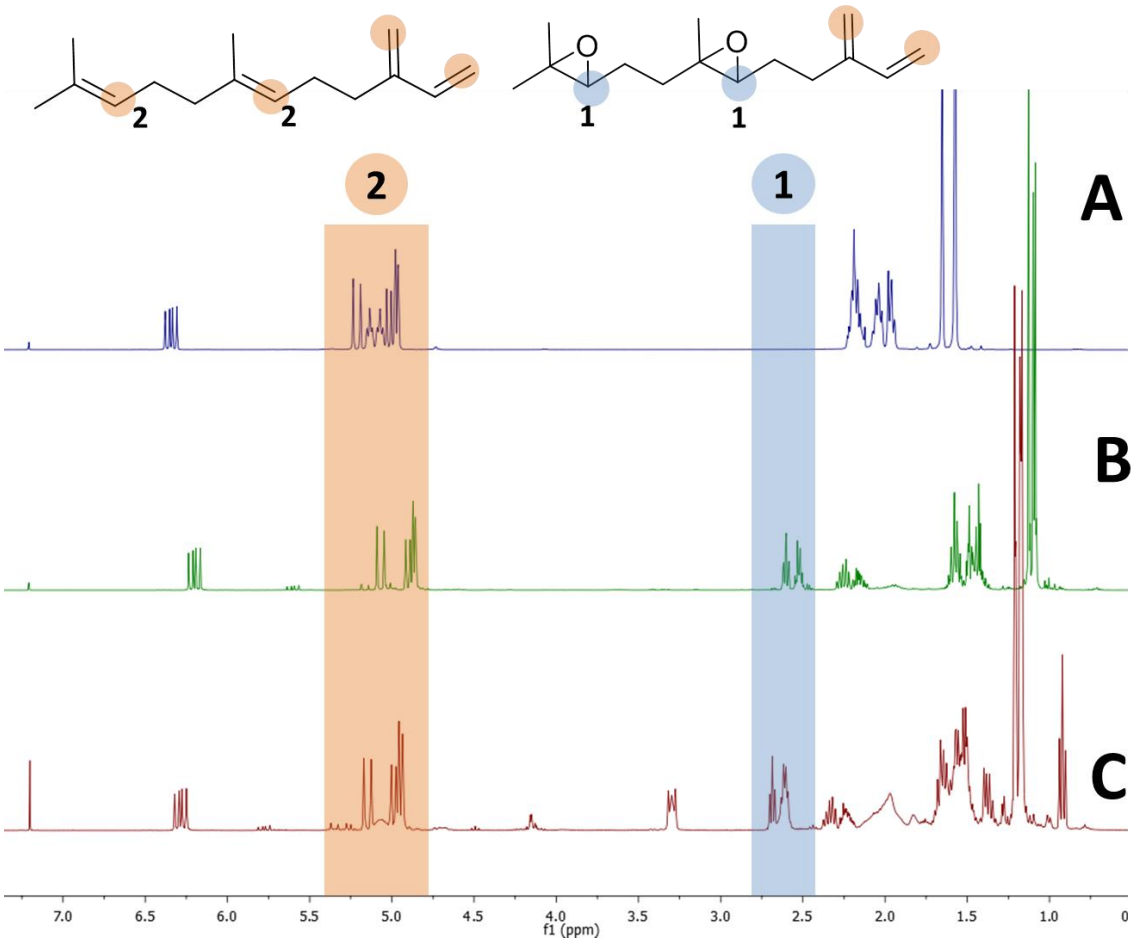

Figure 4.66 Changes in ^{1}H NMR (400 MHz, $CDCl_3$)spectra between farnesene (A), purified FBO (B) and a crude reaction mixture produced via carbonation presented on Figure 4.35 (C). The signal at 3.30 ppm corresponds to Bu_4NBr.

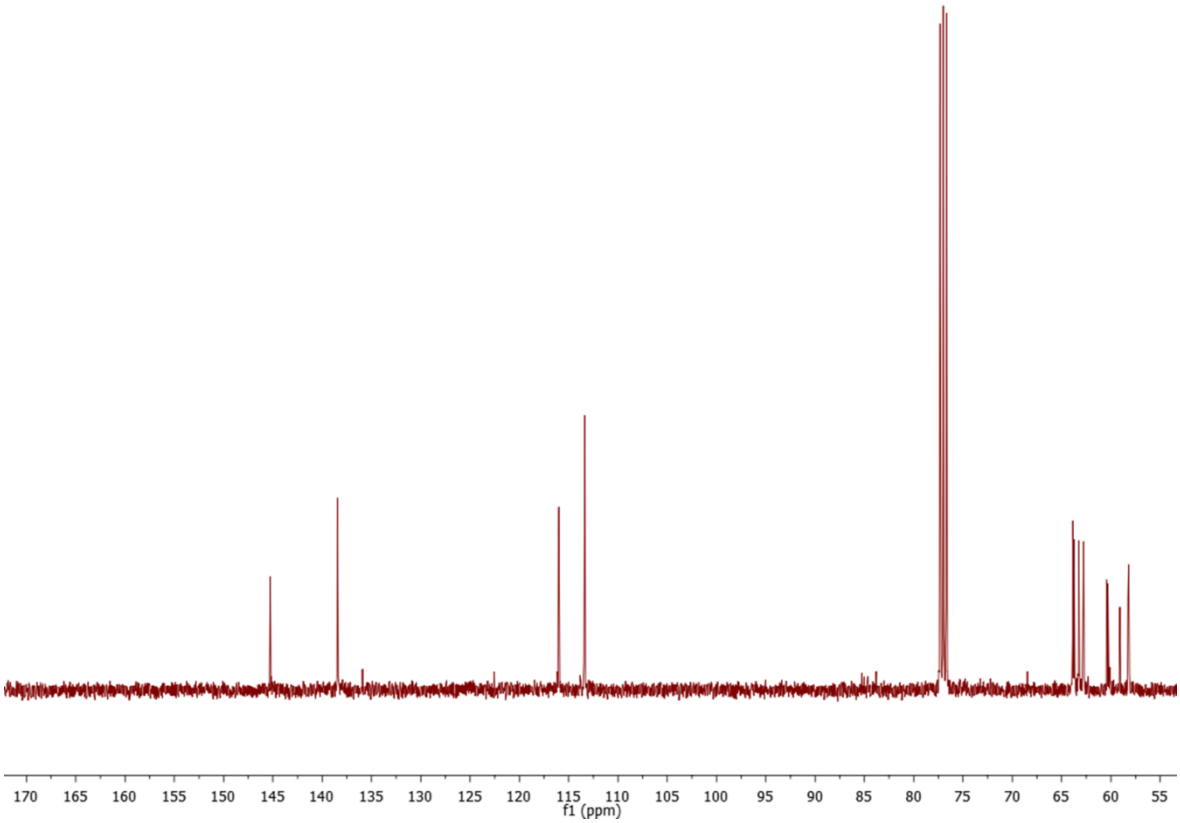

Figure 4.67 $^{13}C\{^{1}H\}$ (101 MHz, $CDCl_3$)NMR spectrum of the crude reaction mixture produced via carbonation presented on Figure 4.35. No signals around 154-155 ppm are visible, indicating that cyclic carbonates are either absent or in concentrations too low to detect.

In summary, farnesene is a promising feedstock with potential for vast availability. An efficient epoxidation protocol has been developed within the Plucinski group, allowing easy access to **FBO**. However, issues with FBO purification and the complex side reactions of **FBO** carbonation make **FBO** a challenging compound for cyclic carbonates synthesis.

4.3 Conclusions and future work

The growing interest in bio-derived NIPU and the commitment of the coating industry to improve their sustainability makes terpene-derived cyclic carbonates desirable compounds.[63, 64] 1,2,8,9-limonene cyclic carbonate has previously been used in NIPU synthesis, showing promising results.[35] Here, novel cyclic carbonates were evaluated in their suitability for NIPU synthesis.

Limonene epoxides (**1,2-LO** and **8,9-LO**) can be selectively synthesised following literature procedures. Both of them can react with CO_2 resulting in **1,2-LC** and **8,9-LC** respectively. The carbonation of 1,2-LO is stereoselective towards ***trans*-1,2-LO** and the use of the polyoxometalate based catalyst **VENT** enhanced reaction rate and shows synergistic interactions between **VENT**

and CO_2. This allows for a telescoped two-step synthesis of **1,2-LC** directly from limonene. The **8,9-LO** is less sterically hindered and both of its isomers react with CO_2 yielding cyclic carbonates.

Considering the wide availability of limonene and well-established scalable epoxidation methods, **1,2-LC** and **8,9-LC** are promising for NIPU synthesis. In this work, **1,2-LC** and **8,9-LC** have been shown to undergo thiol-ene reactions resulting in the bi-functional carbonate species which in combination with polyamines will give an access to novel NIPU with tuneable properties consisting of >50 wt% renewable feedstocks. In this work, novel hydroxyurethanes were synthesised to show their utility as novel monomers. Future work should focus on the synthesis of polymers and varying thiol linkages in order to obtain polymeric coatings with the most desirable properties. Based on available literature, the ring opening with amines can be done regioselectively.[29]

BE represents a valuable terpene feedstock derived via industrial biotechnology. That means it can provide a geographically flexible terpene feedstock with a stable price. The possibilities of scaling up industrial bioprocesses can make β-elemene cost effective feedstock, as has been done by Amyris for farnesene.[49] The β-elemene oxidation methods are still being developed and need improving, but stoichiometric methods such as mCPBA oxidation can yield all three possible epoxides such as **BEMO**, **BEBO**, **BETO**. Multifunctional carbonate species, **BEBO** and **BETO**, were evaluated in the carbonation reactions.

The carbonation of **BEBO** results in bi-functional carbonate **BEBC**. However, the sterically hindered epoxide group requires high reaction temperatures which increase the yield of by-products not usable for NIPU synthesis, such as BEMCMD. The epoxide rearrangement indicated that the epoxide is activated by halide, but either temperature or lack of CO_2 cause it to change selectivity towards the undesirable product. Further investigation into **BEBO** carbonation is required; it should focus on improving CO_2 mass transfer either via a more efficient set up or reducing the viscosity of the reaction by adding solvent. More specific future work can focus on the development of novel catalyst allowing reduction of reaction temperature while maintaining high activity.

BETO is harder to synthesise, but the carbonates synthesised from **BETO** are extremely interesting for NIPU synthesis. **BEBCMO** can be selectively synthesised at 100 °C which is a 40 °C reduction in reaction temperature comparing to **BEBC**. From all β-elemene cyclic carbonates, **BEBCMO** is the most promising due to the relatively low temperature of its synthesis (100 °C) and high selectivity of the reaction. The main focus of future work with **BEBCMO** should be on

synthesising **BEBCMO** derived polymers and investigating additional functionalization or cross-linking via the epoxy group.

The other **BETO** derived cyclic carbonate - **BETC** is a scientifically interesting compound, but the selectivity of the carbonation reaction suffers the same issues as **BEBC** synthesis – high reaction temperature, difficult CO_2 mass transfer and high production of **BEBCMD** which is not a desirable product. Future work should focus on improving **BETC** synthesis, otherwise producing this new monomer for NIPU synthesis in the quantity and purity needed will be significantly limited.

Other terpenes evaluated included carvone and farnesene. Carvone availability is limited (10^4 tonnes annually),[65] but for highly specialised applications it could be investigated for NIPU synthesis. Although no additional work was carried out in this thesis, **8,9-CC** is expected to behave similarly to **8,9-LC**. Farnesene was evaluated because of its availability via industrial biotechnology and efficient epoxidation method, but the difficulties related to farnesene bisepoxde purification and synthesis of farnesene derived cyclic carbonates make it challenging for applications in NIPU.

4.4 Experimental

4.4.1 General consideration

All reagents and NMR solvents were sourced from Sigma Aldrich, Alfa Aesar or Fischer Scientific. All solvents, except NMR solvents, were sourced from VWR and used as received. Liquid CO_2 was obtained from BOC (99.8 % CO_2).

GC-MS spectra were recorded on an Agilent GCMS system (GC: 7890B, MS: 5977A) using a capillary nitroterephtalic acid-modified polyethylene glycol column of high polarity (Agilent Technologies column: DB-FFAP 30 m x 0.250 mm x 0.25) and a flame ionization detector (FID). The sample was prepared in toluene and injected at 250 °C. The oven temperature was increased by 20 °C min^{-1} from 40 °C to 250 °C, where it was kept for 5.5 min. The FID had a temperature of 300 °C. The carrier gas was helium and it was kept at a constant flow rate of 1.2 mL min^{-1} through column.

NMR spectra were obtained on a Bruker Avance III 400 MHz, Agilent ProPulse 500 MHz, Bruker Avance III 500 MHz and Bruker Avance II + 500 MHz Ultrashield equipped with a broadband observe probe. All NMR spectra were referenced against a solvent peak (chloroform-d ^{1}H NMR: 7.26 ppm ^{13}C {1H} NMR 77.16 ppm).

IR spectra were recorded on a Perkin Elmer 100 Fourier transform spectrometer fitted with an ATR accessory. The number of scans was set to 4 and resolution was set to 4 cm^{-1}.

Mass spectrometry data was obtained at the EPSRC UK National Mass Spectrometry Facility at Swansea University and at the University of Bath mass spectrometry facility using Bruker MicrOTOF electrospray time-of-flight mass spectrometer (ESI-TOF) and Bruker MaXis HD ESI-QTOF mass spectrometer for high mass accuracy.

High pressure experiments were carried out in 10 mL stainless steel autoclave equipped with a pressure gauge, a needle valve and 2-way valve. Stirring was provided using a magnetic stir bar. The autoclaves were pressurised at 40 °C using a high pressure CO_2 installation schematically depicted in Figure 4.68. Pressure was controlled by back pressure regulator. The autoclaves were heated up to the reaction temperature using an aluminium heating block, the temperature of which was controlled using a hotplate equipped with electronic thermometer.

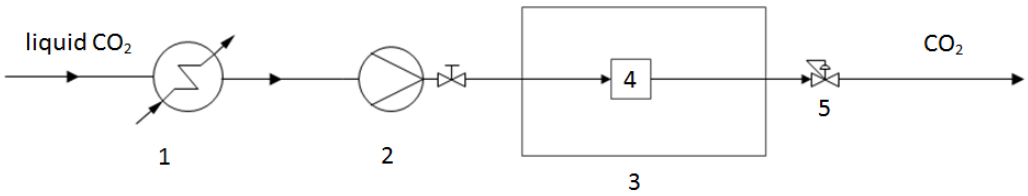

Figure 4.68 High pressure CO2 instalation.[66]
1) cooler (Julabo FL300 Recirculating Cooler); 2) liquid CO2 pump (JASCO PU-2088-CO2); 3) oven set at 40 °C; 4) 10 mL stainless steel autoclave; 5) back pressure regulator (JASCO BP-2080 plus)

4.4.2 Venturello catalyst (VENT) preparation

$$4\ H_2WO_4 + 8\ H_2O_2 + H_3PO_4 \xrightarrow{H_2O} H_3PW_4O_{24} \quad \text{[Solution 1]}$$

$$3\ [(C_8H_{17})_3NCH_3]Cl + H_3PW_4O_{24} \xrightarrow{H_2O/CH_2Cl_2} [(C_8H_{17})_3NCH_3]_3(PW_4O_{24})$$

The Venturello catalyst for olefin epoxidation was prepared according to the original Venturello preparation method with minor changes.[67] 25g tungstic acid was suspended in 80 mL 30 % wt hydrogen peroxide solution and stirred for 30 min at 70 °C leading to a colour change from yellow to light green. The light green solution was cooled down to room temperature and 6 mL 40 % phosphoric acid was added, followed by 20 min stirring. Next, this solution was diluted with 220

mL distilled water and stirred for another 15-20 min (this solution is further referred as a Solution 1).

For the cation exchange, the commercially available Aliquat 336 was used, which is an ammonium salt mixture consisting mostly of methyltrioctylammonium chloride. 21 g Aliquat 336 was dissolved in 400 mL DCM and the resulting solution was added dropwise to Solution 1 under magnetic stirring followed by 30 min additional stirring. The resulting bi-phasic mixture was separated using a separating funnel. The organic phase was collected and washed with 2x150 mL saturated NaCl water solution. After washing, the organic solution was dried over $MgSO_4$, filtered and evaporated *in vacuo*. The yield of resulting yellow oil varied between 26 and 29g (67 % -74 %).

4.4.3 Epoxidation of 1,2-LO in microreactor

Epoxidation was carried out in a microreactor with preheating channels and an integrated static mixer (Little Things Factory, XXL-ST-04, 4.5 mL reaction volume). The reaction was carried out at 50 °C. The temperature controlled by a recirculating heat exchanger (Fisher Scientific ISO UK 6200). The substrates were delivered to the reactor using syringe pumps. The first syringe was charged with 30 wt % hydrogen peroxide solution with the pH adjusted to 7 using 1M NaOH. The second syringe was charged with pure limonene containing 1 mol % Venturello catalyst. For the hydrogen peroxide solution, a plastic syringe was used. For the limonene and the catalyst solution, a stainless steel syringe was used. Both reactants were delivered to the reactor in equal volume ratios at an overall flow rate of 27 mL/h (13.5 mL/h for each syringe), 10 min residence time. Products were analysed by NMR spectroscopy and GC-MS. Conversion was 83 % and selectivity to **1,2-LO** was 90 %. The reaction yielded a mixture of **1,2-LO** isomers (59 % *cis*-**1,2-LO** and 41 % *trans*-**1,2-LO**).

Characteristic ^{1}H NMR spectroscopy signals: *trans*-**1,2-LO** doublet at 2.98 ppm; *cis*-**1,2-LO** multiplet at 3.03 ppm

4.4.4 Kinetic resolution of trans- and cis-1,2-LO

a) *Cis*-1,2-limonene oxide

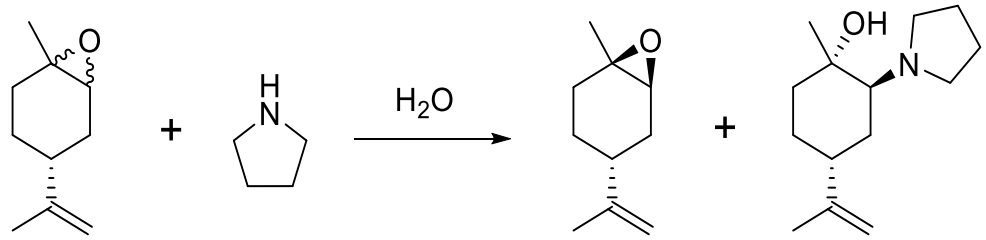

Figure 4.69 Kinetic resolution of 1,2-LO by selective opening of trans-1,2-LO.[44]

***Cis*-1,2-LO** was isolated from commercially available **1,2-LO** following the literature procedure (Figure 4.69).[44] 16.4 mL **1,2-LO**, 1.5 mL water and 8.35 mL pyrrolidine were placed in a 100 mL round bottom flask. The mixture was heated under reflux (100 °C) for 24 h. After cooling to room temperature, the mixture was dissolved in 50 mL diethyl ether (Et_2O) and washed twice with 50 mL water. The Et_2O was evaporated and ***cis*-1,2-LO** was purified by silica column chromatography using 20% Et_2O and 80 % petroleum spirit 40-60 °C as a solvent. TLC plates were developed using a solution of phosphomolybdic acid in ethanol (EtOH). Yield after chromatography: 7 mL of colourless oil containing 96% *cis* isomer and 4 % *trans* isomer. 100 % ***cis*-1,2-LO** can be obtained by repeating the procedure with a shorter reflux time of 1.5 h.

b) *Trans*-1,2-limonene oxide

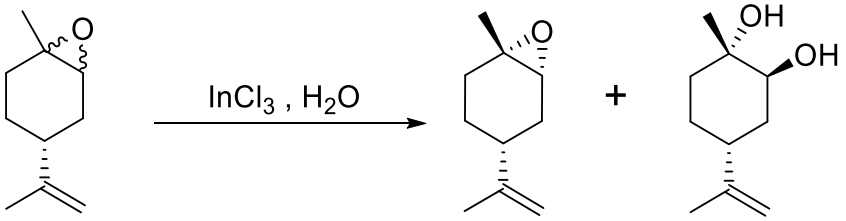

Figure 4.70 Kinetic resolution of 1,2-LO using indium chloride.[43]

Following a previously reported method,[43] 0.664 g $InCl_3$ and 50 mL water were placed in a 100 mL round bottom flask. Then, 4.5 g commercially available **1,2-LO** (58 % ***trans*-1,2-LO**) was added and the reaction was stirred at room temperature for 24 h. After the reaction, the ***trans*-1,2-LO** was extracted with dichloromethane three times (3x50 mL). Finally, ***trans*-1,2-LO** was purified using column chromatography using 20% Et_2O and 80 % petroleum spirit 40-60 °C as a solvent. TLC plates were developed using a solution of phosphomolybdic acid in ethanol. Yield: 1.37 g of colourless oil consisting of 95% ***trans*-1,2-LO** and 5 % ***cis*-1,2-LO**. High purity (100 %) ***trans*-1,2-LO** can be obtained by repeating kinetic resolution catalysed by $InCl_3$ on 95% ***trans*-1,2-LO** with a shorter reaction time of 8 h.

c) Large scale synthesis of *trans*-1,2-LO

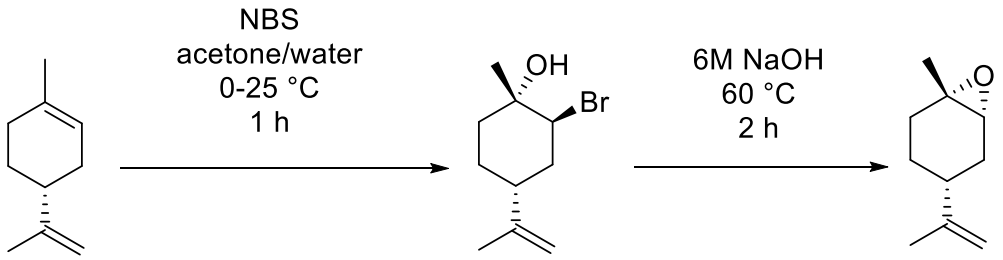

Figure 4.71 Synthesis of trans-1,2-LO using NBS. [68]

Following the literature procedure (Figure 4.71):[68] 60 mL limonene, 225 mL acetone, 50 mL water and a large magnetic stirrer bar were placed in a 500 mL round bottom flask and cooled in an ice bath. Then, 75 g N-bromosuccinimide (NBS) was added over 30 min followed by 1 h stirring. After the reaction, acetone was evaporated on a rotary evaporator. The bromohydrin was extracted with 150 mL Et_2O and separated from the aqueous phase, followed by washing with 60 mL water and evaporation of Et_2O. The bromohydrin was placed in a 250 mL round bottom flask with 100 mL 6 M aqueous solution of NaOH and stirred for 2 h at 60 °C. After the reaction, the mixture was left to cool down and the NaOH solution was removed using a separating funnel. The remaining organic phase was dissolved in 150 mL Et_2O and washed with 45 mL saturated aqueous solution of $NaHCO_3$ and 45 mL water. After the evaporation of Et_2O, the resulting product is a yellow oil consisting 90 % **1,2-LO** (95 % ***trans*-1,2-LO**).

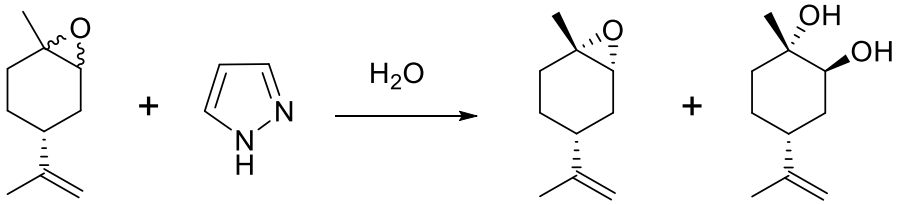

Figure 4.72 Selective hydrolysis of 1,2-LO yielding trans-5. [44]

95 % ***trans*-1,2-LO** was further purified following the literature procedure (Figure 4.72).[44] 20 g **1,2-LO**, 1.50 g pyrazole and 70 mL water was placed in a 250 mL round bottom flask and was heated under reflux (100 °C) for 30 min. The reaction mixture was cooled down to 80 °C, placed in a separating funnel and washed twice with 150 mL water. The synthesised ***trans*-1,2-LO** was purified by distillation yielding 100 % ***trans*-1,2-LO**; no ***cis*-1,2-LO** was observed (90 % purity identified by GCMS).

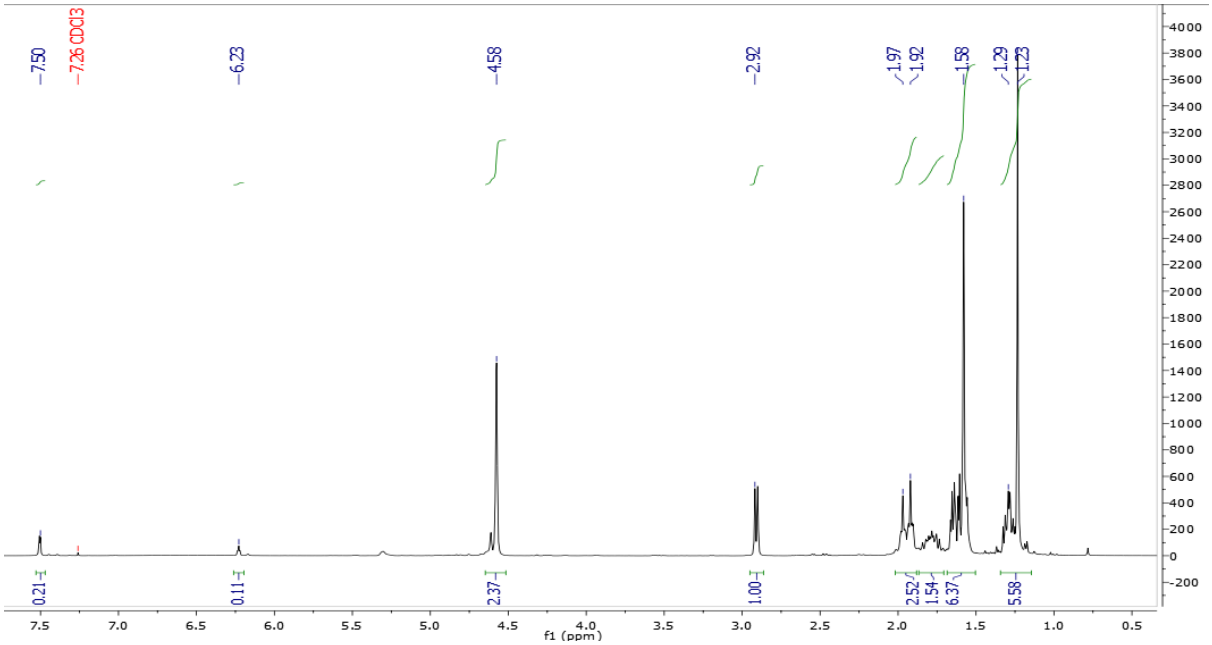

Figure 4.73 ^{1}H NMR spectrum of trans-1,2-LO obtained in large scale synthesis.

4.4.5 Mizuno catalyst (MIZ) preparation and olefin epoxidation

a) Mizuno catalyst preparation

$$H_2WO_4 + Cs(OH) + H_3PO_4 \xrightarrow{H_2O} Cs_6[P_2W_5O_{23}] \times n\,H_2O \longrightarrow Cs_7[PW_{10}O_{36}] \times n\,H_2O \quad \textbf{STEP I}$$

$$Cs_7[PW_{10}O_{36}] \times n\,H_2O + NaVO_3 \xrightarrow{HCl,\ H_2O} Cs_5[\gamma PV_2W_{10}O_{40}] \times n\,H_2O \quad \textbf{STEP II}$$

$$Cs_5[\gamma PV_2W_{10}O_{40}] \times n\,H_2O + TBA\text{-}Cl \xrightarrow[H_2O]{NaVO_3} [TBA]_4[\gamma HPV_2W_{10}O_{40}] \quad \textbf{STEP III}$$

STEP I $Cs_7[PW_{10}O_{36}]$ x nH_2O preparation: Following the previously published method,[69] 6 g of tungstic acid was added to 40 mL water under magnetic stirring, resulting in a yellow slurry. 50 wt %. aqueous CsOH was added dropwise to the slurry under vigorous stirring until pH = 13 (about 11 mL CsOH solution). After CsOH addition, the mixture become cloudy, thus it was filtered over celite yielding a clear colourless filtrate. The pH of the filtrate was adjusted to 7 by adding 85 % H_3PO_4 dropwise (usually about 2.1 mL acid). The solution was stirred for 1 h, filtered again and cooled down in a refrigerator overnight. The resulting white solid ($Cs_6[P_2W_5O_{23}]$ x nH_2O) was recovered by filtration and refluxed in water for 24h. The mass ratio between the solid and water was 1:2 respectively. After reflux, the white solid ($Cs_7[PW_{10}O_{36}]$ x nH_2O) was separated by filtration.

Note: The batch of CsOH solution has crucial impact on the synthesis. The reported synthesis was carried out with Alfa Aesar™ Cesium hydroxide, 50% w/w aq. soln., 99% (metals basis)

STEP II $Cs_5[\gamma PV_2W_{10}O_{40}]$ x nH_2O preparation: Following the previously published method,[69-71] 0.1 g sodium metavanadate ($NaVO_3$) was dissolved in 4 mL water by heating to 70 °C. The solution was cooled down to room temperature and 3 M HCl was added dropwise to adjust the pH to 0.8. The solution became yellow, which indicated the presence of $[VO_2]^+$. 1.25 g $Cs_7[PW_{10}O_{36}]$ was slowly added to the yellow solution. The solution was stirred for an additional 30 min and filtered yielding a yellow solid ($Cs_5[\gamma PV_2W_{10}O_{40}]$ x nH_2O). The resulting yellow solid (γ isomer) is stable at pH 2 and in the presence of $[VO_2]^+$. In the absence of $[VO_2]^+$, isomerisation to the β-isomer occurs which has an orange colour.[69]

STEP III $[TBA]_4[\gamma HPV_2W_{10}O_{40}]$ preparation: Following the previously published method,[48] 0.145 g of $NaVO_3$ was dissolved in 120 mL water at 70 °C, cooled down to room temperature and acidified to pH 2 using 3 M HCl (about 0.8 mL 3 M HCl was needed). 3.8 g $Cs_5[\gamma\text{-}PV_2W_{10}O_{40}]$ was added. The resulting solution was filtered in order to remove insoluble solids and 1.55 g Bu_4N-Cl was added in one portion. The reaction was stirred for 10 min and filtered, yielding yellow solid which will be referred as the Mizuno catalyst (**MIZ**). IR analysis results were in accordance with previously published data.[48, 69]

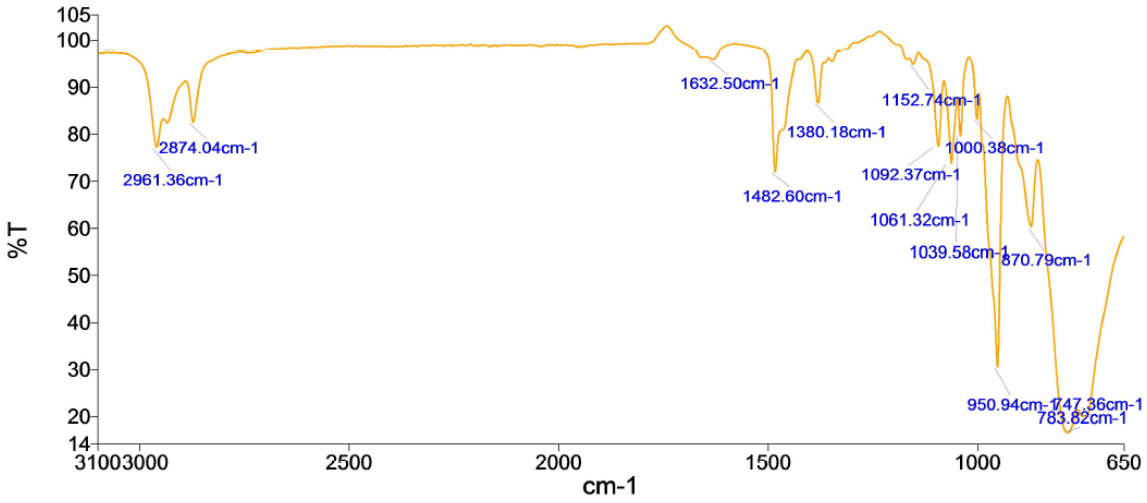

Figure 4.74 IR of the final Mizuno catalyst $[TBA]_4[\gamma HPV_2W_{10}O_{40}]$ (MIZ).

b) limonene epoxidation using Mizuno catalyst

The epoxidation of limonene to 8,9-limonene oxide (**8,9-LO**) was conducted according to the previously reported method.[48] The 0.1 mmol Mizuno catalyst (358 mg), magnetic stirrer bar and a 60 mL mixture of acetonitrile (MeCN) and tert butanol (t-BuOH) (1:1 volume) was placed in a 100

mL round bottom flask. The catalyst was activated by adding 14 mg of 70 % $HClO_4$ (about 1-2 drops). Finally, 20 mmol limonene (3.2 mL) was added to the round bottom flask. The mixture was warmed up to 32 °C and a 30 % hydrogen peroxide solution was added to the reaction mixture in 5 portions every 10 min (5 x 0.41 mL). After complete hydrogen peroxide addition, the reaction mixture was stirred for 30 min. After the reaction, organic solvents were removed *in vacuo* until a precipitate of catalyst was formed. 60 mL Et_2O was added to the resulting mixture and **8,9-LO** was filtered from the precipitate, followed by evaporation of Et_2O. The resulting oil was purified by silica column chromatography using a mixture of Et_2O and petroleum spirit as a solvent (2:98 Et_2O : petroleum spirit). TLC plates were developed using solution of phosphomolybdic acid in EtOH. The obtained product was a mixture of 8,9-limonene oxide stereoisomers 36 % **4R,8R-8,9-LO** and 64 % **4R,8S-8,9-LO**.[72]

4.4.6 Carbonation using high pressure CO_2

High pressure cyclic carbonate synthesis was performed in a 10 mL stainless steel autoclave with a glass liner. Epoxide, biphenyl and catalyst were placed in the glass liner, which was placed in the pre-heated to 40 °C autoclave. The autoclave was sealed and pressurised with CO_2 to the desired pressure at 40 °C and then the autoclave was placed in an aluminium heating block, preheated to the reaction temperature. After the reaction, the autoclave was cooled to room temperature and the pressure was slowly released over 20 minutes. Conversion and selectivity were calculated by ^1H NMR spectroscopy using biphenyl as an internal standard.

4.4.7 General procedure of β-elemene epoxidation using mCPBA

5 g **BE** (24.5 mmol) and magnetic stir bar was placed in a round bottomed flask, then DCM was added (the volume of DCM depends on the amount of mCPBA used, about 30 mL DCM per 1 g of mCPBA). The solution was cooled down to 0 °C using an ice bath and it was kept at 0 °C through the first 2 hours of reaction. mCPBA was added when the solution was at 0 °C, 1.2 mol eq mCPBA per each double bond to oxidise. For example, to obtain **BETO** 3.6 mol eq mCPBA were added (about 22 g of 70 % mCPBA). The reaction was periodically monitored via TLC using phosphomolybdic acid stain to develop the TLC and it was stopped when full conversion of BE was observed. The reaction time depends on the desired epoxide. **BEMO** and **BEBO** oxidise within 6 h, **BETO** is slower and it needs 24 h reaction time. After achieving the desired epoxide, the reaction was quenched with an aqueous solution of Na_2SO_3. The reaction was filtered and the solution containing DCM and **BE epoxides** was washed with saturated aqueous solution of Na_2CO_3 (3 x 150 mL). The epoxides can be purified using column chromatography in a mixture of EtOAc

and petroleum spirit 40 – 60. The polarity of the solvent depends on the epoxide that was purified. For the highest polarity **BETO** 40 % EtOAc and 60 % petroleum spirit was used.

4.4.8 Carvone oxide preparation (8,9-CO)

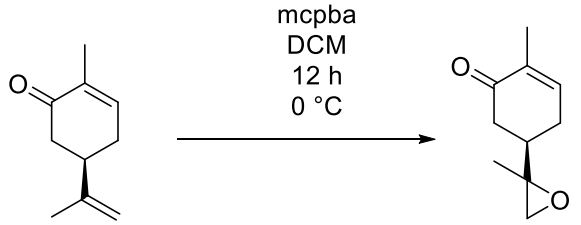

Figure 4.75 Carvone oxidation using mCPBA.

Carvone-8,9-oxide (8,9-CO) was prepared according to previously reported procedure (Figure 4.75).[58] 5 g (33.3 mmol) carvone was placed in round bottomed flask with 200 mL DCM. The flask was cooled down to 0 °C and 8.21 g of 70 % mCPBA was added slowly. The reaction was left in the fridge overnight (about 12 h). When reaction was completed 50 mL of 10 % aqueous Na_2SO_3 was added and stirred for 10 min. The reaction mixture was filtered and solids were washed with DCM three times. All DCM fractions were collected together and washed three times with saturated aqueous solution of Na_2CO_3 and once with saturated aqueous solution of NaCl. DCM was evaporated and products were purified by column chromatography using mixture of 35 % ethyl acetate and 65 % petroleum spirit 40-60 as eluent yielding 3.486 g (21 mmol) of pure carvone-8,9-epoxide. Purity was confirmed by NMR spectroscopy. The reaction yields two isomers in a ratio of about 56:44 (if using epoxide peaks at 2.32 and 2.30 ppm), which is consistent with literature data, or in a ratio 50:50 if using methyl groups at 1.05 and 1.04 ppm, which is slightly different then 57:43 reported.[58] The stereoisomers were not further assigned.

4.4.9 Thiol-ene reactions

a) The synthesis of BI-1,2-LC

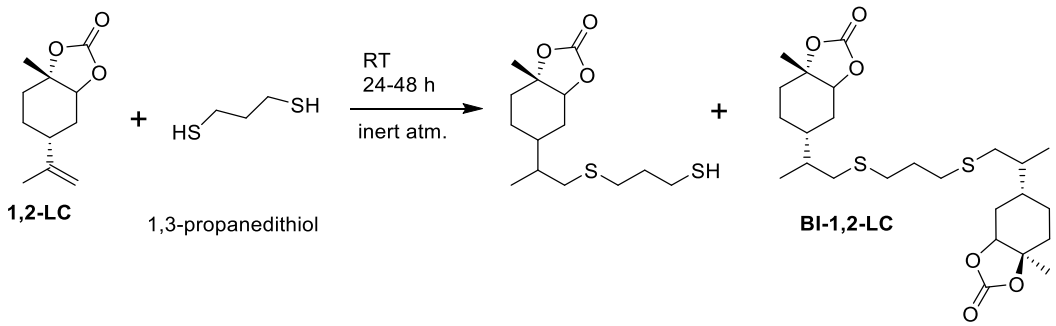

Figure 4.76 Synthesis of compound BI-1,2-LC.

The synthesis of **BI-1,2-LC** was performed using the method developed by Meier *et al.* which does not require using radical initiator.[38] 2.076 g (10.59 mmol) of **1,2-LC** was placed in a round bottom

flask and put under inert atmosphere of Ar. Then, 0.53 mL of 1,3-propanedithiol was added to the flask and the flask was flushed with Ar. The reaction was stirred at room temperature for 24 h. The progress of the reaction can be monitored by ^{1}H NMR spectroscopy using the signal from the double bond at 4.75 ppm. After 24 h, 80 % of **1,2-LC** reacted. To fully react the remaining **1,2-LC**, another 0.53 mL of 1,3-propanedithiol was added and stirred for another 24 h.

The crude reaction mixture was purified by silica column chromatography using a mixture of ethyl acetate and petroleum spirit as a solvent (40:60 ethyl acetate : petroleum spirit). Isolated yield of **BI-1,2-LC**: 1.568 g (3.13 mmol), 59 %

b) Radical addition of 8,9-limonene cyclic carbonate

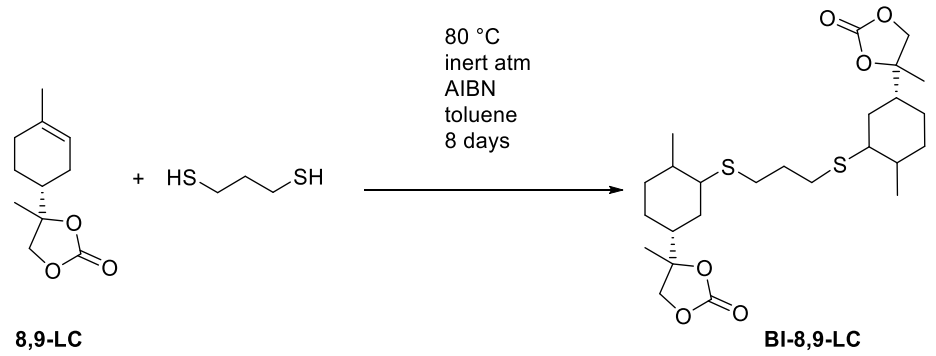

Figure 4.77 Synthesis of compound BI-8,9-LC.

The double bond in **8,9-LC** is less reactive than the double bond in **1,2-LC**, thus the method without a radical initiator did not yield the desired product.

2.741 g (13.4 mmol) **8,9-LC** was placed in a round bottom flask and put under an inert atmosphere of Ar. 0.229 g AIBN was dissolved in 7 mL dry toluene and added to **8,9-LC**. The flask was flushed with Ar a few times and 0.7 mL 1,3-propanedithiol was added to the mixture in the flask. The reaction was stirred for 8 days at 80 °C. After this time 72 % of **8,9-LC** reacted.

The reaction mixture was purified using silica column chromatography using ethyl acetate and petroleum spirit (40:60 respectively) as a solvent. Isolated yield of **8,9-LC**: 1.169 g (2.34 mmol), 35 %.

4.4.10 Carbonate ring opening with amines for compounds BI-1,2-LC and BI-8,9-LC

a) the synthesis of compound BI-1,2-LC-HU

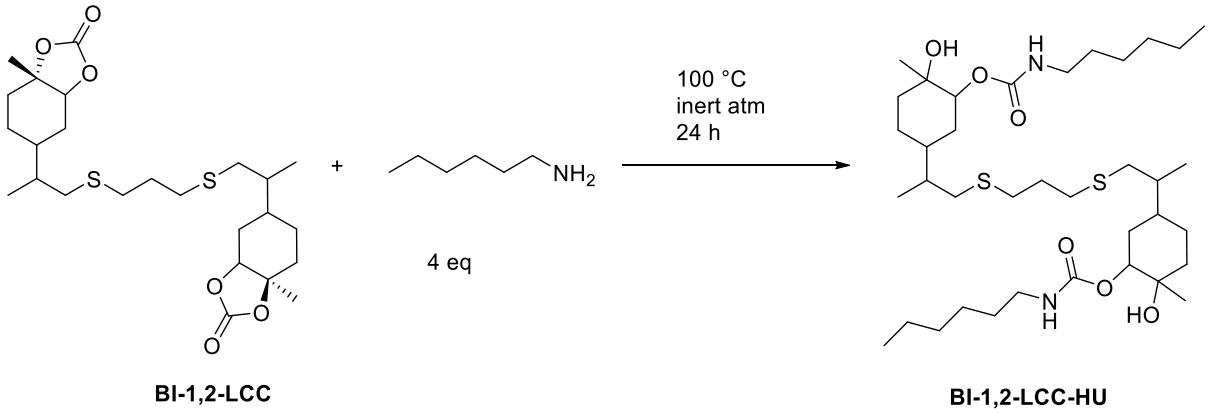

Figure 4.78 Urethane synthesis from BI-1,2-LC.
Note: This reaction will yield a mixture of isomers, for clarity only one is presented.

0.432 g of **BI-1,2-LC** and magnetic stirrer bar was placed in round bottom flask attached to a reflux condenser. **BI-1,2-LC** was put in an inert atmosphere of argon. 0.5 mL of hexyl amine (4 molar equivalents) was added to the round bottom flask and the temperature was increased to 100 °C. The reaction was left for 24 h. After the reaction, the excess of amine was evaporated *in vacuo*. The resulting yellow-brown oil was analysed by NMR spectroscopy, mass spectrometry and FT-IR.

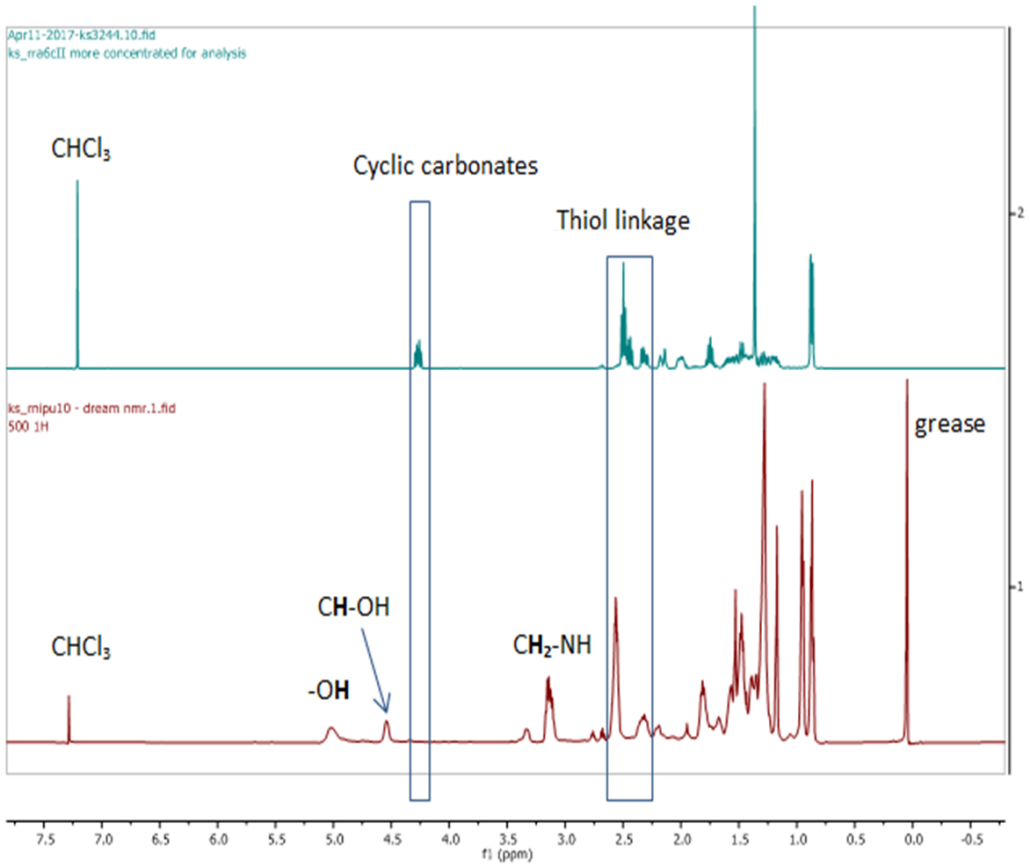

Figure 4.79 ^{1}H NMR spectra of BI-1,2-LC (top) and BI-1,2-LC-HU (bottom). BI-1,2-LC-HU was not further purified, the presented spectrum is a spectrum of crude reaction mixture after evaporating an excess of amine.

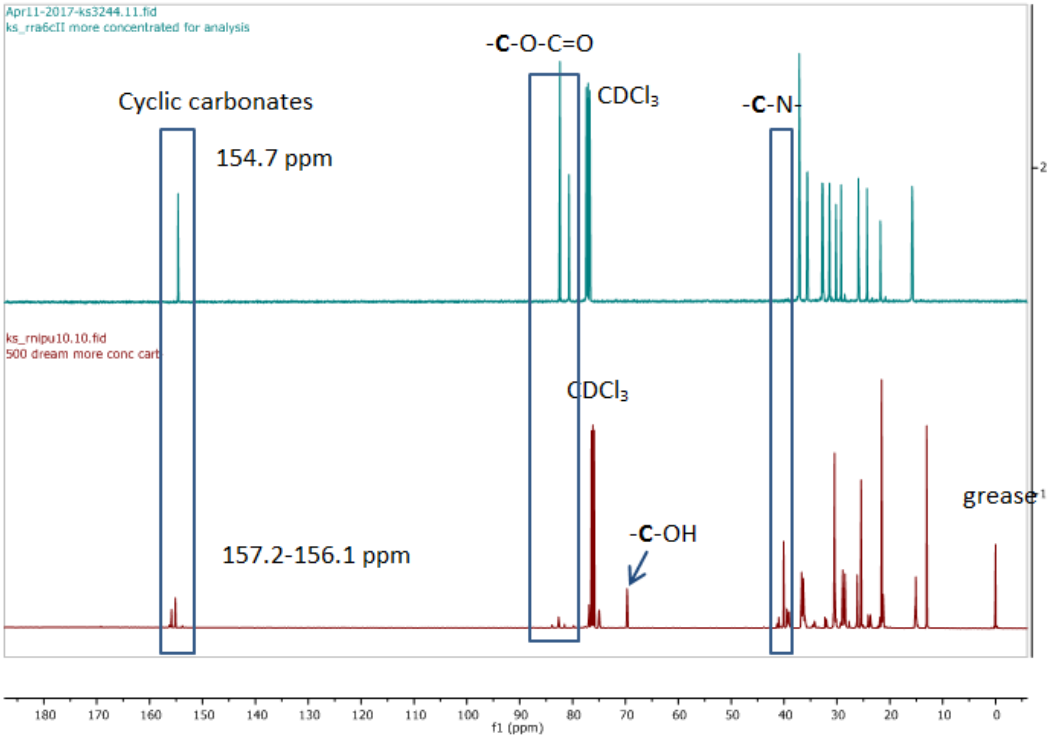

Figure 4.80 ^{13}C {^{1}H} NMR spectra of BI-1,2-LC (top) and BI-1,2-LC-HU (bottom). BI-1,2-LC-HU was not further purified, the presented spectrum is a spectrum of crude reaction mixture after evaporating an excess of amine.

MS ESI-TOF+

Calculated $[M+H]^+$ = 703.4748, $[M+Na]^+$ = 725.4573

Found $[M+H]^+$ = 703.4752, $[M+Na]^+$ = 725.4690

FT-IR: 1689 cm^{-1} (C=O)

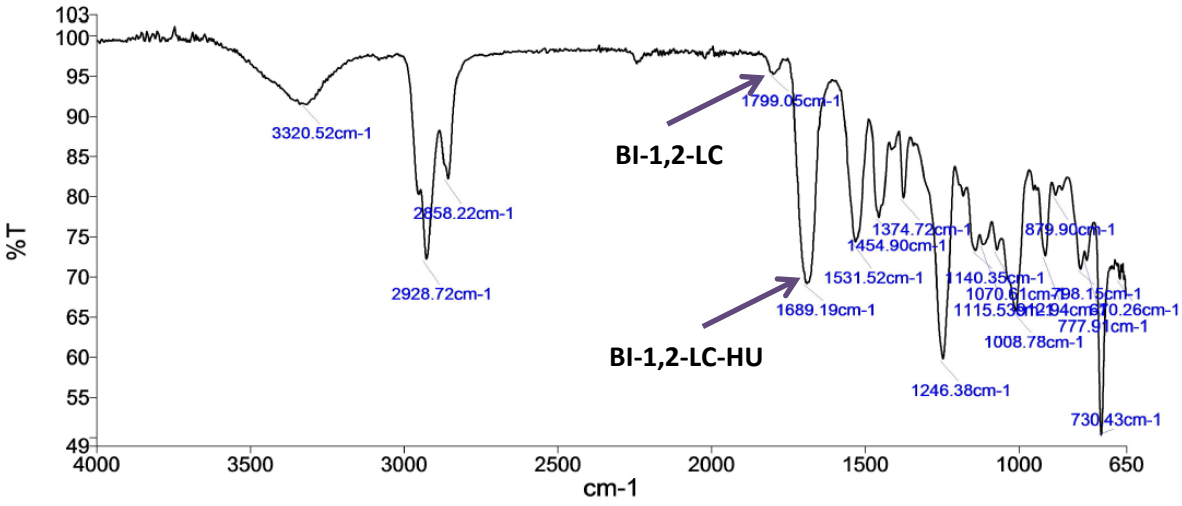

Figure 4.81 IR of crude reaction mixture from the synthesis of BI-1,2-LC-HU after evaporation of the excess of amine.

b) the synthesis of BI-8,9-LC-HU

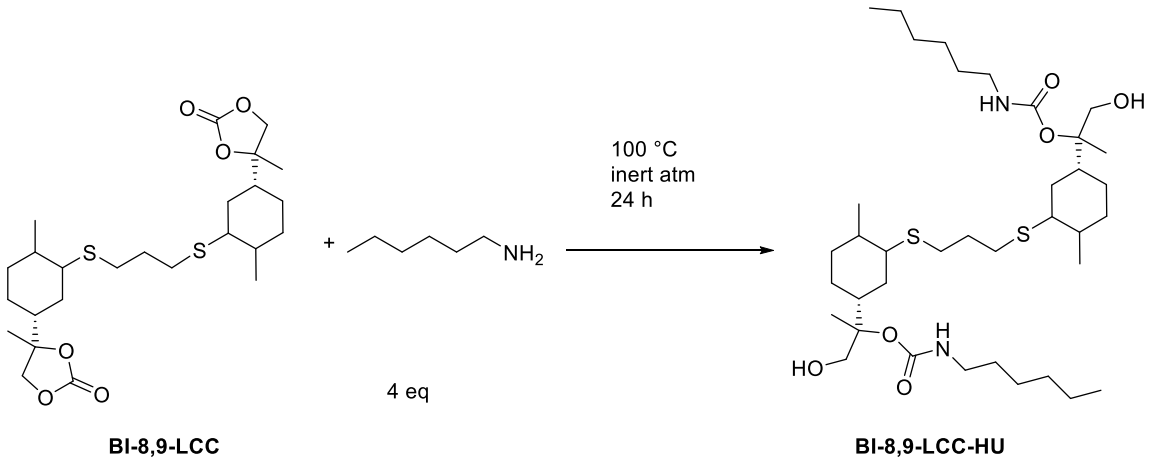

Figure 4.82 Urethane synthesis from BI-8,9-LC.
Note: This reaction will yield a mixture of isomers, for clarity only one is presented.

0.739 g of **BI-8,9-LC** and a magnetic stirrer bar were placed in a round bottom flask attached to a reflux condenser. **BI-8,9-LC** was put in an inert atmosphere of argon. 0.8 mL of hexyl amine (4 molar equivalents) was added to the round bottom flask and the temperature was increased to 100

°C. The reaction was left for 24 h. After the reaction, the excess of amine was evaporated *in vacuo*. The resulting yellow-brown oil was analysed by NMR spectroscopy, mass spectrometry and FT-IR.

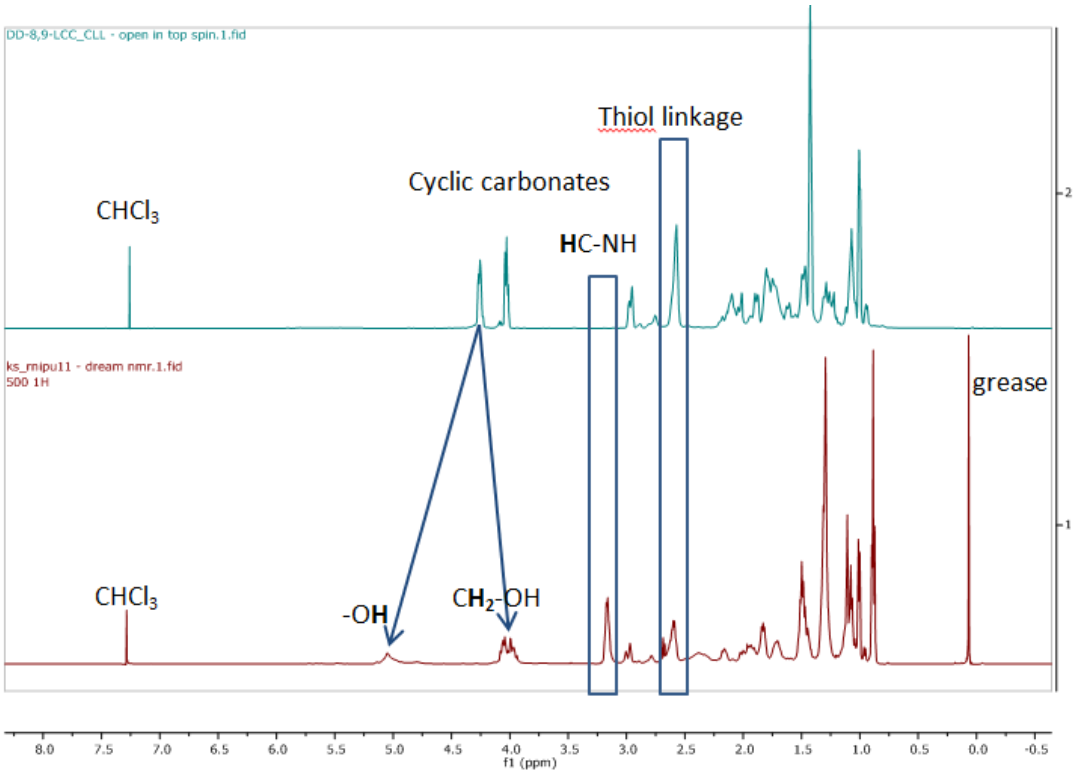

Figure 4.83 ^{1}H NMR spectra of BI-8,9-LC (top) and BI-8,9-LC-HU (bottom). BI-8,9-LC-HU was not further purified, the presented spectrum is a spectrum of crude reaction mixture after evaporating an excess of amine.

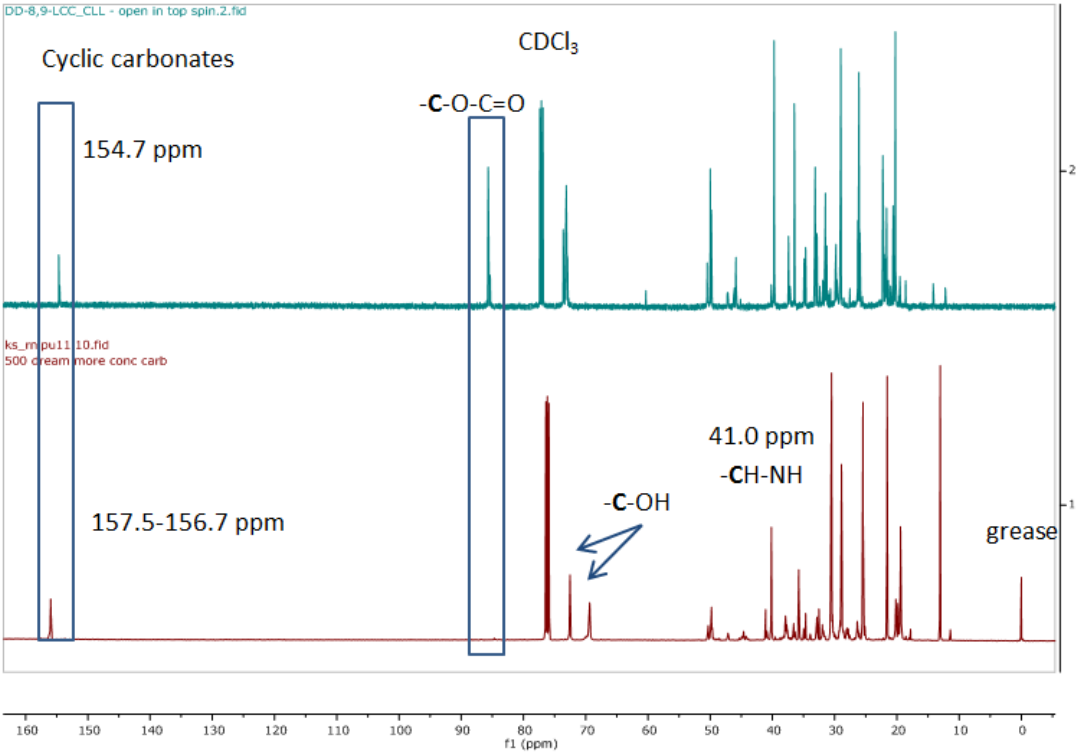

Figure 4.84 $^{13}C\{^{1}H\}$ NMR spectra of BI-8,9-LC (top) and BI-8,9-LC-HU (bottom). BI-8,9-LC-HU was not further purified, the presented spectrum is a spectrum of crude reaction mixture after evaporating an excess of amine.

MS ESI-TOF+

Calculated $[M+H]^+$ = 703.4748, $[M+Na]^+$ = 725.4573

Found $[M+H]^+$ = 703.4774, $[M+Na]^+$ = 725.4624

FT-IR: 1698 cm^{-1} (C=O)

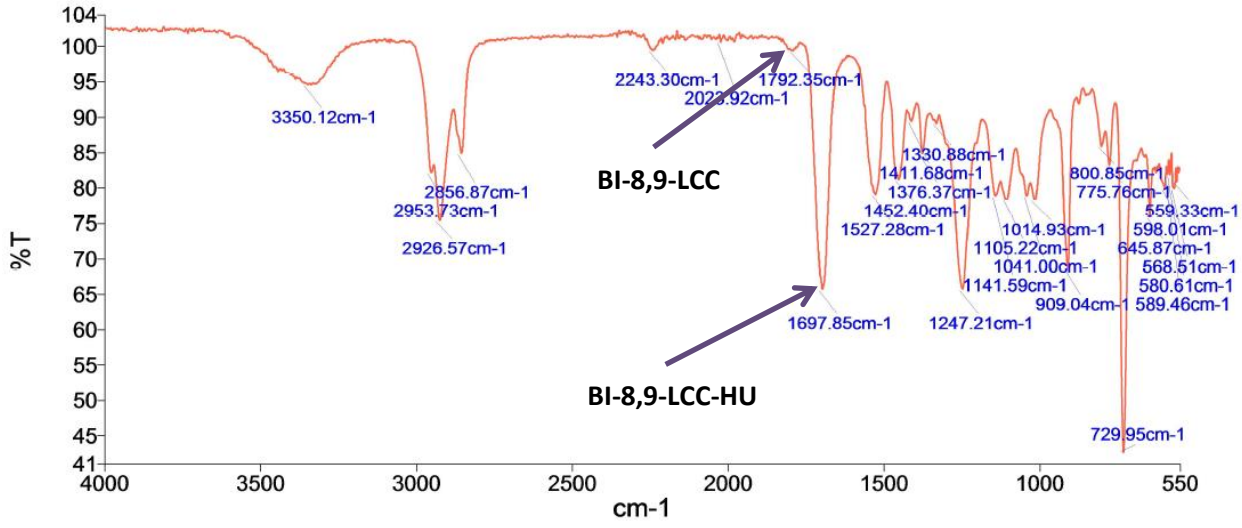

Figure 4.85 IR of crude reaction mixture from the synthesis of BI-8,9-LC-HU after evaporation of the excess of amine.

4.4.11 Ring opening of BEBC crude reaction mixture with amines

A crude reaction mixture of BEBC was prepared according to the high pressure cyclic carbonates synthesis procedure. BEBO was placed in an autoclave with 6 mol % TBA-Br and stirring was provided using magnetic stirrer bar. The autoclave was pressurised to 50 bar CO_2 at 40 °C and then heated to the desired reaction temperature of 140 °C.

All ring opening reactions were performed using the same batch of crude reaction mixture. A large batch of crude reaction mixture was prepared by performing the same cyclic carbonates synthesis multiple times. The ^{1}H NMR spectrum is presented in Figure 4.80. The carbonate content was estimated using integration of carbonate region 4.2 – 3.6 ppm and it was assumed 80 %.

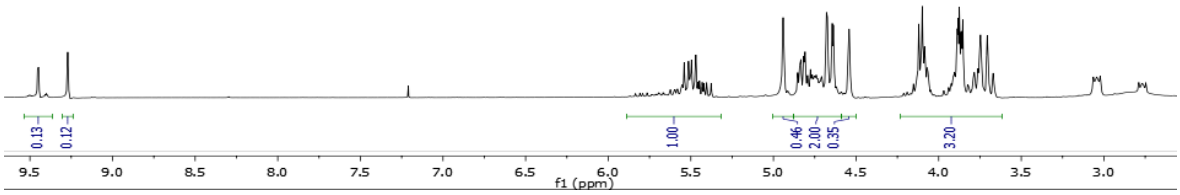

Figure 4.86 ^{1}H NMR spectrum of crude reaction mixture containing BEBC.

The crude reaction mixture with carbonates was placed in a 10 mL round bottomed flask, the magnetic stir bar was added and the flask was heated at 60 °C. The crude reaction mixture was dried from any residual solvents by applying three cycles of vacuum and argon, each of them 5 min long. An amine was added using a plastic syringe, with the amount of amine needed calculated by volume (see Table 4.11 for the exact conditions). It is worth noting that all amines were stored in air and amine C8 and C4 are solid at room temperature. They had to be melted before use and the syringe used to add them to reaction had to be preheated. Upon amine addition a change of colour from yellow to dark orange was observed. Immediately after amine addition, a reflux condenser was placed on the round bottomed flask and the whole apparatus was kept under argon atmosphere. The temperature was increased by 20 °C every time when magnetic stir bar was stopping to rotate. The maximum reaction temperature was 105 °C.

Table 4.11 Exact conditions for ring opening.

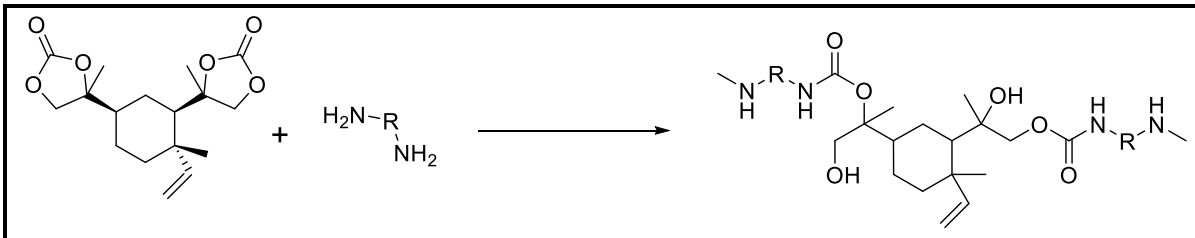

	Mass of crude reaction mixture	amount of amine	temperature	time	comments
NIPU-PRI	1.110 g	3.32 mmol 0.878 g 0.98 mL	60 – 105 °C	18 h	kept under Ar atmosphere
NIPU-IP	1.110 g	3.32 mmol 0.565 g 0.62 mL	60 – 100 °C	16 h	kept under Ar atmosphere
NIPU-C8	1.110 g	3.32 mmol 0.478 g 0.58 mL	60 – 100 °C	16 h	kept under Ar atmosphere
NIPU-C4	1.110 g	3.32 mmol 0.293 g 0.33 mL	60 – 100 °C	18 h	kept under Ar atmosphere

4.4.12 Compounds analysis

The analysis of β-elemene derived oxides is included in Chapter 3.

Trans-1,2-limonene oxide (trans-1,2-LO)

Trans-**1,2-LO** is a previously known compound [44, 73]

***trans*-1,2-LO**

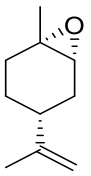

^{1}H NMR (400 MHz, $CDCl_3$) δ = 4.76 – 4.59 (m, 2H), 2.99 (d, $^{3}J_{H\text{-}H}$ =5.4 Hz, 1H), 2.20 – 1.97 (m, 2H), 1.93 – 1.79 (m, 1H), 1.76 – 1.61 (m, 3H+2H), 1.48 – 1.12 (m, 3H+2H).

^{13}C {^{1}H} NMR (101 MHz, $CDCl_3$) δ = 149.2, 109.2, 59.3, 57.5, 40.8, 30.9, 30.0, 24.4, 23.2, 20.3.

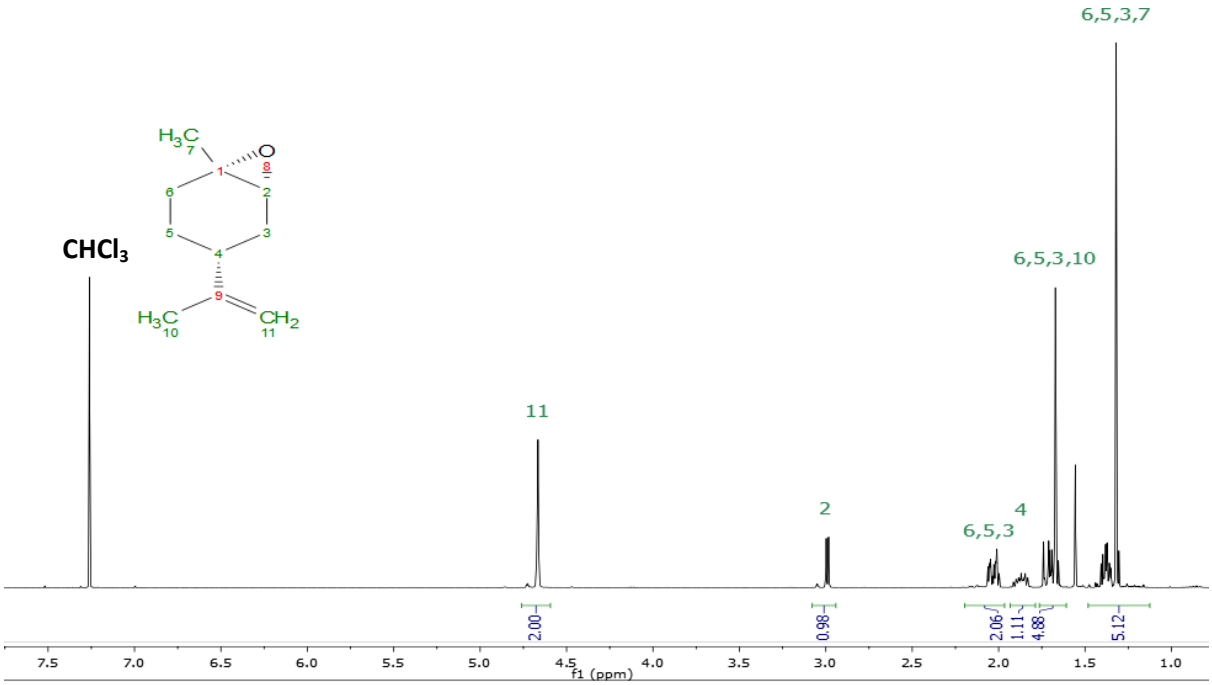

Figure 4.87 ^{1}H NMR of 95 % trans-1,2-LO.

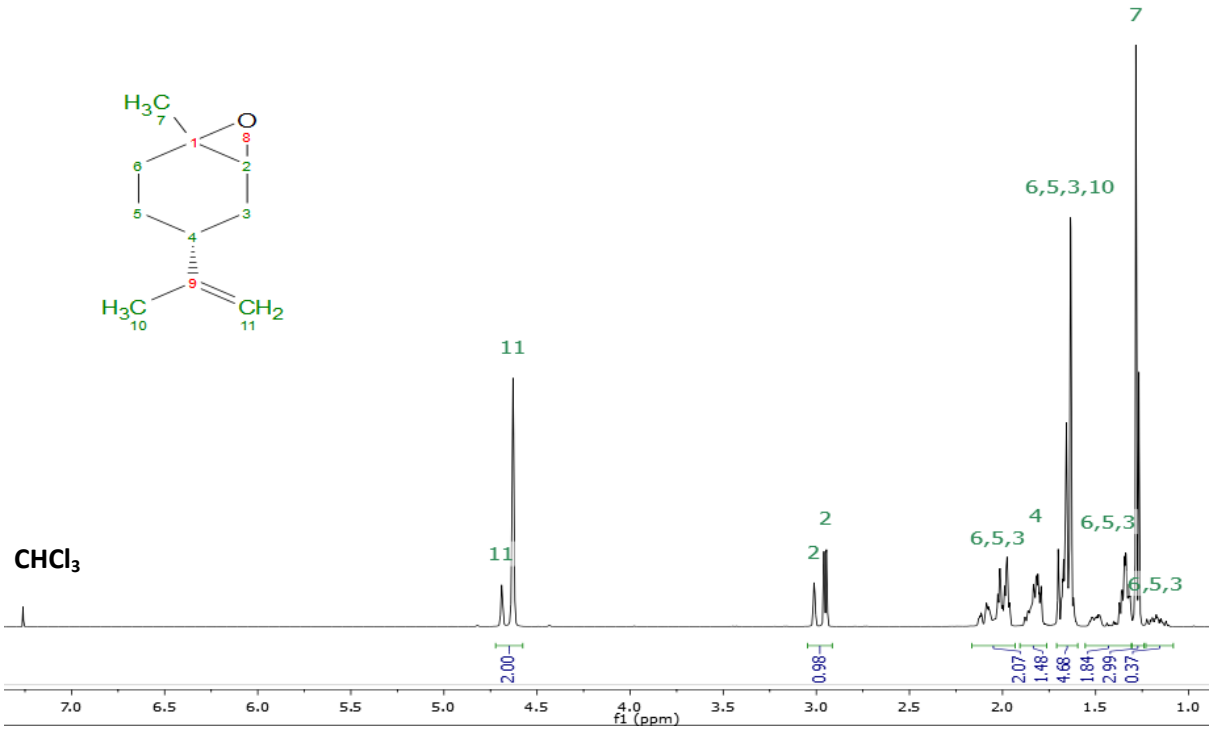

Figure 4.88 ^{1}H NMR of 1,2-LO, 70 % trans-1,2-LO 30 % cis-1,2-LO.

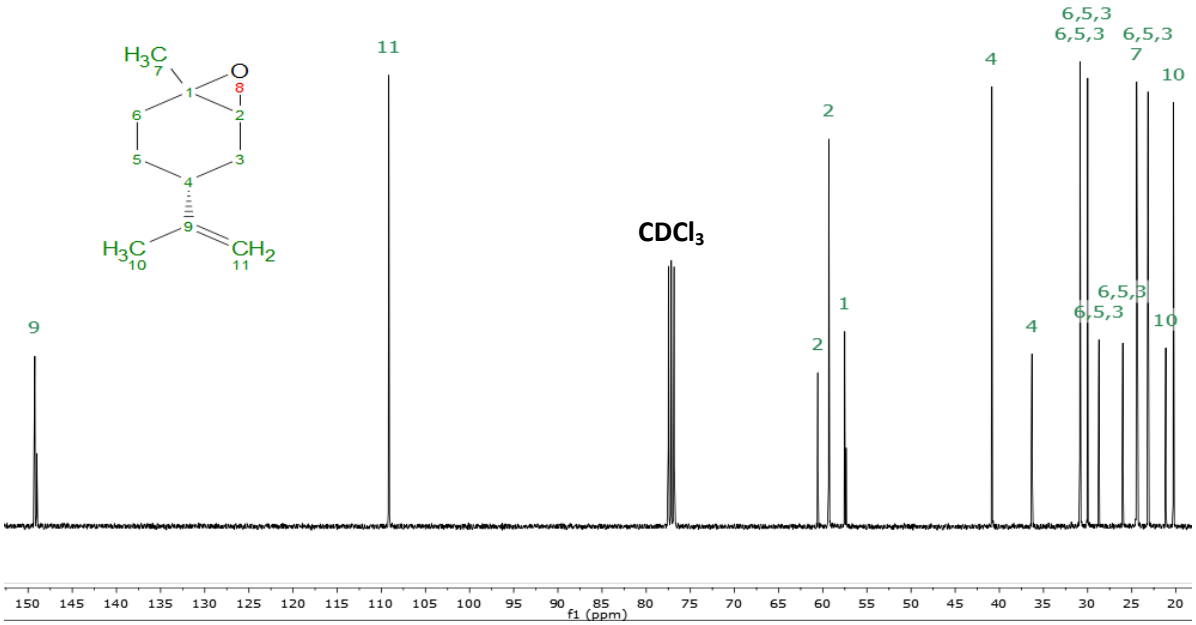

Figure 4.89 $^{13}C\{^{1}H\}$ NMR of 1,2-LO 70 % trans-1,2-LO 30 % cis-1,2-LO

Cis-1,2-limonene oxide (cis-1,2-LO)

Cis-**1,2-LO** is a previously known compound[44, 73]

***cis*-1,2-LO**

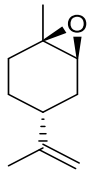

^{1}H NMR (400 MHz, $CDCl_3$) δ = 4.73 – 4.58 (m, 2H), 3.04 – 2.91 (m, 1H), 2.15 – 1.93 (m, 2H), 1.87 – 1.72 (m, 2H), 1.72 – 1.56 (m, 4H), 1.54 – 1.31 (m, 1H), 1.30 – 1.23 (m, 3H), 1.24 – 1.06 (m, 1H).

$^{13}C\{^{1}H\}$ NMR (101 MHz, $CDCl_3$) δ = 149.0, 109.1, 60.5, 57.3, 36.3, 30.8, 28.7, 26.0, 24.3, 21.1.

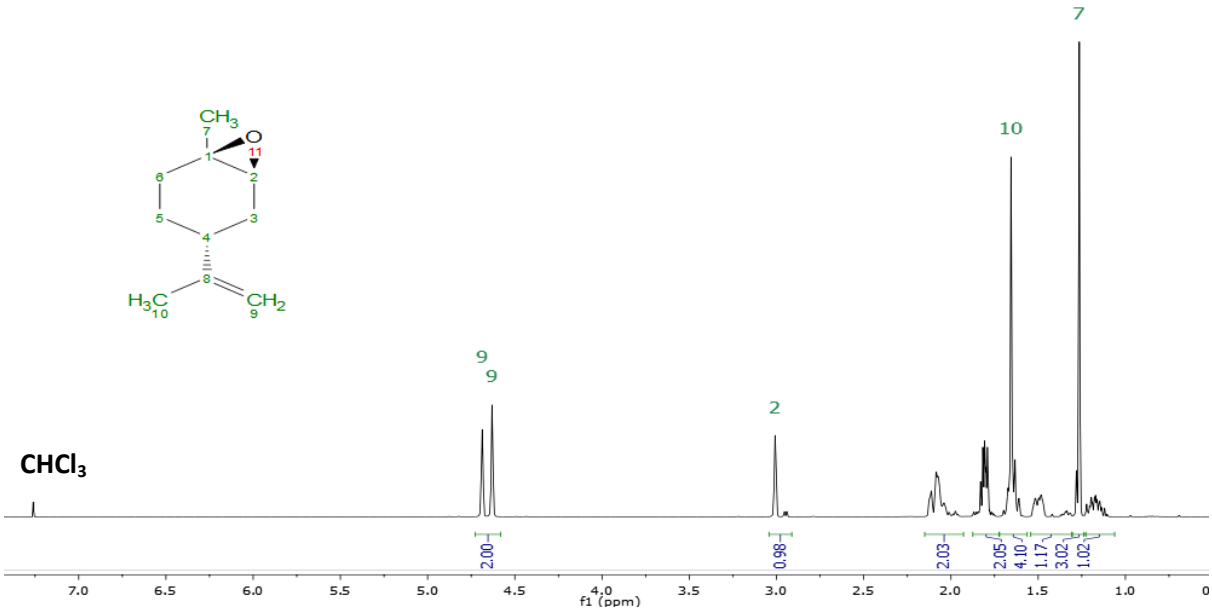

Figure 4.90 ^{1}H NMR of 92 % cis-1,2-LO

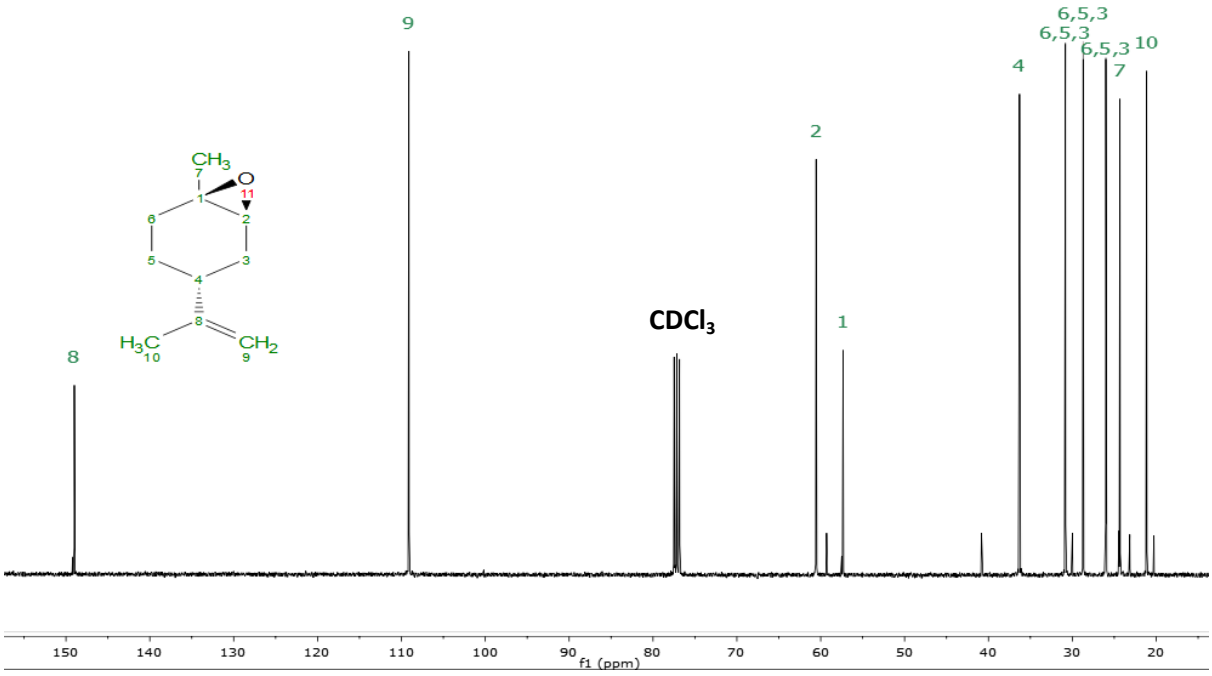

Figure 4.91 ^{13}C {^{1}H} NMR of 92 % cis-1,2-LO

8,9-limonene oxide (8,9-LO)

8,9-limonene oxide

4R,8R-8,9-LO **4R,8R-8,9-LO**

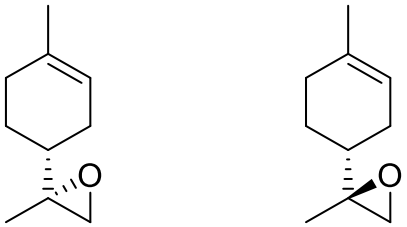

8,9-LO is a previously known compound[48, 72]

mixture of isomers:

^{1}H NMR (400 MHz, $CDCl_3$) δ = 5.32 (m, 1H), 2.62 – 2.57 (m, 1H), 2.53 – 2.47 (2xd, 1H), 1.93 (m, 5H), 1.60 (m, 3H), 1.22 (m, 5H).

^{13}C {^{1}H} NMR (101 MHz, $CDCl_3$) δ = 134.1, 133.9, 120.1, 119.9, 59.4, 59.2, 53.4, 52.7, 40.2, 39.7, 30.4, 30.1, 27.5, 27.5, 25.0, 24.9, 23.5, 23.4, 18.8, 18.1.

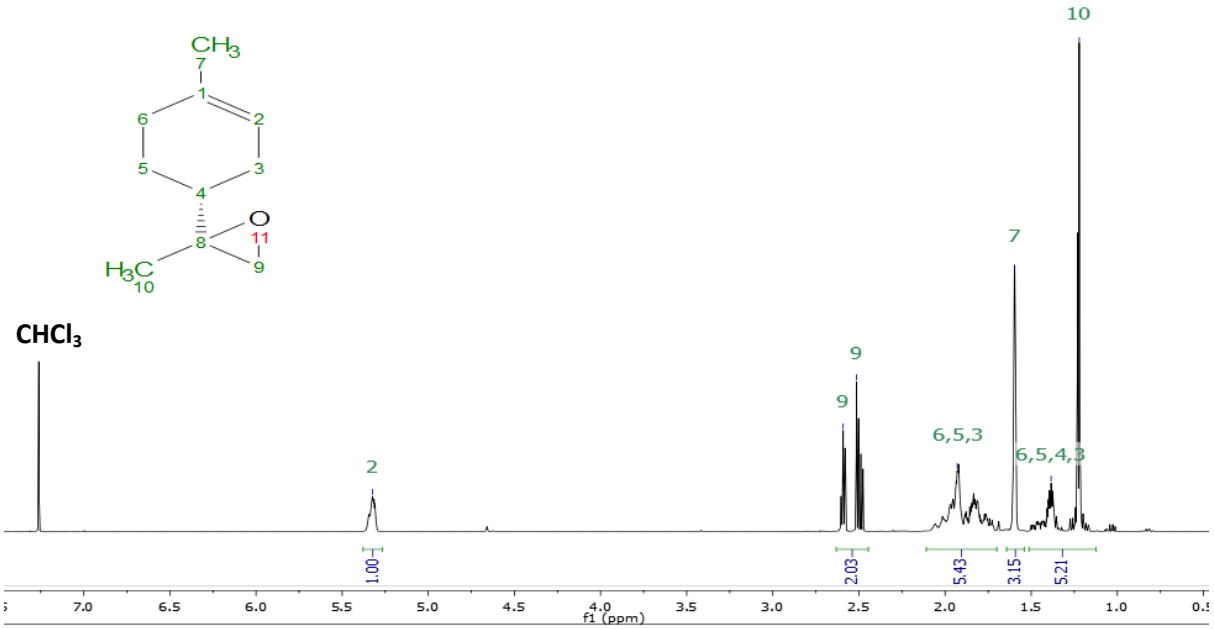

Figure 4.92 ^{1}H NMR of 8,9-LO

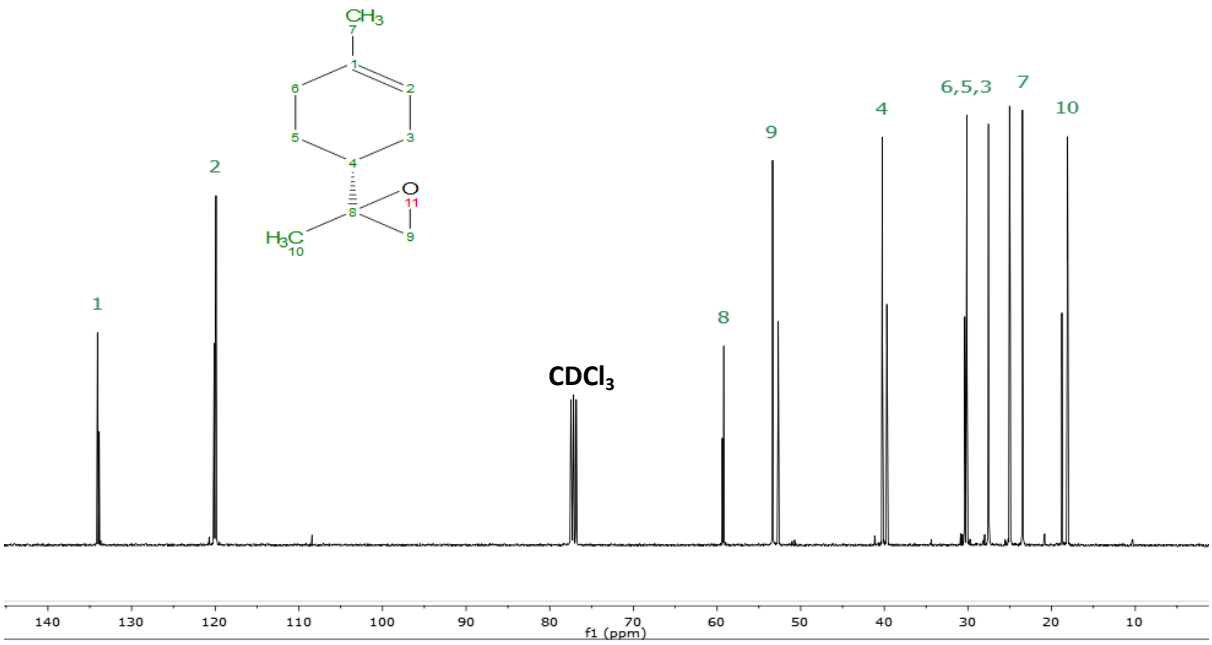

Figure 4.93 $^{13}C\{^{1}H\}$ NMR of 8,9-LO

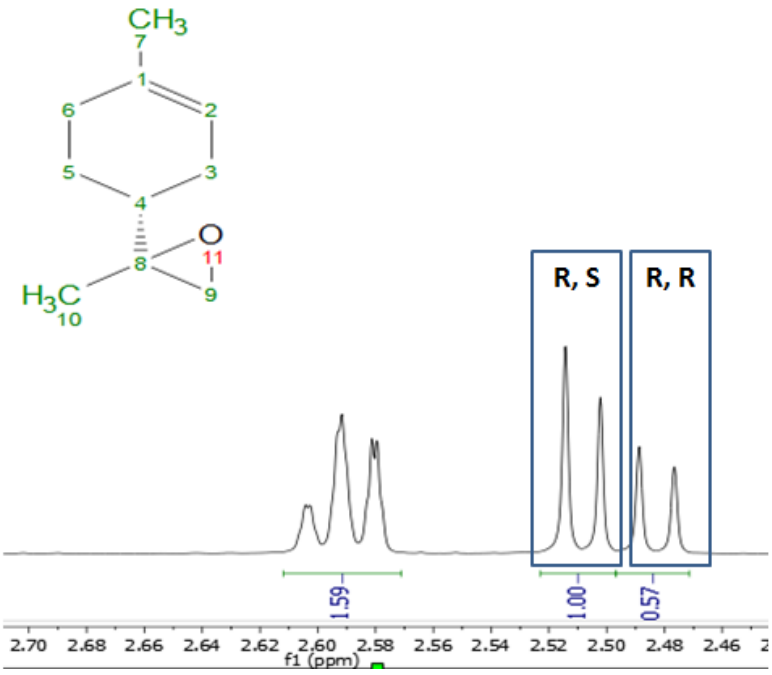

Figure 4.94 ^{1}H NMR spectra of protons in position 9 with characteristic stereoisomers peaks[72]

trans-1,2-limonene cyclic carbonate (trans-1,2-LC)

***trans*-1,2-limonene cyclic carbonate (*trans*-1,2-LC)**

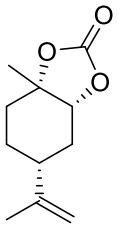

Trans-**1,2-LC** is a previously known compound[14]

^{1}H NMR (500 MHz, $CDCl_3$) δ = 4.77 – 4.63 (m, 2H), 4.35 (dd, $^{3}J_{H\text{-}H}$ =9.5 Hz, $^{3}J_{H\text{-}H}$ = 7.0 Hz, 1H), 2.31 – 2.14 (m, 2H), 1.95 – 1.83 (tt, $^{3}J_{H\text{-}H}$ = 11.8 Hz, $^{3}J_{H\text{-}H}$ = 3.2 Hz, 1H), 1.74 – 1.55 (m, 3H+2H), 1.53 – 1.32 (m, 3H+2H).

^{13}C {^{1}H} NMR (126 MHz, $CDCl_3$) δ = 154.8, 147.4, 110.1, 82.2, 80.5, 39.8, 34.0, 33.0, 26.1, 25.7, 20.6.

MS ESI-TOF+

Calculated $[M+Na]^+$ = 219.0992

Found $[M+Na]^+$ = 219.1017

FT-IR: 1790 cm^{-1} (C=O)

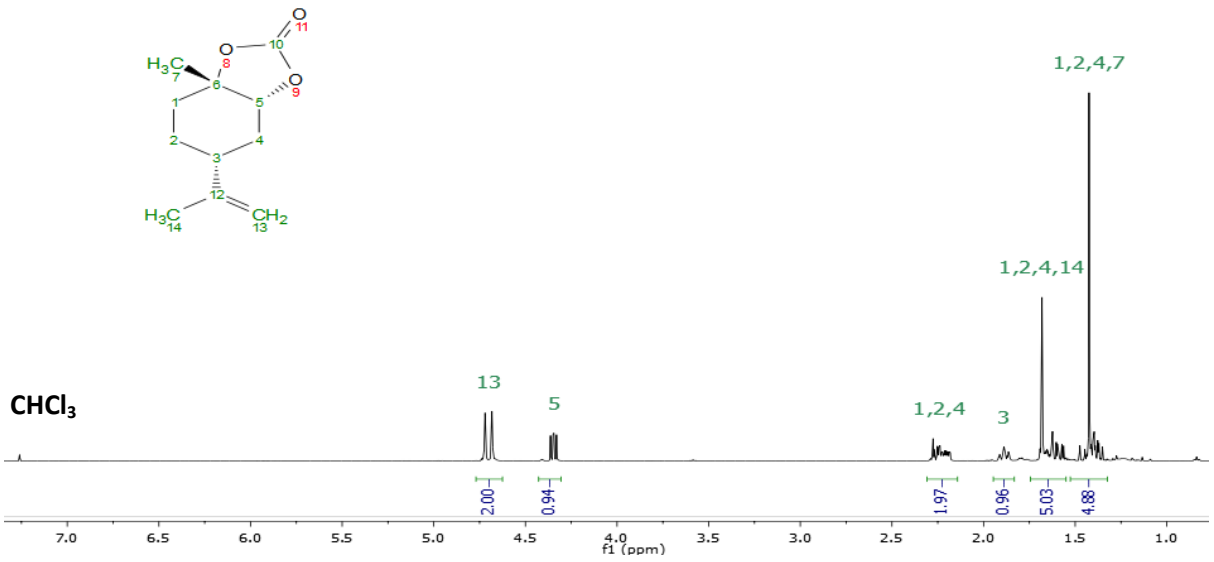

Figure 4.95 ^{1}H NMR of trans-1,2-LC

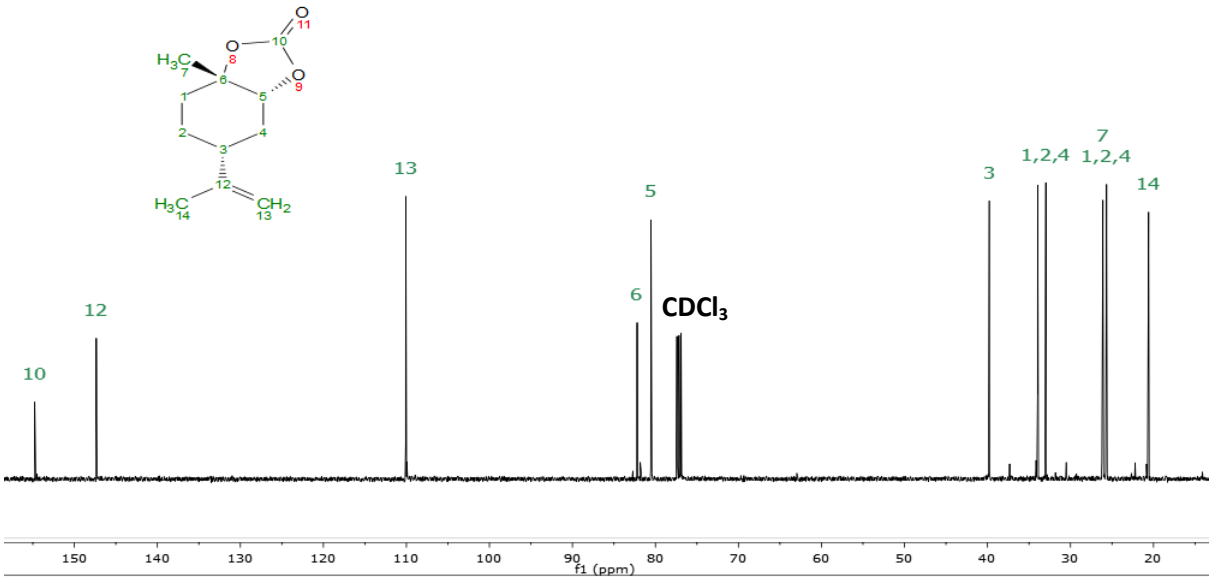

Figure 4.96 $^{13}C\{^{1}H\}$ NMR of trans-1,2-LC

***cis*-1,2-LC** has never been isolated and fully characterised. However, the presence of ***cis*-1,2-LC** has been reported by other research grups.[14, 74] The isomers ratio between ***trans*-1,2-LC** and ***cis*-1,2-LC** was calculated using ^{1}H NMR (Figure 4.91). The ^{1}H NMR spectrum was consistent with previously published data.[74]

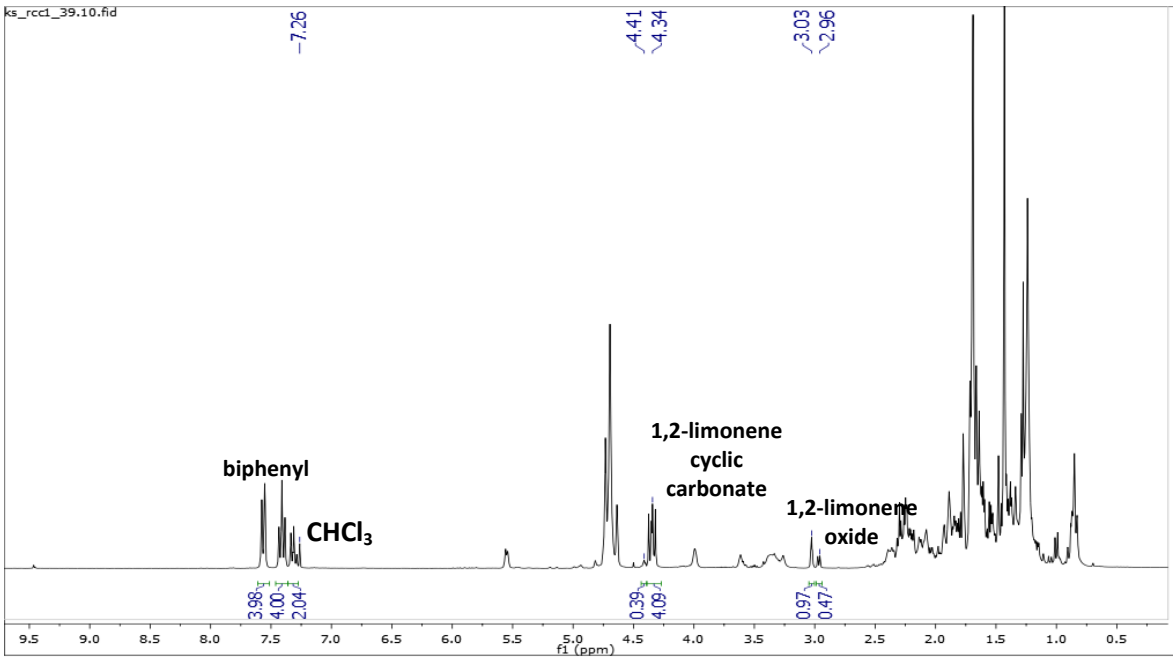

Figure 4.97 Calculation of isomers ratio in 1,2-LC. Cis isomer: 4.41 ppm (m), trans isomer: 4.34 ppm (dd)

8,9-limonene cyclic carbonate (8,9-LC)

8,9-limonene cyclic carbonate

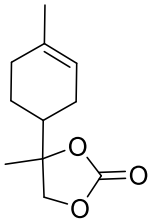

4R,8R-8,9-LC

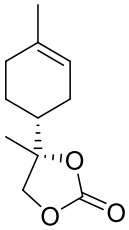

4R,8S-8,9-LC

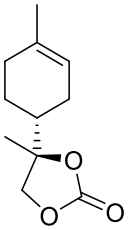

Mixture of isomers

^{1}H NMR (500 MHz, $CDCl_3$) δ = 5.40 – 5.27 (m, 1H), 4.33 – 3.94 (m, 2H), 2.14 – 1.67 (m, 6H), 1.62 (m, 3H), 1.44 (**(4R,8R)-8,9-LC**) and 1.43 (**(4R,8S)-8,9-LC**) (s, 3H), 1.30 (m, 1H).

^{13}C NMR (126 MHz, $CDCl_3$) δ = 154.8, 154.8, 134.4, 134.2, 119.0, 118.9, 85.9, 73.1, 72.8, 41.8, 41.7, 30.0, 30.0, 25.7, 25.6, 23.3, 23.0, 23.0, 22.2, 21.9.

TOF MS EI+

Calculated [M] = 196.1099

Found [M] = 196.1102

FT-IR: 1786 cm^{-1} (C=O)

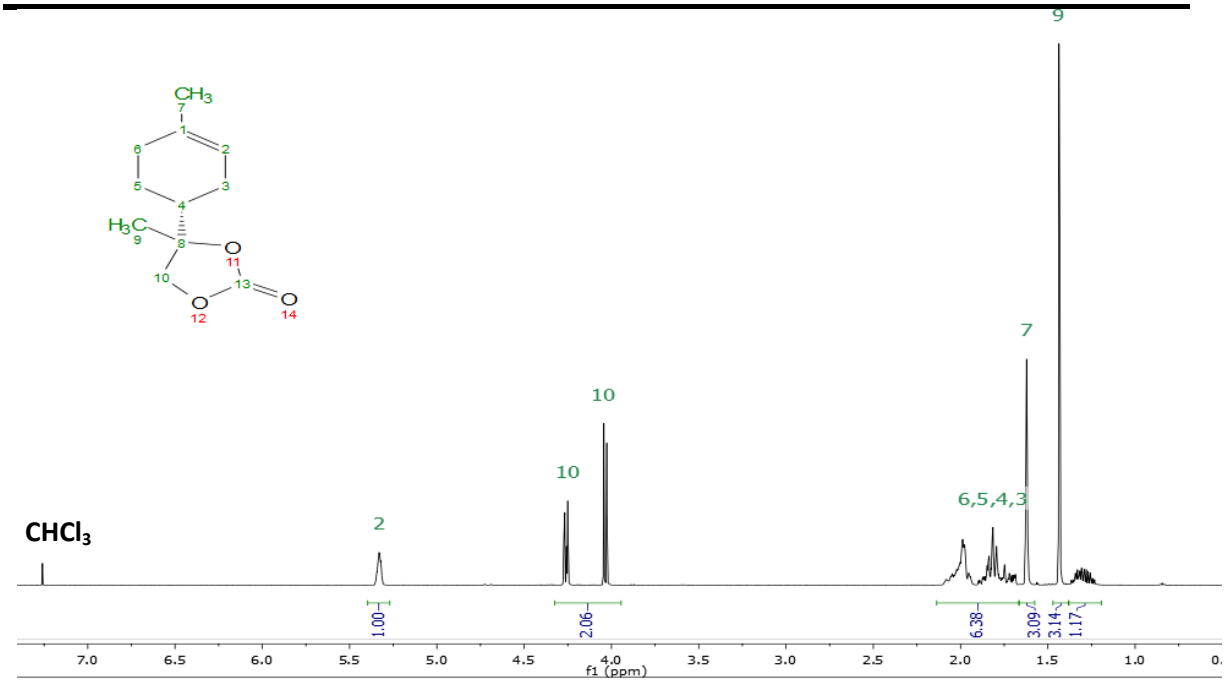

Figure 4.98 ^{1}H NMR of 8,9-LC, mixture of isomers.

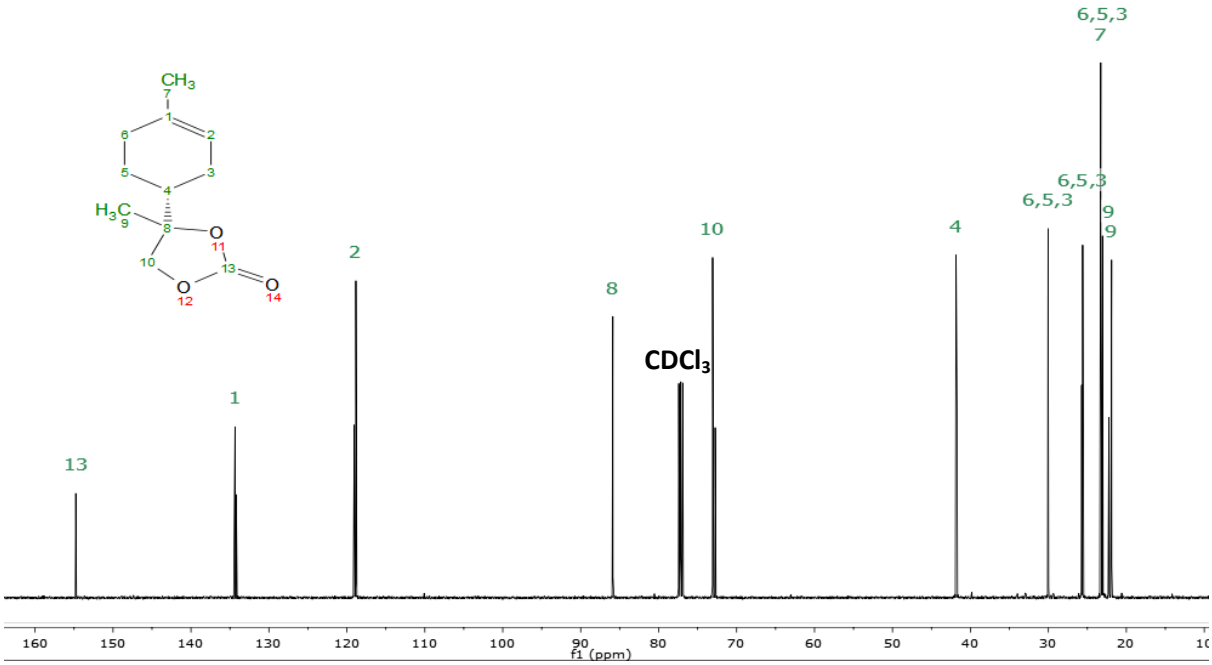

Figure 4.99 $^{13}C\ \{^{1}H\}$ NMR of 8,9-LC, mixture of isomers

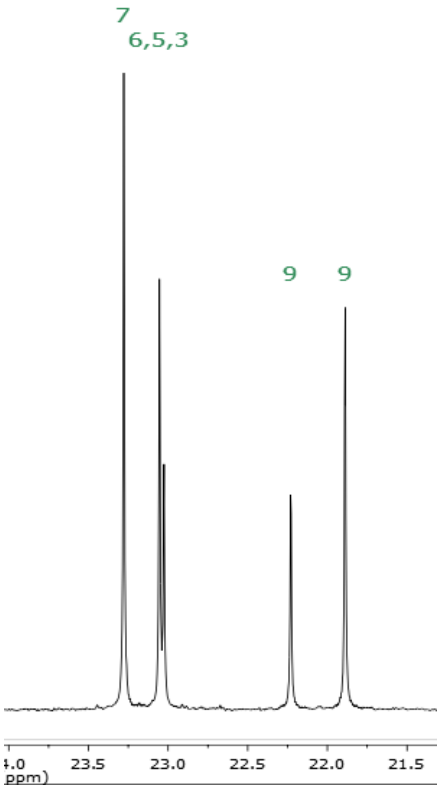

Figure 4.100 Zoom in on the $^{13}C\ \{^{1}H\}$ NMR of 8,9-LC in the range of 23.5-21.5 ppm

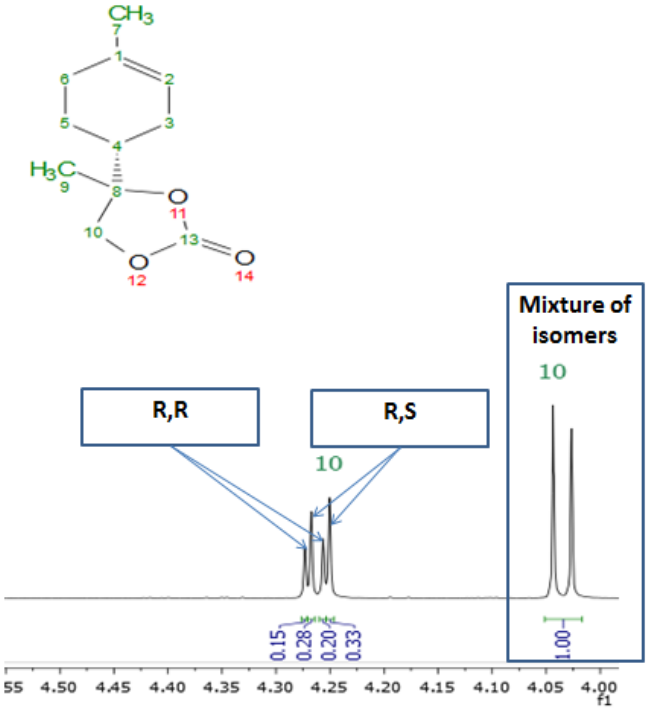

Figure 4.101 4R, 8R-8,9-LC and 4R, 8S-8,9-LC assignments using ^{1}H NMR and signal from protons at the position 10

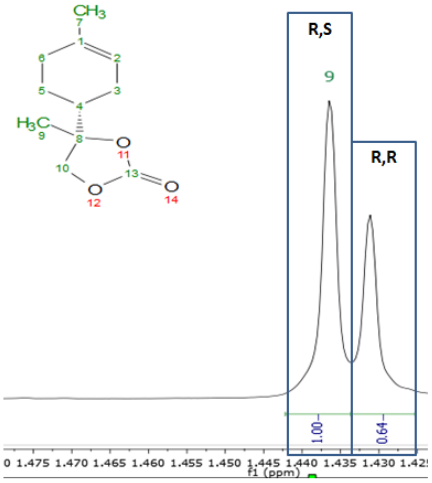

Figure 4.102 4R, 8R-8,9-LC and 4R, 8S-8,9-LC assignments using ^{1}H NMR and signal from methyl group at the position 9

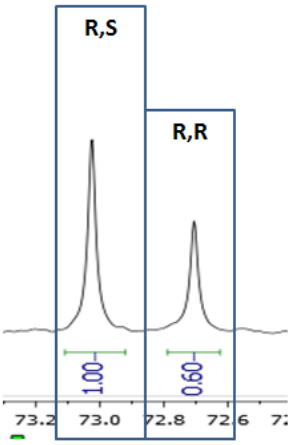

Figure 4.103 4R, 8R-8,9-LC and 4R, 8S-8,9-LC assignments using inverse gated $^{13}C\{^{1}H\}$ NMR and signal from carbon at the position 10

Calculations of 8,9-LC stereoisomers [% RR : %RS]			
	^{1}H NMR (H10)	^{1}H NMR (H9)	Inverse gated $^{13}C\{^{1}H\}$ NMR (C10)
4R, 8R : 4R, 8S	36:64	39:61	38:62

The isomers assignments are based on the assumption that the carbonation follows the double inversion pathway and the stereoisomers of **8,9-LO** yield corresponding stereoisomers of **8,9-LC**.

Characterisation of compound BI-1,2-LC

Compound **BI-1,2-LC**

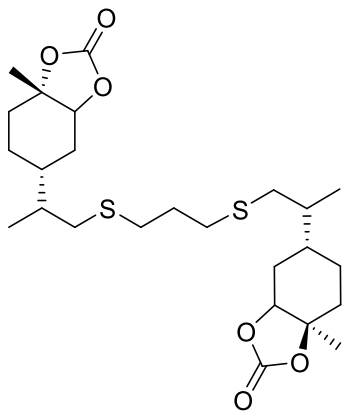

^{1}H NMR (400 MHz, $CDCl_3$) δ = 4.36 – 4.26 (m, 2H), 2.58 – 2.32 (m, 8H), 2.26 – 2.01 (m, 4H), 1.80 (m, 2H), 1.70 – 1.18 (m, 18H), 0.92 (2xd, *J*=6.9, 6H).

^{13}C {^{1}H} NMR (101 MHz, $CDCl_3$) δ = 154.7, 82.5, 80.8, 80.7, 37.3, 37.2, 37.1, 35.7, 35.7, 32.9, 32.8, 32.7, 31.7, 31.5, 31.5, 30.3, 29.4, 29.3, 28.6, 26.0, 26.0, 24.5, 24.4, 23.4, 21.9, 15.9, 15.8.

TOF MS ASAP+

Calculated $[M+H]^+$ = 501.2345

Found $[M+H]^+$ = 501.2343

FT-IR: 1792 cm^{-1} (C=O)

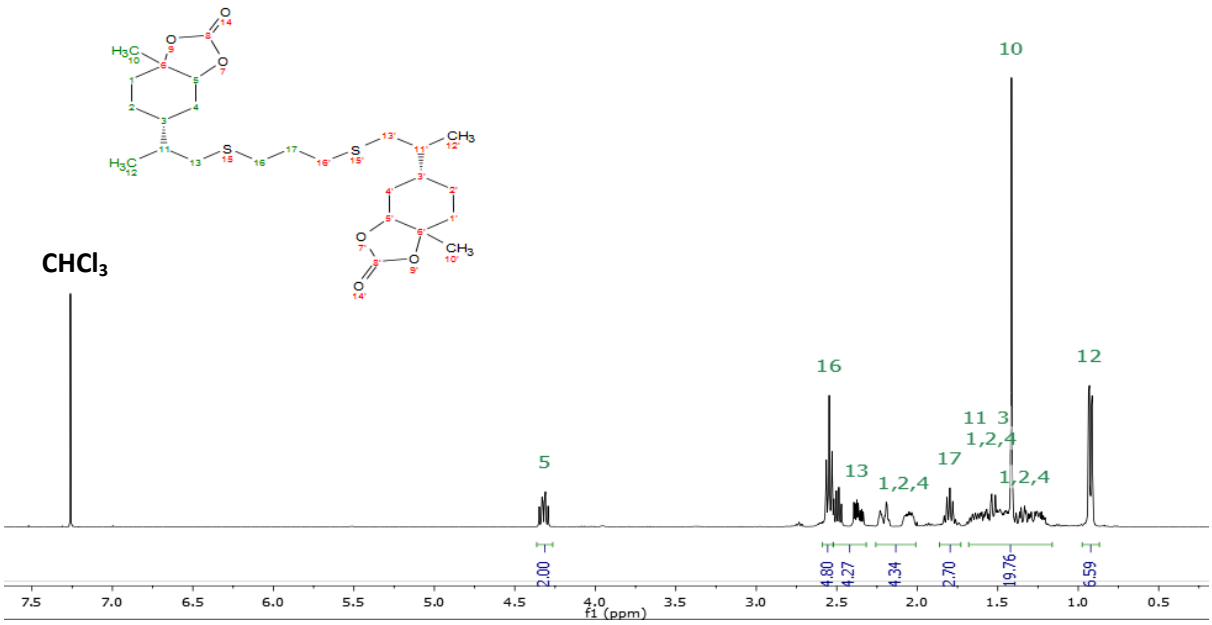

Figure 4.104 ^{1}H NMR of BI-1,2-LC.

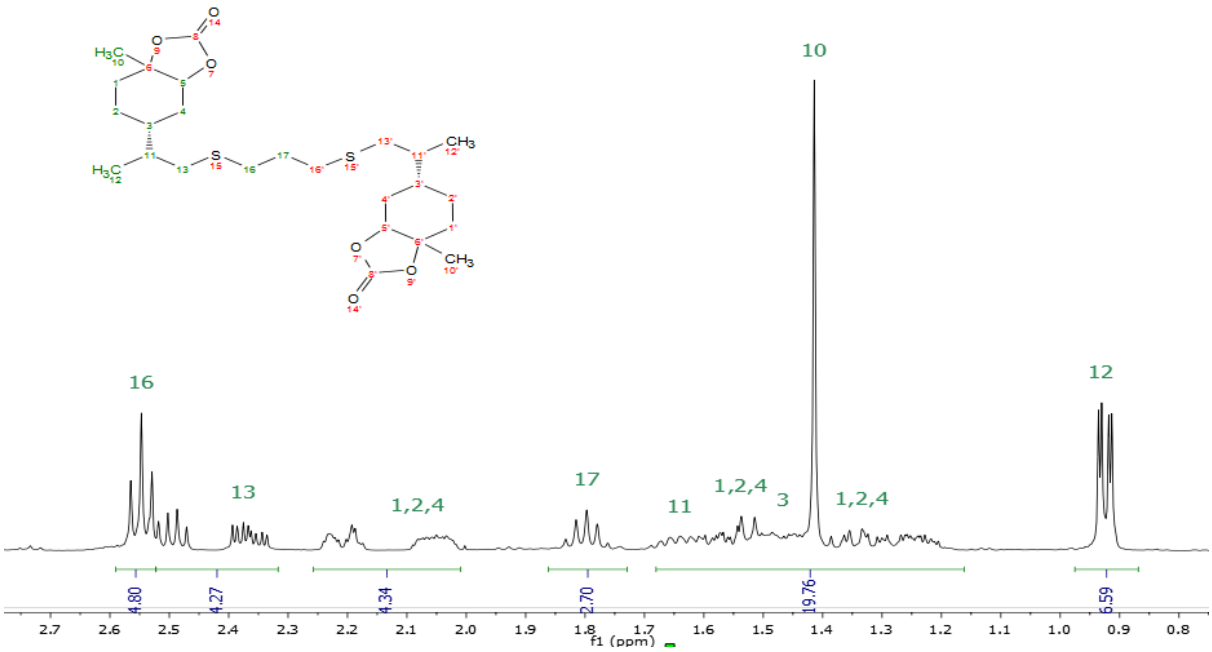

Figure 4.105 Zoom in on ^{1}H NMR spectrum of BI-1,2-LC in the range of 2.7 ppm – 0.8 ppm.

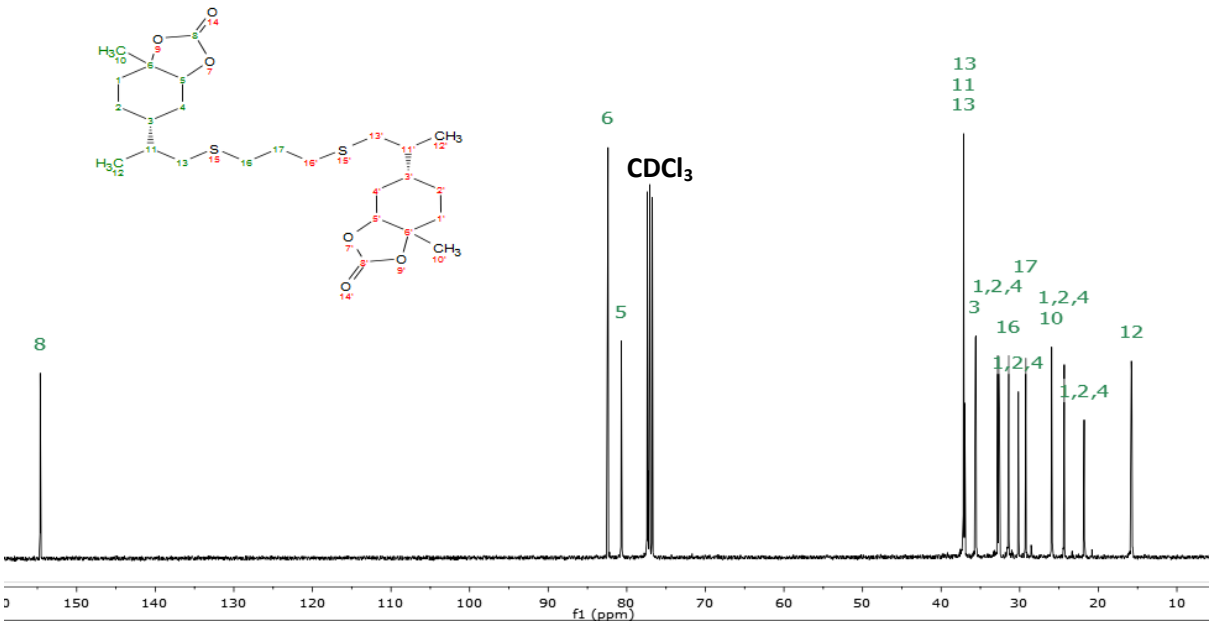

Figure 4.106 ^{13}C {^{1}H} NMR of BI-1,2-LC.

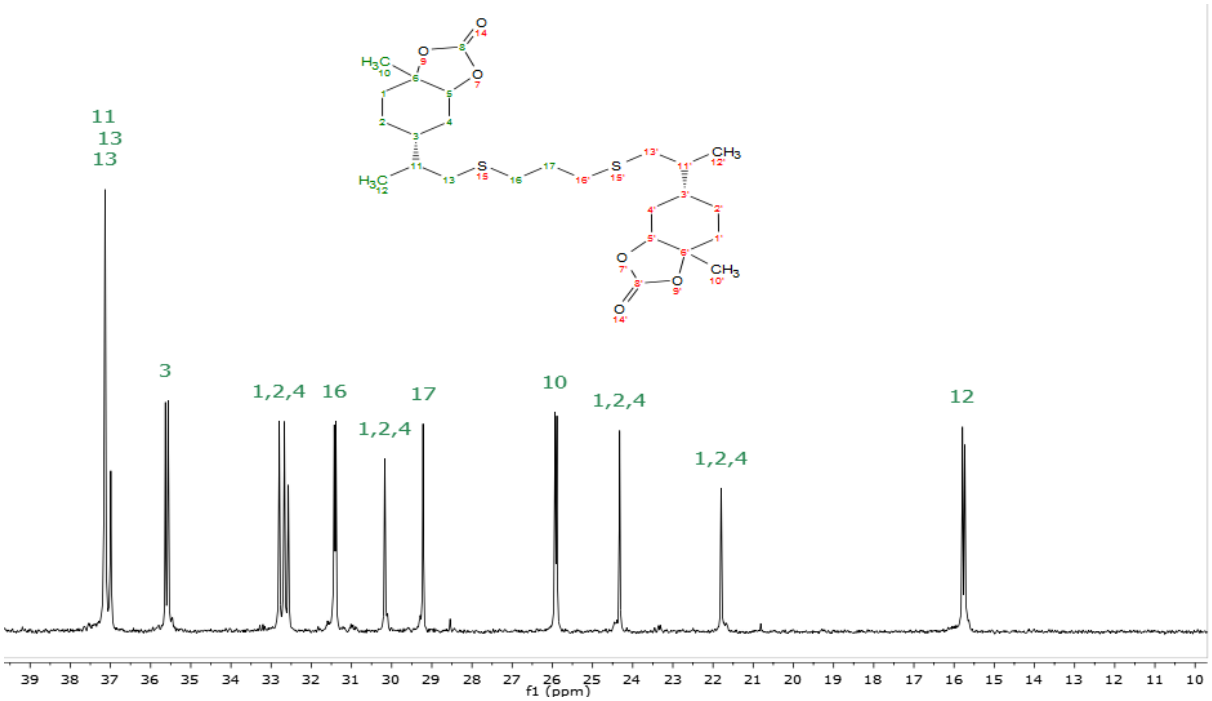

Figure 4.107 Zoom in on $^{13}C\{^{1}H\}$ NMR spectrum of 17 in the range 39 ppm – 10 ppm.

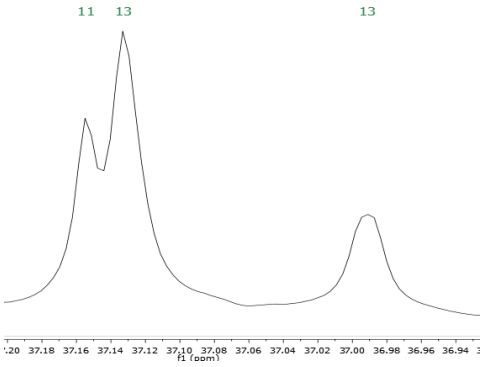

Figure 4.108 Zoom in on $^{13}C\{^{1}H\}$ NMR spectrum of 17 in the region 37.2 ppm – 36.9 ppm.

Characterisation of compound BI-8,9-LC

Compound **BI-8,9-LC**

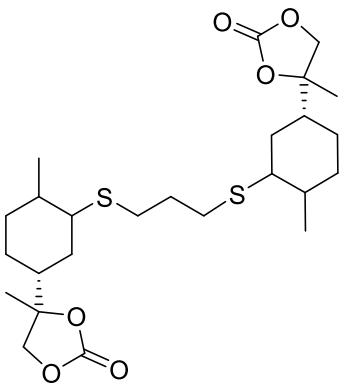

^{1}H NMR(400 MHz, $CDCl_3$): δ = 4.36 – 4.19 (m, 2H), 4.02 (m, 2H), 3.03 – 2.51 (m, 6H), 2.14 – 2.03 (m, 2H), 1.98 – 0.90 (m, 28H) ppm

^{13}C {^{1}H} NMR (126 MHz, $CDCl_3$) δ = 154.7, 85.7, 73.7, 73.2, 50.5, 50.0, 49.9, 45.9, 39.8, 37.4, 36.5, 34.7, 33.2, 31.5, 29.1, 26.2, 22.3, 21.7, 20.7, 20.3, 19.6, 18.6, 12.3.

TOF MS ASAP+

Calculated $[M+H]^+$ = 501.2345

Found $[M+H]^+$ = 501.2344

FT-IR: 1788 cm^{-1} (C=O)

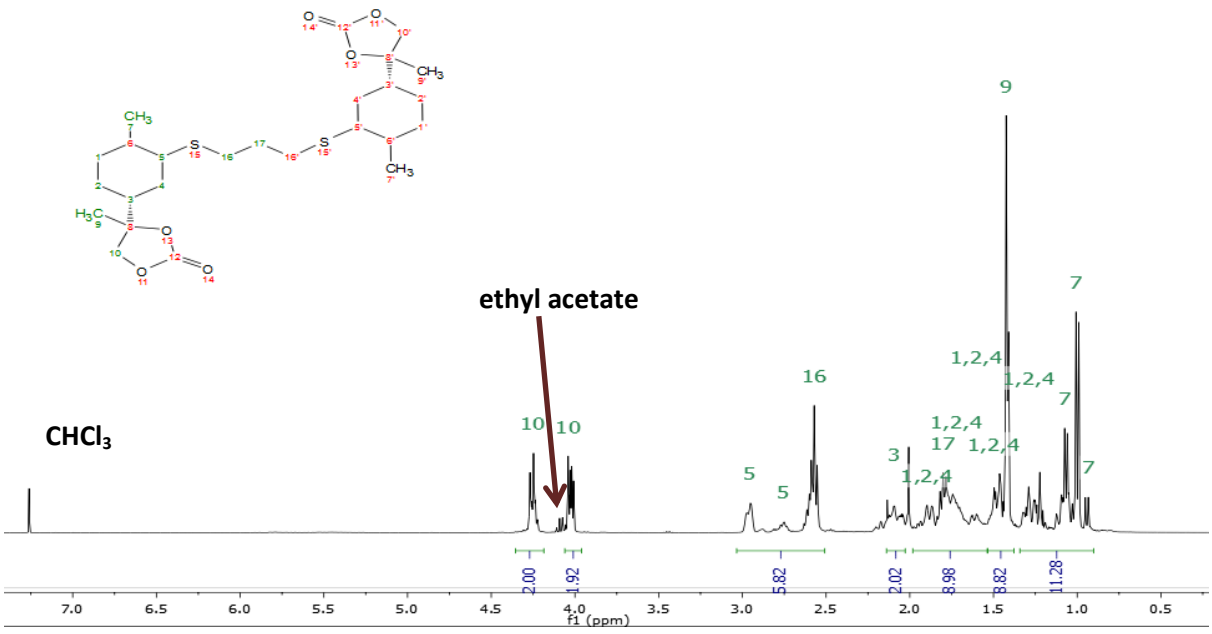

Figure 4.109 ^{1}H NMR spectrum of BI-8,9-LC.

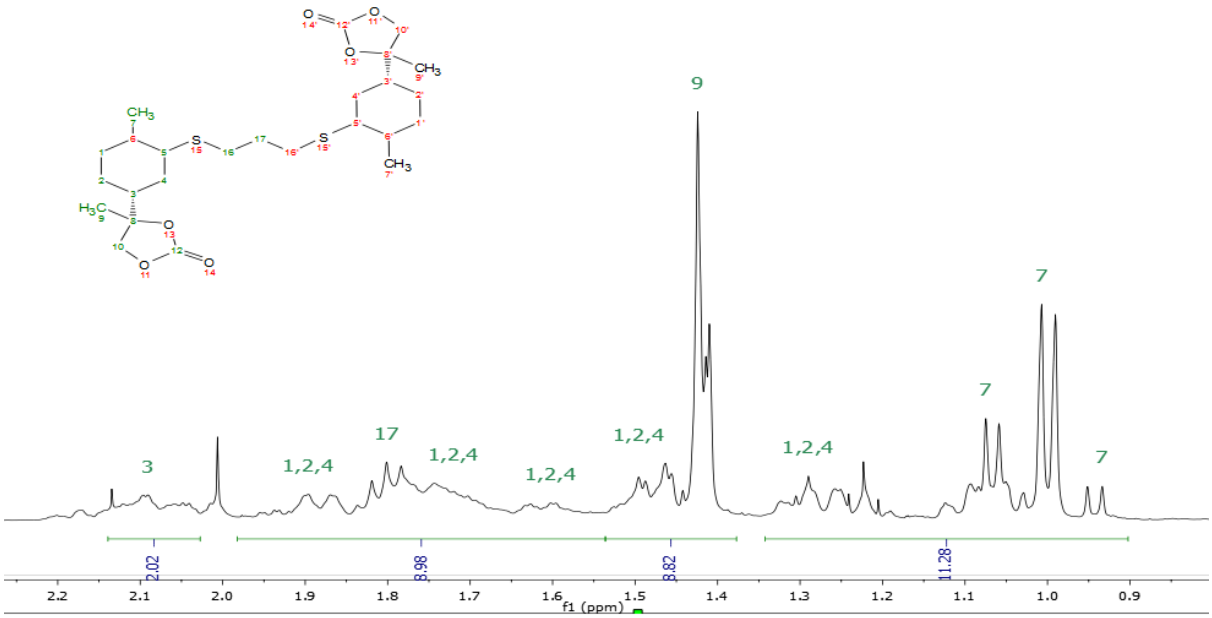

Figure 4.110 Zoom in on ^{1}H NMR spectrum in the range of 2.2 ppm – 0.9 ppm.

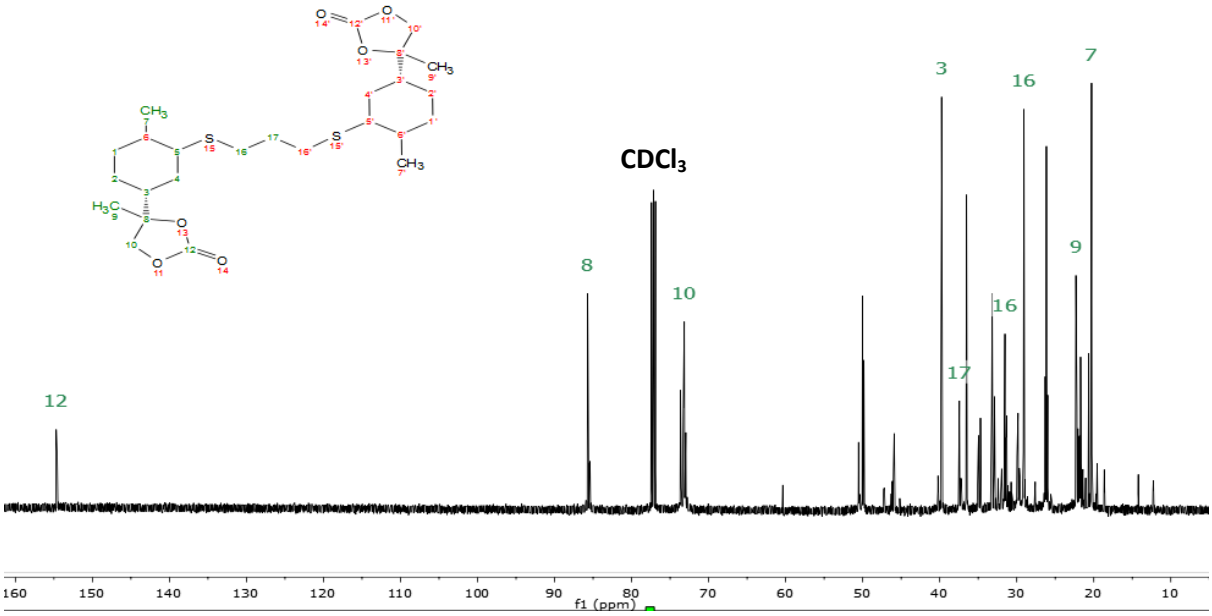

Figure 4.111 ^{13}C {^{1}H} NMR of BI-8,9-LC

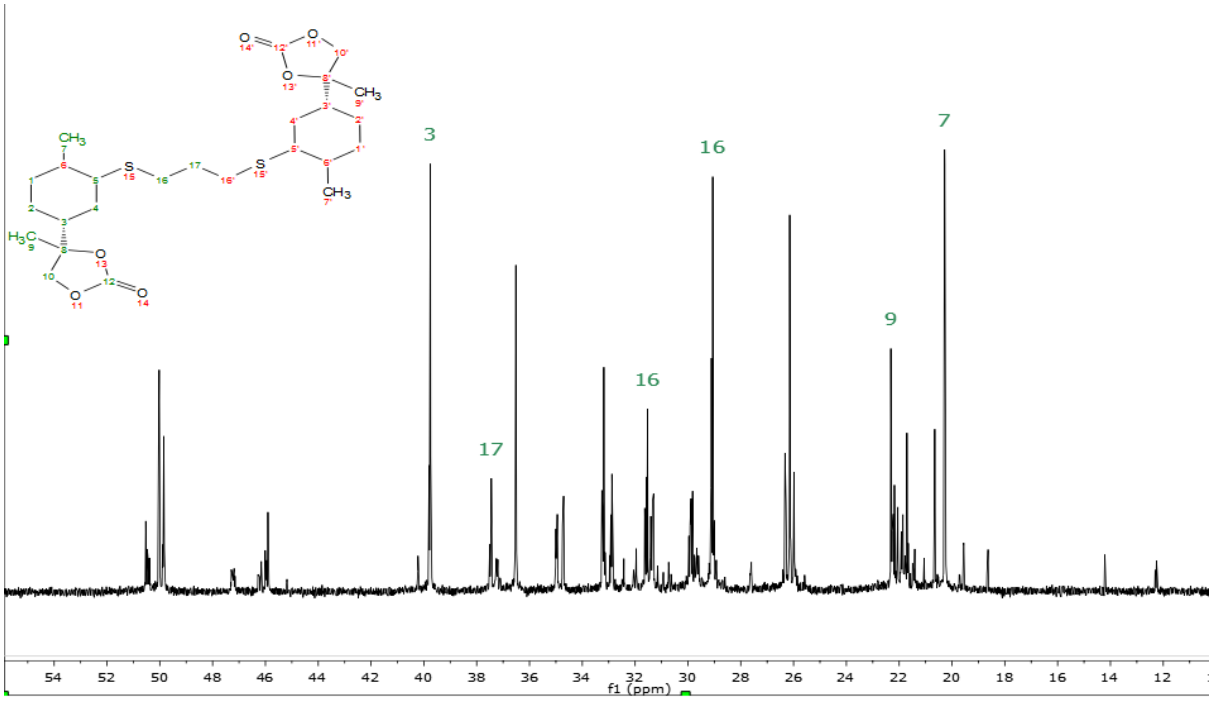

Figure 4.112 Zoom in on spectrum in the range of 54 ppm - 11.5 ppm.

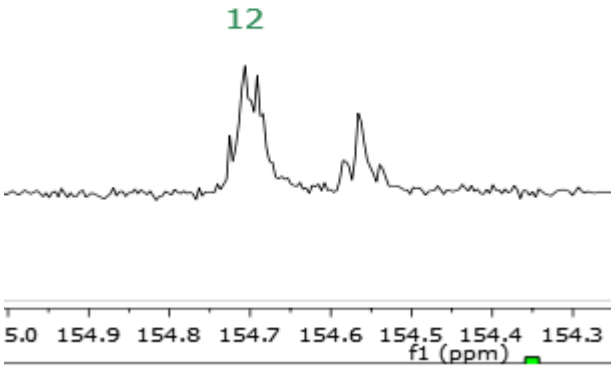

Figure 4.113 Zoom in on $^{13}C\{^{1}H\}$ NMR spectrum in the carbonyl region. The complexity of C=O signal indicates presence of isomers mixture.

8,9-limonene aldehyde (8,9-LA)

Compound **8,9-LA**

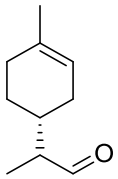

^{1}H NMR (400 MHz, $CDCl_3$) δ = 9.65 (2xd, $^{3}J_{H-H}$ = 2.5 Hz, 1H), 5.35 (m, 1H), 2.26 (m, 1H), 2.13 - 1.54 (m, 5H+3H), 1.35 (m, 2H), 1.06 (2xd, $^{3}J_{H-H}$ =7.0 Hz, 3H).

^{13}C {^{1}H} NMR (101 MHz, $CDCl_3$) δ = 205.5, 205.4, 134.2, 134.2, 120.1, 120.0, 51.1, 50.8, 34.5, 34.4, 30.8, 30.3, 30.1, 29.8, 28.2, 27.4, 25.6, 23.6, 23.5, 10.5, 10.4.

ESI QTOF MS-

Calculated $[M-H]^-$ = 151.1117
Found $[M-H]^-$ = 151.1134

FT-IR: 1707 cm^{-1} (C=O)

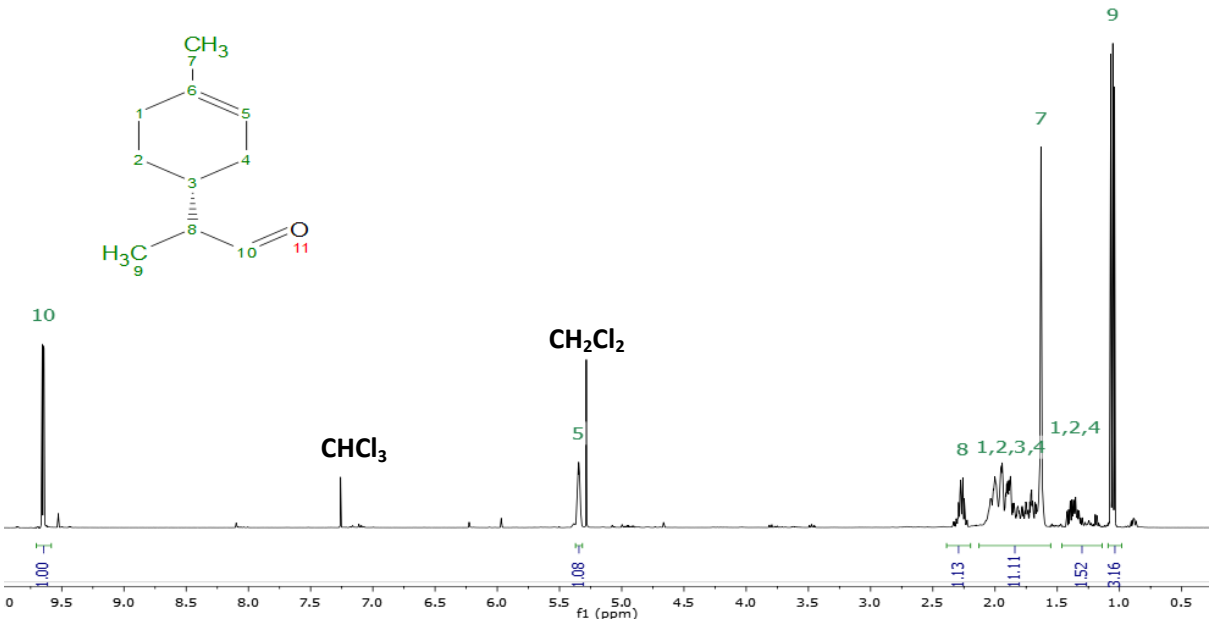

Figure 4.114 ^{1}H NMR of 8,9-LA

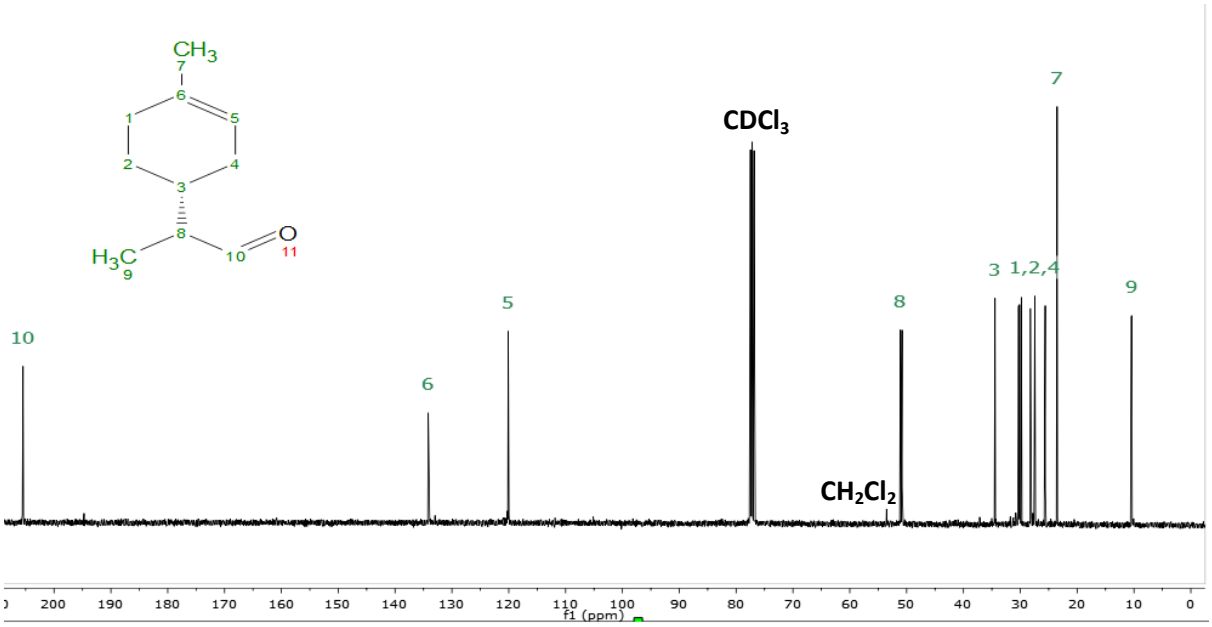

Figure 4.115 $^{13}C\{^{1}H\}$ NMR of 8,9-LA

8,9-Carvone oxide (8,9-CO)

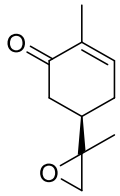

Carvone oxide is a previously known compound [58]

^{1}H NMR(Chloroform-d, 400 MHz): δ = 6.53 (m, 1H), 2.53 – 1.79 (m, 7H), 1.53 (m, 3H), 1.10 (m, 3H) ppm

$^{13}C\{^{1}H\}$ NMR (101 MHz, $CDCl_3$) δ = 198.2, 198.1, 143.8, 143.6, 135.1, 135.1, 57.5, 57.4, 52.3, 52.1, 40.9, 40.5, 39.9, 39.6, 27.6, 27.4, 18.5, 18.1, 15.3.

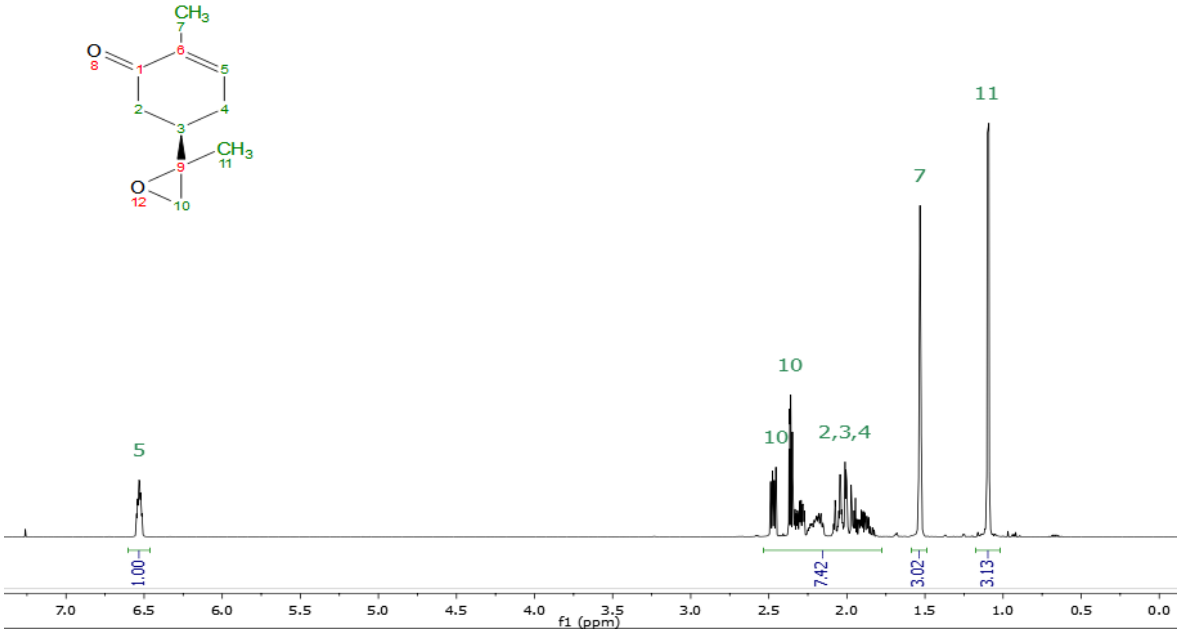

Figure 4.116 ^{1}H NMR spectrum of 8,9-CO.

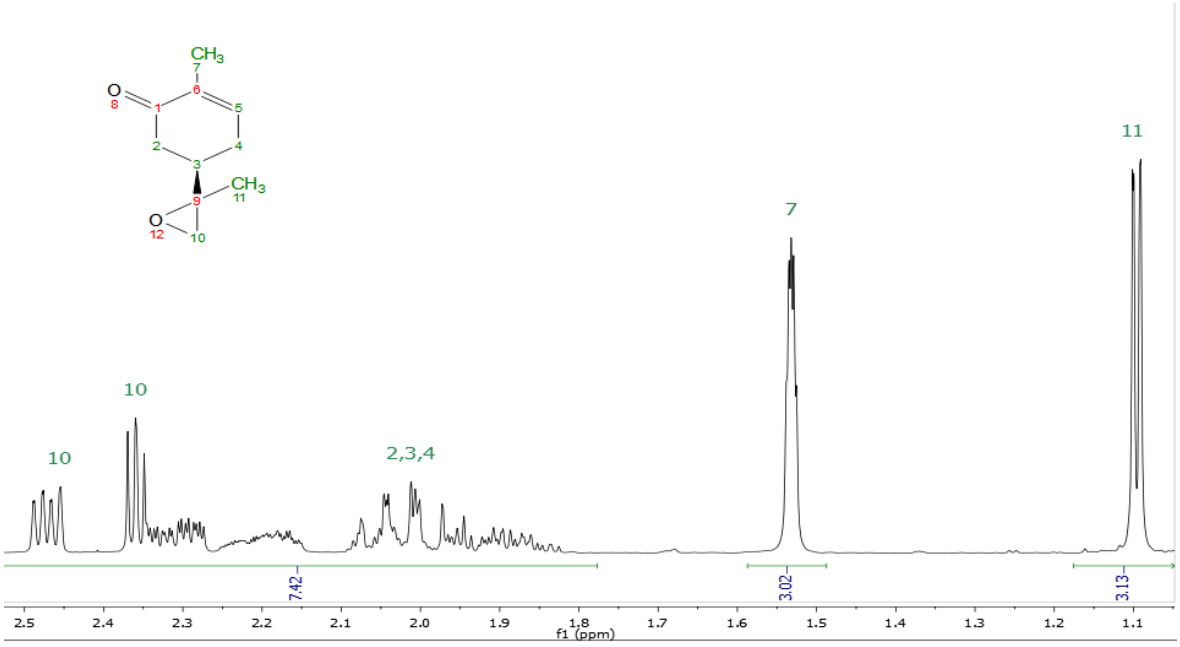

Figure 4.117 ^{1}H NMR spectrum of 8,9-CO in the range of 2.5 – 1.1 ppm.

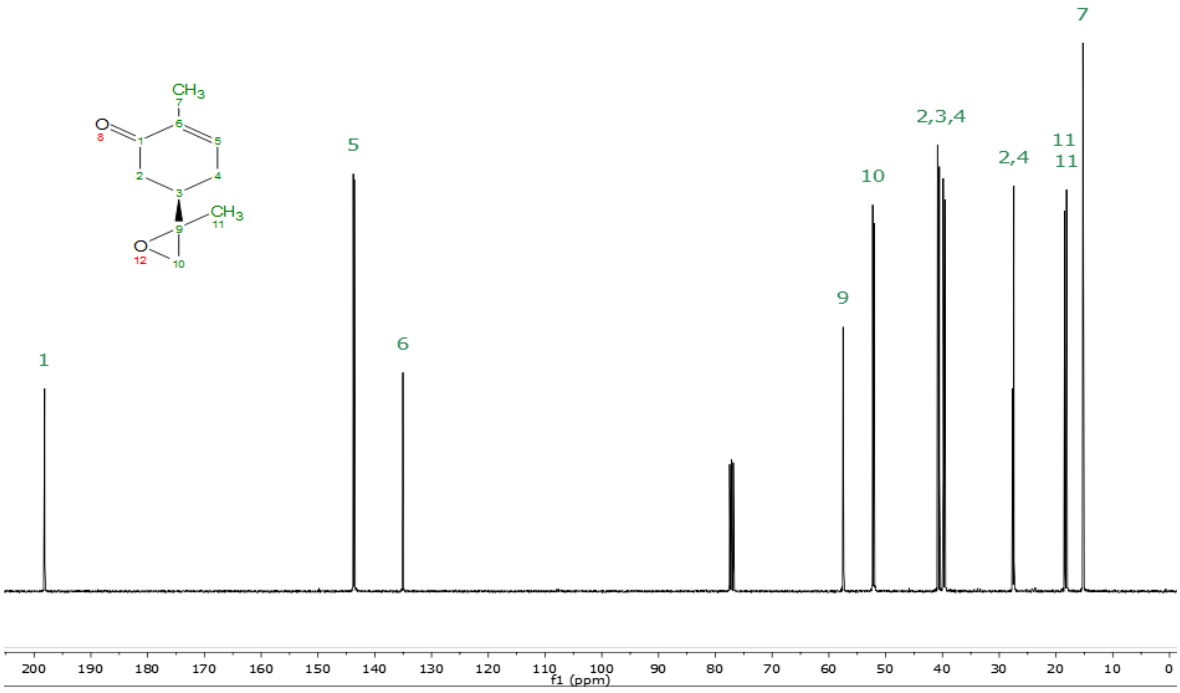

Figure 4.118 ^{13}C NMR spectrum of 8,9-CO.

8,9-carvone carbonate (8,9-CC)

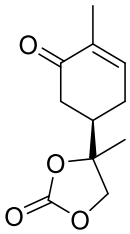

8,9-CC

^{1}H NMR(400 MHz, $CDCl_3$): δ = 6.66 (m, 1H, J=7.8, 6.4, 3.2, 1.8 Hz), 4.27 (m, 1H), 4.04 (m, 1H), 2.54 – 2.03 (m, 5H), 1.73 – 1.54 (s, 3H), 1.41 (2 x s, 3H) ppm

^{13}C {^{1}H} NMR (101 MHz, $CDCl_3$) δ = 197.2, 196.9, 154.0, 143.3, 143.0, 135.5, 135.5, 84.1, 84.0, 72.6, 72.2, 60.1, 42.5, 42.5, 38.1, 38.1, 37.9, 26.0, 26.0, 22.1, 21.5, 20.8, 15.3, 14.0.

MS-ESI^{+}

Calculated $[M+H]^{+}$ = 211.0965

Found $[M+H]^{+}$ = 211.0969

Calculated $[M+Na]^{+}$ = 233.0784

Found $[M+Na]^{+}$ = 233.0789

FT-IR: 1800 cm^{-1} (C=O)

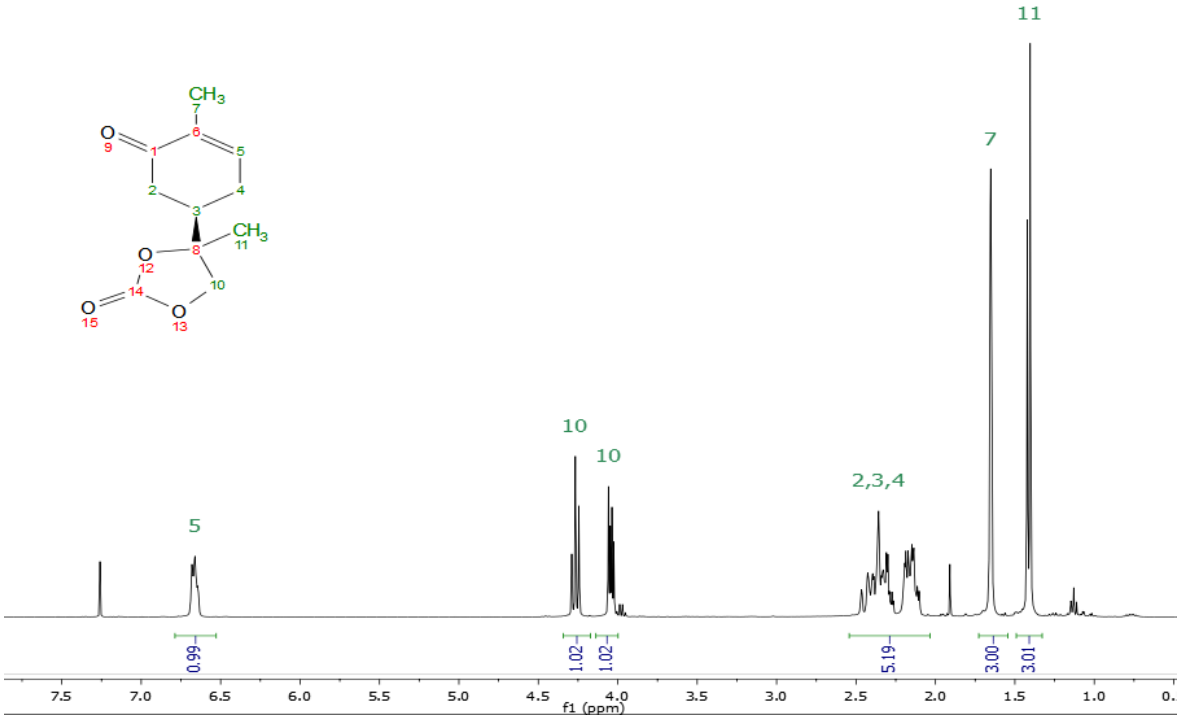

Figure 4.119 ^{1}H NMR spectroscopy of 8,9-CC.

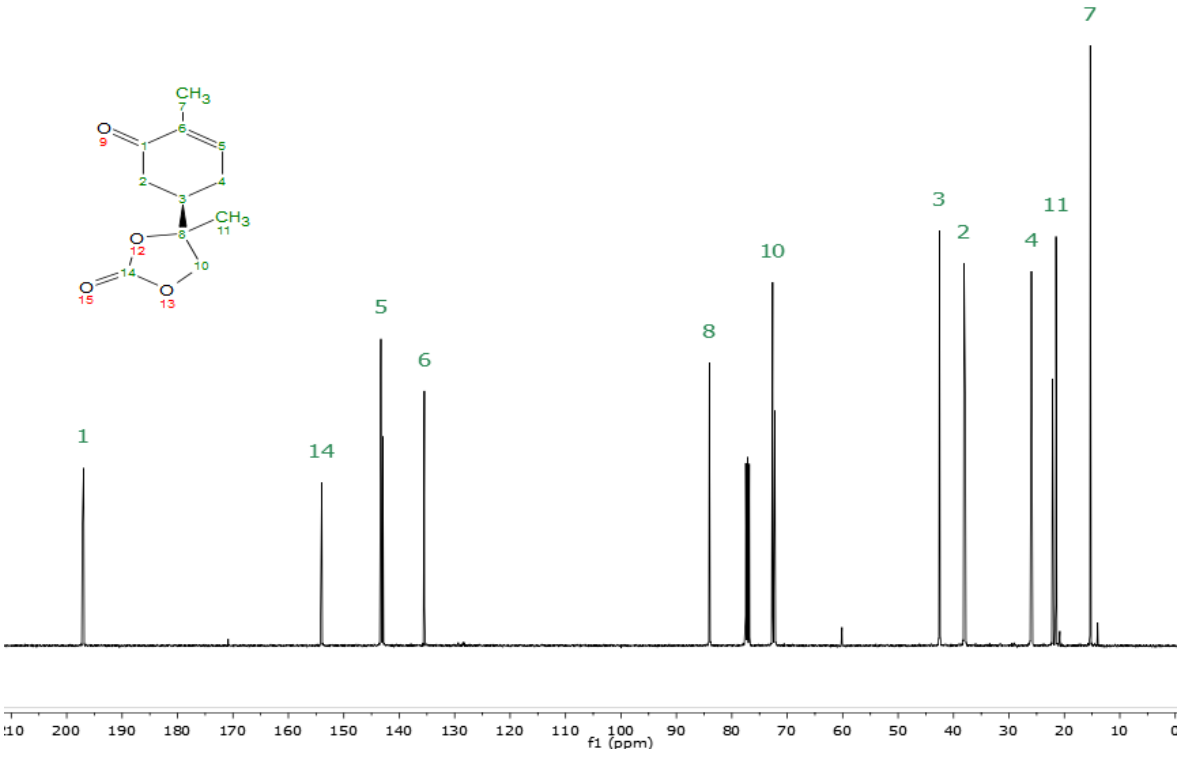

Figure 4.120 ^{13}C NMR spectroscopy of 8,9-CC.

β-elemene monocarbonate monoepoxide (BEMCMO)

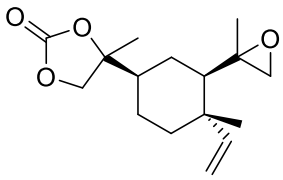

BEMCMO

^{1}H NMR(400 MHz, $CDCl_3$): δ = 5.73 (m, 1H), 5.08 – 4.90 (m, 2H), 4.39 – 3.98 (m, 2H), 2.70 – 2.35 (m, 2H), 1.88 – 0.98 (m, 17H) ppm

^{13}C {^{1}H} NMR (101 MHz, $CDCl_3$) δ = 154.7, 154.6, 154.6, 149.7, 149.6, 148.3, 148.3, 111.4, 111.3, 110.5, 110.4, 85.6, 85.5, 85.5, 73.6, 73.3, 73.1, 72.8, 58.3, 58.2, 57.7, 56.3, 56.2, 53.0, 53.0, 52.8, 52.7, 50.6, 50.5, 45.7, 45.6, 45.6, 45.4, 40.8, 40.2, 39.7, 39.1, 39.1, 24.3, 24.1, 23.9, 23.7, 23.1, 22.8, 22.8, 22.1, 22.0, 21.9, 21.9, 21.8, 21.5, 21.5, 19.8, 19.7, 17.5, 17.4, 17.1, 17.0.

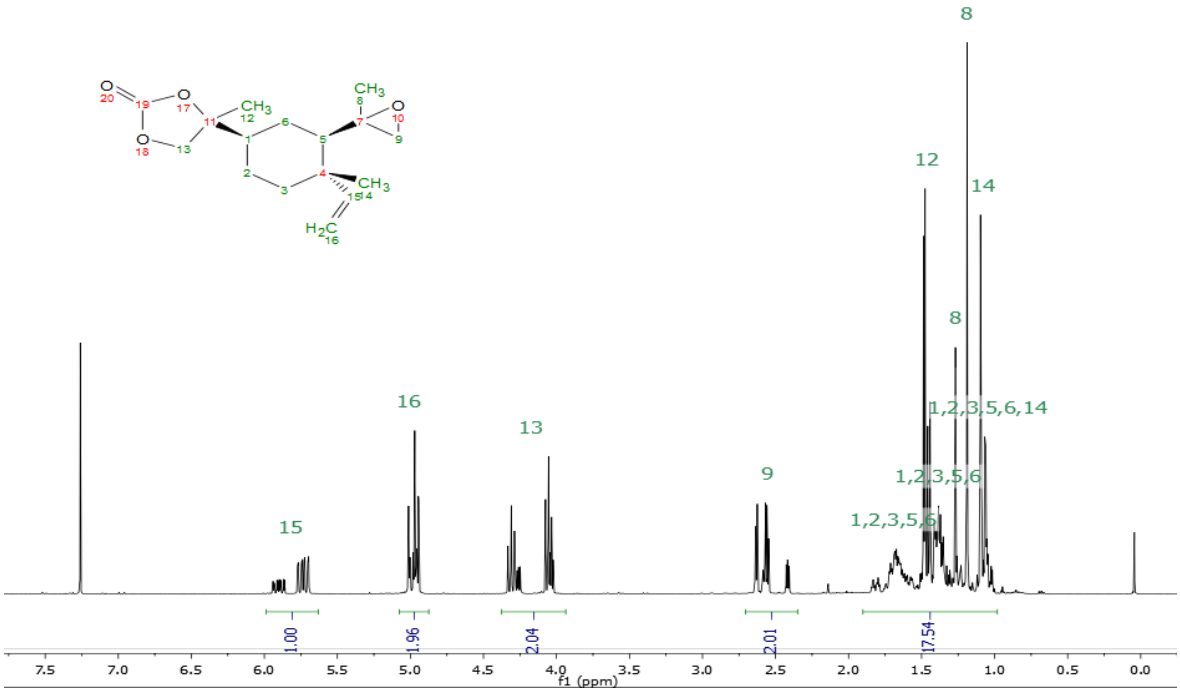

Figure 4.121 ^{1}H NMR spectrum of BEMCMO.

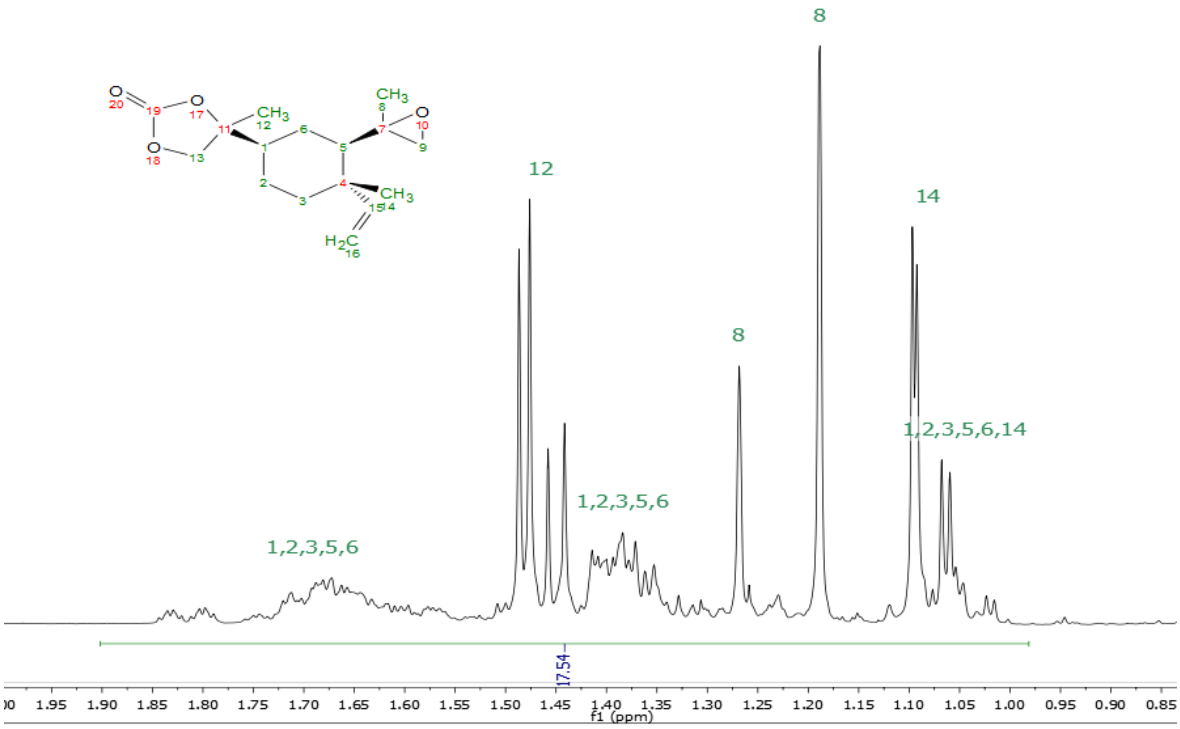

Figure 4.122 ^{1}H NMR spectrum of BEMCMO in the range of 2 – 0.9 ppm.

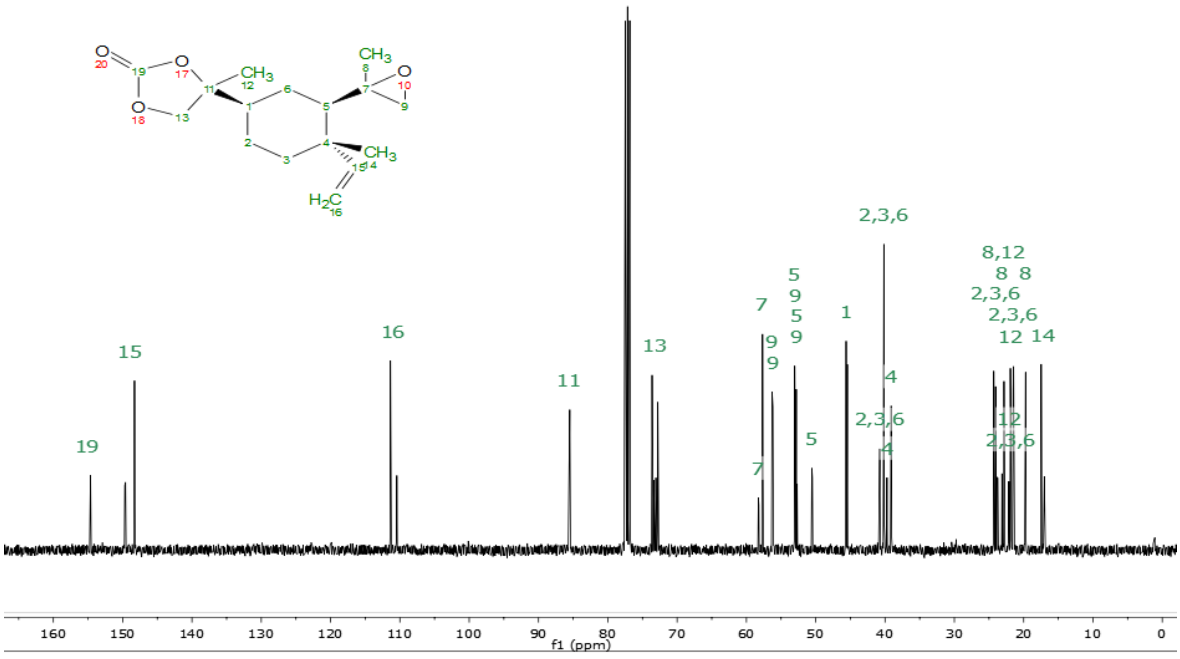

Figure 4.123 ^{13}C NMR spectrum of BEMCMO.

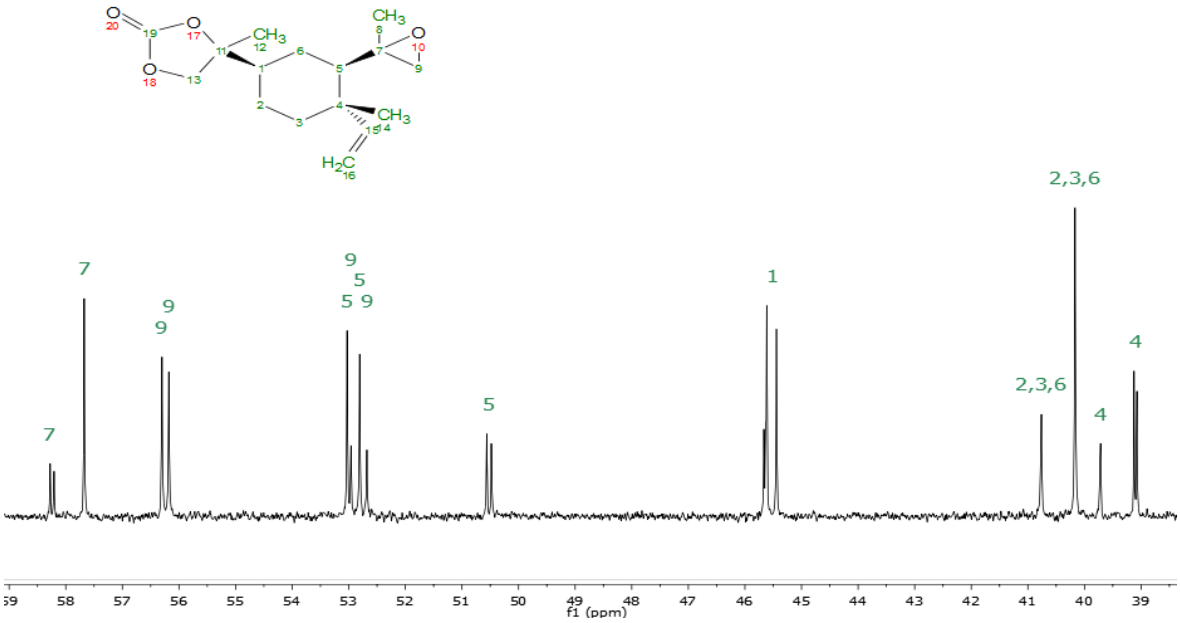

Figure 4.124 ^{13}C NMR spectrum of BEMCMO in the range of 59 – 39 ppm.

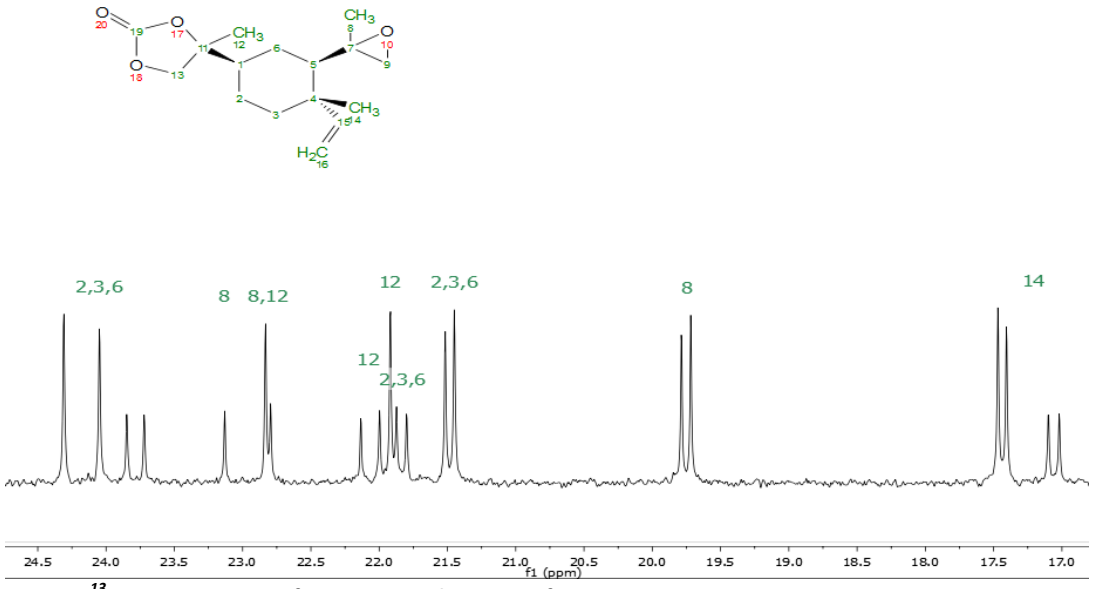

Figure 4.125 ^{13}C NMR spectrum of BEMCMO in the range of 24 – 17 ppm.

β-elemene biscarbonate (BEBC)

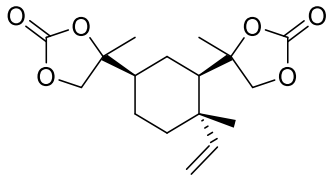

BEBC

^{1}H NMR(400 MHz, $CDCl_3$): δ = 5.96 – 5.65 (m, 1H), 5.11 – 4.91 (m, 2H), 4.46 – 3.87 (m, 4H), 1.98 – 1.02 (m, 17H) ppm

^{13}C {1H} NMR (101 MHz, $CDCl_3$) δ = 154.5, 154.5, 154.4, 154.1, 154.0, 149.9, 149.9, 148.6, 148.4, 112.2, 112.0, 110.8, 110.7, 87.2, 87.0, 86.9, 86.8, 85.3, 85.3, 85.2, 75.8, 75.7, 73.5, 73.4, 73.3, 73.1, 72.9, 52.9, 52.6, 51.4, 51.3, 45.6, 45.4, 45.4, 45.3, 42.0, 42.0, 42.0, 42.0, 39.5, 39.4, 39.4, 24.0, 23.3, 23.2, 23.1, 23.1, 22.8, 22.7, 22.2, 22.0, 21.9, 21.9, 21.8, 21.7, 21.5, 17.1, 17.0, 16.9, 16.8.

MS-ESI^{+}
Calculated $[M+Na]^{+}$ = 347.1470
Found $[M+Na]^{+}$ = 347.1465

FT-IR: 1789 cm^{-1} (C=O)

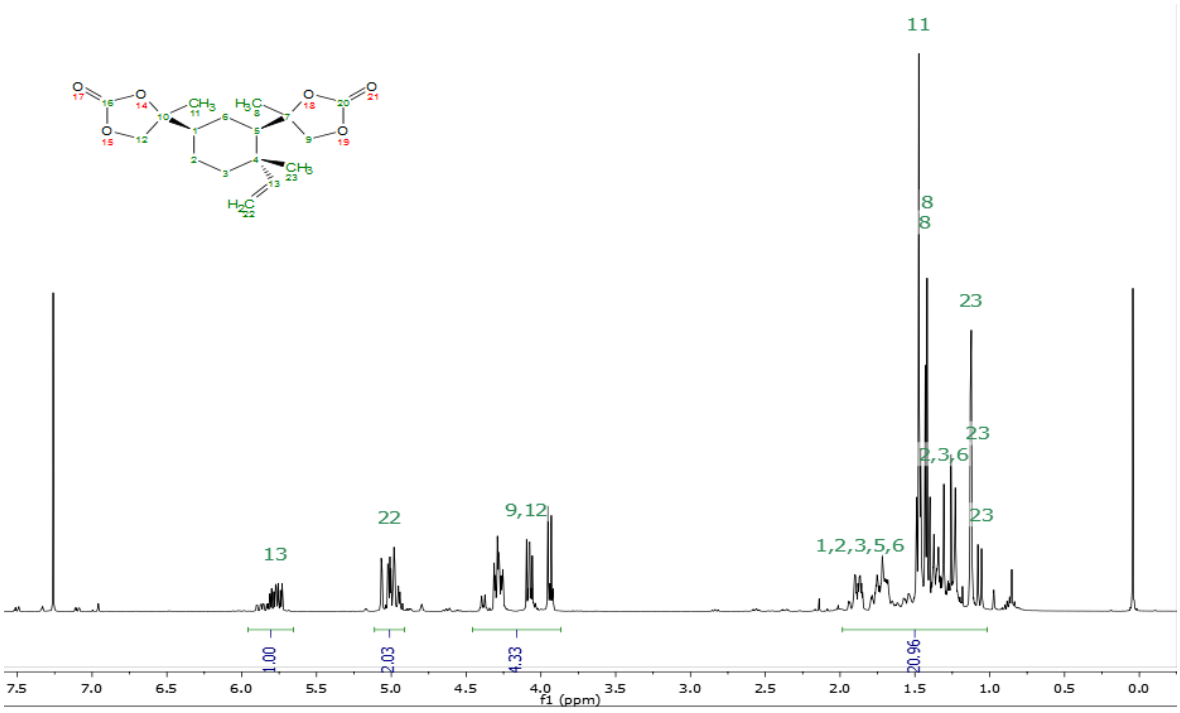

Figure 4.126 ^{1}H NMR spectrum of BEBC.

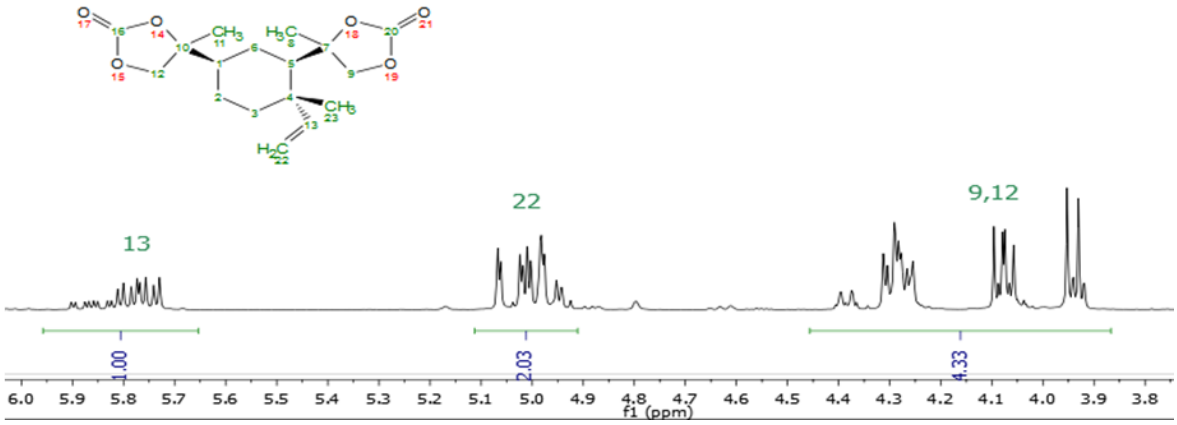

Figure 4.127 ^{1}H NMR spectrum of BEBC in the range of 6.0 – 3.8 ppm.

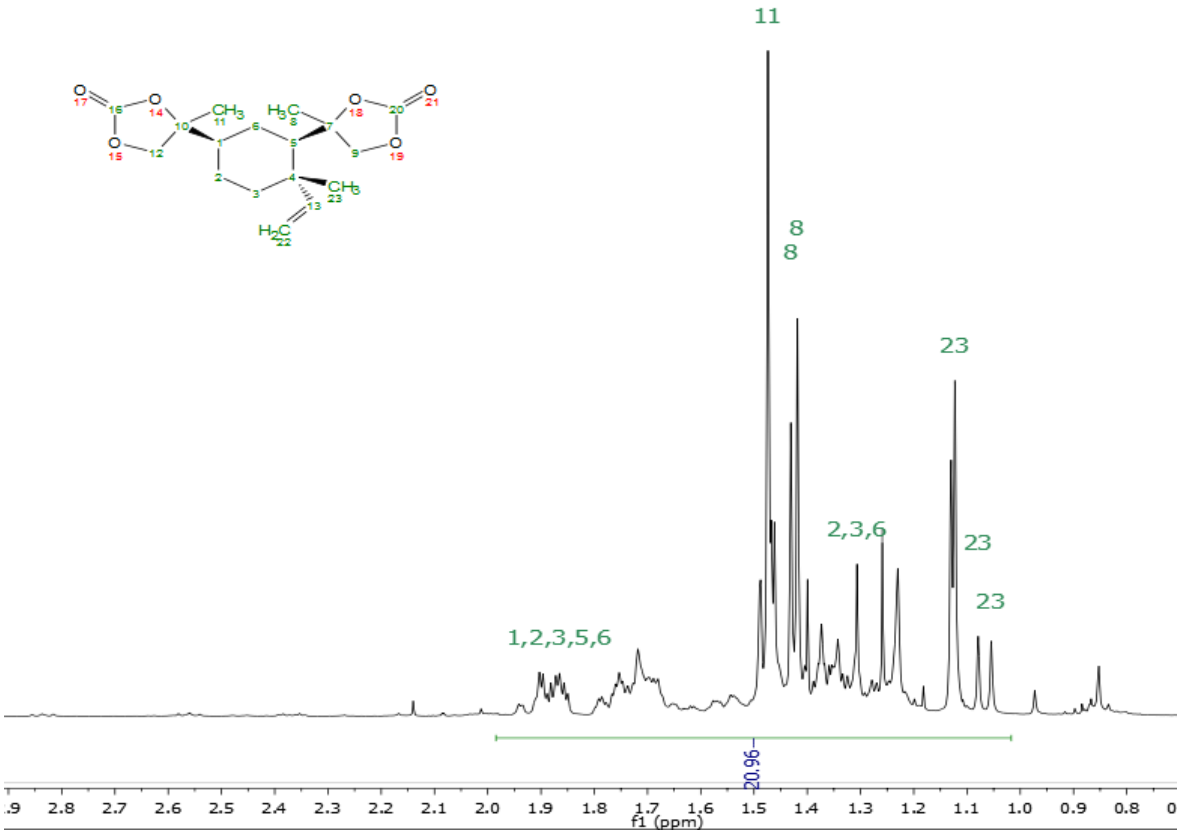

Figure 4.128 ^{1}H NMR spectrum of BEBC in the range of 2.8 – 0 ppm.

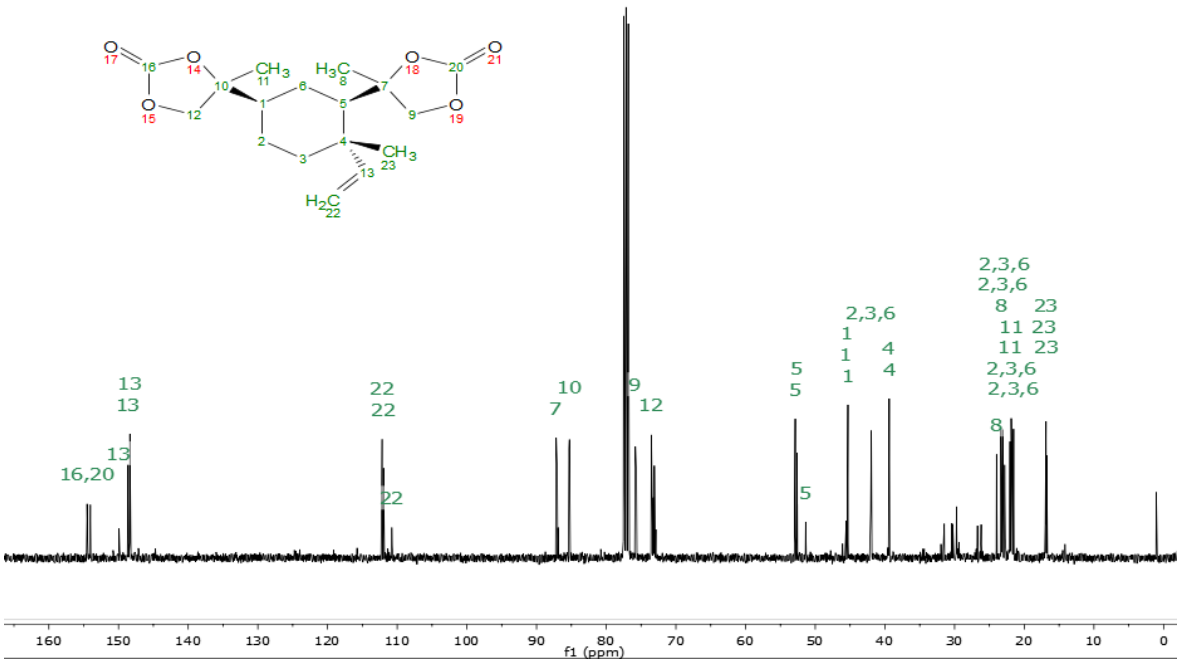

Figure 4.129 ^{13}C NMR spectrum of BEBC.

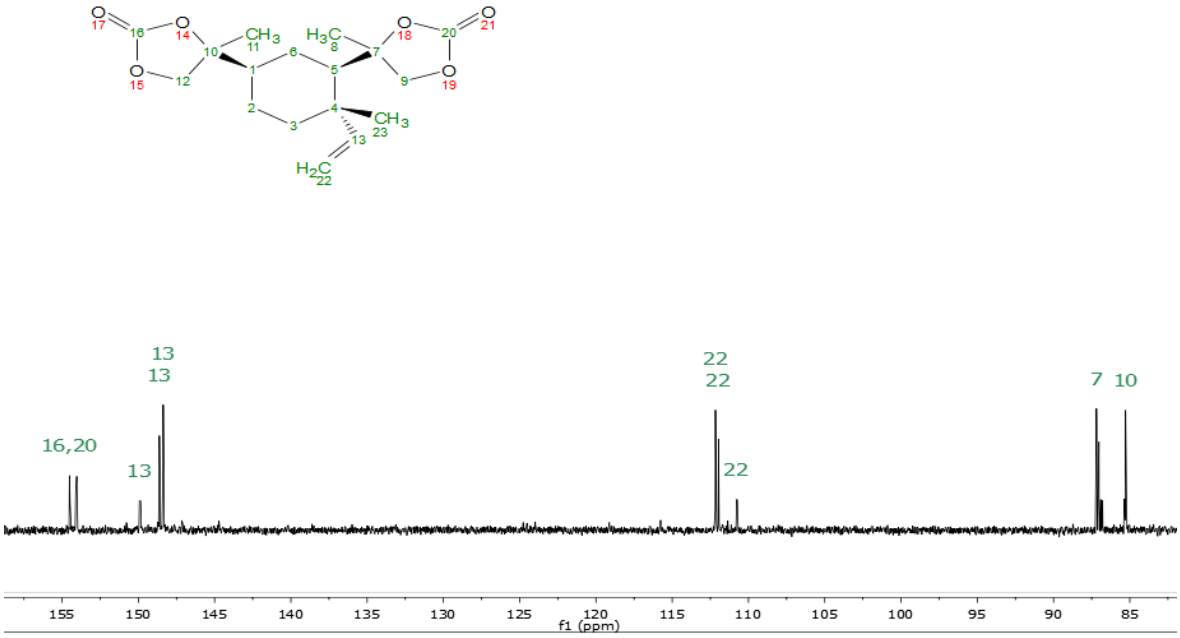

Figure 4.130 ^{13}C NMR spectrum of BEBC in the range of 155 – 85 ppm.

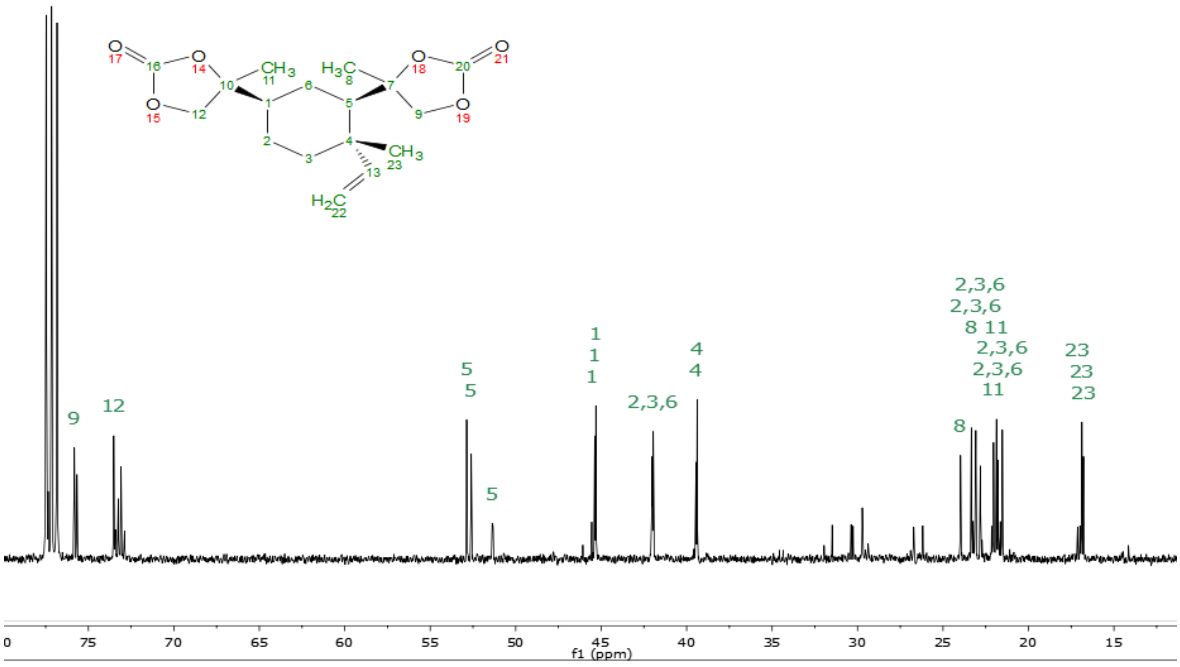

Figure 4.131 ^{13}C NMR spectrum of BEBC in the range of 77 – 15 ppm.

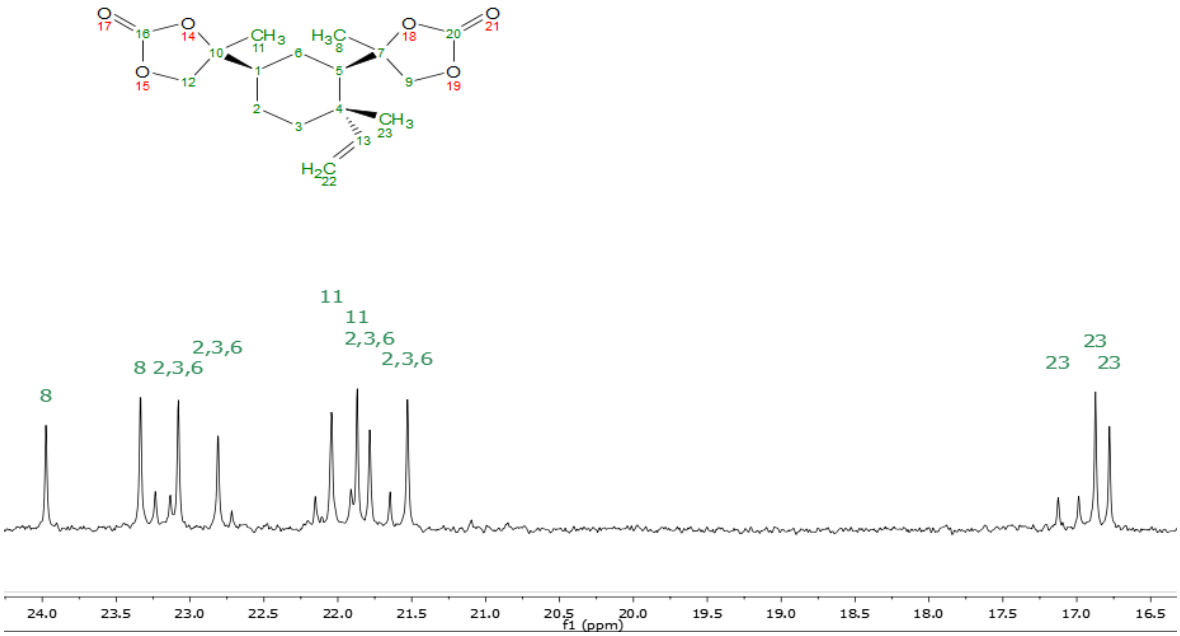

Figure 4.132 ^{13}C NMR spectrum of BEBC in the range of 24 – 16.5 ppm.

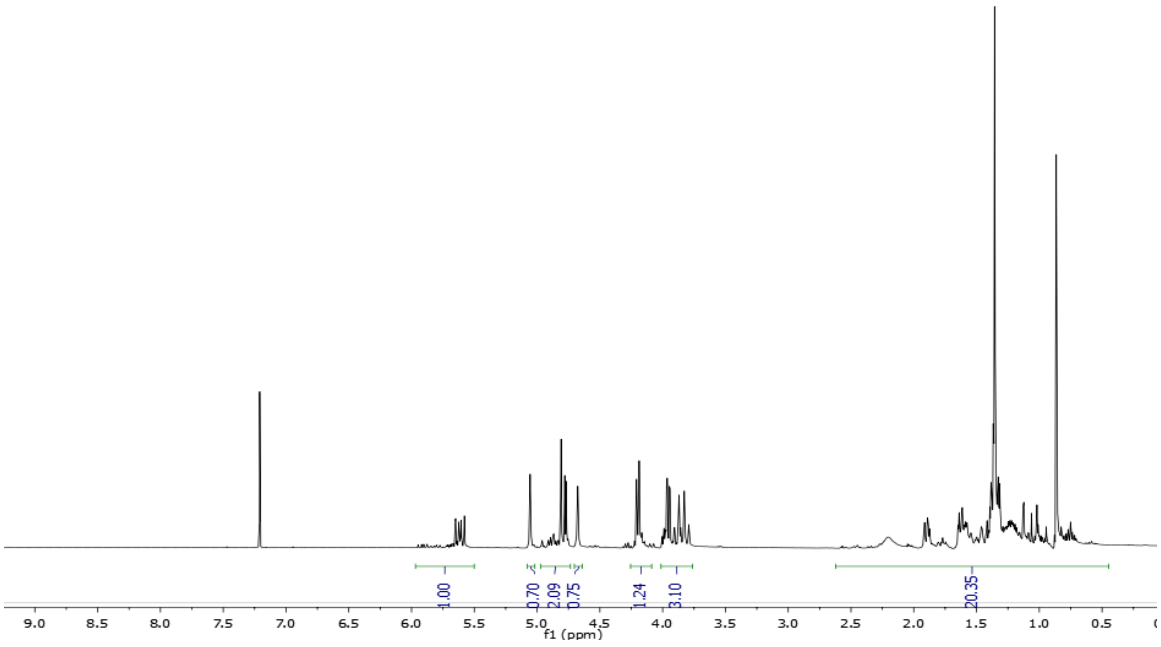

Figure 4.133 Example of mixture of BEBC with BEMCMD, estimated composition 73 % BEMCMD and 27 % BEBC

β-elemene monocarbonate monoaldehyde (BEMCMA)

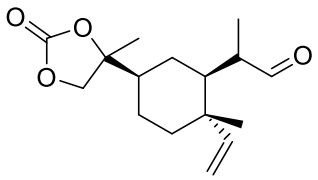

BEMCMA

^{1}H NMR(400 MHz, $CDCl_3$): δ = 9.84 – 9.27 (m, 1H), 5.80 – 5.50 (m, 1H), 5.21 – 4.91 (m, 2H), 4.38 – 3.92 (m, 2H), 2.70 – 2.30 (m, 1H), 2.09 – 0.60 (m, 17H) ppm

^{13}C {^{1}H} NMR (101 MHz, $CDCl_3$) δ = 205.5, 205.4, 204.3, 204.3, 154.7, 154.7, 154.6, 148.5, 148.3, 148.3, 113.6, 113.6, 113.2, 85.7, 85.6, 85.6, 85.5, 73.4, 73.3, 49.3, 49.2, 46.9, 46.9, 46.8, 46.7, 46.6, 46.5, 45.9, 45.8, 41.5, 41.4, 40.7, 40.6, 40.5, 40.5, 40.0, 40.0, 39.8, 39.8, 23.8, 23.7, 23.5, 23.4, 22.2, 22.1, 22.0, 21.9, 21.9, 21.8, 21.7, 21.6, 16.8, 16.8, 16.6, 16.6, 15.2, 15.1, 10.7, 10.5.

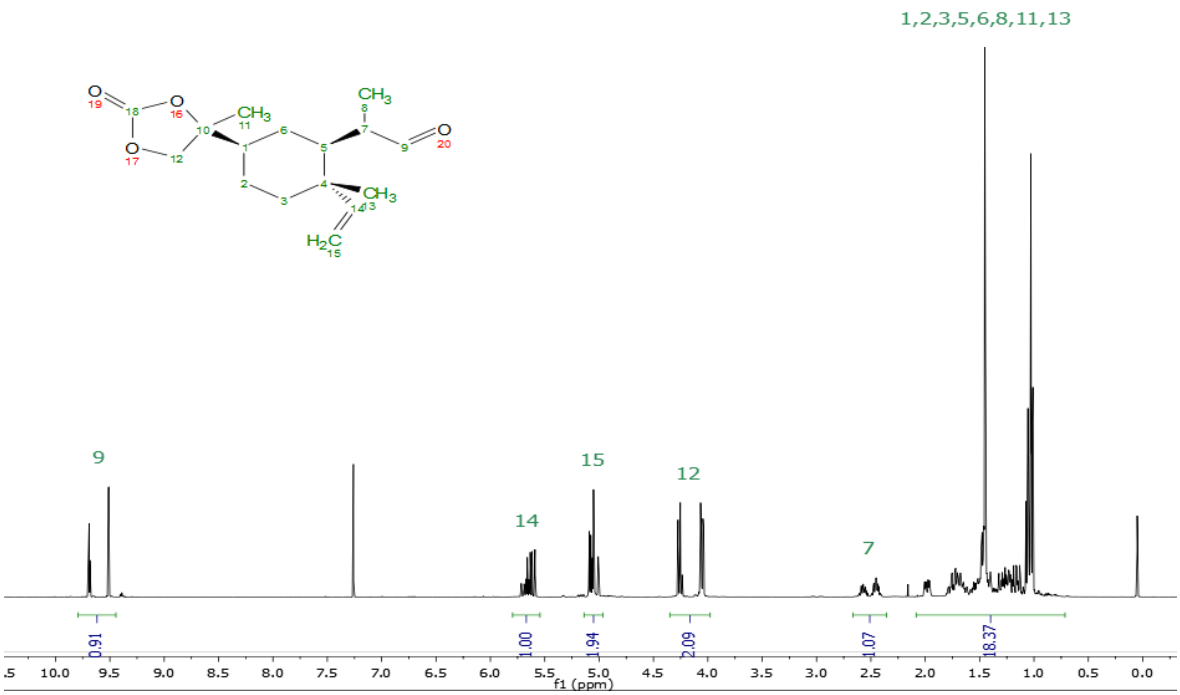

Figure 4.134 ^{1}H NMR spectrum of BEMCMA.

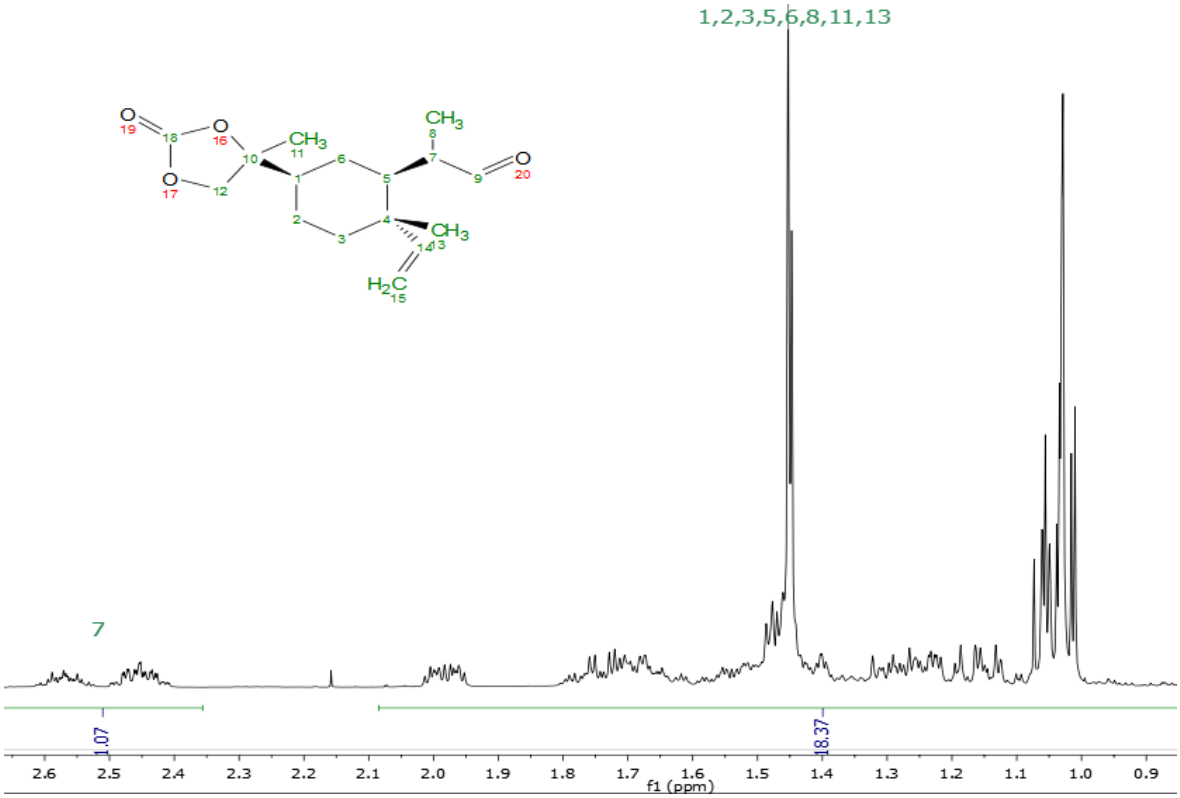

Figure 4.135 [1]H NMR spectrum of BEMCMA in the range of 2.6 – 0.9 ppm.

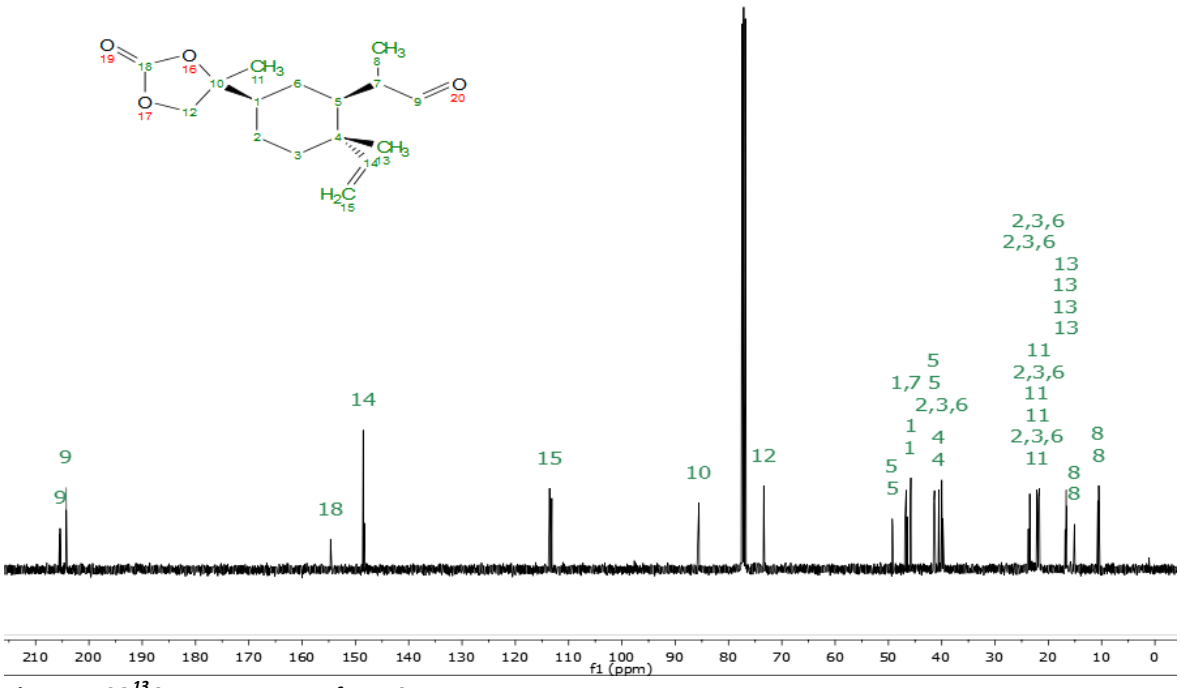

Figure 4.136 [13]C NMR spectrum of BEMCMA.

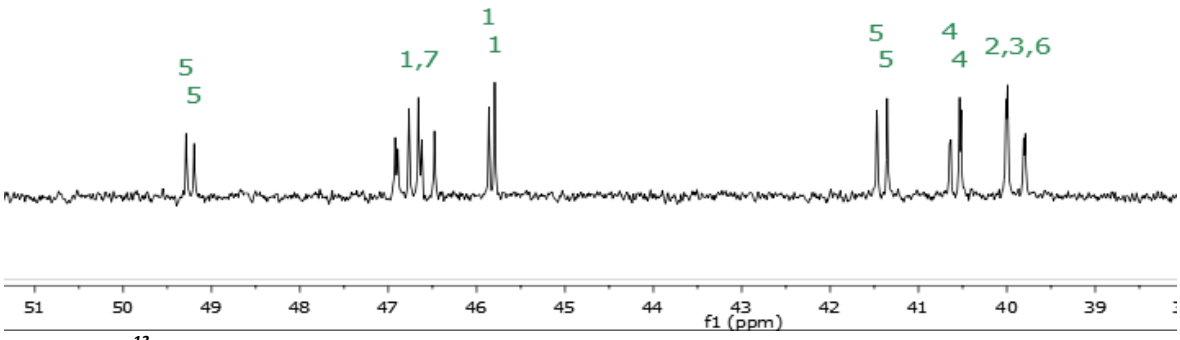

Figure 4.137 ^{13}C NMR spectrum of BEMCMA in the range of 51 – 39 ppm.

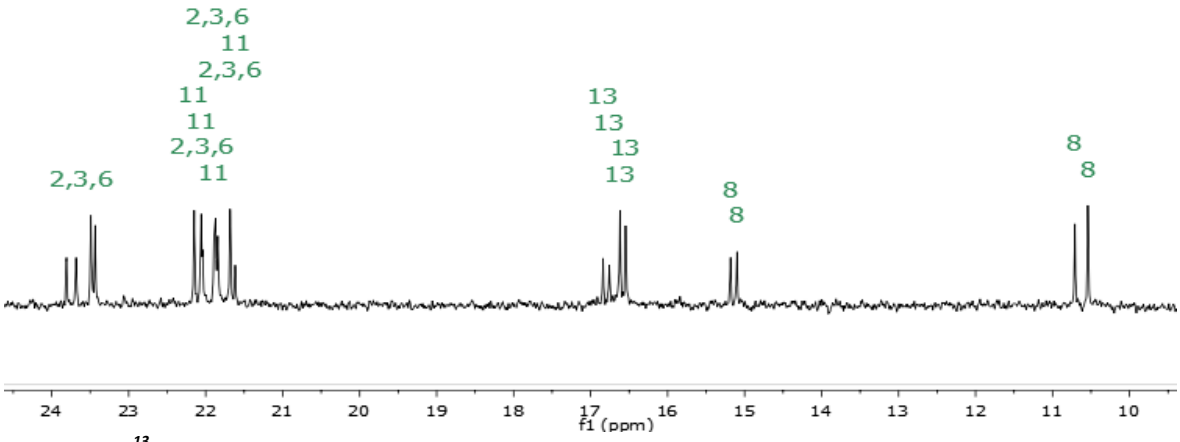

Figure 4.138 ^{13}C NMR spectrum of BEMCMA in the range of 24 – 10 ppm.

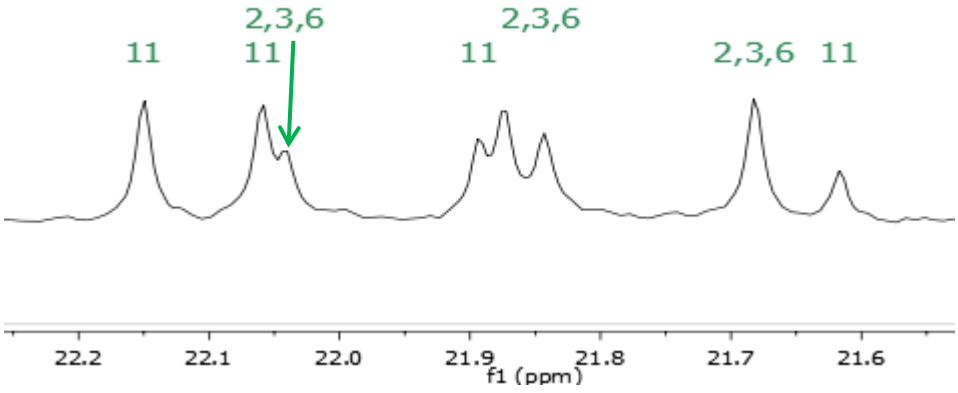

Figure 4.139 ^{13}C NMR spectrum of BEMCMA in the range of 22 – 21.6 ppm.

β-elemene biscarbonate monoepoxide (BEBCMO)

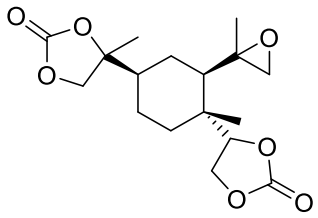

^{1}H NMR(400 MHz, $CDCl_3$): δ = 4.55 (m, 1H), 4.38 (m, 1H), 4.27 (m, 2H), 4.09 – 4.00 (m, 1H), 2.79 – 2.53 (m, 2H), 2.02 – 0.69 (m, 17H) ppm

^{13}C {^{1}H} NMR (101 MHz, $CDCl_3$) δ = 154.8, 154.5, 154.4, 85.1, 85.1, 85.0, 83.7, 83.6, 73.5, 73.4, 73.0, 72.7, 65.3, 65.2, 64.8, 57.8, 57.8, 56.6, 56.4, 54.7, 54.5, 52.9, 52.8, 52.3, 45.2, 45.2, 45.0, 44.9, 38.9, 38.9, 38.6, 33.4, 33.3, 30.7, 30.6, 24.3, 24.3, 24.0, 22.6, 21.7, 20.8, 20.6, 20.5, 19.9, 19.9, 19.8, 15.0, 13.4, 13.2.

MS-ESI^{+}

Calculated $[M+Na]^{+}$ = 363.1414

Found $[M+Na]^{+}$ = 363.1457

FT-IR: 1785 cm^{-1} (C=O)

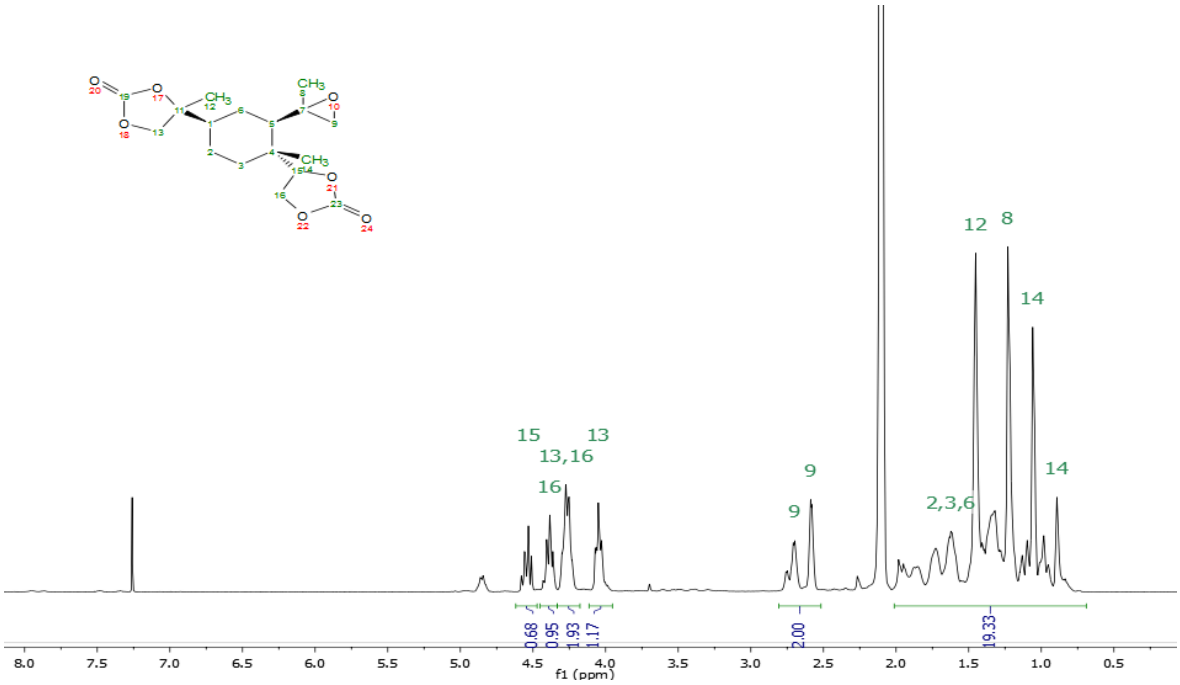

Figure 4.140 ^{1}H NMR spectrum of BEBCMO. The signal at 2.05 is an impurity from acetone, confirmed by HSQC.

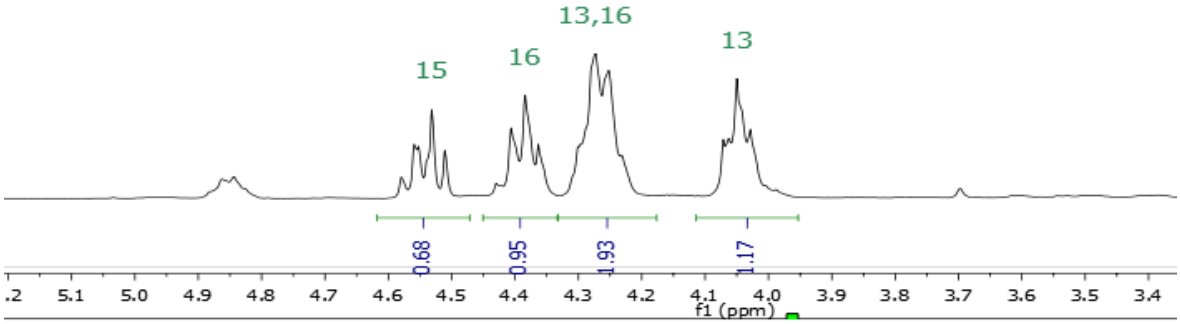

Figure 4.141 ^{1}H NMR spectrum of BEBCMO in the range of 5.1 – 3.4 ppm.

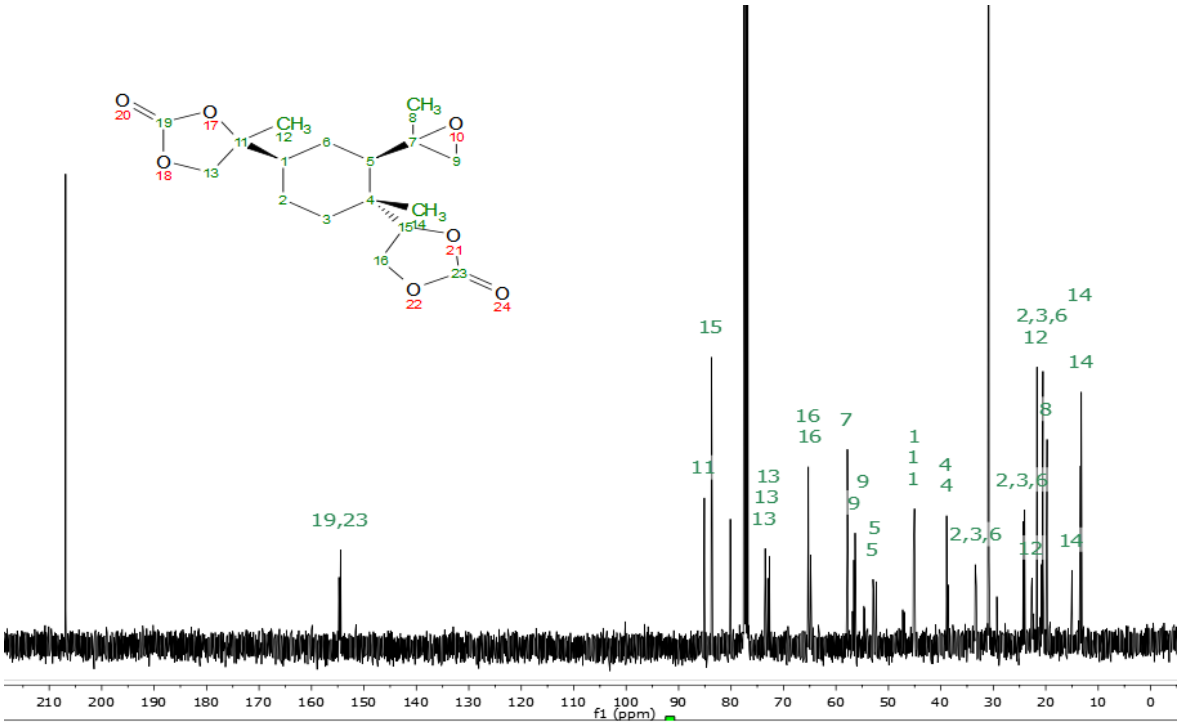

Figure 4.142 ^{13}C NMR spectrum of BEBCMO. The signal at 208 ppm is acetone and carbon at 80 ppm is an unidentified impurity probably originating from BETO carbonation.

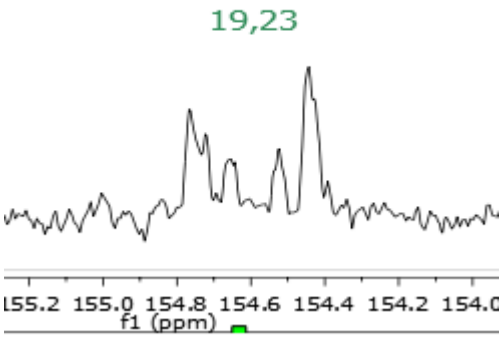

Figure 4.143 ^{13}C NMR spectrum of BEBCMO in the carbonyl region.

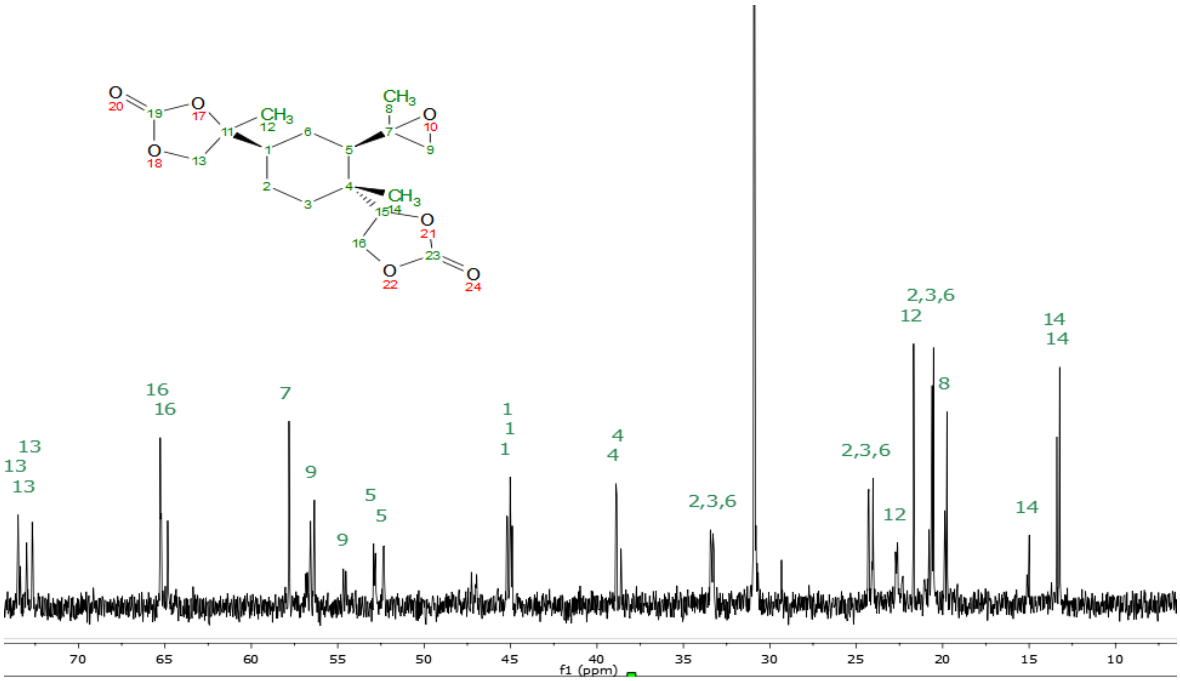

Figure 4.144 ^{13}C NMR spectrum of BEBCMO in the region of 74 – 10 ppm.

4.5 References

1. T. Sakakura and K. Kohno, *Chem. Commun.*, 2009, 1312-1330.
2. M. Tamura, M. Honda, Y. Nakagawa and K. Tomishige, *J. Chem. Technol. Biotechnol.*, 2014, **89**, 19-33.
3. A. J. Kamphuis, F. Picchioni and P. P. Pescarmona, *Green Chem.*, 2019, **21**, 406-448.
4. N. Yadav, F. Seidi, D. Crespy and V. D'Elia, *ChemSusChem*, 2019, **12**, 724-754.
5. J. A. Castro-Osma and M. North, *Curr. Green Chem.*, 2014, **1**, 257-272.
6. M. North and R. Pasquale, *Angew. Chem. Int. Ed.*, 2009, **48**, 2946-2948.
7. L.-N. He, J.-Q. Wang and J.-L. Wang, *Pure Appl. Chem.*, 2009, **81**, 2069-2080.

8. J. Langanke, L. Greiner and W. Leitner, *Green Chem.*, 2013, **15**, 1173-1182.
9. H. Yasuda, L.-N. He, T. Sakakura and C. Hu, *J. Catal.*, 2005, **233**, 119-122.
10. F. Chen, X. Li, B. Wang, T. Xu, S.-L. Chen, P. Liu and C. Hu, *Chem.: Eur. J.*, 2012, **18**, 9870-9876.
11. S. H. Szczepankiewicz, C. M. Ippolito, B. P. Santora, T. J. Van de Ven, G. A. Ippolito, L. Fronckowiak, F. Wiatrowski, T. Power and M. Kozik, *Inorg. Chem.*, 1998, **37**, 4344-4352.
12. M. North, S. C. Z. Quek, N. E. Pridmore, A. C. Whitwood and X. Wu, *ACS Catal.*, 2015, **5**, 3398-3402.
13. X. Wu and M. North, *ChemSusChem*, 2017, **10**, 74-78.
14. G. Fiorani, M. Stuck, C. Martín, M. M. Belmonte, E. Martin, E. C. Escudero-Adán and A. W. Kleij, *ChemSusChem*, 2016, **9**, 1304-1311.
15. D. E. Heath and S. L. Cooper, in *Biomaterials Science (Third Edition)*, eds. B. D. Ratner, A. S. Hoffman, F. J. Schoen and J. E. Lemons, Academic Press, 2013, pp. 79-82.
16. Statista, Polyurethanes Sales Volume in The United Kingdom, http://www.statista.com/statistics/348940/polyurethanes-sales-volume-in-the-united-kingdom-uk/, (accessed 04/02/2019).
17. B. Nohra, L. Candy, J.-F. Blanco, C. Guerin, Y. Raoul and Z. Mouloungui, *Macromolecules*, 2013, **46**, 3771-3792.
18. M. Blain, A. Cornille, B. Boutevin, R. Auvergne, D. Benazet, B. Andrioletti and S. Caillol, *J. Appl. Polym. Sci.*, 2017, **134**, 44958.
19. M. Blain, L. Jean-Gérard, R. Auvergne, D. Benazet, S. Caillol and B. Andrioletti, *Green Chem.*, 2014, **16**, 4286-4291.
20. B. Ochiai, S. Inoue and T. Endo, *J. Polym. Sci. Pol. Chem.*, 2005, **43**, 6282-6286.
21. A. Cornille, R. Auvergne, O. Figovsky, B. Boutevin and S. Caillol, *Eur. Polym. J.*, 2017, **87**, 535-552.
22. A. Rudin, in *Elements of Polymer Science and Engineering (Second Edition)*, ed. A. Rudin, Academic Press, San Diego, 1999, pp. 155-188.
23. R. H. Lambeth and T. J. Henderson, *Polymer*, 2013, **54**, 5568-5573.
24. A. Cornille, M. Blain, R. Auvergne, B. Andrioletti, B. Boutevin and S. Caillol, *Polym. Chem.*, 2017, **8**, 592-604.
25. R. M. Garipov, V. A. Sysoev, V. V. Mikheev, A. I. Zagidullin, R. Y. Deberdeev, V. I. Irzhak and A. A. Berlin, *Dokl. Phys. Chem.*, 2003, **393**, 289-292.
26. H. Tomita, F. Sanda and T. Endo, *J. Polym. Sci. Pol. Chem.*, 2001, **39**, 3678-3685.
27. M. S. Kathalewar, P. B. Joshi, A. S. Sabnis and V. C. Malshe, *RSC Adv.*, 2013, **3**, 4110-4129.
28. F. D. Bobbink, A. P. van Muyden and P. J. Dyson, *Chem. Commun.*, 2019, **55**, 1360-1373.
29. S. Sopeña, V. Laserna, W. Guo, E. Martin, E. C. Escudero-Adán and A. W. Kleij, *Adv. Synth. Catal.*, 2016, **358**, 2172-2178.
30. J. Guan, Y. Song, Y. Lin, X. Yin, M. Zuo, Y. Zhao, X. Tao and Q. Zheng, *Ind. Eng. Chem. Res.*, 2011, **50**, 6517-6527.
31. British Coatings Federation, VOCs, https://www.coatings.org.uk/VOCs.aspx, (accessed 01/05/2019).
32. R. Gautam, A. S. Bassi and E. K. Yanful, *Appl. Biochem. Biotechnol.*, 2007, **141**, 85-108.
33. G. T. Howard, *Int. Biodeter. Biodeg.*, 2002, **49**, 245-252.
34. M. Bähr, A. Bitto and R. Mülhaupt, *Green Chem.*, 2012, **14**, 1447-1454.
35. V. Schimpf, B. S. Ritter, P. Weis, K. Parison and R. Mülhaupt, *Macromolecules*, 2017, **50**, 944-955.
36. UNICA, New Amyris plant in Brazil points to expanding business opportunities for sugarcane, http://www.unica.com.br/news/22317484920343585770/new-amyris-plant-in-brazil-points-to-expanding-business-opportunities-for-sugarcane/, (accessed 16/05/2019).

37. H. Tomita, F. Sanda and T. Endo, *J. Polym. Sci. Pol. Chem.*, 2001, **39**, 4091-4100.
38. M. Firdaus, L. Montero de Espinosa and M. A. R. Meier, *Macromolecules*, 2011, **44**, 7253-7262.
39. M. Hutchby and W. Cunningham, unpublished work.
40. M. Vezzoli, unpublished work.
41. CSCT, Terpene-based Manufacturing for Sustainable Chemical Feedstocks, http://www.bath.ac.uk/csct/research/projects/20130201-terpenes.html, (accessed 30/08/2016).
42. K. Smug, MRes Dissertation, Univeristy of Bath, 2015.
43. S. C. S. Kumar, J. R. Manjunatha, P. Srinivas and B. K. Bettadaiah, *J. Chem. Sci.*, 2014, **126**, 875-880.
44. D. Steiner, L. Ivison, C. T. Goralski, R. B. Appell, J. R. Gojkovic and B. Singaram, *Tetrahedron-Asymmetr.*, 2002, **13**, 2359-2363.
45. C.-X. Miao, J.-Q. Wang and L.-N. He, *Open Org. Chem. J.*, 2008, **2**, 68-82.
46. J.-Q. Wang, J. Sun, W.-G. Cheng, K. Dong, X.-P. Zhang and S.-J. Zhang, *Phys. Chem. Chem. Phys.*, 2012, **14**, 11021-11026.
47. C. Li, R. J. Sablong and C. E. Koning, *Eur. Polym. J.*, 2015, **67**, 449-458.
48. K. Kamata, K. Sugahara, K. Yonehara, R. Ishimoto and N. Mizuno, *Chem. Eur. J.*, 2011, **17**, 7549-7559.
49. K. R. Benjamin, I. R. Silvab, J. P. Cherubimc, D. McPheea and C. J. Paddon, *J. Braz. Chem. Soc.*, 2016, **27**, 1339-1345.
50. Isobionics, Natural Beta Elemene, http://www.isobionics.com/index-Beta%20Elemene.html, (accessed 12/04/2019).
51. S. Federle, MRes, University of Bath, 2017.
52. N. Kindermann, À. Cristòfol and A. W. Kleij, *ACS Catal.* 2017, **7**, 3860-3863.
53. L. Pena Carrodeguas, J. Gonzalez-Fabra, F. Castro-Gomez, C. Bo and A. W. Kleij, *Chem. Eur. J.*, 2015, **21**, 6115-6122.
54. D. Choquesillo-Lazarte and J. M. Garcia-Ruiz, *J. Appl. Crystallogr.*, 2011, **44**, 172-176.
55. Croda, Priamine™ 1074, https://www.crodacoatingsandpolymers.com/en-gb/products-and-applications/product-finder/product/448/Priamine_1_1074, (accessed 19/10/2019).
56. J. Ke, X. Li, S. Jiang, C. Liang, J. Wang, M. Kang, Q. Li and Y. Zhao, *Polym. Int.*, 2019, **68**, 651-660.
57. I. Javni, D. P. Hong and Z. S. Petrović, *J. Appl. Polym. Sci.*, 2008, **108**, 3867-3875.
58. K. K. W. Mak, Y. M. Lai and Y.-H. Siu, *J. Chem. Educ.*, 2006, **83**, 1058.
59. K. Smug, MRes Disertation, Univeristy of Bath, 2015.
60. C. Mangeon, F. Thevenieau, E. Renard and V. Langlois, *ACS Sustain. Chem. Eng.*, 2017, **5**, 6707-6715.
61. A. Behr and L. Johnen, *ChemSusChem*, 2009, **2**, 1072-1095.
62. N. Bauer, J. Brunke and G. Kali, *ACS Sustain. Chem. Eng.*, 2017, **5**, 10084-10092.
63. British Coatings Federation, Sustainable Development, https://www.coatings.org.uk/Sustainable_Development.aspx, (accessed 05/09/2019).
64. M. F. Cunningham, J. D. Campbell, Z. W. Fu, J. Bohling, J. G. Leroux, W. Mabee and T. Robert, *Green Chem.*, 2019, **21**, 4919-4926.
65. J. R. Lowe, M. T. Martello, W. B. Tolman and M. A. Hillmyer, *Polym. Chem.*, 2011, **2**, 702-708.
66. U. Hintermair, C. Roosen, M. Kaever, H. Kronenberg, R. Thelen, S. Aey, W. Leitner and L. Greiner, *Org. Process Res. Dev.*, 2011, **15**, 1275-1280.
67. C. Venturello and R. Daloisio, *J. Org. Chem.*, 1988, **53**, 1553-1557.
68. O. Hauenstein, M. Reiter, S. Agarwal, B. Rieger and A. Greiner, *Green Chem.*, 2016, **18**, 760-770.

69. P. J. Domaille, in *Inorg. Synth.*, eds. G. Hervéa and A. Téazéa, John Wiley & Sons, Inc., 1990, vol. 27, pp. 96-104.
70. W. H. Knoth and R. L. Harlow, *J. Am. Chem. Soc.*, 1981, **103**, 1865-1867.
71. P. J. Domaille and R. L. Harlow, *J. Am. Chem. Soc.*, 1986, **108**, 2108-2109.
72. R. M. Carman, J. J. Devoss and K. L. Greenfield, *Aust. J. Chem.*, 1986, **39**, 441.
73. C. M. Byrne, S. D. Allen, E. B. Lobkovsky and G. W. Coates, *J. Am. Chem. Soc.*, 2004, **126**, 11404-11405.
74. L. Longwitz, J. Steinbauer, A. Spannenberg and T. Werner, *ACS Catal.*, 2018, **8**, 665-672.

4.6 Appendix – Polymerisation of BEBO using Al cat

Aluminium amino-tris(phenolate) catalyst (Al cat) in combination with PPNCl was previously used in the synthesis of poly(1,2-limonene carbonate).[1] In this section, the potential of creating poly(b-elemene carbonate) and poly(8,9-limonene carbonate) was tested. For the purpose of experiments performed in this section, PPNCl was sourced from Sigma Aldrich and Al cat was prepared by Dr Paul McKeown according to the previously published procedure.[2] The synthesised Al cat was stored in a glove box under argon atmosphere.

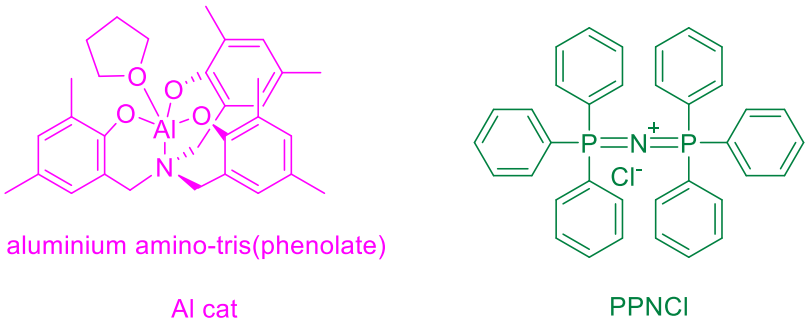

Figure A4_1 Structure of Al cat and PPNCl

Published reaction conditions:[1] 4 mL 1,2-limonene oxide (commercial mixture of isomers), 74 mg Al catalyst and 40 mg PPNCl were placed in the reactor vessel, purged with CO_2 and the pressure was stabilised at 15 bar at room temperature, then reactor was heat up to 45 °C for 48 h.

After the reaction, the mixture was dissolved in $CHCl_3$ and MeOH was added dropwise until no furthered precipitation was observed. Finally, a few drops of water were added to complete the precipitation. The obtained solid was suspended in MeOH and sonicated for up to 30 min, filtered and dried in vacuo for 1 day.

The reported results for 1,2-limonene oxide are:

a) dry 1,2-limonene oxide was used, GPC of purified polymer M_n = 9.92 kg mol^{-1} Đ 1.27
b) not dry 1,2-limonene oxide was used, GPC of purified polymer M_n = 3.13 kg mol^{-1} Đ 1.27

In this work: Based on previous experience gained during cyclic carbonates synthesis, all reactions performed in this work were conducted in slightly higher pressure than it was reported (reactors were pressurised to 30 bar at 40 °C). First, control reactions have been done to check if the catalyst and available high pressure reactors perform similar to equipment used in the previous publication (Table A4_1 Entry 1 and 2). The sample with dry 1,2-LO used (Entry 1) showed M_n = 12 kg mol^{-1} and Đ 1.23 which is comparable to published results. The sample with commercial 1,2-LO used without drying showed lower M_n, but the conversion and selectivity was not affected. This is consistent with previously published results and shows that catalyst can handle some contamination from air and moisture.

Then, reactions with BEBO were performed (Entry 3 – 5). BEBO was pre-dried using azeotropic drying with MeCN. The characteristic signals for polycarbonates were not present in any of the samples. At 50 °C a small conversion to cyclic carbonates was observed, at lower temperature (30 °C) with longer reaction time only traces of cyclic carbonates were observed and at high temperature (70 °C) about 40 % of the epoxide groups were converted to cyclic carbonates. In summary, no polymerisation was observed and conversion to cyclic carbonates was slow, with the most promising results achieved at 70 °C.

Another substrate that was investigated (Table A4_1 Entry 6 – 9), 8,9-LO is easier to purify and the NMR analysis is simpler. It performed the same as BEBO, no polycarbonates signals were observed on ^{1}H NMR and ^{13}C NMR. Cyclic carbonates production was strongly dependent on temperature, with the highest yield of cyclic carbonates obtained at 70 °C.

Table A4_1 Polymerisation attempts for 1,2-LO, 8,9-LO and BEBO

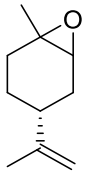

1,2-LO

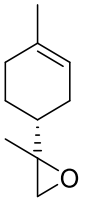

8,9-LO

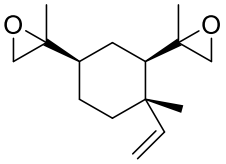

BEBO

entry	substrate	catalyst loading	T [°C]	p[a] [bar]	t [h]	Conv.[b] [%]	Yield CC[c]	Yield polyC[d]	Purified polymer
1	1 mL 1,2-LO (dry)[f]	21.9 mg Al cat 10 mg PPNCl	50	30	50	73	0	73	GPC[e] 12 kg mol^{-1} Đ 1.23
2	1 mL 1,2-LO	18.5 mg Al cat 15 mg PPNCl	50	30	48	77	0	70	GPC[e] 7.8 kg mol^{-1} Đ 1.18
3	1 mL BEBO[g]	20 mg Al cat 10 mg PPNCl	50	30	48	10	9	0	No precipitation
4	1 mL BEBO[g]	20 mg Al cat 20 mg PPNCl	30	30	67	<2	<2	0	No precipitation
5	1 mL BEBO[g]	18.5 mg Al cat 24 mg PPNCl	70	30	66	38	40[h]	0	No precipitation
6	1 mL 8,9-LO	20 mg Al cat 12 mg PPNCl	50	30	48	16	16	0	Precipitation not done
7	1 mL 8,9-LO[g]	18.5 mg Al cat 12 mg PPNCl	30	30	66	7	<1	0	No precipitation
8	1 mL 8,9-LO[g]	18.5 mg Al cat 19 mg PPNCl	70	30	66	46	44	0	No precipitation
9	1 mL 8,9-LO[g]	18.5 mg Al cat 13 mg PPNCl	50	30	4	20	0	0	No precipitation

a) pressurised at 40 °C b) conversion of epoxy groups based on ^{1}H NMR c) yield of cyclic carbonate groups based on ^{1}H NMR d) yield of polycarbonate groups based on ^{1}H NMR e) GPC of purified via precipitation polycarbonate f) distilled over CaH and stored in glove box g) azeotropic drying using dry MeCN h) yield higher than conversion, but it is within error of NMR analysis

Examples of NMR analysis:

1,2-LO: Figure 4A_2 and 4A_3 present NMR spectra of the crude reaction mixture for the reaction of commercial 1,2-LO at 50 °C (Table 4A_1 Entry 2). In Figure 4A_2, the signals at 4.6 ppm correspond to a double bond in 1,2-LO, signals around 3.0 ppm correspond to epoxide groups in 1,2-LO and signals at 5.0 ppm correspond to linear polycarbonates. Conversion was calculated by

referencing the whole spectrum against the signal at 4.6 ppm. The full assignments are available in the supporting information of previously published literature.[1]

In Figure 4A_3, the signals at 153.5 ppm, 151.8 ppm and 150.5 ppm correspond to carbonate linkages in region-irregular polycarbonates.[3] There is no signal at 154.8 ppm, which corresponds to 1,2-limonene cyclic carbonate.

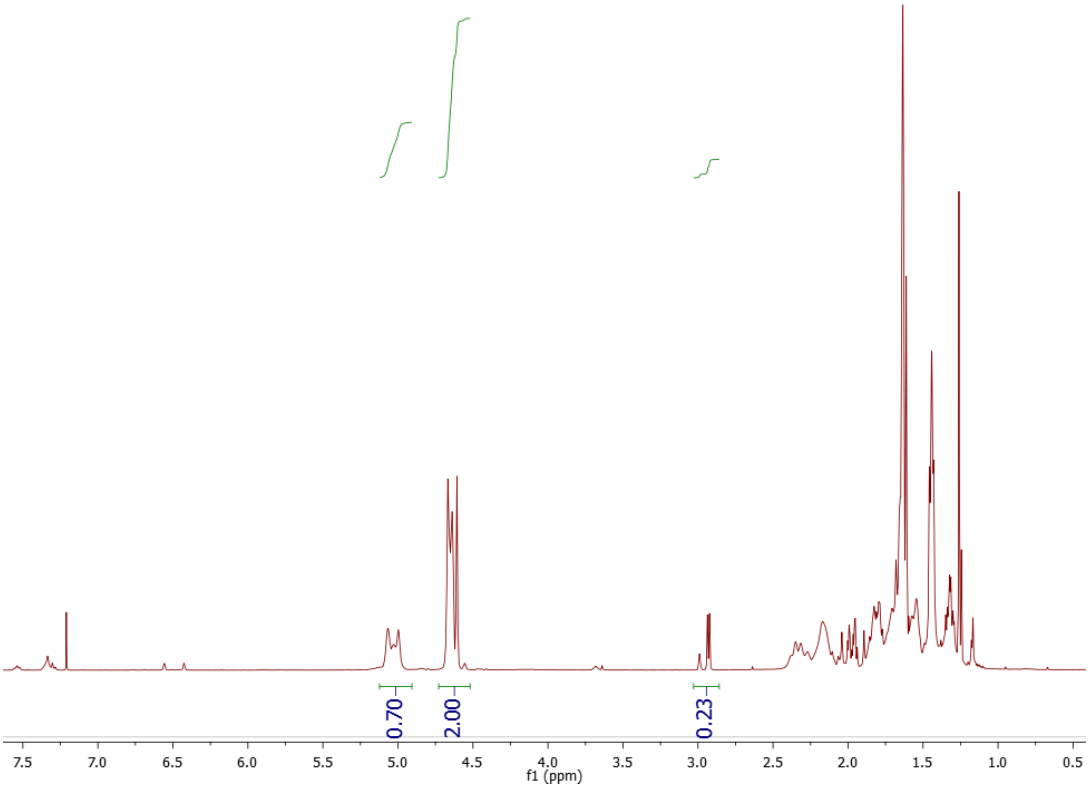

Figure 4A_2 ^{1}H NMR spectrum of reaction between 1,2-LO and CO_2 in the presence of Al cat and PPNCl at 50 ℃ and 30 bar CO_2

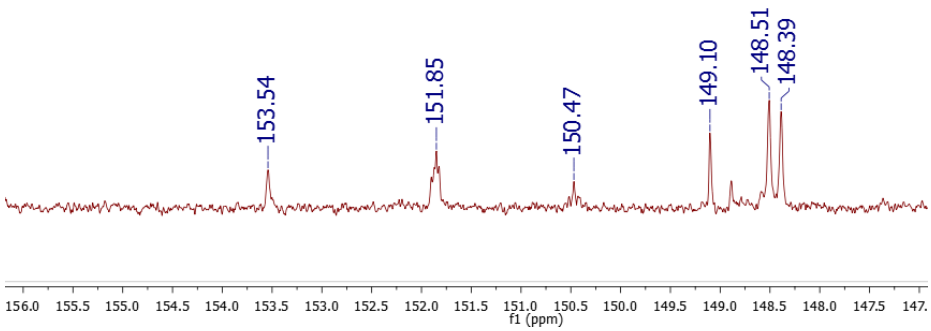

Figure 4A_3 ^{13}C NMR spectrum of reaction between 1,2-LO and CO_2 in the presence of Al cat and PPNCl at 50 ℃ and 30 bar CO_2

BEBO: Figures 4A_4 and 4A_5 present NMR spectra of the crude reaction mixture for the reaction of BEBO at 70 °C (Table 4A_1 Entry 5). In the Figure 4A_4, the signals at 5.85 – 5.54 ppm correspond to CH of vinyl group in BEBO, 4.84 ppm corresponds to CH_2 from double bonds, 4.19 and 3.93 ppm are signals from cyclic carbonates and 2.58 – 2.19 ppm correspond to epoxide groups. Conversion was calculated by referencing the whole spectrum against the signal at 5.85 – 5.54 ppm. The full assignments of BEBC are available in the experimental section of Chapter 4.

In Figure 4A_5 the signals at 154.7 ppm and 154.5 ppm correspond to cyclic carbonates. There are no signals in the region of 153 – 151 ppm which can be assigned to polycarbonates.

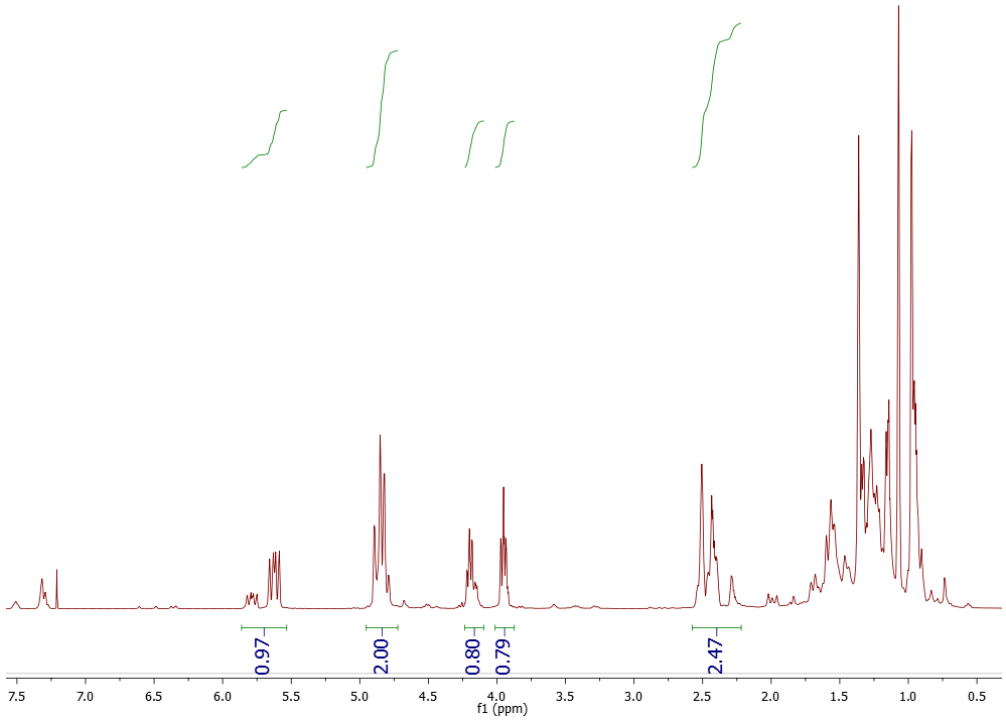

Figure 4A_4 ^{1}H NMR spectrum of reaction between BEBO and CO_2 in the presence of Al cat and PPNCl at 70 °C and 30 bar CO_2

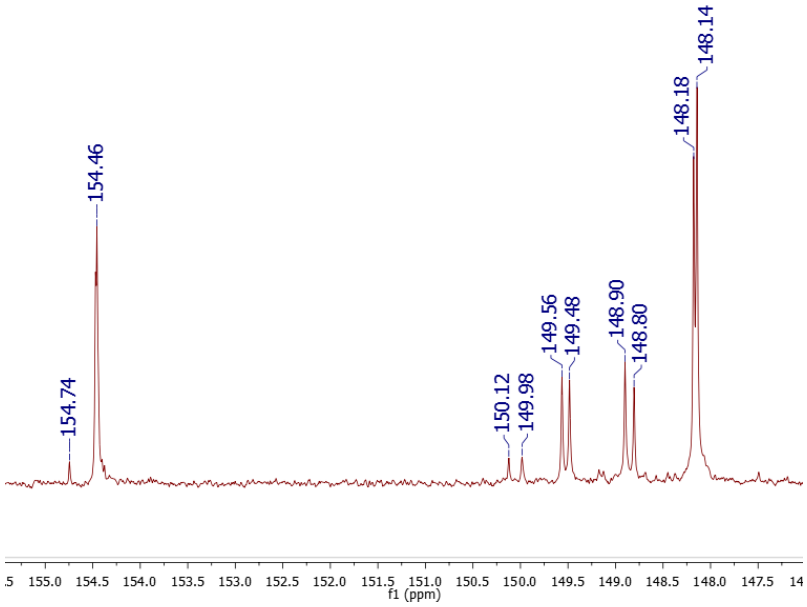

Figure 4A_5 ^{13}C NMR spectrum of reaction between BEBO and CO_2 in the presence of Al cat and PPNCl at 70 ℃ and 30 bar CO_2

8,9-LO: Figures 4A_6 and 4A_7 present NMR spectra of the crude reaction mixture for the reaction of 8,9-LO at 50 ℃ (Table 4A_1 Entry 6). In the Figure 4A_6, the signal at 5.28 ppm corresponds to the CH double bond in 8,9-LO, signals around 2.59 – 2.39 ppm correspond to epoxide groups in 8,9-LO and signals at 4.20 and 3.95 ppm correspond to linear polycarbonates. Conversion was calculated by referencing the whole spectrum against the signal at 5.28 ppm. The full assignments of 8,9-LC are available in the experimental section of Chapter 4.

In the Figure 4A_7, the signal at 154.7 ppm corresponds to 8,9-LC. No signals indicating the presence of polycarbonates were present.

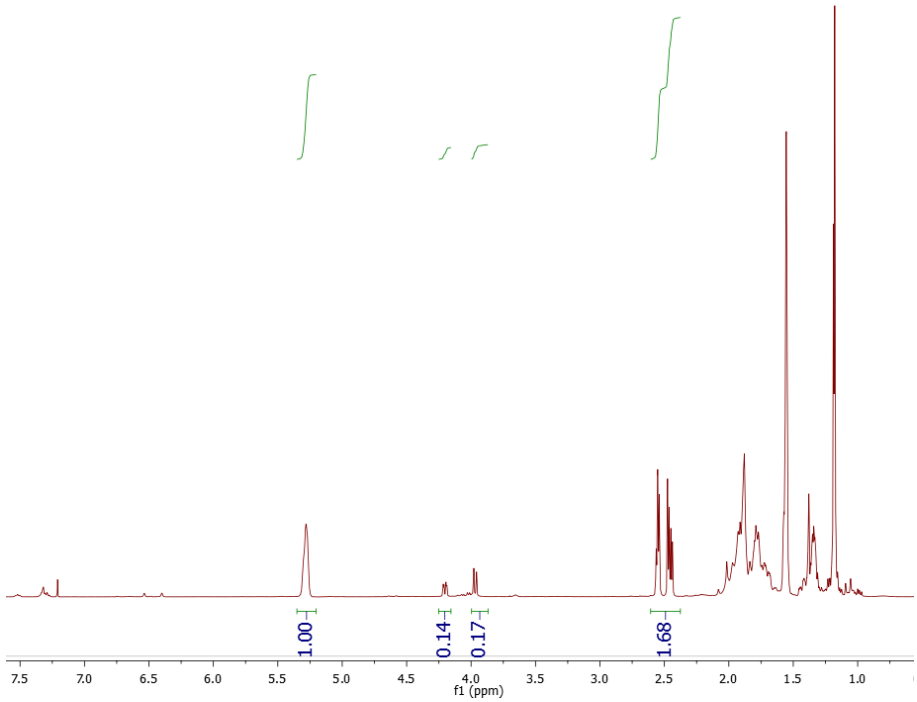

Figure 4A_6 ^{1}H NMR spectrum of reaction between BEBO and CO_2 in the presence of Al cat and PPNCl at 70 ℃ and 30 bar CO_2

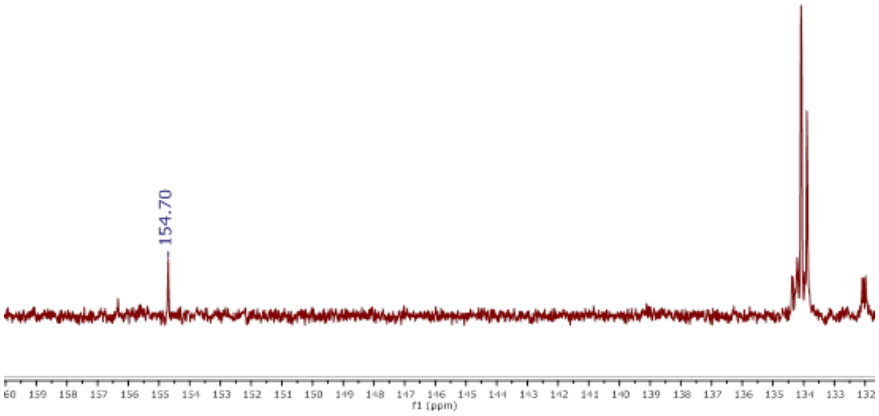

Figure 4A_7 ^{13}C NMR spectrum of reaction between BEBO and CO_2 in the presence of Al cat and PPNCl at 70 ℃ and 30 bar CO_2

References

1. N. Kindermann, À. Cristòfol and A. W. Kleij, *ACS Catal.*, 2017, **7**, 3860-3863.
2. A. L. Johnson, M. G. Davidson, Y. Perez, M. D. Jones, N. Merle, P. R. Raithby and S. P. Richards, *Dalton Trans.*, 2009, 5551-5558.
3. L. Pena Carrodeguas, J. Gonzalez-Fabra, F. Castro-Gomez, C. Bo and A. W. Kleij, *Chem. Eur. J.*, 2015, **21**, 6115-6122.

5. Conclusions and future work

This chapter includes overall conclusions and future work. It is divided into three parts. First, conclusions and future work related to the β-elemene epoxidation (Chapter 3). Second, conclusions and future work related to the carbonation of 1,2-limonene oxide and 8,9-limonene oxide (Chapter 4, section 4.2.1). Third, conclusions and future work related to the carbonation of β-elemene epoxides (Chapter 4, section 4.2.2).

5.1 Conclusions and future work - β-elemene epoxidation

BE epoxidation catalysed by **VENT** is a bi-phasic reaction which could be performed in flow. It is performed in relatively low temperature (50 °C) and in solventless conditions which is within green chemistry principles. As it was shown in the introduction to Chapter 3, flow processes allow for easier scale up and better process control, which makes them highly desirable for developing new catalytic epoxidations.

All possible **BE** epoxides were achieved by epoxidations catalysed by **VENT**, but **BETO** was never observed in flow epoxidation. As **BETO** was observed in batch epoxidations after 3 h, it might indicate slow kinetics of epoxidising **BEBO** into **BETO**. Future work should include further investigation into achieving **BETO** in flow. A higher excess of H_2O_2 (min 4.8 mol eq) and longer residence time are expected to improve the epoxide yield based on the results presented in Table 3.3.

The results showed that the **VENT** catalysed reaction was kinetically limited and not mass transfer limited when 3.2 mol eq H_2O_2 was used. When more H_2O_2 was used (4.8 mol eq), the flow reactor showed improved conversion by 30 % and improved epoxide yield (**BEMO** and **BEBO**) by 23 % compared to the same reaction performed in a batch reactor. With high excess of H_2O_2 the reaction followed pseudo-first order reaction kinetics, but applying longer residence time (above 33.2 min) resulted in some catalyst degradation which should be addressed in future work. Other researchers working on **VENT** catalysed terpene epoxidation showed that **VENT** degrades if it is recycled[1] and the maximum TON achieved for **VENT** was reported to be up to 500.[2] The reports of deactivation of polyoxometalates during epoxidation reactions are present within research articles and so far 500 TON is the highest reported. An alternative approach to extending the lifetime of the catalyst is to reuse the catalyst in a different reaction, for example carbonation. Transition metal polyoxometalates were previously reported to coordinate to CO_2[3-5] and it is postulated that in a carbonation reaction they can activate CO_2.[6] This approach has been described in Chapter 4.2.1 and the main findings are presented in Section 5.3 of this chapter. Investigations into heterogeneous PW-Amberlite (a catalyst described in detail in the introduction to Chapter 3 Section 3.1.4) could

be another approach to increase catalyst stability, as the full activity of the heterogeneous catalyst was recovered by simple rinsing with acetone after reaction. However, the heterogeneous catalysts still have to be improved to achieve faster conversion.

MIZ epoxidation of **BE** yielded **BEMO** and **BEBO**, but no **BETO** was observed under any reaction conditions. It has been shown **MIZ** decomposes H_2O_2 even in the absence of an alkene, which might be the reason why MIZ is not able to yield **BETO** considering the slow rate of reaction for oxidising **BEBO** to **BETO**. Moreover, **MIZ** is sensitive to the amount of water present in the system. Improvements could be made by changing the Bu_4N^+ cation for a longer chain quaternary ammonium salt and investigating this system in bi-phasic conditions. However, considering other catalytic procedures showed better performance in **BE** epoxidation it is not recommended to focus future work on improving **MIZ** epoxidation.

The third catalyst tested was the organocatalyst **TFAP** which is the only commercially available catalyst tested. Although only a few preliminary reactions were done, **TFAP** showed high selectivity to epoxides (99 %). It is the only catalyst tested which showed high selectivity toward **BETO**, which is a highly desirable epoxide for polymer synthesis (see Section 5.3). The reaction is a bi-phasic system which uses relatively mild solvents such as t-BuOH, iPrOH or MeCN. The well described mechanism of reaction (Figure 3.18)[7] is a helpful tool for following the catalyst at the reaction conditions via flow NMR, which can give a further insight into the mechanism.[8] No catalyst degradation studies or product inhibition experiments have been done and they should be addressed in the future work. Even though it is in bi-phasic conditions it still runs at relatively high dilution (1 g **BE** required 20 mL MeCN and 20 mL aqueous pH buffer). Potentially the use of flow microreactors in future work could allow for reducing the dilution levels to a minimum. This catalyst is an interesting alternative to the metal-based catalysts.

BE is a relatively new, yet unexplored terpene feedstock, and because it is produced via industrial biotechnology processes it can be supplied at a stable price in various geographical locations. Exploring catalytic epoxidation of **BE** is vital for implementing **BE** in the polymer industry. In the Introduction (Chapter 1) a wide range of polymers synthesised from epoxides is presented, such as polycarbonates, polyesters, polyethers or non-isocyanate polyhydroxyurethanes. It is worth noting that comparing to the most widely investigated limonene-derived polymers, β-elemene-derived alternatives have an additional double bond which potentially allows for more post-functionalisation options or highly crosslinked polymers.

5.2 Conclusions and future work – 1,2-limonene oxide and 8,9-limonene oxide carbonation

LIM contains trisubstituted and disubstituted alkenes in its structure and by selective epoxidation of one of them it is possible to synthesise **1,2-LO** and **8,9-LO** with an additional double bond available for further functionalisation. Both limonene epoxides were investigated in reactions with CO_2. It was shown that only one isomer of **1,2-LO** is reactive in the carbonation reaction yielding ***trans*-1,2-LCC**. The stereo selective behaviour was caused by the steric hindrance of **cis-1,2-LO**, and it was the same for all catalysts tested. Among the quaternary ammonium salts tested, the most efficient was Bu_4NCl. Moreover, expanding of the catalyst used showed that an addition of **VENT** to Bu_4NBr allowed increased cyclic carbonates yields. These results showed the possibility of telescoping a green epoxidation catalysed by **VENT** directly into the synthesis of cyclic carbonates.

The mono-functionalised ***trans*-1,2-LC** and **8,9-LC** were further reacted with a dithiol and an amine as a proof of concept for implementing them in the NIPU synthesis. The polymers were not synthesised, which could be a part of future work. However, the large-scale sustainable epoxidation protocols for ***trans*-1,2-LO** and **8,9-LO** are a significant constraint for this technology.

In future work, the developed protocol could be further applied to β-elemene-derived cyclic carbonates (Figure 5.1), as **BE** can be epoxidised with **VENT**. Using **VENT** in the carbonation of β-elemene-derived epoxides could have multiple positive effects on the carbonation reaction. First, it is expected that it will enhance reaction rates. Second, it was shown that polyoxometalates can coordinate to CO_2, thus **VENT** can improve selectivity by allowing double substrate activation (epoxide activated by Bu_4NX and CO_2 activated by **VENT**). Third, **VENT** might decrease the high viscosity of the reaction, which potentially is one of the causes for epoxide rearrangement. The high viscosity reduces the amount of available CO_2 and when CO_2 is unavailable, the epoxide is being activated, but the carbonation yields by-products instead of cyclic carbonates as it has been shown in Table 4.5 for ***trans*-1,2-LO**.

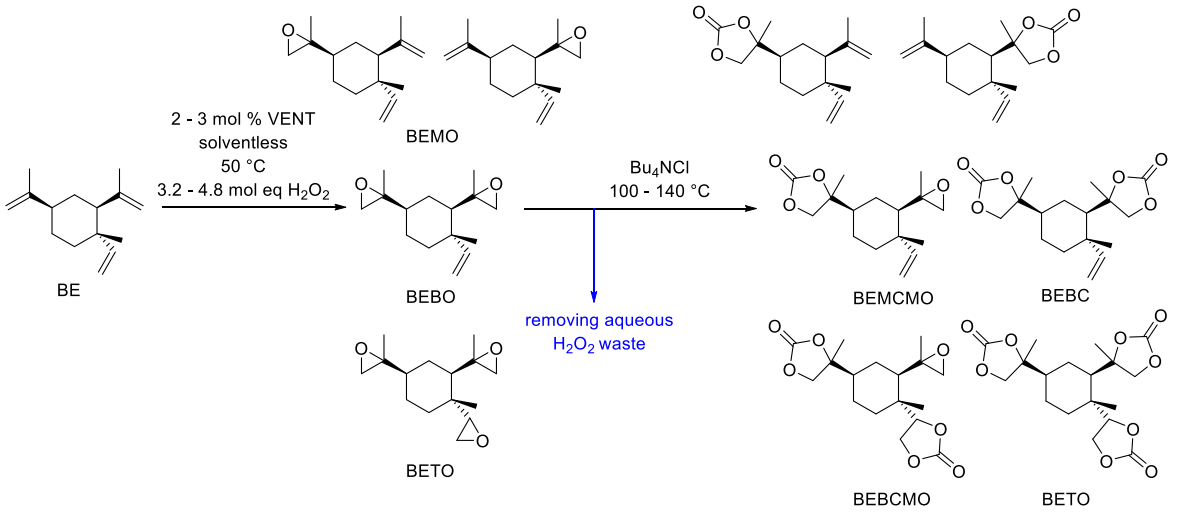

Figure 5.1 Future work: a strategy for implementing the catalytic carbonation system developed for 1,2-LC and 8,9-LC into BE.

5.3 Conclusions and future work - β-elemene cyclic carbonates

The activity of β-elemene epoxide groups in the carbonation reactions was highly dependent on the temperature of reaction (Figure 5.2). At low temperatures (100-120 °C) in 24 h only the less sterically hindered groups were able to react (Figure 5.2 yellow dots). The more sterically hindered epoxide (Figure 5.2 red dot) was able to open at temperatures in the range of 120-140 °C, but it required long reaction times of 65 h at 120 °C. Moreover, the carbonation of sterically hindered epoxide groups also suffered from high production of **BEMCMD** and **BEBCMD** which is a result of epoxide rearrangements. This can occur due to a lack of available CO_2 related to high conversion and high viscosity of the reaction, or due to high temperature of reaction, or by the combination of both of these factors.

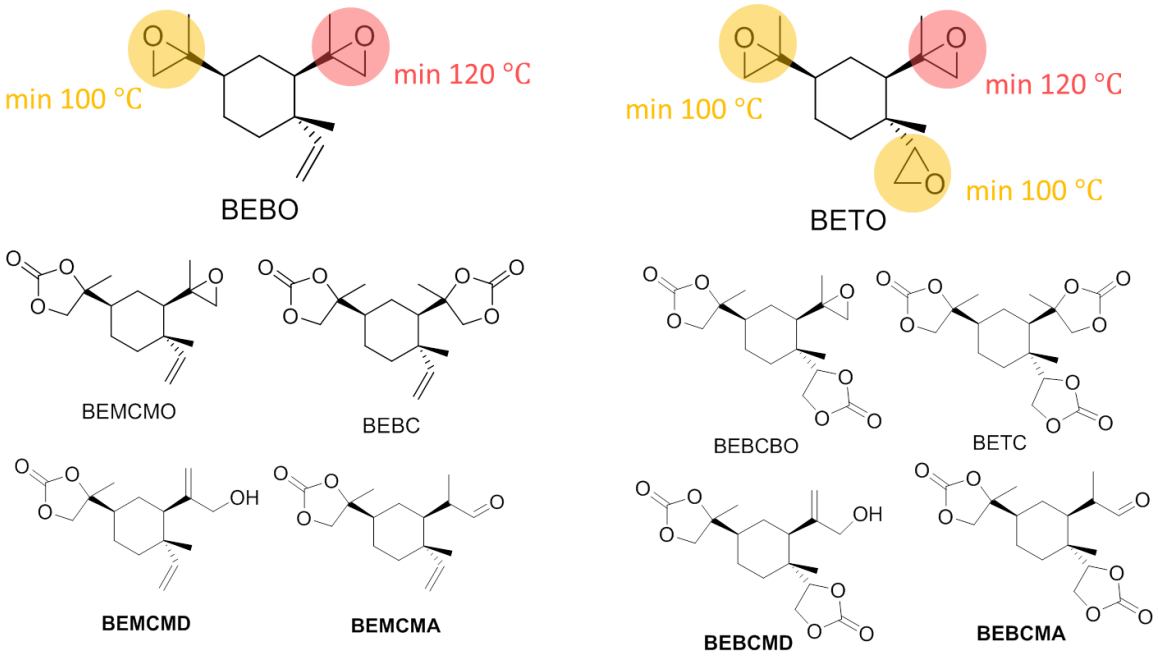

Figure 5.2 The activity of BE epoxide groups depending on the carbonation reaction temperature and the carbonation products achieved in this report.

Probably the most promising cyclic carbonate derived from β-elemene is **BEBCMO** as it can be synthesised at temperature as low as 100 °C in 24 h, which is a 40 °C reduction in the reaction temperature compared to the other multifunctional carbonates such as **BEBC**, **BETC** or **BEBCMD**. In future work, the two cyclic carbonates functionalities in **BEBCMO** could be used in NIPU synthesis and additional epoxide could be used for post-functionalisation (Figure 5.3). Future work should also include expanding the scope of carbonation catalyst in order to lower the temperature required for the synthesis of β-elemene-derived cyclic carbonates. The improvement in catalytic **BETO** synthesis should be addressed in the future work of developing green epoxidation protocols.

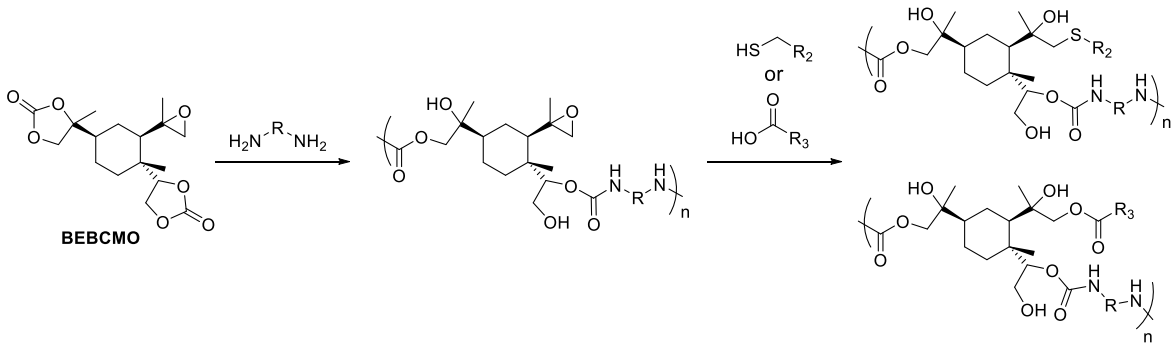

Figure 5.3 Future work: Implementing BEBCMO in NIPU synthesis and possible postfunctionalisation.

As it has been described in the introduction in Chapter 4, most NIPU syntheses are reported neat. However, controlling stoichiometric ratio on small laboratory scale without solvent might be difficult, thus a use of solvent is recommended. A polar solvent, such as methanol, can improve the conversion of cyclic carbonate aminolysis by increasing the positive charge on a carbonyl carbon.[9] Additionally, the use of catalyst could be investigated to further improve the aminolysis. Among reported catalysts, organocatalyst TBD was consistently reported as one of the most efficient.[10] Moreover, TBD might have an effect on regioselectivity of the aminolysis, as it was shown by Kleij and co-workers in ring opening of **1,2,8,9-LC** using TBD and allyl amine.[11] It is worth noting this effect was strongly dependent on the carbonate and amine structures.

5.4 Closing remarks

To summarise, **BE** epoxidation allows for delivering novel epoxides which in the future could be used in the polymer industry. Implementing **BE** epoxidation as a green industrial epoxidation require developing easily scalable catalytic protocols with a minimal waste production. The synthesised β-elemene-derived epoxides were used in the carbonation reaction yielding novel β-elemene-derived cyclic carbonates. However, future work is required to improve the carbonation of the sterically hindered epoxide in **BE**. The use of β-elemene-derived cyclic carbonates in NIPU synthesis still have to be investigated, but the low temperature, selective synthesis of **BEBCMO** showed great potential for delivering new monomer for NIPU synthesis.

5.5 References

1. W. B. Cunningham, J. D. Tibbetts, M. Hutchby, K. A. Smug, M. G. Davidson, U. Hintermair, P. Plucinski and S. D. Bull, *under review*.
2. D. C. Duncan, R. C. Chambers, E. Hecht and C. L. Hill, *J. Am. Chem. Soc.*, 1995, **117**, 681-691.
3. H. Yasuda, L.-N. He, T. Sakakura and C. Hu, *J. Catal.*, 2005, **233**, 119-122.
4. F. Chen, X. Li, B. Wang, T. Xu, S.-L. Chen, P. Liu and C. Hu, *Chem. Eur. J.*, 2012, **18**, 9870-9876.
5. S. H. Szczepankiewicz, C. M. Ippolito, B. P. Santora, T. J. Van de Ven, G. A. Ippolito, L. Fronckowiak, F. Wiatrowski, T. Power and M. Kozik, *Inorg. Chem.*, 1998, **37**, 4344-4352.
6. J. Langanke, L. Greiner and W. Leitner, *Green Chem.*, 2013, **15**, 1173-1182.
7. D. Limnios and C. G. Kokotos, *J. Org. Chem.*, 2014, **79**, 4270-4276.
8. A. M. R. Hall, P. Dong, A. Codina, J. P. Lowe and U. Hintermair, *ACS Catal.*, 2019, **9**, 2079-2090.
9. M. Blain, A. Cornille, B. Boutevin, R. Auvergne, D. Benazet, B. Andrioletti and S. Caillol, *J. Appl. Polym. Sci.*, 2017, **134**, 44958.
10. M. Blain, L. Jean-Gérard, R. Auvergne, D. Benazet, S. Caillol and B. Andrioletti, *Green Chem.*, 2014, **16**, 4286-4291.
11. S. Sopeña, V. Laserna, W. Guo, E. Martin, E. C. Escudero-Adán and A. W. Kleij, *Adv. Synth. Catal.*, 2016, **358**, 2172-2178.